Energy Transfer Between the Geosphere and Biosphere

by

Peter Anthony Canovas III

A Dissertation Presented in Partial Fulfillment
of the Requirements for the Degree
Doctor of Philosophy

Approved October 2016 by the
Graduate Supervisory Committee:

Everett L. Shock, Chair
Hilairy E. Hartnett
Thomas G. Sharp
James A. Tyburczy
Arjun M. Heimsath

ARIZONA STATE UNIVERSITY

December 2016

ABSTRACT

One goal of geobiochemistry is to follow geochemical energy supplies from the external environment to the inside of microbial cells. This can be accomplished by combining thermodynamic calculations of energy supplies from geochemical processes and energy demands for biochemical processes. Progress towards this goal is summarized here. A critique of all thermodynamic data for biochemical compounds involved in the citric acid cycle (CAC) and the formulation of metabolite properties allows predictions of the energy involved in each step of the cycle as well as the full forward and reverse cycles over wide ranges of temperature and pressure. These results allow evaluation of energy demands at the center of many microbial metabolic systems. Field work, sampling, and lab analyses from two low-temperature systems, a serpentinizing system, and a subglacial setting, provide the data used in these thermodynamic analyses of energy supplies. An extensive literature summary of microbial and molecular data from serpentinizing systems found is used to guide the evaluation and ranking of energy supplies used by chemolithoautotrophic microbes. These results constrain models of the distribution of microbial metabolisms throughout the low-temperature serpentinization systems in the Samail ophiolite in Oman (including locales of primary and subsequent alteration processes). Data collected from Robertson Glacier in Alberta, Canada, together with literature data from Lake Vida in Antarctica and bottom seawater, allowed thermodynamic analyses of low-temperature energy supplies in a glacial system. Results for 1460 inorganic redox reactions are used to fully inventory the geochemical energy sources that support the globally extensive cold biosphere.

I dedicate this dissertation to my parents, Pete and Sally, who stood by and supported me through a tumultuous academic career. Without them, I would not have made it nearly this far.

ACKNOWLEDGMENTS

All of my interactions with people, both good and bad, have had a profound effect on not only this dissertation, but also my personal and professional development. From early on, in my undergraduate career, I was fortunate enough to have the encouragement and support of academic advisors such as Drs. Joe Loter, David McKee, Gene Billiot, George Tintera and many others. This support continued on through my work as a masters student with guidance from Wolfgang Bach and Katrina Edwards as well as Tim Grove, Rob Sohn, Ken Sims, and Chris Reddy and many others. Here at ASU I was lucky enough to have the supervisory committee and advisor that I had as well as the rest of the GEOPIG lab group. Through my years working on my dissertation their patience and guidance is what allowed all of this to happen. I'm especially indebted to my committee: Hilairy Hartnett, Tom Sharp, Jim Tyburczy, and Arjun Heimseth, as well as my advisor Everett Shock for their guidance, support and patience. Everett Shock in particular was invaluable in his constant support and instruction as well as introducing me to field work in Yellowstone National Park, Oman, Iceland, and Robertson Galcier. All of which were truly wonderful and unique experiences that allowed me to craft a course of study that was interesting, intriguing and multidisciplinary in approach. Further help and instruction came from Tori Hoehler and Mike Kubo at NASA-Ames, Eric Boyd at MSU, as well as Freider Klein, Tom McCollom, and Mitch Schulte.

The support of the GEOPIG lab group was also instrumental and I'll never forget the insightful conversations and help I've received from all of its members, including but not limited to Tod Windman, Jeff Havig, Jeff Dick, Tucker Elly, Jessie Hobbs, Tracy Lund, Jordan Okie, Kris Fectue, Chris Glein, Alta Howells, Kristin Johnson, Chris

Lawler, Jeremy Melton, Grayson Boyer, Apar Prasad, Alysia Cox, Vince Debes, Panjai Prapaipong, Ziming Yang, Kirt Robinson, Brian St. Clair, and Kristin Paris. Other friends, collegues, coworkers, and researchers at ASU were also a constant pillar of support as well, such as Allie Rutlidge, John-Francois Smekens, Mike Rutkowski, Greg Breneka, Jorge Nunez, Carolina Londono, Misha and Natasha Zolotov, Wyatt, DuFrane, Danny Foley, David Haddad, Kurt Leinenweber, Stan Klonowski, Alicia Mangosing, Becky Polley, and Becca Dial.

Finally I'd like to thank my roommates Tyler Thompson, Zack Bowles and Sean Merrit for all their support and help during some of the less fortunate occurances I went through during my graduate career. They got me through some of the toughest times of my life and encouraged me to stick with it and not let anything get me down. Finally, I must thank all of my family especially my parents, Pete and Sally and my uncle Roger as well.

TABLE OF CONTENTS

Page

CHAPTER Page

CHAPTER Page

APPENDIX Page

LIST OF TABLES

Table Page

LIST OF FIGURES

Figure Page

Figure Page

Figure Page

I. INTRODUCTION

Understanding the effect the geochemical environment has on microbial populations is critical for evaluating the viability of potential metabolic strategies, growth potential of populations, community structure and global elemental and nutrient cycling. The disequilibria in geochemical environments provides the supply of energy used by microorganisms to transfer extracellular redox potential into cells to drive energy production for growth and maintenance. This, in turn, is directly linked to the energetic demands of microorganisms through their metabolic strategies, maintenance energy requirements, and ability to subsist when resources and/or competition limits their productivity. A diverse variety of geochemical environments have been studied, and lab investigations across a wide range of temperatures and pressures have been pursued (Fig.1). Fig. 1A displays the temperature and depth where microbial activity (or evidence for it) has been recorded; note that geotherms are given to 4km depth. While depth may be a physical barrier for microbes to overcome, it is not necessarily a physiochemical barrier. This makes it crucial to look at temperature vs. pressure to investigate what the real extremes of life are, as is depicted in Fig. 1B. As may be inferred from this figure, increasing pressure seems to facilitate microbial tolerance to elevated temperatures. This has been observed in laboratory experiments where maximum growth and/or survival temperatures of microorganisms can be increased by culturing at elevated pressures (Collins et al., 2010; Takai et al., 2008). For this reason, results from laboratory experiments should also be considered when evaluating the extent to which the deep biosphere may extend. As can be seen in Fig.1C, microbes are capable of persisting to slightly higher temperatures than what is found in nature, but the most startling result is

the high pressures to which they may be able to survive when temperatures are as great as ~125 ^{o}C at 1000 bars. This indicates the deep biosphere may extend much deeper than was previously thought. Depths up to 50 km on continental margins where subduction zones inject cold, altered oceanic crust into the mantle at temperatures ranging from 90 – 120 °C could provide a stable and habitable zone for microorganisms to thrive. This depth could be even greater at fast, cold subduction zones with high slab dip angles such as those occurring at Tonga or Kermadec (Syracuse et al., 2010).

Given the diverse range of temperatures, pressures, and geochemical environments that microorganisms inhabit, it is necessary to understand the energetic needs and the potential bioenergetic costs to running their metabolisms. As a step in reaching this goal, the thermodynamics of the citric acid cycle (CAC), also known as the tricarboxylic acid cycle (TCA), or Krebs cycle, were examined, and are presented in Chapter 2. The CAC is unique in that every organism either utilizes it, or at the very least parts of it, in order to survive and propagate. Under aerobic conditions (or when there is a suitable electron acceptor) the CAC is a major metabolic pathway in organisms for the aerobic oxidation of sugars, fatty acids and some amino acids. It can also be run in reverse to synthesize important biomolecules through carbon fixation. Defining the standard partial molal thermodynamic properties of species in the CAC over wide ranges of temperatures and pressures will contribute to answering questions about energy *demands* in geobiochemical systems.

Quantifying energy *supplies* available in geochemical systems can complete the study of energy transfers from the geosphere to the biosphere. The low-temperature continental serpentinizing system at the Samail Ophiolite in the Sultanate of Oman offers

an opportunity to investigate and quantify the geochemical supply of energy at a distinct type of system that is far from equilibrium, as described in Chapter 3. In serpentinizing systems, ultramafic rocks are at or near the Earth's surface and are out of equilibrium with respect to the atmosphere and hydrosphere with which they interact. During serpentinization, water reacts with reduced ferrous iron minerals to generate highly-reduced fluids often enriched with hydrogen, methane, and other reduced solutes such as ammonia and hydrogen sulfide. Disequilibria are enhanced when reduced fluids in the subsurface interact with oxidized meteoric waters and the atmosphere. Due to the sluggish kinetics involved in redox transformations at low temperatures, microorganisms are able to capitalize on and exploit the potential energy available due to the disequilibria of the system. By quantifying the amounts of disequilibria, combined with inferences from studies that report microbial and molecular data for serpentinizing systems, qualitative and quantitative predictions and modeling helps to evaluate the habitability and potential metabolic strategies of serpentinizing systems.

Serpentinizing systems are only one type of low-temperature system on Earth (or arguably on other planets with the potential for life). In fact, the largest fraction of Earth's biosphere is the cold biosphere ($\leq 5°C$). In order to ascertain the supply of energy from geochemical processes in the cold biosphere, geochemical data were collected from Robertson Glacier in Alberta, Canada and combined with data from Lake Vida in Antarctica and from the global mean characterization of oceanic bottom seawater, as presented in Chapter 4. By utilizing the data from these model systems to encompass the greater cold biosphere in conjunction with 1460 inorganic redox reactions, the abundance of energy throughout the cold biosphere was quantified, and the results

used to depict geochemical energy supplies that can be used to predict the occurrence of various diverse metabolic strategies. Linking these reactions in each model system to the amount of energy per milliliter of cold fluid allows a visualization of the amount of energy cold geochemical processes deliver to microbial populations.

A summary of future directions for research expandincy based on these studies is presented in Chapter 5.

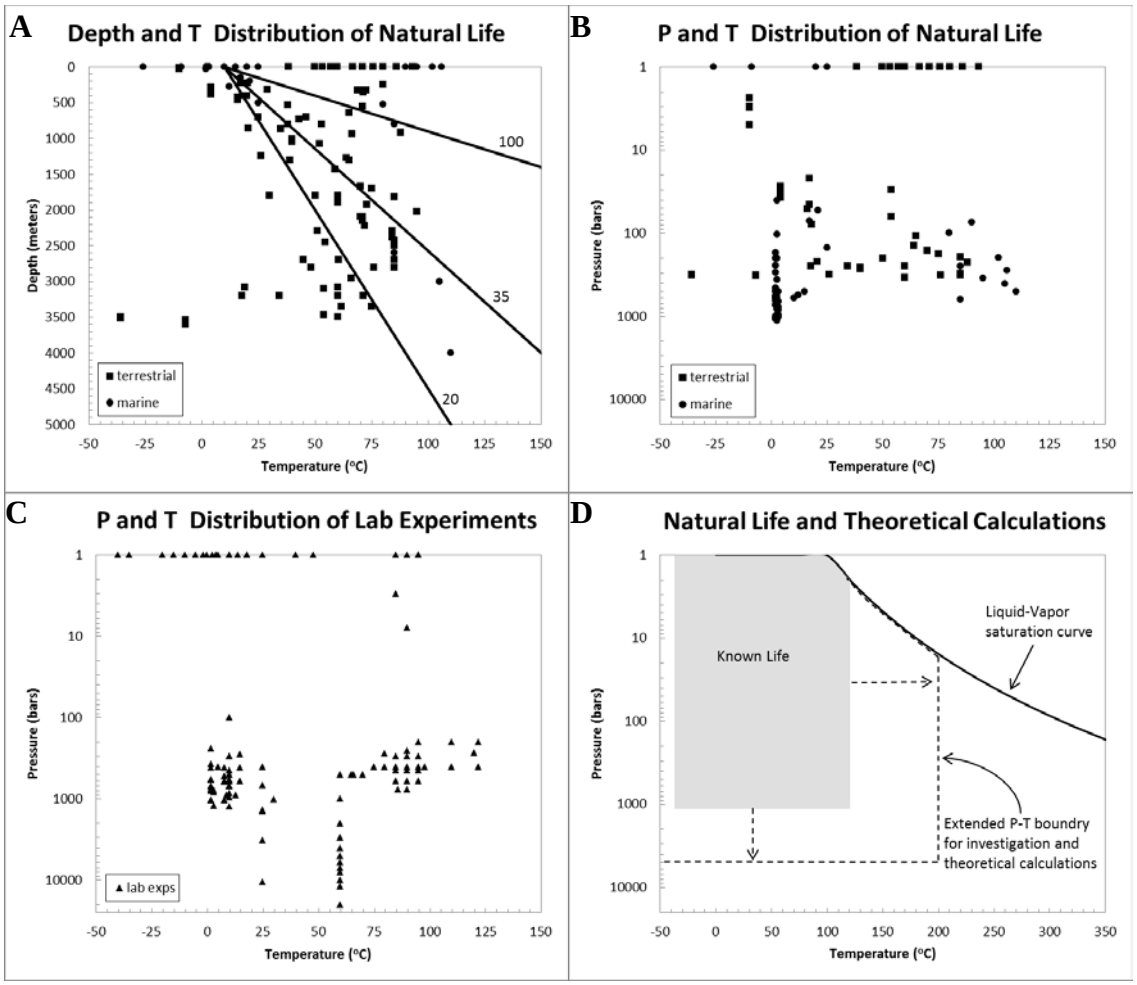

Figure 0. Figures depicting the extent to which known life persists in natural systems (A, B) and in the laboratory (C) and the scope of the theoretical calculations performed in the context of what we already know about the persistence of life (D). Figure 1A compares subsurface habitats with geothermal gradients plotted as depth vs. temperature for 20, 30, and 100°C /km. Symbols show the depth (excluding that of seawater) and temperature of subsurface samples. Continental symbols are filled squares while marine samples are filled circles. Figure 1B shows the recalculation of data from Fig. 1A from depth to pressure. Pressures were calculated based on the respective depth for each sampling environment based on each overlying geologic setting. It should be noted that many of the depths in Fig. 1A had no readily available pressure data correlated with them. When possible, the pressures were estimated, but many could not be predicted with great accuracy and thus were left out of the plot. Fig. 1C displays the temperatures and pressures at which microbes have been documented to persist in laboratory cultures. Fig. 1D displays the extent to which theoretical calculations for metabolic process can be addressed at elevated temperatures and pressures, such as those used for the citric acid cycle in Chapter 2. For references and details concerning the construction of these plots, see Appendix I.

II. GEOBIOCHEMISTRY OF METABOLISM: STANDARD STATE THERMODYNAMIC PROPERTIES OF THE CITRIC ACID CYCLE

2.1. Integrating Biochemical Cycles with Geochemical Processes

Microbial metabolisms take advantage of a huge diversity of geochemical energy sources. Electron donors (reductants) include hydrogen, methane and other light hydrocarbons, hydrogen sulfide, sulfur, thiosulfate, $S_4O_6^{2-}$, polysulfides, sulfide minerals, ferrous iron and ferrous minerals, carboxylic acids, hydroxy acids, alcohols, amino acids, and other organic compounds. Many organic compounds can also be fermented through disproportionation reactions. Electron acceptors (oxidants) range from oxygen to carbon dioxide and carbon monoxide, ferric iron, nitrate, nitrite, nitrous and nitric oxide, sulfate, thiosulfate, sulfite, and sulfur. Chemotrophic microorganisms can be aerobic or anaerobic, and autotrophic, heterotrophic, or mixotrophic. Considerable progress has been made by examining hundreds of reactions that couple electron donors and acceptors and generating frameworks for calculating energy and power supplies in diverse geochemical environments (McCollom and Shock, 1997; McCollom, 2000; 2007; Amend and Shock, 2001; Amend et al., 2003; 2004; 2011; 2013; Shock et al., 2005; 2010; Rogers and Amend, 2006; Windman et al., 2007; Skoog et al., 2007; Costa et al., 2009; Dodsworth et al., 2012; Frank et al., 2015). Meanwhile, less is known about the energy or power demands of microbes over wide ranges of temperature, pressure, and composition. With this in mind, we shift our focus inside the cell and onto the thermodynamics of the citric acid cycle (CAC), also known as the tricarboxylic acid cycle or the Krebs cycle, because it is central to many other biochemical processes.

Through the citric acid cycle, redox potential is captured from extracellular electron donors and acceptors that are far from equilibrium with one another and is used to provide the energy needed for biomolecule synthesis. Run in one direction, conventionally referred to as forward, the CAC is a major catabolic pathway in organisms for the aerobic oxidation of sugars, fatty acids, and amino acids, as shown in Fig 1.

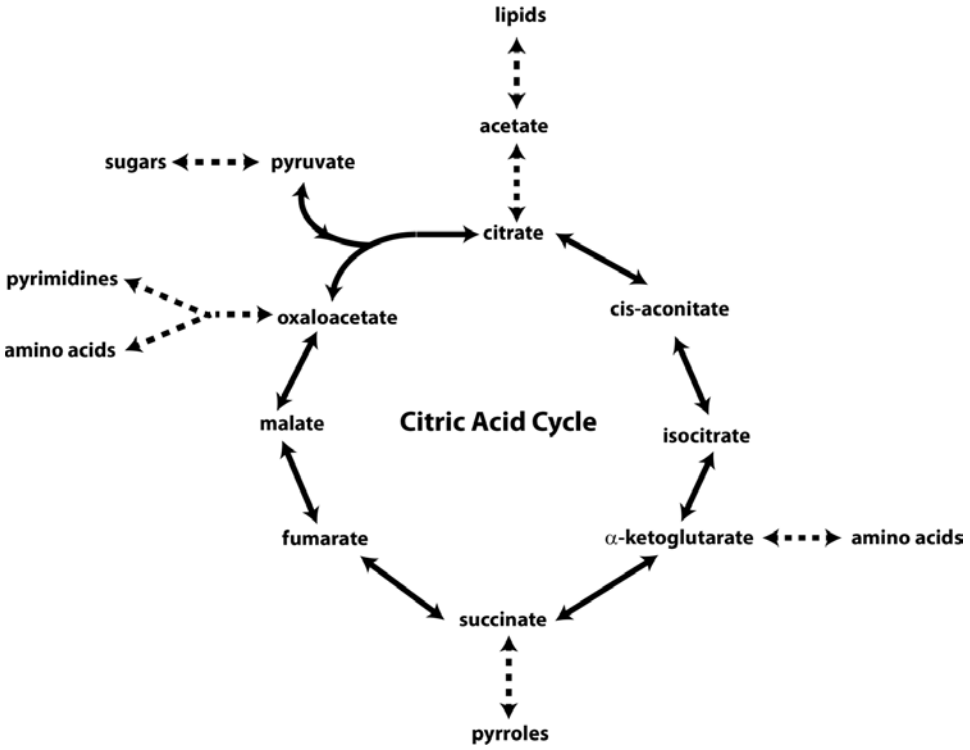

Figure 1. Schematic depiction of the citric acid cycle. Clockwise corresponds to the forward (catabolic) direction, and counterclockwise to the reverse (anabolic) direction, either of which is possible depending on the organism or the environment. Solid arrows indicate steps in the cycle. Dashed arrows indicate how the cycle connects to various processes integral to other metabolic pathways. The CAC is an integral part of overall metabolism and when run in reverse it is a powerful carbon fixation pathway connected to the production of lipids from citrate, sugars through pyruvate, amino acids through alpha-ketoglutarate and oxaloacetate, pyrroles through succinate, and pyrimidines through oxaloacetate.

Run in the opposite direction the reverse citric acid cycle (rCAC) is involved in anabolic CO_2 fixation into these and other organic metabolites. In the present study we developed

an internally consistent set of standard state[1] thermodynamic properties and equation-of-state coefficients for compounds used in the citric acid cycle that are compatible with data for biomolecules that are linked to the CAC, as well as thermodynamic data for inorganic and organic aqueous species widely used in geochemical calculations. Implications of the thermodynamics of various steps in the CAC are discussed below, following an explanation of how internally consistent thermodynamic data were obtained.

2.2. Standard Partial Molal Thermodynamic Properties

Energy changes in geochemical reactions can be calculated by combining analytical data from natural environments with standard state thermodynamic properties of minerals, gases, organic compounds, and aqueous solutes. The approach often taken in theoretical geochemistry is to evaluate chemical affinities (A) using the relation

$$A = 2.303RT\ log(K/Q)\ , \quad (1)$$

where *R* stands for the gas constant, *T* indicates temperature in Kelvin, *Q* represents the activity product for a given reaction, and *K* designates the equilibrium constant, which is related to the standard partial molal Gibbs energy of a reaction ($\Delta_r \bar{G}^o$) via

$$\Delta_r \bar{G}^o = -2.303RT\ logK\ . \quad (2)$$

In turn, the standard partial molal Gibbs energy of a reaction is related to the standard partial molal Gibbs energies of the *ith* species in the reaction ($\bar{G}_i^o$) by

$$\Delta_r \bar{G}^o = \sum_i^r \nu_{i,r}\, \bar{G}_i^o \quad (3)$$

[1] The aqueous solution standard state adopted in this study is a hypothetical one molal solution referenced to infinite dilution at any temperature and pressure. The standard state for gases is the pure gas at any temperature and 1 bar, and that for liquid H_2O is the pure liquid at any temperature and pressure.

where $\nu_{i,r}$ represents the stoichiometric reaction coefficient of the *ith* species in the *rth* reaction, which is positive for products and negative for reactants. Values of $\bar{G}_i^o$ at elevated and pressures temperatures, $\bar{G}_{i,P,T}^o$, are calculated from

$$\bar{G}_{i,P,T}^o = \bar{G}_{i,P_r,T_r}^o - \bar{S}_{i,P_r,T_r}^o(T - T_r) + \int_{T_r}^{T} \bar{C}_{P,i}^o \, dT - T \int_{T_r}^{T} \bar{C}_{P,i}^o \, dlnT + \int_{P_r}^{P} \bar{V}_i^o \, dP \quad , \qquad (4)$$

where $\bar{G}_{i,P_r,T_r}^o$ and $\bar{S}_{i,P_r,T_r}^o$ stand for the standard partial molal Gibbs energy and entropy of the *ith* species at the reference pressure of 1 bar and temperature of 298.15K, and $\bar{V}_i^o$ and $\bar{C}_{P,i}^o$ represent the standard partial molal volume and isobaric heat capacity of the *ith* species, which are both functions of temperature and pressure. When the standard partial molal Gibbs energy of formation from the elements at the reference conditions, $\Delta\bar{G}_f^o$, is used in place of $\bar{G}_{i,P_r,T_r}^o$then Eqn 4 represents the *apparent* standard partial molal Gibbs energy of formation of the *ith* chemical species at any temperature and pressure (Helgeson et al., 1981; Anderson, 2005). In addition, we make use of standard state enthalpies of reaction $\Delta_r\bar{H}^o$ that are related to standard state Gibbs energies of reaction by

$$\Delta_r\bar{G}^o = \Delta_r\bar{H}^o - T\Delta_r\bar{S}^o \quad , \qquad (5)$$

where

$$\Delta_r\bar{S}^o = \sum_i^r \nu_{i,r} \, \bar{S}_i^o \quad . \qquad (6)$$

In the rest of this paper, we use the following abbreviations: $\bar{S}^o = \bar{S}_{i,P_r,T_r}^o$, $\bar{V}^o = \bar{V}_i^o$, and $\bar{C}_P^o = \bar{C}_{P,i}^o$.

The present study builds on efforts to maintain internal consistency among standard state thermodynamic properties of aqueous biomolecules (Dick et al., 2005; 2006; LaRowe and Helgeson, 2006a; 2006b; 2007), dissolved gases and organic

compounds (Shock et al., 1989; Shock and Helgeson, 1990; Shock, 1992; 1993; 1995; Shock and McKinnon, 1993; Schulte and Shock, 1993; Dale et al., 1997; Amend and Helgeson, 1997a; 1997b; 2000; Haas and Shock, 1999; Plyasunov and Shock, 2000a; 2000b; 2001a; 2001b; Amend & Plyasunov, 2001; Schulte et al., 2001; Plyasunov et al., 2004; 2006a; 2006b; Plyasunova et al., 2005), inorganic ions and complexes (Shock and Helgeson, 1988; Haas et al., 1995; Sverjensky et al., 1997; Shock et al., 1997a; 1997b; Sassani and Shock, 1998; Murphy and Shock, 1999; Sverjensky et al., 2014), metal-organic complexes (Shock and Koretsky, 1993; 1995; Prapaipong et al., 1999; Prapaipong and Shock, 2001), and pure organic gases, liquids, and solids (Helgeson et al., 1998; Richard and Helgeson, 1998; Richard, 2001; LaRowe and Dick, 2012). In the case of aqueous species, predictions at elevated temperatures and pressures (up to 5kb and 1000°C) are made with the revised Helgeson-Kirkham-Flowers (HKF) equations of state (Helgeson et al., 1981; Tanger and Helgeson, 1988; Shock and Helgeson, 1988; Shock et al., 1992). An additional feature of the revised HKF equations is the existence of methods that allow estimation of standard partial molal properties of solutes at the reference conditions of 25°C and 1 bar, as well as the various revised-HKF parameters that allow predictions at other temperatures and pressures (Shock, 1995; Shock et al., 1997a; Sverjenksy et al., 1997; 2014; Plyasunov and Shock, 2001a). Correlations among standard state properties and HKF parameters from Shock and Helgeson (1988), Shock (1995), and Shock et al. (1997a) were used in the present study.

Standard state thermodynamic data and HKF parameters are already established for citric acid and its anions (LaRowe and Helgeson, 2006a), and succinic acid and its anions (Shock, 1995). Maintaining consistency is facilitated further through reactions

connecting CAC species with amino acids, inorganic solutes and gases, and biomolecules for which standard state data have already been evaluated. These reactions are listed in Table 1, together with reaction properties selected in this study. Another set of essential data is the standard state dissociation constants and other thermodynamic properties of acid dissociation reactions listed in Table 2. As described below, the experimentally derived data in Tables 1 and 2, together with newly proposed estimation methods, provide the means for obtaining standard state thermodynamic data for all of the acids and anions involved in the CAC.

Table 1. Reactions used to obtain the standard partial molal thermodynamic properties of citric acid cycle species, together with experimental data from the literature at 298.15K and 1 bar.

Reaction		log K	$\Delta_r \bar{H}^{o}$ [a]	$\Delta_r \bar{C}_P^{o}$ [b]
A	aspartate$^-$ = fumarate^{2-} + NH_4^+	-2.830[c]	5860.[c]	-35.1[c]
B	fumarate^{2-} + H_2O = malate^{2-}	0.623[d]	-3745.2[d]	-8.60[d]
C	oxaloacetate^{2-} + NAD^{2-}_{red} + H^+ = malate^{2-} + NAD^-_{ox}	12.190[e]	-21505.[f]	
D	aspartate$^-$ + α-ketoglutarate^{2-} = oxaloacetate^{2-} + glutamate$^-$	-0.845[g]	454.[g]	
E	alanine + α-ketoglutarate^{2-} = pyruvate$^-$ + glutamate$^-$	0.134[h]	1410.[h]	
F	isocitrate^{3-} = citrate^{3-}	1.069[i]		
G	*cis*-aconitate^{3-} + H_2O = citrate^{3-}	1.49[j]		

[a] cal mol^{-1}, [b] cal mol^{-1} K^{-1}, [c]Goldberg et al. (1986), [d]Gajewski et al. (1985), [e]Jesperson (1976), [f]adjusted from the value reported by Jesperson (1976) to maintain consistency with the standard enthalpy of dissociation of phosphoric acid from Shock et al. (1997a) (see text), [g]Kishore et al. (1998), [h]Tewari et al. (1998), [i]calculated from data reported by Blair (1969) (see text), [j]Krebs (1953).

The framework provided by the revised-HKF equations and estimation methods makes it possible to calculate standard state thermodynamic properties of individual species in the CAC at elevated temperatures and pressures. As a result, standard state properties can be estimated for reactions that make up the cycle, as well as reactions that

connect the CAC with relevant further steps of biomolecule synthesis and reactions that link the CAC to the geochemical composition of environments outside microbial cells. These types of integration allow the results reported here to be used to evaluate the energetics of abiotic synthesis, microbial metabolism, and other biogeochemically relevant processes at any conditions where life occurs.

Table 2. Standard state properties for dissociation reactions involving citric acid cycle species selected from the literature.

Acid dissociation	pKa	$\Delta_r\overline{H}^{o}$ [a]	$\Delta_r\overline{C}_P^{o}$ [b]
citric, first	3.128[c]	997.[c]	-26.43[c]
second	4.760[c]	583.[c]	-39.33[c]
third	6.396[c]	803.[c]	-50.87[c]
cis-aconitic, first	1.9[d]		
second	4.3[d]		
third	6.4[d]		
isocitric, first	3.287[e]		
second	4.714[e]		
third	6.396[e]		
α-ketoglutaric, first	2.24[f]	3346.[g]	
second	5.12[f]	1912.[g]	
succinic, first	4.29[h]	760.[h]	-44.[h]
second	5.68[h]	40.[h]	-59.8[h]
fumaric, first	3.093[i]	110.[i]	-37.[j]
second	4.603[i]	-680.[i]	-52.8[j]
malic, first	3.460[k]	706.[k]	-37.[k]
second	5.096[k]	-282.[k]	-52.8[k]
oxaloacetic, first	2.555[l]	3824.[f]	
second	4.370[l]	956.[f]	
pyruvic	2.490[l]	2900.[k]	

[a]cal mol^{-1}, [b]cal mol^{-1} K^{-1}, [c]LaRowe and Helgeson (2006a) ($\Delta_r\overline{C}_P^{o}$ values corrected, see Table 3), [d]Schloss et al. (1984), [e]Hitchcock (1958), [f]Martell et al. (1997), [g]estimated in Kishore et al. (1998) by assuming that the values of the standard molar entropy changes were the same as those of the respective oxaloacetic acid reactions, [h]Shock (1995), [i]Christensen et al. (1967), [j]estimated by Gajewski et al. (1985) by using the same values for malic acid species, [k]Eden and Bates (1959), [l]Pedersen (1952), [k]Christensen et al. (1976).

In the following discussion, details are given of the selection of data that permit the maintenance of internal consistency, and the methods used or developed in this study to fill gaps in experimental data. The approach taken for each major acid constituent of the cycle is summarized, and the resulting standard state data and HKF parameters are compiled in Table 3. These data and parameters can be used with the SUPCRT92 (Johnson et al., 1992) and CHNOSZ (Dick, 2008) computer codes to explore the consequences of including the CAC in geobiochemical calculations.

2.2.1 Succinic and Citric Acids

Standard state thermodynamic properties and HKF equation-of-state parameters for succinic acid and its anions were adopted from Shock (1995) where experimental partial molal volumes for Na-succinate solutions and equilibrium constants for the first and second dissociation of succinic acid were used to constrain standard state data and to test predictions at elevated temperatures. Data for citric acid and its anions were taken from LaRowe and Helgeson (2006a) where high-temperature heat capacity measurements were used to constrain HKF parameters. LaRowe and Helgeson (2006a) provide values of the standard partial molal volume ($\bar{V}^o$) at the reference conditions of 298.15K and 1 bar, but not the $a_1 - a_4$ nonsolvation HKF parameters that allow $\bar{V}^o$ calculations at elevated temperatures and pressures. These parameters were estimated in the present study using correlations from Shock (1995).

Table 3. Summary of standard partial molal thermodynamic data at 25°C and 1 bar for aqueous species in the citric acid cycle, along with equation of state parameters required to calculate the corresponding properties at high temperatures and pressures. Unless otherwise indicated, revised-HKF equation-of-state parameters were estimated in this study using the correlation algorithms of Shock and Helgeson (1988) and Shock (1995) (see Appendix B).

Species	$\Delta\overline{G}^o_f$ [a]	$\Delta\overline{H}^o_f$ [a]	$\overline{S}^o$ [b]	$\overline{C}^o_p$ [b]	$\overline{V}^o$ [c]	$a_1\times10^1$ [c]	$a_2\times10^{-2}$	a_3 [e]	$a_4\times10^{-4}$	c_1 [b]	$c_2\times10^{-4}$	$\omega_e\times10^{-5}$
citric acid	-297180.[g]	-364527.[g]	78.89[g]	73.47[h]	112.98[h]	17.2019	32.2622	-2.7285	-4.1127	96.43[g]	-11.57[g]	-0.06[g]
H_2-citrate$^-$	-292912.[g]	-363530.[g]	67.92[g]	47.04[h]	102.48[h]	16.3576	30.3484	-2.2931	-4.0336	89.40[g]	-14.12[g]	1.50[g]
H-citrate^{2-}	-286417.[g]	-362947.[g]	48.09[g]	7.71[h]	91.08[h]	15.1704	27.6579	-1.6828	-3.9224	73.14[g]	-21.06[g]	2.48[g]
citrate^{3-}	-277690.[g]	-363750.[g]	16.13[g]	-43.16[h]	74.08[h]	12.9466	22.6175	-0.5371	-3.7140	31.50[g]	-24.41[g]	2.75[g]
cis-aconitic acid	-236200.[av]	-291400.[aw]	63.9[l]	64.0[ay]	108.7[ao]	16.5766	30.8449	-2.4072	-4.0541	59.7379	1.3622	-0.1640
H_2-*cis*-aconitate$^-$	-233600.[av]	-290480.[ax]	58.2[l]	37.6[az]	98.2[an]	15.4873	28.3760	-1.8452	-3.9521	51.8298	-3.6503	0.7477
H-*cis*-aconitate^{2-}	-227700.[av]	-289900.[ax]	40.4[l]	-1.7[az]	86.8[an]	14.6306	26.4342	-1.4046	-3.8718	30.3757	-4.1266	2.6010
cis-aconitate^{3-}	-218970.[au]	-290700.[ax]	8.4[l]	-52.6[az]	69.8[an]	13.0954	22.9544	-0.6139	-3.7279	-0.2807	-4.7435	4.6843
isocitric acid	-295880.[j]	-363960.[p]	76.4[l]	74.5[af]	114.3[af]	17.3743	32.6530	-2.8170	-4.1289	68.8768	2.3996	-0.0820
H_2-isocitrate$^-$	-291390.[j]	-362960.[k]	64.7[l]	48.1[ag]	103.8[ah]	16.2126	30.0199	-2.2197	-4.0200	61.1741	-3.5230	0.6493
H-isocitrate^{2-}	-284960.[j]	-362380.[k]	45.1[l]	8.8[ag]	92.4[ah]	15.3672	28.1034	-1.7830	-3.9408	39.9770	-3.9993	2.5298
isocitrate^{3-}	-276230.[i]	-363180.[k]	13.1[l]	-42.1[ag]	75.4[ah]	13.8316	24.6230	-0.9928	-3.7969	9.3108	-4.6163	4.6132
α-ketoglutaric acid	-201800.[o]	-245700.[o]	76.1[l]	39.9[aq]	95.7[aq]	14.8287	26.8831	-1.5061	-3.8903	41.2055	-1.0189	-0.0840
H-α-ketoglutarate$^-$	-198800.[o]	-242300.[o]	77.1[l]	2.9[ar]	88.9[al]	14.1054	25.2437	-1.1337	-3.8226	15.3765	-4.0709	0.4615
α-ketoglutarate^{2-}	-191800.[n]	-240400.[n]	60.1[n]	-49.9[ar]	82.7[al]	13.9562	24.9058	-1.0570	-3.8086	-19.3472	-4.7108	2.3026
succinic acid	-177800.[q]	-218000.[q]	62.3[q]	53.3[q]	82.44[q]	12.9872[q]	22.7109[q]	-0.5623[q]	-3.7178[q]	51.0740[q]	0.3050[q]	-0.1744[q]
H-succinate$^-$	-172060.[q]	-217350.[q]	45.2[q]	9.3[q]	69.99[q]	11.6617[q]	19.7057[q]	0.1226[q]	-3.5935[q]	26.1173[q]	-3.9932[q]	0.9446[q]
succinate^{2-}	-164380.[q]	-217350.[q]	19.5[q]	-50.5[q]	56.32[q]	10.4577[q]	15.8622[q]	3.5716[q]	-3.4346[q]	-14.0383[q]	-4.7180[q]	2.9170[q]
fumaric acid	-154820.[z]	-186260.[z]	60.62[l]	47.00[z]	77.9[ab]	12.3542	21.2748	-0.2318	-3.6585	45.9510	-0.3174	-0.1860
H-fumarate$^-$	-150600.[z]	-186150.[z]	46.83[l]	10.0[z]	65.4[y]	11.0637	18.3498	0.4327	-3.5376	26.4785	-3.9848	0.9199
fumarate^{2-}	-144320.[x]	-186830.[x]	23.48[x]	-42.8[ae]	51.7[y]	9.9248	15.7683	1.0191	-3.4309	-7.3722	-4.6247	2.8572
malic acid	-213530.[s]	-259310.[s]	68.21[s]	56.43[t]	82.22[ad]	12.9644	22.6577	-0.5461	-3.7157	53.9427	0.6143	-0.1360
H-malate$^-$	-208810.[s]	-258610.[s]	54.75[s]	19.4[u]	75.40[ac]	12.3867	21.3482	-0.2490	-3.6615	34.5541	-3.8709	0.8000
malate^{2-}	-201860.[r]	-258890.[r]	30.48[r]	-33.4[u]	69.19[ac]	12.2779	21.1017	-0.1928	-3.6513	0.8264	-4.5108	2.7512
oxaloacetic acid	-200000.[ai]	-235100.[ai]	72.9[l]	29.1[as]	79.1[as]	12.5492	21.7168	-0.3324	-3.6768	32.3818	-2.0859	-0.1050
H-oxaloacetate$^-$	-196600.[ai]	-231300.[ai]	74.0[l]	-7.9[at]	72.3[ap]	11.8516	20.1357	0.0269	-3.6114	5.2703	-4.2017	0.5084
oxaloacetate^{2-}	-190600.[aa]	-230300.[aa]	57.2[aa]	-60.7[at]	66.1[ap]	11.7014	19.7949	0.1041	-3.5973	-29.4812	-4.8417	2.3465
pyruvic acid	-117000.[w]	-140300.[m]	62.1[l]	36.3[aj]	64.6[aj]	10.5381	17.1584	0.7032	-3.4883	37.4903	-1.3746	-0.1760
pyruvate$^-$	-113600.[v]	-137400.[v]	60.4[v]	-3.7[ak]	51.5[ak]	9.0836	13.8620	1.4526	-3.3521	11.2428	-4.1508	0.7144

[a]cal mol^{-1}, [b]cal mol^{-1} K^{-1}, [c]cm^3 mol^{-1}, [d]cal mol^{-1} bar^{-1}, [e]cal K mol^{-1} bar^{-1}, [f]cal K mol^{-1}, [g]LaRowe and Helgeson (2006a) [h]corrected values from LaRowe and Helgeson (2006a) where $\overline{C}_p^o$ and $\overline{V}^o$ entries are switched in their table B1, [i]calculated using log K for reaction (F) from Table 1, and $\Delta\bar{G}_f^o$ of citrate^{3-} from the table. [j]calculated using $\Delta\bar{G}_f^o$ of isocitrate^{3-} in the table, pKa values from Table 2 and properties of H^+ from Shock et al. (1997a), [k]calculated by assuming the Δ_rH^o for dissociation of isocitric acid species are equivalent to those of citric acid species (to four significant figures), [l]calculated using $\Delta\bar{G}_f^o$ and $\Delta\bar{H}_f^o$ listed in the table along with $\overline{S}^o$ for the elements from Cox et al. (1989) and the relation $\Delta\bar{G}_f^o = \Delta\bar{H}_f^o - T(\bar{S}^o - \sum\bar{S}_{elements}^o)$, [m]calculated using $\Delta\bar{H}_f^o$ of pyruvate$^-$ in the table and Δ_rH^o from Table 2, [n]calculated using properties for reaction (D) in Table 1, properties for aspartate$^-$ and glutamate$^-$ from Dick et al. (2006), and properties for oxaloacetate^{2-} in the table, [o]calculated from the values of α-ketoglutarate^{2-} in the table, and dissociation reaction properties from Table 2, [p]calculated from an estimation of Δ_rH^o for reaction (F) in Table 1 as described in the text, [q]Shock (1995), [r]calculated using the properties of reaction (B) in Table 1, properties of H_2O consistent with Shock et al. (1992), and the properties of fumarate^{2-} in the table, [s]calculated using the properties of malate^{2-} in the table, and reaction properties of dissociation from Table 2, [t]Sijpkes et al. (1989), [u]calculated using the property of malic acid in the table and dissociation properties in Table 2, [v]calculated using properties of reaction (E) in Table 1, data for alanine and glutamate$^-$ from Dick et al. (2006), and the properties of α-ketoglutrate^{2-} in the table, [w]calculated using the values of pyruvate$^-$ in the table and the pKa in Table 2, [x]calculated using properties of reaction (A) in Table 1, data for aspartate$^-$ from Dick et al. (2006), and properties of NH_4^+ from Shock et al. (1997a), [y]given by Dalla-Beta and Schulte (2009) from Yokoyama et al. (1988), [z]calculated using the values in the table for fumarate^{2-} and dissociation reaction properties from Table 2, [aa]calculated using properties of reaction (C) from Table 1, NAD^{2-}_{red} and NAD^-_{ox} from LaRowe and Helgeson (2006b), and H^+ from Shock et al (1997a), [ab]estimated from $\overline{V}^o$ of H-fumarate$^-$ assuming the volume change of the first dissociation reaction is equal to that of succinic acid, [ac]Apelblat and Manzurola (1990), [ad]Manzurola and Apelblat (1985), [ae]calculated using $\Delta_rC_p^o$ for reaction (B) in Table 1, $\overline{C}_p^o$ of malate^{2-} from the table, and $\overline{C}_p^o$ of H_2O consistent with Shock et al. (1992), [af]estimated from citric acid by analogy to the differences in the properties of 2-pentanol and 3-pentanol (see text), [ag]estimated by assuming the same $\Delta_rC_p^o$ of dissociation as that of citric acid, [ah]calculated by assuming the same Δ_rV^o of dissociation as that of citric acid, [ai]estimated assuming the same Δ_rV^o of dissociation as that of malic acid, [aj]estimated using $\overline{C}_p^o$ values of lactic acid from Shock (1995), acetone from Shock & Helgeson (1990), and 2-propanol from Origlia-Luster and Woolley (2003) as described in the text, [ak]estimated by assuming the same $\Delta_rC_p^o$ of dissociation as that of lactic acid from Shock (1995), [al] calculated using the values in the table for oxaloacetate^{2-} and dissociation reaction properties from Table 2, [am]estimated by assuming that Δ_rV^o of dissociation is the same as that of lactic acid from Shock (1995), [an]estimated assuming the same change in volume of dissociation as that of citric acid species, [ao]estimated from $\overline{V}^o$ of citric acid in the table using the difference in volume between fumaric acid and malic acid, [ap]estimated by assuming that Δ_rV^o of dissociation is equal to that of malic acid, [aq]estimated using the properties of pyruvic acid in the table, and propanoic acid and glutaric acid from Shock (1995) as described in the text, [ar]estimated from the value for α-ketoglutaric acid in the table and assuming the same $\Delta_rC_p^o$ of dissociation as that of the corresponding malic acid species, [as]estimated using the properties of pyruvic acid in the table, together with propanoic acid and succinic acid from Shock (1995) as described in the text, [at]estimated from the property of oxaloacetic acid in the table assuming the same $\Delta_rC_p^o$ of dissociation as that of the corresponding malic acid species, [au]calculated using log K for reaction (G) in Table 1, $\Delta\bar{G}_f^o$ of citrate^{3-} in the table and H_2O consistent with Shock et al. (1992), [av]calculated using the pK_a value in Table 2, [aw]estimated from $\Delta\bar{H}_f^o$ of citric acid in the table using the difference in enthalpy between fumaric acid and malic acid, [ax]estimated assuming the same enthalpy of dissociation as that of citric acid species from Table 2, [ay]estimated from $\overline{C}_p^o$ of citric acid in the table using the difference in heat capacity between fumaric acid and malic acid, [az]estimated assuming the same change in heat capacity of dissociation as that of citric acid species from Table 2.

2.2.2 Fumaric and Malic Acids

In addition to adopting existing data for succinic and citric acid species, another way of establishing internal consistency with existing standard state data and HKF parameters is to use data for reactions that link species in the CAC to amino acids and other biomolecules for which data have already been obtained. As an example, Goldberg et al. (1986) provide data that yield equilibrium constants, as well as enthalpies and heat capacities of reaction for

$HOOCCH_2CHNH_2COO^-$ (aspartate$^-$) ⇔ $^-OOC(CH)_2COO^-$ (fumarate^{2-}) + NH_4^+ , (A)

and values at the reference conditions are listed in Table 1. These data, together with $\Delta\bar{H}_f^o$ and $\Delta\bar{G}_f^o$ of aspartate$^-$ from Dick et al. (2006) and NH_4^+ from Shock et al. (1997a) were used to calculate $\Delta\bar{H}_f^o$ and $\Delta\bar{G}_f^o$ for fumarate^{2-} listed in Table 3. In turn, these results were used with the data in Table 1 for the reaction

$^-OOC(CH)_2COO^-$ (fumarate^{2-}) + H_2O ⇔ $^-OOCCH_2CHOHCOO^-$ (malate^{2-}) (B)

to obtain consistent values of $\Delta\bar{H}_f^o$ and $\Delta\bar{G}_f^o$ for malate^{2-}. Corresponding properties of the monovalent (H-fumarate$^-$, H-malate$^-$) and fully protonated fumaric and malic acid species were calculated from the dissociation reaction properties given in Table 2. Combining $\Delta\bar{G}_f^o$ values for fumarate^{2-} and succinate^{2-} from Table 3 yields a standard Gibbs energy of reaction of −20060 cal mol^{-1} for: fumarate^{2-} + 2 H^+ + 2 e^- = succinate^{2-}, which is within 0.5% of the value of −20140 cal mol^{-1} calculated from the potential obtained by Borsook and Schott (1931a; 1931b) (0.437 V) for the same reaction using methylene blue, a platinum electrode, and succinate dehydrogenase to catalyze the reaction.

The value of $\Delta_r \bar{C}_P^o$ for reaction A in Table 1 reported by Goldberg et al. (1986) has a large uncertainty leading to an unacceptably large uncertainty in $\bar{C}_P^o$ of fumarate^{2-}. Therefore, $\bar{C}_P^o$ of fumarate^{2-} was determined from $\Delta_r \bar{C}_P^o$ for reaction B in Table 1, together with the $\bar{C}_P^o$ of H_2O consistent with Shock et al. (1992), and the $\bar{C}_P^o$ of malate^{2-}, which is independently determined from the measured $\bar{C}_P^o$ of malic acid listed in Table 3 and the $\Delta_r \bar{C}_P^o$ values for the dissociation reactions to form H-malate$^-$ and malate^{2-} from Table 2. Values of $\bar{C}_P^o$ for the monovalent (H-fumarate$^-$) and fully protonated fumaric acid species were calculated from the dissociation reaction properties in Table 2.

The standard partial molal volumes of malic acid species in Table 3 are all from experimental measurements, as are the $\bar{V}^o$ values for fumarate^{2-} and H-fumarate$^-$. An estimate of $\bar{V}^o$ of fumaric acid was made by assuming that the change in volume for the first fumaric acid deprotonation reaction can be estimated by that for succinic acid. The resulting value is listed in Table 3.

2.2.3 Oxaloacetic, α-ketoglutaric, and Pyruvic Acids

The three keto-acids involved in the CAC are treated together owing to the similarities in the methods we propose to estimate data that are not available from experiments. Values of $\Delta \bar{G}_f^o$, and $\Delta \bar{H}_f^o$, for oxaloacetate^{2-} ($^-$OOCC=OCH$_2$COO$^-$) were calculated from the properties in Table 1 for the reaction:

$$\text{oxaloacetate}^{2-} + \text{NAD}^{2-}_{\text{red}} + \text{H}^+ \Leftrightarrow \text{malate}^{2-} + \text{NAD}^-_{\text{ox}} \qquad \text{(C)}$$

using the properties for malate^{2-} obtained as described above and H$^+$ from Shock et al. (1997a), following the hydrogen ion convention, together with data for the reduced (NAD$^{2-}_{\text{red}}$) and oxidized (NAD$^-_{\text{ox}}$) forms of nicotinamide adenine dinucleotide from LaRowe and Helgeson (2006b). In the process of obtaining $\Delta \bar{H}_f^o$ for oxaloacetate^{2-}, the

selected value of $\Delta_r \bar{H}^o$ was re-evaluated to be consistent with the enthalpic contribution of the phosphate buffer, which is 105 cal mol^{-1} more negative in Shock et al. (1997a) than the value used by Jesperson (1976). The corresponding properties for protonated forms of oxaloacetic acid species were calculated using dissociation reaction data from Table 2. The standard state thermodynamic properties $\Delta \bar{G}_f^o$ and $\Delta \bar{H}_f^o$ for α-ketoglutarate^{2-} listed in Table 3 were calculated from the properties of the reaction

aspartate$^-$ + α-ketoglutarate^{2-} ⇔ oxaloacetate^{2-} + glutamate$^-$ (D)

listed in Table 1 using the properties of oxaloacetate^{2-} from Table 3 and those of aspartate$^-$ and glutamate$^-$ from Dick et al. (2006) to maintain internal consistency[2]. Corresponding properties for the protonated forms of α-ketoglutarate^{2-} were calculated using the standard state thermodynamic properties for the dissociation reactions listed in Table 2. Internally consistent standard state values of $\Delta \bar{G}_f^o$ and $\Delta \bar{H}_f^o$ for pyruvate$^-$ were calculated at the reference conditions from the reaction properties for

alanine + α-ketoglutarate^{2-} ⇔ pyruvate$^-$ + glutamate$^-$ (E)

listed in Table 1 using the properties of α-ketoglutarate^{2-} determined as described above and listed in Table 3, and corresponding values for the amino acids from Dick et al. (2006). Properties of pyruvic acid were calculated from the resulting properties of pyruvate$^-$ using properties of the dissociation reaction listed in Table 2.

No values of $\bar{C}_P^o$ or $\bar{V}^o$ of any aqueous forms of the three keto-acids are available from experiments, requiring the development of an estimation strategy. Functional-group contributions quantified by regression of multiple sets of experimental data often can be used to estimate standard state properties when data are lacking for individual

[2] See Appendix for a discussion of other experimental constraints on $\Delta \bar{G}_f^o$ of α-ketoglutarate^{2-}.

compounds. However, the presence of multiple functional groups in small organic molecules leads to interactions among those groups that are in close proximity. As a consequence, estimation methods based on group contributions are complicated by higher-order interaction terms that are typically poorly known if quantified at all (Plyasunov et al., 2004; 2006a; Plyasunova et al., 2005). This problem plagues efforts to develop group-contribution approaches for hydroxy- and keto-acids, opening the need for alternative estimations methods. Here we propose methods based on the quantitative similarity of reaction properties for analogous chemical reactions. As an example, $\Delta_r \bar{C}_P^o$ and $\Delta_r \bar{V}^o$ for the oxidative hydration of succinic acid ($HOOCCH_2CH_2COOH$) to malic acid ($HOOCCH_2CHOHCOOH$) given by

$$HOOCCH_2CH_2COOH + H_2O \Leftrightarrow HOOCCH_2CHOHCOOH + H_2(aq) \quad (7)$$

are 25.0 cal mol^{-1} K^{-1} and 7.5 cm^3 mol^{-1}, respectively, using data in Table 3, data for $H_2(aq)$ from Shock et al. (1989) and data for H_2O consistent with Shock et al. (1992). In turn, $\Delta_r \bar{C}_P^o$ and $\Delta_r \bar{V}^o$ for the oxidative hydration of malic acid to tartaric acid ($HOOCCHOHCHOHCOOH$)

$$HOOCCH_2CHOHCOOH + H_2O \Leftrightarrow HOOCCHOHCHOHCOOH + H_2(aq) \quad (8)$$

are 25.5 cal mol^{-1} K^{-1} and 7.7 cm^3 mol^{-1}, respectively, using data from the same sources, together with $\bar{C}_P^o$ and $\bar{V}^o$ of tartaric acid (60.0 cal mol^{-1} K^{-1}, and 83.4 cm^3 mol^{-1}) from Sijpkes et al. (1989). The similarity of these reaction properties means that the calorimetric and volumetric consequences of these analogous reactions are quite similar. It also means that $\Delta_r \bar{C}_P^o$ and $\Delta_r \bar{V}^o$ for the hypothetical reaction that compares structurally similar compounds

$$2\ HOOCCH_2CHOHCOOH \Leftrightarrow HOOCCH_2CH_2COOH + HOOCCHOHCHOHCOOH \quad (9)$$

should be close to zero, which, at 0.5 cal mol^{-1} K^{-1}, and 0.2 cm^3 mol^{-1}, they are. As a consequence, if we assume that $\Delta_r \bar{C}_P^o = 0$ and $\Delta_r \bar{V}^o = 0$ for a reaction balanced in this way, we could estimate unknown values of $\bar{C}_P^o$ or $\bar{V}^o$ for one compound given $\bar{C}_P^o$ or $\bar{V}^o$ values for the others. In the case of estimates for tartaric acid using properties of succinic and malic acids, the uncertainty in $\bar{C}_P^o$ is 0.5 cal mol^{-1} K^{-1} relative to a value of 60.0 cal mol^{-1} K^{-1} (Sijpkes et al., 1989), or 0.83%, which is nearly the same as the reported experimental uncertainty of ~0.8%, and the uncertainty in $\bar{V}^o$ is 0.2 cm^3 mol^{-1} relative to a value of 83.4 cm^3 mol^{-1} (Sijpkes et al., 1989) or 0.2%, which rivals the experimental uncertainty of 0.1%.

Extending the comparison of structurally similar compounds to keto-acids allows us to propose an estimation method for pyruvic acid based on assuming that $\Delta_r \bar{C}_P^o = 0$ and $\Delta_r \bar{V}^o = 0$ for the hypothetical reaction

$$CH_3CHOHCOOH + CH_3C{=}OCH_3 \Leftrightarrow CH_3CHOHCH_3 + CH_3C{=}OCOOH \quad . \qquad (10)$$

lactic acid acetone 2-propanol pyruvic acid

This assumption, together with experimentally determined $\bar{C}_P^o$ and $\bar{V}^o$ values for lactic acid (Shock, 1995), acetone (Shock and Helgeson, 1990), and 2-propanol (Origlia-Luster and Woolley, 2003) leads to 36.3 cal $mol^{-1}K^{-1}$ and 64.6 cm^3 mol^{-1} as estimates for $\bar{C}_P^o$ and $\bar{V}^o$ of pyruvic acid, as listed in Table 3. These values were used to estimate $\bar{C}_p^o$ and $\bar{V}^o$ for pyruvate$^-$ by assuming that $\Delta_r \bar{C}_P^o$ and $\Delta_r \bar{V}^o$ for dissociation of pyruvic acid can be approximated by that of lactic acid.

Following the same strategy for the other keto-acids in the CAC is thwarted by the lack of experimental partial molal properties of α-hydroxyglutaric acid, which eliminates the possibility of estimating data in an analogous way for α-ketoglutaric acid.

Therefore another strategy was developed. The oxidative hydration of propanoic acid to yield pyruvic acid is given by

$$CH_3CH_2COOH + H_2O \Leftrightarrow CH_3C{=}OCOOH + 2\ H_2(aq)\ , \qquad (11)$$

which is closely analogous to reactions (7) and (8). Using the values of $\bar{C}_P^o$ and $\bar{V}^o$ for propanoic acid from Shock (1995) and pyruvic acid estimated as described above, $\Delta_r\bar{C}_P^o$ and $\Delta_r\bar{V}^o$ for this reaction are 37.6 cal $mol^{-1}K^{-1}$ and 29. cm^3 mol^{-1}, respectively, at the reference conditions. We propose using these reaction properties for the analogous oxidative hydration reactions

$$\text{succinic acid} + H_2O \Leftrightarrow \text{oxaloacetic acid} + 2\ H_2(aq) \qquad (12)$$

and

$$\text{glutaric acid} + H_2O \Leftrightarrow \alpha\text{-ketoglutaric} + 2\ H_2(aq) \qquad (13)$$

to estimate $\bar{C}_P^o$ and $\bar{V}^o$ for oxaloacetic acid and α-ketoglutaric acid, using corresponding properties for succinic acid and glutaric acid from Shock (1995). The results are listed in Table 3, together with estimates for the anions of these acids based on assuming that $\Delta_r\bar{C}_P^o$ and $\Delta_r\bar{V}^o$ of the dissociation reactions can be approximated by those of malic acid.

2.2.4 Isocitric and Cis-aconitic Acids

Isocitric acid (1-hydroxypropane-1,2,3-tricarboxylic acid) is an isomer of citric acid (3-carboxy-3-hydroxypentane-1,5-dioic acid), differing by the location of a hydroxyl group, so it can be anticipated that its standard state thermodynamic properties will be similar to those of citric acid. It follows that the magnitude of thermodynamic properties for the isomerization reaction

$$\text{isocitrate}^{3-} \Leftrightarrow \text{citrate}^{3-} \qquad (F)$$

will be small, as confirmed by the available experimental data. Blair (1969) obtained an apparent equilibrium constant for reaction (F) in experiments designed to study Mg complex formation. In that set of experiments the concentrations of both species were measured with spectrophotometry and apparent K values were calculated using a set of equations (Blair, 1968) that relate the apparent equilibrium constant obtained at finite Mg concentrations to that at zero magnesium. Experiments were carried out at an ionic strength of 0.1 M and by maintaining the ionic strength with Na^+ while diluting the concentration of Mg^{2+} toward zero. Assuming that the activity coefficients of citrate^{3-} and isocitate^{3-} are equal leads to the standard state equilibrium constant listed in Table 1, which can be combined with the thermodynamic data from LaRowe and Helgeson (2006a) for citrate^{3-} to obtain $\Delta\bar{G}_f^o$ of isocitrate^{3-} given in Table 3. Dissociation constants from Hitchcock (1958) listed in Table 2, were used to calculate values of $\Delta\bar{G}_f^o$ for the other isocitric acid species in Table 3.

Without experimental evidence of the enthalpy change for isomerization reaction (F), a value was estimated by comparison with another isomerization reaction in which a hydroxyl group effectively moves from one carbon to another,

$$\text{2-pentanol (aq)} \Leftrightarrow \text{3-pentanol (aq)} \quad . \qquad (14)$$

The standard enthalpy change for reaction (14) was calculated from the value of $\Delta\bar{H}_f^o$ for aqueous 2-pentanol (-90663. cal mol^{-1}) from Plyasunov and Shock (2000a), and a value of $\Delta\bar{H}_f^o$ for aqueous 3-pentanol calculated from

$$\Delta\bar{H}_f^o(aq) = \Delta_{hyd}\bar{H}° + \Delta_{vap}\bar{H}° + \Delta\bar{H}_f^o(l) \qquad (15)$$

where $\Delta\overline{H}_f^o(aq)$ stands for the standard partial molal enthalpy of formation of the aqueous species, $\Delta_{hyd}\overline{H}°$ represents the standard partial molal enthalpy of hydration (-15970. cal mol^{-1} from Cabani et al., 1975), $\Delta_{vap}\overline{H}°$ indicates the standard partial molal enthalpy of vaporization (12910. cal mol^{-1} from Majer and Svoboda, 1985), and $\Delta\overline{H}_f^o(l)$ corresponds to the standard partial molal enthalpy of formation of the pure liquid (-88170. cal mol^{-1} from Pedley et al., 1986). The resulting value of $\Delta\overline{H}_f^o$ for aqueous 3-pentanol (-91230. cal mol^{-1}) leads to a value of -567. cal mol^{-1} for the standard enthalpy of hydroxide isomerization used to estimate $\Delta\overline{H}_f^o$ of aqueous isocitric acid with the value of $\Delta\overline{H}_f^o$ for citric acid from Table 3. The $\Delta\overline{H}_f^o$ values of isocitric acid anions were estimated by assuming the same standard enthalpies of dissociation as citric acid.

Values of $\bar{C}_p^o$ and $\bar{V}^o$ for isocitric acid were estimated from those of citric acid by using the corresponding properties of the 2-pentanol/3-pentanol isomerization reaction (14) using data from Fenclová et al. (2004). As shown in Table 3, these differences are minor. The $\bar{C}_p^o$ and $\bar{V}^o$ of isocitric acid anions were estimated by assuming that $\Delta_r\bar{C}_p^o$ and $\Delta_r\bar{V}^o$ of the dissociation reactions could be approximated by the corresponding properties of citric acid.

The isomerization of citrate^{3-} to isocitrate^{3-} passes through an intermediate of *cis*-aconitate^{3-}, which forms from citrate^{3-} by dehydration and yields isocitrate^{3-} through hydration. Internal consistency in $\Delta\bar{G}_f^o$ of *cis*-aconitate^{3-} was maintained by using log K for

$$\textit{cis}\text{-aconitate}^{3-} + H_2O \Leftrightarrow \text{citrate}^{3-} \qquad \text{(G)}$$

at 25°C and 1 bar listed in Table 1, together with $\Delta\bar{G}_f^o$ of citrate^{3-} from Table 3 and $\Delta\bar{G}_f^o$ of H_2O consistent with Shock et al (1992). The resulting value of $\Delta\bar{G}_f^o$ for *cis*-aconitate^{3-} (in Table 3) was used to calculate $\Delta\bar{G}_f^o$ for H-*cis*-aconitate^{-2}, H_2-*cis*-aconitate^{-} and *cis*-aconitic acid (also in Table 3) using values of pKa from Table 2. In the absence of experimental enthalpy data, $\Delta\bar{H}_f^o$ of *cis*-aconitic acid was estimated from that of citric acid by analogy with the dehydration reaction between malate^{2-} and fumarate^{2-} (reaction B), and the assumption that $\Delta_r\bar{H}^o$ for reaction (G) could be approximated using the corresponding property for reaction (B) in Table 1. Values of $\Delta\bar{H}_f^o$ for deprotonated species were estimated by assuming the same $\Delta_r\bar{H}^o$ values for dissociation as each of the corresponding citric acid species from Table 2. The same strategy was used to estimate values of $\bar{C}_p^o$ and $\bar{V}^o$ for *cis*-aconitic acid using the differences between the $\bar{C}_p^o$ and $\bar{V}^o$ values of fumaric acid and malic acid. Likewise, values of $\bar{C}_p^o$ and $\bar{V}^o$ for deprotonated *cis*-aconitic acid species were estimated by assuming that $\Delta_r\bar{C}_P^o$ and $\Delta_r\bar{V}^o$ of each dissociation reaction could be approximated with those of the corresponding citric acid reaction.

2.2.5 Estimating Revised-HKF Parameters

Based on the preceding discussion, values at the reference conditions of $\bar{C}_p^o$, $\bar{V}^o$, $\Delta\bar{H}_f^o$, $\Delta\bar{G}_f^o$, and values of $\bar{S}^o$ calculated from the latter two properties using $\bar{S}^o$ of the elements from Cox et al. (1989), are compiled in Table 3 along with parameters in the revised-HKF equation of state for aqueous solutes (see Appendix A). Revised-HKF parameters, which allow prediction of the same standard state properties at elevated temperatures and pressures, were estimated in this study using the approach proposed by

Shock (1995) for aqueous organic acids, owing to the general absence of experimental data that would permit obtaining parameters through regression (see Appendix B). This approach yields results consistent with revised-HKF parameters for aqueous inorganic ions and complexes (Shock et al., 1997a; Sverjensky et al., 1997), metal-organic complexes (Shock and Koretsky, 1993; 1995; Prapaipong et al., 1999), amino acids and unfolded proteins (Dick et al., 2006), as well as aqueous forms of NAD, NADP, ATP, ADP, and other nucleic bases, nucleosides, and nucleotides (LaRowe and Helgeson, 2006a; 2006b; 2007). Thermodynamic data and parameters in Table 3 can be used to estimate the energetic consequences of reactions in the citric acid cycle and with data and parameters from these other sources to other aqueous species involved in geochemical and biochemical processes throughout the conditions where life exists and beyond.

2.3. Thermodynamic Predictions for the Citric Acid Cycle

Data and parameters summarized in Table 3 were applied in this study to estimate how equilibrium constants for acid dissociations change with temperature and pressure, which is a first step to determining the speciation of the acids involved in the CAC in biochemical and geochemical fluids. In addition, standard Gibbs energies of each of the forward steps in the CAC were predicted over wide ranges of temperature and pressure, extending well beyond the currently known limits of microbial life. Each of these applications is described in this section, which also includes a comparison of the results obtained here with previous thermodynamic analyses of the CAC.

2.3.1 Acid Dissociations

The organic acids in the CAC all undergo dissociation, and their speciation in solution will depend on pH. The influence of temperature and pH at pressures

corresponding to vapor-liquid equilibrium for H_2O (Psat) are shown in Figure 2. These plots of predicted pKa values for each of the acids in the CAC were calculated with data and parameters given in Table 3 using the revised-HKF equation of state. The numbered curves correspond to the order of the dissociation reactions, which in the case of citric acid refer to the reactions

$$1: \text{citric acid} \Leftrightarrow H_2\text{-citrate}^- + H^+ \quad (16)$$

$$2: H_2\text{-citrate}^- \Leftrightarrow \text{H-citrate}^{2-} + H^+ \quad (17)$$

$$3: \text{H-citrate}^{2-} \Leftrightarrow \text{citrate}^{3-} + H^+ \quad . \quad (18)$$

Also shown in these plots are pH values of neutrality for H_2O. These figures can be used to assess how changes in pH and temperature determine the dissociation state of each acid present in solution. It should be kept in mind that in a homogeneous solution all aqueous species are present at all temperatures and pH values, but their relative predominance can be determined quantitatively by comparing pKa values.

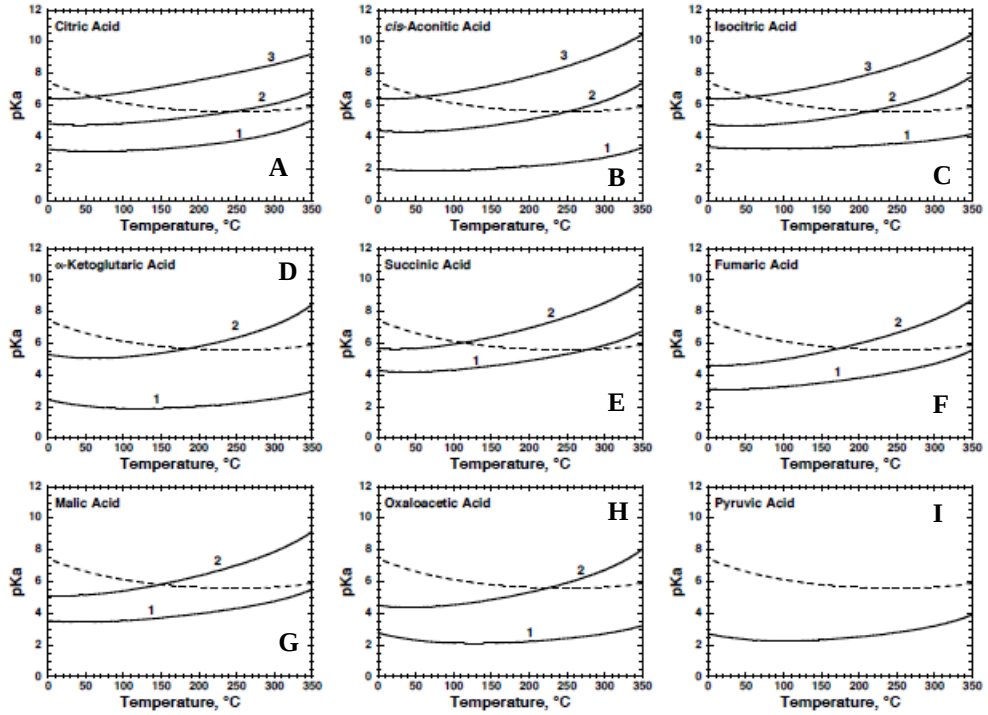

Figure 2. Plots of predicted dissociation constants (solid curves) for all of the organic acids in the CAC as functions of temperature at Psat (pKa = - log K for successive acid dissociation reactions indicated by number, see text). The dashed curve in each plot shows neutral pH for H_2O (on the pKa scale), calculated from log K for the reaction $H_2O = H^+ + OH^-$. Increasing temperature favors increased association as illustrated for the changes along the neutral pH trajectory.

At the reference conditions, as well as mammalian body temperatures and pressures, the form of each acid that dominates at neutrality is the completely dissociated anion (citrate^{3-}, succinate^{2-}, pyruvate$^-$, etc.). The same would be true in hyperalkaline fluids generated by low-temperature serpentinization at continental or seafloor settings. As temperature increases, the dominant form at neutrality of several of the acids can change, and, as shown in Fig 2, dominant forms at 100°C and Psat include H-citrate^{2-}, H-*cis*-aconotate^{2-}, and H-isocitrate^{2-}. Associated forms of the acids will dominate the speciation at strongly acidic conditions, but some anionic forms would still be relatively abundant in a pH = 2, boiling continental hot spring (especially, H_2-*cis*-aconitate$^-$, H-α-

ketoglutarate$^-$, H-oxaloacetate$^-$ and pyruvate$^-$). At circum-neutral environments around submarine hydrothermal systems (~350°C) CAC acid speciation would be dominated by monovalent anions with the exception of succinic acid, and possibly fumaric and malic acids.

2.3.2 Stepwise Changes in Standard State Gibbs Energies of Reaction

As the preceding discussion illustrates, the way that reactions in the CAC are depicted should vary depending on the speciation of the acids in the environment of interest. Here we follow the convention from biochemistry of writing the reactions for each step as involving the completely dissociated anionic forms, which reflects humanity's self-centered fixation on mammalian body temperature and neutral pH. An example of a charge-and-mass-balanced version of the forward CAC, composed of reactions including coupled metabolites and coenzymes, is shown in Fig 3, and the reactions corresponding to each step are listed in Table 4.

Table 4. Individual reactions representing forward steps in the citric acid cycle, balanced by mass and charge, as illustrated in Fig 3 and 4, using the biochemical convention of fully dissociated anions.

1. $citrate^{3-} \Rightarrow$ *cis*-$aconitate^{3-} + H_2O$

2. *cis*-$aconitate^{3-} + H_2O \Rightarrow isocitrate^{3-}$

3. $isocitrate^{3-} + NAD^-_{ox} \Rightarrow$ α-$ketoglutarate^{2-} + NAD^{2-}_{red} + CO_2(aq)$

4. α-$ketoglutarate^{2-} + NAD^-_{ox} + ADP^{3-} + HPO_4^{2-} \Rightarrow succinate^{2-} + NAD^{2-}_{red} + CO_2(aq) + ATP^{4-}$

4A. α-$ketoglutarate^{2-} + CoA + NAD^-ox \Rightarrow$ succinyl-$CoA^- + NAD^{2-}$red $+ CO_2(aq)$

4B. succinyl-$CoA^- + ADP^{3-} + HPO_4^{2-} \Rightarrow CoA + ATP^{4-} + succinate^{2-}$

5. $succinate^{2-} \Rightarrow fumarate^{2-} + H_2(aq)$

5A. $succinate^{2-} + FAD \Rightarrow fumarate^{2-} + FADH_2$

6. $fumarate^{2-} + H_2O \Rightarrow malate^{2-}$

7. $malate^{2-} + NAD^-_{ox} \Rightarrow oxaloacetate^{2-} + NAD^{2-}_{red} + H^+$

0. $pyruvate^- + NAD^-_{ox} + oxaloacetate^{2-} + H_2O \Rightarrow citrate^{3-} + NAD^{2-}_{red} + CO_2(aq) + H^+$

0A. $pyruvate^- + NAD^-_{ox} + CoA \Rightarrow$ acetyl-$CoA + NAD^{2-}_{red} + CO_2(aq)$

0B. acetyl-$CoA + oxaloacetate^{2-} + H_2O \Rightarrow citrate^{3-} + CoA + H^+$

Overall forward citric acid cycle resulting in pyruvate oxidation, NAD and FAD reduction, and ATP generation:

$pyruvate^- + 4NAD^-_{ox} + ADP^{3-} + HPO_4^{2-} + 2H_2O + FAD \Rightarrow 3CO_2(aq) + 4NAD^{2-}_{red} + 2H^+ + ATP^{4-} + FADH_2$

Substituting reaction 5 for 5A as a proxy for the reduction of FAD, as in Fig 4:

$pyruvate^- + 4NAD^-_{ox} + ADP^{3-} + HPO_4^{2-} + 2H_2O \Rightarrow 3CO_2(aq) + 4NAD^{2-}_{red} + 2H^+ + ATP^{4-} + H_2(aq)$

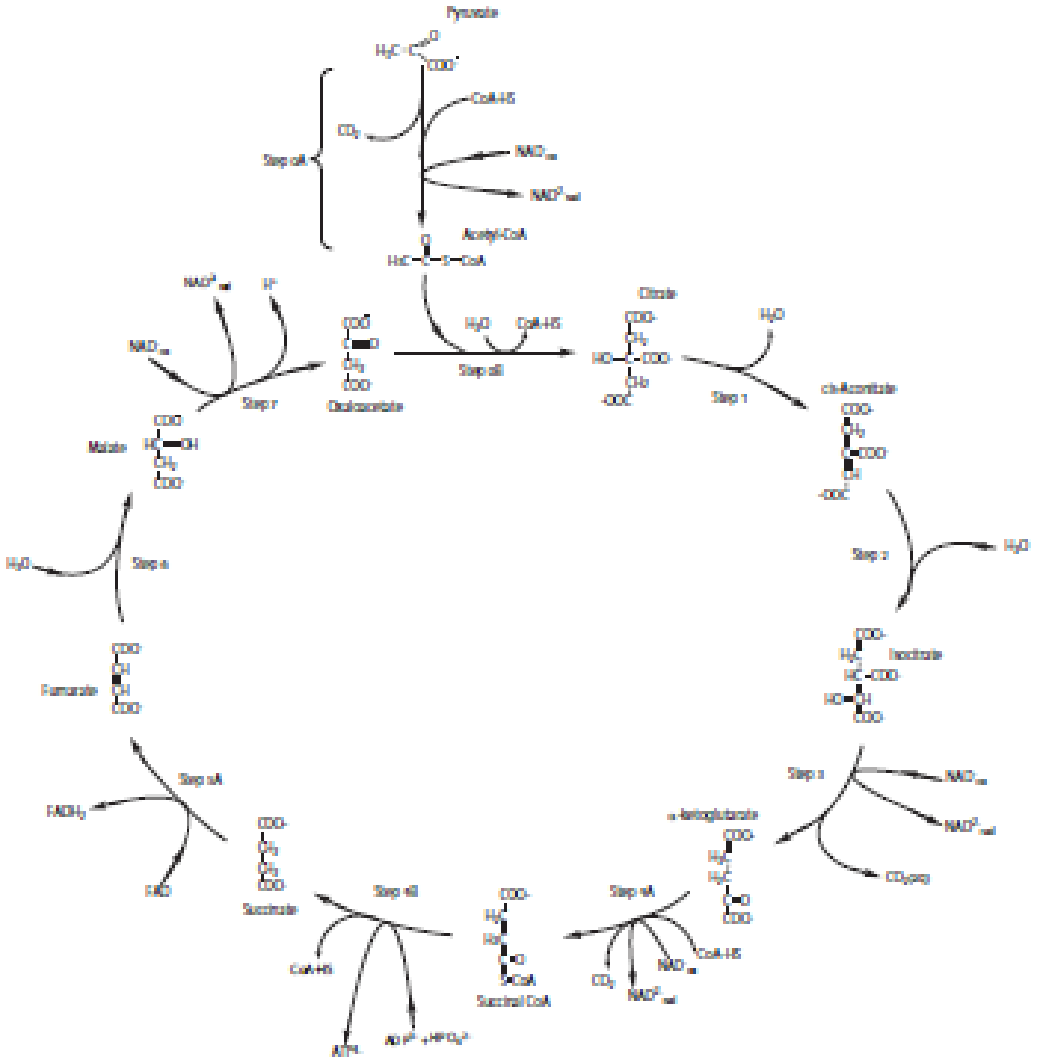

Figure 3. A CAC depiction that includes mass- and charge-balanced reactions involving acid anions, major intermediaries, and coenzymes for each numbered step as outlined in Table 4. The clockwise direction indicated by the arrows corresponds to the catabolic CAC. The catalytic coenzyme Co-A helps to lower the activation energies of several steps, but ultimately does not contribute to the thermodynamic properties of the corresponding reactions. Molecular structures are provided in Appendix C.

The forward cycle begins with two primer steps. In the first (step 0A), pyruvate decarboxylates and reacts with coenzyme A (CoA-HS) to form acetyl-CoA (see molecular structures in Appendix C), via reduction of NAD^-_{ox}. Acetyl-CoA is then coupled to oxaloacetate and dehydrates to form citrate (step 0B). The primer steps in the CAC involve the transfer of a pyruvate-derived acetyl group ($-COCH_3$) from acetyl-CoA

to oxaloacetate to form citrate. From there, an isomerization process takes place through the *cis*-aconitate intermediary (often left out in representations of the cycle) resulting in the transfer of the hydroxyl group in citrate one carbon over to yield isocitrate via sequential dehydration (step 1) and hydration (step 2) reactions. This sets the stage for step 3 where α-ketoglutarate is produced through decarboxylation and oxidation coupled to production of NAD^{-2}_{red}, which leaves the cycle and is coupled to adenosine triphosphate (ATP) synthesis elsewhere in cellular metabolism. Meanwhile, α-ketoglutarate continues in the cycle and is decarboxylated to succinyl-CoA and coupled (Step 4A) to the production of another NAD^{-2}_{red}. The conversion of succinyl-CoA to succinate is coupled to the production of ATP from adenosine diphosphate (ADP) and inorganic phosphate in step 4B. Succinate is oxidized to fumarate, coupled to the reduction of flavin adenine dinucleotide (FAD) in step 6, and the double bond in fumarate is hydrated to yield the hydroxyl group in malate in step 7. Oxidation of the hydroxyl group in malate to the keto group in oxaloacetate coupled to the reduction of NAD^{-}_{ox} (step 8) and release of a proton closes the cycle by providing one of the reactants leading to citrate in step 0B.

In summary, during a complete turn of the forward CAC coenzyme-A is involved twice, once between pyruvate and citrate, and again between α-ketoglutarate and succinate. Three oxidation reactions are coupled to reduction of NAD^{-}_{ox} or FAD cofactors, and there is one step in which ATP is generated from ADP. In their reduced forms, NAD^{-2}_{red} and $FADH_2$ serve as energy-rich transport molecules and diverge from the CAC to take part in the production of ATP through oxidative phosphorylation. In addition, three decarboxylation reactions, three hydration reactions, one dehydration

reaction and one deprotonation reaction are included in the forward cycle. One complete forward cycle yields one $FADH_2$, one ATP, two CO_2 molecules and three NAD^{-2}_{red} (or four, including the primer step of creating acetyl-CoA from pyruvate). Run in the opposite direction the reverse citric acid cycle (rCAC) is involved in anabolic CO_2 fixation into organic metabolites, and the oxidized compounds NAD^{-}_{ox} and FAD can be products.

In a thermodynamic treatment the CAC can be simplified by omitting the co-enzymes acetyl-CoA and succinyl-CoA that lower the activation energy of steps 0 and 4, and therefore do not influence the thermodynamic properties of the cycle. The resulting thermodynamically relevant representation of the process is shown in Figure 4 in which steps 0A and 0B in Table 4 are replaced by step 0, and step 4 replaces steps 4A and 4B to permit an overall energetic analysis. We have also substituted step 5 in Table 4 for step 5A, as internally consistent standard state thermodynamic data and HKF parameters are not available for FAD and $FADH_2$.

Predicted values of the standard Gibbs energies of reaction ($\Delta_r G°$) for the 8 steps in the forward CAC shown in Fig 4 and listed in Table 4, as well as the overall forward reaction given at the end of Table 4, are shown as functions of temperature at the vapor-liquid saturation pressures (Psat, or boiling curve) of H_2O in Figure 5. All of the curves in Fig 5 were calculated with standard state thermodynamic data and parameters from Table 3 using the revised-HKF equations of state (Appendix A). Standard Gibbs energies of steps 0, 2, and 8 are predicted to become increasingly positive with increasing temperature in more-or-less monotonic fashions. Note that the ranges of the ordinates of the plots in Fig 5 differ, as do the magnitudes of the changes in $\Delta_r G°$. The changes in

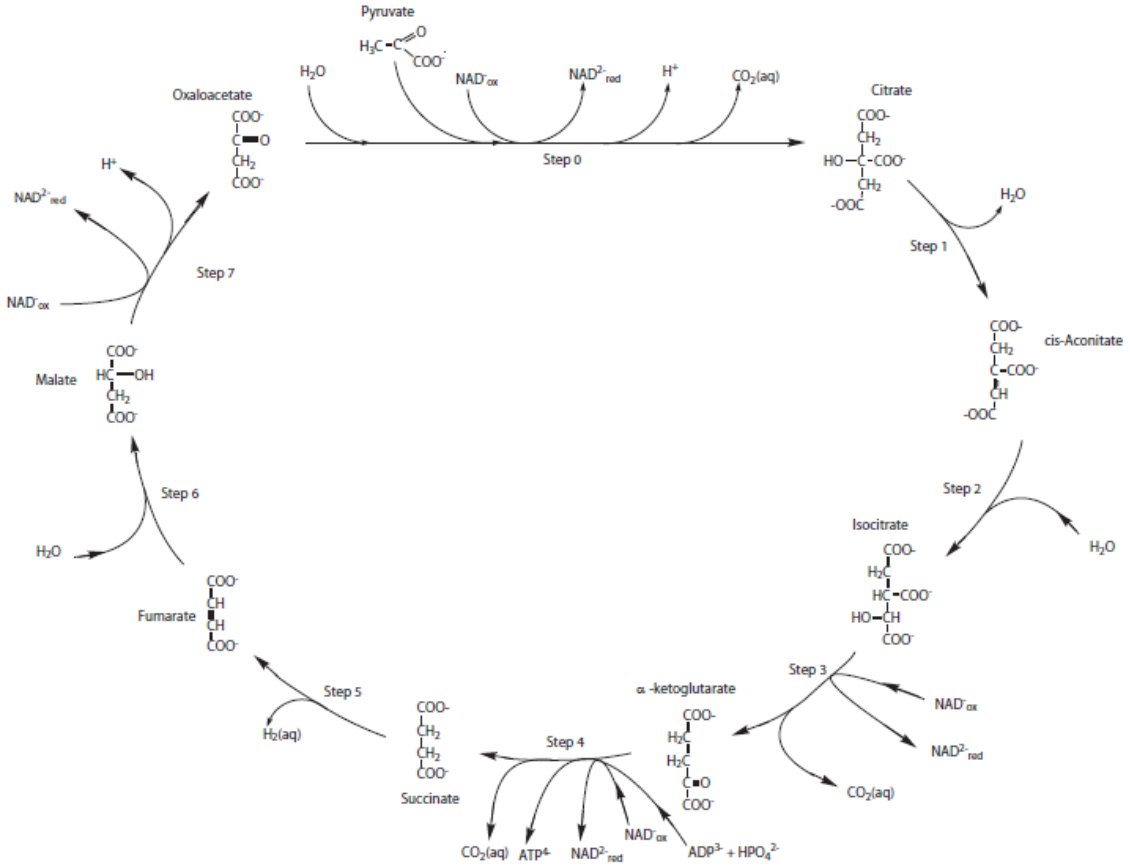

Figure 4. A thermodynamic depiction of the CAC used to assess the standard state changes associated with individual steps, as well as the energetics of the overall metabolic pathway. Some of the numbered steps represent condensed or alternative versions of steps shown in Fig 3.

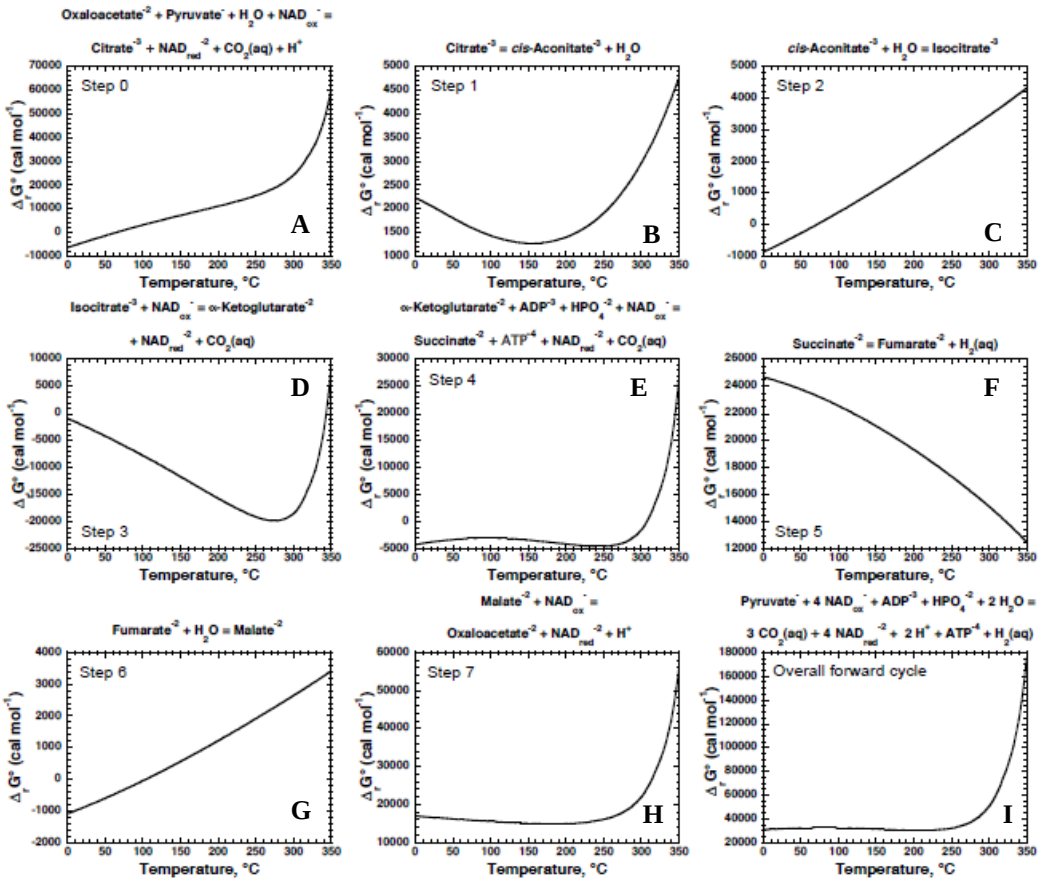

Figure 5**.** Plots of the standard partial molal Gibbs energy of reaction ($\Delta_r \bar{G}°$) for each step in the CAC depicted in Fig 4 and listed in Table 4, starting in the upper left with step 0 and ending in the lower middle with step 7, as functions of temperature at Psat. The overall reaction for the CAC is depicted in the lower right corner as a function of Psat. The curves were calculated with the revised-HKF equations of state using standard state data and parameters generated in this study and listed in Table 3.

steps 2 and 6 are less dramatic than those in step 0 over any temperature range. All three of these forward steps are exergonic at low temperatures, becoming endergonic as temperatures exceed 50° – 100°C. The predicted effects of temperature at Psat on $\Delta_r G°$ for steps 1, 4, and 7, as well as the overall forward reaction, all show minor fluctuations as temperature increases to ~250°C, beyond which all curves turn dramatically to more positive values of $\Delta_r G°$. Of these forward steps, only step 4 is predicted to be exergonic at any temperature at Psat. Step 4 is predicted to stay exergonic at all temperatures < 300°C.

In contrast, values of $\Delta_r G°$ for step 5 are predicted to become less endergonic with increasing temperature at Psat, and predicted values of $\Delta_r G°$ for step 3 are predicted to become increasingly exergonic until temperatures exceed ~275°C. It should be noted that despite the complexity of the CAC, $\Delta_r G°$ of the complete forward cycle is predicted to remain approximately constant from 0° to 250°C at roughly 30 kcal mol^{-1}. It should also be kept in mind that values of $\Delta_r G°$ for the steps in the reverse CAC would be opposite in sign to the results shown in Fig 5. As an example, step 5, which has a large positive value of $\Delta_r G°$ in the forward direction, would be strongly exergonic in the reverse direction at all temperatures. Likewise, the overall rCAC would be exergonic at all temperatures at Psat.

Predictions with the revised-HKF equations of state can be made at elevated temperatures and pressures well beyond Psat. Results for $\Delta_r G°$ at temperatures to 500°C and pressures to 5kb are depicted in Fig 6. Curves showing values of $\Delta_r G°$ at 0.5, 1.0 and 5.0 kb are indicated in all of the plots in Fig 6, and the increment between curves is 500 bar. In general, the predicted changes evident in Fig 6 are similar to those shown in Fig 5, although the scales of plots for individual steps may differ between the two figures. As examples, the ranges in $\Delta_r G°$ for steps 4 and 7 in Fig 6 were selected to be much smaller than the ranges for the same steps in Fig 5 so that pressure differences could be resolved. Note that in some cases the pressure dependence at low temperatures is opposite to that at elevated temperatures. Forward step 1 is an example of a reaction for which $\Delta_r G°$ is predicted to become increasingly positive with increasing pressure at lower temperatures, but to flip over and become less positive with increasing pressure at higher temperatures. Once again, it should be noted that $\Delta_r G°$ for the complete forward cycle stays remarkably

constant over wide ranges of temperature and that the effect of pressure is to extend the near constancy of $\Delta_r G°$ for this reaction to higher temperatures.

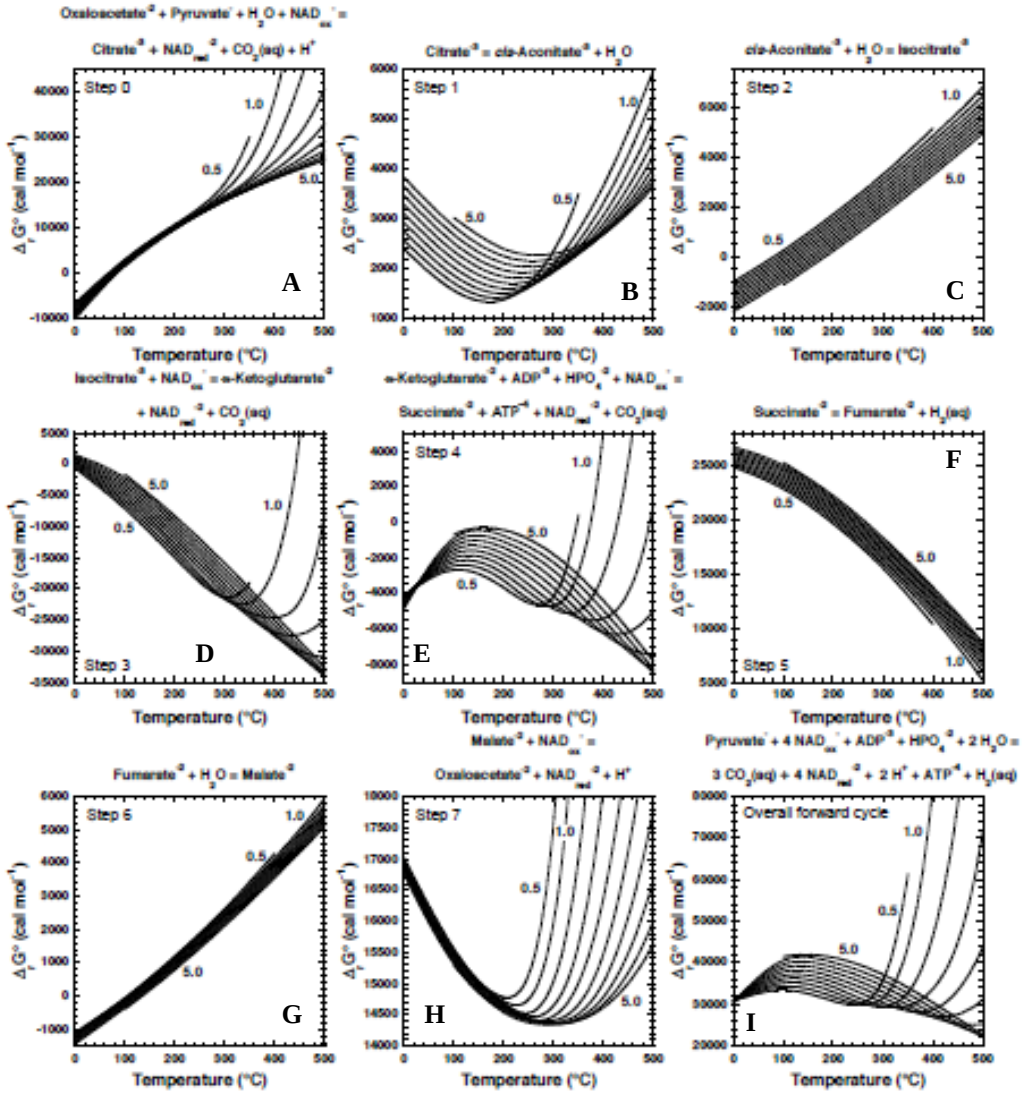

Figure 6. Values of $\Delta_r \bar{G}°$ for the same steps in the CAC shown in Fig 5, but for temperatures to 500°C and pressures to 5 kilobars. The 5.0 kilobar isobar is truncated at low temperatures owing to its proximity to the stability field of a high-pressure isomorph of ice, and the 0.5 kilobar isobar is truncated at high temperature where it encounters the upper-temperature applicability limit of the revised-HKF equations (Johnson and Norton, 1991; Shock et al., 1992).

2.3.3 Comparison with Other Thermodynamic Analyses of the CAC

Central to the development of thermodynamic data for the CAC is the goal of maintaining internal consistency in those data such that properties of any reaction can be

calculated without introducing new sources of uncertainty. This has been done, to varying degrees, for species in the CAC (Burton and Krebs, 1953; Burton and Wilson, 1953; Burton 1955; 1957; Krebs and Kornberg, 1957; Decker et al., 1970; Thauer et al., 1977; Miller and Smith-Magowan, 1990; Alberty, 1997; 1998a; 1998b; 1998c; 2004; 2005; Ishida and Okuno, 2004; Goldberg et al., 2007; Dalla-Betta and Schulte, 2009; among others), but despite how robust some of these thermochemical cycles are for quantifying reactions among various CAC species, thermodynamic consistency with species outside the cycle is often limited. In addition, few of these efforts allow estimates at elevated pressures and temperatures, or if they do may not maintain internal consistency with thermodynamic properties of biomolecules generated via pathways that branch from the CAC, or those that are ancillary to it. Finally, when data are missing or unreliable from experiments, some of these efforts introduce inconsistencies in the way individual properties are estimated (Appendix D).

The most complete compilations and critiques of CAC data preceding the present study are those by Burton (1957), Thauer et al. (1977), Miller and Smith-Magowan (1990), Alberty (2005), and Dalla-Betta and Schulte (2009). Differences among these studies and the present study are examined in Appendix D, but a few general details are worthy of note here. The earlier studies do not include $\Delta\bar{G}_f^o$ values for ATP^{4-}, ADP^{3-}, or species of NAD(P), which inhibits evaluation of $\Delta_r G°$ for several of the steps in the CAC. Miller and Smith-Magowan (1990) attempted to overcome the lack of $\Delta\bar{G}_f^o$ values for species of NAD(P) by arbitrarily setting values of $\Delta\bar{G}_f^o$ for the oxidized forms to 100 kcal mol^{-1} and using the potentiometric measurements from experimental investigations to calculate $\Delta\bar{G}_f^o$ of the reduced forms. This decision allows reaction properties to be

evaluated when oxidation-reduction reactions are coupled to NAD or NADP redox reactions, but do not allow consistent evaluation of the thermodynamics of the biosynthesis of these compounds from other organic compounds or inorganic constituents. These authors also do not consider data for any forms of ADP or ATP. In contrast, Alberty (2005) includes various forms of ADP and ATP, but arbitrarily sets $\Delta\bar{G}_f^o$ of NAD^-_{ox} to zero, which is not an improvement over the arbitraty choice of 100 kcal mol^{-1} made by Miller and Smith-Magowan (1990). As in the case of the present study, Dalla-Betta and Schulte (2009) built on efforts by LaRowe and Helgeson (2006a; 2006b, 2007) who evaluated thermodynamic properties of several NAD, NADP, ADP and ATP species, among other biomolecules. Data for isocitric acid and *cis*-aconitic acid species were not included by Dalla-Betta and Schulte (2009), and uncertainties induced by their choice of properties of the keto-acids discussed in Appendix D hinder the general applicability of their results.

2.4. Concluding Remarks

One goal of the emerging field of geobiochemistry is to attain a quantitative capability for predicting the flows of energy and transformations of matter that constitute habitability (Shock and Canovas, 2010; Dick and Shock, 2011; 2013; Amend et al., 2011; 2013; LaRowe et al., 2012; 2014; LaRowe and Amend, 2015; Shock and Boyd, 2015). A path toward reaching this goal is to integrate the thermodynamics of biochemical pathways within those of overall geochemical processes. As illustrated here, that process begins with assessment and critique of available experimental data, and continues with development of estimation methods to cope with gaps in the data, and production of methods to extrapolate calculations to temperatures and pressures that are habitable but

well beyond the ranges covered by experimental work. Completing the last step is assisted by the revised HKF equations of state for aqueous solutes (Shock et al., 1992), which is increasingly applied to the problem of incorporating biomolecules into geochemical calculations (LaRowe and Helgeson, 2006a; 2006b; 2007; Dick et al., 2006; Shock et al., 2013). The results described above make it possible to integrate the citric acid cycle into geobiochemical calculations, and applications of this type are the subjects of our ongoing research.

Future improvements that will enhance the accuracy and usefulness of geobiochemical modeling involving the CAC include:

1) Experimental measurements leading to dissociation constants that can test predictions such as those shown in Fig 2.

2) Replacing the estimates of standard state properties made in this study at the reference conditions with values determined by experiment. The most pressing need is for the keto-acids for which we were unable to find any experimentally determined standard partial molal volumes or heat capacities. We encourage a renewed effort to improve and update standard state data for major biochemical compounds at 298.15K and 0.1 MPa, many of which have not been determined for many decades, if at all. Recent efforts for solutions including citrate ions are promising in this regard (Sadeghi and Ziamajidi, 2007; Sadeghi and Goodarzi, 2008; Sadeghi et al., 2010; Zafarani-Moattar and Izadi, 2011; Apelblat et al., 2013).

3) Determining high-temperature standard partial molal volumes and heat capacities of aqueous species involved in the CAC either as associated acid molecules or as anions in electrolyte solutions. Promising efforts for succinic acid are provided by Criss and Wood (1996) and Ingelse et al. (1996), and experimental methods for aqueous nonelectrolytes have improved in the intervening 20 years.

4) Renewed efforts to reconcile the diverse results for standard state Gibbs energies of individual steps in the citric acid cycle. As an example, the experimentally determined value of $\Delta_r G°$ for step 3 of the CAC by Londesborough and Dalziel (1968) differs considerably from the value calculated here using independent experimental constraints (see Appendix D). Other researchers have articulated the ambiguities associated with interpreting the experimental results for step 3 (Miller and Smith-Magowan, 1990; Alberty, 2005), but reach other conclusions reflected in their choice of thermodynamic data.

5) Quantifying the thermodynamic properties of interactions among CAC species and other aqueous biomolecules. Recent progress on interactions between citrate and amino acids hints at the directions this work could take (Kumar et al., 2013a; 2013b; 2016; Jamal et al., 2015).

6) Building on the results presented here to include aqueous metal-organic complexes of all of the anions involved in the CAC so that their speciation can be assessed inside microbial cells and in the external geochemical environment where there is renewed interest in the

influence of organic acids to the mobilization and immobilization of metals and the dissolution of minerals (Wolff-Boenisch et al., 2011; Declercq et al., 2013; Li et al., 2014; Braunschweig et al., 2014; Lawrence et al., 2014; Bray et al., 2015).

2.5. Acknowledgments

The research reported was supported through NSF grants OCE-0937406 and EAR-1123649, as well as NASA grants NNX12AB38G and NNA15BB02A. We thank Jeff Dick, Mitch Schulte, and Chris Glein for useful discussions about estimating thermodynamic data and maintaining consistency with other sources of geochemical and biochemical data. This paper represents a portion of the first author's PhD thesis work at Arizona State University.

III. GEOCHEMICAL BIOENERGETICS DURING LOW-TEMPERATURE SERPENTINIZATION: AN EXAMPLE FROM THE SAMAIL OPHIOLITE, SULTANATE OF OMAN

3.1 Serpentinization as a Link Between Geologic and Biologic Processes

When water and rock react at low temperatures, the fluids generated are in disequilibria with the rest of the environment and define the energy supplies harvested by chemolithotrophic microbes. Inorganic supplies of redox energy contribute to the habitability of water-rock systems, and allow the biosphere to extend to considerable depths into the Earth's crust. When and where these energy supplies are substantial, the subsurface biosphere can operate independently of photosynthesis at the surface.

Chemosynthetic microbial communities that operate independent of light driven photosynthesis can be found in marine and continental hydrothermal systems. They are also found in serpentinizing systems where ultramafic rocks and water are far from equilibrium across a wide range of temperatures. The process of serpentinization has attracted considerable attention as a model for how planets may support life without photosynthesis, leading to suggestions that water-rock reactions within terrestrial planets, icy moons, and ocean worlds may support microbial habitability in the dark (Jakosky and Shock, 1997; Shock, 1998; McCollom, 1999; Zolotov and Shock, 2003; 2004; an others). On Earth, serpentinization yields novel habitats in continental and marine settings that feature hyperalkaline pH (>11) and extremely reduced conditions. Serpentinization could be a mechanism for life to infiltrate deep into subduction zones. Arguments for the ultramafic nature of the crust and upper mantle of the early Earth lead to the suggestion that the emergence of life was hosted in serpentinizing systems (Weiss et al., 2016). In

the present study, inorganic energy supplies were quantified in surface waters and hyperalkaline springs that constitute the surface expression of active serpentinization in the Samail ophiolite of Oman. The Samail ophilite is one of several sites around the world where geobiochemical connections from water-rock reactions to biomolecular compositions are being studied.

The Samail ophiolite has received considerable attention from geologists and petrologists who consider it to be a prime example of a continental exposure of rocks that corresponding to the upper mantle and to oceanic crust formed at a mid-ocean ridge. It contains the largest block of mantle peridotite emplaced on the continents (~15000 km^3) with a depth of a few km (Nicolas et al., 2000; Kelemen and Matter, 2008). Compared to other ophiolites, the Samail ophiolite is well-ordered and displays overlying sediments, pillow lavas, sheeted dykes, layered gabbros, and mantle peridotites (Glennie et al., 1973). Approximately 70 Ma, after a relatively short accretion time (95-93 Ma), part of the crustal sequence at the spreading center of the Tethys Sea obducted onto the Arabian plate as the sea closed (Glennie et al., 1973; Coleman, 1981; Tilton et al., 1981; Tippit et al., 1981; Hacker et al., 1996; Goodenough et al., 2010; Rioux et al., 2013). The metamorphic sole beneath the mantle section is composed of a thin sheet of metamorphosed oceanic sediment and volcanic rocks that were heated and welded against the mantle rocks during the thrusting event. Relatively unmetamorphosed oceanic sediments and volcanic rocks of the allochthonous Hawasina nappes were driven in front of and beneath the leading edge of the advancing ophiolite resulting in the autochthonous continental shelf, parautochthonous continental slope deposits, and carbonate deposits resting on pre-Permian crystalline basement (Glennie et al., 1974;

Falk, 2014). Following emplacement, shallow marine limestones were deposited on the ophiolite sequence and, subsequently, partly eroded after the uplift of the Oman Mountains generating the current exposures of the Samail ophiolite (Glennie et al., 1973).

In the arid climate of Oman, mafic and ultramafic rocks that underwent alteration in seafloor hydrothermal systems, as well as during the process of obduction of oceanic lithosphere onto the continents, continue to be altered by low-temperature water-rock reactions including active serpentinization of harzburgites and peridotites. Natural water compositions in the ultramafic-dominated Samail ophiolite terranes diverge either toward surface streams and shallow groundwaters of neutral to slightly basic pH, low overall salinity, enriched in Mg^{+2} and HCO_3^-, or toward more deeply circulated fluids emerging at springs with higher pH, somewhat higher salinity, and elevated concentrations of Ca^{+2} and OH^- (Fig 7). Several hyperalkaline seeps and springs precipitate calcium carbonate mineral as crusts, terraces, or aprons. Carbonate precipitation can be extensive, especially where hyperalkaline and surface waters mix. The surface water and shallow groundwater compositions are interpreted to result from open system reactions between meteoric waters and altered ultramafic rock. In contrast, the hyperalkaline fluids are thought to result from serpentinization in a mostly closed system (Barnes et al., 1978; Neal and Stanger, 1983; 1985; Stanger, 1986; Keleman and Matter, 2008; Paukert et al., 2012). Hyperalkaline springs can be found along the basal contact between autochthonous sediments and mantle peridotites, as well as at the contacts between mantle peridotites and gabbroic cumulates from the crustal section. However, there are high-pH springs located within the crustal or mantle sections in addition to those found at

discontinuities (Boulart et al., 2013). The pH of these systems ranges up to 12.1 with temperatures similar to the annual mean air temperature (between 25 and 36°C).

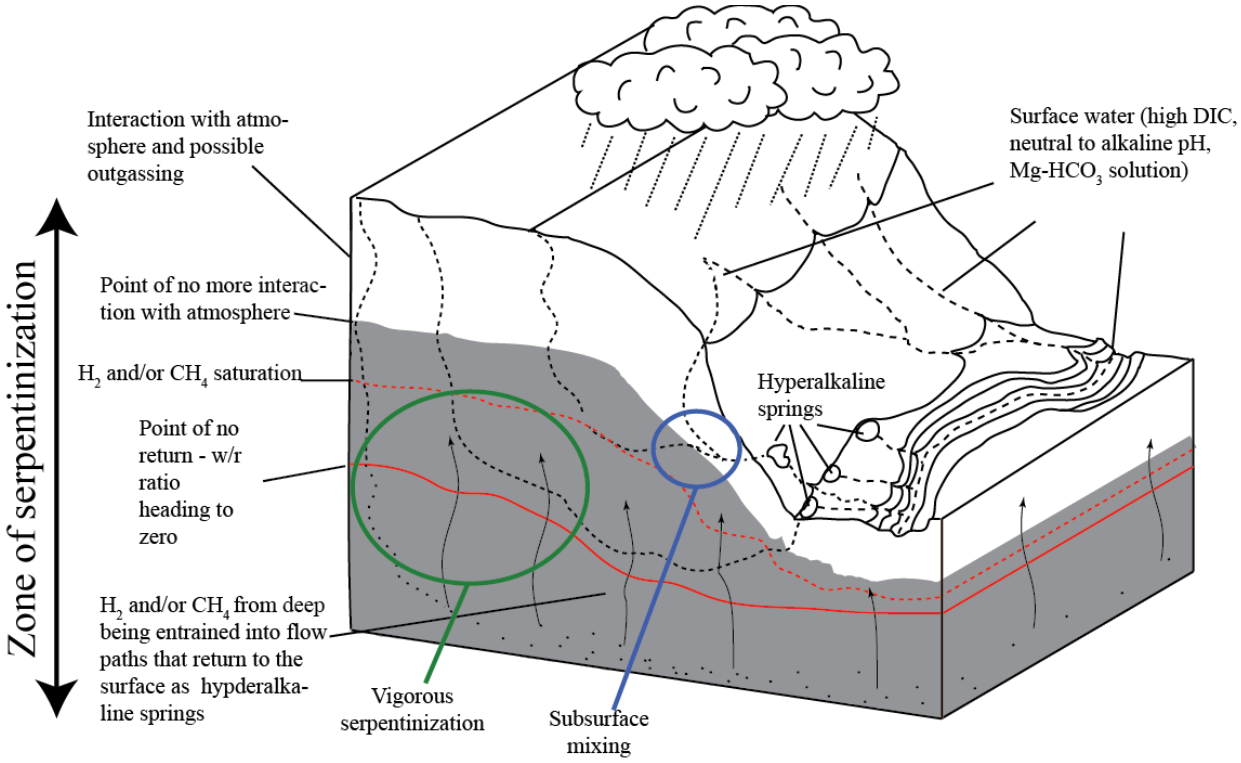

Figure 7. Schematic block diagram depicting possible flow paths and interaction of fluids at depth in hyperalkaline systems. As meteoric water infiltrates into the host rock a variety of different paths are possible. Some paths can take a parcel of water deep into the subsurface where it can react with ultramafic minerals through the process of serpentinization to such an extent that all of the water is consumed and portioned into primary and secondary alteration phases and the generation of hydrogen gas. The hydrogen could then be entrained back into flow paths that reemerge at the surface. Other paths may not infiltrate as deep and return to the surface as hyperalkaline Ca-OH fluids with high concentrations of hydrogen and methane. Shallower flow paths can produce Mg-carbonate waters of intermediate pH that may still be in contact with the atmosphere with low hydrogen and methane concentrations. Comingling between different flow paths may also create a diverse range of geochemical compositions expressed at the surface. This system provides a variety of unique habitats and geochemical compositions with disequilibria that microorganisms could exploit. It also produces environments conducive to the abiotic organic synthesis of a variety of compounds that could be precursors to those necessary to facilitate the processes for the origin of life.

The dissolved hydrogen and methane concentrations in these springs are nanomolar to micromolar and low concentrations of short-chain hydrocarbons are reported (Barnes et al., 1978; Neal and Stanger, 1983; Bath et al., 1987; Fritz et al., 1992; Boulart et al., 2013; Chavagnac et al., 2013b). Bubbling gas exsolving from springs and streambeds where springs are submerged can be seen at various locales. Pockmarks are also apparent in precipitates along the stream beds where discharge has occurred (Chavagnac et al., 2013a). Neal and Stanger (1983) estimated gas flows from 10 ml/s to 10 l/s at several seeps at Nizwa and B'lad.

3.2 Molecular Evidence for Microbial Metabolisms from Hyperalkaline Serpentinizaing Ecosystems

Geologic processes allow many ways that combinations of inorganic compounds can be brought together in far-from-equilibrium states. Ideally, we would turn to what is known about the microbial inhabitants of serpentinizing systems to determine which of many plausible chemolithotrophic energy supplies are being used. Possibly the most convincing evidence (Class I) would come from the physiologies of isolates obtained from the water-rock system that would be further enhanced if genomic data from those isolates revealed their biochemical pathways of energy harvesting. Similarly compelling results could come from experiments conducted in natural settings or in the lab that show rates of redox processes that are enhanced relative to abiotic rates, or isotopic labeling experiments that show uptake and transformation of specific compounds (Class II). Nearly as useful would be transcriptomic, proteomic, or biomarker data from natural environments (Class III) that yield compelling evidence for the expression of genes involved in specific metabolic processes. Less convincing, but highly suggestive, would

be identification of genes in natural samples that are indicative of the capacity for the microbes in a water-rock system to conduct specific metabolic processes (Class IV), that would mean the process is possible, although perhaps, not directly observed. Finally, the least compelling molecular evidence for active metabolisms (Class V) comes from ribosomal RNA sequencing, gathered to identify the representatives of microbial communities and to explore their relatedness to other microbes in the same or other systems, from which inferences about metabolism can be made generally and with unknown reliability. In the case of serpentinization, the overwhelming majority of currently available molecular data yield Class V results. In the present study molecular results from the literature, together with analytical geochemical data from sites of active serpentinization in Oman, were used to construct a general quantitative framework for how geochemical processes during serpentinization support microbial communities. This framework can be used to guide the development of investigations that reveal how geochemical energy supplies are accessed and consumed throughout hyperalkaline ecosystems.

In the following discussion, evidence is assembled by the class of data that supports the presence of various chemolithotrophic metabolic strategies in serpentinizing ecosystems. The first occurrence of each of these strategies is given in bold font, which should help to judge the strength of evidence for each type of metabolism. Chemical reactions corresponding to these metabolisms are listed in Table 5, together with additional reactions that are plausible energy sources based on geochemical data (see below).

Table 5. Proposed reactions that include known chemolithotrophic strategies used by microbes in serpentinizing systems, based on various classes of microbial/molecular data, together with plausible reactions based on geochemical data.

Name	Balanced Reaction
Class I	
Hydrogen Oxidation	$H_2(aq) + 0.5O_2(aq) = H_2O$
Class II	
Carbon Monoxide Oxidation	$CO(aq) + 0.5O_2(aq) = CO_2(aq)$
Autotrophic Methanogenesis	$CO_2(aq) + 4H_2(aq) = CH_4(aq) + 2H_2O$
Anaerobic Methanotrophy (SO_4^{-2})	$CH_4(aq) + SO_4^{-2} = HCO_3^- + HS^- + 2H_2O$
Anaerobic Methanotrophy (NO_3^-)	$8NO_3^- + 8H^+ + 5CH_4(aq) = 4N_2(aq) + 5CO_2(aq) + 14H_2O$
Anaerobic Methanotrophy (NO_2^-)	$8NO_2^- + 8H^+ + 3CH_4(aq) = 4N_2(aq) + 3CO_2(aq) + 10H_2O$
Class III	
Ammonia Oxidation	$NH_4^+ + 2O_2(aq) = NO_3^- + 2H^+ + H_2O$
Sulfate Reduction	$SO_4^{-2} + 4H_2(aq) + H^+ = HS^- + 4H_2O$
Class IV	
Sulfide Oxidation	$HS^- + 2O_2(aq) = SO_4^{-2} + H^+$
Nitrogen Reduction	$N_2(aq) + 3H_2(aq) = 2NH_3(aq)$
Class V	
Aerobic Methanotrophy	$CH_4(aq) + 2O_2(aq) = CO_2(aq) + 2H_2O$
Nitrite Oxidation	$NO_2^- + 0.5O_2(aq) = NO_3^-$
Geochemistry	
Nitrate Reduction	$NO_3^- + 4H_2(aq) + 2H^+ = NH_4^+ + 3H_2O$
Anammox	$NO_2^- + NH_4^+ = N_2(aq) + 2H_2O$
Water-Gas Shift	$CO(aq) + H_2O = CO_2(aq) + H_2(aq)$
Carbon Monoxide Reduction	$3H_2(aq) + CO(aq) = CH_4(aq) + H_2O$

At present, most of the isolates from serpentinizing systems with well-characterized physiologies that provide Class I data are heterotrophs. These include numerous aerobic Gram-positive isolates, as well as the Gram-negative *Chimaereicella alkaliphila*, *Microcella putealis*, and *Phenylobacterium falsum*, obtained from groundwater samples from the artesian borehole at Cabeço de Vide, Portugal (Tiago et al. 2004; 2005a; 2005b; 2006). Takai et al. (2005) isolated a facultative anaerobic heterotroph, *Marinobacter alkaliphilus*, from serpentine mud at South Chamorro seamount along the Marianas forearc, that uses nitrate or fumarate as an electron acceptor during anaerobic growth, and oxygen during aerobic growth. Strain PROH2 of the genus *Clostridium* (Mei et al., 2014) and *Acetoanaerobium pronyense* (Bes et al., 2015) were both isolated from an internal section of an active chimney taken from the Needle of Prony (Prony Bay, New Caledonia), and were shown to generate H_2 via fermentation using a variety of carbohydrates and yeast extract. Fermentation and acetogenesis characterize the metabolisms of *Alkaliphilus hydrothermalis* and *Vallitalea pronyensis* isolated from another chimney sample from Prony Bay by Ben Aissa et al. (2014; 2015). Recently, Cohen et al. (2015) reported the genome of a facultative anaerobe from The Cedars (Somona County, California, USA), *Cellulomonas* strain FA1, that catabolizes polysaccharides from plants, and possesses numerous gene homologs to glycosyl hydrolase and glycosyl transferase. In contrast to the copious evidence for heterotrophs, three microbial strains capable of autotrophic growth on H_2 and O_2, using calcite as a carbon source, were isolated from The Cedars by Suzuki et al. (2014). These alkaliphilic, mixotrophic organisms that can also pursue heterotrophic metabolisms are among the *Betaproteobacteria*. A new genus, *Serpentinomonas*, was proposed that includes them.

These results provide Class I evidence for **hydrogen oxidation** as a chemolithotrophic lifestyle in serpentinizing ecosystems. The isolation and characterization of autotrophs in serpentinizing systems is in its infancy. The scarcity of data on autotrophs belies the likely magnitude of their involvement in primary productivity.

A somewhat greater diversity of chemolithotrophic lifestyles is provided by Class II evidence from lab experiments that track reactions using isotopic labels on samples collected at various field sites. Evidence for **CO oxidation** is provided by Morrill et al. (2014) who showed decreasing concentrations of CO and O_2 in growth experiments starting with substrates from the Tablelands in Newfoundland, Canada. Isotopically labeled experiments showed that most of the CO was oxidized and little was incorporated into microbial lipids. **Methanogenesis**, both autotrophic and heterotrophic, was demonstrated using ^{13}C-labeled substrates in laboratory experiments with samples from the serpentinizing system at The Cedars (Kohl et al., 2016). Substrates converted to methane included bicarbonate, methanol, formate, and acetate. Acetogenesis also occurred, but was thought to involve fermentation. Methanogenesis and **anaerobic oxidation of methane** were detected in ^{13}C-labeled experiments on samples from carbonate chimneys from the Lost City Hydrothermal Field, on the Atlantic Massif approximately 15 km from the Mid-Atlantic Ridge (Brazelton et al., 2011). High-temperature portions of chimneys at Lost City are typically coated in biofilms dominated by a single phylotype of *Archaea* known as Lost City *Methanosarcinales* (LCMS; Schrenk et al., 2004; Brazelton et al., 2006) that appear to be responsible for both methane production and consumption (Brazelton et al., 2011). The oxidant coupled to

anaerobic methane oxidation by LCMS was not specified, but sulfate, nitrate, and nitrite from seawater may all be possibilities at Lost City.

Evidence for gene expression (Class III) complements and expands the list of chemolithotrophic metabolisms supported by serpentinizing ecosystems. Extracts of chimneys from Lost City yielded biomarker evidence that allowed Bradley et al. (2009a; 2009b) to interpret isotopic data and state that LCMS is a methanogen, supporting the idea that autotrophic methanogenesis can be an active microbial metabolism in serpentinizing systems. Additional Class III evidence for methanogenesis is provided by Postec et al. (2015) who documented autofluorescence of the F_{420} cofactor used by methanogens in samples from Prony Bay, New Caledonia. Bradley et al. (2009a) cite isotopic evidence from archaeol in one sample from Lost City as evidence that microbes were consuming methane. Lincoln et al. (2013) further suggest that some of the glycerol dialkyl glycerol tetraether biomarkers from Lost City were produced by ANME-1, an anaerobic methanotroph. In addition, **ammonia oxidation** is suggested by the presence of crenarchaeol in several of the same Lost City samples (Lincoln et al., 2013). Crenarchaeol is currently thought to be synthesized by ammonia-oxidizing Archaea. Other types of biomarker evidence (branched monoenoic and mid-chain branched phospholipid fatty acids, and phospholipid-derived diphytanyl diethers) led Mottl et al. (2003) to suggest the presence of **sulfate reduction** at South Chamorro Seamount, consistent with profiles of sulfate, sulfide, ammonia and carbonate in Ocean Drilling Program Hole 1200E. Bradley et al. (2009b) suggest that sulfate reducing bacteria may be the source for some of the diether lipids they detected in Lost City samples that appear to not have archaeal origins. Finallly, Klein et al. (2015) provide fossil evidence for

similar lipids in altered rocks from the Ibera margin that once hosted serpentinizing ecosystems.

Evidence for several of the chemolithotrophic strategies mentioned above are complemented by searches for marker genes for various metabolic processes. These Class IV results include putative evidence for CO oxidation (carbon monoxide dehydrogenase) and H_2 oxidation (novel [Ni,Fe] and [Fe,Fe] hydrogenase sequences) reported by Brazelton et al. (2012; 2013) from metagenomic analyses of samples from Lost City and Tablelands. they also include *mcrA* genes, involved in both methanogenesis and anaerobic methane oxidation in samples from Prony Bay (Quéméneur et al., 2014; Postec et al., 2015) one of which is closer to the corresponding gene from LCMS than to that from ANME-3 organisms. Additional *mcrA* discoveries from Del Puerto Ophiolite in California by Blank et al. (2009), who also found gene evidence for sulfate reduction (*dsrAB* sequences); *dsrB* reported from Prony Bay samples (Quéméneur et al., 2014), and *aprA* genes related to sulfate reducers from Cabeço de Vide (Tiago and Verrissimo, 2013). Additional styles of metabolism are indicated by *Sox* and *SQR* genes, indicative of the potential for **sulfide oxidation,** that were discovered in metagenomic data from Lost City samples (Brazelton and Baross, 2010), and by genes related to the CVA-aprA-cluster 3 in sulfide oxidizers that were found in metagenomic data from Cabeço de Vide (Tiago and Verrissimo, 2013) also provide class IV evidence. Furthermore, Brazelton et al. (2011) identified *nifH* genes involved in **nitrogen reduction** (fixation) in metagenomic data from Lost City samples, and Lang et al. (2013) argue that the presence of nitrogen fixation also helps to explain N isotopic data from Lost City.

Finally, inferences have been drawn from 16S rRNA sequences for a variety of metabolisms. These Class V data can only be taken as suggestions for possible chemolithotrophic metabolisms until more solid evidence is developed. Nevertheless, they point to the possibility for CO oxidation (Brazelton et al., 2013), hydrogen oxidation (Brazelton et al., 2013; Suzuki et al., 2013; Tiago and Verissimo, 2013; Sanchez-Murillo et al., 2014; Quéméneur et al., 2014; 2015; Miller et al., 2016), methanogenesis (Brazelton et al., 2006; Blank et al., 2009; Sanchez-Murillo et al., 2014; Quéméneur et al., 2014; 2015; Baculi et al., 2015; Woycheese et al., 2015; Miller et al., 2016), anaerobic methane oxidation (Curtis et al., 2013; Quéméneur et al., 2014; 2015; Miller et al., 2016), nitrogen reduction (Quéméneur et al., 2015); sulfate reduction (Brazelton et al., 2006; Blank et al., 2009; Tiago & Verissimo, 2013; Curtis et al., 2013; Quéméneur et al., 2014; Postec et al., 2015; Miller et al., 2016), sulfide oxidation (Quéméneur et al., 2014), and ammonia oxidation (Quéméneur et al., 2014; 2015; Baculi et al., 2015). In addition, Class V evidence for **aerobic methanotrophy** is offered by Sanchez-Murillo et al. (2014) in samples from the Santa Elena Ophiolite in Costa Rica, by Quéméneur et al. (2014) for samples from Prony Bay, and by Quéméneur et al. (2015) from samples from the Voltri Massif in Italy. Furthermore, the suggestion of **nitrite oxidation** at Cabeço de Vide is made by Tiago and Verissimo (2013), and at the Leka Ophiolite in Norway by Daae et al. (2013).

In summary, the biological evidence for chemolithotrophic metabolisms in serpentinizing ecosystems includes: Class I data for H_2 oxidation, Class II evidence for CO oxidation, methanogenesis, and anaerobic methanotrophy, which are joined by Class III evidence for ammonia oxidation and sulfate reduction, Class IV evidence for genes

involved in sulfide oxidation and nitrogen reduction, and Class V eveidence for aerobic methanotrophy and nitrite oxidation. Reactions corresponding to these twelve chemolithotrophic energy sources are listed in Table 5, including three versions of anaerobic methanotrophy coupled to sulfate, nitrate, and nitrite. These twelve reactions are joined by four more reactions (nitrate reduction, anammox, water-gas shift, CO reduction) inferred to be plausible based on analysis of the geochemical data described below. The order in which reactions are listed in Table 5 derives from the subsequent thermodynamic analysis of the geochemical data. In addition to the chemolithotrophic metabolic reactions listed in Table 5, circumstantial evidence for autotrophic growth via thiosulfate reduction with H_2 was obtained from microcosm experiments and subsequent sequencing by Crespo-Medina et al. (2014) working at the Coast Range Ophiolite Microbial Observatory (CROMO) site in California.

The purpose of the present study is to take the biological evidence summarized above as a starting point for unveiling the structure of how geochemistry influences bioenergetics during low-temperature serpentinization. By structure, we mean assessing the relative abundance of chemotrophic energy supplies that can support microbial metabolism. In this case, our attention is focused on the reactions listed in Table 5, and our goal is to evaluate the energy supplied by each of these reactions in the specific case of low-temperature serpentinization in the Samail ophiolite of the Sultanate of Oman. There are several steps needed to reach this goal, including geochemical field measurements and sampling, laboratory analysis of the samples, and thermodynamic calculations to clarify the extent to which each reaction in Table 5 is out of equilibrium and therefore able to provide energy for microbial life. The following review of the

thermodynamic background underscores the data requirements for field and laboratory work.

3.3. Quantification of Available Energy

The quantification of energy and its availability for microbial communities helps reveal the viability of different metabolic strategies, the potential for growth and biomass production, and the overall biogeochemical cycling of elements within the system. A thermodynamic framework for this type of analysis is predicated on the fact that only reactions that are out of equilibrium can provide energy for metabolic processes of chemotrophic microorganisms. As an example, let us consider the metabolic strategy of aerobic methane oxidation given by:

$$CH_4(aq) + 2O_2(aq) \rightarrow CO_2(aq) + 2H_2O \quad (1)$$

The amount of energy that can be harnessed by catalyzing this reaction (r) corresponds to the chemical affinity (A_r) for the reaction (Helgeson, 1979) which quantifies how the overall Gibbs energy ($\Delta_r G$) changes with respect to a change in reaction progress (ξ_r) and is given by (de Donder, 1927; de Donder and Van Rysselberghe, 1936; Helgeson, 1979; Kondepudi and Prigogine, 1998):

$$A_r \equiv -\left(\frac{d\Delta_r G}{d\xi_r}\right)_{P,T} \quad . \quad (2)$$

The overall Gibbs energy of a reaction will be influenced by both the standard state thermodynamic properties of the reaction itself and by the activities of the reactants and products in the geochemical environment of interest. This is reflected by:

$$\Delta_r G = \Delta_r G^\circ + RT\, lnQ_r \quad (3)$$

where $\Delta_r G°$ represents the standard Gibbs energy of the reaction, R is the ideal gas constant, T is the temperature in Kelvin, and Q_r is the activity product, or reaction quotient, expressed as:

$$Q_r = \prod_i (a_i)^{\nu_{i,r}} \quad (4)$$

where a_i represents the activity of the i^{th} compound in the reaction raised to its stoichiometric coefficient in the r^{th} reaction, $\nu_{i,r}$, which is positive for products and negative for reactants. Activities are calculated from molal concentrations (m_i) via:

$$a_i = m_i \gamma_i \quad (5)$$

using activity coefficients (γ_i) calculated with one of several activity coefficient models. In this study we used an extended Debye-Huckel equation (Helgeson, 1968; Helgeson et al., 1981). The standard Gibbs energy of the reaction is related to the equilibrium constant for the reaction (K_r) by:

$$\Delta_r G° = -RTlnK_r \quad . \quad (6)$$

Combining equations 3, 4, and 6 yields the following expression for the chemical affinity:

$$A_r = RTln\left(\frac{K_r}{Q_r}\right) \quad . \quad (7)$$

It follows that the chemical affinity for a particular reaction can be evaluated by calculating $\Delta_r G°$ using standard state thermodynamic data at the temperature and pressure of interest, measuring the concentrations of all reactants and products in the reaction, and determining their activities from those concentrations with activity coefficients. For the example of aerobic methanotrophy represented by reaction (1), the final expression for affinity is:

$$A_r = RTln\left(\frac{K_r}{\left(\frac{\left(a_{CO_2(aq)}\left(a_{H_2O}\right)^2\right)}{\left(a_{CH_4(aq)}\left(a_{O_2(aq)}\right)^2\right)}\right)}\right) \quad , \quad (8)$$

which expands to

$$A_r = RT\ (lnK_r\ - ln\ a_{CO_2(aq)} - 2\ln a_{H_2O} + \ln a_{CH_4(aq)} + 2\ln a_{O_2(aq)}) \quad . \quad (9)$$

Standard state data leading to evaluation of K_r at each temperature and pressure of interest can be obtained for reaction (1) using reference state data and equation-of-state parameters from Shock et al. (1989), and Shock and Helgeson (1990), together with the revised Helgeson-Kirkham-Flowers equation of state (Shock et al., 1992). Evaluating the activities of solutes starts with analytical data from field samplesas described in the next section.

3.4. Field and Laboratory Measurements

Samples of surface water and hyperalkaline fluids, together with dissolved gases, sediments, and biofilms were collected at several locations in the Samail ophiolite as shown in Fig 8. Field blanks were collected daily using deionized water (18.2 MΩ cm) and the same equipment and methods used to collect samples. The following describes the sampling and analytical methods used to obtain the composition data summarized in tables 6-8.

3.4.1. Sample Site Descriptions

Six locales were sampled: Masibt, Falej, Qafifah, Al-Banah, Shmait, and Sudari; the images in Fig 9 offer some geological context for the sample collection. Masibt is hosted in gabbro while the others are hosted in peridotite or near the peridotite-gabbro

transition (Nicolas et al. 2000). At or near most of these sites rock outcrops show extensive evidence for serpentinization, with cross-cutting veins bearing carbonate minerals and serpentine (Fig 9a).

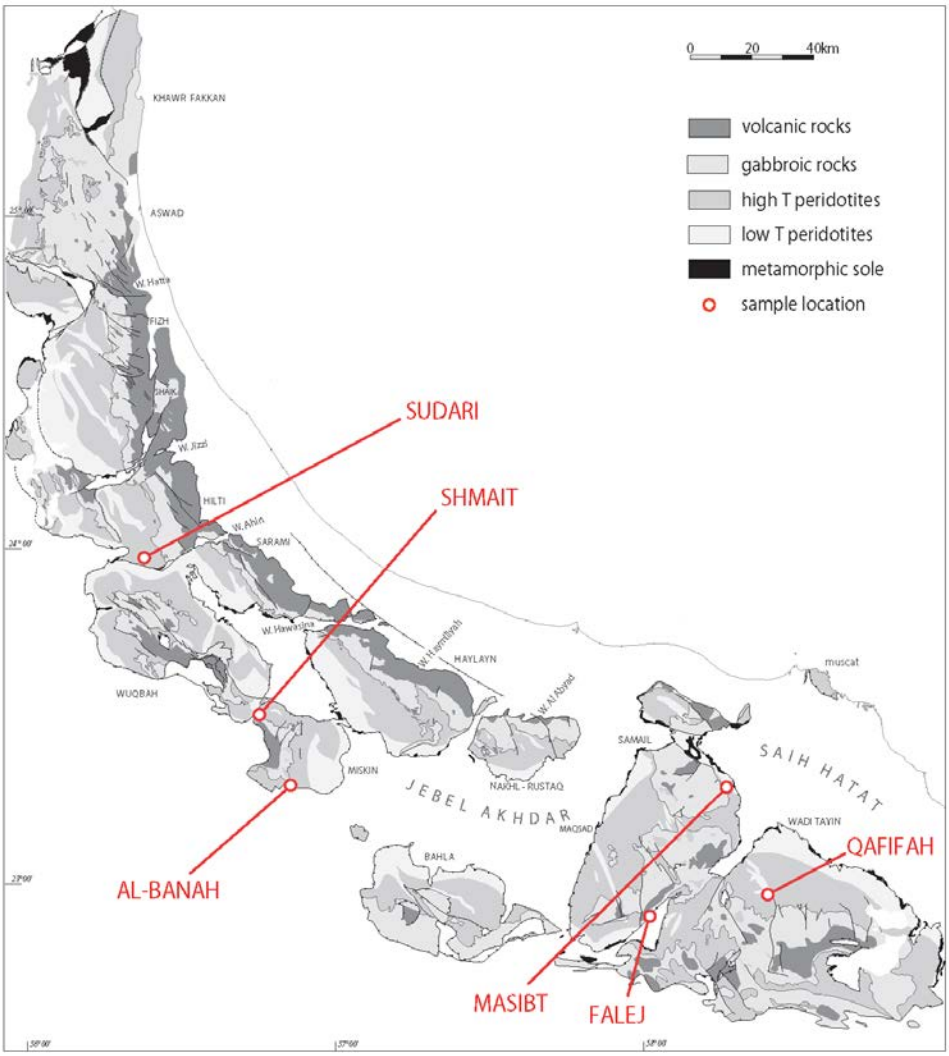

Figure 8. Geologic map of the Samail Ophiolite in the Sultanate of Oman depicting the northern and southern massifs where field samples were collected in 2010. It should be noted that Masibt is the only gabbro-hosted locale while all the others are hosted in peridotite. Map after Paukert et al. (2012) and Nicolas et al. (2000).

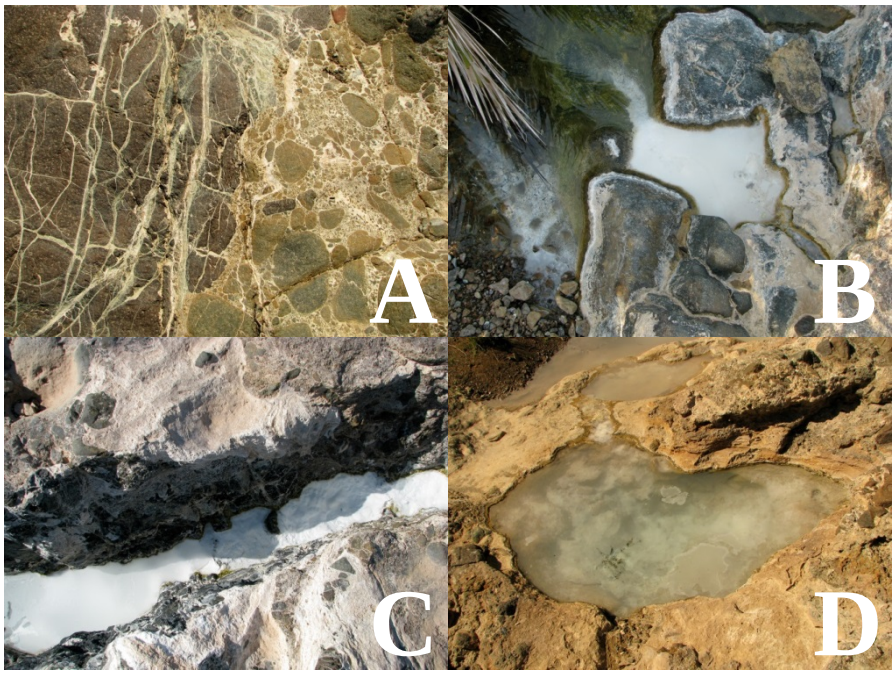

Figure 9. Photographs displaying typical context of samples that are prevalent across the sampling locales at the Samail Ophiolite. Fig. 9A shows typical cross-cutting of ultramafic host rock by carbonate and serpentinite veins; B and C depict mixing zone where hyperalkaline source water from a spring is mixing with wadi water, note the white carbonate flock precipitating upon mixing as the two water meet; D displays a source spring that has become capped by calcite as the hyperalkaline Ca-OH rich water interacts with carbon dioxide dissolving into the fluid eventually isolating it (photo credit: Peter Canovas and Everett Shock).

Hyperalkaline fluids emerge from gently flowing springs or from slowly seeping sources, and either can be located at or near streambeds (e.g. Masibt, Qafifah, Shmait, Sudari), or on the flanks of peridotite outcrops (e.g. Falej, Al-Banah). At zones of mixing between shallow groundwaters or surface waters with hyperalkaline fluids, precipitation of carbonate occurs as terraces or suspended flocs (Fig 9b,c), and a thin glaze of calcite can cover the water of slowly seeping springs (Fig 9d).

3.4.2. Field Measurements

Measurements performed in the field included temperature, pH, conductivity, titrations for alkalinity, and spectrophotometric analyses of redox-sensitive species. Field

measurements from all sampling sites can be found in Table 6. Temperature, pH, and conductivity were measured with YSI 30 and Orion 290Aplus meters and glass pH electrodes that were calibrated daily using buffer solutions of pH 4, 7, and 10. Redox potential (ORP) was also measured in situ at each field site. Dissolved oxygen (DO), nitrate, nitrite, total ammonia, total sulfide, dissolved silica, and ferrous iron were measured on site using portable spectrophotometers and commercially supplied reagents (Hach, Inc.). Colorimetric methods included DO via indigo carmine, nitrate by cadmium reduction, nitrite via diazotization, total ammonia by salicylate, total sulfide by methylene blue, dissolved silica via silicomolybdate, and ferrous iron with 1,10-phenanthroline. Alkalinity was determined in the field by titration with sulfuric acid using colorimetric indicators and a manual titrator (Hach, Inc). The first titration to the phenolphthalein endpoint is dominated by hydroxide alkalinity, and the second titration with bromocresol green/methyl red includes carbonate. The difference between the two titration alkalinity totals yields the carbonate alkalinity.

Table 6. Field measurements from Samail ophiolite hyperalkaline spring waters and wadi waters. Spectrophotometric measurements of dissolved oxygen (O_2(aq)), nitrate, and total ammonia (ΣNH_3) are in ppm, total sulfide (ΣS^{-2}) is in ppb; Alkalinity by titration is reported in mg/kg as $CaCO_3$ and carbonate alkalinity can be calculated by subtracting the second alkalinity from the first in the table. (-, not determined).

Sample Number	T (°C)	pH	Co- (µS)	ORP (mV)	O_2 (aq) (ppm)	NO_3^- (ppm)	ΣS^{-2} (ppb)	ΣNH_3 (ppm)	1st Alkalinity	2ns Alkalinity
100107A	32.5	11.29	1900	-398	0.089	19.8	3885	0.37	176	188
100107B	30.7	11.31	1848	-401	1.5	13.8	2755	1.31	173	187
100107C	25.8	9.31	778	-169	8	16.5	228	0.81	0	149
100107D	25.8	8.56	809	77	-	-	-	-	0	157
100107E	27.1	10.15	910	-294	-	-	-	-	68	153
100108J	24.2	11.72	2214	-253	6	3.5	187	0.5	273	285
100108K	24.9	11.71	2266	-188	5.5	5.2	166	0.44	280	293
100108L	28.6	11.60	2442	-136	0.327	0.8	197	0.54	282	292
100109S	22.4	11.76	1685	-	2.6	2.9	64	0.2	233	242
100109T	23.7	9.62	685	13	7	3.1	18	-	61	235
100109U	24.9	11.71	1778	-139	0.4	3.3	217	0.47	246	258
100109X	23.3	8.94	664	57	6.3	4.6	13	-	0	228
100111AA	28.5	11.65	3400	-247	1.9	5.3	258	1.02	317	330
100111AB	25.4	11.74	2770	-287	6	5.7	92	1.96	314	323
100111AC	16.5	11.55	1873	70	8.7	3	8	0.27	123	177
100111AD	32.9	11.61	3235	-213	1	4.4	179	1.27	437	448
100111AE	19.1	11.89	2468	-70	8	1.6	8	0.75	310	335
100112AG	37.7	11.14	1421	-160	0.312	2.1	106	0.16	168	177
100112AH	38.4	11.16	1537	-343	1.6	2.9	115	0.35	194	202
100112AJ	33.4	11.46	1782	-231	-	-	101	-	255	255
100112AM	31.5	11.53	1772	-323	0.42	2.5	105	0.25	248	253
100113AN	28.6	10.18	720	-31	6.1	4.1	45	-	65	187
100113AO	27.4	10.43	734	-39	5.4	2.4	25	0.19	57	150
100113AP	27	7.90	723	-8	3.2	5.2	-	-	0	233
100114AR	21.5	8.76	923	-110	9.1	0.8	9	-	0	162
100114AS	18.2	11.27	1013	-210	8.2	0.8	30	-	60	89
100114AT	30.4	11.61	1893	-296	3.4	8.3	66	0.03	243	249
100114AU	20.1	11.56	1258	-232	7.8	1.8	33	-	112	137

Due to the time-sensitive nature of these samples, analyses were performed within a few minutes after sample collection. Water samples were filtered except when filtering would compromise the analysis, such as DO and sulfide. We used protocols to minimize uncertainty developed through laboratory simulations of diverse natural systems. Uncertainties in the spectrophotometry data include the analytical method itself, differences in the way individual researchers perform the measurements over the field season, and the quirks of performing such analyses in the field. Taking into account all of the sources of uncertainty, our estimate of error for field spectrophotometry and titrations is ± 5-10 %. While this may be relatively large compared to data produced in a laboratory setting, this error is still quite low with respect to the environment in which the analyses are being performed and has little effect on the uncertainties in thermodynamic calculations, which employ the logarithm of the activities.

3.4.3. Water Analyses

Samples for analysis of major ions were filtered in the field through a series of 0.8 and 0.2 μm filters (Acrodisc® 32 mm PF Syringe Filter with 0.8/0.2 mm Supor® membrane) and collected (after rinsing the filter with 20 milliliters of sample) in 60 ml polypropylene bottles that were acid washed, cleaned, and oven dried in the lab before sampling. Upon returning to the lab, major cation (Na^+, K^+, Ca^{+2}, Mg^{+2}) and anion (SO_4^{-2}, Cl^-, Br^-, F^-) concentrations were measured via ion chromatography. Cation analyses used a Dionex DX-120 ion chromatograph with Dionex IonPac CS12A analytical and IonPac SG11 guard columns. Cations were separated isocratically with 18 mM methanesulfonic acid. Anion analyses used a Dionex DX-600 ion chromatograph consisting of a chromatography oven (LC25), eluent generator (EG 40), gradient pump (GP 50),

electrochemical detector (ED 50), and used Dionex IonPac AS11 analytical and IonPac AG11 guard columns. The column was equilibrated for 10 minutes with 0.5 mM KOH before each injection. After injection, the mobile phase concentration was held at 0.5 mM for 5 minutes, at which point the concentration gradient was increased to 5 mM over a duration of 4 minutes and then 38.25 mM over 13 minutes. Cation and anion samples were injected twice using a Dionex autosampler (AS 40). Data for these analyses can be found in Table 7; analytical uncertainties are estimated to be on the order of ± 5%.

Water samples for dissolved inorganic carbon (DIC) and dissolved organic carbon (DOC) were filtered as those for major ion analyses, with the additional modification of > 350 mL filter rinse before sampling, and collection in 40 ml amber borosilicate vials. DOC vials were acidified with 1 ml of concentrated phosphoric acid and sealed with silicone, Teflon-lined septa; DIC vials were sealed with black butyl rubber septa without acidification. Sample vials were completely filled to minimize headspace upon sealing, thereby inhibiting degassing and atmospheric contamination. Analyses were performed using an OI Analytical Model 1010 Wet Oxidation TOC Analyzer coupled with a Finnigan Delta Plus isotope ratio mass spectrometry (IRMS) to measure CO_2 concentrations along with $\delta^{13}C$ values obtained from reaction of the sample with either phosphoric acid (DIC) or sodium persulfate (DOC; St. Jean, 2003). Resulting data can be found in Table 8.

Table 7. Major cation and anion data for Samail ophiolite hyperalkaline spring waters and wadi waters. Field measurements of temperature and pH from Table 1 are combined with lab measurements by ion chromatography and/or ICP-MS reported in micromolality. (*, indicates value from ICP-MS; -, not determined).

Sample Number	T (°C)	pH	F^- (μmol)	Cl^- (mmol)	SO_4^{-2} (μmol)	NO_2^- (μmol)	Na^+ (mmol)	K^+ (μmol)	Mg^{+2} (mmol)	Ca^{+2} (mmol)
100107A	32.5	11.29	-	7.25	69.89	-	7.18	115.63	0.02*	2.06
100107B	30.7	11.31	0.56	7.31	63.67	-	7.16	136.11	0.02*	1.91
100107C	25.8	9.31	1.74	3.71	734.1	4.26	3.81	90.40	1.51	0.33
100107D	25.8	8.56	3.14	2.98	822.1	348.	3.24	73.66	1.67	0.84
100107E	27.1	10.15	1.05	4.86	497.7	-	4.89	97.43	0.95	0.14
100108J	24.2	11.72	-	8.58	6.51	0.14	10.37	218.67	0.03*	1.89
100108K	24.9	11.71	-	8.35	4.77	-	10.41	218.68	0.03*	1.87
100108L	28.6	11.60	-	8.44	5.05	-	10.61	220.29	0.02*	1.94
100109S	22.4	11.76	1.26	5.32	3.71	-	7.03	125.34	0.02*	1.59
100109T	23.7	9.62	0.50	2.38	334.2	-	2.83	46.03	2.00	0.04
100109U	24.9	11.71	-	5.06	4.57	-	6.90	109.97	0.02*	1.51
100109X	23.3	8.94	0.94	1.71	381.0	0.40	1.76	25.16	2.39	0.40
100111AA	28.5	11.65	-	12.0	4.10	2.01	15.12	262.28	0.03*	1.66
100111AB	25.4	11.74	1.01	12.3	9.54	-	15.68	279.82	0.03*	1.61
100111AC	16.5	11.55	0.75	11.6	123.1	-	14.63	289.85	0.26*	0.33*
100111AD	32.9	11.61	-	13.1	2.08	-	18.11	266.87	0.03*	2.18
100111AE	19.1	11.89	-	13.4	12.77	-	18.28	294.85	0.02*	0.73
100112AG	37.7	11.14	8.06	5.73	1.13	-	6.14	149.88	0.01*	1.73
100112AH	38.4	11.16	1.13	5.77	0.93	-	6.75	136.03	0.02*	1.58
100112AJ	33.4	11.46	0.57	5.58	1.30	-	7.13	120.29	0.02*	1.90
100112AM	31.5	11.53	0.59	5.51	1.04	-	7.13	120.17	0.02*	1.92
100113AN	28.6	10.18	0.60	3.32	398.5	-	3.83	105.93	1.49	0.52*
100113AO	27.4	10.43	0.46	3.56	362.1	-	4.18	108.35	1.20	0.22*
100113AP	27	7.9	1.58	1.43	727.4	0.77	1.16	78.01	2.79	0.58
100114AR	21.5	8.76	-	5.19	518.7	-	5.43	104.96	1.62	0.45
100114AS	18.2	11.27	0.28	6.12	220.8	-	7.42	137.36	0.34	0.30*
100114AT	30.4	11.61	-	6.33	12.11	-	8.40	138.85	0.02*	1.72
100114AU	20.1	11.56	-	6.24	154.9	-	7.80	139.32	0.02*	0.29

Table 8. Dissolved gas and carbon data for Samail ophiolite hyperalkaline spring waters and wadi waters. Field measurements of temperature and pH from Table 1 are combined with lab measurements by EA-IRMS, RGA and, GC-FID reported.

Sample Number	T (^{o}C)	pH	DIC (ppm)	DOC (ppm)	H_2 (aq) (μmol)	CO (aq) (nmol)	CH_4 (aq) (μmol)
100107A	32.5	11.29	1.37	0.30	0.73	145.3	99.7
100107B	30.7	11.31	1.29	0.42	0.13	267.6	38.8
100107C	25.8	9.31	23.2	0.89	0.03	246.32	2.10
100107D	25.8	8.56	37.0	0.30	0.02	154.9	0.08
100107E	27.1	10.15	8.16	0.21	0.03	183.1	4.25
100108J	24.2	11.72	0.65	0.12	1.61	274.6	0.81
100108K	24.9	11.71	0.86	0.19	11.0	265.8	2.95
100108L	28.6	11.60	0.82	0.27	159.4	92.87	16.2
100109S	22.4	11.76	1.23	0.25	22.70	140.9	51.9
100109T	23.7	9.62	42.8	0.42	3.19	121.7	14.1
100109U	24.9	11.71	1.41	0.10	111.2	78.0	131.6
100109X	23.3	8.94	53.9	0.35	0.06	161.1	1.05
100111AA	28.5	11.65	0.50	0.22	106.7	58.36	6.19
100111AB	25.4	11.74	1.57	0.38	7.26	129.9	1.46
100111AC	16.5	11.55	8.33	0.52	0.68	187.8	0.42
100111AD	32.9	11.61	0.55	0.20	104.3	100.7	11.0
100111AE	19.1	11.89	0.83	0.30	0.14	152.2	0.09
100112AG	37.7	11.14	0.53	0.63	273.4	64.67	37.7
100112AH	38.4	11.16	0.63	0.26	157.8	35.15	20.1
100112AJ	33.4	11.46	0.56	0.13	321.3	65.65	26.2
100112AM	31.5	11.53	0.48	0.23	258.6	83.87	21.0
100113AN	28.6	10.18	19.9	0.28	42.06	117.7	3.65
100113AO	27.4	10.43	16.8	0.38	7.95	185.5	4.63
100113AP	27	7.90	62.1	0.43	0.07	214.3	0.03
100114AR	21.5	8.76	36.5	0.43	0.03	110.7	0.01
100114AS	18.2	11.27	5.63	0.27	0.03	87.74	1.31
100114AT	30.4	11.61	0.46	0.28	10.06	138.4	10.8
100114AU	20.1	11.56	0.89	0.24	0.20	131.2	1.01

3.4.4. Dissolved Gas Measurements

Samples of dissolved gas were collected with a battery-powered peristaltic pump to pull water at a slow rate through tubing with very low gas permeability. Before sampling, water is pumped for several minutes to clear out the tubing and to make sure that no bubbles cling to its inner wall. A luer-lok^{TM} fitting at the end of the tube allows connection to a 60 ml syringe via a 3-way stopcock. The syringe is flushed with sample water three times before taking a sample. The positive pressure of the pump is used to fill the syringe through the stopcock to slightly over 50 ml. The tubing is then disconnected leaving the stopcock attached to the syringe. Sample is pushed out of the syringe so that 50 ml of water remains. Separately, but without letting the sample sit for more than a few 10's of seconds, a 10 ml syringe is used to accurately measure and deliver the carrier gas to the 60 ml syringe. The preferred carrier gas is N_2 that has had H_2, CO, CO_2 and hydrocarbons scrubbed from it. However, in Oman lecture canisters of clean N_2 are hard to acquire. As an alternative, ambient air can be as the carrier gas. Each day at each site we collected ~500 ml of air about 0.5 km upwind of each sampling area to use as the carrier gas and to make blanks. The blanks were analyzed to determine the amounts of trace gases imparted to the sample from ambient air so that uncontaminated sample concentrations could be calculated. The 60 ml syringe with 50 ml of water and 10 ml of carrier gas is agitated for 60 seconds. A needle is attached to the syringe, about 1 ml of gas pushed through the needle, and the remaining gas in the syringe is pushed into a gas-impermeable sample bag. We use 100-ml, mylar bags (Calibrated Instruments).

Dissolved gas samples were analyzed at NASA Ames by gas chromatography (GC). For analyses of hydrogen and carbon monoxide an RGA-3 reduced gas analyzer

(RGA) utilizing mercuric oxide detection made by Trace Analytical was used with 99.99995% pure N_2 carrier gas. Methane and other light hydrocarbons were analyzed on a GC with a flame ionization detector (GC-FID), run with the same carrier gas as the RGA and using ultra-high purity H_2 for the FID. Based on comparisons of standards prepared by independent dilutions of analytes the accuracy and precision are estimated to be ± 2% for the chromatographic analyses (Hoehler et al. 1998). Hydrogen, methane, and other light hydrocarbons are at higher concentrations in the samples from Oman, allowing replicate 100 µl injections from each 10 ml sample. Results are compiled in Table 8.

3.5. Aqueous Geochemistry

The surface water, shallow groundwaters, hyperalkaline fluids and their surface or subsurface mixtures sampled provided a range in pH from 7.9 to 11.89, conductivities from 664 to 3400 µS cm^{-1}, and oxidation-reduction potentials from -401 to 77 millivolts. Sample temperatures ranged from 16.5°C at a holding pond for hyperalkaline fluid to 38.4°C at one of the degassing hyperalkaline spring sources at Al-Banah. In general, temperatures of all spring sources were elevated relative to air temperatures in January, possibly reflecting values closer to the average ambient temperature or possibly some heating from the geothermal gradient during circulation in the subsurface. The temperature and pH data obtained in this study fall within the ranges of previous studies (Neal and Stanger, 1984b; Stanger, 1985; Boulart et al., 2012; 2013; Chavagnac et al., 2013b) and are in line with investigations of other hyperalkaline spring systems resulting from serpentinization (Barnes et al., 1978; Neal and Shand, 2002; Cipolli et al., 2004; Boschetti and Toscani, 2008; Margues et al., 2008; Boulart et al., 2012; 2013; Morrill et

al., 2013; Monnin et al., 2014a; b; Cardace et al., 2015; Woycheese et al., 2015; and many others). In general, as pH increases the concentrations of reduced species increase while those of oxidized species decrease.

3.5.1. Major Ions

Compositional data on major solutes are shown in Fig 10 plotted against pH. The highest pH values are from springs emitting hyperalkaline fluids resulting from serpentinization, the lowest pH values correspond to surface waters in contact with already serpentinized material, and intermediate pH values come from locations where fluid mixing occurs at the surface. As shown in Fig 10, many solutes correlate with pH despite it being a nonconservative tracer for mixing owing to the precipitation of calcite. Concentrations of total dissolved Mg are highest in the near-neutral surface waters. In contratst, Mg is so severely depleted in the hyperalkaline fluids as to be below detection by ion chromatography and required analysis by inductively coupled plasma mass spectrometry. Carbonate alkalinity data exhibit a pattern similar to that of Mg. Some scatter in the carbonate alkalinity can be seen in the hyperalkaline range, which is greater than the scatter in the Mg data owing to the vagaries of titrating high-pH, carbonate-depleted fluids in the field. Both Mg^{2+} and HCO_3^- enter surface waters through weathering of already serpentinized material by precipitation .

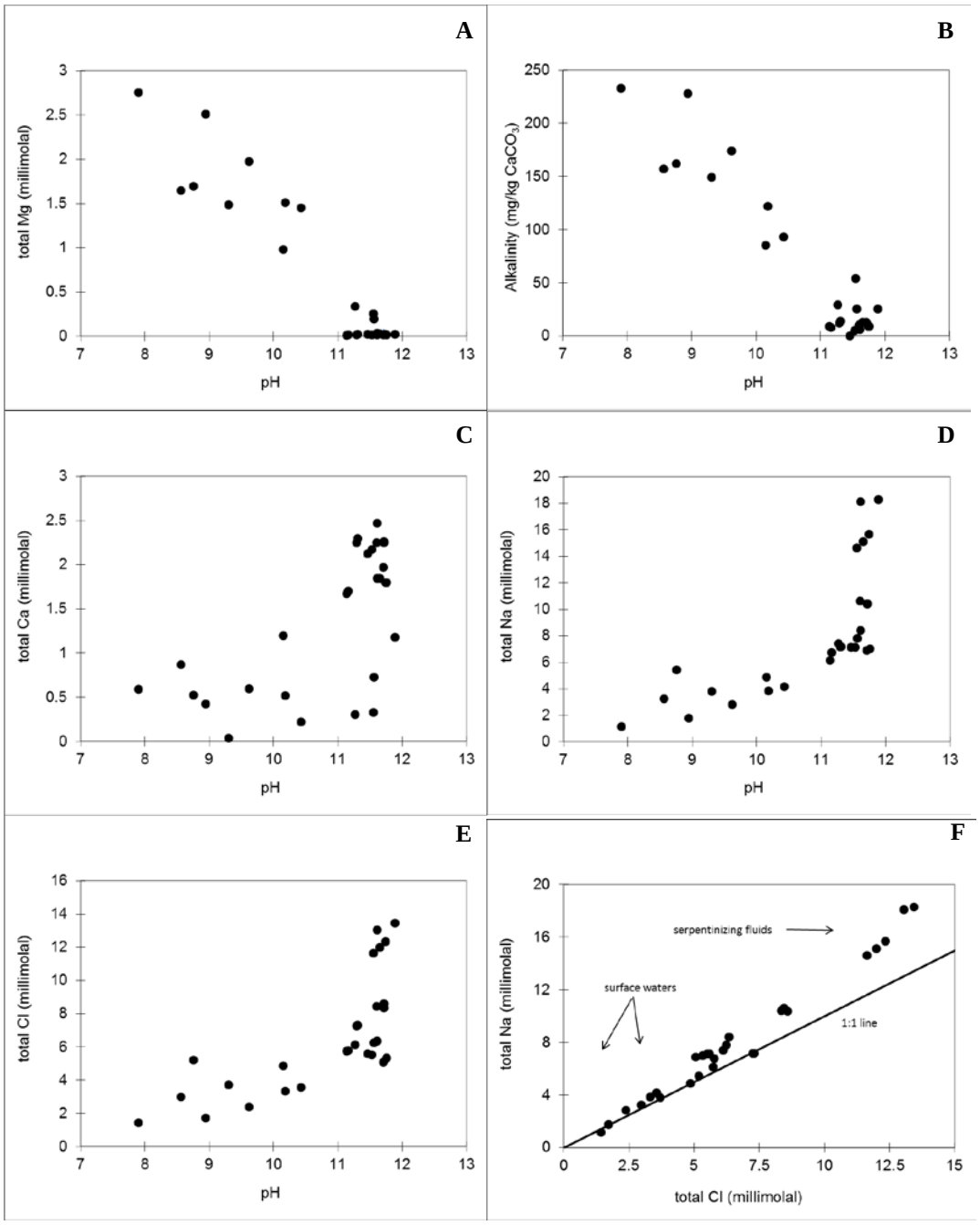

Figure 10. Composition data for major solutes plotted as a function of pH.

In contrast, the calcium concentration tends to be greater in the hyperalkaine fluids than in the near-neutral surface waters. These differences result from the serpentinization process where the formation of serpentine minerals (antigorite, lizardite, chrysotile) creates a sink for magnesium and allows a buildup of calcium ions that do not fit into the alteration products and thus accumulate in solution. Scatter in calcium concentration data, especially at high pH, results from hyperalkaline fluids interacting with the atmosphere and/or with Mg-carbonate waters. At some point as hyperalkaline fluids approach the surface, they start to encounter the atmosphere; when this occurs, carbon dioxide readily dissolves into the Ca-OH rich fluids causing the rapid precipitation of calcium carbonate minerals. Similar precipitation also occurs where surface-derived Mg-carbonate fluids mix with the deeper circulating Ca-OH rich serpentinizing fluids.

Both sodium and chloride increase with increasing pH and seem to become more enriched as the serpentinization process proceeds. Molal abundances of sodium and chloride plot very close to a 1:1 line for surface water samples and serpentinizing fluids show a sodium enrichment. One interpretation of the correlation between Na and Cl is that there is a contribution from NaCl that may reside in the alteration assemblages formed during alteration on the seafloor, or in sedimentary rocks that are encountered along the deep flow paths. Another is that evaporation has allowed small initial contribution from NaCl to increase along the 1:1 slope. Neither of these explanations can account for the excess in Na documented in several samples, which may be a contribution from ongoing water-rock reactions. This may indicate sodium (and even chloride to a lesser extent) is a more conservative tracer with respect to the extent of water-rock

interaction and the subsurface alteration that has taken place to produce the hyperalkaline serpentinizing fluids emerging from the springs.

3.5.2. Nutrients

Concentrations of several nutrients that can be involved in energy-supplying reactions are shown in Fig 11 plotted Vs. pH. Data for dissolved inorganic carbon bear a similarity to the data for total Mg shown in Fig 10, and lack the scatter at high pH seen in the field-based alkalinity titration data. In addition to carbonate mineral precipitation, reducing conditions that prevail during serpentinization can create a thermodynamic drive for inorganic carbon to be converted to methane, which may help explain the carbon balance for dissolved species that are not completely removed from the system via precipitation of carbonate minerals at the onset of the serpentinization process. This is in accord with Chavagnac et al. (2013a; b), Sader et al. (2007), and Boulart et al. (2013) and interpretations of work by Hellevang et al. (2011) and follow suit with measurements made by Boulart et al. (2013) that indicated no CO_2 in either the gaseous or aqueous phases coming from spring sources.

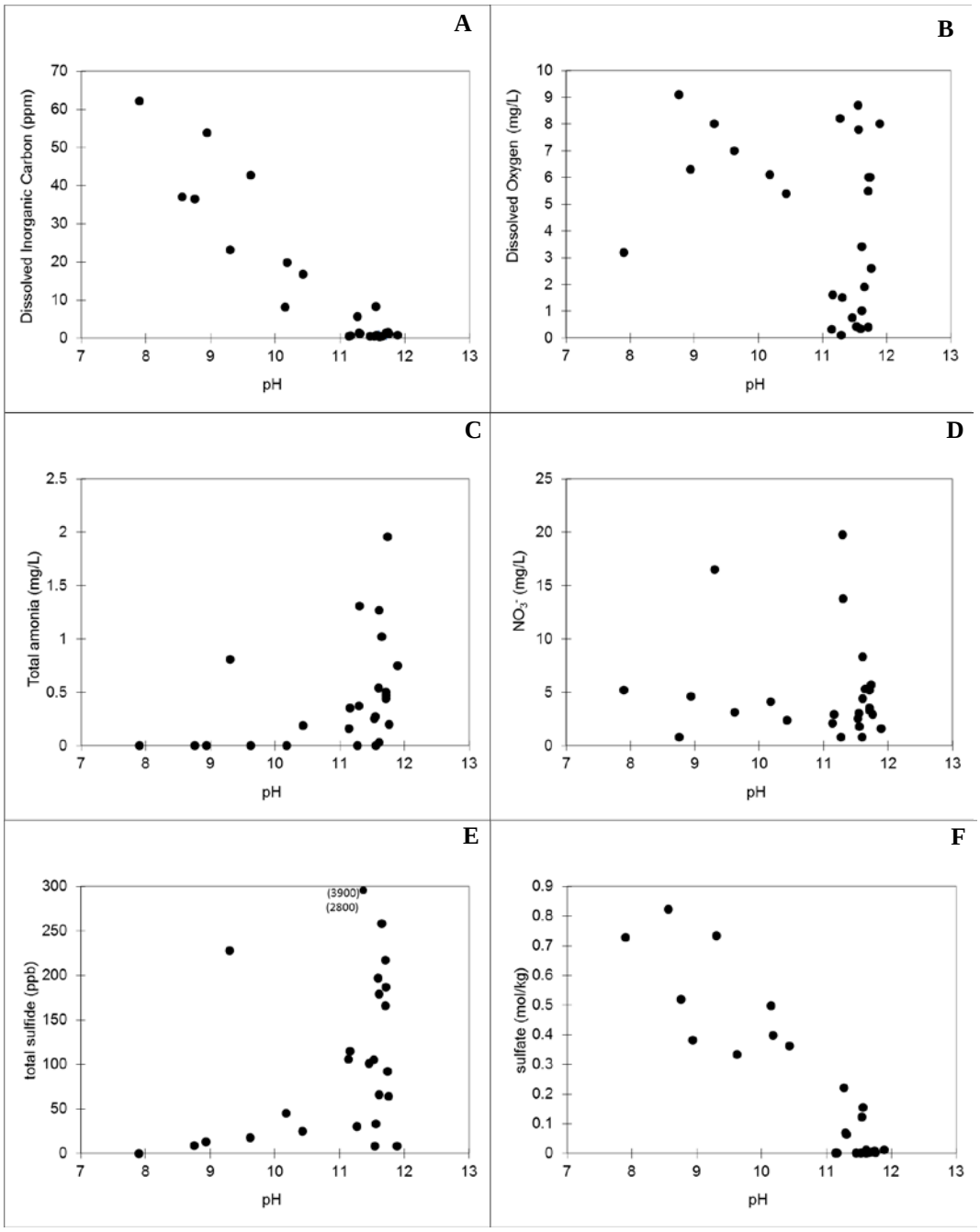

Figure 11. Concentrations of several nutrients that can be involved in energy supplying reactions as a function of pH.

Dissolved oxygen data from field spectrophotometry are diverse, with some samples near saturation with respect to the atmosphere at ambient temperatures (8 to 10 mg L^{-1}), while other samples across the pH range show lower concentrations. By far, the lowest concentrations of dissolved oxygen are found in samples of serpentinizing fluids from flowing hyperalkaline spring sources, many of which exceed 100 μmolar dissolved H_2. Total ammonia concentrations, dominated by NH_3(aq) in this pH range, are low in the surface waters, but can be considerably higher in hyperalkaline fluids. Nitrate concentrations are generally at or below 5 mg L^{-1} in surface waters, hyperalkaline fluids, and their mixtures, although a few locations show elevated abundances. Total dissolved sulfide, dominated by HS- in this pH range, bears some resemblance to the ammonia data with elevated abundances in many of the hyperalkaline samples. It should be noted that two of the samples can not be plotted at the scale of the plot in Fig 11, both are from Masibt, where high-pH fluids may be derived from alteration of gabbros rather than peridotites . In contrast to the behavior of sulfide, concentration of sulfate are lowest in the hyperalkaline fluids, and elevated in the surface waters. Note that the plot for sulfate displays the same trend as that of total Mg, carbonate alkalinity, and dissolved inorganic carbon.

3.5.3. Dissolved Reduced Gases: Hydrogen, Methane, and Carbon Monoxide

Concentrations of the dissolved reduced gases measured in this study are plotted against the pH of each sample in Fig 12. Data for dissolved hydrogen and methane show similarities to the plots for total ammonia and total sulfide shown in Fig 10, which also the same trend as the plot for total Ca in Fig 9. This suggests that all of these solutes are products of the serpentinization process. Concentrations of dissolved hydrogen and

methane are highest in some of the hyperalkaline springs, but other fluids are relatively enriched in one or the other of these dissolved reduced gases. Samples in which the molal concentration of dissolved hydrogen exceeds that of methane are predominantly from the Falaj and Al-Banah areas. In most other samples the molal abundance of dissolved methane exceeds that of hydrogen. Sample locations that are exposed to the atmosphere for long periods of time (holding ponds) or are involved in turbulent mixing with surface waters have among the lowest abundances of dissolved hydrogen and methane. This could be a result of microbial consumption of these reductants, or because the dissolved hydrogen and methane have exsolved from solution. Dissolved hydrogen and methane concentrations are comparable to those of other continental serpentinizing systems (Abrajano et al., 1988; Taran et al., 2010; Etiope et al., 2011, 2013a,b; Boulart et al., 2012, 2013; Szponar et al., 2012; Boschetti et al., 2013; Cardace et al., 2015). Springs in the Samail Ophiolite fall into what Boulart et al. (2013) consider a hydrogen-dominated regime with an average H_2/CH_4 value of 3.99.

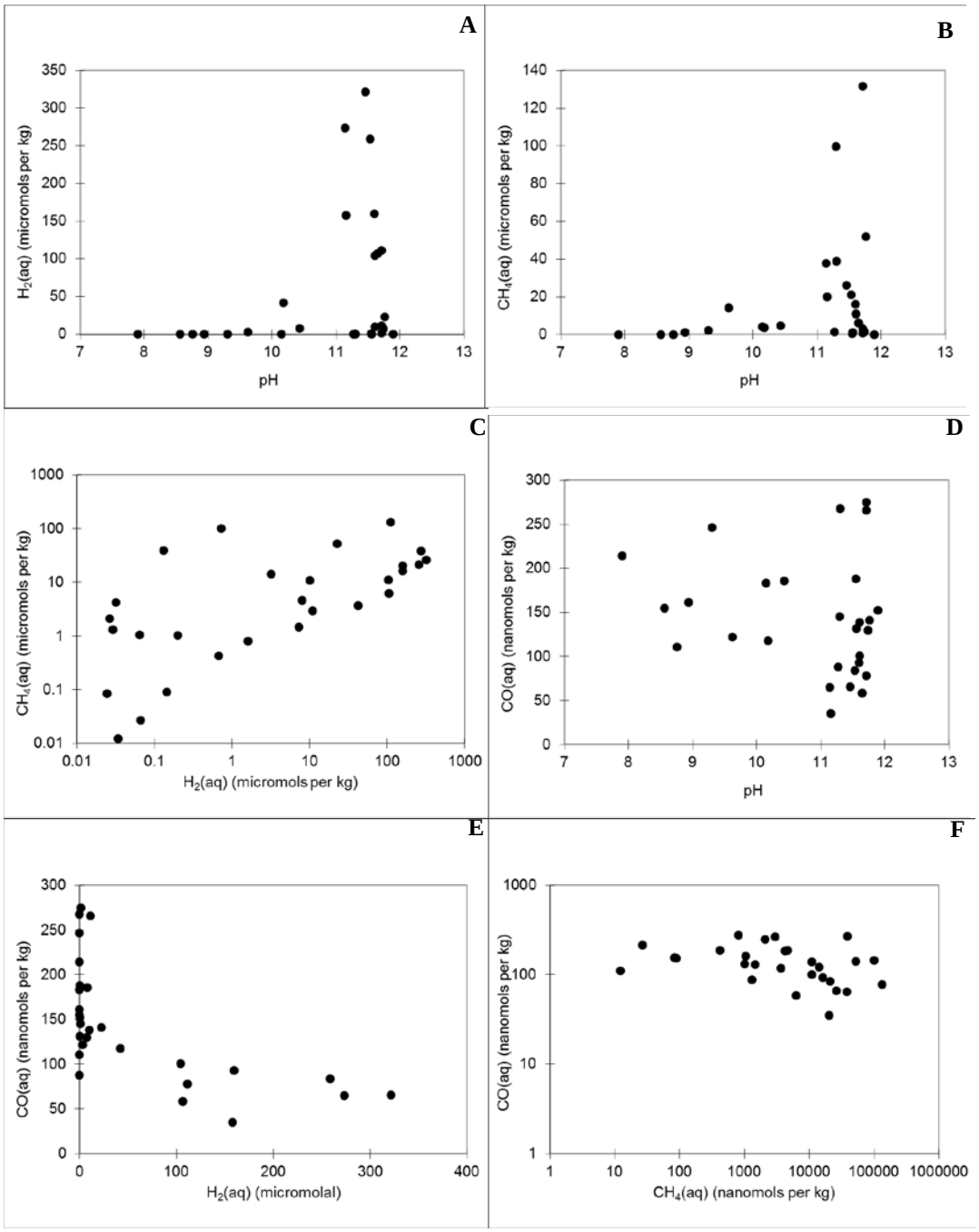

Figure 12. Concentrations of dissolved reduced gases plotted against pH and each other.

Concentrations of dissolved carbon monoxide are highly variable as shown in Fig 12, which obscures the effects of serpentinization. Plotting dissolved carbon monoxide against hydrogen indicates that higer concentrations of CO(aq) tend to occur where H_2(aq) concentrations are lowest. At dissolved hydrogen concentrations greater than ~50 μmolal, carbon monoxide does not reach concentrations greater than ~100 nanomolal. The lack of a positive correlation with H_2(aq) suggests that elevated CO(aq) concentrations are neither abiotic products of the process of serpentinization nor products of deep-seated microbial processes that take advantage of the reducing thermodynamic drive from serpentinization. This observation, together with the lack of a correlation between CO(aq) and CH_4(aq) concentrations suggests that CO(aq) is related to surficial processes. We suggest that CO(aq) is sourced in microbial processes in near-surface environments where reduced fluids encounter CO_2 from the atmosphere or organic solutes in surface waters.

3.6. Geochemical Bioenergetics of Serpentinization

The geochemical data presented above makes it possible to quantify Q_r via Eqn (4) and, in turn, the disequilibria present as redox reactions that could be exploited by microbial metabolisms in serpentinizing ecosystems. The speciation of each constituent measured in the water samples was calculated with standard state thermodynamic data for aqueous ions, neutral solutes, and complexes (Shock et al., 1989; 1997; Shock & Helgeson, 1990; Shock & McKinnon, 1993; Sverjensky et al., 1997) at the temperature of the sample. Activity coefficients were evaluated with an extended Debye-Hückel equation (Helgeson, 1969; Helgeson et al., 1981). Calculations were facilitated with the EQ3/6 computer program (Wolery and Jarek, 2003) using a customized database.

Equilibrium constants were evaluated with the same standard state thermodynamic data via the SUPCRT code (Johnson et al., 1992) using the revised Helgeson-Kirkham-Flowers equation of state (Shock et al. 1992), and are consistent with standard Gibbs energies for metabolic reactions summarized by Amend and Shock (2001). Resulting affinities for the reactions listed in Table 5 are discussed in this section. Affinities for all reactions are shown in terms of energy per mole of electrons involved in each reaction. This approach can be used to compare energy sources within and among ecosystem environments (McCollom and Shock, 1997; Shock et al., 2010; and others), consistent with the approach taken here.

Affinities for metabolisms for which Class I and II evidence are summarized above are depicted in Fig 13 as functions of the pH values of the samples. Dashed horizontal lines in some figures show where affinity = 0, the point where no energy is available from the designated reaction as written. The solid symbols represent affinity values that can be calculated with data provided in Tables 6-8. The open symbols mean that an estimate was needed to complete the affinity calculation. In cases where N_2(aq) appears, the unmeasured abundance of N_2(aq) was estimated to be in equilibrium with the atmosphere. Since N_2(aq) is a product in both cases, the affinities would be greater if the N_2(aq) concentration is in fact less than the value set by atmospheric equilibrium. Note that abundant energy is available for the Class I, hydrogen oxidation metabolism in the serpentinizing systems of the Samail ophiolite. The lowest affinities, around 25 kcal (mole e^-)$^{-1}$, in the hyperalkaline fluids are similar to values in the surface waters, and the greatest affinities are within 10% of the lowest values overall.

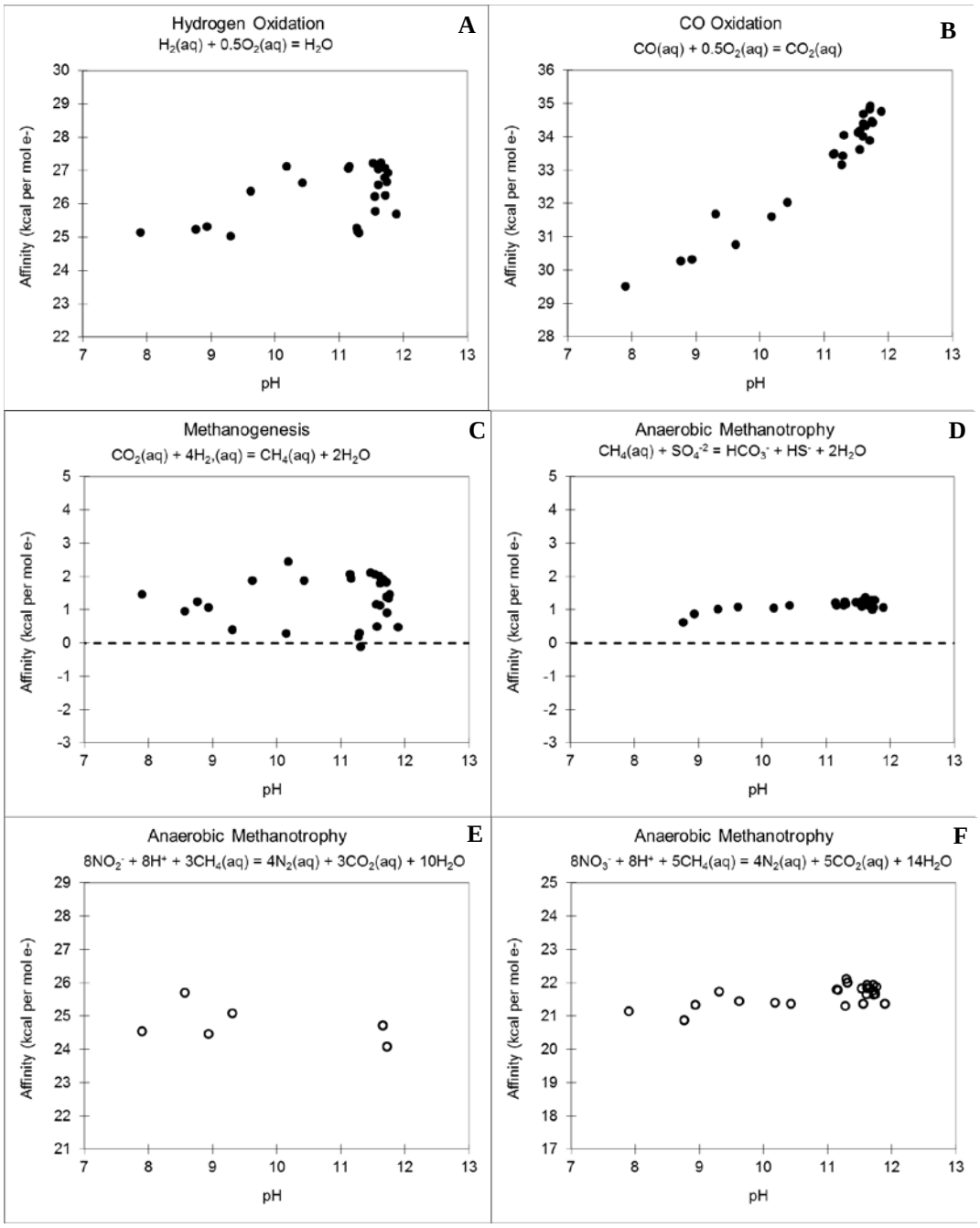

Figure 13. Affinities plotted against pH for metabolisms for which there are Class I and II evidence.

Even greater affinities are shown for the Class II, carbon monoxide oxidation reaction, and in contrast to hydrogen oxidation, there is a discernable trend of increasing affinity with increasing pH. Values range from > 29 kcal (mole e^-)$^{-1}$ at the lowest pH to > 35 kcal (mole e^-)$^{-1}$ at nearly the highest pH. Given the scatter in O_2(aq) data in Fig 11, and CO(aq) data shown in Fig 12, the trend in the affinity for CO oxidation is driven by the steeply decreasing abundance of DIC with increasing pH (Fig 11). This is a case where the product of the reaction has an exceptional influence over the distribution of energy from an overall metabolic reaction.

In contrast to hydrogen and carbon monoxide oxidations, affinities for the Class II autotrophic methanogenesis reaction are considerably lower, from slightly negative to just greater than 2 kcal (mole e^-)$^{-1}$, and the pattern of affinity Vs. pH has much in common with the pattern for hydrogen oxidation, despite being an order of magnitude lower. In both cases, the abundance of H_2(aq) dominates the resulting distributions of the affinity values. The final Class II reaction is anaerobic methane oxidation. Because the evidence from Lost City for this process is isotopic, and not definitive for the oxidant involved, we calculated affinities for the reactions involving sulfate, nitrite, and nitrate. Affinities for anaerobic oxidation of methane using sulfate as the oxidant are the lowest of the three, and hover around 1 ± 0.5 kcal (mole e^-)$^{-1}$ regardless of pH. In contrast, the reactions involving nitrite and nitrate have much greater affinities even though they are nearly pH independent. As mentioned above, no data were collected on the concentration of N_2(aq), and affinities were calculated by setting N_2(aq) to equilibrium with the atmosphere, so it should be kept in mind that these values would be conservative if N_2(aq) concentrations are below atmospheric equilibrium. Note that only six nitrite

measurements were obtained in the field, but they cover the entire obtainable pH range in this system so the resulting affinities may be representative for many serpentinizing ecosystems in the Samail ophiolite.

The affinities shown in Fig 14 are for the metabolisms for which Class III, IV, and V evidence is reported. Of the two Class III reactions, the affinities for ammonia oxidation are about three times greater than those for sulfate reduction per mole of electrons. The latter distribution of datapoints resembles those for the affinities of the hydrogen oxidation and autotrophic methanogenesis reactions shown in Fig 13. Again, it appears that the abundances of H_2(aq) determine this pattern. Comparison with Fig 13 shows that, per mole of electrons, the affinities for sulfate reduction tend to be slightly greater than those for autotrophic methanogenesis. The affinities for ammonia oxidation, while greater, are intermediate between the extremely low values for sulfate reduction, autotrophic methanogenesis, and anaerobic methane oxidation with sulfate, and the much greater affinities for the other Class I and II reactions in Fig 13. Note that there are several samples for which we did not obtain ammonia data (see Table 6).

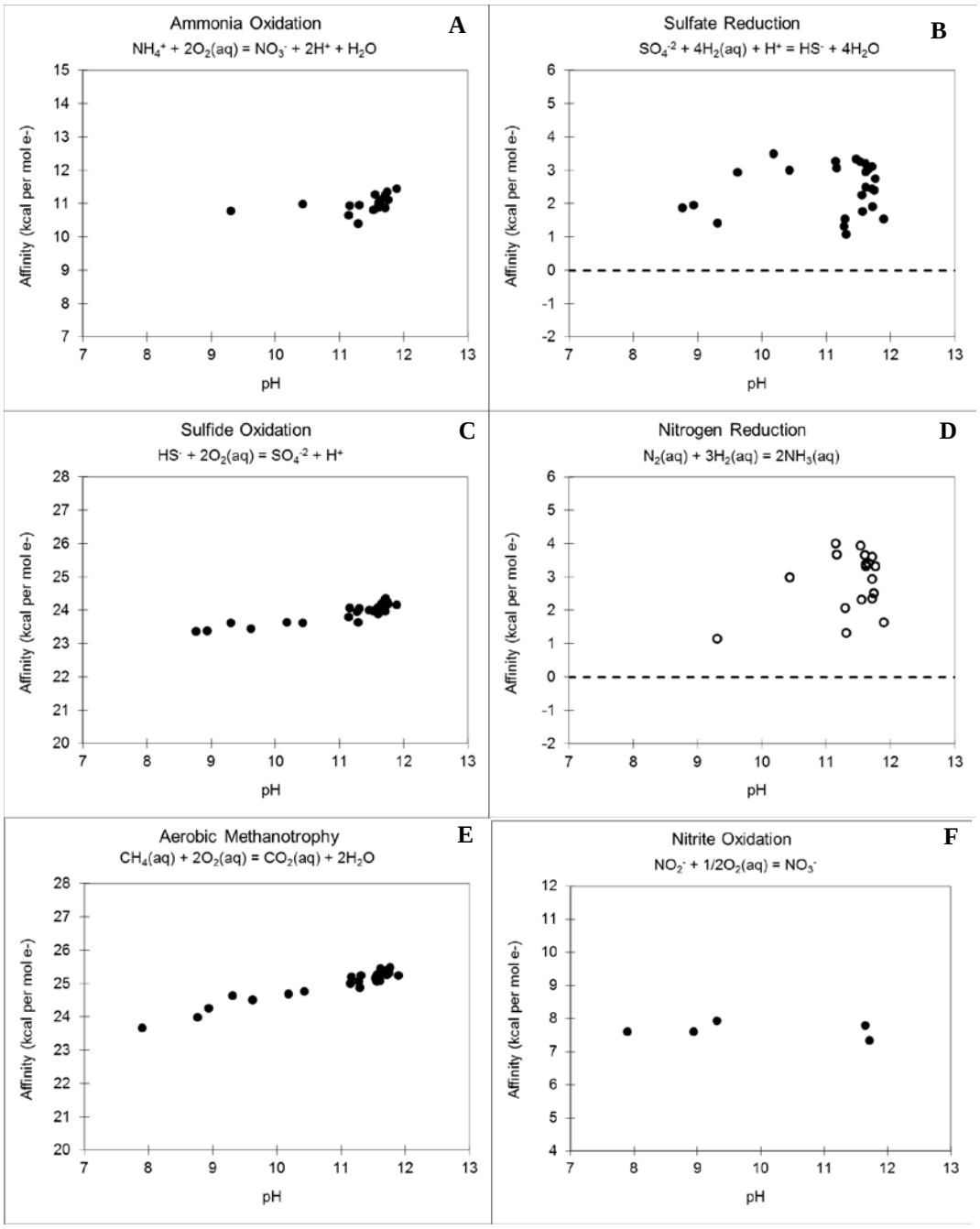

Figure 14. Affinities plotted against pH for metabolisms for which there is Class III, IV, and V evidence reported.

Sulfide oxidation and nitrogen reduction are both Class IV reactions, but the corresponding affinities differ dramatically, with those for sulfide oxidation exceeding by factors from 6 to 10 those for nitrogen reduction. The affinities for sulfide oxidation are of about the same magnitude as those for hydrogen oxidation shown in Fig 13. Unlike the affinities for hydrogen oxidation, those for sulfide oxidation are more closely distributed, and show a slight increase with increasing pH. Although the pattern of nitrogen reduction affinities is missing some datapoints owing to the incomplete coverage of the ammonia measurements, the existing distribution of points is reminiscent of the pattern for sulfate reduction, as well as hydrogen oxidation and autotrophic methanogenesis shown in Fig 13, adding to the evidence for the influence of H_2(aq) abundances on resulting affinities for reactions in which it is a reactant.

Affinities for the two Class V reactions, aerobic methanotrophy and nitrite oxidation are shown at the bottom of Fig 14. The tight distribution of affinities for aerobic methanotrophy is like that for sulfide oxidation (note that the ranges of the ordinates are the same for these plots), and , in fact the values are quite close for these two reactions. The dependence on pH is somewhat greater in the case of aerobic methanotrophy, and affinities at the highest pH values are somewhat greater. Intermediate affinities, somewhat less than those for ammonia oxidation, are attained for nitrite oxidation, which once again are limited by the availability of nitrite data. As in the case of nitrite-driven methane oxidation, the near independence of these affinities with respect to pH suggests the small number of values obtained in this study may be representative of the serpentinizing ecosystems of the Samail ophiolite in general.

Finally, we suggest four additional metabolic strategies that may be capable of supporting microbial metabolisms during serpentinization, despite the lack of molecular evidence. These are shown in Fig 15. Nitrate reduction is selected owing to its geochemical similarity (though biologically different) to nitrogen reduction, which is a Class IV reaction. Affinities for nitrate reduction range from 16 to 19 kcal (mole e^-)$^{-1}$, considerably greater than the 1 to 4 kcal (mole e^-)$^{-1}$ available from nitrogen reduction. The anammox process (anaerobic ammonia oxidation), through which nitrite and ammonia combine to yield N_2, also seems to be a likely candidate given the substantial affinities shown by other reactions in the nitrogen cycle. Even though we are only able to estimate three affinities for the anammox reaction, owing to the incomplete coverage of nitrite measurements and the estimated abundances of N_2(aq), these values rival those for nitrite reduction shown here, and exceed those for nitrite oxidation, nitrogen reduction, and ammonia oxidation shown in Fig 14 for which molecular evidence exists. Two additional geochemically based selections are influenced by the large affinities for CO oxidation shown in Fig 13, as both reactions involve CO as a reactant. Affinities for the water-gas shift reaction range from 4 to 9 kcal (mole e^-)$^{-1}$, and show a trend of increasing affinity with increasing pH. These results are complementary to the CO oxidation affinities shown in Fig 13 that also increase with increasing pH. Oxygen is a stronger oxidant than H_2O, and it follows that affinities for CO oxidation exceed those for the water-gas shift reaction, which, as a source for H_2(aq) could be linked with hydrogen oxidation in some serpentinizing ecosystems. To complete the CO cycle, we suggest CO reduction as a plausible metabolic strategy in these systems, and note that the affinities ranging from about 3 to 5 kcal (mole e^-)$^{-1}$, while small, exceed those for autotrophic

methanogenesis, sulfate-driven methane oxidation, sulfate reduction, and nitrogen reduction for which molecular evidence is reported.

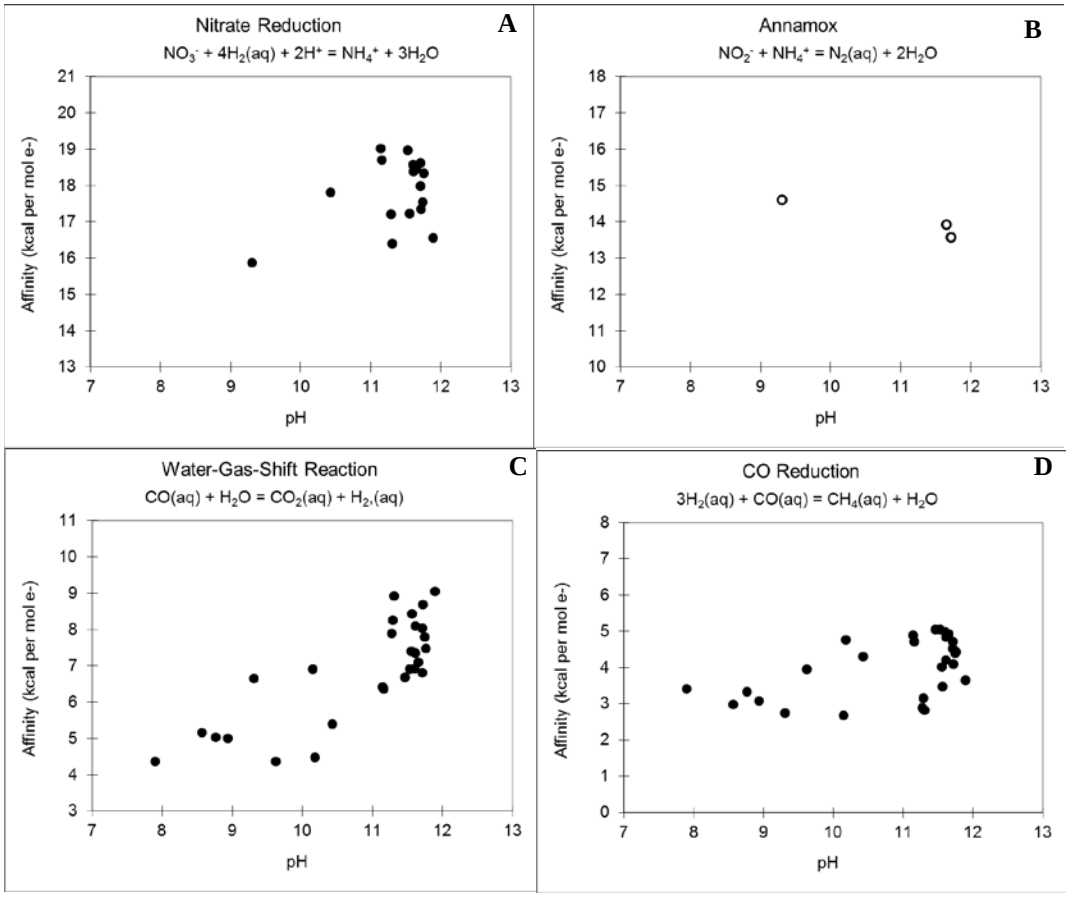

Figure 15. Affinities of metabolic strategies without molecular evidence plotted against pH.

3.7. Predicting Energy Supplies at the Surface and in the Subsurface

Affinities obtained for the 16 reactions illustrated in Figs 13 to 15 are summarized and compared in Fig 16 at a pH of 11 (selected to represent conditions as hyperalkaline fluids generated by serpentinization first encounter the atmosphere). Individual distributions of affinities determine the lengths of the segments for each reaction, and they are ranked by the maximum affinity each attains. It can be seen that this set of reactions provides a cascade of energy sources ranging from 34 to 0 kcal (mole e^-)$^{-1}$ in

hyperalkaline serpentinizing fluids. Four of the top five reactions are oxidations involving O_2, as are reactions 9 and 11, reflecting the disequilibria induced when reduced solutions enriched in CO(aq), H_2(aq), CH_4(aq), HS^- , NH_3(aq) and NO_2^- encounter the oxidized atmosphere. Reactions 4, 6, 7, and 8 all involve either nitrite or nitrate as oxidants and H_2(aq), CH_4(aq), or ammonia as reductants. The H_2-producing water-gas shift reaction ranks tenth, followed by reactions in which H_2(aq) is oxidized by CO(aq), N_2(aq), SO_4^{-2} and CO_2. The oxidation of CH_4(aq) with oxygen, nitrite, or nitrate ranks considerably higher than its oxidation with sulfate, which completes the list of reactions.

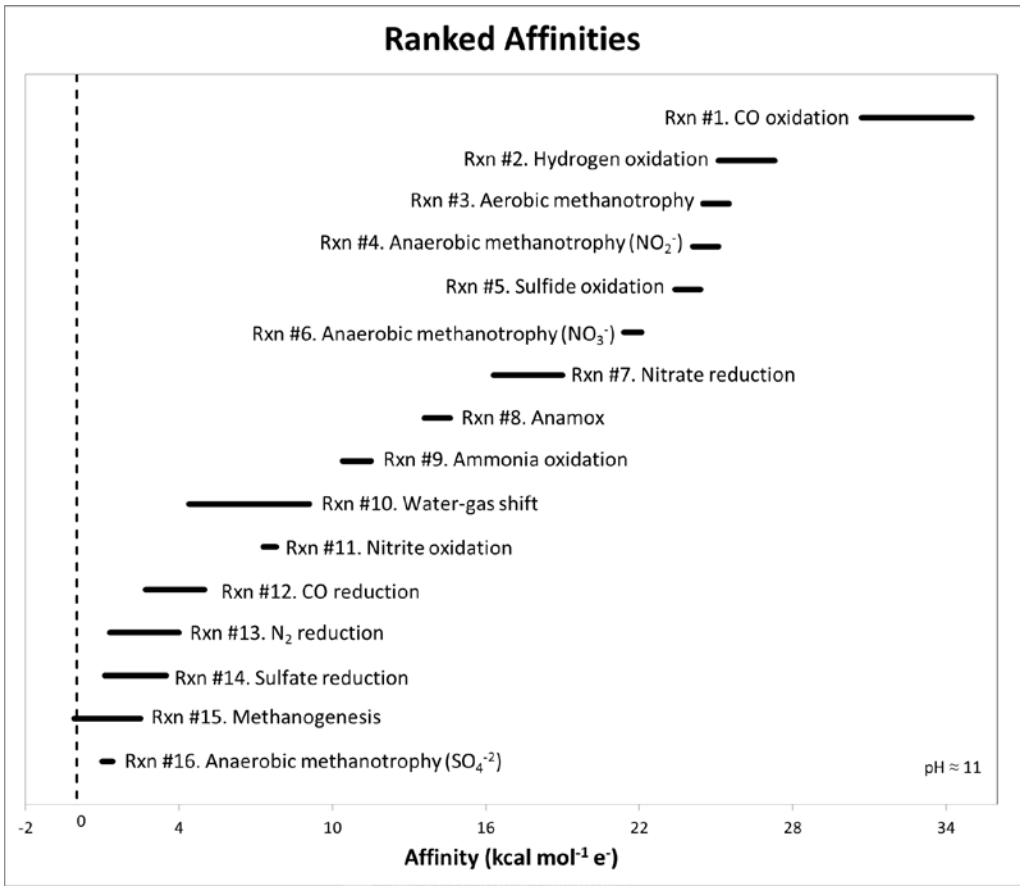

Figure 16. Summary of affinities of reactions in Figs 13-15 at pH = 11.

The results summarized in Fig 16 emphasize how the supply of oxidants and reductants interact to provide structure for the energy supply in serpentinizing

ecosystems. The example in Fig 16 is one of many that can be generated from the affinity calculations summarized above, but all will be limited quantitatively to the easily accessible conditions at the Earth's surface. Nevertheless, these observations allow us to speculate about the distributions of microbial metabolisms that may be encountered in the subsurface, where active low-temperature serpentinization occurs as surface waters infiltrate into mantle-derived peridotites. In the following discussion, we considered two subsurface environments: a shallow setting where abundant oxidants are transported into conditions where the rocks are mostly altered and reductants are supplied through diffusion from deeper-seated reactions, and a deeper setting where active serpentinization supplies abundant reductants but surface-derived oxidants may be limited. These scenarios are chosen to provide predictions of the likelihood of encountering active metabolisms in the subsurface, which may be tested by sampling wells (Paukert et al., 2012; Miller et al., 2016) or by drilling and subsurface sampling (Kelemen et al., 2013).

Examples of predicted distributions of energy supplies are shown in Fig 17 for the 16 reactions listed in Table 5, and ranked as shown in Fig 16. The vertical dimension of these plots is meant to depict depth, which is relative depending on the dynamics of fluid transport, fracture density, progress of water-rock reactions, and actions of subsurface microbial communities in the shallow and deeper settings. The shading is meant to depict our predictions of the relative depths at which each microbial metabolism may be encountered based on availability of energy supplies. Many other metabolic strategies should be anticipated, including heterotrophic processes not considered in this study, and direct oxidation of ferrous iron in primary or secondary minerals during serpentinization.

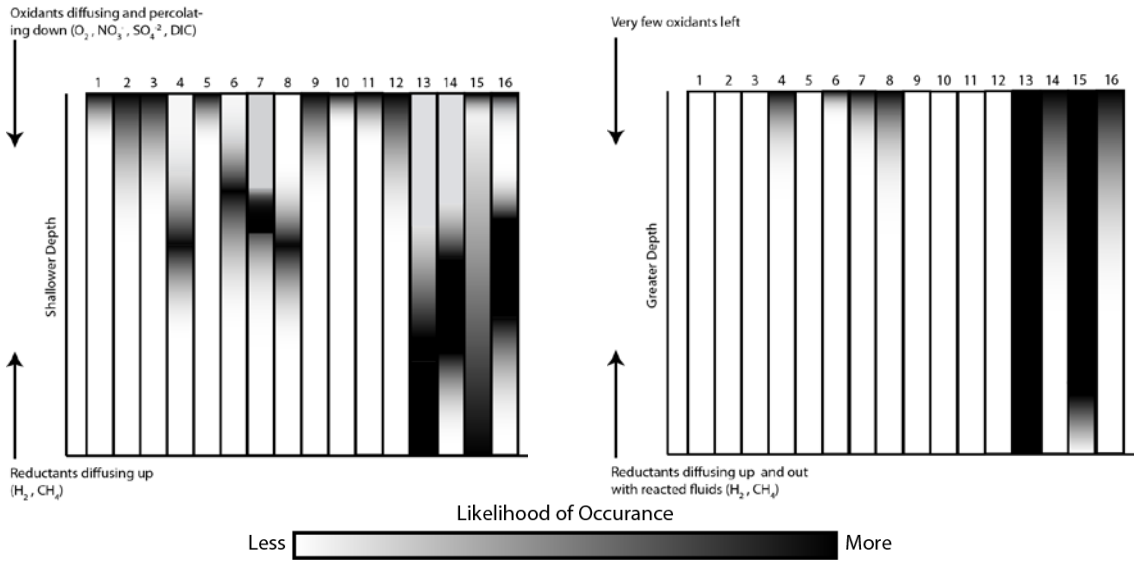

Figure 17. Predicted Distributions of Energy Supplies.

The panel on the left shows predictions for shallow environments in altered rocks where oxidants are delivered from the surface (top) and reductants are diffusing upward from deeper in the system (bottom). Reactions 1, 2, 3, 5, 9, and 11 all involve O_2, which is sourced from the atmosphere. As a consequence, we predict that all of these metabolic strategies will supply ample energy at near-surface environments, but that their distribution with depth may be limited. In detail, we anticipate that oxidation of hydrogen (2), methane (3), ammonia (9), and possibly sulfide (5), all of which can be correlated with high pH and therefore active serpentinization, may extend to greater depths than the oxidation of carbon monoxide (1) and nitrite (11), which we interpret to be derived from near-surface environments given their distributions with pH. It follows that other reactions involving CO are also expected to support microbial metabolism at relatively shallow depths, but we anticipate the water-gas shift reaction (10), which produces H_2 and CO_2, will be encountered shallower than CO reduction (12), which consumes H_2 that would be supplied from depth. At intermediate depths, below conditions where O_2 is

readily available, we anticipate reactions 4, 6, 7, and 8 all involving nitrogen-bearing species to be able to support microbial communities. In general, we expect that nitrite and nitrate are derived from the surface, but that they may be able to infiltrate deeper than O_2. In addition, we assume that nitrite may infiltrate more deeply because it is reduced relative to nitrate. This means that nitrite-driven methanotrophy (4) and anammox (8) may occur at greater relative depths than nitrate-driven methanotrophy (6) or nitrate reduction (7). The depth of occurrence of the anammox process, which consumes NH_3(aq), may be influenced by the progress of nitrogen reduction (13) in which NH_3(aq) is produced. We anticipate that sulfate reduction (14), autotrophic methanogensis (15) and sulfate-driven methane oxidation (16), like nitrogen reduction (13), will be encountered at greater relative depths in this shallow-system scenario. Several of these reactions depend on the availability of H_2(aq), which we anticipate to increase in concentration with depth. Anaerobic methane oxidation with sulfate provides limited energy at surface conditions (see Fig 14), but may be one of the few strategies left if sulfate can infiltrate to deeper environments where elevated concentrations of methane may exist. One deep source for methane may be autotrophic methanogenesis if carbonate minerals that occur as part of the alteration assemblage can be reduced owing to the flux of hydrogen from deeper active serpentinization. We also anticipate that methanogenesis will be encountered in shallow reaches of altered rocks where hydrogen from deep meets CO_2 from the atmosphere. If so, anaerobic oxidation of methane with sulfate (or nitrite or nitrate) may be fueled by near such near-surface methanogenesis.

The plot on the right in Fig 17 shows our predictions for metabolisms that will be encountered in regions of active serpentinization, which we imagine to be deeper-seated

than the near-surface environments discussed above. In this scenario, very few surface-derived oxidants remain in the fluids that are enriched in reductants derived from serpentinization. Note that all of the reactions that depend on O_2 (1, 2, 3, 5, 9, and 11) are envisioned to be absent from this deep scenario. Likewise, the CO-consuming reactions (10, 12) are predicted to be absent if, as we argue, CO has a near-surface source. Reactions dependent on nitrite (4, 8) or nitrate (6, 7) are predicted to be possible energy sources at the upper reaches, assuming that these surface-derived solutes can infiltrate deeper than conditions where O_2 and CO are effectively scrubbed. We expect the anammox reaction (8) to extend deeper than the others if ammonia production is driven by nitrogen reduction (13), which is a candidate to persist throughout deep reaches of active serpentinization. Similarly, we envision that autotrophic methanogenesis (15) will persist to considerable depths until carbonate minerals are lost from the rocks. Finally, sulfate reduction (14) and sulfate-driven methane oxidation (16) may also support microbial communities into deep zones of active serpentinization.

3.8. Concluding Remarks

This study was designed to seek the geochemical and thermodynamic underpinnings for the microbial metabolisms supported by serpentinization. The summary of existing molecular lines of evidence allowed a focus on a subset of reactions that appear to supply energy in serpentinizing ecosystems. Geochemical data from serpentinizing systems in the Samail ophiolite were used to quantify those energy sources, provide rankings of energy supplies, and develop hypotheses for how those energy supplies may be distributed in the subsurface, both in shallow systems where substantial serpentinization has already occurred, and in deep systems where active

serpentinization proceeds. These hypotheses can be tested by sampling existing wells in peridotite and by drilling to obtain subsurface rock, water, and molecular samples. Given the myriad flow paths, water-rock ratios, and residence times that could characterize fluid flow within these systems, it should be anticipated that mapping energy supplies onto actual subsurface environments will require considerable attention to geologic details.

It should not be assumed that the energy sources evaluated in this study are the only ways that serpentinization supports microbial metabolism. As an example, we did not quantify the abundances of any organic compounds, which precludes inclusion of any heterotrophic metabolic strategies. It should also be kept in mind that we did not measure concentrations of N_2(aq), but estimated values based on equilibrium with the atmosphere. Nor did we attempt to measure thiosulfate, polysulfides, N_2O(aq), or other inorganic solutes that could be involved in microbial metabolism. Likewise, we have not conducted analyses of primary and secondary minerals that would enable including Fe-redox reactions in the evaluation of energy supplies. Nevertheless, we anticipate that the involvement of Fe oxidation in determining the abundance of H_2(aq) and, indirectly, CH_4(aq) may indicate a direct role for Fe-based reactions in supporting microbial metabolism throughout the process of serpentinization. Specific details emerging from this study include: 1) the likelihood that nitrogen-cycle reactions are capable of supporting microbial metabolism during serpentinization in the subsurface, 2) that diverse CO-based metabolisms may flourish in near-surface environments, and 3) that autotrophic methanogenesis may occur both very close to the surface where H_2(aq) from depth encounters CO_2 from the atmosphere, and again deep in the system where H_2(aq) generated through serpentinization reactions encounters carbonate minerals formed in

earlier stages of alteration. It is hoped that the results obtained here, as well as the general approach illustrated, will help guide the exploration of the subsurface biosphere supported by serpentinization wherever it occurs.

3.9. Acknowledgments

The authors thank Jeff Havig, Amelia Paukert, Lisa Streit, Jurg Matter, Peter Kelemen, and Sobhi Nasser for assistance with field work and logistics of working in Oman; Kris Fecteau, Natasha Zolotova and Panjai Prapaipong for help with laboratory analyses, as well as Tori Hoehler, Mike Kubo, and Dawn Cardace at NASA AMES. This work was supported by NASA Exobiology, the NAI Rock-Powered Life project, and NSF grant EAR-1515513.

IV. SUBGLACIAL AND LOW TEMPERATURE BIOENERGETICS

4.1. Introduction

4.1.1. The Cold Biosphere

The majorty of the Earth's biosphere can be considered a cold biosphere, with more than 80% of it below 5 ^{o}C. This includes the 14% at polar latitudes and the nearly 11% of the continental landmass that is covered by ice. In addition to both of those locales, 90% (by volume) of the known biosphere is cold ocean water (Cavicchioli et al., 2000; Christner et al., 2008; Patterson 1994; Priscu and Christner 2004). The enormity of the cold biosphere is more easily grasped via a map of the cold (<5 ^{o}C) biosphere (Fig. 18). Understanding the energy supplies available to microorganisms in the largest portion of the biosphere is necessary to evaluate how microbes affect the global cycling of carbon, nitrogen, sulfur, iron, and trace nutrients. This type of knowledge would also be indisposable for assessing the potential for life on icy moons and satelites as well as ocean worlds.

Over geologic time, the advance and retreat of glaciers across continents has had a profound impact on the geology and biology of different regions through physical and biogeochemical processes. Retreat and advance of ice during glacial-interglacial cycles may have driven taxa toward habitats with more stable conditions enabling biodiversity to persist (Hamilton et al. 2013; Hodson et al. 2008). It has recently been suggested that glacial beds are comparatively more stable than surface environments (Skidmore et al. 2005) and may have provided refuges for biodiversity during periods of inclement geologic, climatic or atmospheric conditions (Hodson et al. 2008).

Subglacial systems receive continual exposure to fresh mineral surfaces and chemical species that serve as an energy supply as well as replenishment of nutrients through mechanical and chemical weathering processes; this can support functionally-diverse assemblages of microorganisms over periods of geologic time (Sharp et al., 1999; Skidmore et al., 2000, 2005). The release of iron, sulfide, carbonate, and organic matter into subglacial environments is the result of comminution of minerals in the underlying bedrock of these systems (Tranter et al., 2005). Hydrogen production in subglacial systems is also thought to be the result of rock comminution (Telling et al., 2015) and can provide an important reductant for microorganisms to exploit. In many subglacial systems microbial oxidation of metal sulfides is thought to be important to the biogeochemical cycling of iron and sulfur in both oxic and anoxic settings. There is also evidence that pyrite and its oxidation products influence the structure and composition of microbial communities (Bottrell and Tranter, 2000; Mitchell et al., 2013; Tranter et al., 2002). Also of note is that approximately 90% of atmospheric methane is produced by methnogenic archaea (Conrad, 1996; Thauer et al., 2008); subglacial methane production might be significant in the global carbon cycle and may have had an important role during the Laurentide glaciation (Weitemeyer and Buffett, 2006; Wadham et al., 2008). There is evidence for redox transformations of nitrogenous compounds that could have an impact on the global nitrogen cycle as well in subglacial sediments and other glacial environments (Foght et al., 2004; Skidmore et al., 2005; Boyd et al., 2011)

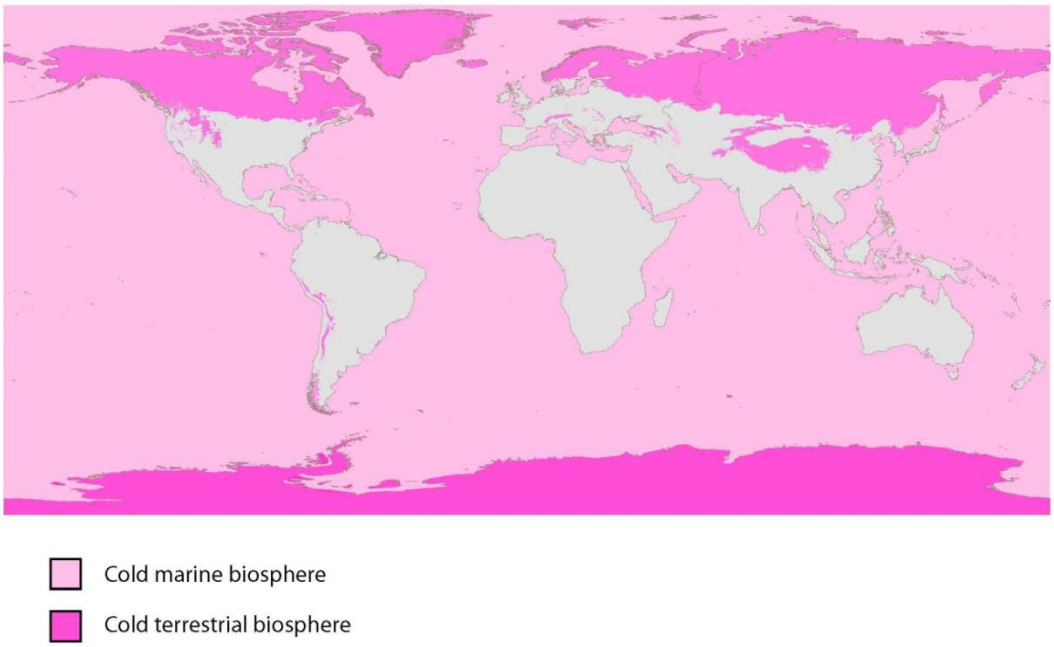

Figure 18. Quantitative depiction of the Earth's cold biosphere (<5 ^{o}C) displaying the cold marine biosphere in light pink and the cold terrestrial biosphere in dark pink. Seventy percent of the Earth's surface is covered by bottom seawater at ~ 2^{o}C and over 10% of the Earth's land surface is ice covered, which means that at least 80% of the surface biosphere is cold (Patterson 1994, Christner et al. 2008). In addition, cold temperatures are likely to prevail in a large volume of the subsurface biosphere, but the extent is presently unknown. Map generated in ARCGIS V10.0 using ocean and continental shape files from ESRI and high resolution (1 km spatial resolution) global landmass climate data from Hijmans et al. (2005) and includes all terrestrial regions that fall into this category including the polar regions, glaciers, and areas of high altitude, as well as the cold marine biosphere.

4.1.2. Microbial Activity

Cold marine sediments, basement rocks, and the overlying bottom seawater, to be referred to from here on out collectively as BSW, host a wide variety of microorganisms performing a myriad of different autotrophic and heterotrophic metabolisms. Microorganisms capable of utilizing iron have received considerable attention due to their role in the cycling of iron and their contribution to the weathering of basement rocks. Psychrophilic iron-oxidizing α- and γ-*Proteobacteria* have been isolated from

weathering habitats in the area of the Juan de Fuca mid-ocean ridge system (Edwards et al., 2003). Iron-oxidizing *Acidiferrobacter* were also detected in the cold oxic crustal aquifer at North Pond, a sedimented basin along the Mid-Atlantic ridge (Meyer et al., 2016; Orcutt et al., 2013). Genomic and geochemical evidenced indicate the presence of iron reducing microorganisms in marine sediments in the central oceanic area and marine sediments from continental margins (Burdige, 1993; D'Hondt et al., 2004; Monien et al., 2014; Wehrmann et al., 2014). Microorganisms involved in nitrogen cycling have been characterized in cold marine settings and include nitrifying *Pseudomonas, Psychromonas, Arcobacter*, and *Herminiimonas* as well as *Shewanella, Enterobacter* sp., and *Vibrio* sp. that perform dissimilatory nitrate reduction to ammonium (Bonin, 1996; Canion et al., 2013). Sulfur cycling microorganisms in marine sediments that have been observed include (but are not limited to) psychorotrophic sulfate-reducing bacteria (Isaksen and Jorgensen, 1996), thiosulfate-reducing and thiosulfate-disproportionating bacteria (Jorgensen and Bak, 1991). Microorganisms from the genus *Sulfurimonas*, that typically use reduced sulfur compounds or molecular hydrogen as electron donors and nitrate, nitrite, or oxygen as electron acceptors, have also been characterized (Meyer et al. 2016). Methane cycling is also observed and methanogenic archaea (Purdy et al., 2003) have been observed in a variety of cold sediment and basement rock habitats. The presence of methanogens is balanced by analyses by research from Knittel et al. (2005). That work compared 16S rRNA gene sequences and the investigators purport that methanotropphic archaea are present in almost all methan environment regardless of temperature, depth, pressure, and methane and sulfate concentrations. The potential for

hydrogen oxidation has also been indicated from sediment cores collected from the Barents Sea, equatorial Pacific, and the Gulf of Mexico (Adhikari et al., 2016).

An extensive review of the available literature indicates that microbial activity has been confirmed at a variety of different (sub)glacial settings (Abyzov et al., 1998; Amato et al., 2007; Boyd et al., 2010, 2011; Brinkmeyer et al., 2003; Christner et al., 2000, 2001, 2003, 2006, 2008; Foght et al., 2004; Gaidos et al., 2004, 2009; Hamilton et al., 2013; Karl et al., 1999; Mikucki and Priscu, 2007; Mikucki et al., 2004, 2009, 2016; Miteva and Brenchley, 2005; Miteva et al., 2004; Murray et al., 2007, 2012; Priscu et al., 1999; Rogers et al., 2013; Sharp et al., 1999; Skidmore et al., 2000, 2005; Ward et al., 2003; Xiang et al., 2005; and others). One particular setting that has received attention in recent years is the Antarctic subglacial lakes. Over 400 subglacial lakes in the Antarctic have been identified (Wright and Siegert 2011). Some of the best characterized are Lakes Vida, Vostok, Bonney, and Whillans. These lakes span a range of dissolved oxygen concentration, from anoxic (Lake Vida), to suboxic (Lakes Bonney and Whillans), to oxic Lake Vostok where very high (2.51 liters (kg water) $^{-1}$) dissolved gas levels have been estimated to exist and the dissolved oxygen concentration has been predicted to be ~50 times higher than water equilibrated with the atmosphere (Christner et al. 2008; Lee et al. 2004; McKay et al. 2003; Mikucki et al. 2016; Mousis et al. 2013; Murray et al. 2012; Ward et al. 2003). Microorganisms that have been found in Antarctic subglacial lakes include bacteria, archaea, and eukarya. The bacterial sequences indicate the presence of firmicutes proteobacteria, actinobacteria, and fungi. Based on the sequence data, this mixture of heterotrophs and autotrophs has the potential to perform nitrogen cycling and carbon fixation, while using hydrogen, reduced forms of N, S, Fe

and methane as energy sources (Christner et al. 2001, 2014; Karl et al. 1999; Mikucki et al. 2016; Murray et al. 2012 and supplemental material; Priscu et al. 1999; Rogers et al. 2013; and others).

Many cold biosphere habitats have been characterized i.e., Lake Vida Brine (LVB), bottom seawater (BSW), etc.; but there are few well characterized glacial or subglacial systems. Robertson Glacier (RG), Figure 19, is a well characterized model system for measurements, calculations, and comparison to other low temperature systems in the cold biosphere (Bhatia, 2004; Boyd et al. 2010, 2011; Hamilton et al. 2013; McMechan, 1988; Mitchell et al. 2013; Sharp et al. 2002). Therefore, it was selected for retrieval of samples that were analyzed. Results from analyses were used to perform intensive bioenergetic investigations as part of a suite of analyses for comparison with BSW and LVB. Its structure is similar to that of other glaciers (Figure 20) and could have a redox zonation as shown in Figure 21. This zonation could support a series of different ecosystems throughout the subglacial regime from anoxic far beneath the glacier to oxic toward the outflow zone of the subglacial meltwater stream. Microbial investigations performed at RG indicate the presence of methanogens, methanotrophs, nitrate reducers and nitrifiers, lithotrophic bacteria, and heterotrophic eukarya and microorganisms associated with metabolism of iron and/or sulfur (Boyd et al. 2010, 2011, Hamilton et al. 2013; Mitchell et al. 2013)

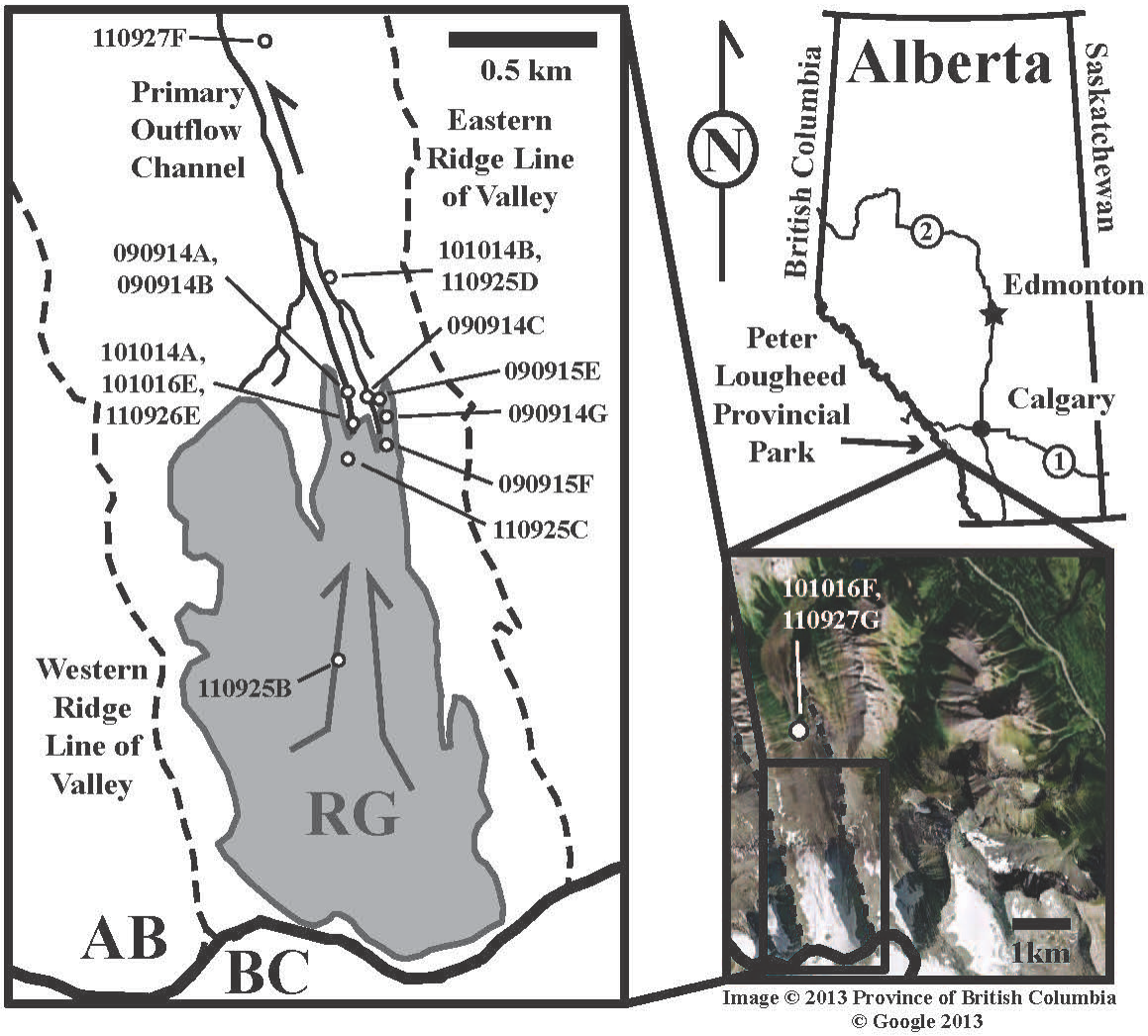

Figure 19. Map illustrating the location of Robertson Glacier and sample locations. The inset photograph is of Robertson Glacier and its location relative to the overview map of Alberta, Canada.

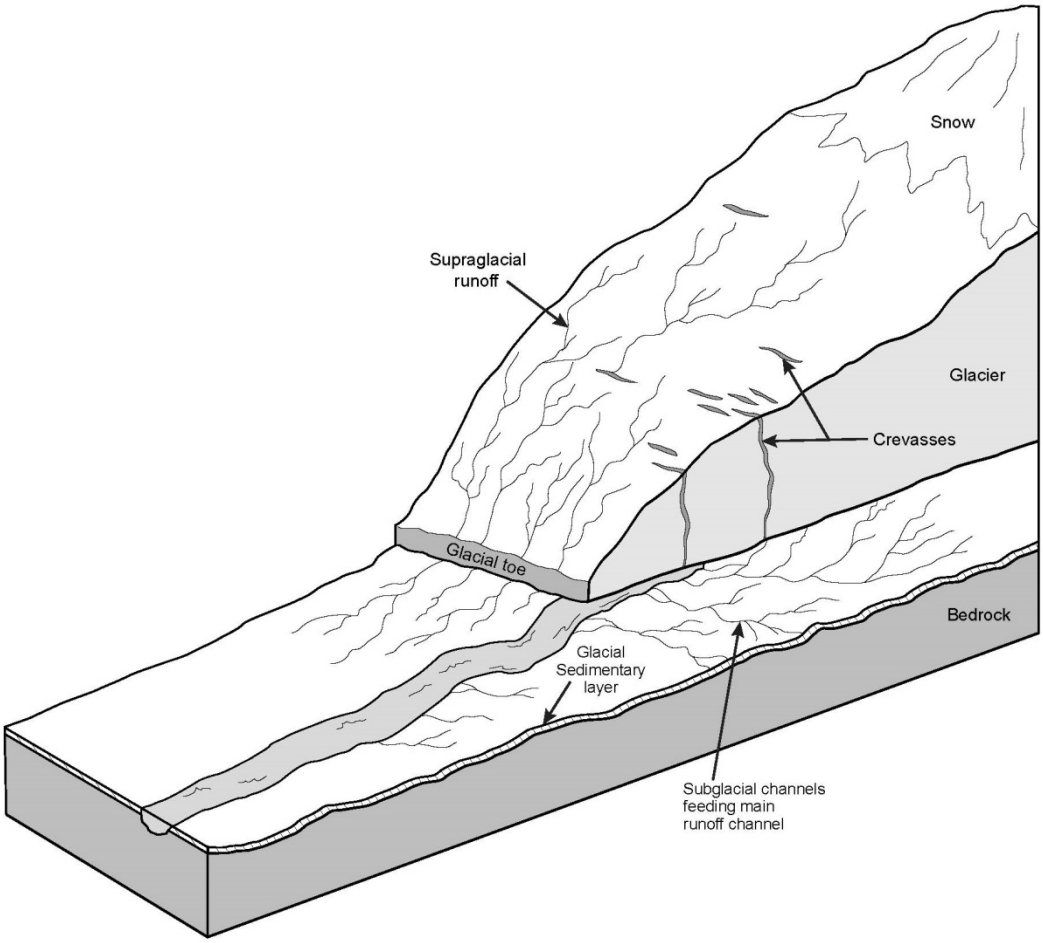

Figure 20. Simplified schematic block diagram of the Robertson Glacier structure (modified from Rennermalm et al. 2013).

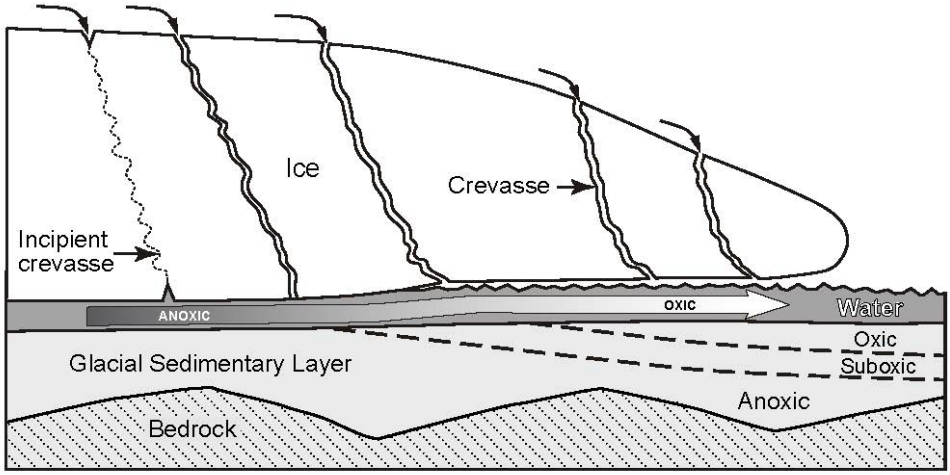

Figure 21. Cartoon depicting biogeochemical zonation in the Robertson Glacier system (after Kivimäki 2005 and Montross 2007).

Despite previous work, only recently have advances in drilling, geochemistry, microbiology, and genetics allowed the scientific community to delve deeper into the subglacial and low temperature biogeochemical processes occurring at these unique sites. In addition, there are very few qualitative analyses of available energy, or the bioenergetics of metabolic strategies that may be prevalent in these systems, and no quantitative analyses of energy availability. The characterization of microbial communities, estimation of rates of metabolisms and identification of potential metabolic pathways in different environments (Cheng and Foght 2007; Christner et al. 2001; Skidmore et al. 2005; Tung et al. 2006) helps reveal how microorganisms may influence their local chemical environment (Bhatia et al. 2006; Gaidos et al. 2004; Kaštovská et al. 2007) and influence geochemical cycles involved with carbon, nitrogen, sulfur, and iron (Bottrell and Tranter 2002; Christner et al. 2008; Gaidos et al. 2004; Hodson et al. 2008; Mikucki et al. 2004; Sharp et al. 1999; Skidmore et al. 2000; Wadham et al. 2004; Wynn

et al. 2007). This is of great consequence considering the plethora of possible metabolisms that have not been investigated or taken into account for the biogeochemical cycling of elements and nutrients. Furthermore, according to work by Price and Sowers (2004) concerning the temperature dependence of metabolic rates for microbial growth, maintenance, and survival: "There is no evidence of a minimum temperature for metabolism". This means the extent (both the depth and the volume) of the cold biosphere may have been vastly underestimated in the past. The effect of a large cold biosphere could reshape perceptions of its influence on the biogeochemical cycling of major elements and nutrients to the rest of the biosphere.

4.2. Material and Methods

4.2.1. Study Site

Robertson Glacier (115°20'W, 50°44'N) is an alpine glacier in the Canadian Rockies that drains the northern flank of the Haig Icefield in Peter Lougheed Provincial Park, Kananaskis County in Alberta Canada (Figure 19). For over a decade it has been studied as a model system to investigate biogeochemical processes in glacial systems (Boyd et al. 2010, 2011, Hamilton et al. 2013, Mitchell et al. 2013, Sharp et al. 2002). Robertson Glacier is a north facing glacier, approximately 2 km long, that ranges in elevation from 2370 to 2900 m. Glacially-smoothed bedrock surfaces occur along the glacier margins and it terminates on a flat till plane. Drainage from beneath the ice front occurs vai two main subglacial meltwater streams, one on the east side and one on the west side. Local bedrock is upper Devonian in age and is composed of dolomitic limestones, dolostones, and impure limestone with interbeds of sandstone, shale, and siltstone (McMechan, 1988). A few of the bedrock surfaces carry a veneer of

subglacially precipitated calcite (Hallet, 1976) and are incised by discontinuous "Nye channels" (e.g., Walder, 1979).

4.2.2. Field and Laboratory Measurements

4.2.2.1 Field Measurements

Sample locations were recorded using GPS and can be found on the map in Figure 19. The sample codes include a year-month-day identifer and a unique letter. A brief description of the sampling sites can be found in Table 1. Field blanks were performed daily using 18.2 MΩ cm deionized water with the same equipment and techniques used on routine samples. Nested water, gas, sediment, and biological samples were collected during the fall of 2009 and 2010. Field measurements included: temperature, pH, conductivity, titrations for alkalinity, and spectrophotometric analyses of redox-sensitive species. Temperature, conductivity, and pH were measured with YSI 30 and Orion 290A meters and glass pH electrodes that were calibrated daily using buffer solutions of pH 4, 7, and 10. Dissolved oxygen (DO), nitrate, nitrite, total ammonia, total sulfide, dissolved silica, and ferrous iron were measured on site using portable spectrophotometers (Hach, Inc.). Dissolved oxygen was measured with an indigo carmine method, nitrate by cadmium reduction, nitrite through diazotization, total ammonia with a salicylate method, total sulfide with methylene blue, dissolved silica by a silicomolybdate method, and ferrous iron via 1,10-phenanthroline. Alkalinity was titrated with sulfuric acid using colorimetric indicators and a Hach digital titrator. Due to the redox-sensitive nature of these species, measurements were performed within a few minutes after sample collection. Water samples were filtered except when filtering would compromise the analysis (e.g., DO and sulfide). Results of the field measurements can be found in Table

10. Sources of uncertainty in the spectrophotometry data stem from the analytical method itself, difficulties of performing such analyses at subfreezing conditions, and possible differences in the way individual researchers perform the measurements during the two field seasons. With these sources of uncertainty in mind, our estimate of error for field spectrophotometry and titrations is $\leq \pm$ 10 %. While this error may be relatively large compared to data produced in a laboratory setting, it is quite low considering the environment in which the analyses were performed, and has little effect on the uncertainties in subsequent thermodynamic calculations.

Table 9. Quick reference description of sampling sites, * denotes pore water/sediment sample.

Sample Number	Site Description
090914A	Primary glacial outwash 20 meters from the edge of the glacier
090914B*	Pore water from 090914A
090914C	East-side outflow
090915E	East-side subglacial flow
090915F	Supraglacial water from the middle of the glacier
090915G	Flowing, but ponded melt water from east portion of glacier
101014A	Primary outwash at glacial edge
101014A*	Pore water from 101014A
101014B	Valley side seep fed by subsurface ice with filamentous algae
101016E	Primary outwash at glacial edge, same spot as 101014A
101016F	Glacial outwash 2.5 miles downstream from site 101014A

Table 10. Field measurements from Robertson Glacier. Spectrophotometric measurements of dissolved oxygen (O_2(aq)), nitrate, nitrite, total sulfide (ΣS^{-2}), total ammonia (ΣNH_3), aqueous silica (SiO_2(aq)) and ferrous iron, are μmolar; (*, porewater/sediment samples; bdl, below detection limit; nd, not determined, usually because of turbidity). Alkalinity by titration is reported in mg/kg as $CaCO_3$.

Sample Number	T (^oC)	pH	Cond (μS)	O_2 (aq) (μmol)	NO_3^- (μmol)	NO_2^- (μmol)	ΣS^{-2} (μmol)	ΣNH_3 (μmol)	SiO_2 (aq) (μmol)	Fe^{+2} (μmol)	Alk
090914A	0.30	8.8	32.5	353.	50.0	1.80	6.05	18.3	88.2	bdl	19.8
090914B*	nd	nd	nd	nd	nd	nd	nd	13.9	nd	bdl	nd
090914C	0.10	8.7	32.0	341.	32.3	8.19	8.05	bdl	76.6	bdl	24.8
090915E	0.10	8.8	31.5	356.	16.1	6.09	3.56	0.6	145.	bdl	24.3
090915F	0.10	8.6	18.7	nd	32.3	9.56	0.44	bdl	68.2	0.18	15.4
090915G	0.10	8.4	50.9	nd	48.4	nd	0.50	12.8	79.9	0.54	40.2
101014A	0.30	8.1	112.	347.	71.4	1.21	0.312	bdl	73.2	0.90	41.0
101014B	2.8	8.2	156.	250.	21.4	0.79	0.218	bdl	574.0	bdl	77.0
101016E	0.30	8.1	101.	334.	50.0	1.93	0.530	bdl	178.0	bdl	40.0
101016F	0.80	8.1	133.	nd	nd	nd	nd	nd	71.6	nd	82.0

4.2.2.2 Laboratory Measurements

4.2.2.2.1 Major Ions from Ion Chromatography:

Samples for analysis of major ions were filtered in the field through a series of 0.2 and 0.8 μm filters (Acrodisc® 32 mm PF Syringe Filter with 0.2/0.8 mm Supor® membrane) and collected (after rinsing the filter with 20 milliliters of sample) in 60 ml polypropylene bottles that were acid washed, cleaned, and oven dried in the lab before sampling. Upon returning to the lab, major cation (Na^{+}, K^{+}, Ca^{+2}, Mg^{+2}) and anion (SO_4^{-2}, Cl^{-}, Br^{-}, F^{-}) concentrations were measured via ion chromatography. Cation analyses used Dionex IonPac CS12A analytical and IonPac SG11 guard columns while anion analyses used Dionex IonPac AS11 analytical and IonPac AG11 guard columns. Data for these analyses can be found in Table 11; analytical uncertainties are on the order of 5%.

4.2.2.2.2 DIC/DOC:

Water samples for dissolved inorganic carbon (DIC) and dissolved organic carbon (DOC) were filtered analogous to those for major ion analyses, with the additional modification of a > 350 mL filter rinse with sample, and collected in 40 ml amber borosilicate vials. DOC vials were acidified with 1 ml of concentrated phosphoric acid and sealed with silicone Teflon-lined septa; DIC vials were sealed with black butyl rubber septa and were not acidified. All sample vials were completely filled to minimize headspace volumes, degassing, and atmospheric contamination. Analyses were performed using an OI Analytical Model 1010 Wet Oxidation TOC Analyzer coupled with a Finnigan Delta Plus IRMS to measure CO_2 concentrations along with $\delta^{13}C$ CO^2 values obtained from reaction of the sample with either phosphoric acid (DIC) or sodium persulfate (DOC; St-Jean, 2003). DIC and DOC results are listed in Table 12

Table 11. Major cation and anion data for Robertson Glacier. Field measurements of temperature and pH from Table 1 are combined with lab measurements by ion chromatography reported in micromolality. (*, porewater/sediment samples; bdl, below detection limit; nd, not determined).

Sample Number	T (^{o}C)	pH	F^{-} (μmolar)	Cl^{-} (μmolar)	SO_4^{-2} (μmolar)	Na^{+} (μmolar)	K^{+} (μmolar)	Mg^{+2} (μmolar)	Ca^{+2} (μmolar)
090914A	0.30	8.8	0.570	5.54	75.1	7.09	4.70	44.14	364.0
090914B*	nd	nd	16.8	24.7	82.1	26.5	11.2	61.51	449.0
090914C	0.10	8.7	3.16	1.44	33.3	bdl	bdl	38.08	357.0
090915E	0.10	8.8	0.46	3.00	22.8	bdl	bdl	30.06	359.0
090915F	0.10	8.6	0.07	1.72	1.25	bdl	bdl	7.62	248.0
090915G	0.10	8.4	8.79	3.17	54.7	4.69	7.11	78.23	540.0
101014A	0.30	8.1	2.47	2.85	571.0	6.56	7.25	284.0	675.0
101014B	2.8	8.2	3.05	4.01	403.0	8.06	15.2	448.0	720.0
101016E	0.30	8.1	2.26	2.40	461.0	4.28	7.08	245.0	595.0
101016F	0.80	8.1	2.37	4.17	531.0	5.54	7.57	439.0	825.0

Table 12. Dissolved gas and carbon data for Robertson Glacier. Field measurements of temperature and pH from Table 1 are combined with lab measurements by EA-IRMS, RCP and GC-FID reported. (bdl, below detection limit; nd, not determined, * refers to porewater/sediment samples).

Sample Number	T (^{o}C)	pH	DIC (ppm)	DOC (ppm)	H_2 (nmolar)	CO (aq) (nmolar)	CH_4 (aq) (nmolar)
090914A	0.30	8.8	5.72	0.40	nd	nd	nd
090914B*	nd	nd	8.76	1.6	nd	nd	nd
090914C	0.10	8.7	6.24	0.29	nd	nd	nd
090915E	0.10	8.8	7.24	0.19	nd	nd	nd
090915F	0.10	8.6	4.86	0.15	nd	nd	nd
090915G	0.10	8.4	10.8	0.35	nd	nd	nd
101014A	0.30	8.1	11.9	0.31	41.6	102.0	10.8
101014A*	0.30	8.1	nd	nd	82.5	217.0	742.0
101014B	2.80	8.2	23.1	off scale	50.3	106.0	8.52
101016E	0.30	8.1	11.9	off scale	nd	nd	nd
101016F	0.80	8.1	21.4	off scale	55.0	127.0	13.7

4.2.2.2.3 Dissolved Gas Collection and Analyses:

Dissolved gas sampling (Table 12) used a battery-powered peristaltic pump to pull water at a slow rate through tubing with very low gas permeability. Before sampling, water is pumped for several minutes to clear out the tubing and to make sure that no bubbles cling to its inner wall. A luer-lok^{TM} fitting at the end of the tube allows connection to a 60 ml syringe via a 3-way stopcock. The syringe is flushed with sample water three times before filling. The positive pressure of the pump is used to fill the syringe through the stopcock to slightly over 50 ml. The tubing is then disconnected leaving the stopcock attached to the syringe. Sample is pushed out of the syringe so that 50 ml of water remains. Separately, but without letting the sample sit for more than a few 10's of seconds, a 10 ml syringe is used to accurately measure and deliver the carrier gas to the 60 ml syringe. The preferred carrier gas is N_2 that has had H_2, CO, CO_2 and

hydrocarbons scrubbed from it. The blanks were analyzed to determine the amounts of trace gases imparted to the sample from all nitrogen canisters used so that actual sample concentrations could be calculated. The 60 ml syringe with 50 ml of sample water and 10 ml of carrier gas is agitated for 60 seconds. A needle is attached to the syringe, about 1 ml of gas pushed through the needle, and then the remaining gas in the syringe is pushed into a gas-impermeable sample bag. One hundred milliliter mylar bags from Calibrated Instruments were used. Sediment/pore water samples involved the collection of 30 ml of sediment/ pore water and addition of 20 ml of 18.2 MΩ cm deionized water to bring the total volume to 50 ml. The rest of the process was analogous to that for a typical water sample and calculations that ensue take into account of the addition of the18.2 MΩ deionized water with respect to the smaller sample of the actual sediment/pore water that was used.

Dissolved gas samples were analyzed at Arizona State University's GEOPIG Laboratory by gas chromatography (GC). For analyses of hydrogen and carbon monoxide a Peak Performer 1 reducing compound photometer (RCP) utilizing mercuric oxide detection (Peak Laboratories, LLC) and a 99.99995% pure N_2 carrier gas. Methane and other light hydrocarbons were analyzed on a GC with a flame ionization detector (Peak Performer 1 FID; Peak Laboratories, LLC), run with the same carrier gas as the RCP and using ultra-high purity H_2 for the FID. Based on comparisons of standards prepared by independent dilutions of analytes both the accuracy and precision are estimated to be ± 2% for the chromatographic analyses (Hoehler et al. 1998). These instruments are extremely sensitive, and have a detection limit of about 500 parts per trillion if 1.00 ml of bulk gas is injected. Hydrogen, methane, and other light hydrocarbons are at high

enough concentrations in the samples to allow replicate 100 µl injections from each 10 ml gas sample.

4.3 Quantification of Energy

The quantification of energy and its availability for microbial communities is crucial to assess the viability of different metabolic strategies, the potential for growth and biomass production, and the overall biogeochemical cycling of elements within systems. In order to do this, a thermodynamic framework that is capable of evaluating factors in the geochemical environment must be adopted. Only reactions that are out of equilibrium will provide energy for microorganisms to utilize for various metabolic processes. As an example, let us consider the metabolic strategy of aerobic hydrogen oxidation (Rxn 1 in Appendix E).

$$2H_2(aq) + O_2(aq) \rightarrow 2H_2O,\ 4\ e^-\ \text{transferred} \qquad \text{Rxn 1}$$

The amount of energy that can be harnessed through catalyzing this reaction (r) corresponds to the chemical affinity (A_r) for the reaction (Helgeson, 1979) which is defined as the change in the overall Gibbs energy ($\Delta_r G$) with respect to the change in reaction progress (ξ_r) and is given by (de Donder, 1927; de Donder and Van Rysselberghe, 1936; Helgeson, 1979; Kondepudi and Prigogine, 1998):

$$A_r = -\left(\frac{\partial \Delta_r G}{\partial \xi}\right)_{P,T} \qquad \text{Eqn 1}$$

where A_r is the affinity, $\partial \Delta_r G$ is the change in Gibbs energy of the reaction, and $\partial \xi$ is the change in reaction progress. The overall Gibbs energy of a reaction will be influenced by both the standard state thermodynamic properties of the reaction itself and that of the

activities of the reactants and products in the geochemical environment of interest. This is reflected in the following expression:

$$\Delta_r G = \Delta_r G^o + RTlnQ_r$$

Eqn 2,

where $\Delta_r G^o$ is the standard Gibbs energy of the reaction, R is the ideal gas constant, T represents the temperature in Kelvin. Q_r is the activity product expressed as:

$$Q_r = \prod_i a_i^{\nu_{i,r}}$$

Eqn 3,

where a_i represents the activity of the *ith* compound in the reaction raised to its stoichiometric coefficient in the r'th reaction, $\nu_{i,r}$, and is positive for products and negative for reactants. Activities for analytes that take part in the reaction are calculated from the molal concentration (m_i) in the geochemical environment of interest using activity coefficients (γ_i) via the following relation:

$$a_i = m_i \gamma_i$$

Eqn 4

The standard Gibbs energy of the reaction is related to the equilibrium constant for the reaction (K_r) in the following way:

$$\Delta_r G^\circ = -RTlnK_r$$

Eqn 5

By combining Eqns 2, 3, and 5 (4 is implicit to and already folded into Eqn 3) the following expression for calculating chemical affinity is attained:

$$A_r = RTln\left(\frac{K_r}{Q_r}\right)$$

Eqn 6

or

$$A_r = 2.303RT(logK_r - logQ_r)$$

Eqn 7

Therefore, in order to quantify the chemical affinity for a particular reaction it is necessary to calculate the standard Gibbs energy of the reaction ($\Delta_r G^o$) from standard state thermodynamic data at the temperature and pressure of interest, ascertain the concentration of each of the reactants and products in the reaction, and determine their activities via the appropriate activity coefficient for each reactant and product in the reaction. For the example of aerobic hydrogen oxidation (Rxn 1):

$$A_r = 2.303RT\left(logK_r - log\left(\frac{a_{H_2O}}{\left(a_{H_2(aq)}\right)^2\left(a_{O_2(aq)}\right)}\right)\right)$$

Eqn 8

or

$$A_r = 2.303RT\left(logK_r - loga_{H_2O} + 2loga_{H_2(aq)} + loga_{O_2(aq)}\right)$$

Eqn 9

In order to compute the expression, it is necessary to have actual measurements from the geochemical environment for the aqueous composition. This will entail measurements of dissolved gases, solutes, and in the case of other reactions, rock and sediment composition as well. The speciation and ionic strength of the aqueous solution also needs to be considered to evaluate the activity coefficients and determine activities for species in the expression. Doing so provides a quantitative assessment of the chemical

affinity of a reaction in a given geochemical environment and allows an evaluation of the energy available for microbial communities to exploit.

The availability of the standard partial molal thermodynamic properties and data for thousands of minerals, gases, organic and inorganic aqueous solutes exist that make it possible to calculate the equilibrium constant for a nearly endless number of reactions across a variety of temperatures and pressures (Amend and Shock, 2001). The thermodynamic data used to perform calculations in this study were taken from Helgeson et al. (1978), Shock et al. (1989; 1997), Shock and McKinnon (1993), and Sverjensky et al. (1997); they are all part of an internally consistent database of thermodynamic properties for use with the SUPCRT92 computer code (Johnson et al., 1992) using the revised Helgeson-Kirkham-Flowers equation of state (Shock et al., 1992, 1997) and are consistent with standard Gibbs energies for metabolic reactions summarized by Amend and Shock (2001). The standard partial molar properties for dissolved nitrous and nitric oxide as well as lepidocrocite, maghemite, and ferrihydrite were derived in a way that is consistent with aforementioned references and can be found in Appendices F and G respectively for nitrogen and iron species. Speciation calculations and the corresponding activities for analytes were computed using the computer software package EQ3/6 (Wolery and Jarek, 2003) using a customized thermodynamic database consistent with the above mentioned references and using the extended Debye-Hückel equation for activity coefficients (Helgeson, 1969).

4.4 Construction of Affinity Maps

One way to present energetic calculations is in the form of affinity maps. Equation 7 can be re-written in terms of a line equation where activities of species in Q_r can be used as the dependent and independent variables.

$$logQ_r = logK_r - \left(\frac{A_r}{2.303RT}\right)$$

Eqn 10

For the example of aerobic hydrogen oxidation (Rxn 1), the following can be derived:

$$loga_{H_2O} - 2loga_{H_2(aq)} - loga_{O_2(aq)} = logK_r - \left(\frac{A_r}{2.303RT}\right)$$

Eqn 11

For pure substances, i.e., minerals and water, activities are unity by definition. Although this is not the case in natural systems, it is convenient to make this assumption because it reduces the number of variables, and thus, the number of dimensions necessary to view the results. Therefore Eqn 11 further reduces to:

$$-2loga_{H_2(aq)} - loga_{O_2(aq)} = logK_r - \left(\frac{A_r}{2.303RT}\right)$$

Eqn 12

Rearranging Eqn 12 so that dissolved oxygen is the independent variable and dissolved hydrogen is the dependent variable yields:

$$loga_{H_2(aq)} = -(1/2)logK_r + \left((1/2)\frac{A_r}{2.303RT}\right) - (1/2)loga_{O_2(aq)}$$

Eqn 13

By picking suitable values for the affinity of the reaction, contours can be made in activity space to represent the available energy with respect to the measured geochemical

data (Figure22, upper left). In order to compare the energetics between vastly different reactions, values of affinity are reported in kcal per mole of electrons transferred in the reaction. This convention was adopted by McCollom and Shock (1997) and subsequently by many others (Amend and Shock, 1998, 2001; Shock et al., 2000, 2005, Amend et al., 2003; Shock and Holland, 2004; Meyer-Dombard et al., 2005; Windman et al., 2007; Smith and Shock, 2007; Shock, 2009; and others)

Affinity maps were constructed using activities calculated by the geochemical modeling software eq3nr and data from Table 13 (a compendium of data for the sites examined in this work). All the affinity maps presented here are isothermal with calculations performed at 0.3 ^{o}C. If a reaction is pH sensitive, two sets of contours were made to provide context for the effects, one at a pH=6 (dashed lines) and one at pH=8 (solid lines). The two sets of pH contours were crafted so that all lines are equa-distant from each other. Because of this, the two sets contours can be used to evaluate the available energy at virtually any pH. The energetic unit is kcal per mol e^- transferred. If the activity of an analyte was not available, a range of plausible activities was used to constrain the available energy in affinity space.

Table 13. Typical Robertson Glacier (RG) outwash water and pore water chemistry compared to that of bottom seawater (BSW) and Lake Vida Brine (LVB). All values are reported in μmol l^{-1} unless otherwise specified.

Parameter	RG water	RG pore water	BSW	LVB
T (^{o}C)	0.300	-	2.00	-13.4
pH	8.4	-	7.8	6.2
O_2 (aq)	350.0	-	100.0	bdl
N_2 (aq)	627.0[a]	-	590.0	-
N_2O (aq)	-	-	-	58.8
NO_3^-	60.7	7.60	30.0	904.
NO_2^-	1.51	-	< 0.01	23.7
ΣS^{-2}	3.18	-	< 0.3	bdl
ΣNH_3	18.3	13.9	0.3	3885.2
SiO_2 (aq)	80.71	-	160	-
Fe^{+2}	0.90	-	0.001[b]	307.9[b]
F^-	1.52	16.8	68	1500
Cl^-	4.20	24.7	546000	3318000
SO_4^{-2}	323.0	82.1	27900	58400
Na^+	6.83	26.5	464000	1914000
K^+	5.97	11.2	9800	82800
Mg^{+2}	164.0	61.5	52700	664900
Ca^{+2}	520.0	449.0	10200	30100
DIC	735.	729.0	~2000	61200
DOC	30.0	133.0	308	48200
ΣCO_2	-	-	2300[c]	8860[d]
H_2 (aq) (nmol)	41.6	82.5	0.4	10470
CO (aq) (nmol)	102.	217.0	0.2	bdl
CH_4 (aq) (nmol)	10.8	742.0	0.3	<1000

Bottom seawater values taken from McCollom (2007), Shock and Canovas (2010), Wheat et al. (2010), Cowen et al. (2003), Wei et al (2005), Edwards et al. (2005), Simoneit and Sparrow (2002), Canyon et al. (1999), Tsunogai et al. (2005), Rogers and Schulte (2012), Lake Vida Brine composition taken from Murray et al 2012 and its supporting information. [a] calculated assuming equilibrium with the atmosphere, [b] total iron, [c] CO_3^{-2} + HCO_3^- + CO_2 (aq), [d] CO_2 (aq).

4.5. Summary of Constraints on Analyte Concentrations and Activities Based on Locale and Analyte Used for Calculations and Affinity Maps

For some analytes (i.e., thiosulfate) there is no measured data available in these systems. In order to investigate the viability of a metabolic strategy in these cases a range of log activities is considered. These ranges are intended to provide reasonable upper and lower bounds on analyte activities. Many analytes never reach levels as high as millimolal and below picomolal levels scarcity can limit microbial uptake. However, most reactions can be constrained by comparing of available data from similar or adjacent systems. Examples of how this was done for analytes lacking data in each system follow and are the basis for how calculations were performed and affinity maps constructed.

4.5.1 Robertson Glacier Water (RGW)

We lack data for dissolved nitrogen, nitric oxide, nitrous oxide, and thiosulfate in RGW samples. The dissolved nitrogen was calculated by assuming equilibrium between the water and the atmosphere. Nitric oxide, nitrous oxide, and thiosulfate were given activity ranges of -6.0 to -12.0 for use in affinity plots and subsequent calculations. Attention should be given to affinities involving dissolved oxygen (DO) in the system, since measurements could only be obtained at the outflow. Further underneath the glacier the environment is most likely anoxic (see Fig. 21 cross section). Measurements of DO from RGW indicate DO present in the outwash at the toe of the glacier. It is likely this DO derives from atmospheric interaction via cracks and fissures that provide a delivery mechanism for dissolved oxygen to regions partially underneath the glacier.

4.5.2. Robertson Glacier Pore Water (RGPW)

RGPW lacks data for pH, DO, dissolved nitrogen, nitrite, sulfide, iron, nitric oxide, nitrous oxide, and thiosulfate. The lack of pH data is not essential for the construction of the affinity plots because they assume fixed pH values. As for missing analytes described above, in some cases boundaries for these concentrations can be established using data from RGW. For instance, the maximum DO corresponds to RGW because this water will be the source for oxygen diffusing into the pore water; while the minimum has been set to a log activity of -12.0. A similar arguement can be made for sulfide and iron where the source for RGW is diffusion from the RGPW; therefore, the concentrations of iron and sulfide in RGW can serve as a minimum value for RGPW. For instance, despite a lack of iron data for RGPW, realistic constraints can be applied by utilizing the data from RGW. The source of iron for RGW is most likely from pyrite dissolution and/or pyrite oxidation (Mitchell et al., 2013); therefore, it is appropriate that the minimum iron concentration for RGPW be set equal to that of RGW in order to calculate the associated activity. The maximum log activity of iron for RGPW may be as high as -3.0; this is indicated in affinity plots with arrows showing the direction symbols might move in affinity space. A similar approach was taken to examine reactions involving sulfide in RGPW, because the source and distribution of sulfide is analogous to that of iron. The maximum log activity of sulfide was set to -3.0. Dissolved nitrogen was assumed to be in equilibrium with the atmosphere; although, the actual dissolved nitrogen in the system could be lower or higher depending on microbial activities and other geochemical processes. Therefore, arrows have been added to the affinity plots to

indicate this. Nitrite was approximated by using the value obtained from RGW, and thiosulfate was given a range of log activities from -6.0 to -12.0.

4.5.3. Lake Vida Brine (LVB)

Data for dissolved nitrogen, ferrous iron and thiosulfate are absent for LVB. Concentrations of DO and sulfide, and CO were below the detection limit. Total iron data is available and its corresponding activity is used as the maximum amount for calculations involving ferrous iron. Dissolved nitrogen was assumed to be in equilibrium with the atmosphere. Dissolved nitrogen was assumed to be in equilibrium with the atmosphere; although, the actual dissolved nitrogen in the system could be lower or higher depending on microbial activities and other geochemical processes. Therefore, arrows have been added to the affinity plots to indicate this. Dissolved oxygen, sulfide, thiosulfate, and nitric oxide, were given a range of log activities from -6.0 to -12.0. Dissolved carbon monoxide was given a log activity range of -4.44 (to correspond to the 1 mg L^{-1} detection limit of Murray et al., 2012 and supplemental materials) to -12.0.

4.5.4. Bottom Seawater (BSW)

Bottom seawater lacks robust data for thiosulfate, dissolved nitric oxide and dissolved nitrous oxide; therefore, log activity ranges of -6.0 to -12.0 were used for calculations involving these species. Data for nitrite was also variable with many values being less than 10 nmol kg^{-1}. For this reason, the value was set to a conservative log activity of -9.0.

4.5.5. A Note on Solids for Various Calculations

At times, it can be beneficial to examine the amount of energy available per unit volume of fluid; this is easily done by calculating the affinity for a reaction in terms of

the limiting reagent and multiplying by the total amount of that reactant in aliquot chosen. Investigating a system in terms of energy available per unit volume of fluid can provide information about the potential for biomass production, turnover rate, etc. However, in order to perform bioenergetics calculations in terms of energy per unit volume of fluid, limits on the concentrations of solids need to be set. For example, elemental sulfur is not likely to be present in any of these systems. However numerical values are still needed for affinity calculations to be performed; therefore, the concentration was set to 10^{-24} mol for all systems. Fayalite and ferrosilite are also not expected to be present in these systems and would have the same concentration applied to them as that of elemental sulfur.

Investigations of iron oxyhydroxides in the form of colloidal and nanoparticules in (sub)glacial systems similar to LVB, RGPW, and RGW (Bhatia et al., 2013; Death et al., 2014; Hawkings et al., 2014) had a range of concentrations between 3 and 322 micromols L^{-1}. Therefore, we use the same range for iron oxyhydroxides in the form of colloidal and nanoparticules in calculations of affinity per unit volume fluid involving goethite, hematite, magnetite, lepidocrocite, maghemite, and ferrihydrite. Iron oxyhydroxides in the form of colloidal and nanoparticulates in BSW are very low and often times have concentrations that center around 0.4 nanomols L^{-1} (Bruland and Lohan, 2004; Rue and Bruland, 1995; Rickard and Luther, 2007); therefore, this value has applied to calculations of affinity per unit volume fluid involving goethite, hematite, magnetite, lepidocrocite, maghemite, and ferrihydrite. Pyrite is an abundant mineral at LVB, RGPW, and RGW; therefore, it should not be a limiting reagent in calculations of affinity per unit volume fluid. Instead, another reactant involved in the reaction was used

as the limiting reagent. Pyrite has such a low abundance in BSW that it is usually undetectable (Rickard and Luther, 2007); therefore, the concentration used in this work is the same as that adopted for elemental sulfur, fayalite, and ferrosilite.

4.6 Minimum Energy Constraints

The minimum energy microorganismsrequire to subsist has been a topic of interest for quite some time and can provide information on the limits of life, turnover of cells, biomass production, etc. (Thauer et al., 1977; Lancaster, 1989; Thauer, 1990; Muller et al., 1993; Hoehler et al., 1998; Schafer et al., 1999; Hoehler et al., 2001; Schink and Thauer, 1988; Schink, 1997; Curtis, 2003; Hoehler, 2004; LaRowe et al., 2012; Hoehler and Jorgensen, 2013; LaRowe and Amend, 2015a,b, 2016; and others) . However, minimum energy is difficult to assess; it is much more complex than simply having positive affinity for a reaction utilized as a microbial metabolic strategy. Threshold levels of energy exist and have been explored in many models for microbial systems (Schink and Thauer, 1988; Schink, 1997; Curtis, 2003; Hoehler, 2004; LaRowe et al., 2012; LaRowe and Amend, 2015a,b, 2016 and others). The minimum thresholds for the energy yield of reactions can be dependent on the organism, growth phase, temperature, pH, environment, etc (Hoehler and Jorgensen 2013). For example, thermodynamic analyses indicate the theoretical minimum biosynthetic cost in reducing environments is 13 times lower than in oxic environments (McCollom and Amend, 2005). Most investigations to determine minimum energy are done in laboratory experiments utilizing nutrient-rich cultures, and do not reflect what may be happening in low energy environments where extant microbial communities subsist on energy fluxes as much as 1000 times lower (Hoehler and Jorgensen, 2013). Field and laboratory

experiments have yielded a minimum energy range from 0.9 – 11.9 kcal per reaction turnover (Hoehler et al., 2001, Hoehler, 2004; Schink, 1997; Curtis, 2003). To put this in perspective, in the context of the affinity maps presented in this work (i.e., kcal per mol e^- transferred), we take as an example the apparent minimum energy requirements of methanogenic Archaea and sulfate-reducing bacteria in Hoehler et al. (2001). Hoehler et al. (2001) indicate the minimum energy requirements are ~2.53 kcal per reaction turnover for methanogenesis and 4.57 kcal per reaction turnover for sulfate-reducing bacteria. Dividing these quantities by the number of electrons transferred in the reaction (in this case 8 e^- for both reactions) puts this in terms of per mol e^- transferred. The minimum energy levels for methanogenesis and sulfate reducation are 0.32 and 0.57 kcal per mol e^- transferred, respectively.

4.7. Bioenergetics in the Cold Biosphere

The affinities for 1460 reactions (Appendix E) were evaluated for the four model systems in this work. Of these, several sets of reactions were evaluated using affinity maps to explore the energetic landscape (Figures 22-24 & 26-30). Another set of reactions were put in the form of ranked reaction lists (in affinity in cal ml^{-1}) from each of the four model systems (Figures 31-41). The energetics depicted in the affinity maps range from always having positive affinities regardless of the analyte activities to always having negative affinities and all ranges in between.

4.7.1. Affinity Maps for Aerobic Reations

Oxygen is one of the strongest oxidants in the natural environment and reactions that use it are often highly energetic. The aerobic oxidation of dissolved hydrogen and carbon monoxide, top panels of Fig. 22, are some of the most energetic reactions in the

suites of aerobic reactions. Both reactions are independent of pH, and have the potential to provide more than enough energy for growth and maintenance of microbial populations. Lack of data for dissolved oxygen at LVB and RGPW mean we must assume a range of energies is possible; the ranges are indicated by the dashed horizontal lines. The dissolved oxygen activity for RGW will decrease at greater distances underneath the glacier. This is demonstrated with an arrow indicating the direction the reaction would be driven as the activity of dissolved oxygen decreases. Affinity plots for the aerobic oxidation of dissolved hydrogen and carbon monoxide indicate that even activities of dissolved oxygen corresponding to picomolar concentrations only decrease the affinity by ~2 kcal per mole e^- transferred. In neither case should this affect the microbe's ability to capitalize metabolically on this reaction. The only factor that could stop them would be if the concentrations were so low, that scarcity directly limited uptake of the reactants. The oxidation of carbon monoxide in LVB has the added complication that neither the dissolved carbon monoxide nor dissolved oxygen concentrations are known. In this instance, a shaded box indicates the most probable range of energy that could be exploited by this reaction. Moving diagonally from the bottom right to the top left a maximum change of ~ -6 kcal per mole e^- occurs, but considering how energetic the reaction is, ~ -6 kcal per mole e^- should not affect microorganisms trying to perform the type of metabolism.

Figures 22C&D display oxidation routes for ammonium. They are pH dependent and the affinity for both increases by ~ 0.5 kcal per mole e^- transferred for each unit pH. Both reactions are still quite energetic as is that of nitrite oxidation to nitrate (Fig. 22E), which is not pH dependent. These three reactions also have the potential to be

metabolically viable in each of the four model systems as long as the reactants involved have concentrations high enough that uptake is not impeded. In contrast to the previous reactions, the oxidation of dissolved nitrous oxide to dissolved nitric oxide (Fig. 22F) is energetically very unfavorable. Only at the highest dissolved oxygen activities and the lowest ratios of dissolved nitrous to nitric oxide is the affinity positive. At best, the reaction is feeble, and in most cases across the natural environments investigated here, microorganisms performing this particular reaction would need to couple it to a more energetically favorable reaction for it proceed.

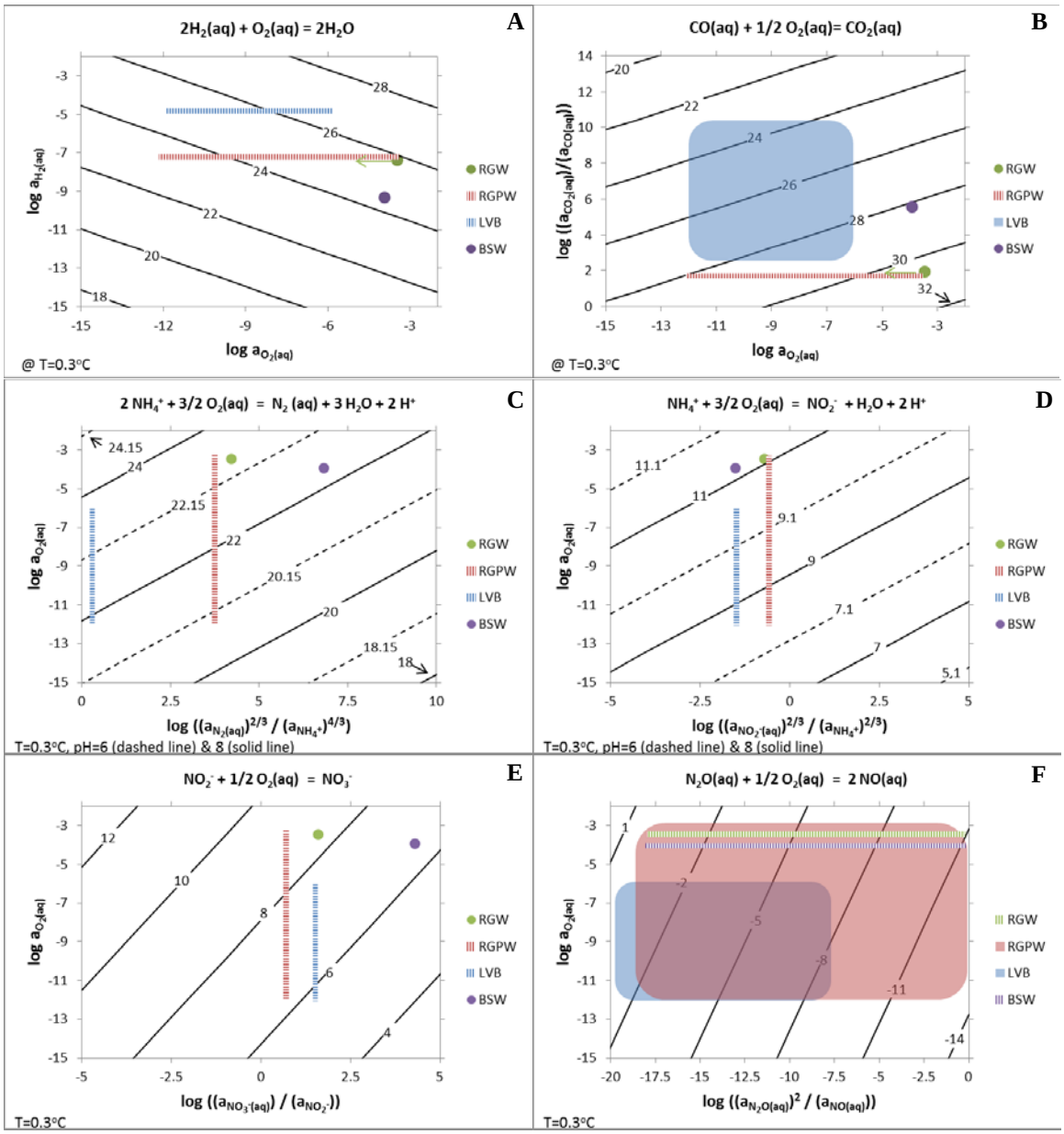

Figure22. Affinity maps depicting energetic landscape for selected aerobic reactions. All contours are in kcal per mole e^- transferred. Panel **A** depicts oxidation of dissolved hydrogen, **B** depicts oxidation of dissolved carbon monoxide, **C** ammonium oxidation to dissolved nitrogen, **D** oxidation of ammonium to nitrite, **E** oxidation of nitrite to nitrate, and, **F** oxidation of dissolved nitrous oxide to dissolved nitric oxide. Dashed lines and shaded boxes indicate the range of affinities possible for sites when analyte concntrations were not known. Except for the oxidation of dissolved nitrous oxide to nitric oxide all of the reactions depicted are quite energetic. Even given the range of energies corresponding to when analyte activities are not known, the energy available should be more than that necessary for microbial growth and maintenance. The affinity for ammonium oxidation to dissolved nitrogen and nitrite is pH dependent and as pH increases the affinity for the reaction increases by nearly 0.5 kcal per mole e^- per unit pH.

Figure 23 depicts aerobic reactions involving sulfur and iron species and in most cases, the affinities rival that of hydrogen oxidation. Figures 23A&B depict the oxidation of sulfide to sulfate and thiosulfate, respectively. Both are pH dependent and each unit increase in pH corresponds to an ~ 0.25 kcal per mole e^- increase in energy from the reaction. Due to the lack of analytical data for dissolved hydrogen sulfide, oxygen, and thiosulfate fields of possible affinity are depicted for LVB and RGPW. Despite the lack of data for thiosulfate in each system, it is apparent that ample energy is available from reactions involving it in the aerobic reactions examined here. Figures 23C&D depict the energetics of pyrite oxidation, which in these systems is speculated to be an important process, but probably utilizes oxidized nitrogen species as the major electron acceptor (Mitchell et al., 2013). Due to this, reactions pertaining to the use of nitrogen species as an electron acceptor are addressed in a later section. Although BSW has the highest affinity for aerobic pyrite oxidation it should be noted that the majority of bottom seawater is not be in contact with pyrite, a necessary condition for this process to proceed. Areas where pyrite deposition has previously occurred, such as off axis oceanic crust that previously experienced hydrothermal alteration or floc from hydrothermal vents that has settled on the cold ocean floor, would be some of the only places where this reaction is expected to occur. It could also occur occur if sediments where pyrite has previously formed are later exposed to BSW. While RGW, RGPW, and LVB all probably have plenty of reduced iron and sulfur species to donate electrons, the low abundance of dissolved oxygen in these systems likely diminishes the viability of aerobic oxidation of pyrite as a key process. The oxidation of thiosulfate to sulfate suffers from a similar set of circumstances as the previous two reactions discussed where the lack of

information on the abundance of thiosulfate is a major constraint for the evaluation of the reaction affinity. The last three reactions concerning the aerobic oxidation of ferrous iron to ferrihydrite, goethite, and hematite are limited in BSW by the lack of dissolved iron in the ocean while in RGW, RGPW, and LVB it will be the lack of dissolved oxygen in the system that modulates the energy available to microorganisms.

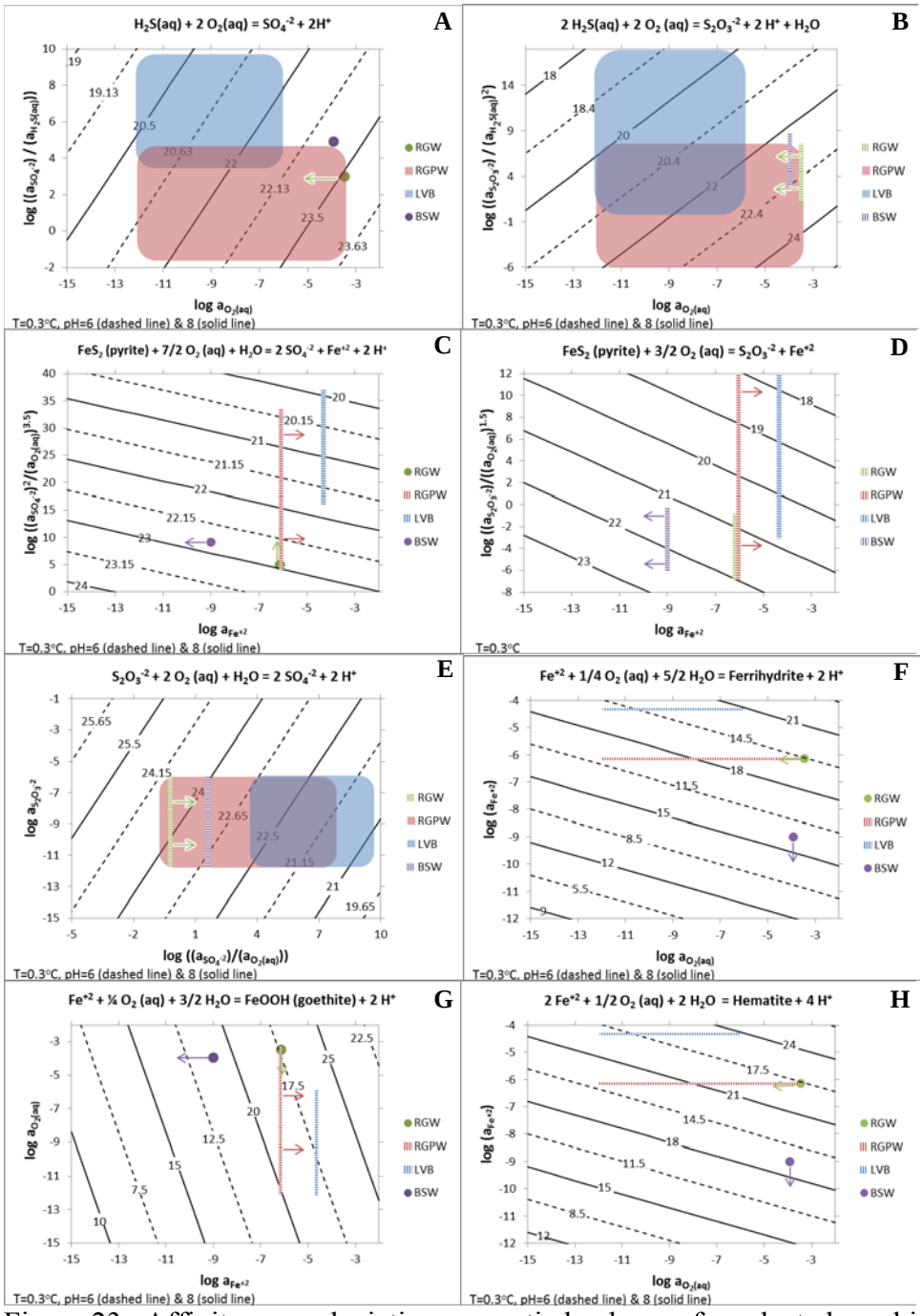

Figure 23. Affinity maps depicting energetic landscape for selected aerobic reactions. Panel **A** depicts the oxidation of sulfide to sulfate, **B** depicts the oxidatioin of sulfide to thiosulfate, **C** depicts the oxidation of pyrite to sulfate and ferrous iron, **D** depicts the oxidation ooof pyrite to thiosulfate and ferrous iron, **E** depicts the oxidation of thiosulfate to sulfate, and panels **F**, **G**, and **H** depict the oxidation of ferrous iron to ferrihydrite, goethite, and hematite respectively. Dashed lines and shaded boxes indicate the range of affinities possible for sites when analyte concntrations were not known. Arrows indicate the direction the reaction is most likely driven based on the analytical constraints

previously discussed in the text. Aerobic oxidation of sulfur and iron species is associated with high affinities, but will be constrained by the amount of oxygen as an electron acceptor in RGW, RGPW, and LVB while in BSW it will be the availability of iron and/or sulfur species constraining the affinity for the reactions.

4.7.2. Affinity Maps for Methane Cycling

Hydrogenotrophic methanogenesis, Figs. 24A&B, (whether utilizing dissolved carbon monoxide or carbon dioxide) yields low affinities relative to all methanotrophic reactions except those using sulfate as an electron acceptor. This means it is not predicted that it would be one of the more prevelant microbial strategies at those sites. Calculations using dissolved carbon dioxide typically yield affinities ~ 1 kcal per mole e^- transferred greater than those using dissolved carbon monoxide. This may be due to the relatively low concentrations of dissolved carbon monoxide in these systems compared to carbon dioxide. Meaning, there is not as much of a thermodynamic drive for the use of carbon monoxide. Affinities for methanogenesis are quite low for all sites, indicating this particular reaction has already been driven towards equilibrium, most likely by microorganisms utilizing these metabolic strategies. Deeper in the RGPW, and further beneath the glacier for RGW, it would be expected that there is a greater thermodynamic drive for methanogenesis to occur because microbes have not yet exploited this reaction and driven its affinity toward zero. BSW has the lowest affinity for methanogenesis due to the low activity of dissolved hydrogen, while LVB has the highest due to higher activities of both reactants.

Affinities for aerobic methanotrophy (Fig. 24C) are some of the highest values of all reactions and are the only methanotrophic reaction that is not dependent on pH. Even at very low oxygen conditions, this reaction has positive affinities for all sites investigated, making it what some would classify as a low-yield but efficient process given the activities of reactants at these sample locales. Conversely, anaerobic oxidation of methane (AOM) coupled to sulfate reduction (Fig. 24D) has very low affinities at all

sites and would be considered a high-yield but inefficient metabolism (Boettger et al., 2013). Part of the reason for this type of classification is due to the inefficiency of AOM (Jørgensen et al., 2001) and low energy yield; others have reported values of ~ 25 kJ per mol methane oxidized (Valentine and Reeburgh, 2000). This equates to about 0.75 kcal per mol e^- transferred and is in the range of the four sites examined in this study. Despite the low affinity, AOM is presumed to be the major sink for methane in sediments and responsible for the removal of ~80% of methane released from ocean sediments (Reeburgh, 2007; Geprägs et al., 2016; Hatzenpichler et al., 2016). Anaerobic oxidation of methane typically works through a syntrophic consortium of sulfate reducing bacteria and methanotrophic archaea that mediate the process (Hinrichs et al., 1999; Boetius et al., 2000; Orphan et al., 2001a, b,; Michaelis et al., 2002; Joye et al., 2004).

AOM coupled to nitrate and nitrite (Figs. 24E&F) is a very energetic process at the sites evaluated. Affinities for these reactions are as high or higher than that of aerobic methanotrophy. Nitrate reduction coupled to AOM (Deutzmann and Schink, 2011; Haroon et al., 2013; Segarra et al., 2013; á Norði and Thamdrup, 2014) has been shown to be a viable metabolism for microorganisms across a variety of environments. In the cold biosphere AOM coupled to nitrate or nitrite could be an important process linking the nitrogen and carbon cycles. Especially true in cold anoxic sediments at the seafloor as well as in other anaerobic settings such as LVB and the basal waters beneath glacial outflows where oxygen would be limiting as an electron acceptor. The use of nitrate as an electron acceptor for AOM is pH dependent and corresponds to a ~0.25 kcal per mole e^- increase in energy per unit pH decrease in environment. This, along with the greater dissolved methane and nitrate concentrations in LVB, cause it to have greater energy

available than at RGW, RGPW, and BSW. The low concentration of dissolved methane and relatively low concentration of nitrate in BSW is responsible for it have the lowest amount of energy available from AOM coupled to nitrate reduction. Arrows on the figures indicate there is an uncertainty in the amount of energy available from this process due to the estimation of the dissolved nitrogen at LVB, RGW, and RGPW. Nitrite reduction coupled to AOM provides ~3.5 kcal per mole e^- more energy in each environment than nitrate reduction coupled to AOM. Nitrite reduction coupled to AOM is also a pH dependent process with each unit decrease in pH corresponding to an increase of ~0.8 kcal per mole e^-. The relative differences in energy for nitrate reduction coupled to AOM are approximately the same as nitrate reduction coupled to AOM across the sites compared here for the same reasons discussed for the energy patterns displayed for nitrate coupled to AOM.

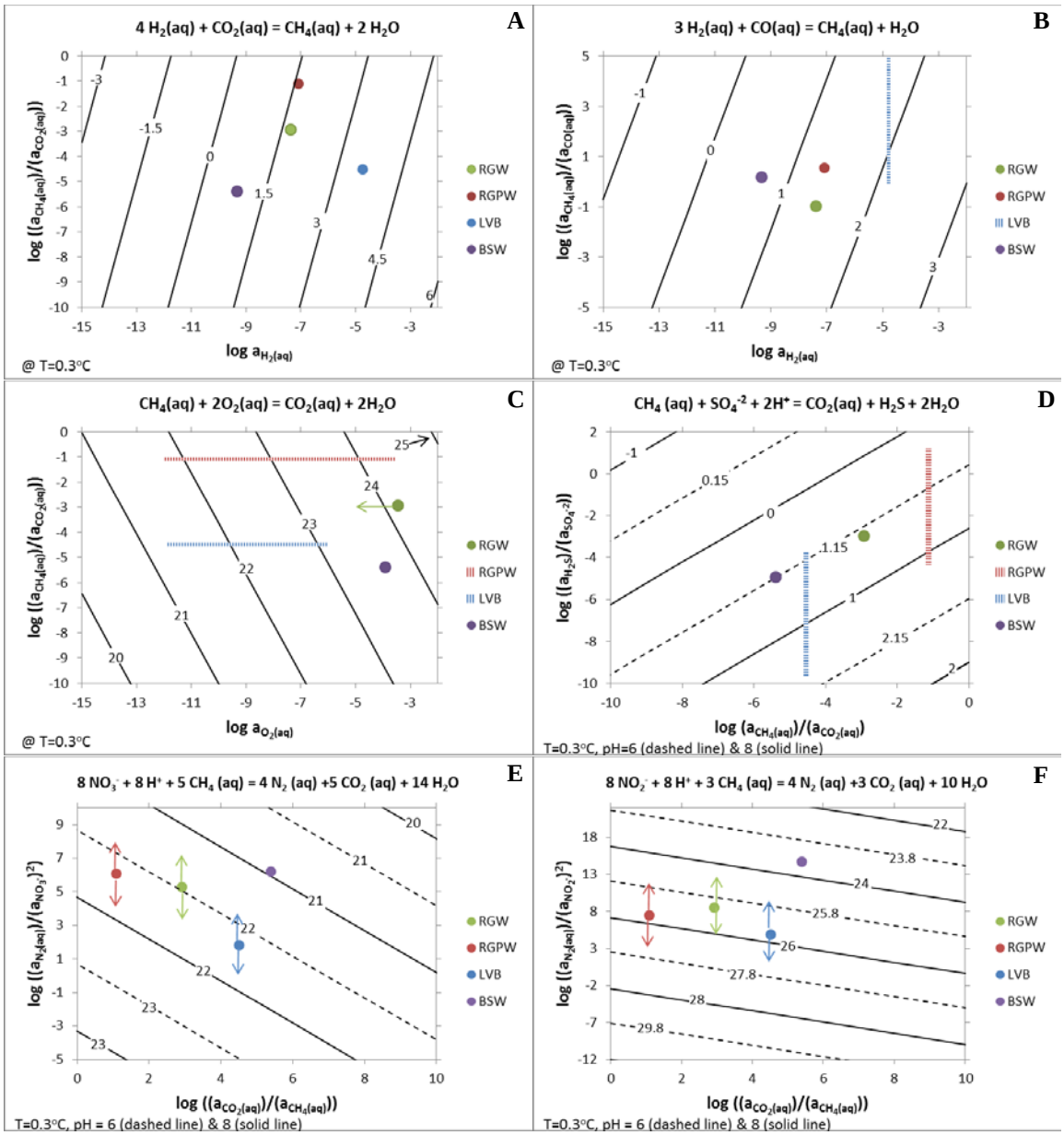

Figure 24. Affinity maps depicting energetic landscape for selected reactions in methane cycling. Figure 24A depicts hydrogenotrophic methanogenesis using dissolved carbon dioxide, 24B depicts hydrogenotrophic methanogenesis using dissolved carbon monoxide, 24C depicts aerobic methanotrophy, 24D depicts anaerobic oxidation of methane (AOM) using sulfate, 24E depicts AOM using nitrate, and 24F depicts AOM using nitrite. Dashed lines indicate the range of affinities possible for sites when analyte concntrations were not known. Arrows indicate the direction the reaction is most likely driven based on the analytical constraints previously discussed in the text. Methanogenesis using either dissolved carbon dioxide or monoxide has the lowest affinity other than that of AOM coupled to sulfate reduction. The reason for this in the case of dissolved carbon dioxide is likely that the microorganisms in these environments have already utilized the majority of the energy for this reaction and driven it further

towards equilibrium. In the case of using dissolved carbon monoxide this is likely due to the low concentration of the analyte in these environments meaning there is not as much thermodynamic drive for the process. Methanotrophy using dissolved oxygen, nitrate, and nitrite are usually very energetic, whereas that utilizing sulfate is traditionally a lower energetic process regardless of whichever environment it has been evaluated in.

4.7.3. Affinity Maps for Nitrogen Cycling

Fixed nitrogen is a limiting reagent in the ocean (Codispoti et al., 2001); there is also evidence for nitrogen limitation at RG (Boyd et al., 2011) making the cycling of nitrogen within the cold biosphere an important process and the energetics behind it essential to understand. Figure 25 displays a asic nitrogen cycle schematic linking the reactions in the nitrogen cycle to reactions in Appendix E. Figures 26 and 27 depict the energetics of the processes listed in Figure 25. Figure 26A depicts the first step of denitrification; nitrate reduction to nitrite. In all environments evaluated, this process is highly energetic with BSW, RGW, and RGPW having very similar affinities for the process and LVB being ~1 kcal per mol e^- greater. As represented by the reaction (# 45 in Appendix E) evaluated at these spots, the affinity per mol e^- is very similar; however, BSW most likely has fewer occurrences for the process due to the low concentrations of dissolved hydrogen, which would limit microbial ability to fulfill the reaction as written. Figure 26B depicts the overall process of denitrification and is quite energetic in all environments evaluated. RGW and RGPW have very similar affinity values (i.e. ~23 kcal per mol e^- transferred), LVB has an affinity ~10% higher (~2.5 kcal per mol e^-) than that of RGW or RGPW. BSW has the lowest affinity at ~ 22 kcal per mol e^- due to the low concentration of dissolved hydrogen available for the reaction to proceed. Similar to other affinity plots, arrows are included on the symbols for the different sites to indicate there could be a change in the affinity due to the uncertainty in the activity of dissolved nitrogen. The reaction in Fig. 26B is pH dependent and for every unit increase in pH the affinity decreases by ~0.25 kcal per mol e^-.

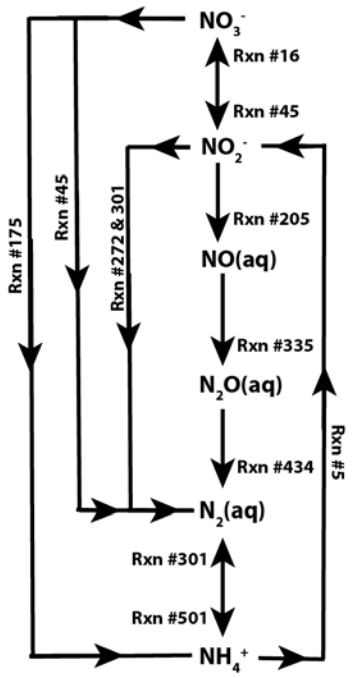

Figure 25. Generalized schematic depicting nitrogen cycling in natural systems and the corresponding reaction number representing transformations between related species (after Amend and Shock, 2001).

The affinity map for the reduction of nitrate (N with +5 valence) to ammonium (N with -3 valence), Fig. 26C, is an important reaction that has been studied in cold marine sediments for quite some time (Sørensen, 1978). The arrangement of the affinities for the different sites is similar to the previous two affinity maps described for the same reasons. The reaction is also pH dependent and has the same characteristics as the last reaction described. For those previously mentioned reasons, the actual affinity for LVB (~17.5 kcal per mol e^- transferred) to be slightly higher than that of RGW, RGPW, and BSW which all have affinities close to ~15 kcal per mol e^- transferred. Figure 26D depicts the last stage of nitrification, the oxidation of nitrite to nitrate. Since the concentration of dissolved oxygen (and therefore the activity of dissolved oxygen) is not known for RGPW or LVB a range of probable affinity is given as a hashed line. This gives a range

of ~ 9 to slightly more than ~6 kcal per mol e^- transferred for RGPW and a range of ~ 8 to slightly less than ~6 kcal per mol e^- transferred for LVB. Overall, the process has the lowest affinity of all maps in Fig. 26. Figure 26E depicts the reduction of nitrite to dissolved nitric oxide; a range needed to be used for each site because there were no reliable dissolved nitric oxide values available. The reaction reduction of nitrate to dissolved nitric oxide is pH dependent and there is an increase of ~1.25 kcal per mol e^- transferred for every log unit decrease in pH. BSW has the lowest affinity range due to the lack of hydrogen in the environment. Marine sediments, which also account for a large part of the cold biosphere, could have substantially higher concentrations of dissolved hydrogen, and therefore, higher affinities. RGW and RGPW have very similar affinity ranges (~12.5 to 20 kcal per mol e^- transferred) while LVB has affinities that range from ~17.5 to ~25 kcal per mol e^- transferred, making it the most energetic environment investigated in this study. Figure 26F depicts the energetics associated with the reduction of nitrite to dissolved nitrogen and has the highest affinity of all affinity maps in Fig. 26. This pH dependent reaction has an increase of ~0.75 kcal per mol e^- transferred for every log unit decrease in pH. BSW has the lowest affinity associated with this reaction while that of RGW and RGPW have affinity values that are very close to each other and fall in between that of BSW and LVB which has the highest affinity associated with the reaction. Like many of the reactions previously investigated that use dissolved hydrogen as an electron donor, the ranked energy order follows suit with the site with the lowest concentration having the lowest affinity and the site with the highest concentration having the highest affinity.

Figure 27 displays another set of affinity maps involving nitrogen cycling. All affinities for sites in Fig. 27 are positive, though some are quite low. Figure 27A has a range of values for each site due to the uncertainty of dissolved nitric oxide for all sites and dissolved nitrous oxide for all sites except LVB. The affinity ranges for BSW, RGW, and RGPW span from ~25 to ~37 kcal per mol e^- transferred; the range for LVB is narrower, ~27 to slightly less than 34 kcal per mol e^- transferred. In this case, LVB has the lowest affinity range due to its high dissolved nitrous oxide concentration; high dissolved nitrous oxide concentrations cause the activity product to be lower than that of the other three sites. Thus, BSW, GRW, and RGPW have the potential for higher affinity values despite their lower dissolved hydrogen concentrations relative to LVB. This is the opposite of what is depicted in the affinity map in the upper right of Fig. 27, which depicts the reduction of dissolved nitrous oxide to dissolved nitrogen. The high concentrations of both dissolved hydrogen and nitrous oxide give LVB a greater thermodynamic drive for this reaction to proceed in the forward direction resulting in an affinity of over 39 kcal per mol e^- transferred. Conversely, BSW has the lowest affinity range of all sites (~31 to ~35 kcal per mol e^- transferred) due to low concentrations of dissolved hydrogen and nitrous oxide. RGW and RGPW have similar affinity values and ranges but the increased activity of dissolved hydrogen at RGPW gives it an energetic advantage over RGW of slightly more than one kcal per mol e^- transferred.

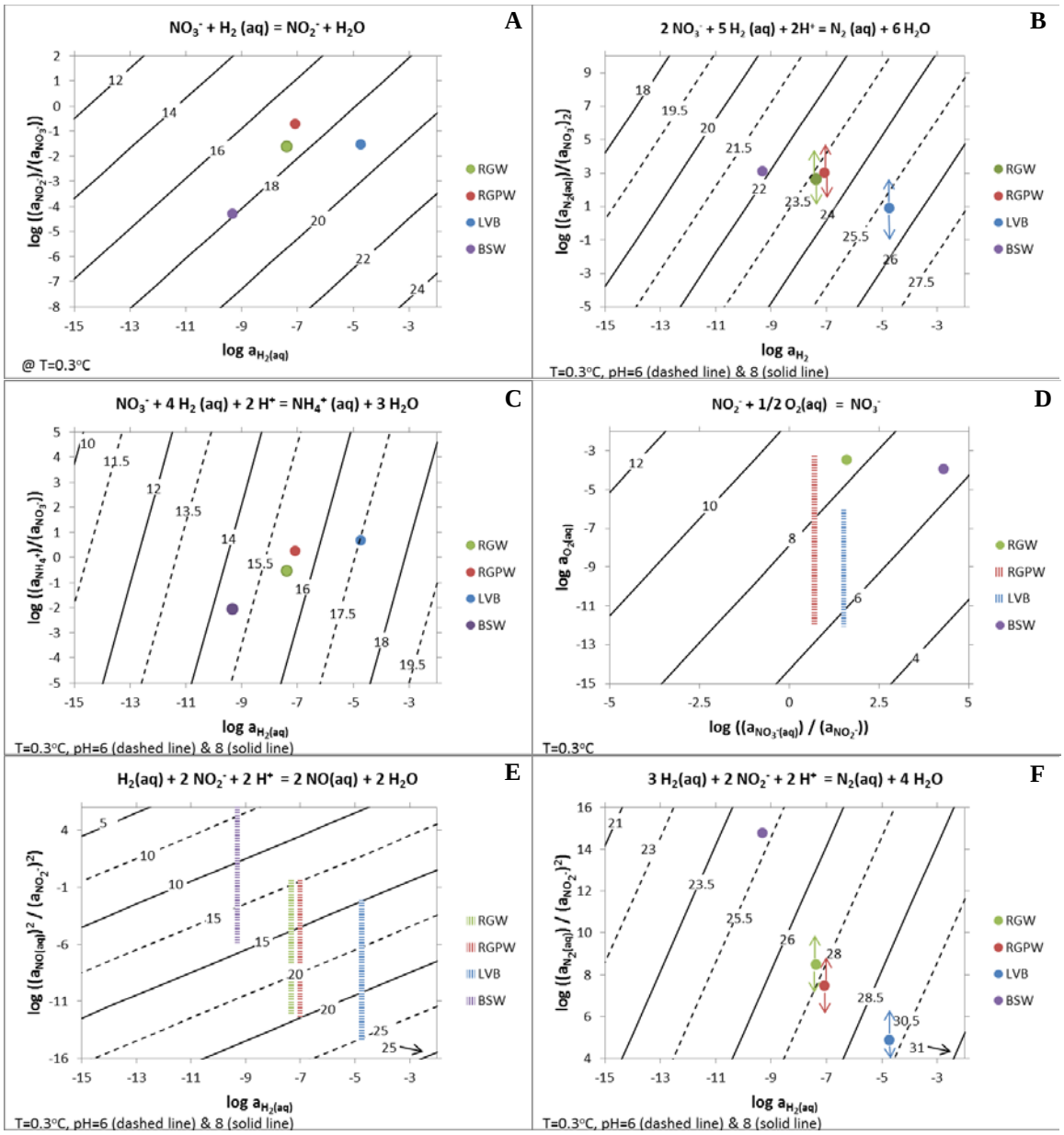

Figure 26. Affinity maps depicting energetic landscapes for reactions involved in nitrogen cycling. Figure 26A depicts the reduction of nitrate to nitrite using dissolved hydrogen, **B** depicts the reduction of nitrate to dissolved nitrogen using hydrogen, **C** depicts the reduction of nitrate to ammonium using dissolved hydrogen, **D** depicts the oxidation of nitrite to nitrate using dissolved oxygen, **E** depicts the reduction of nitrite to dissolved nitric oxide using dissolved hydrogen, **F** depicts the reduction of nitrite to dissolved nitrogen using dissolved hydrogen. Dashed lines indicate the range of affinities possible for sites when analyte concntrations were not known. Arrows indicate the direction the reaction is most likely driven based on the analytical constraints previously discussed in the text. All reactions display positive affinities with the oxidation of nitrite to nitrate having the lowest affinity and the reduction of nitrite to dissolved nitrogen

having the highest affinity. Reactions using hydrogen as an electron donor typically have affinities that increase with increasing hydrogen concentration.

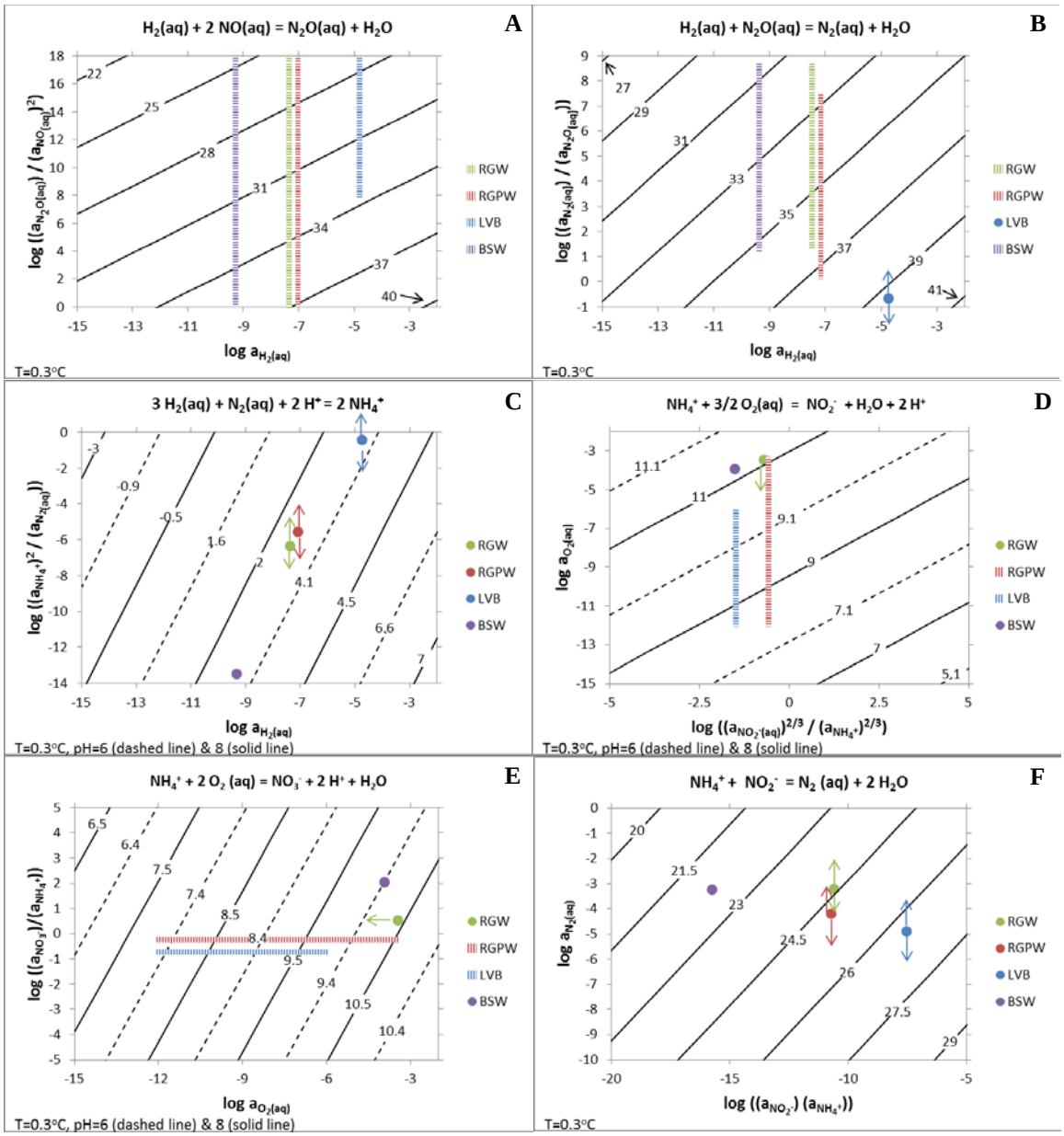

Figure 27. Affinity maps depicting the energetic landscape for reactions involved in nitrogen cycling. Plate **A** depicts the reduction of dissolved nitric oxide to dissolved nitrous oxide using dissolved hydrogen, **B** depicts the reduction of dissolved nitrous oxide to dissolved nitrogen, **C** depicts the recuction of dissolved nitrogen to ammonium, **D** depicts the oxidation of ammonium to nitrite, **E** depicts the oxidation of ammonium to nitrate, **F** depicts anaerobic ammonium oxidation (annamox). Dashed lines indicate the range of affinities possible for sites when analyte concntrations were not known. Arrows indicate the direction the reaction is most likely driven based on the analytical constraints previously discussed in the text. The energetics of all reactions in this plate provide a positive affinity for the reaction to be occurring in the forward direction. Even though nitrogen fixation has low affinity values, they are still positive; meaning nitrogen fixation would not necessarily have to be coupled to another metabolic strategy to proceed.

Surprisingly, the anaerobic oxidation of ammonium yields values that are quite high, and could indicate this is a process that should be investigated at these sites.

Figure 27C (nitrogen fixation) has lower affinities than any other process in the nitrogen cycle depicted in these investigations. The process of nitrogen fixation is seldom thought of as a highly energetic reaction and is more often considered a necessity for some microbial constituent in the community to perform. Nitrogen fixation has been detected in subglacial and cold biosphere environments (Telling et al., 2012; Pearl and Priscu, 1998; Olsen et al., 1998; Grue et al., 1996; Rogers et al., 2013) and based on the positive energetics associated with it in the investigations of these model systems warrents more study. BSW, RGW, and RGPW have very similar affinities at ~3 kcal per mol e^- transferred while LVB is slightly higher with an affinity plotting at ~ 4 kcal per mol e^- transferred. The reaction is pH dependent with a decrease of one pH unit associated with an increase of ~0.85 kcal per mol e^- transferred. Figure 27D depicts the aerobic oxidation of ammonium to nitrite. This process in nitrification has affinity values at RGW and BSW that are just over 11 kcal per mol e^- transferred. LVB and RGPW have lower values due to the lack of measureable dissolved oxygen. The range of affinity for RGPW is ~8.25 to 11 kcal per mol e^- transferred over the range of dissolved oxygen. The affinity at LVB is lower not just because of the low concentration of dissolved oxygen in the system, but also because this is a pH dependent reaction where each log unit decrease in pH corresponds to a drop of 0.45 kcal per mol e^- transferred in affinity giving a range of ~7.8 to 9.6 kcal per mol e^- transferred. Figure 27E depicts the overall process of nitrification oxidizing ammonium all the way to nitrate. RGW may have the highest affinity associated with this reaction (~10.5 kcal per mol e^- transferred) but could be substantially lower further underneath the glacier near the ablation zone. If this process is to occur then, it should be more prevelant toward the glacial toe where there is

more dissolved oxygen in the system. BSW has the second highest affinity with a fixed value of 10 kcal per mol e^- transferred and could therefore provide niches where the process of nitrification should be investigated further to elucidate portential pathways in the nitrogen cycle. RGPW and LVB have ranges of affinity where the affinity could be as low as ~ 7.9 kcal per mol e^- transferred and ~7.3 kcal per mol e^- transferred respectively or as high as ~10.5 kcal per mol e^- transferred and ~9.3 kcal per mol e^- transferred respectively. This pH dependent reaction has a decrease of 0.3 kcal per mol e^- transferred associated with each drop in pH unit; therefore the pH associated with the particular locales in the cold biosphere could directly impact this reaction's vaiability. Figure 27F depicts the anaerobic oxidation of ammonium, also known as anammox. Evidence for anammox has been reported in several subglacial settings and cold biosphere environments (Dalsgaard et al., 2005; Rogers et al., 2013; Shtarkman et al., 2013; Devol et al., 1997; Rysgaard et al., 2004; Gihring et al., 2010; Codispoti 2007; Canion et al., 2013). The reaction is energetically favorable at all sites and could be an important process in cold marine sediments associated with BSW as well as RGPW and RGW locales far beneath the glacier and close to the ablation zone and at LVB which is anoxic. BSW has the lowest affinity for the reaction with a value of ~22.25 kcal per mol e^- transferred, while both RGW and RGPW have values of affinity centering around 24.5 kcal per mol e^- transferred. LVB had the highest affinity for the reaction at over 26 kcal per mol e^- transferred due primarily to the higher concentrations of nitrite and ammonium driving the thermodynamics of the reaction to more positive values. This indicates that the favorable thermodynamic drive for the reaction may indicate that this could be a

potentially important metabolic process in this environment and that attempts at cultures and the proocuremtn of isolates from this environment should be undertaken.

4.7.4. Affinity Maps for Iron and Sulfur Cycling

Iron and sulfur cycling in the cold biosphere are important to understanding the overall global cycling of these elements and are also a valuable source of energy for microbes living within these environments. Figures 28 - 30 depict affinity maps of some of the more salient iron/sulfur redox reactions that could be prominent in the cold biosphere. The basis for the iron/sulfur redox reactions is rooted in the redox chemistry of pyrite in subglacial and low temperature systems. Many glacial waters have high levels of sulfate in meltwaters due to the oxidation of pyrite; and there is evidence pyrite oxidation is the dominant lithogenic control on microbial communities in many subglacial environments (Mitchell et al., 2013). According to Mitchell et al. (2013), pyrite and its oxidation products have a large influence on the structure and composition of microbial communities due to the redox metabolisms of iron and sulfur. With that in mind, and the fact that many different subglacial systems are predominately anaerobic, the majority of the reactions for iron/sulfur redox in Figs. 28-30 are written with nitrate and nitrite as the electron acceptor. The first four affinity maps in Fig. 28 (A-D) depict the dissolution/oxidation of pyrite coupled to nitrate and nitrite reduction. figure 28A depicts the oxidation of pyrite using nitrate as an electron acceptor to ferrous iron, thiosulfate and dissolved nitrogen as the products. In anaerobic systems, this is likely a major pathway for the oxidation of pyrite and could be utilized by microorganisms in the cold biosphere. In all of these systems, the affinity is given by a range due to the lack of data for thiosulfate; arrows indicate the uncertainty in dissolved nitrogen. BSW, RGW,

and RGPW are all very close to each other in terms of affinity and are between 18 and just over 19 (almost 20 for BSW) kcal per mol e^- transferred. LVB on the other hand has a range of affinity of just over 18.5 to ~19.6 kcal per mol e^- transferred. The pH dependency of the reaction as written indicates that there is an increase of ~0.25 kcal per mol e^- transferred per decrease in unit of pH. Figure 28B depicts a reaction similar to 28A except the sulfur from pyrite has been oxidized completely to sulfate. Affinities for this reaction are higher for all sites than those depicted in fig 28A. RGW, RGPW, and BSW all cluster at values of affinity close to 20.25 kcal per mol e^- transferred while that of LVB is at ~20.4 kcal per mol e^- transferred. Arrows indicate the uncertainty associated with the concentration of dissolved nitrogen in the system and in the case of RGPW, the fact that there is probably a greater concentration of ferrous iron in the sediments as a whole than what was measured at the surface. The reaction depicted in Fig. 28B is also pH dependent and for every decrease in pH unit there is an increase of ~0.15 kcal per mol e^- transferred.

Figure 28C is analogous to Figure 28A, with the exception that nitrite is the electron acceptor. Again, affinities are given as ranges due to a lack of data for thiosulfate and arrows are used to indicate the uncertainty associated with the dissolved nitrogen concentration. In every instance, the use of nitrite as an electron acceptor for the reaction is more energetically favorable than the use of nitrate. There is an increase of 0.42 kcal per mol e^- transferred associated with each unit decrease in pH for this reaction, which along with the elevated levels of nitrite help increase the range of affinity for LVB to values more energetically favorable than that of the other sites. The affinity for LVB ranges from 24.34 to ~23 kcal per mol e^- transferred while that for RGW spans from

~21.9 to ~23 kcal per mol e^- transferred. The range of affinity for RGPW is slightly more energetic than that of RGW and ranges from ~22 to 23.4 kcal per mol e^- transferred. BSW has the lowest affinity with a range spanning from ~21.2 to 22.4 kcal per mol e^- transferred most likely due to the very low levels of nitrite in BSW. Figure 28D is similar to the upper right affinity plot, but uses nitrite as the electron acceptor to oxidize pyrite to ferrous iron, dissolved nitrogen, and sulfate; it is also the most energetic of the four reactions depicting pyrite dissolution/oxidation. The pH dependence of this reaction results in an increase in affinity of 0.25 kcal per mol e^- transferred for every decrease in unit of pH. BSW has the lowest affinity (~22.9 kcal per mol e^- transferred) likely due to the relatively low activity of nitrite as opposed to the higher activity of sulfate. RGW and RGPW have similar affinities (~24 and ~24.4 kcal per mol e^- transferred respectively) while LVB has the highest affinity with a value slightly less than 25 kcal per mol e^- transferred. Regardless of the affinities that are presented in Figs. 28A-D, which are all quite high, a limiting factor on a microorganisms ability to perform a reaction is inherent to the concentration of substrate and its availability. In the case of BSW, GRW, and RGPW this means that perhaps on ly the reaction involving nitrate would be oof importance. In LVB however the elevated concentrations of nitrite mean that further investigations using nitrite should be undertaken to get a better understanding of nitrogen-iron-sulfur cycling in subglacial lake settings.

The last four affinity maps in Fig. 28 (E through H) relate to sulfur cycling from the subsequent dissolution and oxidation of pyrite. Figure 28E depicts the oxidation of thiosulfate coupled to nitrate and is one of the more thermodynamically favorable reactions. Figure 38F depicts this reaction utilizing nitrite instead of nitrate. Similar to

the previously described reactions involving nitrate and nitrite, the use of nitrite is more energetically favorable than nitrate, but may not be as widely utilized in BSW, RGW, and RGPW due to the lower concentrations of nitrite. The affinity map depicting the reaction using nitrate has a pH dependence where each unit increase in pH corresponds to a increase of ~0.05 kcal per mol e^- transferred while that of using nitrite corresponds to a decrease of ~0.125 kcal per mol e^- transferred. Coupling the oxidation of thiosulfate to nitrate causes a significant overlap in the affinities of the reaction for all sites. The affinity range for BSW is ~20.4 to ~21.3 kcal per mol e^- transferred while that of RGW is ~21.2 – ~21.9 kcal per mol e^- transferred and RGPW is ~21.1 - ~22 kcal per mol e^- transferred and LVB is ~20.9 – ~21.8 kcal per mol e^- transferred. In each instance, all of these ranges are very close to each other as opposed to using nitrite. The use of nitrite corresponds to ranges of ~23.2 - ~24.1, ~24.9 - ~25.75, ~25 – 26.3, and ~25.25 – 26.5 kcal per mol e^- transferred for BSW, RGW, RGPW, and LVB respectively. The bottom two affinity maps, Figs. 28G&H, address the reduction of oxidized sulfur species to sulfide that are likely to be present in these systems and are coupled to dissolved hydrogen as an electron donor. While both the reduction of thiosulfate and sulfate have positive affinities, they are less energetic than the previously described oxidation reactions using nitrate and nitrite as electron acceptors. Overall, the reduction of thiosulfate is more energetic than the reduction of sulfate and is predicted to be a major metabolic pathway in systems where pyrite oxidation is occuring. The pH dependence for the reduction of thiosulfate corresponds to an increase in affinity by ~0.375 kcal per mol e^- transferred for each unit decrease in pH while that of sulfate reduction corresponds to an increase in affinity of ~0.575 kcal per mol e^- transferred for each unit decrease in

pH. The reduction of thiosulfate to sulfide has ranges of ~2.7 - ~3.6, ~4.4 - ~4.8, ~4.4 - ~5, and ~6.8 – ~7.2 kcal per mol e^- transferred for BSW, RGW, RGPW, and LVB respectively. BSW has the lowest affinity range associated with it most likely because of the low activity of dissolved hydrogen for the system, while the converse is observed for LVB. The affinities for sulfate reduction to sulfide are ~1.45, ~2.4, ~1.7 - ~2.45, and ~4.65 - ~5.65 kcal per mol e^- transferred for BSW, RGW, RGPW, and LVB and the order of their affinities is expectant for the same reasons as that related for the reduction of thiosulfate.

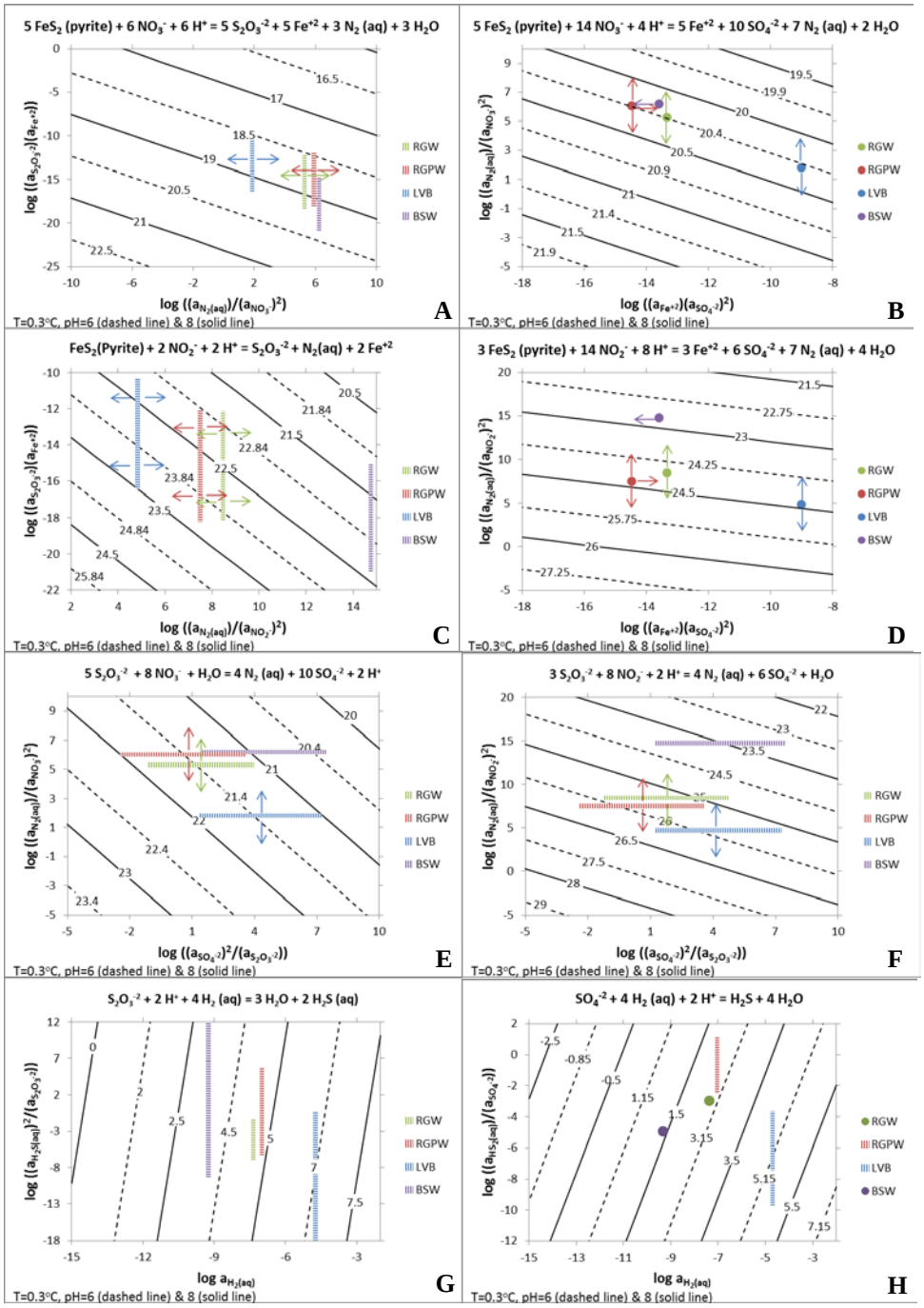

Figure 28. Affinity maps depicting the energetic landscape for selected reactions involved in iron and sulfur cycling. The top four affinity maps depict the oxidation/dissolution of pyrite coupled to the reduction of nitrate and nitrite. Uncertainties in the activity of thiosulfate and dissolved nitrogen necessitate the use of arrows and dashed lines to depict probable ranges for the affinities of these reactions. The bottom four affinity maps depict the energetics related to the cycling of sulfur compounds likely to be present in these systems and include both the oxidation of

thiosulfate coupled to nitrate and nitrite as electron acceptors and the reduction of sulfate and thiosulfate to sulfide.

Figures 29 and 30 explore the energetics associated with anaerobic oxidation of ferrous iron to iron oxides and oxyhydroxides common to cold biosphere settings using nitrate and nitrite (respectively) as electron acceptors. These include magnetite, hematite, maghemite, goethitie, lepidocrocite, and ferrihydrite and in each instance, there is a positive thermodynamic drive for the reaction as written in the forward direction. All of the reactions are pH dependent and in each case, the use of nitrite as an electron acceptor is more energetically favorable than that of nitrate. Using nitrate as an electron acceptor (Fig. 29) the order for increasing affinity for the reactions is: ferrihydrite < magnetite < lepidocrocite < maghemite < goethite ≈ hematite. This is partly a reflection of the relative thermodynamic stability of iron (oxy)hydroxides in these settings; however, it should be noted that less thermodynamically favorable/stable forms of minerals might have a greater instance of utilization by microorganisms in geochemical systems due to the more favorable kinetics associated with their formation. Use of nitrite as an electron acceptor (Fig. 30) has nearly the same order of energetic favorability of formation, except that the formation of goethite seems to be slightly more energetic than that of hematite.

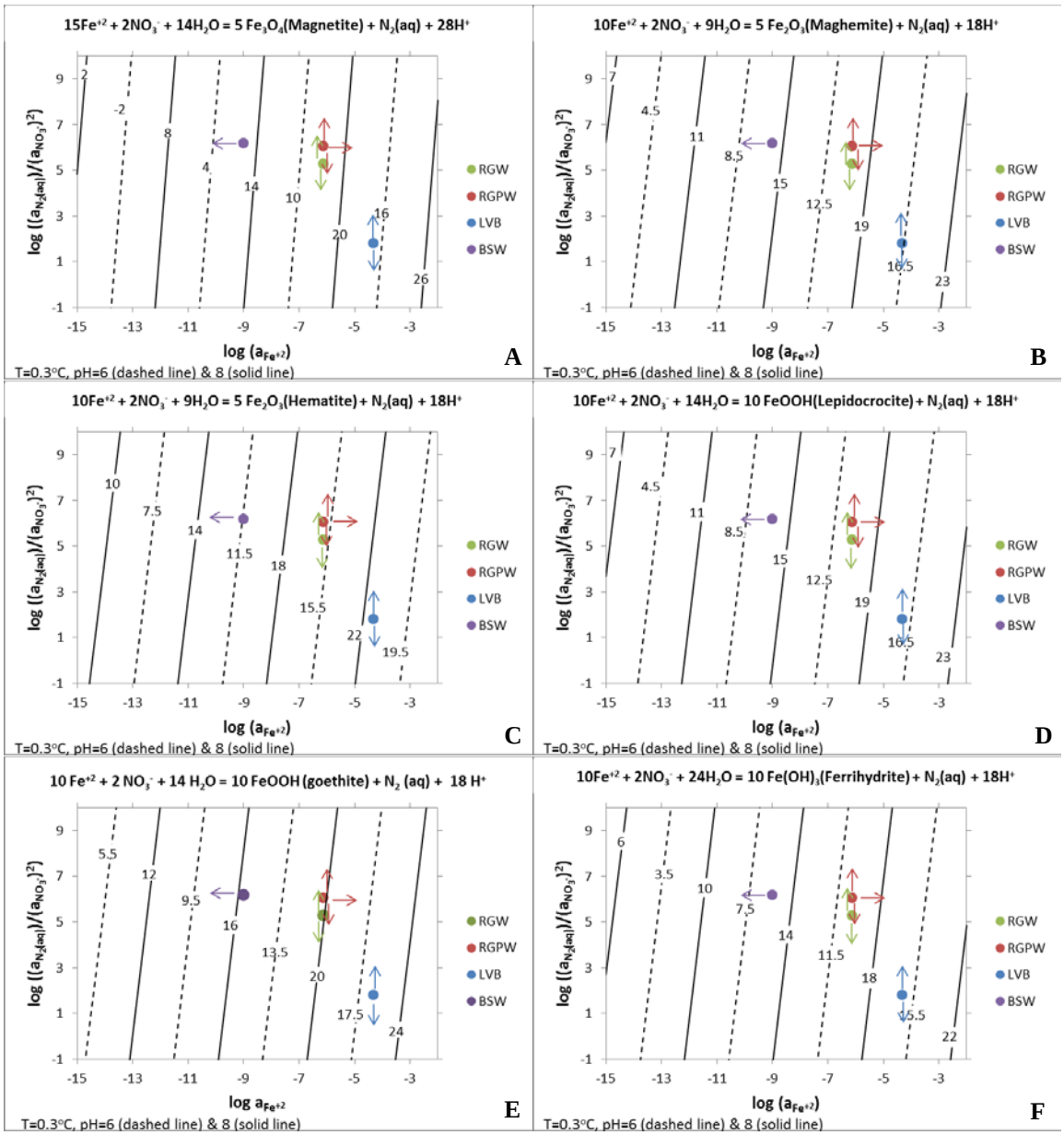

Figure 29. Affinity maps depicting energetic landscape for selected reactions involved in iron cycling with nitrate as an electron acceptor. The ranked thermodynamic drive for the formation of iron minerals is: ferrihydrite < magnetite < lepidocrocite < maghemite < goethite ≈ hematite. Iron minerals with a lower thermodynamic drive for their formation might still be the dominant form in the environment though due to their relatively higher kinetic favorability.

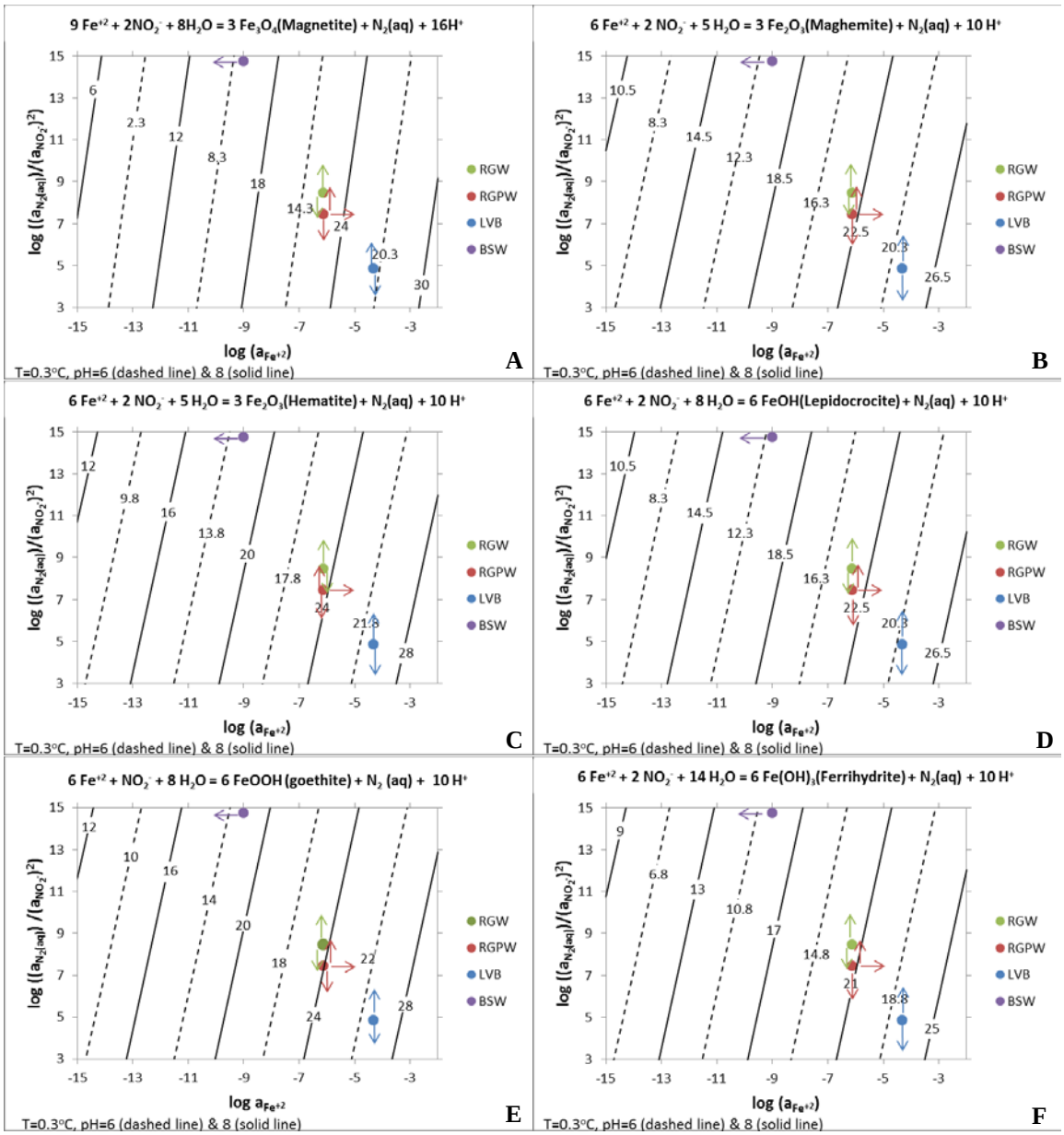

Figure 30. Affinity maps depicting energetic landscape for selected reactions involved in iron cycling with nitrite as an electron acceptor. The ranked thermodynamic drive for the formation of iron minerals is: ferrihydrite < magnetite < lepidocrocite < maghemite < hematite ≤ goethite. Iron minerals with a lower thermodynamic drive for their formation might still be the dominant form in the environment though due to their relatively higher kinetic favorability.

4.7.5. Energy per Unit Volume

It is illustrative to investigate not just the amount of energy per e^- transferred, but also the total amount of energy per unit of volume. This allows one to determine the total amount of energy that is available to a geochemical system per unit volume and can also be used (if desired) to determine the total maximum amount of power the geochemical system is delivering to microorganisms utilizing a particular metabolic strategy if a flow rate or rate of delivery is known. In this section, we analyze the amount of energy per milliliter of solution for a subset of reactions in Appendix E that have positive affinities. They are displayed by affinity ranked according to the ranges portrayed for reactions where there is uncertainty in the concentration of limiting reagents for LVB, RGPW, RGW, and BSW. Dashed lines indicate reactions whose ranges include negative affinities. The full suite of figures for energy per milliliter of solution for the reactions in Appendix E can be found in Apprndix H.

Figure 31 depicts the ranked energies for reactions involving dissolved oxygen as an electron acceptor. The use of dissolved oxygen as an electron acceptor has a much lower energy associated with it for the most energetic reactions at LVB and no values are greater than one μcal per ml. This is likely due to the low concentration of dissolved oxygen associated with this site. The most energy available from a reaction at LVB involves the oxidation of dissolved hydrogen and is the highest ranked due to the large concentration of dissolved hydrogen in LVB despite the miniscule amount of dissolved oxygen. Almost all the reactions for LVB have similar energies. RGPW, RGW, and BSW all have their most energetic reactions in the range of tens or hundreds of μcal ml^{-1}, almost one to two orders of magnitude higher than LVB. Furthermore, these three sites

have a much larger range and variability in shape. While LVB is almost a straight line downward, the other three sites display more changes in slope in the energy distribution. RGPW and RGW are very similar in their energy make up, but BSW shows a wider variability in energy distribution for reactions with several energy transitions across micro and nano calorie régimes. BSW is also the only system with a large number of energies for reactions approaching pcal levels per ml.

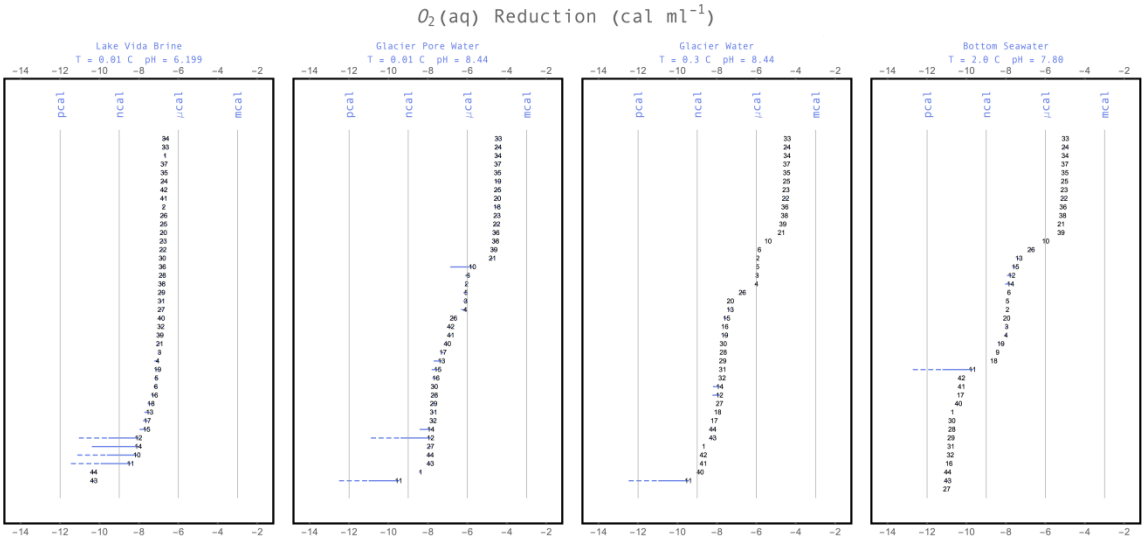

Figure 31. The energetic rankings for reactions involving dissolved oxygen as an electron acceptor. Dashed lines indicate reactions whose range include negative affinities. Note that LVB has similar energetic values for almost all reactions plotted while RGPW, RGW, and BSW have a greater range and more shape in their distribution of energies. BSW also has the most reactions with values approaching pcal per ml levels.

The use of nitrate as an electron acceptor is likely very important to many microorganisms inhabiting these geochemical environments and the energetics of reactions for LVB, RGPW, RGW, and BSW are displayed in Fig. 32. In this instance, reactions at LVB start off with the most energy available per ml and are on average one to two orders of magnitude higher than the other three sites. This is likely due to the relatively high concentration of nitrate at LVB, which can provide a stronger thermodynamic drive for these reactions to proceed in the forward direction. RGPW,

RGW, and BSW only have a moderate amount of nitrate and start off with maximum energies closer to values in the μcal per ml range. Reactions for RGPW drop below the μcal ml^{-1} range earlier than that of RGW and BSW, but unlike BSW and LVB, reactions involving nitrate as an electron acceptor at RGPW and RGW never completely drop below the ncal ml^{-1} energy level. LVB only has ten reactions that drop below the nanocal per mil energy level, but BSW is a different case with nearly half of the reactions shown falling below the ncal ml^{-1} energy value. In contrast to the shape of the energetic decline in LVB, RGW, and BSW; RGPW has more of a linear shape extending from just above the μcal ml^{-1} energy level to the ncal ml^{-1} energy level.

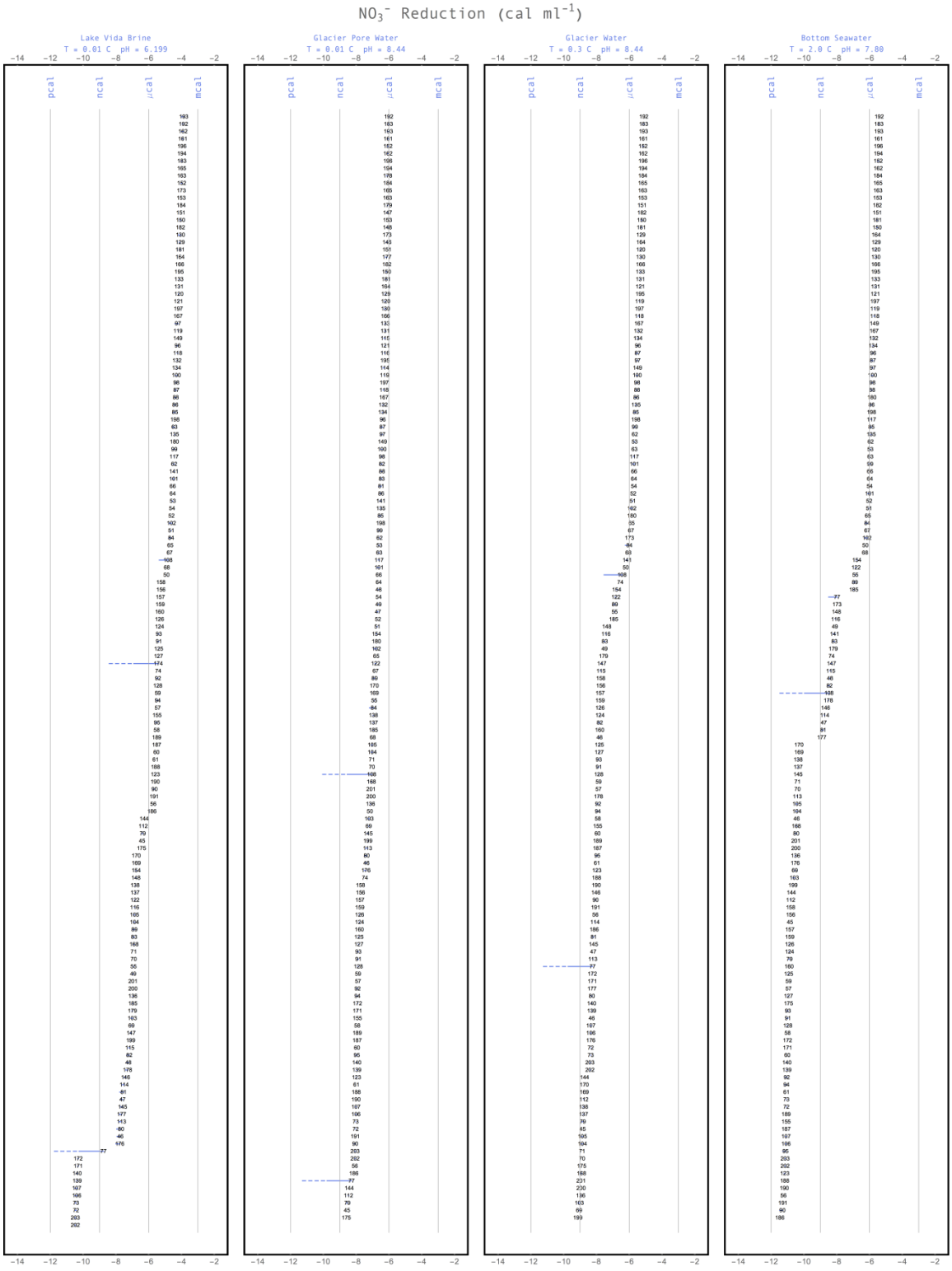

Figure 32. Depiction of nitrate used as an electron acceptor in LVB, RGPW, RGW, and BSW. Dashed lines indicate reactions whose range include negative affinities. LVB has

some of the highest and lowest energies associated for reactions, however BSW overall, has the highest number of reactions that provide less than a ncal ml^{-1}.

Figure 33 depicts the energy available from using nitrite as an electron acceptor. In contrast to many of the affinity maps that indicate that reactions using nitrite as an electron acceptor have more energy (kcal per mol e^- transferred) than nitrate, the opposite is true when viewing the amount of energy in terms of cal per mil of solution. All reactions in Fig. 33 are less energetic on a per ml basis than those depicted in Fig. 32. LVB has the highest energy levels for first several dozen reactions associated with nitrite as an electron acceptor. BSW starts out several orders of magnitude below LVB. Both RGPW and RGW have reactions that are at about the same energetic lever per ml and both have reactions that at their lower levels are similar. LVB has more reactions that are positive for nitrite reduction even though some of them are far below that of RGPW and RGPW (as well as BSW). BSW has the lowest energy associated with reactions due to the low concentrations of nitrite available for reactions to proceed. BSW also has fewer reactions listed in Fig. 33 because they have negative values and cannot be plotted on the axes that have been adopted in this figure. The shape of the curves for the rank ordered reaction is very similar for all sites investigated here, despite the fact that they start at different initial values for reactions that have been evaluated.

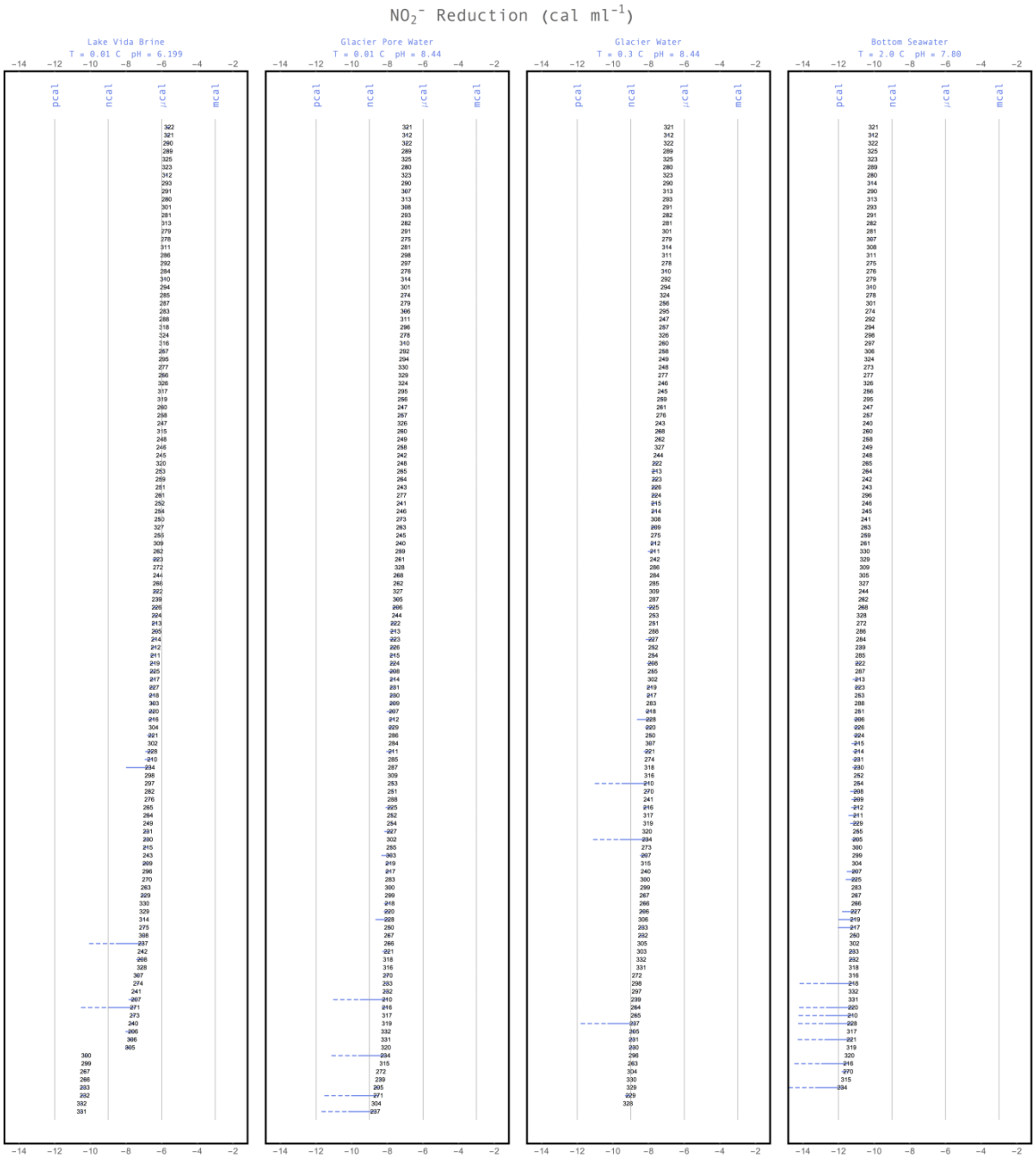

Figure 33. This figure depicts the energetics associated with the use of nitrite as an electron acceptor and in contrast to many of the affinity maps that indicate that reactions using nitrite as an electron acceptor have more energy (kcal per mol e^- transferred) than nitrate, the opposite is true when viewing the amount of energy in terms of cal ml^{-1} of solution. Dashed lines indicate reactions whose ranges include negative affinities.

Sulfate reduction (Fig. 34) for sites investigated in this work has far fewer reactions that are actually viable for energy than other reactions. LVB and BSW have the highest energy available per mil from reactions using sulfate as an electron acceptor, however, while LVB has reactions that drop off sequentially, BSW has the first dozen reactions that maintain high values followed by a large drop in available energy for all other reactions that are evaluated. RGPW has the fewest number of reactions that are energetically favorable, though those that are in the middle range of energy that is available as opposed to BSW whose nearly four magnitude drop in energy nearly segregates the types of reactions that are evaluated. Both RGPW and RGW have ranges of energy for reactions that are very similar, while LVB and BSW each have nearly a dozen reactions that are at or approach energetic levels of mcal ml^{-1}.

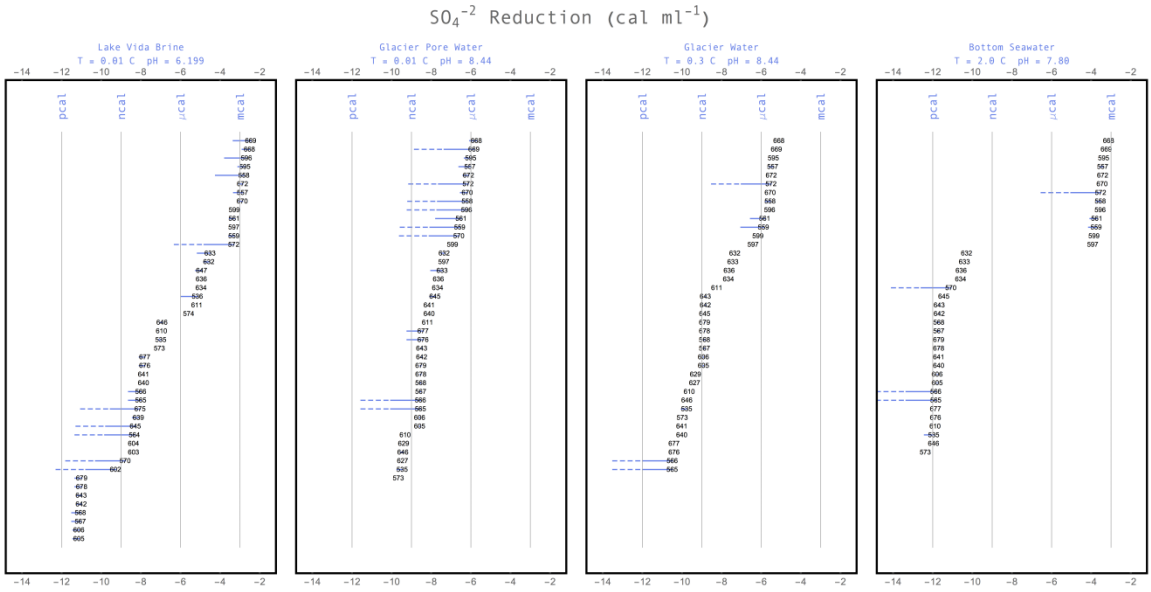

Figure 34. The use of sulfate as an electron acceptor for sites spans several orders of magnitude with LVB and BSW having the highest initial values for reactions ranked in their systems. RGPW and RGW have more tightly centered values than LVB and BSW.

Ferric iron has often been considered a fairly important electron acceptor in aqueous systems, especially those that are anoxic. Figure 35 depicts the ranked

energetics of reactions related to ferric iron in the form of ferrihydrite as an electron acceptor. As may be expected, LVB and RGPW provide environments that are conducive for higher energetic values while RGW is in the middle and BSW has the lowest energies for reactions using ferrihydrite as an electron acceptor. RGPW has nearly twice as many reactions with energies higher than µcal per ml values than the next closest site, LVB. On top of this RGPW does not have any reactions with energies that are lower than nanocal per mil while BSW has several reactions that have negative energies associated with it and subsequently has fewer reactions plotted. LVB has two reactions that are in the hundreds of µcal per ml associated with it and then a smooth taper of reactions that drop from µcal to ncal per ml until there is another large drop in energies past the nanocal per mil value. RGPW and RGW have a smoother grade in decreasing energies for reactions. BSW has three large shifts in energetics associated with reactions evaluated where smoothed transitions in energy shift to discreet drops in energy levels for sets of reactions.

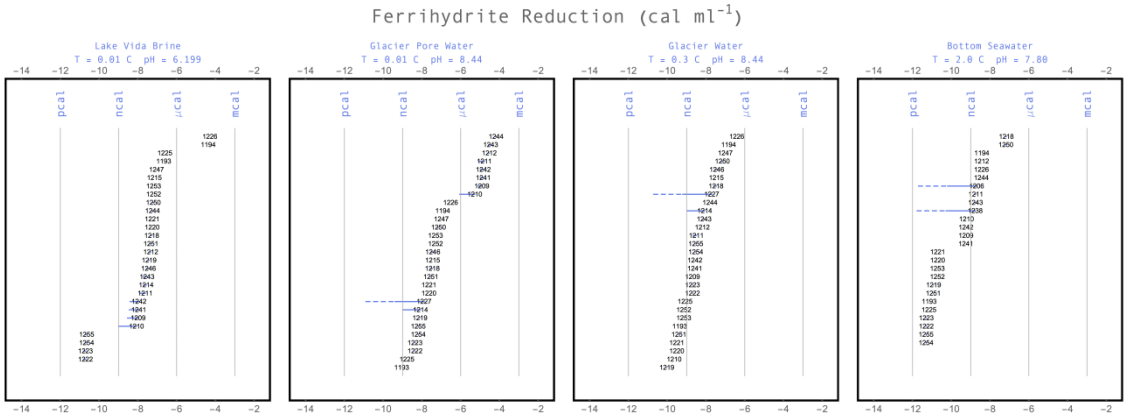

Figure 35. The use of ferric iron in the form of ferrihydrite as an electron acceptor is an important pathway for iron redox reactions. As depicted in the figure RGPW has the most energy associated with reactions using ferrihydrite as an electron acceptor with RGW as a close second overall. LVB has a couple of reactions whose energies rival that of RGPW, but overall the energetics for using ferrihydrite as an electron acceptor are not as energetic as RGW, though they are better than that of these reactions in BSW, which

has the worst energetics and has fewer reactions listed since the others have negative values.

The use of ferric iron as an electron acceptor in the form of goethite (Fig. 36) follows a trend similar to that of ferrihydrite for these systems. One thing to note is how few reactions are able to be plotted in Fig. 36 as opposed to how many reactions involving goethite as an electron acceptor are evaluated in Appendix E. This indicates a greater drive for ferrihydrite to be used as an electron acceptor in these systems than goethite. Both LVB and RGPW have some of the highest energetic values for reactions plotted, while RGW and BSW start off with lower maximum values. Despite this, the lowest energetic values for reactions at LVB are nearly as low as those for BSW. The reactions with the highest energetic values are those involving ammonium, sulfide and thiosulfate as electron donors for goethite across all sites.

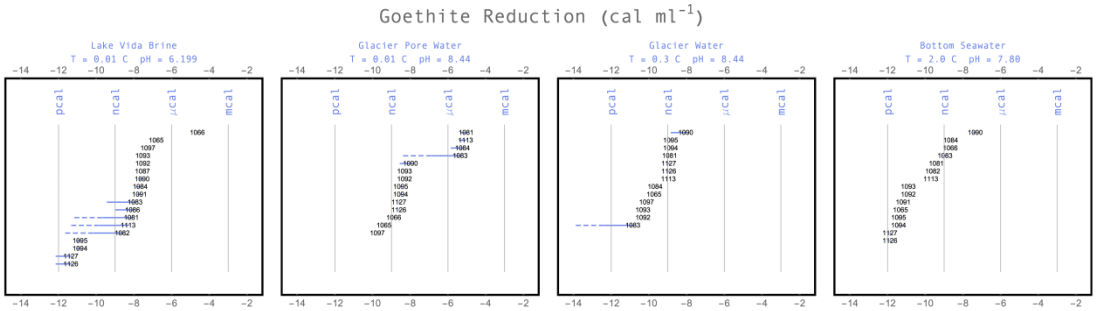

Figure 36. One thing to note is how few reactions are able to be plotted as opposed to how many reactions involving goethite as an electron acceptor are evaluated in Appendix E. This indicates a greater drive for ferrihydrite to be used as an electron acceptor in these systems than goethite. Both LVB and RGPW have some of the highest energetic values for reactions plotted, while RGW and BSW start off with lower maximum values. Despite this, the lowest energetic values for reactions at LVB are nearly as low as those for BSW.

Methane oxidation is typically one of the highest energy yielding reactions across different environments depending on the electron acceptor it is paired with. Figure 37 depicts all methane oxidation reactions compiled in Appendix E. LVB has the highest

range of values for methane oxidation as might be expected since it has a relatively high concentration of dissolved methane in solution while BSW has the lowest overall range of energies due to its low concentration of dissolved methane. RGPW has its top ranked methane oxidation reactions coupled to oxygen as an electron acceptor, but surprisingly, LVB, RGW, and BSW have the highest ranked methane oxidation reactions coupled to dissolved nitrous oxide despite low range given for it in those settings, excluding LVB where it is quite elevated. The low values at RGW and BSW for methane oxidation are approximately three orders of magnitude lower than that for RGPW and LVB and that is likely a reflection of the relatively high values of methane at LVB and RGPW that are able to provide more energy per ml.

Ammonia oxidation (Fig. 38) has its most energetic values per ml at LVB in part due to the high concentration while BSW has the lowest values for the converse reason. LVB also has nearly half a dozen more reactions that have positive values associated with it than any other system. At LVB ammonium oxidation coupled to nitrate has the highest energy yield followed by it being coupled to ferrihydrite reduction to magnetite. At both RGPW and RGW ammonium oxidation coupled to dissolved oxygen have the most energetic return per mil. In BSW ammonium oxidation coupled to dissolved nitric and nitrous oxide have the two highest energetic yields per mil despite the low range of concentration for both of those electron acceptors. However, these values are in line with that of RGW and RGPW, though the value for LVB is much higher due to the elevated concentration of dissolved nitrous oxide.

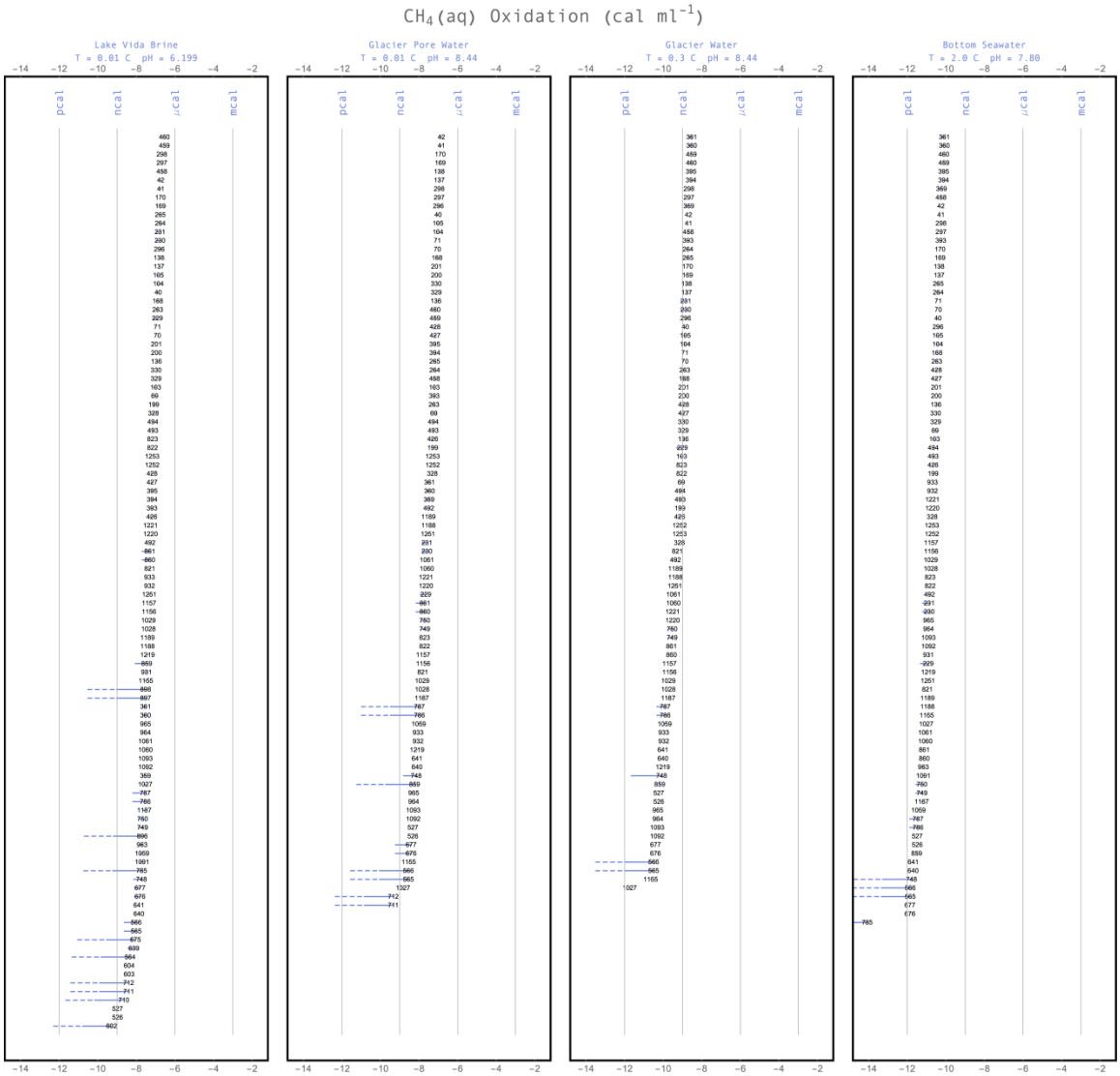

Figure 37. Methane oxidation at LVB and RGPW is more energetically favorable for LVB and RGPW due to the relatively higher concentration of methane in both of those systems, while that of BSW and RGW are much lower in general due to the relatively lower concentration. LVB has the highest overall energetic yield for methane oxidation per ml while BSW has the lowest.

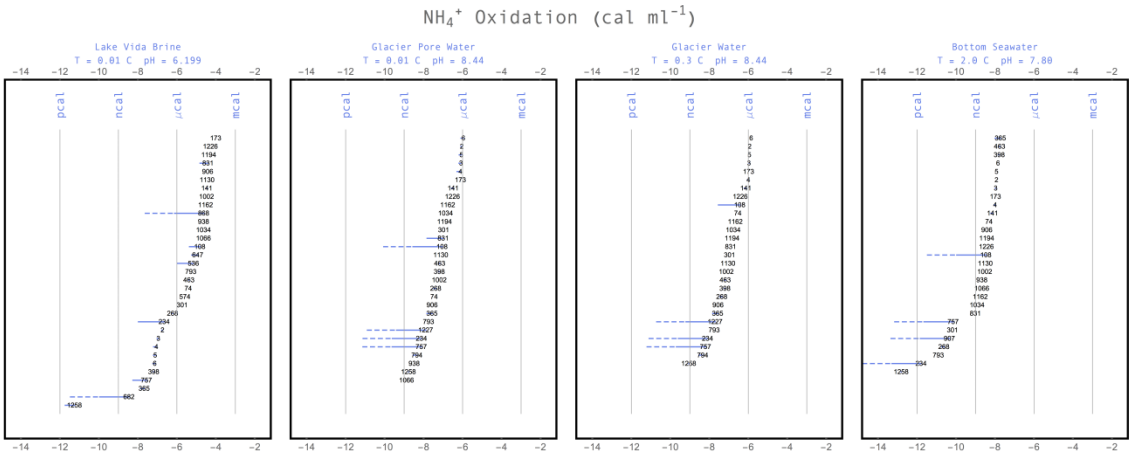

Figure 38. The oxidation for ammonium in these systems tends to be driven by the total amount of ammonium available to interact with electron acceptors. In this respect, LVB with its high concentration of ammonium has the highest values while that of BSW has the lowest values of energy per ml.

The energy for oxidation of sulfide across these systems (Fig. 39) tends to be a function of sulfide concentration, since it is the limiting reagent for this reaction. RGPW has the highest values for sulfide oxidation and also has the highest potential concentration of sulfide, given the sediment structure there. On the other hand, BSW and LVB (where sulfide was below the detection limit) have some of the lowest energy values per mil for each reaction. The cal per ml for RGW is only slightly better than that of BSW and LVB, but the majority of the reactions have values greater than ncal ml^{-1}. LVB has nearly half a dozen fewer reactions that are positive for sulfide oxidation. LVB, RGW and BSW all have sulfide oxidation coupled to dissolved nitrous oxide as the highest yielding reaction for their systems. This could be expected for LVB, which has a high concentration of dissolved nitrous oxide; however, this is somewhat out of the ordinary for BSW and RGW though the same reaction for RGPW has approximately the same value as that of BSW and RGW.

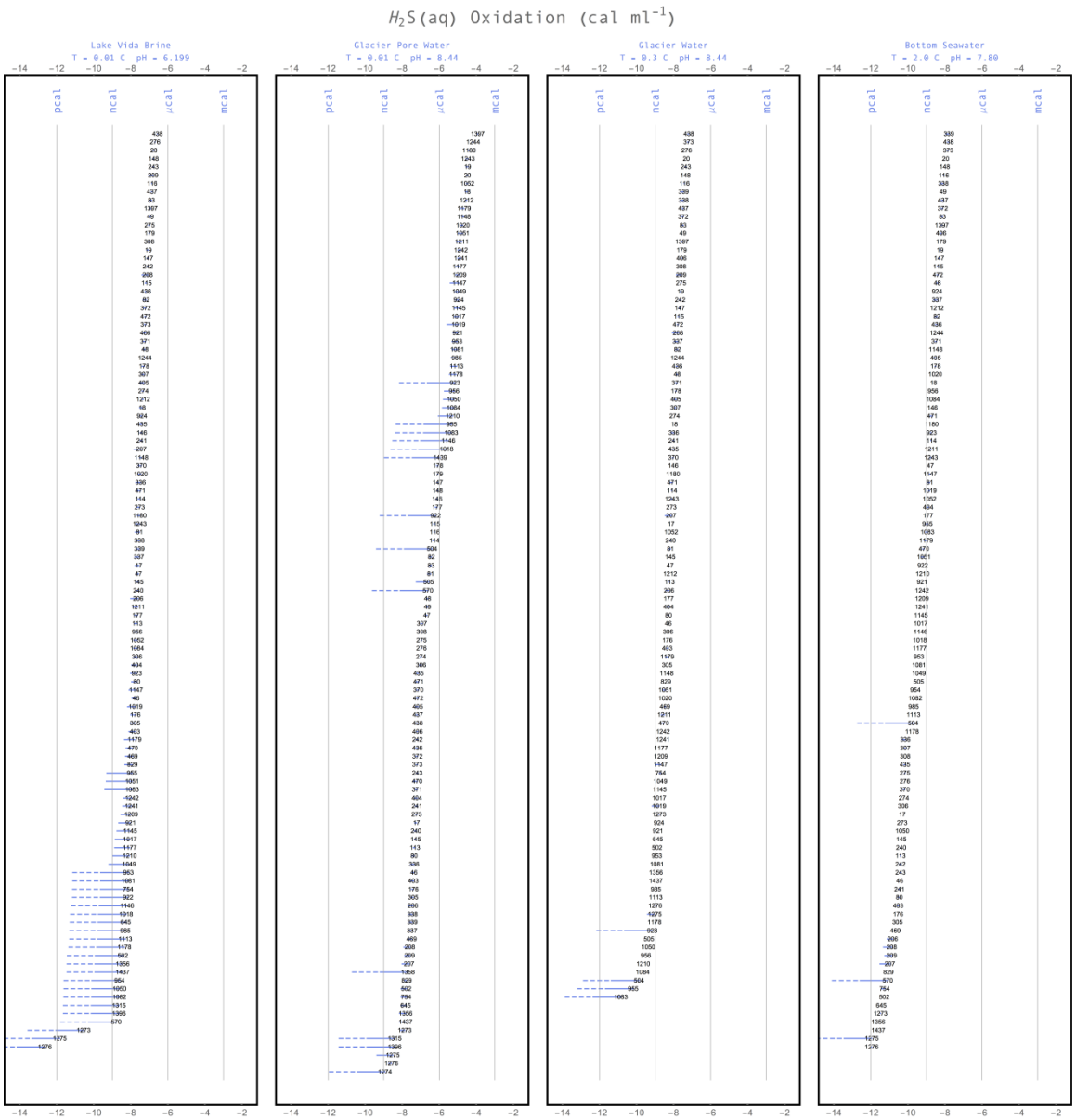

Figure 39. The energy for oxidation of sulfide across these systems tends to be a function of sulfide concentration, since it is the limiting reagent for this reaction. RGPW has the highest values for sulfide oxidation and also has the highest potential concentration of sulfide. On the other hand, BSW and LVB (where sulfide was below the detection limit) have some of the lowest energy values per ml for each reaction.

Ferrous iron oxidation (Fig. 40) is generally enhanced in systems that have the highest concentrations of ferrous iron since most of these systems have enough electron acceptors to be coupled to it. In this respect, LVB has the highest overall number of reactions that have energies greater than μcal ml^{-1} values while BSW has some of the lowest values. RGPW and RGW fall in the middle for these reactions and BSW crosses over to lower than pcal ml^{-1} energies before any other system and also has fewer reactions that are even positive. LVB also falls off before RGPW and RGW, but does so with remaining values well past the ncal ml^{-1} level. RGPW and RGW follow suit very closely with regard to their order of reactions and the shape of the overall energy trends for their systems.

Pyrite is a common mineral in cold biosphere environments and its oxidation (Fig. 41) typically provides energy for microbial metabolic strategies. There are a variety of oxidants that can be coupled to pyrite oxidation and in Fig. 41 these are rank ordered. All sites have reactions that are in the tens to hundreds of μcal ml^{-1} energy levels. LVB has the most energetic reactions associated with it while BSW has the fewest. LVB also has more than half a dozen reactions that still have positive energetics associated with it than any other site. BSW overall has the lowest energies associated with reactions for pyrite oxidation and is the only site where values dip below the ncal ml^{-1} value. In RGPW, RGW, and BSW the oxidation of pyrite with dissolved oxygen as an electron acceptor either to sulfate or thiosulfate are the most energetically favorable reactions. In LVB where oxygen is more scarce, the oxidation of pyrite couple to nitrate reduction has the highest energetic yield of all reactions.

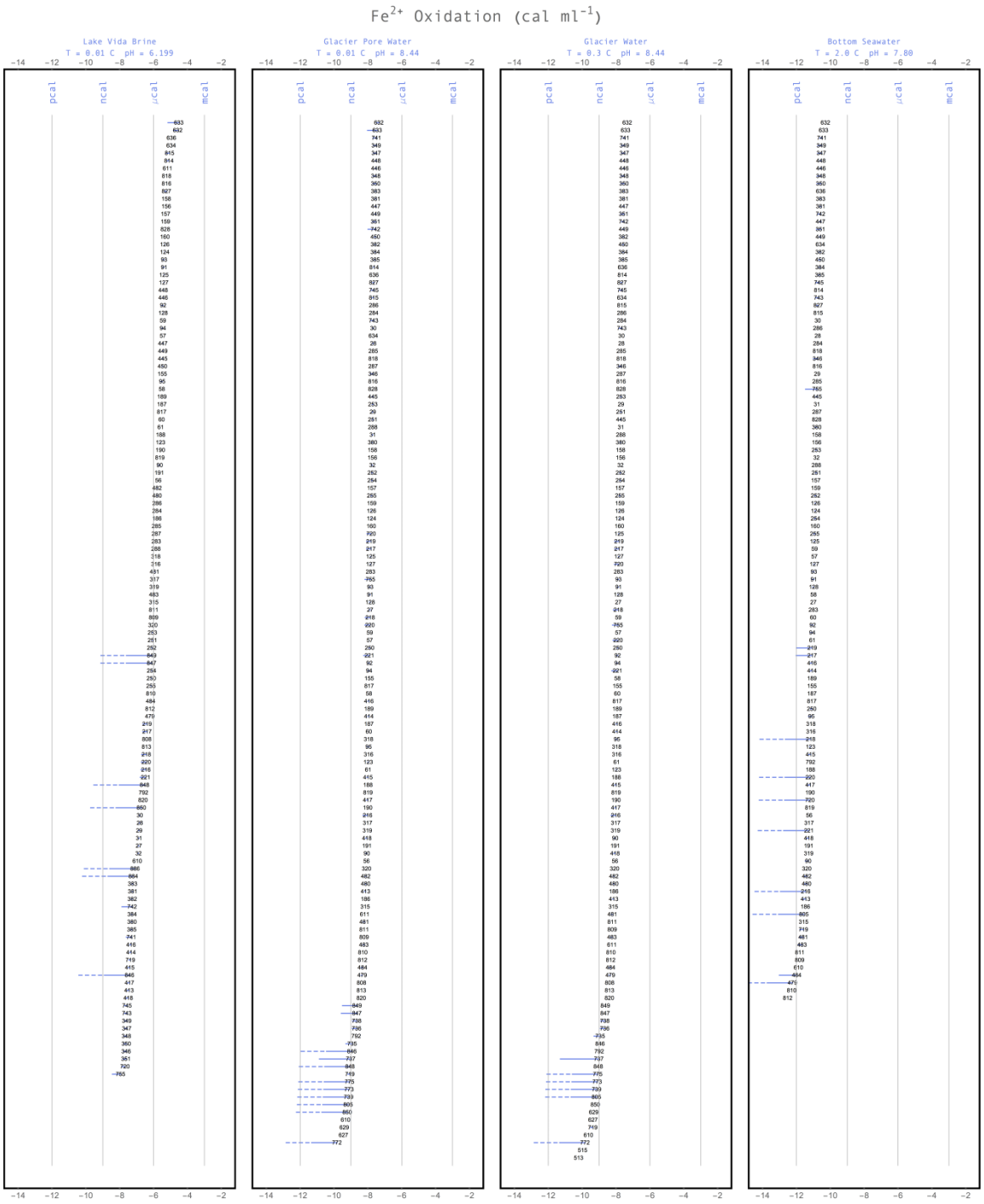

Figure 40. The energetics of ferrous iron oxidation across these four systems is driven mainly by the amount of ferrous iron that is available as an electron donor. LVB therefore has the highest energetic values while that of BSW has the lowest. RGPW and RGW are very similar in their energetics, though RGPW may be more energetically favorable due to enhanced ferrous iron concentrations in the pore waters that are unable to be accommodated for in the calculations here.

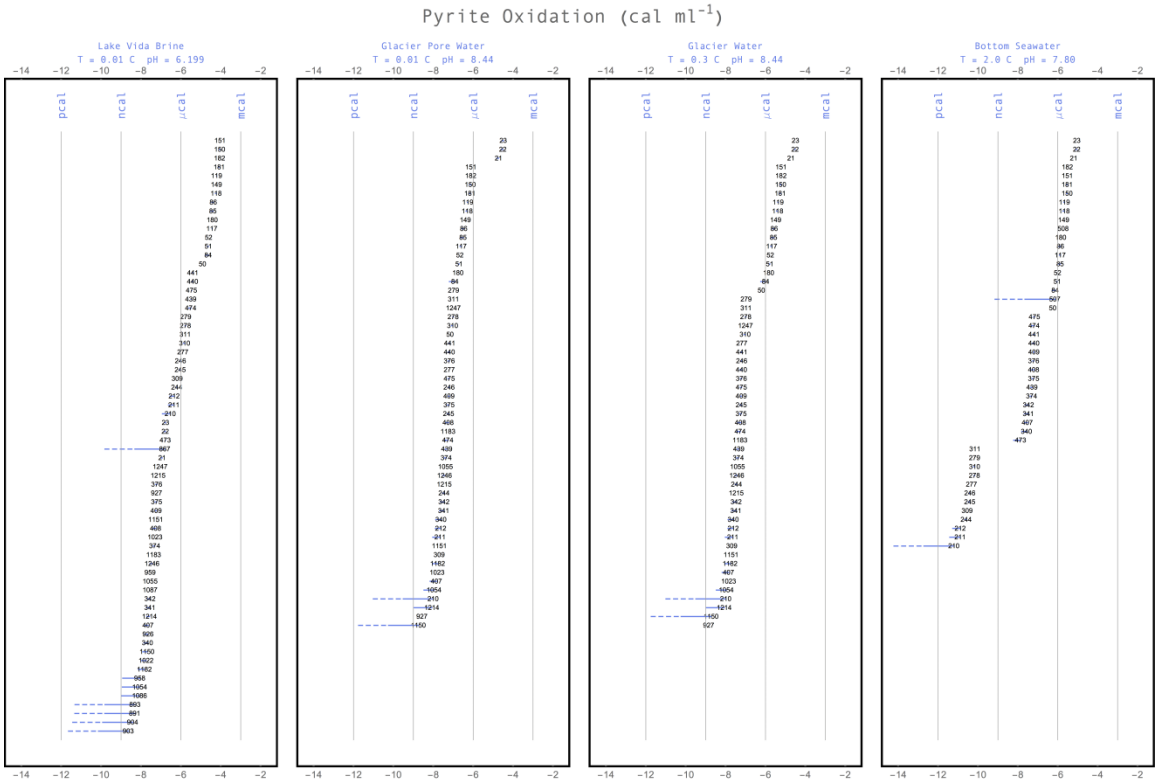

Figure 41. Depiction of the oxidation of pyrite across LVB, RGPW, RGW, and BSW. All sites have reactions that are in the tens to hundreds of μcal per mil energy levels. In RGPW, RGW, and BSW the oxidation of pyrite with dissolved oxygen as an electron acceptor either to sulfate or thiosulfate are the most energetically favorable reactions. In LVB where oxygen is more scarce, the oxidation of pyrite couple to nitrate reduction has the highest energetic yield of all reactions.

4.8. Concluding Remarks

The study described above was designed to more definitively define the extent and energetics of the cold biosphere and the flow of energy through it by using geochemical data from representative/model portions of the cold biosphere and converting it to bioenergetics of chemolithoautotrophic metabolisms that could be occurring there. Heterotrophy was not addressed and niches could exist for a much more diverse overall microbial consortia. However, the data and calculations used here can still be extended to address primary productivity in these systems and be translated into

power to examine the effect the geochemical environment has on primary microbial productivety.

There is still much to address concerning the cold biosphere and this work would have benefitted from more samples from subglacial lakes, species analyses of dissolved nitrous and nitric oxide, and thiosulfate (across all model sites used), and culturing and characterization of more microbial isolates. It is hoped that this work will not only help define the extent of the cold biosphere here on Earth and the bioenergetic processes occurring in it, but could also aid in assessing the habitability and potential for life on other planets and planetismals as well.

4.9. Acknowledgements

This work benefited from help in the field from Jeff Havig, Allie Rutledge, and Eric Boyd and many other colleages from Montana State University as well as numerous discussions with Eric Boyd regarding microbial processes in the cold biosphere.

V. FUTURE DIRECTIONS

The flow of energy from the geosphere to the biosphere can be quantified by accounting for energy supplies in geochemical systems that are far from equilibrium, and energy demands of microbes that reside in those systems, as described in the preceding chapters. Specifically, the work summarized above allows calculation of the energy demands to fuel microbial metabolism via the citric acid cycle (CAC) and provides two examples of how energy supplies in geochemical environments can be quantified in both serpentinizing ecosystems and the cold, dark biosphere. As a result there are many new paths of investigation to be pursued. With regard to the CAC, the predictions made in Chapter 2 can be tested with new experimental measurements. In particular, the estimations at temperatures > 250°C have the greatest uncertainties and are most susceptible to experimental challenge. As a logical follow-up to the summary of standard state data and prediction of equilibrium constants, it should be possible to constrain activity products for the same reactions using metabolite concentrations inside cells during various growth phases from many types of microorganisms. Right now, the most complete metabolome is for *E. coli*, which can help put some aspects of the CAC into perspective across P-T-affinity space.

Using data from Bennett et al. (2009), Peng et al. (2004), and Phillips et al. (2008), together with the *E. coli* metabolome database (http://ecmdb.ca/), affinity calculations can be made for all of the steps in the CAC and the overall cycle (Fig. 42). An example in Fig. 42A shows how the affinity for the conversion of *cis*-aconitate to isocitrate changes at temperatures from 0-200°C and pressures of ~1-5000 bars. The reaction is more energetically favorable at higher temperatures and pressures and has

negative affinities at low temperatures and pressures, which means that the reverse reaction is favorable. Analogous calculations done with all of the steps in the CAC can be summed to give an overall representation of the CAC. This is shown in Fig. 42B, where it can be seen that the overall CAC as a catabolic metabolism is more energetically favorable at higher temperature and lower pressures. In fact, the majority of P-T space where extremophiles dominate the microbial population would be energetically favorable for the reverse CAC (rCAC) and there are many documented cases (e.g. Campbell and Cary, 2004; Hügler et al., 2005; 2007) where extremophiles have been observed to use the rCAC. Once the metabolomes of extremophiles, barophiles, and psychrophiles are better known, similar calculations will clarify and quantify the anabolic and catabolic processes operating throughout the biosphere. Meanwhile, we can model plausible metabolome compositions and make predictions of how geochemical energy supplies are dissipated by microbial metabolism throughout the deep biosphere. It will also become possible to predict how metabolic strategies of microbial communities will shift in response to geochemical changes. Predictions of this type can help guide research in the cold biosphere where climate change is likely to have some of its strongest effects as glaciers and ice sheets melt.

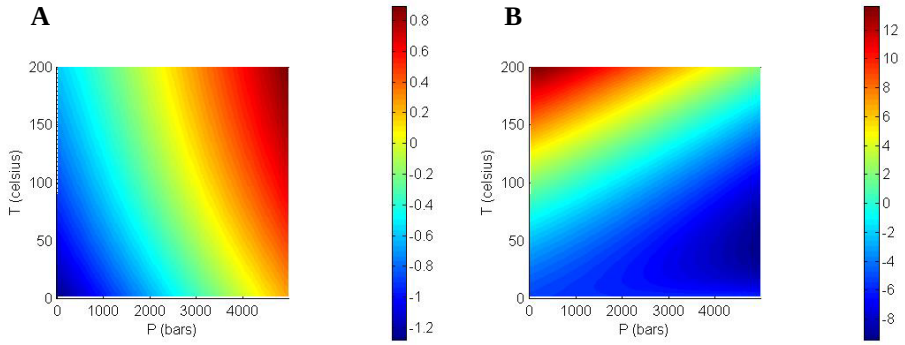

Figure 42. (A) Affinity of the conversion of cis-aconitate to isocitrate in the CAC and (B) the overall affinity of the CAC in the forward direction. Scale bar is in kcal per reaction turnover. Negative values of affinity mean that the reverse reaction is favorable, suggesting the release of energy as isocitrate is converted to cis-aconitate at all temperatures and low pressures, and identifying the rCAC as the energy-releasing direction for the cycle at psychrophilic and mesophilic conditions at low pressures, extending throughout thermophilic temperatures at the elevated pressures of the deep biosphere.

The results described in Chapter 3 for serpentinizing systems provide a foundation for expanded quantitative analyses of redox states, potentials for energetic processes, and resulting predictions for dominant metabolisms at all conditions where ultramafic rocks are altered. For instance, predictions of energy supplies in Fig. 17 can be combined with geochemical reaction path modeling to determine the extents to which water infiltration, fluid mixing, or water-rock reaction progress provide habitat for each type of metabolism. As shown in figure 43, carbon speciation is predicted to change as a function of the extent of mixing of surface water into water already present in a serpentinite aquifer (Fig. 43A), as well as during the serpentinization of fresh ultramafic rock (harzburgite) (Fig. 43B). During mixing, the thermodynamic drive to generate or maintain carbon in the form of dissolved methane decreases dramatically as surface water infiltrates into the aquifer. This indicates that the potential for methanogenesis in this

type of system is best maintained at the interface between the two fluids. During serpentinization, the percent of carbon present as bicarbonate diminishes at early stages of reaction progress, and is equal to dissolved methane when less than 0.1 moles of harzburgite have reacted with surface water. This indicates that the geochemical influences from the serpentinization process could start at relatively shallow depths and high water-to-rock ratios. If this is true, the depth at which methanogens are residing in the serpentinzing system would be relatively shallow. If methanogens are commonly present in serpentinizing systems, and if they inhabit near-surface environments, claims of abiotic methane production during serpentinization may need to be reconsidered (Etiope and Sherwood Loller, 2013; Etiope & Schoell, 2014; Etiope et al., 2016), especially in light of the experimental difficulties attending abiotic methane formation (McCollom, 2016). Predictions can be made based on the entire composition of aqueous fluids and for numerous metabolic strategies that can be verified through drilling and sampling of wells across serpentinizing systems, such as those planned to begin in 2017 through the Oman Drilling Project.

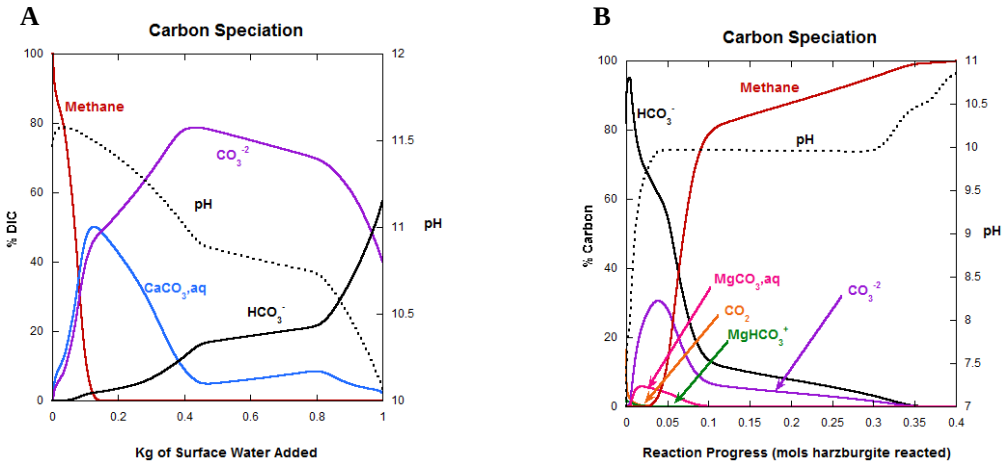

Figure 43. Carbon speciation during mixing of surface and hyperalkaline spring water (A), and during serpentinization (B) as revealed by reaction path calculations. Changes in the predicted speciation of dissolved inorganic carbon (DIC, including methane) are

monitored during the mixing process as the increased addition of surface water to a kilogram of water in a serpentine aquifer. Similarly, changes in aqueous carbon speciation are predicted as harzburgite reacts with a kilogram of surface water. In effect, the calculations in (B) reflect the processes that generate the serpentinized fluid involved in the mixing processes illustrated in (A).

Results for the cold biosphere, as described in Chapter 4, can be converted from affinity, and energy per fluid volume, to geochemical power supplies using fluid flow data. Subglacial fluid flow is highly variable with the seasons, maximizing in late summer and minimizing in mid-winter when fluid flow can nearly stop. Currents at the bottom of the ocean are likely to move fluids considerably more quickly that fluids flowing upward or outward through compacting sediments. Fluid flow into and out of lakes below the ice in Antarctica and elsewhere can be used to evaluate seasonal and decadal trends in geochemical power supplies. Each geochemical system of interest can be tested to determine when and where it can provide minimum power requirements for individual microbial metabolic processes or consortia of microbes. Because extreme cold can slow growth and doubling times in many of these systems, the minimum power supply requirements from the geochemical system may be far less than expected in warmer parts of the biosphere. The framework outlined in Chapter 4 can be used to design a comparative study that quantifies power supplies in cold environments with variable fluid-flow rates, and tests predictions about the resulting microbial responses.

Examining the power provided to microorganisms from geochemical processes is now possible for any system for which analytical geochemical data exist or can be gathered and for which flow rates are known or measurable. In the serpentinizing systems of the Samail Ophiolite many of the flow rates were measured or can be estimated for the springs described in Chapter 3. Even in cases where flow rates are not

known, geochemical power can be estimated using flow rate as a variable, which can be generalized throughout the cold biosphere and hydrothermal ecosystems as well. As a result of the work described above, combining calculations of geochemical energy and power supplies and connecting them with the intracellular metabolic processes of the CAC through speciation modeling of the cytoplasm of microbial cells is now a reality. These efforts pave the way for modeling the energy/power cost of intermembrane transport for various classes of microorganisms, and have the potential to provide powerful insights into the limits of known life, as well the potential for life and habitability elsewhere.

REFERENCES

Abrajano, T. A., Sturchio, N. C., Bohlke, J. K., Lyon, G. L., Poreda, R. J., & Stevens, C. M. (1988). Methane-hydrogen gas seeps, Zambales Ophiolite, Philippines: Deep or shallow origin?. *Chemical Geology*, **71**, 211-222.

Abyzov, S. S., Mitskevich, I. N. and Poglazova, M. N. (1998). Microflora of the deep glacier horizons of central Antarctica. *Microbiology*, **67**, 451-458.

Adhikari, R. R., Glombitza, C., Nickel, J. C., Anderson, C. H., Dunlea, A. G., Spivack, A. J., Murray, R.W., D'Hondt, S. and Kallmeyer, J. (2016). Hydrogen utilization potential in subsurface sediments. *Frontiers in microbiology*, **7**.

Alberty R. A. (1992a). Equilibrium calculations on systems of biochemical reactions at specified pH and pMg. *Biophysical Chemistry* **42**, 117-131.

Alberty R. A. (1992b). Calculation of transformed thermodynamic properties of biochemical reactants at specified pH and pMg. *Biophysical Chemistry* **43**, 239-254.

Alberty R. A. (1997). Apparent equilibrium constants and standard transformed Gibbs energies of biochemical reactions involving carbon dioxide. *Archives of Biochemistry and Biophysics* **348**, 116-124.

Alberty R. A. (1998a). Calculation of standard transformed Gibbs energies and standard transformed enthalpies of biochemical reactants. *Archives of Biochemistry and Biophysics* **353**, 116-130.

Alberty R. A. (1998b). Calculation of standard transformed entropies of formation of biochemical reactants and group contributions at specified pH. *Journal of Physical Chemistry A* **102**, 8460–8466.

Alberty R. A. (1998c). Calculation of standard transformed formation properties of biochemical reactants and standard apparent reduction potentials of half reactions. *Archives of Biochemistry and Biophysics* **358**, 25-39.

Alberty R. A. (2004). Equilibrium concentrations for pyruvate dehydrogenase and the citric acid cycle at specified concentrations of certain coenzymes. *Biophysical Chemistry*, **109**, 73-84.

Alberty, R. A. (2005). *Thermodynamics of biochemical reactions*. John Wiley & Sons.

Allen, D. E. and Seyfried, W. E. (2004). Serpentinization and heat generation: constraints from Lost City and Rainbow hydrothermal systems. *Geochimica et Cosmochimica Acta*, **68**, 1347-1354.

Amato, P., Hennebelle, R., Magand, O., Sancelme, M., Delort, A. M., Barbante, C., Boutron, C. and Ferrari, C. (2007). Bacterial characterization of the snow cover at Spitzberg, Svalbard. *FEMS Microbiology Ecology*, **59**, 255-264.

Amend J. P. and Helgeson H. C. (1997a). Group additivity equations of state for calculating the standard molal thermodynamic properties of aqueous organic species at elevated temperatures and pressures. *Geochimica et Cosmochimica Acta* **61**, 11-46.

Amend, J. P. and Helgeson, H. C. (1997b). Calculation of the standard molal thermodynamic properties of aqueous biomolecules at elevated temperatures and pressures Part 1L-α-Amino acids. *Journal of the Chemical Society, Faraday Transactions*, *93*(10), 1927-1941.

Amend, J. P. and Helgeson, H. C. (2000). Calculation of the standard molal thermodynamic properties of aqueous biomolecules at elevated temperatures and pressures II. Unfolded proteins. *Biophysical chemistry*, *84*(2), 105-136.

Amend J. P. and Plyasunov A. V. (2001). Carbohydrates in thermophile metabolism: Calculation of the standard molal thermodynamic properties of aqueous pentoses and hexoses at elevated temperatures and pressures. *Geochimica et Cosmochimica Acta* **65**, 3901–3917.

Amend, J. P. and Shock, E. L. (1998). Energetics of amino acid synthesis in hydrothermal ecosystems. *Science*, **281**, 1659-1662.

Amend J. P. and Shock E. L. (2001). Energetics of overall metabolic reactions in thermophilic and hyperthermophilic Archaea and Bacteria. *FEMS Microbiology Reviews* **25**, 175-243.

Amend J. P., Rogers K. L., Shock E. L., Gurrieri S. and Inguaggiato S. (2003). Energetics of chemolithoautotrophy in the hydrothermal system of Vulcano Island, southern Italy. *Geobiology* **1**, 37-58.

Amend J. P., Rogers K. L. and Meyer-Dombard D. R. (2004). Microbially mediated sulfur-redox: Energetics in marine hydrothermal vent systems. In *Sulfur Biogeochemistry: Past and Present* (eds J. P. Amend, K. J. Edwards and T. W. Lyons) Geological Society of America Boulder, CO. pp. 17–34.

Amend J. P., McCollom T. M., Hentscher M. and Bach W. (2011). Catabolic and anabolic energy for chemolithoautotrophs in deep-sea hydrothermal systems hosted in different rock types. *Geochimica et Cosmochimica Acta* **75**, 5736–5748.

Amend J. P., LaRowe D. E., McCollom T. M. and Shock E. L. (2013). The energetics of organic synthesis inside and outside the cell. *Philosophical Transactions of the Royal Society B* **368**, 20120255.

á Norði, K. and Thamdrup, B. (2014). Nitrate-dependent anaerobic methane oxidation in a freshwater sediment. *Geochimica et Cosmochimica Acta*, **132**, 141-150.

Anderson G. M. (2005). *Thermodynamics of Natural Systems*, 2nd edition. Cambridge University Press. Cambridge.

Apelblat, A., & Manzurola, E. (1990). Apparent molar volumes of organic acids and salts in water at 298.15 K. *Fluid Phase Equilibria*, *60*(1), 157-171.

Apelblat, A., Korin, E., & Manzurola, E. (2013). Thermodynamic properties of aqueous solutions with citrate ions. Compressibility studies in aqueous solutions of citric acid. *The Journal of Chemical Thermodynamics*, *64*, 14-21.

Apps, J. (2010). Geohydrological Studiies for Nculear Waste Isolation at the Hanford Reservation-Vol. I: Executive Summary; Vol. II: Final Report. *Lawrence Berkeley National Laboratory*.

Arcuri, E. J. and Ehrlich, H. L. (1977). Influence of hydrostatic pressure on the effects of the heavy metal cations of manganese, copper, cobalt, and nickel on the growth of three deep-sea bacterial isolates. *Applied and Environmental Microbiology*, **33**, 282-288.

Ash, C. H. and Arksey, R. L. (1989). The listwanite-lode gold association in British Columbia. *Geological fieldwork*, 359-364.

Ask, D., Stephansson, O., and Cornet, F.H ., 2001. Integrated stress analysis of hydraulic stress data in the Äspö region, Sweden. Analysis of hydraulic fracturing stress data and hydraulic test s on pre-existing fractures (HTPF) in boreholes KAS02, KAS03, and KLX02. *SKB International Progress Report*, IPR-01-26, Stockholm.

Bakermans, C., Ayala-del-Río, H. L., Ponder, M. A., Vishnivetskaya, T., Gilichinsky, D., Thomashow, M. F. and Tiedje, J. M. (2006). Psychrobacter cryohalolentis sp. nov. and Psychrobacter arcticus sp. nov., isolated from Siberian permafrost. *InternationalJournal of Systematic and Evolutionary Microbiology*, **56**, 1285-1291.

Bale, S. J., Goodman, K., Rochelle, P. A., Marchesi, J. R., Fry, J. C., Weightman, A. J. and Parkes, R. J. (1997). *Desulfovibrio profundus* sp. nov., a novel barophilic sulfate-reducing bacterium from deep sediment layers in the Japan Sea. *International Journal of Systematic Bacteriology*, **47**, 515-521.

Barnes, I., LaMarche, V. C. and Himmelberg, G. (1967). Geochemical evidence of present-day serpentinization. *Science*, **156**, 830-832.

Barnes, I. and O'Neil, J. R. (1969). The relationship between fluids in some fresh alpine-type ultramafics and possible modern serpentinization, western United States. *Geological Society of America Bulletin*, **80**, 1947-1960.

Barnes, I., O'neil, J. R. and Trescases, J. J. (1978). Present day serpentinization in New Caledonia, Oman and Yugoslavia. *Geochimica et Cosmochimica Acta*, **42**, 144-145.

Barrett, T. J. and Spooner, E. T. C. (1977). Ophiolitic breccias associated with allochthonous oceanic crustal rocks in the East Ligurian Apennines, Italy—a comparison with observations from rifted oceanic ridges. *Earth and Planetary Science Letters*, **35**, 79-91.

Bartlett, D. H. (2002). Pressure effects on in vivo microbial processes. *Biochimica et Biophysica Acta (BBA)-Protein Structure and Molecular Enzymology*, **1595**, 367-381.

Bath, A. H., Christofi, N., Neal, C., Philp, J. C., Cave, M. R., McKinley, I. G. and Berner, U. (1987). *Trace element and microbiological studies of alcaline groundwaters in Oman, Arabian Gulf: a natural analogue for cement pore-waters*. Nationale Genossenschaft fuer die Lagerung Radioaktiver Abfaelle (NAGRA), Baden (Switzerland).

Ben-Naim A. (1987) *Solvation Thermodynamics.* Plenum Press.

Bennett, B. D., Kimball, E. H., Gao, M., Osterhout, R., Van Dien, S. J. and Rabinowitz, J. D. (2009). Absolute metabolite concentrations and implied enzyme active site occupancy in Escherichia coli. *Nature Chemical Biology*, **5**, 593-599.

Benton, L. D., Ryan, J. G. and Tera, F. (2001). Boron isotope systematics of slab fluids as inferred from a serpentine seamount, Mariana forearc. *Earth and Planetary Science Letters*, **187**, 273-282.

Bernhardt, G., Jaenicke, R., Lüdemann, H. D., König, H. and Stetter, K. O. (1988). High pressure enhances the growth rate of the thermophilic archaebacterium Methanococcus thermolithotrophicus without extending its temperature range. *Applied and Environmental Microbiology*, **54**, 1258-1261.

Bhatia, M. (2004) *Molecular characterization of bacterial communities associated with a high Arctic polythermal glacier*. MSc thesis, Edmonton, Alberta, Canada: University of Alberta.

Bhatia, M., Sharp, M. and Foght, J. (2006). Distinct bacterial communities exist beneath a high Arctic polythermal glacier. *Applied and Environmental Microbiology*, **72**, 5838-5845.

Bhatia, M. P., Kujawinski, E. B., Das, S. B., Breier, C. F., Henderson, P. B. and Charette, M. A. (2013). Greenland meltwater as a significant and potentially bioavailable source of iron to the ocean. *Nature Geoscience*, **6**, 274-278.

Bill, M., O'Dogherty, L., Guex, J., Baumgartner, P. O. and Masson, H. (2001). Radiolarite ages in Alpine-Mediterranean ophiolites: Constraints on the oceanic

spreading and the Tethys-Atlantic connection. *Geological Society of America Bulletin*, **113**, 129-143.

Blackman D. K., Karson J. A., Kelley D. S., Cann J. R., Fru¨h- Green G. L., Gee J. S., Hurst S. D., John B. E., Morgan J., Nooner S. L., Ross D. K., Schroeder T. J. and Williams E. A. (2002). Geology of the Atlantis Massif (Mid-Atlantic Ridge, 30^{o}N): implications for the evolution of an ultramafic oceanic core complex. *Marine Geophysical Research* 23, 443–469.

Blackman, D. K., Slagle, A., Guerin, G. and Harding, A. (2014). Geophysical signatures of past and present hydration within a young oceanic core complex. *Geophysical Research Letters*, **41**, 1179-1186.

Blair J. M. (1968). Metal ions and enzyme equilibria: A mathematical treatment. *FEBS Letters* **1**, 100-103.

Blair, J. M. (1969). Magnesium and the aconitase equilibrium: Determination of apparent stability constants of magnesium substrate complexes from equilibrium data. *European Journal of Biochemistry*, *8*(2), 287-291.

Blank, J. G., Green, S. J., Blake, D., Valley, J. W., Kita, N. T., Treiman, A. and Dobson, P. F. (2009). An alkaline spring system within the Del Puerto Ophiolite (California, USA): a Mars analog site. *Planetary and Space Science*, **57**, 533-540.

Boetius, A., Ravenschlag, K., Schubert, C. J., Rickert, D., Widdel, F., Gieseke, A., Amann, R., Jorgensen, B.B., Witte, U. and Pfannkuche, O. (2000). A marine microbial consortium apparently mediating anaerobic oxidation of methane. *Nature*, **407**, 623-626.

Boettger, J., Lin, H. T., Cowen, J. P., Hentscher, M. and Amend, J. P. (2013). Energy yields from chemolithotrophic metabolisms in igneous basement of the Juan de Fuca ridge flank system. *Chemical Geology*, **337**, 11-19.

Bomatí-Miguel, O., Mazeina, L., Navrotsky, A., and Veintemillas-Verdaguer, S. (2008) Calorimetric study of maghemite nanoparticles synthesized by laser-induced pyrolysis. *Chemistry of Materials* **20**, 591-598.

Bonch-Osmolovskaya, E. A., Miroshnichenko, M. L., Lebedinsky, A. V., Chernyh, N. A., Nazina, T. N., Ivoilov, V. S., Belyaev, S.S., Boulygina, E.S., Lysov, Y.P., perov, A.N., Mirzabekov, A.D., Hippe, H., Stakebrandt, E., L'Haridon, S. and Jeanthon, C. (2003). Radioisotopic, culture-based, and oligonucleotide microchip analyses of thermophilic microbial communities in a continental high-temperature petroleum reservoir. *Applied and Environmental Microbiology*, **69**, 6143-6151.

Böning, P., Brumsack, H. J., Böttcher, M. E., Schnetger, B., Kriete, C., Kallmeyer, J. and Borchers, S. L. (2004). Geochemistry of Peruvian near-surface sediments. *Geochimica et Cosmochimica Acta*, **68**, 4429-4451.

Bonin, P. (1996). Anaerobic nitrate reduction to ammonium in two strains isolated from coastal marine sediment: a dissimilatory pathway. *FEMS Microbiology Ecology*, **19**, 27-38.

Born M. (1920) Volumen und Hydratationsw ärmen der Ionen. *Z. Phys.***1,** 45–48.

Borsook H. and Schott H. F. (1931a). The role of the enzyme in the succinate-enzyme-fumarate equilibrium. *Journal of Biological Chemistry* **92**, 535-557.

Borsook H. and Schott H. F. (1931b). The free energy, heat, and entropy of formation of L-malic acid. *Journal of Biological Chemistry* **92**, 559-567.

Boschetti, T. and Toscani, L. (2008). Springs and streams of the Taro–Ceno Valleys (Northern Apennine, Italy): Reaction path modeling of waters interacting with serpentinized ultramafic rocks. *Chemical Geology*, **257**, 76-91.

Boschetti, T., Etiope, G. and Toscani, L. (2013). Abiotic methane in the hyperalkaline springs of Genova, Italy. *Procedia Earth and Planetary Science*, **7**, 248-251.

Bottrell, S. H. and Tranter, M. (2002). Sulphide oxidation under partially anoxic conditions at the bed of the Haut Glacier d'Arolla, Switzerland. *Hydrological Processes*, **16**, 2363-2368.

Boulart, C., Chavagnac, V., Delacour, A., Monnin, C., Ceuleneer, G., Hoareau, G., (2012) New insights into gas compositions from hyperalkaline springs in Oman, Italy and New Caledonia. Presented at the Serpentine Days 2012, Porquerolles, France.

Boulart, C., Chavagnac, V., Monnin, C., Delacour, A., Ceuleneer, G. and Hoareau, G. (2013). Differences in gas venting from ultramafic-hosted warm springs: The example of Oman and Voltri ophiolites. *Ofioliti*, *38*(2), 143-156.

Boyd, E. S., Skidmore, M., Mitchell, A. C., Bakermans, C. and Peters, J. W. (2010). Methanogenesis in subglacial sediments. *Environmental Microbiology Reports*, **2**, 685-692.

Boyd, E. S., Lange, R. K., Mitchell, A. C., Havig, J. R., Hamilton, T. L., Lafrenière, M. J., Shock, E.L., Peters, J.W. and Skidmore, M. (2011). Diversity, abundance, and potential activity of nitrifying and nitrate-reducing microbial assemblages in a subglacial ecosystem. *Applied and Environmental Microbiology*, **77**, 4778-4787.

Bradley, A. S., Fredricks, H., Hinrichs, K. U. and Summons, R. E. (2009). Structural diversity of diether lipids in carbonate chimneys at the Lost City Hydrothermal Field. *Organic Geochemistry*, **40**, 1169-1178.

Braunschweig J., Klier C., Schröder C., Händel M., Bosch J., Totsche K.U. and Meckenstock R. U. (2014). Citrate influences microbial Fe hydroxide reduction via a dissolution-disaggregation mechanism. *Geochimica et Cosmochimica Acta* **139**, 434-446.

Bray A. W., Oelkers E. H., Bonneville S., Wolff-Boenisch D., Potts N. J., Fones G. and Benning L. G. (2015). The effect of pH, grain size, and organic ligands on biotite weathering rates. *Geochimica et Cosmochimica Acta* **164**, 127-145.

Brazelton, W. J., Schrenk, M. O., Kelley, D. S. and Baross, J. A. (2006). Methane-and sulfur-metabolizing microbial communities dominate the Lost City hydrothermal field ecosystem. *Applied and Environmental Microbiology*, **72**, 6257-6270.

Brazelton, W. J. and Baross, J. A. (2009). Abundant transposases encoded by the metagenome of a hydrothermal chimney biofilm. *The ISME Journal*, **3**, 1420-1424.

Brazelton, W. J. and Baross, J. A. (2010). Metagenomic comparison of two Thiomicrospira lineages inhabiting contrasting deep-sea hydrothermal environments. *PLoS One*, **5**, e13530.

Brazelton, W. J., Ludwig, K. A., Sogin, M. L., Andreishcheva, E. N., Kelley, D. S., Shen, C. C., Edwards, L.R. and Baross, J. A. (2010). Archaea and bacteria with surprising microdiversity show shifts in dominance over 1,000-year time scales in hydrothermal chimneys. *Proceedings of the National Academy of Sciences*, **107**, 1612-1617.

Brazelton, W. J., Mehta, M. P., Kelley, D. S. and Baross, J. A. (2011). Physiological differentiation within a single-species biofilm fueled by serpentinization. *MBio*, **2**, e00127-11.

Breezee, J., Cady, N. and Staley, J. T. (2004). Subfreezing growth of the sea ice bacterium "Psychromonas ingrahamii". *Microbial Ecology*, **47**, 300-304.

Brinkmeyer, R., Knittel, K., Jürgens, J., Weyland, H., Amann, R. and Helmke, E. (2003). Diversity and structure of bacterial communities in Arctic versus Antarctic pack ice. *Applied and Environmental Microbiology*, **69**, 6610-6619.

Brouwer, F. M., Vissers, R. L. and Lamb, W. M. (2002). Metamorphic history of eclogitic metagabbro blocks from a tectonic mélange in the Voltri Massif, Ligurian Alps, Italy. *Ofioliti*, **27**, 1-16.

Bruland, K. W.; Lohan, M. C. Controls on trace metals in seawater. In *Treatise on Geochemistry*; Elderfield, H. Ed.; Elsevier: Amsterdam, 2004; Vol. 6, pp 23-47.

Bruni J, Canepa M, Chiodini G, Cioni R, Cipolli F, Longinelli A, Marini L, Ottonello G, Zuccolini MV (2002). Irreversible water-rock mass transfer accompanying the generation of the neutral, Mg-HCO3 and high-pH, Ca-OH spring waters of the Genova province, Italy. *Applied Geochemistry*, **17,** 455-474.

Burdige, D. J. (1993). The biogeochemistry of manganese and iron reduction in marine sediments. *Earth-Science Reviews*, **35**, 249-284.

Burton K. (1955). The free energy change associated with the hydrolysis of the thiol ester bond of acetyl coenzyme A. *Biochemical Journal* **59**, 44-46.

Burton K. (1957). Free energy data of biological interest. *Ergebnisse der Physiologie, biologischen Chemie und Experimentellen Pharmakologie* **49**, 275-298.

Burton K. and Krebs H. A. (1953). The free-energy changes associated with the individual steps of the tricarboxylic acid cycle, glycolysis and alcoholic fermentation and with the hydrolysis of the pyrophosphate groups of adenosinetriphosphate. *Biochemical Journal* **54**, 94-107.

Burton K. and Wilson T. H. (1953). The free-energy changes for the reduction of diphosphopyridine nucleotide and the dehydrogenation of L-malate and L-glycerol 1-phosphate. *Biochemical Journal* **54**, 86-94.

Byers, H. K., Stackebrandt, E., Hayward, C. and Blackall, L. L. (1998). Molecular investigation of a microbial mat associated with the great artesian basin. *FEMS Microbiology Ecology*, **25**, 391-403.

Cabani S., Conti G., Mollica V. and Lepori L. (1975). Thermodynamic study of dilute aqueous solutions of organic compounds. Part 4. — Cyclic and straight chain secondary alcohols. *Journal of the Chemical Society, Faraday Transactions 1: Physical Chemistry in Condensed Phases* **71**, 1943-1952.

Cabani, S. and Gianni, P. (1986). Gas-liquid and solid-liquid phase equilibria in binary aqueous systems of nonelectrolytes. In *Thermodynamic Data for Biochemistry and Biotechnology* (pp. 259-275). Springer Berlin Heidelberg.

Campbell, B. J., & Cary, S. C. (2004). Abundance of reverse tricarboxylic acid cycle genes in free-living microorganisms at deep-sea hydrothermal vents. *Applied and Environmental Microbiology*, **70**, 6282-6289.

Canganella, F., Gonzalez, J. M., Yanagibayashi, M., Kato, C. and Horikoshi, K. (1997). Pressure and temperature effects on growth and viability of the hyperthermophilic archaeon Thermococcus peptonophilus. *Archives of Microbiology*, **168**, 1-7.

Canion, A., Prakash, O., Green, S. J., Jahnke, L., Kuypers, M. M. and Kostka, J. E. (2013). Isolation and physiological characterization of psychrophilic denitrifying bacteria from permanently cold Arctic fjord sediments (Svalbard, Norway). *Environmental Microbiology*, **15**, 1606-1618.

Canyon, N., De Stigter, H. C. And Party, S. Shipboard Report Of Cruise 64pe138 With Rv “Pelagia” Texel To Texel, The Netherlands 8 May–1 June, 1999.

Cao, X., Liu, X. and Dong, X. (2003). Alkaliphilus crotonatoxidans sp. nov., a strictly anaerobic, crotonate-dismutating bacterium isolated from a methanogenic environment. *International Journal of Systematic and Evolutionary Microbiology*, **53,** 971-975.

Cardace, D., Hoehler, T., McCollom, T., Schrenk, M., Carnevale, D., Kubo, M. and Twing, K. (2013). Establishment of the Coast Range ophiolite microbial observatory (CROMO): drilling objectives and preliminary outcomes. *Scientific Drilling*, **16**, 45-55.

Cardace, D., D'Arcy, R., Woycheese, K. M. and Arcilla, C. A. (2015). Feasible metabolisms in high pH springs of the Philippines. *Frontiers in microbiology*, **6**. 10.

Carvalho, V. M. L. (2013). *Metagenomic analysis of Mariana Trench sediment samples* (Doctoral dissertation).

Chase, M.W.Jr. (1998). NIST-JANAF Thermochemical Tables. Fourth Edition, Part I, Al-Co. *Journal of Physical and Chemical Reference Data*, Mongraph No. 9.

Chavagnac, V., Ceuleneer, G., Monnin, C., Lansac, B., Hoareau, G. and Boulart, C. (2013a). Mineralogical assemblages forming at hyperalkaline warm springs hosted on ultramafic rocks: a case study of Oman and Ligurian ophiolites. *Geochemistry, Geophysics, Geosystems*, **14**, 2474-2495.

Chavagnac, V., Monnin, C., Ceuleneer, G., Boulart, C. and Hoareau, G. (2013b). Characterization of hyperalkaline fluids produced by low-temperature serpentinization of mantle peridotites in the Oman and Ligurian ophiolites. *Geochemistry, Geophysics, Geosystems*, **14**, 2496-2522.

Chivian, D., Brodie, E. L., Alm, E. J., Culley, D. E., Dehal, P. S., DeSantis, T. Z., Gihring, T.M., Lapidus, A., Lin,L-H, Lowry, S.R., Moser, D.P., Richardson, P.M., Southman, G., Wanger, G., Pratt, L.M., Anderson, G.L., Hazen, T.C., Brockman, F.J., Arkin, A.P. and Onstott, T. C. (2008). Environmental genomics reveals a single-species ecosystem deep within Earth. *Science*, **322**, 275-278.

Cavicchioli, R., Thomas, T. and Curmi, P. M. (2000). Cold stress response in Archaea. *Extremophiles*, **4**, 321-331.

Cheng, S. M. and Foght, J. M. (2007). Cultivation-independent and-dependent characterization of bacteria resident beneath John Evans Glacier. *FEMS Microbiology Ecology*, **59**, 318-330.

Christensen J. J., Izatt R. M. and Hansen L. D. (1967). Thermodynamics of proton ionization in dilute aqueous solution. VII. ΔH° and ΔS° values for proton ionization from carboxylic acids at 25°. Journal of the *American Chemical Society* **89**, 213-222.

Christensen J. J., Hansen L. D. and Izatt R. M. (1976). *Handbook of Proton Ionization Heats and Related Thermodynamic Quantities*. Wiley and Sons, New York.

Christner, B. C., Mosley-Thompson, E., Thompson, L. G., Zagorodnov, V., Sandman, K. and Reeve, J. N. (2000). Recovery and identification of viable bacteria immured in glacial ice. *Icarus*, **144**, 479-485.

Christner, B. C., Mosley-Thompson, E., Thompson, L. G. and Reeve, J. N. (2001). Isolation of bacteria and 16S rDNAs from Lake Vostok accretion ice. *Environmental Microbiology*, **3**, 570-577.

Christner, B. C., Mosley-Thompson, E., Thompson, L. G. and Reeve, J. N. (2003). Bacterial recovery from ancient glacial ice. *Environmental Microbiology*, **5**, 433-436.

Christner, B. C., Royston-Bishop, G., Foreman, C. M., Arnold, B. R., Tranter, M., Welch, K. A., Lyons W.B., Tsapin, A.I., Studinger, M. and Priscu, J. C. (2006). Limnological conditions in subglacial Lake Vostok, Antarctica. *Limnology and Oceanography*, **51**, 2485-2501.

Christner, B. C., Skidmore, M. L., Priscu, J. C., Tranter, M. and Foreman, C. M. (2008). Bacteria in subglacial environments. In *Psychrophiles: From Biodiversity to Biotechnology* (pp. 51-71). Springer Berlin Heidelberg.

Christner, B. C., Priscu, J. C., Achberger, A. M., Barbante, C., Carter, S. P., Christianson, K., Michaud, A.B., Mikucki, J.A., Mitchell, C., Skidmore, M.L., Vick-Majors, T. J. and the WISSARD Science Team (2014). A microbial ecosystem beneath the West Antarctic ice sheet. *Nature*, **512**, 310-313.

Cipolli, F., Gambardella, B., Marini, L., Ottonello, G. and Zuccolini, M. V. (2004). Geochemistry of high-pH waters from serpentinites of the Gruppo di Voltri (Genova, Italy) and reaction path modeling of CO 2 sequestration in serpentinite aquifers. *Applied Geochemistry*, **19**, 787-802.

Clark, I. D. and Fontes, J. C. (1990). Paleoclimatic reconstruction in northern Oman based on carbonates from hyperalkaline groundwaters. *Quaternary Research*, **33**, 320-336.

Clark, I. D., Fontes, J. C. and Fritz, P. (1992). Stable isotope disequilibria in travertine from high pH waters: laboratory investigations and field observations from Oman. *Geochimica et Cosmochimica Acta*, **56**, 2041-2050.

Clarke, E. C. W. and Glew, D. N. (1980). Evaluation of Debye–Hückel limiting slopes for water between 0 and 150° C. *Journal of the Chemical Society, Faraday Transactions 1: Physical Chemistry in Condensed Phases* **76**, 1911-1916.

Codispoti, L. A. (2007). An oceanic fixed nitrogen sink exceeding 400 Tg N a? 1 vs the concept of homeostasis in the fixed-nitrogen inventory. *Biogeosciences*, **4**, 233-253.

Codispoti, L. A., Brandes, J. A., Christensen, J. P., Devol, A. H., Naqvi, S. W. A., Paerl, H. W. and Yoshinari, T. (2001). The oceanic fixed nitrogen and nitrous oxide budgets: Moving targets as we enter the anthropocene?. *Scientia Marina*, **65**, 85-105.

Coleman, R. G. (1981). Tectonic setting for ophiolite obduction in Oman. *Journal of Geophysical Research: Solid Earth (1978–2012)*, **86**, 2497-2508.

Collins, R. E., Rocap, G. and Deming, J. W. (2010). Persistence of bacterial and archaeal communities in sea ice through an Arctic winter. *Environmental Microbiology*, **12**, 1828-1841.

Conrad, R. (1996). Soil microorganisms as controllers of atmospheric trace gases (H_2, CO, CH_4, OCS, N_2O, and NO). *Microbiological Reviews*, **60**, 609-640.

Cornell, R. M. and Schwertmann, U. (2003). *The Iron Oxides: Structure, Properties, Reactions, Occurrences and Uses*. John Wiley and Sons.

Costa, K.C., Navarro, J.B., Shock, E.L. Zhang, C.L., Soukup, D. and Hedlund, B.P. (2009). Microbiology and geochemistry of Great Boiling and Mud Hot Springs in the United States Great Basin. *Extremophiles* **13**, 447-459.

Cowen, James P.; Giovannoni, Stephen J.; Kenig, Fabien; Johnson, H. Paul; Butterfield, David; Rappe, Michael S.; Hutnak, Michael; Lam, Phyllis (2003). Fluids from aging ocean crust that support microbial life. *Science* **299**, 120-123.

Cox, M. E., Launay, J. and Paris, J. P. (1982). Geochemistry of low temperature geothermal systems in New Caledonia. In *Proceedings of Pacific Geothermal Conference* (pp. 453-459).

Cox J. D., Wagman D. D. and Medvedev V.A. (1989). *CODATA Key Values for Thermodynamics*. Hemisphere, New York.

Criss, C. M., & Wood, R. H. (1996). Apparent molar volumes of aqueous solutions of some organic solutes at the pressure 28 MPa and temperatures to 598 K. *The Journal of Chemical Thermodynamics*, *28*(7), 723-741.

Curtis, G. P. (2003). Comparison of approaches for simulating reactive solute transport involving organic degradation reactions by multiple terminal electron acceptors. *Computers and Geosciences*, **29**, 319-329.

Curtis, A. C. and Moyer, C. L. (2005, December). Mariana Forearc serpentine mud volcanoes harbor novel communities of extremophilic Archaea. In *AGU Fall Meeting Abstracts* (Vol. 1, p. 1510).

Curtis, A. C., Wheat, C. G., Fryer, P. and Moyer, C. L. (2013). Mariana Forearc serpentinite mud volcanoes harbor novel communities of extremophilic archaea. *Geomicrobiology Journal*, **30**, 430-441.

D'Elia, T., Veerapaneni, R. and Rogers, S. O. (2008). Isolation of microbes from Lake Vostok accretion ice. *Applied and Environmental Microbiology*, **74**, 4962-4965.

D'Hondt, S., Jørgensen, B. B., Miller, D. J., Batzke, A., Blake, R., Cragg, B. A., Cypionka, H., Dickens, G.R., Ferdelman, T., Hinrichs, K., Holm, N. G., Mitterer, R., Spivack, A., Wang, G., Bekins, B., Engelen, B., Ford, K., Gettemy, G., Rutherford, S.D., Sass, H., Skilbeck, C.G., Aiello, I.W., Gurin, G., House, C.H., Inagaki, F., Meister, P., Naehr, T., Niitsuma, S., Parkes, R.J., Schippers, A., Smith, D.C., Teske, A., Wiegel, J., Padilla, C.N., Acosta, J.L.S. (2004). Distributions of microbial activities in deep subseafloor sediments. *Science*, **306**, 2216-2221.

Dale, J. D., Shock, E. L., Macleod, G., Aplin, A. C. and Larter, S. R. (1997). Standard partial molal properties of aqueous alkylphenols at high pressures and temperatures. *Geochimica et Cosmochimica Acta* **61**, 4017-4024.

Dalla-Betta P. and Schulte M. (2009). Calculation of the aqueous thermodynamic properties of citric acid cycle intermediates and precursors and the estimation of high temperature and pressure equation of state parameters. *International Journal of Molecular Sciences* **10**, 2809-2837.

Dalsgaard, T., Thamdrup, B. and Canfield, D. E. (2005). Anaerobic ammonium oxidation (anammox) in the marine environment. *Research in Microbiology*, **156**, 457-464.

Daumas, S., Lombart, R. and Bianchi, A. (1986). A bacteriological study of geothermal spring waters dating from the Dogger and Trias period in the Paris basin. *Geomicrobiology Journal*, **4**, 423-433.

Daumas, S., Cord-Ruwisch, R. and Garcia, J. L. (1988). Desulfotomaculum geothermicum sp. nov., a thermophilic, fatty acid-degrading, sulfate-reducing bacterium isolated with H_2 from geothermal ground water. *Antonie van Leeuwenhoek*, **54**, 165-178.

de Donder T. (1927) *L'Affinite*. Gauthiers-Villars, Paris.

de Donder T. and Van Rysselberghe P. (1936) *Affinity*. Stanford University Press, Menlo Park, California.

Death, R., Wadham, J. L., Monteiro, F., Le Brocq, A. M., Tranter, M., Ridgwell, A., Dutkiewicz, S. and Raiswell, R. (2014). Antarctic ice sheet fertilises the Southern Ocean. *Biogeosciences*, **11**, 2635-2643.

Decker K., Jungermann K. and Thauer R. K. (1970). Energy production in anaerobic organisms. *Angewandte Chemie International Edition in English*, **9**, 138-158.

Delacour, A., Früh-Green, G. L., Frank, M., Bernasconi, S. M., Boschi, C. and Kelley, D. S. (2004, December). Fluid-rock interaction in the basement of the Lost City Vent Field: Insights from stable and radiogenic isotopes. In *AGU Fall Meeting Abstracts* (Vol. 1, p. 0198).

Declercq J., Bosc, O. and Oelkers E. H. (2013). Do organic ligands affect forsterite dissolution rates? *Applied Geochemistry* **39**, 69-77.

DeLong, E. F., Franks, D. G. and Yayanos, A. A. (1997). Evolutionary relationships of cultivated psychrophilic and barophilic deep-sea bacteria. *Applied and Environmental Microbiology*, **63**, 2105-2108.

Delwiche M, Colwell FS, Tseng H-Y, Gao G, Onstott TC. (1996) Pressure and temperature adaptation of a bacterium recovered from 2.8 kilometers beneath the surface of the Earth. Abstr. 96th Ann Mtg Am Soc Microbial, New Orleans.

Deming, J. W. and Baross, J. A. (1986). Solid medium for culturing black smoker bacteria at temperatures to 120 C. *Applied and Environmental Microbiology*, **51**, 238-243.

Deming, J. W., Somers, L. K., Straube, W. L., Swartz, D. G. and Macdonell, M. T. (1988). Isolation of an Obligately barophilic bacterium and description of a new genus, *Colwellia* gen. nov. *Systematic and Applied Microbiology*, **10**, 152-160.

Deutzmann, J. S. and Schink, B. (2011). Anaerobic oxidation of methane in sediments of Lake Constance, an oligotrophic freshwater lake. *Applied and Environmental Microbiology*, **77**, 4429-4436.

Devol, A. H., Codispoti, L. A. and Christensen, J. P. (1997). Summer and winter denitrification rates in western Arctic shelf sediments. *Continental Shelf Research*, **17**, 1029-1050.

Dick J. M. (2008). Calculation of the relative metastabilities of proteins using the CHNOSZ software package. *Geochemical Transactions* **9**:10. doi: 10.1186/1467-4866-9-10.

Dick, J.M. and Shock, E.L. (2011). Calculation of the relative chemical stabilities of proteins as a function of temperature and redox chemistry in a hot spring. *PLoS ONE* **6**(8), e22782. doi:10.1371/journal.pone.0022782.

Dick, J.M. and Shock, E.L. (2013) A metastable equilibrium model for the relative abundances of microbial phyla in a hot spring. *PLoS ONE* **8**, e72395. doi:10.1371/journal. pone.0072395.

Dick J. M., LaRowe D. E., and Helgeson H. C. (2005). Group additivity calculation of the standard molal thermodynamic properties of aqueous amino acids, polypeptides and unfolded proteins as a function of temperature, pressure and ionization state. *Biogeosciences Discussions* **2**, 1515-1615.

Dick J., LaRowe D. and Helgeson H. C. (2006) Temperature, pressure, and electrochemical constraints on protein speciation: Group additivity calculation of the standard molal thermodynamic properties of ionized unfolded proteins. *Biogeosciences* **3**, 311-336.

Dodsworth J. A., McDonald A. I. and Hedlund B. P. (2012). Calculation of total free energy yield as an alternative approach for predicting the importance of potential chemolithotrophic reactions in geothermal springs. *FEMS Microbiology Ecology* **81**, 446-454.

ECMDB: The E. coli Metabolome Database. Guo AC, Jewison T, Wilson M, Liu Y, Knox C, Djoumbou Y, Lo P, Mandal R, Krishnamurthy R, Wishart DS. Nucleic Acids Res. 2012 Jan;41(Database issue):D625-30. 23109553.

Eden M. and Bates R. G. (1959) Resolution of the dissociation constants of d,l-malic acid from 0 °C to 50 °C *Journal of Research of the National Bureau of Standards* **62**, 161-170.

Edwards, K. J., Rogers, D. R., Wirsen, C. O. and McCollom, T. M. (2003). Isolation and characterization of novel psychrophilic, neutrophilic, Fe-oxidizing, chemolithoautotrophic α-and γ-Proteobacteria from the deep sea. *Applied and Environmental Microbiology*, **69**, 2906-2913.

Edwards, Katrina J.; Bach, Wolfgang; McCollom, Thomas M. (2005). Geomicrobiology in oceanography: microbe-mineral interactions at and below the seafloor. *TRENDS in Microbiology* **13**, 449-456.

Ehrlich, H. L., W. C. Ghiorse, and G. L. Johnson (1972). Distribution of microbes in manganese nodules from the Atlantic and Pacific oceans. *Developments in Industrial Miccrobiology* **13**, 57-65.

Ekendahl, S. and Pedersen, K. (1994). Carbon transformations by attached bacterial populations in granitic groundwater from deep crystalline bed-rock of the Stripa research mine. *Microbiology*, **140**, 1565-1573.

Ellis, W.L., and Ege, J.R. (1975) Determination of *in situ* stress in U12g tunnel, Rainier Mesa, Nevada Test Site, Nevada: *U.S. Geological Survey report RSGS* – 474- 219, 18.p.

Erauso, G., Reysenbach, A. L., Godfroy, A., Meunier, J. R., Crump, B., Partensky, F., Baross, J.A., Marteinsson, V., Barbier, G., Pace, N.R., and Prieur, D. (1993). *Pyrococcus abyssi* sp. nov., a new hyperthermophilic archaeon isolated from a deep-sea hydrothermal vent. *Archives of Microbiology*, **160**, 338-349.

Etiope, G. and Sherwood Lollar, B. (2013). Abiotic methane on Earth. *Reviews of Geophysics*, **51**, 276-299.

Etiope, G., Schoell, M. and Hosgörmez, H. (2011). Abiotic methane flux from the Chimaera seep and Tekirova ophiolites (Turkey): understanding gas exhalation from low temperature serpentinization and implications for Mars. *Earth and Planetary Science Letters*, **310**, 96-104.

Etiope, G., Tsikouras, B., Kordella, S., Ifandi, E., Christodoulou, D. and Papatheodorou, G. (2013a). Methane flux and origin in the Othrys ophiolite hyperalkaline springs, Greece. *Chemical Geology*, **347**, 161-174.

Etiope, G., Vance, S., Christensen, L. E., Marques, J. M. and da Costa, I. R. (2013b). Methane in serpentinized ultramafic rocks in mainland Portugal. *Marine and Petroleum Geology*, **45**, 12-16.

Etiope, G. and Schoell, M. (2014). Abiotic gas: atypical, but not rare. *Elements*, **10**, 291-296.

Etiope, G., Vadillo, I., Whiticar, M. J., Marques, J. M., Carreira, P. M., Tiago, I., Benavente, J., Jimenez, P. and Urresti, B. (2016). Abiotic methane seepage in the Ronda peridotite massif, southern Spain. *Applied Geochemistry*, **66**, 101-113.

Facq S., Daniel I., Montagnac G., Cardon H. and Sverjensky D. A. (2014) *In situ* Raman study and thermodynamic model of aqueous carbonate speciation in equilibrium with aragonite under subduction zone conditions. *Geochimica et Cosmochimica Acta* **132**, 375-390.

Falk, E. S. (2014). *Carbonation of Peridotite in The Oman Ophiolite* (Doctoral dissertation, Columbia University).

Falk, E. S. and Kelemen, P. B. (2015). Geochemistry and petrology of listvenite in the Samail ophiolite, Sultanate of Oman: Complete carbonation of peridotite during ophiolite emplacement. *Geochimica et Cosmochimica Acta*, **160**, 70-90.

Fardeau, M. L., Magot, M., Patel, B. K., Thomas, P., Garcia, J. L. and Ollivier, B. (2000). *Thermoanaerobacter subterraneus* sp. nov., a novel thermophile isolated from oilfield

water. *International Journal of Systematic and Evolutionary Microbiology*, **50**, 2141-2149.

Fell, J. W. (1967) Distribution of yeasts in the Indian Ocean. *Bulletin of Marine Science* **17**, 454-470.

Fenclová, D., Perez-Casas, S., Costas, M. and Dohnal, V. (2004). Partial molar heat capacities and partial molar volumes of all of the isomeric (C3 to C5) alkanols at infinite dilution in water at 298.15 K. *Journal of Chemical & Engineering Data*, **49**, 1833-1838.

Foght, J., Aislabie, J., Turner, S., Brown, C. E., Ryburn, J., Saul, D. J. and Lawson, W. (2004). Culturable bacteria in subglacial sediments and ice from two southern hemisphere glaciers. *Microbial Ecology*, **47**, 329-340.

Foustoukos, D. I., Savov, I. P. and Janecky, D. R. (2008). Chemical and isotopic constraints on water/rock interactions at the Lost City hydrothermal field, 30 N Mid-Atlantic Ridge. *Geochimica et Cosmochimica Acta*, **72**, 5457-5474.

Frank K. L., Rogers K.L., Rogers D.R., Johnston D.T. and Girguis P.R. (2015). Key factors influencing rates of heterotrophic sulfate reduction in active seafloor hydrothermal massive sulfide deposits. *Frontiers in Microbiology* **6**,1449. doi: 10.3389/fmicb.2015.01449

Friedman, H. L. and Krishnan, C. V. (1973). Thermodynamics of ionic hydration. In *Aqueous Solutions of Simple Electrolytes* (pp. 1-118). Springer US.

Fritz P, Clark ID, Fontes JC, Whiticar MJ, Faber E (1992). Deuterium and ^{13}C evidence for low temperature production of hydrogen and methane in a highly alkaline groundwater environment in Oman. *In:* Proceedings of the 7th International Symposium on Water-Rock Interaction. Kharaka Y, Maest AS (eds), Rotterdam Balkama, p 792-796.

Früh-Green, G. L., Kelley, D. S., Bernasconi, S. M., Karson, J. A., Ludwig, K. A., Butterfield, D. A., Boschi, A. and Proskurowski, G. (2003). 30,000 years of hydrothermal activity at the Lost City vent field. *Science*, **301**, 495-498.

Fryer, P., Ambos, E. L. and Hussong, D. M. (1985). Origin and emplacement of Mariana forearc seamounts. *Geology*, **13**, 774-777.

Fryer, P., Pearce, J.A., Stokking, L.B., Ali, J.R., Arculus, R., Ballotti, D., Burke, M.M., Ciampo, G., Haggerty, J.A., Haston, R.B., Dietrich, H., Hobart, M.A., Ishii, T., Johnson, L.E., Lagabrielle, Y., McCoy, F.W., Maekawa, H., Marlo, M.S., Milner, G., Mottl, M.J., Murton, B.J., Phipps, S.P., Rigsby, C.A., Saboda, K.L., Stabell, B., van der Laan, S., Xu, Y. (1990). Bonin/Marian region covering Leg 125 of the cruises of the drilling vessel JOIIDES Resolution, Apra harbor, Guam, to Tokyo, Japan, sites 778-786. In: Fryer, P., Pearce, J.A., Stokking, L.B., et al. (Eds), *Proceedings of the Ocean Drilling Progra Initial Reports*, 125, pp. 367-380.

Fryer, P., Wheat, C. G. and Mottl, M. J. (1999). Mariana blueschist mud volcanism: Implications for conditions within the subduction zone. *Geology*, **27**, 103-106.

Fryer, P. and Todd, C., (1999) Mariana blueschist mud volcanism sampling the subducted slab. EOS. AGU 80, S349.

Fryer, P., Lockwood,J., Becker, N., Todd, C, Phipps, S. (2000) Significance of serpentine and blueschist mud volcanism in convergent margin settings. In: Dilek, Y., et al. (Ed.), Ophiolites and Oceanic Crust: New Insights from Field Studies and Ocean Drillling Program: Special Papers Geological Socitey of America, 349. pp. 35-51.

Fryer, P. B. and Salisbury, M. H. (2006). Leg 195 synthesis: Site 1200-Serpentinite seamounts of the Izu-Bonin/Mariana convergent plate margin (ODP Leg 125 and 195 drilling results). In *Proceedings of the ODP, Scientific Results* (Vol. 195, pp. 1-30).

Fujii, N., Arcilla, C. A., Yamakawa, M., Pascua, C., Namiki, K., Sato, T., Shikazono,N. and Alexander, W. R. (2010, January). Natural analogue studies of bentonite reaction under hyperalkaline conditions: Overview of ongoing work at the Zambales Ophiolite, Philippines. In *ASME 2010 13th International Conference on Environmental Remediation and Radioactive Waste Management* (pp. 41-50). American Society of Mechanical Engineers.

Gaidos, E., Lanoil, B., Thorsteinsson, T., Graham, A., Skidmore, M., Han, S. K., Rust, R. and Popp, B. (2004). A viable microbial community in a subglacial volcanic crater lake, Iceland. *Astrobiology*, **4**, 327-344.

Gaidos, E., Marteinsson, V., Thorsteinsson, T., Johannesson, T., Rúnarsson, Á. R., Stefansson, A., Glazer, B., Lanoil, B., Skidmoer, M., Han, S., Miller, M., Rusch, A. and Foo, W. (2009). An oligarchic microbial assemblage in the anoxic bottom waters of a volcanic subglacial lake. *The ISME Journal*, **3**, 486-497.

Gajewski E., Goldberg R. N. and Steckler D. K. (1985). Thermodynamics of the conversion of fumarate to L-(-) malate. *Biophysical Chemistry* **22**, 187-195.

Garnier, J. (1871). *Voyage autour du monde: La Nouvelle-Calédonie (côte orientale)*. H. Plon.

Geprägs, P., Torres, M. E., Mau, S., Kasten, S., Römer, M. and Bohrmann, G. (2016). Carbon cycling fed by methane seepage at the shallow Cumberland Bay, South Georgia, sub-Antarctic. *Geochemistry, Geophysics, Geosystems*, **17**, 1401-1418.

Gihring, T. M., Lavik, G., Kuypers, M. M. and Kostka, J. E. (2010). Direct determination of nitrogen cycling rates and pathways in Arctic fjord sediments (Svalbard, Norway). *Limnology and Oceanography*, **55**, 740-752.

Glennie, K. W., Boeuf, M. G. A., Clarke, M. H., Moody-Stuart, M., Pilaar, W. F. H. and Reinhardt, B. M. (1973). Late Cretaceous nappes in Oman Mountains and their geologic evolution. *AAPG Bulletin*, *57*(1), 5-27.

Goldberg, R. N. and Tewari, Y. B. (1991). Thermodynamics of the disproportionation of adenosine 5′-diphosphate to adenosine 5′-triphosphate and adenosine 5′-monophosphate: I. Equilibrium model. *Biophysical Chemistry* **40**, 241-261.

Goldberg R. N., Gajewski E., Steckler D. K. and Tewari Y. B. (1986). Thermodynamics of the conversion of aqueous L-aspartic acid to fumaric acid and ammonia, *Biophysical Chemistry* **24**, 13-23.

Goldberg, R. N., Tewari, Y. B. and Bhat, T. N. (2007). Thermodynamics of enzyme-catalyzed reactions: Part 7—2007 update. *Journal of Physical and Chemical Reference Data*, ***36***(4), 1347-1397.

Goodenough, K. M., Styles, M. T., Schofield, D., Thomas, R. J., Crowley, Q. C., Lilly, R. M., McKervey, J. and Carney, J. N. (2010). Architecture of the Oman–UAE ophiolite: Evidence for a multi-phase magmatic history. *Arabian Journal of Geosciences*, *3*(4), 439-458.

Grabowski, A., Tindall, B. J., Bardin, V., Blanchet, D. and Jeanthon, C. (2005). Petrimonas sulfuriphila gen. nov., sp. nov., a mesophilic fermentative bacterium isolated from a biodegraded oil reservoir. *InternationalJournal of Systematic and Evolutionary Microbiology*, **55**, 1113-1121.

Greene, A. C., Patel, B. K. and Sheehy, A. J. (1997). *Deferribacter thermophilus* gen. nov., sp. nov., a novel thermophilic manganese-and iron-reducing bacterium isolated from a petroleum reservoir. *International Journal of Systematic Bacteriology*, **47**, 505-509.

Grossman, D. and Shulman, S. (1995). The biosphere below. *Earth (Waukesha, Wis.)*, **4**, 34-40.

Grue, A. M., Fritsen, C. H. and Priscu, J. C. (1996). Nitrogen fixation within permanent ice covers on lakes in the McMurdo Dry Valleys, Antarctica. *Antarctic Journal of the United States*, **31**, 218-220.

Haas J. R and Shock E. L. (1999). Halocarbons in the environment: Estimates of thermodynamic properties for aqueous chloroethylene species and their stabilities in natural settings. *Geochimica et Cosmochimica Acta* **63**, 3429-3441.

Haas J. R., Shock E. L. and Sassani D. C. (1995). Rare earth elements in hydrothermal systems: Estimates of standard partial molal thermodynamic properties of aqueous complexes of the REE at high pressures and temperatures. *Geochimica et Cosmochimica*

Acta **59**, 4329-4350.

Hacker BR, Mosenfelder JL, Gnos E (1996). Rapid emplacement of the Oman ophiolite: Thermal and geochronologic constraints. *Tectonics* **15,** 1230-1247. doi:10.1029/96tc01973.

Haggerty JA, Fisher JB (1992). Short-chain organic acids in interstitial waters from Mariana and Bonin forearc serpentinites: Leg 1251. *In:* Proceedings of the Ocean Drilling Program, Scientific Results. Fryer P, Coleman P, Pearce JA, Stokking LB (eds) College Station, Texas Ocean Drilling Program, p 387-395, doi: 10.2973/odp.proc.sr.125.125.1992.

Haldeman, D. L., Amy, P. S., Ringelberg, D. and White, D. C. (1993). Characterization of the microbiology within a 21 m^3 section of rock from the deep subsurface. *Microbial Ecology*, **26**, 145-159.

Hallet, B. (1976). Deposits formed by subglacial precipitation of $CaCO_3$. *Geological Society of America Bulletin*, **87**, 1003-1015.

Hamilton, T. L., Peters, J. W., Skidmore, M. L. and Boyd, E. S. (2013). Molecular evidence for an active endogenous microbiome beneath glacial ice. *The ISME Journal*, **7**, 1402-1412.

Hansen, L. D., Dipple, G. M., Gordon, T. M. and Kellett, D. A. (2005). Carbonated serpentinite (listwanite) at Atlin, British Columbia: A geological analogue to carbon dioxide sequestration. *The Canadian Mineralogist*, **43**, 225-239.

Haroon, M.F., Hu, S., Shi, Y., Imelfort, M., Keller, J., Hugenholtz, P., Yuan, Z. and Tyson, G.W. (2013). Anaerobic oxidation of methane coupled to nitrate reduction in a novel archaeal lineage. *Nature*, **500**, pp.567-570.

Hatzenpichler, R., Connon, S. A., Goudeau, D., Malmstrom, R. R., Woyke, T. and Orphan, V. J. (2016). Visualizing in situ translational activity for identifying and sorting slow-growing archaeal− bacterial consortia. *Proceedings of the National Academy of Sciences*, **113**, E4069-E4078.

Havig, J. R., J. Raymond, D. R. Meyer-Dombard, N. Zolotova, and E. L. Shock (2011), Merging isotopes and community genomics in a siliceous sinter-depositing hot spring, *Journal of Geophysical Research* **116**, G01005, doi:10.1029/2010JG001415.
Hawkings, J. R., Wadham, J. L., Tranter, M., Raiswell, R., Benning, L. G., Statham, P. J., Tedstone, A., Nienow, P., Lee, K. and Telling, J. (2014). Ice sheets as a significant source of highly reactive nanoparticulate iron to the oceans. *Nature communications*, **5**.

Helgeson, H. C. (1969). Thermodynamics of hydrothermal systems at elevated temperatures and pressures. *American Journal of Science*, **267**, 729-804.

Helgeson H. C. and Kirkham D. H. (1976). Theoretical prediction of the thermodynamic properties of aqueous electrolytes at high pressures and temperatures. III. Equation of state for aqueous species at infinite dilution. *American Journal of Science* **276**, 97-240.

Helgeson, H. C. (1979). Mass transfer among minerals and hydrothermal solutions. *Geochemistry of hydrothermal ore deposits*, **2**, 568-610.

Helgeson H. C., Delany J. M., Nesbitt H. W. and Bird D. K. (1978) Summary and critique of the thermodynamic properties of rock-forming minerals. *American Journal of Science* 278A, 1–229.

Helgeson H. C., Kirkham D. H. and Flowers G. C., (1981). Theoretical prediction of the thermodynamic behavior of aqueous electrolytes at high pressures and temperatures: IV. Calculation of activity coefficients, osmotic coefficients, and apparent molal and standard and relative partial molal properties to 600°C and 5 KB. *American Journal of Science* **281**, 1249-1516.

Helgeson H. C., Owens C. E., Knox A. M. and Richard L. (1998). Calculation of the standard molal thermodynamic properties of crystalline, liquid, and gas organic molecules at high temperatures and pressures. *Geochimica et Cosmochimica Acta* **62**, 985-1081.

Hellevang, H., Huang, S. and Thorseth, I. H. (2011). The potential for low-temperature abiotic hydrogen generation and a hydrogen-driven deep biosphere. *Astrobiology*, **11**, 711-724.

Hemingway, B. S., Robie, R. A. and Apps, J. A. (1991). Revised values for the thermodynamic properties of boehmite, AlO (OH), and related species and phases in the system Al-HO. *American Mineralogist;(United States)*, *76*.

Hiemstra, T. (2013). Surface and mineral structure of ferrihydrite. *Geochimica et Cosmochimica Acta*, **105**, 316-325.

Hiemstra T. and Van Riemsdijk W. H. (2009) A surface structural model for ferrihydrite: I. Sites related to primary charge, molar mass, and mass density. *Geochimica et Cosmochimica Acta* **73**, 4423–4436.

Hijmans, R. J., Cameron, S. E., Parra, J. L., Jones, P. G. and Jarvis, A. (2005). Very high resolution interpolated climate surfaces for global land areas. *International Journal of Climatology*, **25**, 1965-1978.

Hinrichs, K. U., Hayes, J. M., Sylva, S. P., Brewer, P. G. and DeLong, E. F. (1999). Methane-consuming archaebacteria in marine sediments. *Nature*, **398**, 802-805.

Hitchcock, D. I. (1958). The Ionization Constants of Isocitric Acid. *The Journal of Physical Chemistry*, ***62***(10), 1337-1339.

Hodson, A., Anesio, A. M., Tranter, M., Fountain, A., Osborn, M., Priscu, J., Laybourn-Perry, J. and Sattler, B. (2008). Glacial ecosystems. *Ecological Monographs*, **78**, 41-67.

Hoehler, T. M. (2004). Biological energy requirements as quantitative boundary conditions for life in the subsurface. *Geobiology*, **2**, 205-215.

Hoehler, T. M. and Jørgensen, B. B. (2013). Microbial life under extreme energy limitation. *Nature Reviews Microbiology*, **11**, 83-94.

Hoehler, T. M., Alperin, M. J., Albert, D. B. and Martens, C. S. (1998). Thermodynamic control on hydrogen concentrations in anoxic sediments. *Geochimica et Cosmochimica Acta*, **62**, 1745-1756.

Hoehler, T. M., Alperin, M. J., Albert, D. B. and Martens, C. S. (2001). Apparent minimum free energy requirements for methanogenic Archaea and sulfate-reducing bacteria in an anoxic marine sediment. *FEMS Microbiology Ecology*, **38**, 33-41.

Holm, N.G. and Neubeck A. (2009). Reduction of nitrogen compounds in oceanic basement and its implications for HCN formation and abiotic organic synthesis. *Geochemical Transactions* 10. doi:10.1186/1467-4866-10-9.

Hosgörmez, H. (2007). Origin of the natural gas seep of Cirali (Chimera), Turkey: Site of the first Olympic fire. *Journal of Asian Earth Sciences*, **30**, 131-141.

Howells, A., Poret-Peterson, A.T., Cox, A., Canovas, P., Shock, E. (June 2015) Geochemical influences on sediment bacterial communities in a serpentinization-hosted ecosystem. At *Astrobiology Science Conference*, Chicago, Illinois.

Hügler, M., Wirsen, C. O., Fuchs, G., Taylor, C. D., & Sievert, S. M. (2005). Evidence for autotrophic CO2 fixation via the reductive tricarboxylic acid cycle by members of the ε subdivision of proteobacteria. *Journal of Bacteriology*, **187**, 3020-3027.

Hügler, M., Huber, H., Molyneaux, S. J., Vetriani, C., & Sievert, S. M. (2007). Autotrophic CO2 fixation via the reductive tricarboxylic acid cycle in different lineages within the phylum Aquificae: evidence for two ways of citrate cleavage. *Environmental Microbiology*, **9**, 81-92.

Hulme, S. M., Wheat, C. G., Fryer, P. and Mottl, M. J. (2010). Pore water chemistry of the Mariana serpentinite mud volcanoes: a window to the seismogenic zone. *Geochemistry, Geophysics, Geosystems*, **11,** .

Imachi, H., Sekiguchi, Y., Kamagata, Y., Loy, A., Qiu, Y. L., Hugenholtz, P., Kimura, N, Wagner, M., Ohashi, A. and Harada, H. (2006). Non-sulfate-reducing, syntrophic

bacteria affiliated with Desulfotomaculum cluster I are widely distributed in methanogenic environments. *Applied and Environmental Microbiology*, **72**, 2080-2091.

Inagaki, F., Takai, K., Hirayama, H., Yamato, Y., Nealson, K. H. and Horikoshi, K. (2003). Distribution and phylogenetic diversity of the subsurface microbial community in a Japanese epithermal gold mine. *Extremophiles*, ***7***, 307-317.

Inglese A., Sedlbauer J. and Wood, R. H. (1996). Apparent molar heat capacities of aqueous s solutions of acetic, propanoic and succinic acids, sodium acetate and sodium propanoate from 300 to 525 K and a pressure of 28 MPa. *Journal of Solution Chemistry* **25**, 849-864.

Isaksen, M. F. and Jorgensen, B. B. (1996). Adaptation of psychrophilic and psychrotrophic sulfate-reducing bacteria to permanently cold marine environments. *Applied and Environmental Microbiology*, **62**, 408-414.

Ishida M. and Okuno K. (2004). Systematic analysis of biochemical processes in cells by applying graphical diagrams. *Energy* **29**, 2461-2472.

Jamal M. A., Khosa M. K., Muneer M., Rehman F.-U., Saif M. J., Bhatti H. N., Naz S. and Javed J. (2015). Acoustical behavior of some amino acids in aqueous disodium citrate solutions over temperature range (298.15-313.15 K). *Pakistan Journal of Pharmaceutical Sciences* **28**, 1613-1617.

Jespersen N. (1976). Thermochemistry of the reaction catalyzed by malate dehydrogenase. *Thermochimica Acta* **17**, 23-27.

Johnson J.W. and Norton D. (1991). Critical phenomena in hydrothermal systems: State, thermodynamic, electrostatic and transport properties of H_2O in the critical region. *American Journal of Science* **291,** 541-548.

Johnson J. W., Oelkers E. H. and Helgeson H. C. (1992). SUPCRT92: A software package for calculating the standard molal thermodynamic properties of minerals, gases, aqueous species, and reactions from 1 to 5000 bar and 0 to 1000 C. *Computers & Geosciences* **18**, 899-947.

Jørgensen, B. B. and Bak, F. (1991). Pathways and microbiology of thiosulfate transformations and sulfate reduction in a marine sediment (Kattegat, Denmark). *Applied and Environmental Microbiology*, **57**, 847-856.

Jørgensen, B. B., Weber, A. and Zopfi, J. (2001). Sulfate reduction and anaerobic methane oxidation in Black Sea sediments. *Deep Sea Research Part I: Oceanographic Research Papers*, **48**, 2097-2120.

Joye, S. B., Boetius, A., Orcutt, B. N., Montoya, J. P., Schulz, H. N., Erickson, M. J. and Lugo, S. K. (2004). The anaerobic oxidation of methane and sulfate reduction in sediments from Gulf of Mexico cold seeps. *Chemical Geology*, **205**, 219-238.

Kahl, W. A., Jöns, N., Bach, W., Klein, F. and Alt, J. C. (2015). Ultramafic clasts from the South Chamorro serpentine mud volcano reveal a polyphase serpentinization history of the Mariana forearc mantle. *Lithos*, **227**, 1-20.

Kaksonen, A. H., Plumb, J. J., Robertson, W. J., Spring, S., Schumann, P., Franzmann, P. D. and Puhakka, J. A. (2006a). Novel thermophilic sulfate-reducing bacteria from a geothermally active underground mine in Japan. *Applied and Environmental Microbiology*, ***72***, 3759-3762.

Kaksonen, A. H., Spring, S., Schumann, P., Kroppenstedt, R. M. and Puhakka, J. A. (2006b). *Desulfotomaculum thermosubterraneum* sp. nov., a thermophilic sulfate-reducer isolated from an underground mine located in a geothermally active area. *International Journal of Systematic and Evolutionary Microbiology*, **56**, 2603-2608.

Karl, D. M., Bird, D. F., Björkman, K., Houlihan, T., Shackelford, R. and Tupas, L. (1999). Microorganisms in the accreted ice of Lake Vostok, Antarctica. *Science*, **286**, 2144-2147.

Karson, J. A., Früh-Green, G. L., Kelley, D. S., Williams, E. A., Yoerger, D. R. and Jakuba, M. (2006). Detachment shear zone of the Atlantis Massif core complex, Mid-Atlantic Ridge, 30 N. *Geochemistry, Geophysics, Geosystems*, **7**(6).

Kaštovská, K., Stibal, M., Šabacká, M., Černá, B., Šantrůčková, H. and Elster, J. (2007). Microbial community structure and ecology of subglacial sediments in two polythermal Svalbard glaciers characterized by epifluorescence microscopy and PLFA. *Polar Biology*, **30**, 277-287.

Kato, C., Sato, T. and Horikoshi, K. (1995). Isolation and properties of barophilic and barotolerant bacteria from deep-sea mud samples. *Biodiversity and Conservation*, **4**, 1-9.

Kato, C. , Masui, N. , Horikoshi, K.,(1996). Properties of obligately barophilic bacteria isolated from a sample of deep-sea sediment from the Izu-Bonin Trench, *Journal of Marine Biotechnology*, **4**, 96-99.

Kato, C., Li, L., Tamaoka, J. and Horikoshi, K. (1997). Molecular analyses of the sediment of the 11000-m deep Mariana Trench. *Extremophiles*, **1**, 117-123.

Kato, C., Li, L., Nogi, Y., Nakamura, Y., Tamaoka, J. and Horikoshi, K. (1998). Extremely barophilic bacteria isolated from the Mariana Trench, Challenger Deep, at a depth of 11,000 meters. *Applied and Environmental Microbiology*, **64**, 1510-1513.

Kelemen, P. B. and Matter, J. (2008). In situ carbonation of peridotite for CO_2 storage. *Proceedings of the National Academy of Sciences*, **105**, 17295-17300.

Kelemen, P. B. and Hirth, G. (2012). Reaction-driven cracking during retrograde metamorphism: Olivine hydration and carbonation. *Earth and Planetary Science Letters*, **345**, 81-89.

Kelemen, P., Al Rajhi, A., Godard, M., Ildefonse, B., Köpke, J., MacLeod, C., Manning, C., Michibayashi, K., Nasir, S., Shock, E., Takazawa, E. and Teagle, D. (2013). Scientific drilling and related research in the Samail ophiolite, Sultanate of Oman. *Scientific Drilling*, **15**, 64-71.

Kelley, D. S., Karson, J. A., Blackman, D. K., Fruh-Green, G. L., Butterfield, D. A., Lilley, M. D., Olson, E. J., Schrenk, M. O., Roe, K. K., Lebon, G.T., Rivizzigno, P. and the AT3-60 Shipboard Part (2001). An off-axis hydrothermal vent field near the Mid-Atlantic Ridge at 30 N. *Nature*, **412**, 145-149.

Kelley, D. S., Karson, J. A., Früh-Green, G. L., Yoerger, D. R., Shank, T. M., Butterfield, D. A., Hayes, J. M., Schrenk, M.O., Olson, E.J., Proskurowski, G., Jakuba, M., Bradley, A., Larason, B., Ludwig, K., Glickson, D., Buckman, K., Bradley, A.S., Brazelton, W.J., roe, K., Elend, M.J., Delacour, A., Bernasconi, S.M., Lilley, M.D., Baross, J.A., Summons, R.,E., Sylva, S. P. (2005). A serpentinite-hosted ecosystem: the Lost City hydrothermal field. *Science*, **307**, 1428-1434.

Kelley, D. S., Fruh-Green, G. L., Karson, J. A. and Ludwig, K. A. (2007). The Lost City hydrothermal field revisited. *Oceanogrphy-Washiington DC-Oceanography Society*, **20**, 90.

Kemmer, G., Keller, S. (2010) Nonlinear least-squares data fitting in Excel spreadsheets. *Nature Protocols*, **5**, 267-281.

Kieft, T. L., Fredrickson, J. K., Onstott, T. C., Gorby, Y. A., Kostandarithes, H. M., Bailey, T. J., ... and Gray, M. S. (1999). Dissimilatory reduction of Fe (III) and other electron acceptors by a *Thermus* isolate. *Applied and Environmental Microbiology*, **65**, 1214-1221.

Kieft, T. L., McCuddy, S. M., Onstott, T. C., Davidson, M., Lin, L. H., Mislowack, B., ... and Heerden, A. V. (2005). Geochemically generated, energy-rich substrates and indigenous microorganisms in deep, ancient groundwater. *Geomicrobiology Journal*, **22**, 325-335.

Kimura, H., Sugihara, M., Yamamoto, H., Patel, B. K., Kato, K. and Hanada, S. (2005). Microbial community in a geothermal aquifer associated with the subsurface of the Great Artesian Basin, Australia. *Extremophiles*, **9**, 407-414.

Kishore N., Tewari Y. B. and Goldberg R. N., (1998). An investigation of the equilibrium of the reaction {L-aspartate(aq)} + 2-oxoglutarate(aq) = oxaloacetate(aq) + L-glutamate(aq)}. *Journal of Chemical Thermodynamics* **30**, 1373-1384.

Kivimäki, A.L. (2005). *Presence of microbial populations in glaciers and their impact on rock weathering at glacial beds*. Doctoral Dissertation. University of Bristol, Department of Earth Science.

Kloysuntia, A.N. (2014). *Physiological and Phylogenetic Studies of the Biogeography of Alkaliphilic Heterotrophic Bacteria from Serpentinizing Habitats* (Master's Thesis, East Carolina University). Retrieved from the Scholarship. (http://hdl.handle.net/10342/4675.)

Klouche, N., Fardeau, M. L., Lascourrèges, J. F., Cayol, J. L., Hacene, H., Thomas, P. and Magot, M. (2007). *Geosporobacter subterraneus* gen. nov., sp. nov., a spore-forming bacterium isolated from a deep subsurface aquifer. *International Journal of Systematic and Evolutionary Microbiology*, **57**, 1757-1761.

Knittel, K., Lösekann, T., Boetius, A., Kort, R., & Amann, R. (2005). Diversity and distribution of methanotrophic archaea at cold seeps. *Applied and Environmental Microbiology*, **71**, 467-479.

Kondepudi D. and Prigogine I. (1998) *Modern Thermodynamics: From Heat Engines to Dissipative Structures*. John Wiley and Sons, New York.

Kotelnikova, S., and Pedersen, K. (1998) Microbial oxygen consumption in Aspo tunnel environment, SKB-PR-HRL-98-1, Swedish Nucl. Fuel Waste Manag. Co.k Stockholm, Sweden.

Kotelnikova, S., Macario, A. J. and Pedersen, K. (1998). Methanobacterium subterraneum sp. nov., a new alkaliphilic, eurythermic and halotolerant methanogen isolated from deep granitic groundwater. *International Journal of Systematic Bacteriology*, **48**, 357-367.

Kotlar, H. K., Lewin, A., Johansen, J., Throne-Holst, M., Haverkamp, T., Markussen, S., Winnberg, A., Ringrose, P., Aakvik, T., Ryeng, E., Jakobseen, K., Brablos, F. and Valla, S. (2011). High coverage sequencing of DNA from microorganisms living in an oil reservoir 2.5 kilometres subsurface. *Environmental Microbiology Reports*, **3**, 674-681.

Krebs H. A. (1953). Equilibria in transamination systems. *Biochemical Journal* **54**, 82-86.

Krebs H. A. and Kornberg H. L. (1957). *Energy Transformations in Living Matter.* Springer Berlin.

Kumar H., Kaur K., Kaur S.P. and Singla M. (2013a). Studies of volumetric and acoustic properties of trisodium citrate and tripotassium citrate in aqueous solutions of N-acetyl glycine at different temperatures. *Journal of Chemical Thermodynamics* **59**, 173-181.

Kumar H., Singla M. and Jindal R. (2013b). Interactions of glycine, L-alanine and L-valine with aqueous solutions of trisodium citrate at different temperatures: A volumetric and acoustic approach. *Journal of Chemical Thermodynamics* **67**, 170-180.

Kumar, H. and Sharma, S. K. (2016). Volumetric and Acoustic Behavior of d (+)-glucose and d (−)-fructose in Aqueous Trisodium Citrate Solutions at Different Temperatures. *Journal of Solution Chemistry*, ***45***(1), 1-27.

L'Haridon, S., Reysenbacht, A. L., Glenat, P., Prieur, D. and Jeanthon, C. (1995). Hot subterranean biosphere in a continental oil reservoir. *Nature*, **377**, 223-224.

Laberty, C. and Navrotsky, A. (1998). Energetics of stable and metastable low-temperature iron oxides and oxyhydroxides. *Geochimica et Cosmochimica Acta*, **62**, 2905-2913.

Lancaster Jr, J. R. (1989). Sodium, protons, and energy coupling in the methanogenic bacteria. *Journal of Bioenergetics and Biomembranes*, **21**, 717-740.

Lang, S. Q., Butterfield, D. A., Schulte, M., Kelley, D. S. and Lilley, M. D. (2010). Elevated concentrations of formate, acetate and dissolved organic carbon found at the Lost City hydrothermal field. *Geochimica et Cosmochimica Acta*, **74**, 941-952.

Lang, S. Q., Früh-Green, G. L., Bernasconi, S. M., Lilley, M. D., Proskurowski, G., Méhay, S. and Butterfield, D. A. (2012). Microbial utilization of abiogenic carbon and hydrogen in a serpentinite-hosted system. *Geochimica et Cosmochimica Acta*, **92**, 82-99.

Lang, S. Q., Früh-Green, G. L., Bernasconi, S. M. and Butterfield, D. A. (2013). Sources of organic nitrogen at the serpentinite-hosted Lost City hydrothermal field. *Geobiology*, **11**, 154-169.

Launay, J. and Fontes, J. C. (1985). Les sources thermales de Prony (Nouvelle--Caledonie) et leurs precipites chimiques. Exemple de formation de brucite primaire. *Geologie de la France*, **1**, 83-100.

LaRowe, D. E. and Amend, J. P. (2015a). Power limits for microbial life. *Frontiers in Microbiology*, *6*.

LaRowe D. E. and Amend J. P. (2015b). Catabolic rates, population sizes and doubling/replacement times of microorganisms in natural settings. *American Journal of Science* **315**, 167-203.

LaRowe, D. E. and Amend, J. P. (2016). The energetics of anabolism in natural settings. *The ISME Journal*, **10**, 1285-1295.

LaRowe D. E. and Dick J. M. (2012). Calculation of the standard molal thermodynamic properties of crystalline peptides. *Geochimica et Cosmochimica Acta* **80**, 70–91.

LaRowe D.J. and Helgeson H.C. (2006a). Biomolecules in hydrothermal systems: Calculation of the standard molal thermodynamic properties of nucleic-acid bases, nucleosides, and nucleotides at elevated temperatures and pressures. *Geochimica et Cosmochimica Acta* **70**, 4680–4724.

LaRowe D. and Helgeson H.C. (2006b). The energetics of metabolism in hydrothermal systems: Calculation of the standard molal thermodynamic properties of magnesium-complexed adenosine nucleotides and NAD and NADP at elevated temperatures and pressures. *Thermochimica Acta* **448**, 82-106.

LaRowe D. E. and Helgeson H. C. (2007). Quantifying the energetics of metabolic reactions in diverse biogeochemical systems: electron flow and ATP synthesis. *Geobiology* **5**, 153-168.

LaRowe D. E., Dale A. W., Amend J. P. and Van Cappellen P. (2012). Thermodynamic limitations on microbially catalyzed reaction rates: *Geochimica et Cosmochimica Acta* **90**, 96–109.

LaRowe D. E., Dale A. W., Aguilera D. R., L'Heureux I., Amend J. P. and Regnier P. (2014). Modeling microbial reaction rates in a submarine hydrothermal vent chimney wall. *Geochimica et Cosmochimica Acta* **124**, 72–97.

Lawrence C., Harden J. and Maher K. (2014). Modeling the influence of organic acids on soil weathering. *Geochimica et Cosmochimica Acta* **139**, 487-507.

Lee, P. A., Priscu, J. C., DiTullio, G. R., Riseman, S. F., Tursich, N. and De Mora, S. J. (2004). Elevated levels of dimethylated-sulfur compounds in Lake Bonney, a poorly ventilated Antarctic lake. *Limnology and Oceanography*, **49**, 1044-1055.

Li, H., Yang, S. Z., Mu, B. Z., Rong, Z. F. and Zhang, J. (2006). Molecular analysis of the bacterial community in a continental high-temperature and water-flooded petroleum reservoir. *FEMS Microbiology Letters*, **257**, 92-98.

Li, H., Yang, S. Z., Mu, B. Z., Rong, Z. F. and Zhang, J. (2007). Molecular phylogenetic diversity of the microbial community associated with a high-temperature petroleum reservoir at an offshore oilfield. *FEMS Microbiology Ecology*, **60**, 74-84.

Li, X. L., Bastiaens, W., Van Marcke, P., Verstricht, J., Chen, G. J., Weetjens, E. and Sillen, X. (2010). Design and development of large-scale in-situ PRACLAY heater test

and horizontal high-level radioactive waste disposal gallery seal test in Belgian HADES. *Journal of Rock Mechanics and Geotechnical Engineering*, **2**, 103-110.

Li J., Zhang W., Li S., Li W. and Lu J. (2014). Effects of citrate on the dissolution and transformation of biotitie, analyzed by chemical and atomic force microscopy. *Applied Geochemistry* **51**, 101-108.

Liesack, W., Weyland, H. and Stackebrandt, E. (1991). Potential risks of gene amplification by PCR as determined by 16S rDNA analysis of a mixed-culture of strict barophilic bacteria. *Microbial Ecology*, **21**, 191-198.

Lin, C. L. and Wood, R. H. (1996). Prediction of the free energy of dilute aqueous methane, ethane, and propane at temperatures from 600 to 1200 C and densities from 0 to 1 g cm^3 using molecular dynamics simulations. *The Journal of Physical Chemistry*, **100**, 16399-16409.

Lin, L. H., Wang, P. L., Rumble, D., Lippmann-Pipke, J., Boice, E., Pratt, L. M., Lollar, B.S., Brodie, E.L., Hazen, T.C., Andersen, G.L., DeSantis, T.Z., Moser, D.P., Kershaw, D. and Onstott, T. C. (2006). Long-term sustainability of a high-energy, low-diversity crustal biome. *Science*, **314**, 479-482.

Lincoln, S. A., Bradley, A. S., Newman, S. A. and Summons, R. E. (2013). Archaeal and bacterial glycerol dialkyl glycerol tetraether lipids in chimneys of the Lost City Hydrothermal Field. *Organic Geochemistry*, **60**, 45-53.

Liu, Y., Karnauchow, T. M., Jarrell, K. F., Balkwill, D. L., Drake, G. R., Ringelberg, D., Clarno, R. and Boone, D. R. (1997). Description of two new thermophilic *Desulfotomaculum* spp., *Desulfotomaculum putei* sp. nov., from a deep terrestrial subsurface, and *Desulfotomaculum luciae* sp. nov., from a hot spring. *International journal of systematic bacteriology*, **47**, 615-621.

Loiacono, S. T., Meyer-Dombard, D. A. R., Havig, J. R., Poret-Peterson, A. T., Hartnett, H. E. and Shock, E. L. (2012). Evidence for high-temperature in situ nifH transcription in an alkaline hot spring of Lower Geyser Basin, Yellowstone National Park. *Environmental Microbiology*, **14**, 1272-1283.

Londesborough J. C. and Dalziel K. (1968). The equilibrium constant of the isocitrate dehydrogenase reaction. *Biochemical Journal* **110**, 217-222.

Love, C. A., Patel, B. K. C., Nichols, P. D. and Stackebrandt, E. (1993) *Desulfotomaculum australicum*, sp. nov., a Thermophilic Sulfate-Reducing Bacterium Isolated from the Great Artesian Basin of Australia. *Systematic and Applied Microbiology*, **16**, 244-251.

Ludwig, K. A., Shen, C. C., Kelley, D. S., Cheng, H. and Edwards, R. L. (2011). U–Th systematics and ^{230}Th ages of carbonate chimneys at the Lost City Hydrothermal Field. *Geochimica et Cosmochimica Acta*, **75**, 1869-1888.

Lueders, T., Pommerenke, B. and Friedrich, M. W. (2004). Stable-isotope probing of microorganisms thriving at thermodynamic limits: syntrophic propionate oxidation in flooded soil. *Applied and Environmental Microbiology*, **70**, 5778-5786.

Lyon, G.L., Giggenbach, W.F., Lupton, J.E. (1990). Compositioin and origin of the hydrogen-rich gas seep, Fiordland, New Zealand. *EOS Trans* V51D-10: 1717.

Magnier, Y. (1979) Une source thermal sous-marine a Prony: le recif de L'aiguill, Rossiniana, **3**, 16-17.

Maier, C. G. and Kelley, K. K. (1932). An equation for the representation of high-temperature heat content data1. *Journal of the American Chemical Society*, **54**, 3243-3246.

Majer V. and Svoboda V. (1985). *Enthalpies of Vaporization of Organic Compounds.* Blackwell Scientific Publications.

Majzlan, J., Lang, B.E., Stevens, R., Navrotsky, A., Woodfield, B.F., Boerio_Goates, J. (2003a). Thermodynamics of Fe oxides: Part I. Entropy at standard temperature and pressure and heat capacity of goethite (α-FeOOH), lepidocrocite (γ-FeOOH), and maghemite (γ-Fe_2O_3). *American Mineralogist*, **88**, 846-854.

Majzlan, J., Grevel, K., Navrotsky, A. (2003b). Thermodynamics of Fe oxides: Part II. Enthalpies of formation and relative stability of goethite (α-FeOOH), lepidocrocite (γ-FeOOH), and maghemite (γ-Fe_2O_3). *American Mineralogist*, **88,** 855-859.

Majzlan, J., Navrotsky, A., Schwertmann, U. (2004). Thermodynamics of iron oxides: Part III. Enthalpies of formation and stability of ferrihydrite (~$Fe(OH)_3$), schwertmannite (~$FeO(OH)_{3/4}(SO_4)_{1/8}$), and ε-$Fe_2O_3$. *Geochimica et Cosmochimica Acta*, **68**, 1049-1059.

Majzlan, J., Mazeina, L., Navrotsky, A., (2007). Enthalpy of water adsorption and surface enthalpy of lepidocrocite (γ-FeOOH). *Geochimica et Cosmochimica Acta*, **71**, 615-623.

Manzurola E. and Apelblat A. (1985). Apparent molar volumes of citric, tartaric, malic, succinic, maleic, and acetic acids in water at 298.15 K. *Journal of Chemical Thermodynamics* **17**, 579-584.

Marques, J. M., Carreira, P. M., Carvalho, M. R., Matias, M. J., Goff, F. E., Basto, M. J., Graca, R.C., Aires-Barros, L. and Rocha, L. (2008). Origins of high pH mineral waters from ultramafic rocks, Central Portugal. *Applied Geochemistry*, **23**, 3278-3289.

Marteinsson, V. T., Moulin, P., Birrien, J., Gambacorta, A., Vernet, M. and Prieur, D. (1997). Physiological Responses to Stress Conditions and Barophilic Behavior of the Hyperthermophilic Vent Archaeon Pyrococcus abyssi. *Applied and Environmental Microbiology*, **63**, 1230-1236.

Marteinsson, V. T., Birrien, J. L., Reysenbach, A. L., Vernet, M., Marie, D., Gambacorta, A., Messner, P., Sleytr, U.B. and Prieur, D. (1999). Thermococcus barophilus sp. nov., a new barophilic and hyperthermophilic archaeon isolated under high hydrostatic pressure from a deep-sea hydrothermal vent. *International Journal of Systematic Bacteriology*, **49**, 351-359.

Marteinsson, V. T., Runarsson, A., Stefánsson, A., Thorsteinsson, T., Johannesson, T., Magnusson, S. H., Reynisson, E., Einarsson, B., Wade, N., Morrison, H.G. and Gaidos, E. (2012). Microbial communities in the subglacial waters of the Vatnajökull ice cap, Iceland. *The ISME journal*, *7*(2), 427-437.

Martell A. E., Smith R. M., Motekatis R. J. (1997). *NIST Critical Stability Constants of Metal Complexes Database: NIST Standard Reference Database 46*. National Institute of Standards and Technology: Gaithersburg, MD.

Mazeina, L., and Navrotsky, A. (2005) Surface enthalpy of goethite. *Clays and Clay Minerals*, **53**, 113-122.

McCollom T. M. (2000). Geochemical constraints on primary productivity in submarine hydrothermal vent plumes. *Deep Sea Research Part I Oceanographic Research Papers* **47**, 85–101.

McCollom T. M. (2007). Geochemical constraints on sources of metabolic energy for chemolithoautotrophy in ultramafic-hosted deep-sea hydrothermal systems. *Astrobiology* **7**, 933-950.

McCollom T. M. (2016). Abiotic methane formation during experimental serpentinization of olivine. *Proceedings of the National Academy of Science* doi: 10.1073/pnas.1611843113.

McCollom TM and Bach W (2009). Thermodynamic constraints on hydrogen generation during serpentinization of ultramafic rocks. *Geochimica et Cosmochimica Acta* **73**,856-875.

McCollom, T. M. and Amend, J. P. (2005). A thermodynamic assessment of energy requirements for biomass synthesis by chemolithoautotrophic micro-organisms in oxic and anoxic environments. *Geobiology*, **3**, 135-144.

McCollom T. M. and Shock E. L. (1997). Geochemical constraints on chemolithoautotrophic metabolism by microorganisms in seafloor hydrothermal systems.

Geochimica et Cosmochimica Acta **61**, 4375-4391.

McCollom TM, Lollar BS, Lacrampe-Couloume G, Seewald JS (2010). The influence of carbon source on abiotic organic synthesis and carbon isotope fractionation under hydrothermal conditions. *Geochimica et Cosmochimica Acta* ***74***, 2717-2740. doi:10.1016/j.gca.2010.02.008

McKay, C. P., Hand, K. P., Doran, P. T., Andersen, D. T. and Priscu, J. C. (2003). Clathrate formation and the fate of noble and biologically useful gases in Lake Vostok, Antarctica. *Geophysical Research Letters*, **30**.

McMechan, M.E. (1988) *Geology of Peter Lougheed Provincial Park, Rocky Mountain Front Ranges, Alberta*. Open File Report 2057. Geological Survey of Canada.

Meersman, F., Daniel, I., Bartlett, D. H., Winter, R., Hazael, R. and McMillain, P. F. (2013). High-pressure biochemistry and biophysics. *Reviews in Mineralogy and Geochemistry* **75**, 607-648.

Meyer, J. L., Jaekel, U., Tully, B. J., Glazer, B. T., Wheat, C. G., Lin, H. T., Hsieh, C., Cowen, J.P., Hulm, S.M., Girguis, P.R. and Huber, J. A. (2016). A distinct and active bacterial community in cold oxygenated fluids circulating beneath the western flank of the Mid-Atlantic ridge. *Scientific reports*, ***6***.

Meyer-Dombard, D. R., Shock, E. L. and Amend, J. P. (2005). Archaeal and bacterial communities in geochemically diverse hot springs of Yellowstone National Park, USA. *Geobiology*, **3**, 211-227.

Meyer-Dombard, D. A. R., Swingley, W., Raymond, J., Havig, J., Shock, E. L. and Summons, R. E. (2011). Hydrothermal ecotones and streamer biofilm communities in the Lower Geyser Basin, Yellowstone National Park. *Environmental Microbiology*, **13**, 2216-2231.

Michaelis, W., Seifert, R., Nauhaus, K., Treude, T., Thiel, V., Blumenberg, M., Knittel, K., Gieseke, A., Peterknecht, K., Pape, T., Boetius, A., Amann, R., Jørgenson, B.B.,Widdel, F., Peckmann, J., Pimenkov, N. and Gulin, M.B. (2002). Microbial reefs in the Black Sea fueled by anaerobic oxidation of methane. *Science*, **297**, 1013-1015.

Michel, F.M., Ehm, L., Antao, S.M., Lee, P.L., Chupas, P.J., Liu, G., Strongin, D.R., Schoonen, M.A.A., Phillips, B.L., and Parise, J.B. (2007a). The structure of ferrihydrite, a nanocrystalline material. *Science*, **316**, 1726–1729.

Michel, F.M., Ehm, L., Liu, G., Han, W.Q., Antao, S.M., Chupas, P.J., Lee, P.L., Knorr, K., Eulert, H., Kim, J., and others. (2007b). Similarities in 2-and 6-line ferrihydrite based on pair distribution function analysis of X-ray total scattering. *Chemistry of Materials*, **19**, 1489–1496.

Michel, F. M., Barrón, V., Torrent, J., Morales, M. P., Serna, C. J., Boily, J. F., Liu, Q., Ambrosini, A., Cismasu, A.C., and Brown, G. E. (2010). Ordered ferrimagnetic form of ferrihydrite reveals links among structure, composition, and magnetism. *Proceedings of the National Academy of Sciences*, **107**, 2787-2792.

Michel, F. M., Barrón, V., Torrent, J., Morales, M. P., Serna, C. J., Boily, J. F., Liu, Q., Ambrosini, A., Cismasu, A.C., and Brown, G. E. (2010). Supporting information for: Ordered ferrimagnetic form of ferrihydrite reveals links among structure, composition, and magnetism. *Proceedings of the National Academy of Sciences*, **107**, 2787-2792.

Mikucki, J. A. and Priscu, J. C. (2007). Bacterial diversity associated with Blood Falls, a subglacial outflow from the Taylor Glacier, Antarctica. *Applied and Environmental Microbiology*, **73**, 4029-4039.

Mikucki, J. A., Foreman, C. M., Sattler, B., Lyons, W. B. and Priscu, J. C. (2004). Geomicrobiology of Blood Falls: an iron-rich saline discharge at the terminus of the Taylor Glacier, Antarctica. *Aquatic Geochemistry*, **10**, 199-220.

Mikucki, J. A., Pearson, A., Johnston, D. T., Turchyn, A. V., Farquhar, J., Schrag, D. P., Anbar, A.D., Priscu, J.C. and Lee, P. A. (2009). A contemporary microbially maintained subglacial ferrous "Ocean". *Science*, **324**, 397-400.

Mikucki, J. A., Lee, P. A., Ghosh, D., Purcell, A. M., Mitchell, A. C., Mankoff, K. D., Fisher, A.T., Tulaczyk, S., Carter, S., Siegried, M.R., Fricker, H. A., Hodson, T., Coenen, J., Powell, R., Scherer, R., Vick-Majors, T., Achberger, A.A., Christner, B.C., Tranter, M., Team WISSARDS (2016). Subglacial Lake Whillans microbial biogeochemistry: a synthesis of current knowledge. *Philosophical Transactions of the Royal Society A*, **374**, 20140290.

Miller S. and Smith-Magowan D. (1990). The thermodynamics of the Krebs cycle and related compounds. *Journal of Physical and Chemical Reference Data* **19**, 1049-1073.

Miller, J. F., Shah, N. N., Nelson, C. M., Ludlow, J. M. and Clark, D. S. (1988). Pressure and temperature effects on growth and methane production of the extreme thermophile Methanococcus jannaschii. *Applied and Environmental Microbiology*, **54**, 3039-3042.

Mikutta C., Mikutta R., Bonneville S., Wagner F., Voegelin A., Christl I. and Kretzschmar R. (2008) Synthetic coprecipitates of exopolysaccharides and ferrihydrite. Part I: characterization. *Geochimica et Cosmochimica Acta* **72**, 1111–1127.

Mitchell, A. C., Lafrenière, M. J., Skidmore, M. L. and Boyd, E. S. (2013). Influence of bedrock mineral composition on microbial diversity in a subglacial environment. *Geology*, **41**, 855-858.

Miteva, V. I. and Brenchley, J. E. (2005). Detection and isolation of ultrasmall microorganisms from a 120,000-year-old Greenland glacier ice core. *Applied and Environmental Microbiology*, **71**, 7806-7818.

Miteva, V. I., Sheridan, P. P. and Brenchley, J. E. (2004). Phylogenetic and physiological diversity of microorganisms isolated from a deep Greenland glacier ice core. *Applied and Environmental Microbiology*, **70**, 202-213.

Miyoshi, T., Iwatsuki, T. and Naganuma, T. (2005). Phylogenetic characterization of 16S rRNA gene clones from deep-groundwater microorganisms that pass through 0.2-micrometer-pore-size filters. *Applied and Environmental Microbiology*, **71**, 1084-1088.

Mochimaru, H., Yoshioka, H., Tamaki, H., Nakamura, K., Kaneko, N., Sakata, S., Imachi, H., Sekiguchi, Y., Uchiyama, H. and Kamagata, Y. (2007). Microbial diversity and methanogenic potential in a high temperature natural gas field in Japan. *Extremophiles*, **11**, 453-461.

Monien, P., Lettmann, K. A., Monien, D., Asendorf, S., Wölfl, A. C., Lim, C. H., Thal, J., Schnetger, B. and Brumsack, H. J. (2014). Redox conditions and trace metal cycling in coastal sediments from the maritime Antarctic. *Geochimica et Cosmochimica Acta*, **141**, 26-44.

Monnin, C., Pelletier, B., Boulart, C., and Quemeneur, M. (2013). Suivi temporal de la temperature et de la composition des equx et des gaz des sources hyperalcalines de la Baie de Prony (Nouvelle-Caledonie), Grand Observatoire de l'Environment et de la Biodoversite (GOPS), Noumea, Nouvelle Caledonie, Unpublished report.

Monnin, C., Chavagnac, V., Boulart, C., Ménez, B., Gérard, M., Gérard, E., Pisapia, C., Quemeneur, M., Erauso, G., Postec, A., Guentas_Dombrowski, L., Payri, C. and Pelletier, B. (2014a). Fluid chemistry of the low temperature hyperalkaline hydrothermal system of Prony Bay (New Caledonia). *Biogeosciences*, **11**, 5687-5706.

Monnin, C., Chavagnac, V., Boulart, C., Ménez, B., Gérard, M., Gérard, E., Quemeneur, M., Erauso, G., Postec, A., Guentas-Dombrowski, L., Payri, C., and Pelletier, B. (2014b). The low temperature hyperalkaline hydrothermal system of the Prony bay (New Caledonia). *Biogeosciences Discuss*, **11**, 6221-6267.

Montross, S.N. (2005). *Geochemical evidence for microbailly mediated subglacial mineral weathering*. Master Thesis. Montana State University, Department of Earth Sciences.

Mori, K., Hanada, S., Maruyama, A. and Marumo, K. (2002). *Thermanaeromonas toyohensis* gen. nov., sp. nov., a novel thermophilic anaerobe isolated from a subterranean vein in the Toyoha Mines. *International Journal of Systematic and Evolutionary Microbiology*, **52**, 1675-1680.

Morita, R. Y. and ZoBell, C. E. (1955). Occurrence of bacteria in pelagic sediments collected during the Mid-Pacific Expedition. *Deep Sea Research (1953)*, **3**, 66-73.

Morrill, P. L., Kuenen, J. G., Johnson, O. J., Suzuki, S., Rietze, A., Sessions, A. L., Fogel, M.L. and Nealson, K. H. (2013). Geochemistry and geobiology of a present-day serpentinization site in California: The Cedars. *Geochimica et Cosmochimica Acta*, **109**, 222-240.

Moser, D. P., Gihring, T. M., Brockman, F. J., Fredrickson, J. K., Balkwill, D. L., Dollhopf, M. E., Lollar, B.S., Pratt, L.M., Boice, E., Southam, G., Wanger, G., Baker, B.J., Pfiffner, S.M., Lin, L-H and Onstott, T. C. (2005). Desulfotomaculum and Methanobacterium spp. dominate a 4-to 5-kilometer-deep fault. *Applied and Environmental Microbiology*, **71**, 8773-8783.

Motamedi, M. and Pedersen, K. (1998). Note *Desulfovibrio aespoeensis* sp. nov., a mesophilic sulfate-reducing bacterium from deep groundwater at äspö hard rock laboratory, Sweden. *International Journal of Systematic Bacteriology*, **48**, 311-315.

Mottl, M.J. (1992). Pore waters from serpentine seamounts in the Mariana and Izu-Bonin forearcs, Leg 125: evednce for volatiles from the subducting slab. In: Fryer,P., Pearce, J.A., Stokking, L.B. et al. (Eds.), Proceedings of the Ocean Drilling Program, Scientific Results, 125, pp. 373-385.

Mottl, M. J., Komor, S. C., Fryer, P. and Moyer, C. L. (2003). Deep-slab fluids fuel extremophilic Archaea on a Mariana forearc serpentinite mud volcano: Ocean Drilling Program Leg 195. *Geochemistry, Geophysics, Geosystems*, **4**(11).

Mottl, M. J., Wheat, C. G., Fryer, P., Gharib, J. and Martin, J. B. (2004). Chemistry of springs across the Mariana forearc shows progressive devolatilization of the subducting plate. *Geochimica et Cosmochimica Acta*, **68**, 4915-4933.

Mousis, O., Lakhlifi, A., Picaud, S., Pasek, M. and Chassefiere, E. (2013). On the abundances of noble and biologically relevant gases in Lake Vostok, Antarctica. *Astrobiology*, **13**, 380-390.

Müller, V., Blaut, M. and Gottschalk, G. (1993). Bioenergetics of methanogenesis. In *Methanogenesis* (pp. 360-406). Springer US.

Murphy W. M. and Shock E.L. (1999). Environmental aqueous geochemistry of actinides. *Reviews in Mineralogy* **38**, 221-253.

Murray, A. E. and Fritsen, C. H. (2007). Microbiota within the perennial ice cover of Lake Vida, Antarctica. *FEMS Microbiology Ecology*, **59**, 274-288.

Murray, A. E., Kenig, F, Fritsen, C.H., McKay, C.P., Cawley, K.M., Edwards, R., Kuhn, E., McKnight, D.M., Ostrom, N.E., Peng, V., Paterson W.S.B. (1994). *The Physics of Glaciers*. Butterworth-Heinemann.

Murray, A. E., Kenig, F., Fritsen, C. H., McKay, C. P., Cawley, K. M., Edwards, R., Kuhn, E., McKnight, D.M., Ostrom, N..E., Peng, V., Ponce, A., Priscu, J.C., Samarkin, V., Townsend, A.T., Wagh, P., Young, S.A., Yung, P.T., Doran, P.T. (2012). Microbial life at− 13 C in the brine of an ice-sealed Antarctic lake. *Proceedings of the National Academy of Sciences*, **109**, 20626-20631, and supplemental material.

Nakai R., Abe T., Takeyama H., Naganuma T. (2011) Metagenomic analysis of 0.2-mm-passable microorganisms in deep-sea hydrothermal fluid. *Mar Biotechnol* (NY) 13:900-908.

Nasir, S., Al Sayigh, A. R., Al Harthy, A., Al-Khirbash, S., Al-Jaaidi, O., Musllam, A., Al-Mishwat, A. and Al-Bu'saidi, S. (2007). Mineralogical and geochemical characterization of listwaenite from the Semail ophiolite, Oman. *Chemie der Erde-Geochemistry*, **67**, 213-228.

Navrotsky, A., Mazeina, L., Majzlan, J. (2008). Size-driven structural and thermodynamic complexity in iron oxides. *Science*, **319**, 1635-1638.

Nazina, T. N., Grigor'Yan, A. A., Shestakova, N. M., Babich, T. L., Ivoilov, V. S., Feng, Q., Ni, F., Wang, J., She, Y., Xiang, T., Luo, Z., Bellyaev, S.S. and Ivanov, M. V. (2007). Microbiological investigations of high-temperature horizons of the Kongdian petroleum reservoir in connection with field trial of a biotechnology for enhancement of oil recovery. *Microbiology*, **76**, 287-296.

Neal, C. and Shand, P. (2002). Spring and surface water quality of the Cyprus ophiolites. *Hydrology and Earth System Sciences*, **6**, 797-817.

Neal, C. and Stanger, G. (1983). Hydrogen generation from mantle source rocks in Oman. *Earth and Planetary Science Letters*, **66**, 315-320.

Neal, C. and Stanger, G. (1984a). Calcium and magnesium hydroxide precipitation from alkaline groundwaters in Oman, and their significance to the process of serpentinization. *Mineralogical Magazine*, **48**, 237-241.

Neal, C., and G. Stanger (1984b), Past and present serpentinization of ultramafic rocks; An example from the Semail ophiolite nappe of Northern Oman, in *Proceedings of the NATO Advanced Research Workshop on the The Chemistry of Weathering*, edited by T. Drever, pp. 249–275, D. Reidel, Dordrecht, Netherlands.

Neal, C. and Stanger, G. (1985). *Past and present serpentinisation of ultramafic rocks; an example from the Semail Ophiolite Nappe of Northern Oman* (pp. 249-275). Springer Netherlands.

Nicolas, A., Boudier, F., Ildefonse, B. and Ball, E. (2000). Accretion of Oman and United Arab Emirates ophiolite–Discussion of a new structural map. *Marine Geophysical Researches*, **21**, 147-180.

Nilsen, R. K. and Torsvik, T. (1996). *Methanococcus thermolithotrophicus* isolated from North Sea oil field reservoir water. *Applied and Environmental Microbiology*, **62**, 728-731.

Nilsen, R. K., Torsvik, T. and Lien, T. (1996a). *Desulfotomaculum thermocisternum* sp. nov., a sulfate reducer isolated from a hot North Sea oil reservoir. *International Journal of Systematic Bacteriology*, **46**, 397-402.

Nilsen, R. K., Beeder, J., Thorstenson, T. and Torsvik, T. (1996b). Distribution of thermophilic marine sulfate reducers in north sea oil field waters and oil reservoirs. *Applied and Environmental Microbiology*, **62**, 1793-1798.

Nogi, Y., Masui, N. and Kato, C. (1998). Photobacterium profundum sp. nov., a new, moderately barophilic bacterial species isolated from a deep-sea sediment. *Extremophiles*, **2**, 1-8.

Nunoura, T., Hirayama, H., Takami, H., Oida, H., Nishi, S., Shimamura, S., Suzuki, Y., Inagaki, F., Takai, K., Nealson, K.H., and Horikoshi, K. (2005). Genetic and functional properties of uncultivated thermophilic crenarchaeotes from a subsurface gold mine as revealed by analysis of genome fragments. *Environmental Microbiology*, **7**, 1967-1984.

Oakley, A. J., Taylor, B., Fryer, P., Moore, G. F., Goodliffe, A. M. and Morgan, J. K. (2007). Emplacement, growth, and gravitational deformation of serpentinite seamounts on the Mariana forearc. *Geophysical Journal International*, **170**, 615-634.

Olson, G. J., Dockins, W. S., McFeters, G. A. and Iverson, W. P. (1981). Sulfate-reducing and methanogenic bacteria from deep aquifers in montana. *Geomicrobiology Journal*, **2**, 327-340.

Olson, J. B., Steppe, T. F., Litaker, R. W. and Paerl, H. W. (1998). N_2-fixing microbial consortia associated with the ice cover of Lake Bonney, Antarctica. *Microbial Ecology*, **36**, 231-238.

Olsson, J., Stipp, S. L. S. and Gislason, S. R. (2014). Element scavenging by recently formed travertine deposits in the alkaline springs from the Oman Semail Ophiolite. *Mineralogical Magazine*, **78**, 1479-1490.

Onstott, T. C., Tobin, K., Dong, H., DeFlaun, M. F., Fredrickson, J. K., Bailey, T., Brockman, F., Kieft, T., Peacock, A., White, D.C., Balkwill, D., Phelps, T.J. and Boone, D. R. (1997, July). Deep gold mines of South Africa: windows into the subsurface

biosphere. In *Optical Science, Engineering and Instrumentation'97* (pp. 344-357). International Society for Optics and Photonics.

Onstott, T. C., Phelps, T. J., Colwell, F. S., Ringelberg, D., White, D. C., Boone, D. R., McKinley, J.P., Stevens, T.O., Loong, P.E., Balkwill, D.L., Griffin, W.T. and Kieft, T. (1998). Observations pertaining to the origin and ecology of microorganisms recovered from the deep subsurface of Taylorsville Basin, Virginia. *Geomicrobiology Journal*, **15**, 353-385.

Orcutt, B. N., Sylvan, J. B., Knab, N. J. and Edwards, K. J. (2011). Microbial ecology of the dark ocean above, at, and below the seafloor. *Microbiology and Molecular Biology Reviews*, **75**, 361-422.

Orcutt, B. N., Wheat, C. G., Rouxel, O., Hulme, S., Edwards, K. J. and Bach, W. (2013). Oxygen consumption rates in subseafloor basaltic crust derived from a reaction transport model. *Nature communications*, **4**.

Origlia-Luster M. L. and Woolley E. M. (2003). Apparent molar volumes and apparent molar heat capacities of dilute aqueous solutions of ethanol, 1-propanol, and 2-propanol at temperatures from 278.15 K to 393.15 K and at the pressure 0.35 MPa. *Journal of Chemical Thermodynamics* **35**, 1101-1118.

Orphan, V. J., Hinrichs, K. U., Ussler, W. I. I. I., Paull, C. K., Taylor, L. T., Sylva, S. P., Hayes, J.M., and DeLong, E. F. (2001a). Comparative analysis of methane-oxidizing archaea and sulfate-reducing bacteria in anoxic marine sediments. *Applied and Environmental Microbiology*, **67**, 1922-1934.

Orphan, V. J., House, C. H., Hinrichs, K. U., McKeegan, K. D. and DeLong, E. F. (2001b). Methane-consuming archaea revealed by directly coupled isotopic and phylogenetic analysis. *Science*, **293**, 484-487.

Paerl, H. W. and Priscu, J. C. (1998). Microbial phototrophic, heterotrophic, and diazotrophic activities associated with aggregates in the permanent ice cover of Lake Bonney, Antarctica. *Microbial Ecology*, **36**, 221-230.

Palandri, J. L. and Reed, M. H. (2004). Geochemical models of metasomatism in ultramafic systems: Serpentinization, rodingitization, and sea floor carbonate chimney precipitation. *Geochimica et Cosmochimica Acta*, **68**, 1115-1133.

Panikov, N. S. and Sizova, M. V. (2007). Growth kinetics of microorganisms isolated from Alaskan soil and permafrost in solid media frozen down to 35 C. *FEMS Microbiology Ecology*, **59**, 500-512.

Pantazis, T. M. (1978). Thermal mineral waters of Cyprus. *Proc. Internat. Congr. on Thermal Waters, Geothermal Energy and Volcanism, Mediterranean Area, Athens*, **2**, 367-386.

Parker, V.B. (1965). Thermal properties of uni-univalent electrolytes. *National Standard Reference Data Series, National Bureau of Standards* 2, p. 66.

Parkes, R. J., Cragg, B. A., Bale, S. J., Getlifff, J. M., Goodman, K., Rochelle, P. A., Fry, J.C., Weightman, A.J. and Harvey, S. M. (1994). Deep bacterial biosphere in Pacific Ocean sediments. *Nature*, **371**, 410-413.

Patterson, W. S. B. (1994). *The Physics of Glaciers*. 480 S.

Paukert, A. N., Matter, J. M., Kelemen, P. B., Shock, E. L. and Havig, J. R. (2012). Reaction path modeling of enhanced in situ CO 2 mineralization for carbon sequestration in the peridotite of the Samail Ophiolite, Sultanate of Oman. *Chemical Geology*, **330**, 86-100.

Pedersen K. J. (1952). The dissociation constants of pyruvic and oxaloacetic acid. *Acta Chemica Scandinavica* **8**, 243-256.

Pedersen, K. (1997). Microbial life in deep granitic rock. *FEMS Microbiology Reviews*, **20**, 399-414.

Pedersen, K. and Ekendahl, S. (1990). Distribution and activity of bacteria in deep granitic groundwaters of southeastern Sweden. *Microbial Ecology*, **20**, 37-52.

Pedley J. B., Naylor R. D. and Kirby S. P. (1986). *Thermochemical Data of Organic Compounds*. Springer Science and Business Media.

Peng, L., Arauzo-Bravo, M. J. and Shimizu, K. (2004). Metabolic flux analysis for a ppc mutant Escherichia coli based on 13C-labelling experiments together with enzyme activity assays and intracellular metabolite measurements. *FEMS Microbiology Letters*, **235**, 17-23.

Pinney, N., Kubicki, J.D., Middlemiss, D.S., Grey, C.P., and Morgan, D. (2009). Density functional theory study of ferrihydrite and related fe-oxyhydroxides. *Chemistry of Materials*, **21**, 5727–5742.

Plyasunov A. V. and Shock E. L. (2000a). Thermodynamic functions of hydration of hydrocarbons at 298.15 K and 0.1 MPa. *Geochimica et Cosmochimica Acta* **64**, 439-468.

Plyasunov A. V. and Shock E. L. (2000b). Standard state Gibbs energies of hydration of hydrocarbons at elevated temperatures as evaluated from experimental phase equilibria studies. *Geochimica et Cosmochimica Acta* **64**, 2811-2833.

Plyasunov A. V. and Shock E. L. (2001a). Correlation strategy for determining the parameters of the revised Helgeson-Kirkham-Flowers model for aqueous nonelectrolytes. *Geochimica et Cosmochimica Acta* **65**, 3879-3900.

Plyasunov A. V. and Shock E. L. (2001b). Group contribution values of the infinite dilution thermodynamic functions of hydration for aliphatic non-cyclic hydrocarbons, alcohols and ketones at 298.15 K and 0.1 MPa. *Journal of Chemical and Engineering Data* **46**, 1016-1019.

Plyasunov, A. V. and Shock, E. L. (2003). Prediction of the vapor–liquid distribution constants for volatile nonelectrolytes in water up to its critical temperature. *Geochimica et Cosmochimica Acta*, **67**, 4981-5009.

Plyasunov, A. V., O'Connell, J. P. and Wood, R. H. (2000a). Infinite dilution partial molar properties of aqueous solutions of nonelectrolytes. I. Equations for partial molar volumes at infinite dilution and standard thermodynamic functions of hydration of volatile nonelectrolytes over wide ranges of conditions. *Geochimica et Cosmochimica Acta*, **64**, 495-512.

Plyasunov, A. V., O'Connell, J. P., Wood, R. H. and Shock, E. L. (2000b). Infinite dilution partial molar properties of aqueous solutions of nonelectrolytes. II. Equations for the standard thermodynamic functions of hydration of volatile nonelectrolytes over wide ranges of conditions including subcritical temperatures. *Geochimica et Cosmochimica Acta*, **64**, 2779-2795.

Plyasunov A. V., Plyasunova N. V. and Shock E. L. (2004). Group contribution values for the thermodynamic functions of hydration of aliphatic esters at 298.15K and 0.1Mpa. *Journal of Chemical and Engineering Data* **49**, 1152–1167.

Plyasunov A. V., Plyasunova N. V. and Shock E. L. (2006a). Group contribution values for the thermodynamic functions of hydration at 298.15 K, 0.1 MPa. 3. Aliphatic monoethers, diethers, and polyethers. *Journal of Chemical and Engineering Data* **51**, 276-290.

Plyasunov A. V., Plyasunova N. V., Shock E. L. (2006b). Group contribution values for the thermodynamic functions of hydration at 298.15 K, 0.1 MPa. 4. Aliphatic nitriles and dinitriles. *Journal of Chemical and Engineering Data* **51**, 1481–90.

Plyasunova N. V., Plyasunov A. V. and Shock, E. L. (2005). Group contribution values for the thermodynamic functions of hydration at 298.15 K, 0.1 MPa. 2. Aliphatic thiols, alkyl sulfides, and polysulfides. *Journal of Chemical and Engineering Data* **50**, 246-253.

Ponce, Adrian; Priscu, John C.; Samarkin, Vladimir; Townsend, Ashley T.; Wagh, Protima; Young, Seth A.; Yung, Pung To; and Doran, Peter (2012) Microbial life at -13 ^{o}C in the brine of an ice-sealed Antarctic lake. *Proceedings of the National Academy of Science*, www.pnas.org/cgi/doi/10.1073/pnas.1208607109.

Pope, D.,H., Smith, W.,P., Swartz, R.,W., Landau, J.,V., (1975). Role of bacterial ribosomes in barotolerance. *Journal of Bacteriology* **121**, 664-669.

Poret-Peterson, A., Schwegel, R., Canovas, P., Shock, E. (2012, September). Microbiological aspects of methane and hydrogen cycling in hyperalkaline springs emerging from ultramafic rocks of the Samail ophiolite in Oman. At *Serpentine Days Conference,* Porquerolles Island, France.

Power, I. M., Wilson, S. A., Thom, J. M., Dipple, G. M. and Southam, G. (2007). Biologically induced mineralization of dypingite by cyanobacteria from an alkaline wetland near Atlin, British Columbia, Canada. *Geochemical Transactions*, **8**, 13.

Power, I. M., Wilson, S. A., Harrison, A. L., Dipple, G. M., McCutcheon, J., Southam, G. and Kenward, P. A. (2014). A depositional model for hydromagnesite–magnesite playas near Atlin, British Columbia, Canada. *Sedimentology*, **61**, 1701-1733.

Prapaipong P. and Shock E. L. (2001). Estimation of standard-state entropies of association for aqueous metal—organic complexes and chelates at 25°C and 1 bar. *Geochimica et Cosmochimica Acta* **65**, 3931-3953.

Prapaipong P., Shock E. L. and Koretsky C. M. (1999). Metal-organic complexes in geochemical processes: Temperature dependence of standard partial molal thermodynamic properties of aqueous complexes between metal cations and dicarboxylate ligands. *Geochimica et Cosmochimica Acta* **63**, 2547-2577.

Price, P. B. and Sowers, T. (2004). Temperature dependence of metabolic rates for microbial growth, maintenance, and survival. *Proceedings of the National Academy of Sciences*, **101**, 4631-4636.

Priscu, J. C. and Christner, B. C. (2004). Earth's icy biosphere. *Microbial Diversity and Bioprospecting*, 130-145.

Priscu, J. C., Adams, E. E., Lyons, W. B., Voytek, M. A., Mogk, D. W., Brown, R. L., McKay, C.P., Takacs, C.D., Welch, K.A., Wolf, C.F., Kirshtein, J.D., Avci, R. (1999). Geomicrobiology of subglacial ice above Lake Vostok, Antarctica. *Science*, **286**, 2141-2144.

Proskurowski, G., Lilley, M. D., Kelley, D. S. and Olson, E. J. (2006). Low temperature volatile production at the Lost City Hydrothermal Field, evidence from a hydrogen stable isotope geothermometer. *Chemical Geology*, **229**, 331-343.

Proskurowski G, Lilley MD, Seewald JS, Frueh-Green G, Olson EJ, Lupton JE, Sylva SP, Kelley DS (2008) Abiogenic hydrocarbon production at Lost City hydrothermal field. *Science* **319,** 604-607.

Purdy, K. J., Nedwell, D. B. and Embley, T. M. (2003). Analysis of the sulfate-reducing bacterial and methanogenic archaeal populations in contrasting Antarctic sediments. *Applied and Environmental Microbiology*, **69**, 3181-3191.

Quéméneur, M., Bes, M., Postec, A., Mei, N., Hamelin, J., Monnin, C., Chavagnac, V., Ollivier, B. and Erauso, G. (2014). Spatial distribution of microbial communities in the shallow submarine alkaline hydrothermal field of the Prony Bay, New Caledonia. *Environmental Microbiology Reports*, **6**, 665-674.

Quéméneur, M., Palvadeau, A., Postec, A., Monnin, C., Chavagnac, V., Ollivier, B. and Erauso, G. (2015). Endolithic microbial communities in carbonate precipitates from serpentinite-hosted hyperalkaline springs of the Voltri Massif (Ligurian Alps, Northern Italy). *Environmental Science and Pollution Research*, 1-12.

Rancourt D. G. and Meunier J. F. (2008). Constraints on structural models of ferrihydrite as a nanocrystalline material. *American Mineralogist* **93**, 1412–1417.

Reeburgh, W. S. (2007). Oceanic methane biogeochemistry. *Chemical Reviews*, **107**, 486-513.

Reid, R. C., Prausnitz, J. M. and Poling, B. E. (1987). The properties of gases and liquids.

Rennermalm, A. K., Moustafa, S. E., Mioduszewski, J., Chu, V. W., Forster, R. R., Hagedorn, B., Harper, J.T., Mote, T.L., Robinson, D.A., Shuman, C.A., Smith, L. C. and Tedesco, M. (2013). Understanding Greenland ice sheet hydrology using an integrated multi-scale approach. *Environmental Research Letters*, **8**, 015017.

Rickard, D. and Luther, G. W. (2007). Chemistry of iron sulfides. *Chemical Reviews*, **107**, 514-562.

Richard L. (2001). Calculation of the standard molal thermodynamic properties as a function of temperature and pressure of some geochemically important organic sulfur compounds. *Geochimica et Cosmochimica Acta* **65**, 3827-3877.

Richard L. and Helgeson H. C. (1998). Calculation of the thermodynamic properties at elevated temperatures and pressures of saturated and aromatic high molecular weight solid and liquid hydrocarbons in kerogen, bitumen, petroleum, and other organic matter of biogeochemical interest. *Geochimica et Cosmochimica Acta*, **62**, 3591-3636.

Rioux, M., Bowring, S., Kelemen, P., Gordon, S., Miller, R. and Dudas, F. (2013). Tectonic development of the Samail ophiolite: High-precision U-Pb zircon geochronology and Sm-Nd isotopic constraints on crustal growth and emplacement. *Journal of Geophysical Research: Solid Earth*, **118**, 2085-2101.

Rivkina, E. M., Friedmann, E. I., McKay, C. P. and Gilichinsky, D. A. (2000). Metabolic activity of permafrost bacteria below the freezing point. *Applied and Environmental Microbiology*, **66**, 3230-3233.

Robie, R.A. and Hemingway, B.S. (1995) Thermodynamic properties of minerals and related substances at 298.15 K and 1 bar (10^5 pascals) and at higher temperatures. *US Geological Survey Bulletin*, **2131**, 461.

Rogers K. L. and Amend J. P. (2006). Energetics of potential heterotrophic metabolisms in the marine hydrothermal system of Vulcano Island, Italy. *Geochimica et Cosmochimica Acta* **70**, 6180–6200.

Rogers, K.L. and Schulte, M.D. (2012) Organic sulfur metabolisms in hydrothermal environments. *Geobiology* **10**, 320-332.

Rogers, S. O., Shtarkman, Y. M., Koçer, Z. A., Edgar, R., Veerapaneni, R. and D'Elia, T. (2013). Ecology of subglacial Lake Vostok (Antarctica), based on metagenomic/metatranscriptomic analyses of accretion ice. *Biology*, **2**, 629-650.

Rosnes, J. T., Torsvik, T. and Lien, T. (1991). Spore-forming thermophilic sulfate-reducing bacteria isolated from North Sea oil field waters. *Applied and Environmental Microbiology*, **57**, 2302-2307.

Rue, E. L. and Bruland, K. W. (1995). Complexation of iron (III) by natural organic ligands in the Central North Pacific as determined by a new competitive ligand equilibration/adsorptive cathodic stripping voltammetric method. *Marine Chemistry*, **50**, 117-138.

Russell, M. J. (2007). The alkaline solution to the emergence of life: Energy, entropy and early evolution. *Acta Biotheoretica*, **55**, 133-179.

Russell, C. E., Jacobson, R., Haldeman, D. L. and Amy, P. S. (1994). Heterogeneity of deep subsurface microorganisms and correlations to hydrogeological and geochemical parameters. *Geomicrobiology Journal*, **12**, 37-51.

Russell, M. J., Hall, A. J., Boyce, A. J. and Fallick, A. E. (2005). 100th Anniversary special paper: On Hydrothermal Convection Systems and the Emergence of Life. *Economic Geology*, **100**, 419-438.

Russell, M. J., Hall, A. J. and Martin, W. (2010). Serpentinization as a source of energy at the origin of life. *Geobiology*, **8**, 355-371.

Russell, M. J., Barge, L. M., Bhartia, R., Bocanegra, D., Bracher, P. J., Branscomb, E., Kidd, R., McGlynn, S., Meier, D.H., Nitschke, W., Shibuya, T., Vance, S., White, L. and Kanik, I. (2014). The drive to life on wet and icy worlds. *Astrobiology*, **14**, 308-343.

Rysgaard, S., Glud, R. N., Risgaard-Petersen, N. and Dalsgaard, T. (2004). Denitrification and anammox activity in Arctic marine sediments. *Limnology and Oceanography*, **49**, 1493-1502.

Sadeghi R. and Goodarzi B. (2008). Volumetric properties of potassium dihydrogen citrate and tripotassium citrate in water and in aqueous solutions of alanine at T = (283.15 to 308.15K). *Journal of Chemical and Engineering Data* **53**, 26-35.

Sadeghi R. and Ziamajidi F. (2007). Thermodynamic properties of tripotassium citrate in water and in aqueous solutions of polypropylene oxide 400 over a range of temperatures. *Journal of Chemical and Engineering Data* **52**, 1753-1759.

Sadeghi R., Golabiazar R. and Parsi E. (2010). Vapor-liquid equilibriua, density, and speed of sound if aqueous solutions of sodium dihydrogen citrate of disodium hydrogen citrate. *Journal of Chemical and Engineering Data* **55**, 5874-5882.

Sader, J. A., Leybourne, M. I., McClenaghan, M. B. and Hamilton, S. M. (2007). Low-temperature serpentinization processes and kimberlite groundwater signatures in the Kirkland Lake and Lake Timiskiming kimberlite fields, Ontario, Canada: Implications for diamond exploration. *Geochemistry: Exploration, Environment, Analysis*, **7**, 3-21.

Sajed, T., Marcu, A., Ramirez, M., Pon, A., Guo, A., Knox, C., Wilson, M., Grant, J., Djoumbou, Y. and Wishart, D. (2015). ECMDB 2.0: A richer resource for understanding the biochemistry of E. coli. Nucleic Acids Res, p.gkv1060. 26481353.

Sahl, J. W., Schmidt, R., Swanner, E. D., Mandernack, K. W., Templeton, A. S., Kieft, T. L., Smith, R.L., Sanford, W.E., Callaghan, R.L., Mitton, J.B. and Spear, J. R. (2008). Subsurface microbial diversity in deep-granitic-fracture water in Colorado. *Applied and Environmental Microbiology*, **74**, 143-152.

Salamatin, A. N., Lipenkov, V. Y., Barkov, N. I., Jouzel, J., Petit, J. R. and Raynaud, D. (1998). Ice core age dating and paleothermometer calibration based on isotope and temperature profiles from deep boreholes at Vostok Station (East Antarctica). *Journal of Geophysical Research: Atmospheres (1984–2012)*, **103**, 8963-8977.

Salisbury, M.H. and ODP 195 Shipboard Scientific Party, 2002: Site 1200. *In,* Scientific Party, *Proceedings of the Ocean Drilling Program Initial Reports*, Vol. 195. (http://www.odp.tamu.edu/publications/195)IR/195TOC.HTM)

Sano, Y., Urabe, A., Wakita, H. and Wushiki, H. (1993). Origin of hydrogen-nitrogen gas seeps, Oman. *Applied Geochemistry*, **8**, 1-8.

Sassani D. C. and Shock E. L. (1992). Estimation of standard partial molal entropies of aqueous ions at 25°C and 1 bar. *Geochimica et Cosmochimica Acta*, **56**, 3895-3908.

Sassani D. C. and Shock E. L. (1998). Solubility and transport of platinum-group elements in supercritical fluids: Summary and estimates of thermodynamic properties for Ru, Rh, Pd, and Pt solids, aqueous ions and aqueous complexes. *Geochimica et Cosmochimica Acta* **62**, 2643-2671.

Schäfer, G., Engelhard, M. and Müller, V. (1999). Bioenergetics of the Archaea. *Microbiology and molecular biology reviews*, **63**, 570-620.

Schink, B. (1997). Energetics of syntrophic cooperation in methanogenic degradation. *Microbiology and Molecular Biology Reviews*, **61**, 262-280.

Schink, B. and Thauer, R. K. (1988). Energetics of syntrophic methane formation and the influence of aggregation. *Granular Anaerobic Sludge*, 5-17.

Schippers, A. and Neretin, L. N. (2006). Quantification of microbial communities in near-surface and deeply buried marine sediments on the Peru continental margin using real-time PCR. *Environmental Microbiology*, **8**, 1251-1260.

Schloss J. V., Emptage M. H. and Cleland W. W. (1984). pH profiles and isotope effects for aconitases from *Saccharomycopsis lipolytica*, beef heart, beef liver. α-Methyl-*cis*-aconitate and *threo*-D_S-α-methylisocitrate as substrates. *Biochemistry* **23**, 4572-4580.

Scholander, P. F., Bradstreet, E. D., Hemmingsen, E. A. and Hammel, H. T. (1965). Sap pressure in vascular plants negative hydrostatic pressure can be measured in plants. *Science*, **148**, 339-346.

Schrenk, M. O., Kelley, D. S., Bolton, S. A. and Baross, J. A. (2004). Low archaeal diversity linked to subseafloor geochemical processes at the Lost City Hydrothermal Field, Mid-Atlantic Ridge. *Environmental Microbiology*, **6**, 1086-1095.

Schrenk, M. O., Brazelton, W. J. and Lang, S. Q. (2013). Serpentinization, carbon, and deep life. *Reviews in Mineralogy and Geochemistry*, **75**, 575-606.

Schulte M. D. and Shock E. L. (1993). Aldehydes in hydrothermal solutions: Standard partial molal thermodynamic properties and relative stabilities at high temperatures and pressures. *Geochimica et Cosmochimica Acta* **57**, 3835-3846.

Schulte M. D., Shock E. L. and Wood R. H. (2001). The temperature dependence of the standard state thermodynamic properties of aqueous nonelectrolytes. *Geochimica et Cosmochimica Acta* **65**, 3919-3930.

Schulte M, Blake D, Hoehler T, McCollom TM (2006). Serpentinization and its implications for life on the early Earth and Mars. *Astrobiology* **6,** 364–376.

Schwarz, J.,R., Colwell, R.,R., (1975) (abstract). In: *Proceedings, 75th annual meeting of the American Society for Microbiology*, American Society for Microbiology, Washington DC, p 162.

Schwarz, J. R. and Colwell, R. R. (1975). Heterotrophic activity of deep-sea sediment bacteria. *Applied Microbiology*, **30**, 639-649.

Schwarz, J. R., Walker, J. D. and Colwell, R. R. (1975). Deep-sea bacteria: Growth and utilization of n-hexadecane at in situ temperature and pressure. *Canadian Journal of Microbiology*, *21*(5), 682-687.

Schwertmann U. (1988) Some properties of soil and synthetic iron oxides In *Iron in Soils and Clay Minerals* (ed. J. W. Stucki et al.); *NATO ASI Ser.* 217, 203–244.

Schwertmann U. and Taylor R. M. (1989) Iron oxides. In: *Minerals in Soil Environments* (eds. J. B. Dixon and S. B. Weed). Soil Science Society of America, pp. 379–438.

Schwarzenbach, E. (2011). *Serpentinization, fluids and life: Comparing carbon and sulfur cycles in modern and ancient environments* (Doctoral dissertation, Diss., Eidgenössische Technische Hochschule ETH Zürich, Nr. 19588, 2011).

Schwarzenbach, E. M., Lang, S. Q., Früh-Green, G. L., Lilley, M. D., Bernasconi, S. M. and Méhay, S. (2013). Sources and cycling of carbon in continental, serpentinite-hosted alkaline springs in the Voltri Massif, Italy. *Lithos*, **177**, 226-244.

Segarra, K. E., Comerford, C., Slaughter, J. and Joye, S. B. (2013). Impact of electron acceptor availability on the anaerobic oxidation of methane in coastal freshwater and brackish wetland sediments. *Geochimica et Cosmochimica Acta*, ***115***, 15-30.

Semhi, K., Abdalla, O. A., Al Khirbash, S., Khan, T., Asaidi, S. and Farooq, S. (2009). Mobility of rare earth elements in the system soils–plants–groundwaters: a case study of an arid area (Oman). *Arabian Journal of Geosciences*, **2**, 143-150.

Sharma, A., Scott, J. H., Cody, G. D., Fogel, M. L., Hazen, R. M., Hemley, R. J. and Huntress, W. T. (2002). Microbial activity at gigapascal pressures. *Science*, **295**, 1514-1516.

Sharp, M., Parkes, J., Cragg, B., Fairchild, I. J., Lamb, H. and Tranter, M. (1999). Widespread bacterial populations at glacier beds and their relationship to rock weathering and carbon cycling. *Geology*, **27**, 107-110.

Sharp, M., Creaser, R. A. and Skidmore, M. (2002). Strontium isotope composition of runoff from a glaciated carbonate terrain. *Geochimica et Cosmochimica Acta*, **66**, 595-614.

Shi, T., Reeves, R. H., Gilichinsky, D. A. and Friedmann, E. I. (1997). Characterization of viable bacteria from Siberian permafrost by 16S rDNA sequencing. *Microbial Ecology*, **33**, 169-179.

Shock E. L. (1992). Stability of peptides in high temperature aqueous solutions.

Geochimica et Cosmochimica Acta **56**, 3481-3491.

Shock E. L. (1993). Hydrothermal dehydration of aqueous organic compounds. *Geochimica et Cosmochimica Acta* **57**, 3341-3349.

Shock E. L. (1994). Erratum to D. C. Sassani and E. L. Shock (1992) "Estimation of standard partial molal entropies of aqueous ions at 25°C and 1 bar" . *Geochimica et Cosmochimica Acta* **58**, 2756-2758.

Shock E. L. (1995). Organic acids in hydrothermal solutions-standard molal thermodynamic properties of carboxylic acids and estimates of dissociation constants at high temperatures and pressures. *American Journal of Science* **295**, 496–580.

Shock, E.L. (2009) Minerals as energy sources. *Economic Geology*, **104**, 1235-1248.

Shock E. L. and Boyd E. S. (2015). Principles of geobiochemistry. *Elements* **11**, 395-401.

Shock E. and Canovas P. (2010). The potential for abiotic organic synthesis and biosynthesis at seafloor hydrothermal systems. *Geofluids* **10**, 161-192.

Shock E. L. and Helgeson H. C. (1988). Calculation of the thermodynamic and transport properties of aqueous species at high pressures and temperatures: correlation algorithms for ionic species and equation of state predictions to 5 kb and 1000°C. *Geochimica et Cosmochimica Acta* **52**, 2009-2036.

Shock E. L. and Helgeson H. C. (1990). Calculation of the thermodynamic and transport properties of aqueous species at high pressures and temperatures: Standard partial molal properties of organic species. *Geochimica et Cosmochimica Acta* **54**, 915-945.

Shock, E. L. and Holland, M. E. (2004). Geochemical energy sources that support the subsurface biosphere. *The subseafloor biosphere at mid-ocean ridges*, 153-165.

Shock E. L. and Koretsky C. M. (1993). Metal-organic complexes in geochemical processes: Calculation of standard partial molal thermodynamic properties of aqueous acetate complexes at high pressures and temperatures. *Geochimica et Cosmochimica Acta* **57**, 4899-4922.

Shock E. L. and Koretsky C. M. (1995). Metal-organic complexes in geochemical processes: Estimation of standard partial molal thermodynamic properties of aqueous complexes between metal cations and monovalent organic acid ligands at high pressures and temperatures. *Geochimica et Cosmochimica Acta* **59**, 1497-1532.

Shock E. L. and McKinnon W. B. (1993). Hydrothermal processing of cometary volatiles-Applications to Triton. *Icarus* **106**, 464-477.

Shock E. L., Helgeson H. C. and Sverjensky D. A. (1989). Calculation of the thermodynamic and transport properties of aqueous species at high pressures and temperatures: Standard partial molal properties of inorganic neutral species. *Geochimica et Cosmochimica Acta* **53**, 2157-2183.

Shock E. L., Oelkers E. H., Johnson J. W., Sverjensky, D. A. and Helgeson H. C. (1992). Calculation of the thermodynamic properties of aqueous species at high pressures and temperatures: Effective electrostatic radii, dissociation constants, and standard partial molal properties to 1000°C and 5 kb. *Journal of the Chemical Society, Faraday Transactions* **88**, 803-826.

Shock E. L., Sassani D. C., Willis M. and Sverjensky D. A. (1997a). Inorganic species in geologic fluids: Correlations among standard molal thermodynamic properties of aqueous ions and hydroxide complexes. *Geochimica et Cosmochimica Acta* **61**, 907-950.

Shock E. L., Sassani D. C. and Betz H. (1997b). Uranium in geologic fluids: Estimates of oxidation potentials and hydrolysis constants at high temperatures and pressures. *Geochimica et Cosmochimica Acta* **61**, 4245-4266.

Shock, E. L., Amend, J. P. and Zolotov, M. Y. (2000). The early Earth vs. the origin of life. *Origin of the Earth and Moon*, 527-543.

Shock E. L., Holland M., Meyer-Dombard D. and Amend J. P. (2005). Geochemical sources of energy for microbial metabolism in hydrothermal ecosystems: Obsidian Pool, Yellowstone National Park, USA. *Geothermal Biology and Geochemistry in Yellowstone National Park* (eds. Inskeep, WP, McDermott, TR), Thermal Biology Institute, Montana State University pp. 95-112.

Shock E. L., Holland M. E., Meyer-Dombard D. R., Amend J. P., Osburn G. R. and Fischer T. (2010). Quantifying inorganic sources of geochemical energy in hydrothermal ecosystems, Yellowstone National Park, USA. *Geochimica et Cosmochimica Acta* **74**, 4005-4043.

Shock E. L., Canovas P., Yang Z., Boyer G., Johnson K., Robinson K., Fecteau K., Windman T. and Cox A. (2013). Thermodynamics of organic transformations in hydrothermal fluids. *Reviews in Mineralogy & Geochemistry* **76**, 311-350.

Shtarkman, Y. M., Koçer, Z. A., Edgar, R., Veerapaneni, R. S., D'Elia, T., Morris, P. F. and Rogers, S. O. (2013). Subglacial Lake Vostok (Antarctica) accretion ice contains a diverse set of sequences from aquatic, marine and sediment-inhabiting bacteria and eukarya. *PLoS One*, *8*(7), e67221.

Sijpkes A. H., Van Rossum P., Raad J. S. and Somsen G. (1989). Heat capacities and volumes of some polybasic carboxylic acids in water at 298.15 K. *Journal of Chemical Thermodynamics* **21**, 1061-1067.

Simoneit, B.R.T. and Sparrow, M.A. (2002) Dissolved organic carbon in interstitial waters from sediments of Middle Valley and Esscanaba Trough, Northeast Pacific, ODP Legs 139 and 169. *Appllied Geochemistry* **17**, 1495-1502.

Skidmore, M. L., Foght, J. M. and Sharp, M. J. (2000). Microbial life beneath a high Arctic glacier. *Applied and Environmental Microbiology*, **66**, 3214-3220.

Skidmore, M., Anderson, S. P., Sharp, M., Foght, J. and Lanoil, B. D. (2005). Comparison of microbial community compositions of two subglacial environments reveals a possible role for microbes in chemical weathering processes. *Applied and Environmental Microbiology*, **71**, 6986-6997.

Skoog A., Vlahos P., Rogers K. L. and Amend J. P. (2007). Concentrations, distributions, and energy yields of dissolved neutral aldoses in a shallow hydrothermal vent system of Vulcano, Italy. *Organic Geochemistry* **38**, 1416–1430.

Sleep NH, Meibom A, Fridriksson T, Coleman RG, Bird DK (2004). H_2-rich fluids from serpentinization: Geochemical and biotic implications. *Proceedings of the National Academy of Sciences* **101**, 12818-12823.

Sleep NH, Bird DK, Pope EC (2011). Serpentinite and the dawn of life. *Philosophical Transactions of the Royal Society B-Biological Sciences* **366**, 2857-2869. doi:10.1098/rstb.2011.0129.

Smith, J. N. and Shock, E. L. (2007). A thermodynamic analysis of microbial growth experiments. *Astrobiology*, **7**, 891-904.

Smith, S. J., Page, K., Kim, H., Campbell, B. J., Boerio-Goates, J. and Woodfield, B. F. (2012). Novel synthesis and structural analysis of ferrihydrite. *Inorganic Chemistry* **51**, 6421-6424.

Snow, C.L., Lilova, K.I., Radha, A.V., Shi, Q., Smith, S., Navrotsky, A., Boerio-Goates, J., Woodfield, B.F. (2013) Heat capacity and thermodynamics of a synthetic two-line ferrihydrite, $FeOOH{\cdot}0.027H_2O$. *Journal of Chemical Thermodynamics* **58**, 307-314.

Sørensen, J. (1978). Capacity for denitrification and reduction of nitrate to ammonia in a coastal marine sediment. *Applied and Environmental Microbiology*, **35**, 301-305.

St-Jean, G. (2003). Automated quantitative and isotopic (^{13}C) analysis of dissolved inorganic carbon and dissolved organic carbon in continuous-flow using a total organic carbon analyser. *Rapid Communications in Mass Spectrometry*, **17,** 419-428.

Stetter, K. O., Huber, R., Blöchl, E., Kurr, M., Eden, R. D., Fielder, M., Cash, H. and Vance, I. (1993). Hyperthermophilic archaea are thriving in deep North Sea and Alaskan oil reservoirs. *Nature*, **365**, 743-745.

Stanger, G. (1985) *The hydrogeology of the Oman Mountains*. Ph.D. Thesis, Open University, London, U.K.

Steurer, J. F. and Underwood, M. B. (2003). Data report: the relation between physical properties and grain-size variations in hemipelagic sediments from Nankai Trough. In *Proceedings of the ODP, Science Results* **190**, 1-25).

Stevens, T. O., McKinley, J. P. and Fredrickson, J. K. (1993). Bacteria associated with deep, alkaline, anaerobic groundwaters in southeast Washington. *Microbial Ecology*, **25**, 35-50.

Stevens, T. O. and McKinley, J. P. (1995). Lithoautotrophic microbial ecosystems in deep basalt aquifers. *Science*, **270**, 450-455.

Stull, D.R., Westrum, E.F., Jr. and Sinke, G.C. (1969) *The Chemical Thermodynamics of Organic Compounds*, John Wiley and Sons, New York.

Sverjensky D. A., Shock E. L. and Helgeson H. C. (1997). Prediction of the thermodynamic properties of aqueous metal complexes to 1000°C and 5 kb. *Geochimica et Cosmochimica Acta* **61**, 1359-1412.

Sverjensky D. A., Harrison B. and Azzolini D. (2014). Water in the deep Earth: The dielectric constant and the solubilities of quartz and corundum to 60 kb and 1200°C. *Geochimica et Cosmochimica Acta* **129**, 125-145.

Syracuse, E. M., van Keken, P. E. and Abers, G. A. (2010). The global range of subduction zone thermal models. *Physics of the Earth and Planetary Interiors*, **183**, 73-90.

Szewzyk, U., Szewzyk, R. and Stenström, T. A. (1994). Thermophilic, anaerobic bacteria isolated from a deep borehole in granite in Sweden. *Proceedings of the National Academy of Sciences* **91**, 1810-1813.

Szewzyk, U., Szewzyk, R. and Stenstroem, T. A. (1997). Thermophilic fermentative bacteria from a deep borehole in granitic rock in Sweden. In *Optical Science, Engineering and Instrumentation'97* (pp. 330-334). International Society for Optics and Photonics.

Szponar, N., Brazelton, W. J., Schrenk, M. O., Bower, D. M., Steele, A. and Morrill, P. L. (2013). Geochemistry of a continental site of serpentinization, the Tablelands Ophiolite, Gros Morne National Park: A Mars analogue. *Icarus*, **224**, 286-296.

Takai, K., Moser, D. P., Onstott, T. C., Spoelstra, N., Pfiffner, S. M., Dohnalkova, A. and Fredrickson, J. K. (2001a). *Alkaliphilus transvaalensis* gen. nov., sp. nov., an extremely

alkaliphilic bacterium isolated from a deep South African gold mine. *International Journal of Systematic and Evolutionary Microbiology*, **51**, 1245-1256.

Takai, K., Moser, D. P., DeFlaun, M., Onstott, T. C. and Fredrickson, J. K. (2001b). Archaeal diversity in waters from deep South African gold mines. *Applied and Environmental Microbiology*, **67**, 5750-5760.

Takai, K., Hirayama, H., Sakihama, Y., Inagaki, F., Yamato, Y. and Horikoshi, K. (2002). Isolation and metabolic characteristics of previously uncultured members of the order Aquificales in a subsurface gold mine. *Applied and Environmental Microbiology*, **68**, 3046-3054.

Takai, K., Moyer, C. L., Miyazaki, M., Nogi, Y., Hirayama, H., Nealson, K. H. and Horikoshi, K. (2005). Marinobacter alkaliphilus sp. nov., a novel alkaliphilic bacterium isolated from subseafloor alkaline serpentine mud from Ocean Drilling Program Site 1200 at South Chamorro Seamount, Mariana Forearc. *Extremophiles*, **9**, 17-27.

Takai, K., Nakamura, K., Toki, T., Tsunogai, U., Miyazaki, M., Miyazaki, J., Hirayama, H., Nakagawa, S., Nunoura, T. and Horikoshi, K. (2008). Cell proliferation at 122 ^{o}C and isotopically heavy CH4 production by a hyperthermophilic methanogen under high-pressure cultivation. *Proceedings of the National Academy of Sciences*, **105**, 10949-10954.

Tanaka, T., Burgess, J. and Wright, P. (2001). High-pressure adaptation by salt stress in a moderately halophilic bacterium obtained from open seawater. *Applied Microbiology and Biotechnology*, **57**, 200-204.

Tanger J. C. IV and Helgeson H. C. (1988). Calculation of the thermodynamic and transport properties of aqueous species at high pressures and temperatures: Revised equations of state for the standard partial molal properties of ions and electrolytes. *American Journal of Science* **288**, 19-98.

Tardy-Jacquenod, C., Magot, M., Patel, B. K. C., Matheron, R. and Caumette, P. (1998). *Desulfotomaculum halophilum* sp. nov., a halophilic sulfate-reducing bacterium isolated from oil production facilities. *International Journal of Systematic Bacteriology*, **48**, 333-338.

Telling, J., Stibal, M., Anesio, A. M., Tranter, M., Nias, I., Cook, J., Bellas, C., Lis, G., Wadham, J.L., Sole, A., Nienow, P. and Hodson, A. (2012). Microbial nitrogen cycling on the Greenland Ice Sheet. *Biogeosciences*, **9**, 2431-2442.

Telling, J., Boyd, E. S., Bone, N., Jones, E. L., Tranter, M., MacFarlane, J. W., Martin, P.G., Wadham, J.L., Lamarche-Gagnon, G., Skidmore, M.L., Hamilton, T. L., Hill, E., Jackson, M. and Hodgson, D.A. (2015). Rock comminution as a source of hydrogen for subglacial ecosystems. *Nature Geoscience*, **8**, 851-855.

Tewari Y. B., Kishore N., Goldberg R. N. and Luong T. N. (1998). An equilibrium and calorimetric study of some transamination reactions. *Journal of Chemical Thermodynamics* **30**, 777-793.

Thauer, R. K. (1990). Energy metabolism of methanogenic bacteria. *Biochimica et Biophysica Acta (BBA)-Bioenergetics*, **1018**, 256-259.

Thauer R. K., Jungermann K. and Decker K. (1977). Energy conservation in chemotrophic anaerobic bacteria. *Bacteriological Reviews* **41**, 100-180.

Thauer, R. K., Kaster, A. K., Seedorf, H., Buckel, W. and Hedderich, R. (2008). Methanogenic archaea: ecologically relevant differences in energy conservation. *Nature Reviews Microbiology*, **6**, 579-591.

Tilton, G. R., Hopson, C. A. and Wright, J. E. (1981). Uranium-lead isotopic ages of the Samail Ophiolite, Oman, with applications to Tethyan ocean ridge tectonics. *Journal of Geophysical Research: Solid Earth* **86**, 2763-2775.

Tippit, P. R., Pessagno, E. A. and Smewing, J. D. (1981). The biostratigraphy of sediments in the volcanic unit of the Samail ophiolite. *Journal of Geophysical Research: Solid Earth* **86**, 2756-2762.

Tobal, G.M., (1993) Master's Thesis, Scripps Institute of Oceanography, University of California, San Diego, La Jolla, CA.

Towe, K. M. and Bradley, W. F. (1967) Mineralogical constitution of colloidal hydrous ferric oxides. *Journal of Colloid and Interface Science* **24**, 384-392.

Tranter, M., Sharp, M. J., Lamb, H. R., Brown, G. H., Hubbard, B. P. and Willis, I. C. (2002). Geochemical weathering at the bed of Haut Glacier d'Arolla, Switzerland—a new model. *Hydrological Processes*, **16**, 959-993.

Tranter, M., Skidmore, M. and Wadham, J. (2005). Hydrological controls on microbial communities in subglacial environments. *Hydrological Processes*, **19**, 995-998.

Trimarco, E., Balkwill, D., Davidson, M. and Onstott, T. C. (2006). In situ enrichment of a diverse community of bacteria from a 4–5 km deep fault zone in South Africa. *Geomicrobiology Journal*, **23**, 463-473.

Tsunogai, U., Nakagawa, F., Gamo, T. and Ishibashi, J. (2005). Stable isotopic compositions of methane and carbon monoxide in the Suiyo hydrothermal plume, Izu–Bonin arc: Tracers for microbial consumption/production. *Earth and Planetary Science Letters*, **237**, 326-340.

Tung, H. C., Price, P. B., Bramall, N. E. and Vrdoljak, G. (2006). Microorganisms metabolizing on clay grains in 3-km-deep Greenland basal ice. *Astrobiology*, **6**, 69-86.

Turley, C. (2000). Bacteria in the cold deep-sea benthic boundary layer and sediment–water interface of the NE Atlantic. *FEMS microbiology ecology*, **33**, 89-99.

Valentine, D. L. and Reeburgh, W. S. (2000). New perspectives on anaerobic methane oxidation. *Environmental Microbiology*, **2**, 477-484.

Vanlint, D., Mitchell, R., Bailey, E., Meersman, F., McMillan, P. F., Michiels, C. W. and Aertsen, A. (2011). Rapid acquisition of gigapascal-high-pressure resistance by *Escherichia coli*. *Mbio*, *2*(1), e00130-10.

Wadham, J. L., Bottrell, S., Tranter, M. and Raiswell, R. (2004). Stable isotope evidence for microbial sulphate reduction at the bed of a polythermal high Arctic glacier. *Earth and Planetary Science Letters*, **219**, 341-355.

Wadham, J. L., Tranter, M., Tulaczyk, S. and Sharp, M. (2008). Subglacial methanogenesis: a potential climatic amplifier?. *Global Biogeochemical Cycles*, **22**.

Wadsö, I., Gutfreund, H., Privalov, P., Edsall, J. T., Jencks, W. P., Armstrong, G. T. and Biltonen, R. L. (1976). Recommendations for measurement and presentation of biochemical equilibrium data. *Journal of Biologiccal Chemistry* **251**, 6879-6885.

Wagman D. D., Evans W. H., Parker V. B., Schumm R. H., Halow I., Bailey S. M., Churney K. L. and Nuttall R. L. (1982). The NBS tables of chemical thermodynamic properties. *Journal of Physical and Chemical Reference Data* **11** (Supplement no. 2).

Wagman, D. D., Evans, W. H., Parker, V. B., Schumm, R. H. and Halow, I. (1982). *The NBS tables of chemical thermodynamic properties. Selected values for inorganic and C1 and C2 organic substances in SI units*. National Standard Reference Data System.

Wagner, W. and Pruß, A. (2002). The IAPWS formulation 1995 for the thermodynamic properties of ordinary water substance for general and scientific use. *Journal of Physical and Chemical Reference Data*, **31**, 387-535.

Walder, J. (1979). Geometry of former subglacial water channels and cavities. *Journal of Glaciology*, **23**, 335-346.

Wanger, G., Moser, D., Hay, M., Myneni, S., Onstott, T. C. and Southam, G. (2012). Mobile hydrocarbon microspheres from 2-billion-year-old carbon-bearing seams in the South African deep subsurface. *Geobiology*, **10**, 496-505.

Ward, B. B., Granger, J., Maldonado, M. T. and Wells, M. L. (2003). What limits bacterial production in the suboxic region of permanently ice-covered Lake Bonney, Antarctica?. *Aquatic Microbial Ecology*, **31**, 33-47.

Wehrmann, L. M., Formolo, M. J., Owens, J. D., Raiswell, R., Ferdelman, T. G., Riedinger, N. and Lyons, T. W. (2014). Iron and manganese speciation and cycling in glacially influenced high-latitude fjord sediments (West Spitsbergen, Svalbard): Evidence for a benthic recycling-transport mechanism. *Geochimica et Cosmochimica Acta*, **141**, 628-655.

Wei, W., Kastner, M., Deyhle, A., Spivack, A. (2005). Geochemical cycling of fluorine, chlorine, bromine, and boron and implications for fluid-rock reactions in Mariana Forearc, South Chamorro Seamount, ODP Leg 195. In *Proceedings of the Ocean Drilling Program, Scientific Results*. Vol. 195. Shinohara, M., Salisbury, M.H., and Richter, C. (Eds.) 1-23.

Weitemeyer, K. A. and Buffett, B. A. (2006). Accumulation and release of methane from clathrates below the Laurentide and Cordilleran ice sheets. *Global and Planetary Change*, **53**, 176-187.

Weyhenmeyer, C. E., Burns, S. J., Waber, H. N., Macumber, P. G. and Matter, A. (2002). Isotope study of moisture sources, recharge areas, and groundwater flow paths within the eastern Batinah coastal plain, Sultanate of Oman. *Water Resources Research*, **38**, 2-1.

Wheat, C. G., Fryer, P., Fisher, A. T., Hulme, S., Jannasch, H., Mottl, M. J. and Becker, K. (2008). Borehole observations of fluid flow from South Chamorro Seamount, an active serpentinite mud volcano in the Mariana forearc. *Earth and Planetary Science Letters*, **267**, 401-409.

Wheat, C. G., Jannasch, H. W., Fisher, A. T., Becker, K., Sharkey, J. and Hulme, S. (2010). Subseafloor seawater-basalt-microbe reactions: Continuous sampling of borehole fluids in a ridge flank environment. *Geochemistry, Geophysics, Geosystems*, *11*(7).

Wheat, C.G., P. Fryer, K. Takai, and S. Hulme. (2010). Spotlight 9: South Chamorro Seamount. *Oceanography* **23,** 174–175, http://dx.doi.org/10.5670/oceanog.2010.81.

Wilhelm, E., Battino, R. and Wilcock, R. J. (1977). Low-pressure solubility of gases in liquid water. *Chemical reviews*, **77**, 219-262.

Windman, T., Zolotova, N., Schwandner, F. and Shock, E. (2007). Formate as an energy source for microbial metabolism in chemosynthetic zones of hydrothermal ecosystems. *Astrobiology* **7**, 873-890.

Winnock, E., and Pontalier, Y., (1970) Lacq Gas Field, France, AAPG Memoir 14: Geology of Giant Petroleum Fields, Tulsa: AAPG, pp. 370-387.

Wolery T. W. and Jarek R. L. (2003) *Software User's Manual EQ3/6, Version 8.0*. U.S. Department of Energy, Office of Civilian Radioactive Waste Management, Office of Repository Development, Software Document Number 10813-UM-8.0-00, 376 pp.

Wolff-Boenisch D., Wenau S., Gislason S. R. and Oelkers E. H. (2011). Dissolution of basalts and peridotite in seawater, in the presence of ligands, and CO_2: Implications for mineral sequestration of carbon dioxide. *Geochimica et Cosmochimica Acta* **75**, 5510-5525.

Wouters, K., Moors, H., Boven, P. and Leys, N. (2013). Evidence and characteristics of a diverse and metabolically active microbial community in deep subsurface clay borehole water. *FEMS Microbiology Ecology*, **86**, 458-473.

Woycheese, K. M., D'Arcy, R., Cardace, D., Argayosa, A. M. and Arcilla, C. A. (2015). Out of the dark: transitional subsurface-to-surface microbial diversity in a terrestrial serpentinizing seep (Manleluag, Pangasinan, the Philippines). *Frontiers in microbiology*, *6*.

Wright, A. and Siegert, M. J. (2011). The identification and physiographical setting of Antarctic subglacial lakes: An update based on recent discoveries. *Geophysical Monograph Series*, **192**, 9-26.

Wynn, P. M., Hodson, A. J., Heaton, T. H. and Chenery, S. R. (2007). Nitrate production beneath a High Arctic glacier, Svalbard. *Chemical geology*, **244**, 88-102.

Wynter, C., Patel, B. K. C., Bain, P., Jersey, J. D., Hamilton, S. and Inkerman, P. A. (1996). A novel thermostable dextranase from a Thermoanaerobacter species cultured from the geothermal waters of the Great Artesian Basin of Australia. *FEMS Microbiology Letters*, **140**, 271-276.

Xiang, S., Yao, T., An, L., Xu, B. and Wang, J. (2005). 16S rRNA sequences and differences in bacteria isolated from the Muztag Ata glacier at increasing depths. *Applied and Environmental Microbiology*, **71**, 4619-4627.

Xu, W., Hausner, D. B., Harrington, R., Lee, P. L., Strongin, D. R. and Parise, J. B. (2011). Structural water in ferrihydrite and constraints this provides on possible structure models. *American Mineralogist*, **96**, 513-520.

Yanagibayashi, M., Nogi, Y., Li, L. and Kato, C. (1999). Changes in the microbial community in Japan Trench sediment from a depth of 6292 m during cultivation without decompression. *FEMS Microbiology Letters*, **170**, 271-279.

Yayanos, A. A., Dietz, A. S. and Van Boxtel, R. (1981). Obligately barophilic bacterium from the Mariana Trench. *Proceedings of the National Academy of Sciences*, **78**, 5212-5215.

Yayanos, A. A. and Dietz, A. S. (1982). Thermal inactivation of a deep-sea barophilic bacterium, isolate CNPT-3. *Applied and Environmental Microbiology*, **43**, 1481-1489.

Yayanos, A. A., Dietz, A. S. and Van Boxtel, R. (1982). Dependence of reproduction rate on pressure as a hallmark of deep-sea bacteria. *Applied and Environmental Microbiology*, **44**, 1356-1361.

Yayanos, A. A. (1986). Evolutional and ecological implications of the properties of deep-sea barophilic bacteria. *Proceedings of the National Academy of Sciences*, **83**, 9542-9546.

Yokoyama H., Mochida M. and Koyama Y. (1988). Molar volumes and electrostriction behavior of dicarboxylate, disulfonate, tartrate, and bis (ethylenediamine) glycinatocobalt (III) ions in water. *Bulletin of the Chemical Society of Japan* **61**, 3445-3449.

Yoshioka, H., Sakata, S., Cragg, B. A., Parkes, R. J. and Fujii, T. (2009). Microbial methane production rates in gas hydrate-bearing sediments from the eastern Nankai Trough, off central Japan. *Geochemical Journal*, **43**, 315-321.

Zafarani-Moattar M. T. and Izadi F. (2011). Effect of KCl on the volumetric and transport properties of aqueous tri-potassium citrate solutions at different temperatures. *Journal of Chemical Thermodynamics* **43**, 552-561.

Zhang, G., Dong, H., Xu, Z., Zhao, D. and Zhang, C. (2005). Microbial diversity in ultra-high-pressure rocks and fluids from the Chinese Continental Scientific Drilling Project in China. *Applied and Environmental Microbiology*, **71**, 3213-3227.

Zhang, G., Dong, H., Jiang, H., Xu, Z. and Eberl, D. D. (2006). Unique microbial community in drilling fluids from Chinese continental scientific drilling. *Geomicrobiology Journal*, **23**, 499-514.

Zimov, S. A., Schuur, E. A. and Chapin III, F. S. (2006). Permafrost and the global carbon budget. *Science*, **312**, 1612-1613.

Zink, K. G., Wilkes, H., Disko, U., Elvert, M. and Horsfield, B. (2003). Intact phospholipids—microbial "life markers" in marine deep subsurface sediments. *Organic Geochemistry*, **34**, 755-769.

ZoBell, C. E. (1952). Bacterial life at the bottom of the Philippine Trench. *Science*, **115**, 507-508.

ZoBell, C. E. and Morita, R. Y. (1957). Barophilic bacteria in some deep sea sediments. *Journal of Bacteriology*, **73**, 563.

ZoBell (1958). Ecology of sulfate-reducing bacteria. *Producers Monthly* **2**, 12-29.

APPENDIX A

SUMMARY OF THE REVISED-HKF EQUATIONS OF STATE

The derivation of the revised-HKF equations of state relies on the notion that aqueous species experience solvation effects from surrounding water molecules, but that solvation alone is insufficient to explain how standard state thermodynamic properties depend on temperature and pressure. This leads to the concept of solvation (*s*) and nonsolvation (*n*) contributions to standard partial molal properties. In the case of the standard partial molal volume ($\bar{V}^0$), it is represented by a sum of these contributions, and is given by

$$\bar{V}^0 = \Delta\bar{V}_n^0 + \Delta\bar{V}_s^0 \tag{A1}$$

The solvation contribution is taken to be accounted for by the classical Born equation (Helgeson & Kirkham, 1976; Shock et al., 1992)

$$\Delta\bar{G}_s^0 = \omega\left(\frac{1}{\varepsilon} - 1\right) \tag{A2}$$

where ε represents the dielectric constant, and ω stands for the Born coefficient given by

$$\omega = \frac{\eta Z^2}{r_e} \tag{A3}$$

where $\eta = 1.66027 \times 10^{-5}$ Å cal mol^{-1}, Z represents the charge of the solute, and r_e stands for the effective electrostatic radius of the solute, which, for ions, is related to the crystallographic radii of monatomic ions (Sassani and Shock, 1992; Shock, 1994). In the revision of the HKF equations it was proposed (Tanger & Helgeson, 1988; Shock et al., 1992) that r_e could be treated as a temperature/pressure dependent parameter, which makes ω also depend on temperature and pressure. The consequences of variable effective electrostatic radii are discussed below; here we continue the discussion for conditions where ω is constant.

As the volume is the isothermal pressure derivative of the Gibbs energy, $\Delta\bar{V}_s^0$ is given by the pressure derivative of Eqn (A2), or

$$\Delta\bar{V}_s^0 = -\omega Q \tag{A4}$$

where Q designates the Born function given by

$$Q = \frac{1}{\varepsilon}\left(\frac{\partial \ln \varepsilon}{\partial P}\right)_T \tag{A5}$$

The nonsolvation contribution to the standard partial molal volume of an aqueous species takes the functional form

$$\Delta\bar{V}_n^0 = \sigma + \frac{\xi}{(T-\theta)} \tag{A6}$$

where σ and ξ stand for solute-dependent equation-of-state parameters and θ represents a solvent property equal to 228K (Tanger & Helgeson, 1988). The Born function Q depends on both temperature and pressure, but there is no explicit pressure dependence in Eqn (A6). This is solved by expanding the σ and ξ parameters as

$$\sigma = a_1 + \frac{a_2}{(\Psi+P)} \tag{A7}$$

and

$$\xi = a_3 + \frac{a_4}{(\Psi+P)} \quad , \tag{A8}$$

where Ψ indicates a solvent property equal to 2600 bar (Tanger & Helgeson, 1988), and a_1, a_2, a_3, and a_4 stand for solute-dependent equation-of-state parameters. Combining Eqns (A1), (A4), (A6), (A7) and (A8) yields

$$\bar{V}^0 = a_1 + \frac{a_2}{\Psi+P} + \left(a_3 + \frac{a_4}{\Psi+P}\right)\left(\frac{1}{T-\theta}\right) - \omega Q \quad . \tag{A9}$$

There are close parallels between the derivation of the revised-HKF equations for $\bar{V}^0$ and those for the standard partial molal heat capacity ($\bar{C}_P^0$). By analogy to Eqn (A1),

$$\bar{C}_P^0 = \Delta\bar{C}_{P,n}^0 + \Delta\bar{C}_{P,s}^0 \quad \text{(A10)}$$

and, similarly to Eqn (A4),

$$\Delta\bar{C}_{P,s}^0 = \omega TX \quad , \quad \text{(A11)}$$

where the X Born function is given by the second isobaric temperature derivative of Eqn (A2) or

$$X = \frac{1}{\varepsilon}\left[\left(\frac{\partial^2 \ln \varepsilon}{\partial T^2}\right)_P - \left(\frac{\partial \ln \varepsilon}{\partial T}\right)_P^2\right] \quad . \quad \text{(A12)}$$

In addition, by analogy to Eqn (A6),

$$\Delta\bar{C}_{P,n}^0 = c_1 + \frac{c_2}{(T-\theta)^2} \quad . \quad \text{(A13)}$$

Calculating values of $\bar{C}_P^0$ at elevated pressures is accomplished by taking account of the nonsolvation analog of

$$\left(\frac{\partial^2 \bar{V}^0}{\partial T^2}\right)_P = -\frac{1}{T}\left(\frac{\partial \bar{C}_P^0}{\partial P}\right)_T , \quad \text{(A14)}$$

which allows expansion of Eqn (A13) to yield

$$\Delta\bar{C}_{P,n}^0 = c_1 + \frac{c_2}{(T-\theta)^2} - 2\mathrm{T}\left(\frac{1}{(T-\theta)}\right)^3\left(a_3(P-P_r) + a_4 \ln\left(\frac{\Psi+P}{\Psi+P_r}\right)\right) \quad , \quad \text{(A15)}$$

and the form of the revised-HKF equation of state for the standard partial molal heat capacity of an aqueous solute at conditions where ω is constant

$$\bar{C}_P^0 = c_1 + \frac{c_2}{(T-\theta)^2} - 2\mathrm{T}\left(\frac{1}{(T-\theta)}\right)^3\left(a_3(P-P_r) + a_4 \ln\left(\frac{\Psi+P}{\Psi+P_r}\right)\right) + \omega TX \quad . \quad \text{(A16)}$$

Although derived for ions and electrolytes the revised-HKF equations were extended to neutral solutes by Shock et al. (1989), who introduced the concepts of effective charge (Z_e) and the effective Born coefficient ω_e, which is assumed to be a constant. Substituting ω_e for ω in Eqn (A9) and (A16) provides the means to solve the integrals in

Eqn (4) in section 2 of the text and arrive at the revised-HKF expression for the standard partial molal Gibbs energy for neutral solutes (Shock et al., 1989), or

$$\bar{G}^{o}_{i,P,T} =$$

$$\bar{G}^{o}_{i,P_r,T_r} - \bar{S}^{o}_{i,P_r,T_r}(T - T_r) - c_1\left(T\ln\frac{T}{T_r} - T + T_r\right) - c_2\left\{\left[\left(\frac{1}{T-\theta}\right) - \left(\frac{1}{T_r-\theta}\right)\right]\left(\frac{\theta-T}{\theta}\right) - \frac{T}{\theta^2}\ln\left(\frac{T_r(T-\theta)}{T(T_r-\theta)}\right)\right\} + a_1(P - P_r) + a_2\ln\left(\frac{\Psi+P}{\Psi+P_r}\right) + \left[a_3(P - P_r) + a_4\ln\left(\frac{\Psi+P}{\Psi+P_r}\right)\right]\left(\frac{1}{T-\theta}\right) + \omega_e\left[Y_{P_r,T_r}(T - T_r) + \left(\frac{1}{\varepsilon} - 1\right) - \left(\frac{1}{\varepsilon_{P_r,T_r}} - 1\right)\right] \quad , \tag{A17}$$

where Y_{P_r,T_r} refers to the value of the Y Born function (-5.7987 × 10^{-5} K^{-1}) given by

$$Y = \frac{1}{\varepsilon}\left(\frac{\partial \ln \varepsilon}{\partial T}\right)_P \tag{A18}$$

at the reference pressure and temperature (0.1 MPa and 298.15K). In this study, Eqn (A17) was applied to calculate $\bar{G}^{o}_{i,P,T}$ of neutral associated forms of the acids involved in the CAC, which maintains consistency with Shock (1995) and LaRowe & Helgeson (2006a).

As mentioned above, the revised-HKF equations include a pressure- and temperature-dependent effective electrostatic radius for aqueous ions (see Eqn A3). As a result, the solvation terms for ions are more involved than Eqns (A4) and (A11), and become

$$\Delta\bar{V}^0_S = -\omega Q + \left(\frac{1}{\varepsilon} - 1\right)\left(\frac{\partial\omega}{\partial P}\right)_T \quad , \tag{A19}$$

and

$$\Delta\bar{C}^0_{P,S} = \omega TX + 2TY\left(\frac{\partial\omega}{\partial T}\right)_P - T\left(\frac{1}{\varepsilon} - 1\right)\left(\frac{\partial^2\omega}{\partial T^2}\right)_P \quad . \tag{A20}$$

The derivatives of ω, as well as consistent values of dielectric constants and Born functions, can be calculated with expressions provided by Shock et al. (1992). Combining Eqn (A19) with Eqns (A1), (A6), (A7) and (A8) yields

$$\bar{V}^0 = a_1 + \frac{a_2}{\Psi+P} + \left(a_3 + \frac{a_4}{\Psi+P}\right)\left(\frac{1}{T-\theta}\right) - \omega Q + \left(\frac{1}{\varepsilon} - 1\right)\left(\frac{\partial \omega}{\partial P}\right)_T \quad , \qquad \text{(A21)}$$

and combining Eqn (A20) with Eqns (A10) and (A15) gives

$$\bar{C}_P^0 = c_1 + \frac{c_2}{(T-\theta)^2} - 2\mathrm{T}\left(\frac{1}{(T-\theta)}\right)^3 \left(a_3(P-P_r) + a_4 \ln\left(\frac{\Psi+P}{\Psi+P_r}\right)\right) + \omega T X + 2TY\left(\frac{\partial \omega}{\partial T}\right)_P -$$

$$T\left(\frac{1}{\varepsilon} - 1\right)\left(\frac{\partial^2 \omega}{\partial T^2}\right)_P \quad . \qquad \text{(A22)}$$

Eqns (A21) and (A22) are the revised-HKF equations of state for the standard partial molal volume and heat capacity of ions, respectively, and allow integration of Eqn (4) in section 2 of the text to yield

$$\bar{G}^o_{i,P,T} =$$

$$\bar{G}^o_{i,P_r,T_r} - \bar{S}^o_{i,P_r,T_r}(T-T_r) - c_1\left(T\ln\frac{T}{T_r} - T + T_r\right) - c_2\left\{\left[\left(\frac{1}{T-\theta}\right) - \left(\frac{1}{T_r-\theta}\right)\right]\left(\frac{\theta-T}{\theta}\right) -\right.$$

$$\left.\frac{T}{\theta^2}\ln\left(\frac{T_r(T-\theta)}{T(T_r-\theta)}\right)\right\} + a_1(P-P_r) + a_2\ln\left(\frac{\Psi+P}{\Psi+P_r}\right) + \left[a_3(P-P_r) + a_4\ln\left(\frac{\Psi+P}{\Psi+P_r}\right)\right]\left(\frac{1}{T-\theta}\right) +$$

$$\omega\left(\frac{1}{\varepsilon} - 1\right) + \omega_{P_r,T_r}\left[Y_{P_r,T_r}(T-T_r) - \left(\frac{1}{\varepsilon_{P_r,T_r}} - 1\right)\right] \quad , \qquad \text{(A23)}$$

which is the revised-HKF equation of state for the standard Gibbs energy of aqueous ions. This expression was used in the present study to calculate standard Gibbs energies of anionic forms of CAC aqueous species at elevated temperatures and pressures, which again maintains consistency with Shock (1995) and LaRowe & Helgeson (2006a).

APPENDIX B

SUMMARY OF PREDICTIVE CORRELATIONS FOR HKF EQUATION-OF-STATE PARMETERS USED IN THE PRESENT STUDY

The power of the revised-HKF equations resides in their versatility. If abundant experimental thermodynamic data are available, then the seven solute-dependent parameters can be retrieved with limited uncertainties through regression. Accuracy is greater for ions and electrolytes, but well-constrained regressions are also possible for nonelectrolytes given abundant data (Plyasunov and Shock, 2001a; Schulte et al., 2001; Facq et al., 2014). However, it is common that experimental data are insufficient either in range or variety to obtain all HKF parameters through regression. In fact, the most common situation for most solutes is that few if any data exist, with the best cases being that experiments yield partial datasets only at the reference conditions. At the same time, geochemical problems that could be explored through thermodynamic modeling involve thousands (or maybe millions) of aqueous species, and the lack of experimental data should not be allowed to impede progress. In an effort to fill the gap, methods have been generated to estimate HKF parameters, as well as standard state data at the reference conditions, for monatomic and polyatomic ions, dissolved gases, polar and nonpolar organic compounds, biomolecules, and organic and inorganic metal-ligand complexes (Shock and Helgeson, 1988; 1990; Shock et al., 1989; 1997a; 1997b; Sassani and Shock, 1992; Shock and Koretsky, 1993; 1995; Shock, 1994; 1995; Amend and Helgeson, 1997a; 1997b, 2000; Sverjensky et al., 1997; 2014; Prapaipong et al., 1999; Amend and Plyasunov, 2001; Plyasunov and Shock, 2001a; Schulte et al., 2001; Prapaipong and Shock, 2001; Dick et al., 2006; LaRowe and Helgeson, 2006a; 2006b; Facq et al., 2014).

In the present study we built on existing revised-HKF parameters and standard state data at the reference conditions for citric acid and its anions from LaRowe & Helgeson (2006a) and succinic acid and its anions from Shock (1995). In doing so we

employed methods for predicting revised-HKF parameters for aqueous organic acids and acid anions from Shock (1995), some of which come from Shock and Helgeson (1988) and Shock et al. (1989). The following discussion outlines how such predictions were made. New methods for estimating standard state data at the reference conditions that are not available from experiments are described in the section 2.2 of the text.

Born coefficients for anions (ω) were calculated from Eqn (A3) using values of the effective electrostatic radius (r_e) estimated from standard partial molal entropies ($\bar{S}°$) at the reference conditions via

$$r_e = \frac{Z^2(\eta Y - 100)}{\bar{S}° - \alpha_Z} \quad , \tag{B1}$$

with α_Z values of 72, 141, and 211 from Shock and Helgeson (1988) for monovalent, divalent, and trivalent anions, respectively. Values of ω_e for neutral associated acid molecules were predicted from (Shock, 1995)

$$\omega_e = 661.98\bar{S}° - 58740. \tag{B2}$$

Estimated values of ω or ω_e were used to calculate values of $\Delta\bar{V}_s^0$ using Eqn (A4) with the Q Born function at the reference conditions (6.6342×10^{-7} bar^{-1}), and the conversion factor 41.8393 cm^3 bar cal^{-1}. Resulting values of $\Delta\bar{V}_s^0$ were combined with values of $\bar{V}^0$ to calculate values of $\Delta\bar{V}_n^0$ with Eqn (A1).

These estimates were used to predict the σ and a_1 equation-of-state parameters from the correlations

$$\sigma = 1.07143\Delta\bar{V}_n^0 + 3.0 \quad , \tag{B3}$$

described by Shock (1995), and

$$a_1 = 1.3684 \times 10^{-2}\left(\frac{\Delta\bar{V}_n^0}{41.8393}\right) + 0.1765 \ , \tag{B4}$$

from Shock & Helgeson (1988). Resulting values of σ and a_1 were combined with Eqn (A7) to calculate the a_2 parameter, and values of a_2 were used with the correlation

$$a_4 = -4.134a_2 - 27790. \quad \text{(B5)}$$

from Shock & Helgeson (1988) to predict the a_4 parameter, which was then used together with values of $\bar{V}^0$, $\Delta\bar{V}_s^0$, a_1, and a_2 to evaluate a_3 from Eqn (A9).

Values of ω or ω_e estimated as described above were used to calculate values of $\Delta\bar{C}_{P,s}^0$ using Eqn (A11) and the X Born function at the reference conditions (-3.0556 × 10^{-7} K^{-2}). Standard partial molal heat capacities at the reference conditions were used to predict the c_2 parameter from

$$c_2 \times 10^{-4} = 0.01212\bar{C}_P^0 - 4.106 \quad \text{(B6)}$$

for acid anions, and

$$c_2 \times 10^{-4} = 0.0988\bar{C}_P^0 - 4.961 \quad \text{(B7)}$$

for neutral acid species, which are both proposed by Shock (1995). Consistent values of the c_1 parameter were obtained from $\bar{C}_P^0$, $\Delta\bar{C}_{P,s}^0$, and c_2, together with Eqns (A10) and (A13).

APPENDIX C

STRUCTURES OF AQUEOUS ORGANIC ACIDS INVOLLVED IN THE CAC, AS WELL AS BIOMOLECULES THAT PARTICIPATE IN STEPS OF THE CYCLE

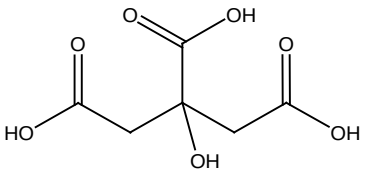

citric acid ($C_6H_8O_7$)

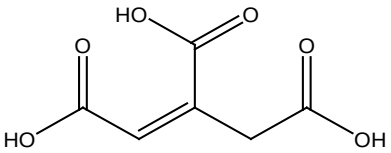

cis-aconitic acid ($C_6H_6O_6$)

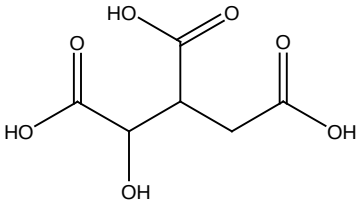

isocitric acid ($C_6H_8O_7$)

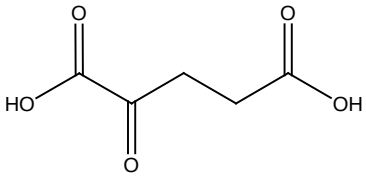

α-ketoglutaric acid ($C_5H_6O_5$)

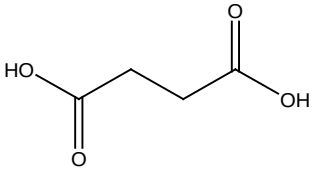

succinic acid ($C_4H_6O_4$)

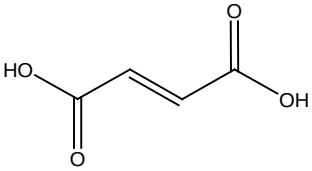

fumaric acid ($C_4H_4O_4$)

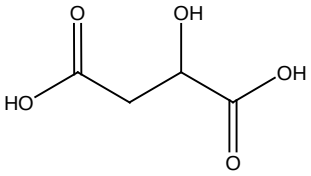

malic acid ($C_4H_6O_5$)

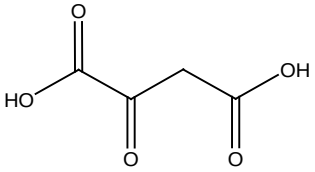

oxaloacetic acid ($C_4H_4O_5$)

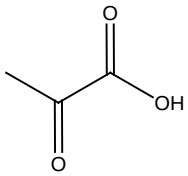

pyruvic acid ($C_3H_4O_3$)

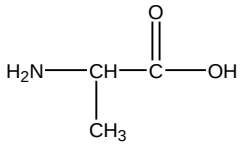

alanine ($C_3H_7NO_2$)

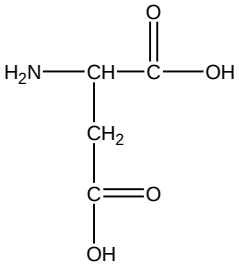

aspartic acid ($C_4H_7NO_4$)

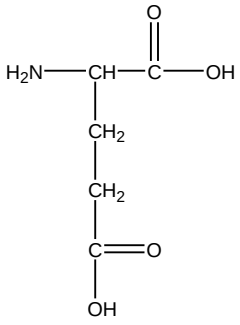

glutamic acid ($C_5H_9NO_4$)

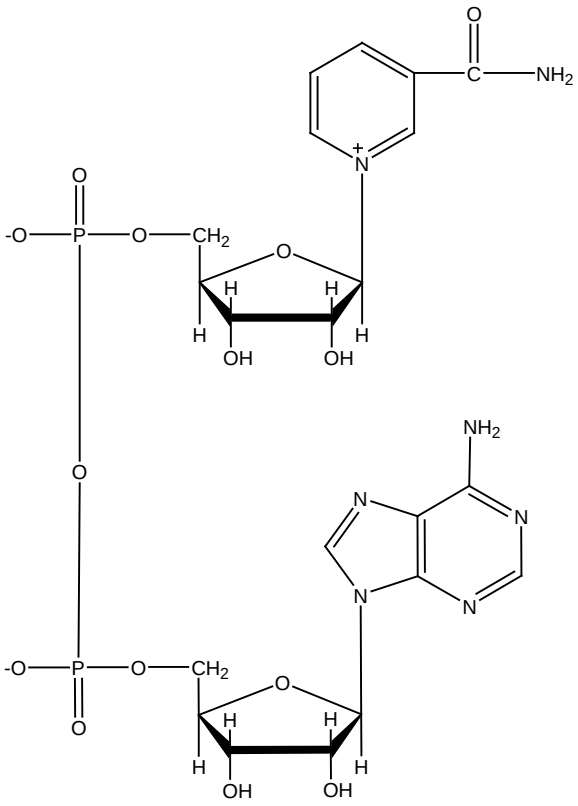

NAD^-_{ox} ($C_{21}H_{26}N_7O_{14}P_2^-$)

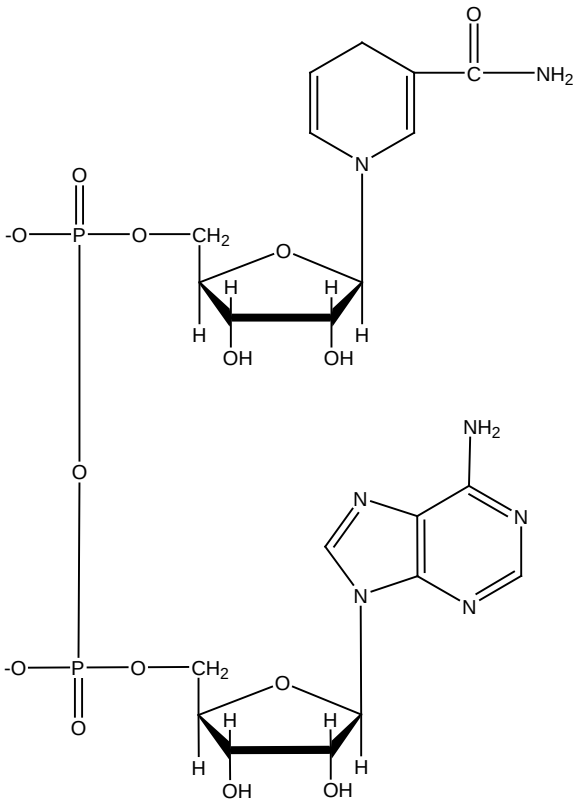

NAD^{2-}_{red} ($C_{21}H_{27}N_7O_{14}P_2^{-2}$)

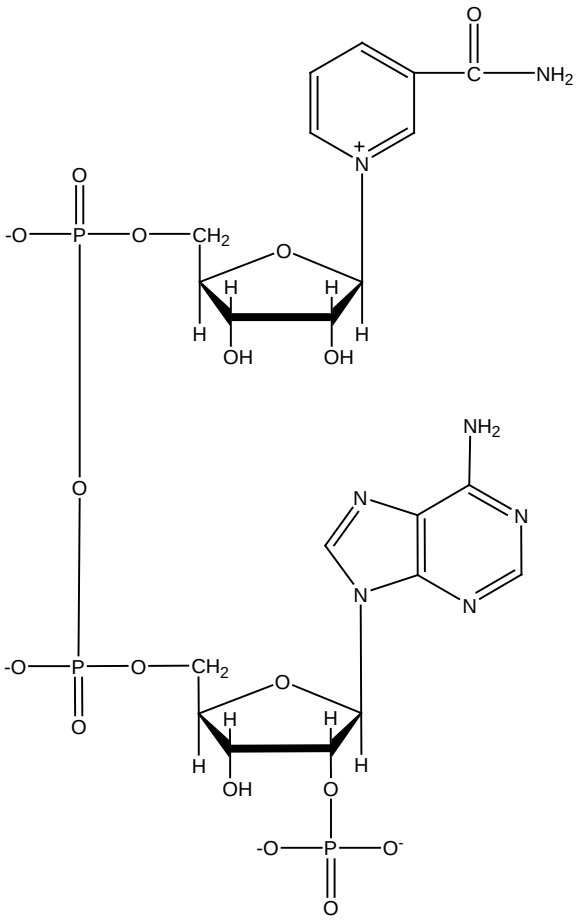

$NADP^{3-}_{ox}$ $(C_{21}H_{25}N_7O_{17}P_3^{-3})$

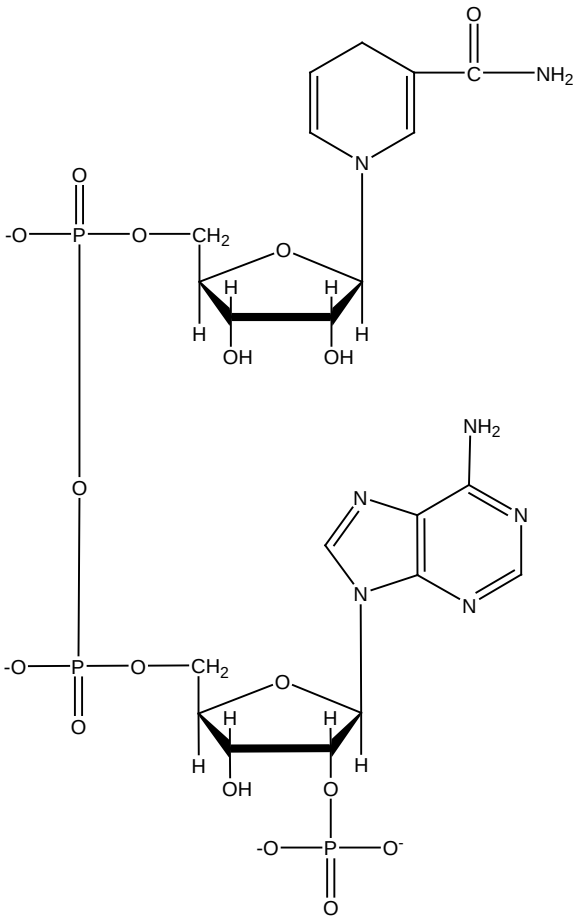

$NADP^{4-}_{red}$ $(C_{21}H_{26}N_7O_{17}P_3^{-4})$

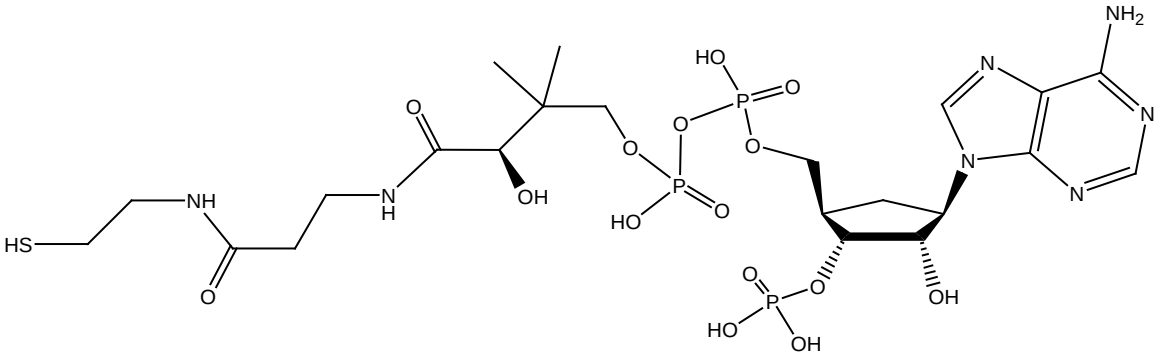

Coenzyme A (CoA) ($C_{21}H_{36}N_7O_{16}P_3S$)

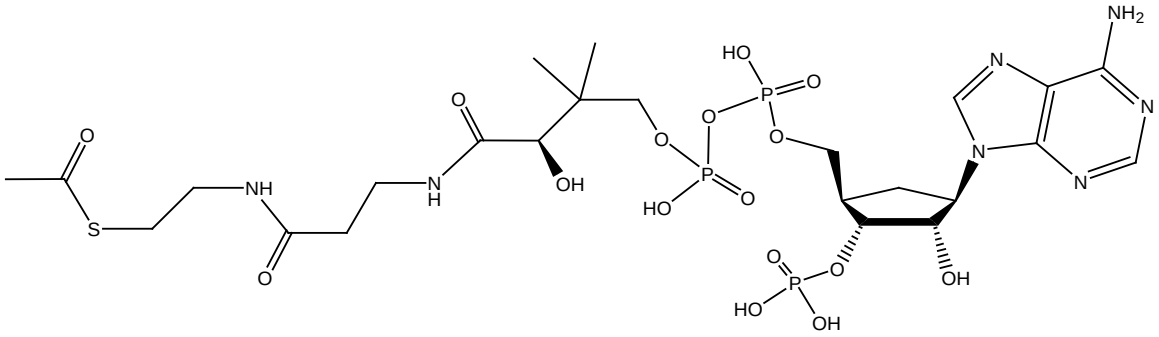

acetyl-CoA ($C_{23}H_{38}N_7O_{17}P_3S$)

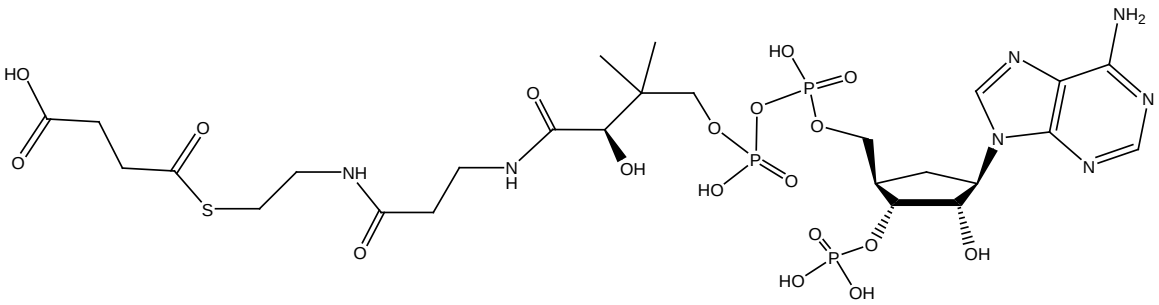

succinyl-CoA ($C_{25}H_{40}N_7O_{19}P_3S^{-1}$)

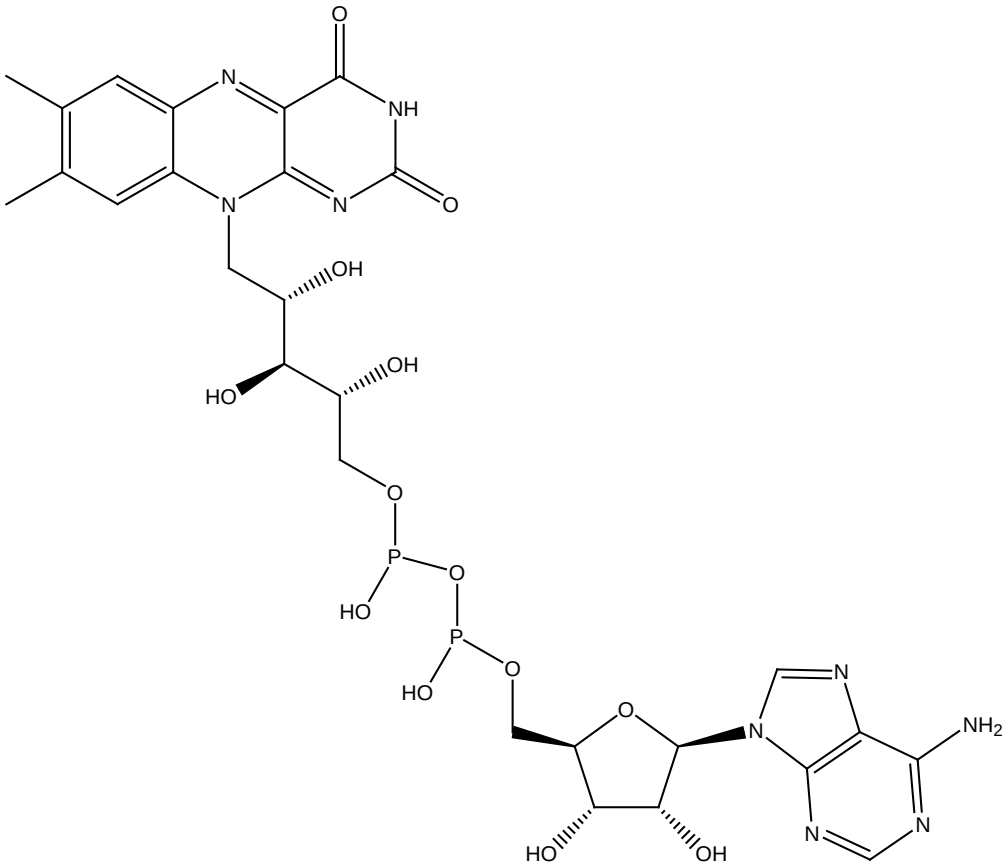

flavin adenine dinucleotide (FAD) ($C_{27}H_{33}N_9O_{15}P_2$)

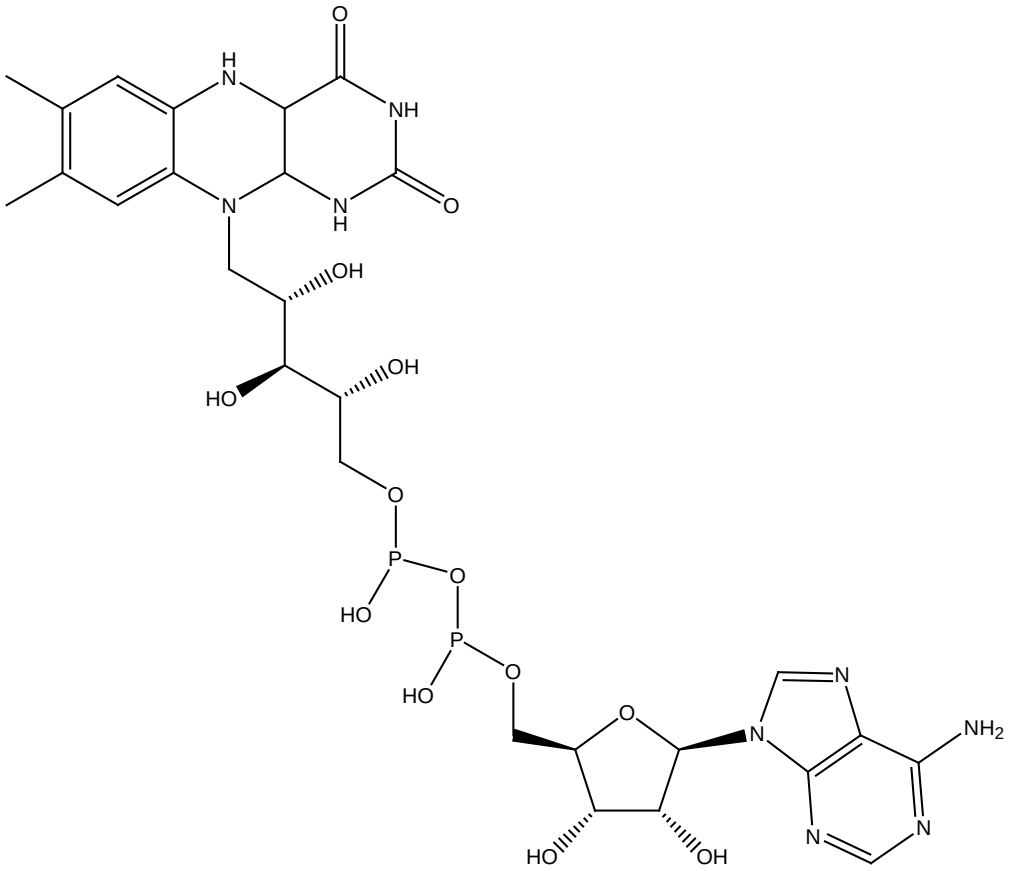

$FADH_2$ ($C_{27}H_{35}N_9O_{15}P_2$)

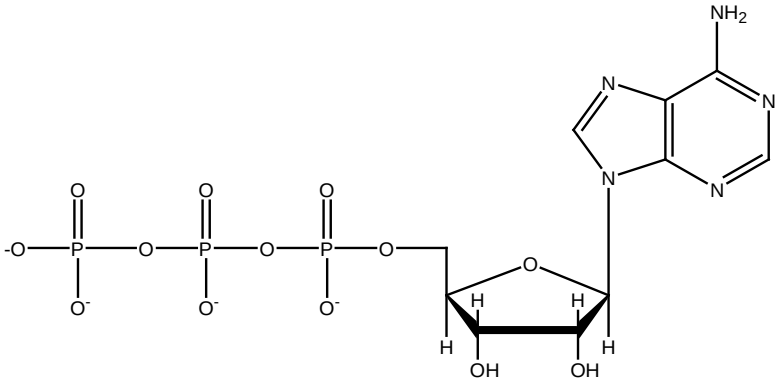

adenosine triphosphate (ATP^{4-}) ($C_{10}H_{12}N_5O_{13}P_3^{-4}$)

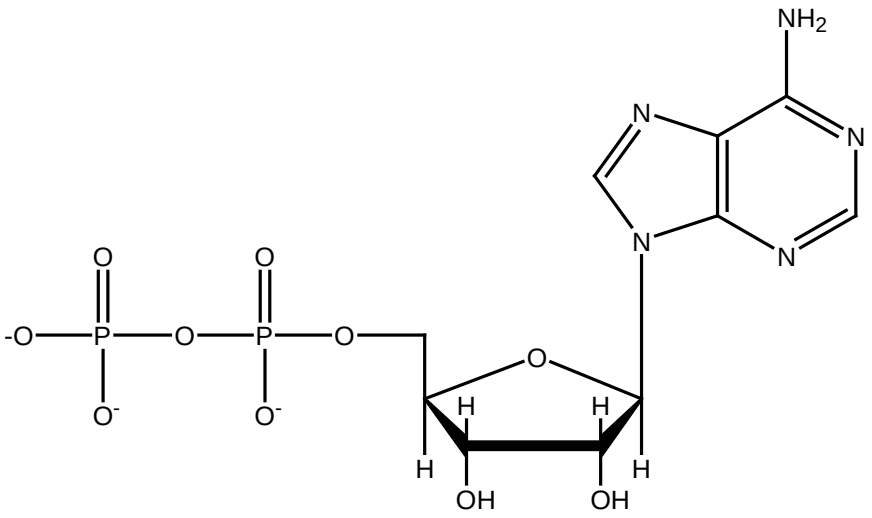

adenosine diphosphate (ADP^{3-}) ($C_{10}H_{12}N_5O_{10}P_2^{-3}$)

APPENDIX D

COMPARISON OF STANDARD STATE GIBBS ENERGIES FOR AQUESOUS CAC SPECIES OBTAINED IN OTHER STUDIES

Several investigators have compiled and/or derived sets of thermodynamic data for CAC species in the form of thermochemical cycles. The most extensive lists and their comparison to the results obtained in this study are presented in Table E1. One of the first attempts was by Burton (1957), which included a set of $\Delta\bar{G}_f^o$ values for some sugars, organic acids (completely associated or dissociated, but not intermediate forms), amino acids, purines and common inorganic solutes (*e.g.,* bicarbonate, sulfate, sulfide) at standard state conditions. Not all of the values in that compilation are entirely self-consistent, though it is improbable that it was possible to make them so at the time. That work was augmented and improved upon by Thauer et al. (1977) who added many more species both organic and inorganic for use in biochemical calculations. Justifiably, the data from Thauer et al. (1977) are widely used in the biochemical, microbiological and geochemical literature. Neither of these early tabulations include intermediate dissociation states of polybasic organic acids, nor do they contain $\Delta\bar{G}_f^o$ values for ATP^{4-}, ADP^{3-}, or species of NAD(P).

The first major compilation to attempt to present a complete assessment for everything in the CAC was that of Miller and Smith-Magowan (1990), although they do not address ATP^{4-} or ADP^{3-} species. These researchers arbitrarily set the values of $\Delta\bar{G}_f^o$ for NAD(P) species in their oxidized forms to 100 kcal mol^{-1} and used literature values of potentiometric measurements to calculate $\Delta\bar{G}_f^o$ values for the reduced forms. It should be noted that it is impossible for these values to be standard Gibbs energies of formation from the elements. Miller and Smith-Magowan (1990) used a network of thermochemical cycles in a complex regression procedure, which employed an equally weighted least-

sums solution together with a least-squares solution for a set of ~40 reactions, to evaluate $\Delta\bar{G}_f^o$ of 26 species in, and related to, the CAC. The benefit of this approach is that the thermochemical network includes multiple reactions involving the same species and yields a set of $\Delta\bar{G}_f^o$ values determined to be the best overall fit. At the same time, the equal weighting means that if certain reaction properties are not as well characterized as others the mathematical analysis can skew the determination of individual $\Delta\bar{G}_f^o$ values away from well-established quantities. Miller and Smith-Magowan (1990) note that the values they present are self-consistent among themselves, but that care needs to be taken when using them in conjunction with other species.

In contrast with the present treatment of CAC species and other efforts discussed here, Miller and Smith-Magowan (1990) performed their work in the context of The Interunion Commission on Biothermodynamics (Wadsö et al., 1976) where all of the values are for 25°C , 1 bar, and an ionic strength (I) of 0.1. Making comparisons with other assessments of thermodynamic data for the CAC necessitates that the values be normalized to standard state conditions (referenced to I=0), which can be done in several ways. In the present study, we used extrapolation methods proposed by Alberty (1998a) and Alberty (2005) resulting in two additional columns for Miller and Smith-Magowan (1990) in Table E1. Alberty (1998a) employs the equation:

$$\Delta_f G_i^{I^\circ}(pH, I) = \Delta_f G_i^\circ(I = 0) - 2.91482\, z_i^2\, I^{1/2}\left(1 + BI^{1/2}\right) - N_H(i)\left[-2.91482 I^{1/2}\left(1 + BI^{1/2}\right) + RT \ln 10^{-pH}\right] \quad \text{(D1)}$$

where $\Delta_f G_i'^{\circ}(pH, I)$ stands for the transformed Gibbs energy of formation (in joules) of a species at 25°C, 1 bar, and a specified pH and ionic strength, $\Delta_f G^{\circ}(I = 0)$ represents the standard Gibbs energy of formation of a species, z_i indicates the charge of the species, B = 1.6 $L^{1/2}$ $mol^{1/2}$, and $N_H(i)$ corresponds to the number of hydrogen atoms in the species. As discussed by Alberty (1998a) the $N_H(i)$ term comes from the Legendre transform that defines the transformed Gibbs energy (Alberty 1992a; 1992b), and the terms concerning ionic strength are of the form used by Clarke and Glew (Clarke and Glew, 1980; Goldberg and Tewari, 1991). Alberty (2005) gives the following equation to relate ionic strength and $\Delta_f G^{\circ}(I = 0)$ using the extended Debye-Hückel theory:

$$\Delta_f G^{\circ}(I) = \Delta_f G^{\circ}(I = 0) - \frac{2.91482 z_i^2 I^{1/2}}{1 + B I^{1/2}} \qquad \text{(D2)}$$

which was used in the present study to provide a second method of extrapolating the Gibbs energies from Miller and Smith-Magowan (1990) to the standard state. The original values from Miller and Smith-Magowan (1990), as well as those extrapolated to the standard state with Eqns (D1) and (D2) are included in Table E1, where it can be seen that the extrapolations modify the values by no more than a few calories, or much less than 1%.

A more extensive and later compilation of CAC species and related compounds was constructed by Alberty (2005) from Alberty (1998a,b,c) and includes associated and dissociated forms of ATP, ADP, and AMP species. In contrast, the approach taken for NAD species is similar to that taken by Miller and Smith-Magowan (1990), but follows the convention that $\Delta \bar{G}_f^o = \Delta \bar{H}_f^o = 0$ for both H^+ and NAD^-_{ox}. In the case of the latter, it

follows that $\Delta\bar{G}_f^o$ of the reduced form (NAD^{2-}_{red}) is calculated from the standard potential between the oxidized and reduced forms, but it is not actually a standard Gibbs energy of formation from the elements. Although earlier efforts also used the same zero convention for $NADP^{3-}_{ox}$, a value appears in Alberty (2005) for this species that we were unable to trace (as indicated by the parentheses in Table E1). As in the case of NAD^{-}_{ox}, the $\Delta\bar{G}_f^o$ value of the reduced form ($NADP^{4-}_{red}$) is calculated from the standard potential between the oxidized and reduced forms, and is again not actually a standard Gibbs energy of formation from the elements. Despite this flaw, the Alberty (2005) compilation has the benefits of 1) listing $\Delta\bar{H}_f^o$ for almost all of the species in the cycle, 2) including all of the protonation states for the acids in the cycle, and 3) being otherwise consistent not only within itself but also with the NBS tables from Wagman et al. (1982).

The comprehensive compilation of Alberty (2005) for CAC species was supplanted by that of Dalla-Betta and Schulte (2009), which includes all acids in their protonated and anionic forms (with the exceptions of *cis*-aconitic and isocitric). Dalla-Betta and Schulte (2009) built on progress by LaRowe and Helgeson (2006a; 2006b; 2007) and included actual $\Delta\bar{G}_f^o$ values for multiple aqueous forms of ATP, ADP, AMP, and NAD(P), which allowed them to maintain internal consistency with thousands of other aqueous species, gases, organic compounds and minerals used in geochemical calculations. In addition, they provide revised-HKF equation-of-state parameters that allow calculations of standard state data at elevated temperatures and pressures. Unfortunately the volume for α-ketoglutaric acid selected by Dalla-Betta and Schulte (2009) is that of the solid and not the aqueous form, which means their volume estimates for the deprotonated species of α-ketoglutaric acid are dependent on this value.

Furthermore, because data for solid α-ketoglutaric acid were used to estimate volumes for pyruvic and oxaloacetic acids and anions, those volumes can not refer to aqueous species. As a result the a_1-a_4 HKF parameters for these species from Dalla-Betta and Schulte (2009) are unlikely to predict the high-temperature/pressure behavior of the aqueous species. These problems were addressed in the present study with new estimation methods described in section 2.2.3 of the text.

Differences in these datasets can be assessed by comparing calculated standard Gibbs energies for reactions, which can, in some cases, be contrasted with data obtained from additional experimental studies. As an example, values of $\Delta_r \bar{G}^o$ for the reaction

$$\text{aspartate}^- + \alpha\text{-ketoglutarate}^{2-} = \text{oxaloacetate}^{2-} + \text{glutamate}^- \qquad \text{(D3)}$$

are listed in Table D2 from various sources including the experimental value adopted in the present study as described in section 2.2.3 of the text. Although there is close agreement between the value adopted in the present study and that consistent with Miller and Smith-Magowan (1990), other values differ considerably, and in the case of Alberty (2005) by more than 100% with a change in sign. This large discrepancy is partly a function of the small magnitude of these numbers. Similar differences attend the values of $\Delta_r \bar{G}^o$ for

$$\text{malate}^{2-} + \text{NAD}^-_{\text{ox}} = \text{oxaloacetate}^{2-} + \text{NAD}^{2-}_{\text{red}} + \text{H}^+ \qquad \text{(D4)}$$

but the magnitudes of these values leads to smaller percent discrepancies, with the possible exception of the value from Thauer et al. (1977). The experimental value for reaction (D4) in Table D2 comes from a different source than the value adopted in the present study. It can be seen that there is a small difference between this alternate value of $\Delta_r \bar{G}^o$ and the one we adopted, but that larger discrepancies attend the other datasets.

As discussed in sections 2.2.2 and 2.2.3 of the text, the choice was made in this study to maintain consistency with thermodynamic data for amino acids by adopting the standard Gibbs energy for reaction (D3) and the deamination of aspartate to yield fumarate. Experimental data yielding a value of $\Delta_r \bar{G}^o$ for

$$\text{fumarate}^{2-} + 2\text{H}^+ + 2\text{e}^- = \text{succinate}^{2-} \qquad \text{(D5)}$$

are also available as discussed in section 2.2 of the text and shown in Table D2. Note that the value obtained by Miller and Smith-Magowan (1990) and the independently calculated value obtained in the present study are closest to the experimental value. It should be kept in mind that this experimental $\Delta_r \bar{G}^o$ value is part of the dataset used by Miller and Smith-Magowan (1990). In contrast, the other compilations show larger disagreements, which stem from their decisions to accept other data for succinate, fumarate, or both.

We encountered difficulties in accommodating all of the experimental data relating to isocitrate and α-ketoglutarate. In the present study we adopted data linking isocitrate with citrate via

$$\text{isocitrate}^{3-} = \text{citrate}^{3-} \ , \qquad \text{(D6)}$$

together with reactions involving *cis*-aconitate^{3-}, but this choice, and the constraints from data for reactions involving α-ketoglutarate, means that the value of $\Delta_r \bar{G}^o$ for

$$\text{isocitrate}^{3-} + \text{NADP}^{3-}_{\text{ox}} = \alpha\text{-ketoglutarate}^{2-} + \text{NADP}^{4-}_{\text{red}} + \text{CO}_2(\text{g}) \qquad \text{(D7)}$$

we obtain differs from the experimental value in Table D2. We note that Alberty (1997) suggests that this reaction should be written as

$$\text{isocitrate}^{3-} + \text{NAD(P)}_{\text{ox}} + \text{H}_2\text{O} = \text{a-ketoglutarate}^{2-} + \text{NAD(P)}_{\text{red}} + \text{TotCO}_2 \ ,$$

where $TotCO_2$ is the total CO_2 formed from the oxidation of isocitrate^{3-} and H_2O is added to the left hand side of the reaction to balance the oxygen for the overall expression, and also discusses the difficulties and uncertainties related to making measurements when dissolved carbon dioxide and carbonic acid species are involved. It should also be noted that thermochemical cycles that incorporate this reaction and its associated value of $\Delta_r \bar{G}^o$ would incorporate uncertainties contributed by this reaction. This is most likely the case for Miller and Smith-Magowan (1990) as the network analysis they used minimizes the residuals for several reactions including (D7).

Table D1. Compilation of $\Delta\bar{G}_f^o$ data (cal mol^{-1}) at 25°C, 1 bar, and I=0 for CAC and related aqueous species. Blank entries indicate values unavailable, and parentheses indicate values unexplained in original sources. Italicized values are not actually standard Gibbs energies of formation from the elements owing to arbitrary choices in original sources.

Species	Thauer et al. (1977)	Miller & Smith-Magowan (1990)[a]	Miller & Smith-Magowan (1990)[b]	Miller & Smith-Magowan (1990)[c]	Alberty (2005)	Dalla-Betta & Schulte (2009)	This project
$citrate^{3-}$	-279240	-280256	-280254	-280248	-277890	-277892	-277690
$cis\text{-}aconitate^{3-}$	-220510	-221537	-221535	-221532	-219199		-218970
$isocitrate^{3-}$	-277650	-278786	-278785	-278778	-276300		-276230
$\alpha\text{-}ketoglutarate^{2-}$	-190620	-191675	-191675	-191673	-189630	-191683	-191800
$succinate^{2-}$	-164970	-164933	-164932	-164930	-165019	-164380	-164380
$fumarate^{2-}$	-144410	-144744	-144744	-144743	-143850	-143858	-144320
$malate^{2-}$	-201980	-202232	-202232	-202229	-201401	-201506	-201860
$oxaloacetate^{2-}$	-190530	-190896	-190896	-190895	-189630	-190894	-190600
$pyruvate^{-}$	-113440	-113492	-113492	-113491	-112875	-113504	-113600
NAD^{-}_{ox}		*-100000*[d]	*-100000*[d]	*-99996*[d]	*0*[d]	-529458	-529458
NAD^{2-}_{red}		*-95000*[e]	*-94999*[e]	*-94984*[e]	*5413*[e]	-524091	-524091
$NADP^{3-}_{ox}$		*-100000*[d]	*-99999*[d]	*-99966*[d]	(*-199613*)	-729109	-729109
$NADP^{4-}_{red}$		*-94737*[e]	*-94735*[e]	*-94674*[e]	(*-193401*)	-722462	-722462
ADP^{3-}					-455576	-452649	-452649
ATP^{4-}					-661592	-657038	-657038
$lactate^{-}$	-123600	-124352	-124352	-124351	-123499	-122530	-122530
alanine	-88800	-88762	-88762	-88762	-88671	-88810	-88810
$aspartate^{-}$	-167140	-167053	-167053	-167052	-166319	-167170	-167170
$glutamate^{-}$	-167200	-166690	-166690	-166688	-166699	-167210	-167210
H^+	0	0	0	0	0	0	0
$H_2(g)$	0	0	0	0	0	0	0
$H_2(aq)$		4238	4238	4238	4207	4236	4236
$CO_2(g)$	-94254	-94257	-94257	-94257	-94254	-94254	-94254
$CO_2(aq)$	-92260	-92256	-92256	-92256	-92250	-92250	-92250
NH_4^+	-18970	-18991	-18991	-18991	-18956	-18990	-18990
H_2O	-56687	-56690	-56690	-56690	-56688	-56688	-56688

[a] Original values from Miller and Smith-Magowan at 25°C, 1 bar, and I=0.1, [b] standard state values using Eqn (D2), [c] standard state values using Eqn (D1), [d] value arbitrarily set by the investigators, [e] value impressed upon that species to maintain consistency for the potentiometric measurement between the oxidized and reduced forms.

Table D2. Comparison of experimental $\Delta_r \bar{G}^o$ values (cal mol^{-1}) from the literature and those obtained through various thermochemical cycles. Missing entries mean that values for that reaction cannot be calculated from that study.

rxn #	Experiment	Thauer et al. (1977)	Miller & Smith-Magowan (1990)[a]	Alberty (2005)	Dalla-Betta & Schulte (2009)	This study
D3	1150[b]	30	1142	-380	749	1150
D4	16674[c]	11450	16347	17185	15979	16627
D5	-20155[d]	-20560	-20188	-21169	-20522	-20060
D6	-1460[e]	-1590	-1470	-1589	---	-1460
D7	-2030[f]	---	-1859	-1372	---	-3177

[a] normalized to 25 ^{o}C, 1 bar, and I=0.0 [b] Kishore et al. (1998), [c] Burton and Wilson (1953), [d] Borsook and Schott (1931a; 1931b), [e] Blair (1968; 1969), [f] Londesborough and Dalziel (1968).

APPENDIX E

BALANCED REACTIONS AND CORRESPONDING ENERGIES FOR LAKE VIDA BRINE (LVB), ROBERTSON GLACIER PORE WATER, ROBERTSON (RGPW) GLACIER WATER (RGW), AND BOTTOM SEA WATER (BSW) AS A FUNCTION OF VOLUME

Table E1. Energetic evaluation for 1460 balanced reactions expressed as calories per ml of solution for Lake Vida Brine (LVB), Robertson Glacier Pore Water (RGPW), Robertson Glacier Water (RGW), and Bottom Sea Water (BSW) displaying number of electrons transferred per reaction as well. If there is not a range of affinity, the explicit value will be listed in the Range (low)/Specific column of the table. If there is a range of affinity for the reaction, both columns will have values listed.

Rxn #	**Overall Reaction**	**# of e- transferred**	**Energy (cal ml^{-1})**							
			LVB		RGPW		RGW		BSW	
	Oxygen as an electron acceptor		Range(low) / Specific	Range(high)	Range(low) / Specific	Range(high)	Range(low) / Specific	Range(high)	Range(low) / Specific	Range(high)
1	$2H_2(aq) + O_2(aq) \rightarrow 2H_2O$	4	1.99E-07	2.14E-01	3.86E-09	4.30E-09	2.15E-09		1.96E-11	
2	$2NH_4^+ + 3/2O_2(aq) \rightarrow N_2(aq) + 2H^+ + 3H_2O$	6	1.69E-07	1.85E-01	8.20E-07	9.24E-01	1.19E-06		1.21E-08	
3	$2NH_4^+ + 2O_2(aq) \rightarrow N_2O(aq) + 2H^+ + 3H_2O$	8	9.77E-08	1.13E-01	6.51E-07	8.39E-01	1.03E-06	1.93E-01	1.03E-08	1.98E-01
4	$2NH_4^+ + 5/2O_2(aq) \rightarrow 2NO(aq) + 2H^+ + 3H_2O$	10	6.40E-08	9.95E-01	5.20E-07	7.92E-01	9.06E-07	1.33E-01	8.95E-09	1.32E-01
5	$NH_4^+ + 3/2O_2(aq) \rightarrow NO_2^- + 2H^+ + H_2O$	6	6.34E-08	7.84E-01	6.71E-07	8.80E-01	1.15E-06		1.21E-08	
6	$NH_4^+ + 2O_2(aq) \rightarrow NO_3^- + 2H^+ + H_2O$	8	5.90E-08	7.45E-01	8.35E-07	1.11E-01	1.43E-06		1.44E-08	
7	$N_2(aq) + 1/2O_2(aq) \rightarrow N_2O(aq)$	2	-1.16E-07	-1.18E-01	-1.63E-06	-8.21E-01	-1.21E-05	-7.42E-01	-3.93E-06	-2.42E-01
8	$N_2(aq) + O_2(aq) \rightarrow 2NO(aq)$	4	-9.36E-08	-4.86E-01	-2.88E-06	-1.28E-01	-1.19E-05	-6.65E-01	-3.46E-06	-1.95E-01
9	$N_2(aq) + 3/2O_2(aq) + H_2O \rightarrow 2NO_2^- + 2H^+$	6	-4.23E-08	-2.73E-01	-1.43E-06	-4.26E-01	-1.29E-06		3.76E-09	

10	$N_2(aq) + 5/2O_2(aq) + H_2O \rightarrow 2NO_3^- + 2H^+$	10	-6.93E-09	8.75E-09	1.45E-07	1.82E-01	3.93E-06		1.05E-06	
11	$N_2O(aq) + 1/2O_2(aq) \rightarrow 2NO(aq)$	2	-7.12E-08	3.82E-09	-2.75E-08	3.35E-01	-2.22E-08	3.59E-01	-2.25E-08	2.36E-01
12	$N_2O(aq) + O_2(aq) + H_2O \rightarrow 2NO_2^- + 2H^+$	4	-5.41E-09	9.59E-09	-4.38E-09	1.38E-01	6.33E-09	1.38E-01	1.22E-08	1.97E-01
13	$N_2O(aq) + 2O_2(aq) + H_2O \rightarrow 2NO_3^- + 2H^+$	8	2.04E-08	3.54E-01	2.08E-08	4.96E-01	3.99E-08	4.74E-01	3.83E-08	4.58E-01
14	$2NO(aq) + 1/2O_2(aq) + H_2O \rightarrow 2NO_2^- + 2H^+$	2	4.38E-11	9.42E-09	4.06E-09	1.42E-01	6.74E-09	1.42E-01	9.76E-09	1.73E-01
15	$2NO(aq) + 3/2O_2(aq) + H_2O \rightarrow 2NO_3^- + 2H^+$	6	1.16E-08	2.47E-01	1.66E-08	3.21E-01	2.35E-08	3.13E-01	2.28E-08	3.37E-01
16	$NO_2^- + 1/2O_2(aq) \rightarrow NO_3^-$	2	4.61E-08	6.11E-01	1.82E-08	2.60E-01	2.53E-08		1.31E-11	
17	$2H_2S(aq) + Fe^{+2} + 1/2O_2(aq) \rightarrow$ pyrite $+ 2H^+ + H_2O$	2	1.74E-08	2.68E-01	4.65E-08	5.93E-01	7.37E-09		4.98E-11	
18	$H_2S(aq) + 1/2O_2(aq) \rightarrow$ sulfur $+ H_2O$	2	3.00E-08	4.13E-01	2.57E-05	3.25E-01	1.09E-08		2.44E-09	
19	$2H_2S(aq) + 2O_2(aq) \rightarrow S_2O_3^{-2} + 2H^+ + H_2O$	8	7.05E-08	8.92E-01	2.80E-05	3.46E-01	2.35E-08	2.45E-01	5.29E-09	5.52E-09
20	$H_2S(aq) + 2O_2(aq) \rightarrow SO_4^{-2} + 2H^+$	8	1.54E-07	1.77E-01	2.95E-05	3.46E-01	4.91E-08		1.10E-08	
21	pyrite $+ 2H^+ + 1/2O_2(aq) \rightarrow$ 2sulfur $+ Fe^{+2} + H_2O$	2	1.01E-07	1.16E-01	1.52E-05	1.89E-01	1.90E-05		6.38E-06	
22	pyrite $+ 3/2O_2(aq) \rightarrow S_2O_3^{-2} + Fe^{+2}$	6	1.42E-07	1.67E-01	2.53E-05	3.76E-01	2.90E-05	3.79E-01	8.48E-06	8.98E-01
23	pyrite $+ 7/2O_2(aq) + H_2O \rightarrow 2SO_4^{-2} + Fe^{+2} + 2H^+$	14	1.56E-07	1.71E-01	2.86E-05	3.23E-01	3.22E-05		9.11E-06	
24	$2sulfur + O_2(aq) + H_2O \rightarrow S_2O_3^{-2} + 2H^+$	4	1.62E-07	1.92E-01	3.03E-05	3.67E-01	3.41E-05	3.67E-01	9.53E-06	1.29E-01
25	sulfur $+ 3/2O_2(aq) + H_2O \rightarrow SO_4^{-2} + 2H^+$	6	1.66E-07	1.88E-01	3.08E-05	3.46E-01	3.44E-05		9.57E-06	
26	$S_2O_3^{-2} + 2O_2(aq) + H_2O \rightarrow 2SO_4^{-2} + 2H^+$	8	1.60E-07	1.83E-01	1.70E-07	1.99E-01	1.90E-07	1.98E-01	1.84E-07	1.92E-01
27	$3Fe^{+2} + 1/2O_2(aq) + 3H_2O \rightarrow$ magnetite $+ 6H^+$	2	1.21E-07	1.36E-01	1.22E-08	1.38E-01	1.38E-08		1.01E-11	

28	$2Fe^{+2} + 1/2O_2(aq) + 2H_2O \rightarrow$ hematite $+ 4H^+$	2	1.40E-07	1.55E-01	1.88E-08	2.12E-01	2.12E-08		1.83E-11	
29	$2Fe^{+2} + 1/2O_2(aq) + 2H_2O \rightarrow$ maghemite $+ 4H^+$	2	1.28E-07	1.43E-01	1.74E-08	1.99E-01	1.98E-08		1.67E-11	
30	$Fe^{+2} + 1/4O_2(aq) + 3/2H_2O \rightarrow$ goethite $+ 2H^+$	1	1.40E-07	1.55E-01	1.88E-08	2.12E-01	2.12E-08		1.83E-11	
31	$Fe^{+2} + 1/4O_2(aq) + 3/2H_2O \rightarrow$ lepidocrocite $+ 2H^+$	1	1.25E-07	1.40E-01	1.71E-08	1.95E-01	1.95E-08		1.64E-11	
32	$Fe^{+2} + 1/4O_2(aq) + 5/2H_2O \rightarrow$ ferrihydrite $+ 2H^+$	1	1.15E-07	1.35E-01	1.61E-08	1.86E-01	1.85E-08		1.53E-11	
33	3fayalite + $O_2(aq) \rightarrow$ 2magnetite + $3SiO_2(aq)$	4	1.84E-07	2.22E-01	3.22E-05	3.74E-01	3.74E-05		1.06E-05	
34	3ferrosilite + $1/2O_2(aq) \rightarrow$ magnetite + $3SiO_2(aq)$	2	1.70E-07	2.30E-01	2.97E-05	3.63E-01	3.64E-05		1.03E-05	
35	2magnetite + $1/2O_2(aq) \rightarrow$ 3hematite	2	1.77E-07	1.93E-01	3.10E-05	3.47E-01	3.47E-05		9.85E-06	
36	2magnetite + $1/2O_2(aq) \rightarrow$ 3maghemite	2	1.40E-07	1.55E-01	2.45E-05	2.82E-01	2.82E-05		8.00E-06	
37	2magnetite + $1/2O_2(aq) + 3H_2O \rightarrow$ 6goethite	2	1.78E-07	1.93E-01	3.12E-05	3.49E-01	3.49E-05		9.90E-06	
38	2magnetite + $1/2O_2(aq) + 3H_2O \rightarrow$ 6lepidocrocite	2	1.32E-07	1.47E-01	2.31E-05	2.69E-01	2.69E-05		7.60E-06	
39	2magnetite + $1/2O_2(aq) + 9H_2O \rightarrow$ 6ferrihydrite	2	1.04E-07	1.19E-01	1.84E-05	2.22E-01	2.22E-05		6.24E-06	
40	$CH_4(aq) + 3/2O_2(aq) \rightarrow CO(aq) + 2H_2O$	6	1.21E-07	1.36E-01	8.76E-08	9.95E-01	1.43E-09	1.43E-09	3.98E-11	3.98E-11
41	$CH_4(aq) + 2O_2(aq) \rightarrow CO_2(aq) + 2H_2O$	8	1.70E-07	1.86E-01	1.29E-07	1.45E-01	2.09E-09		5.67E-11	
42	$CH_4(aq) + 2O_2(aq) \rightarrow HCO_3^- + H^+ + H_2O$	8	1.70E-07	1.86E-01	1.29E-07	1.45E-01	2.09E-09		5.67E-11	
43	$CO(aq) + 1/2O_2(aq) \rightarrow CO_2(aq)$	2	4.52E-11	5.27E-11	1.22E-08	1.34E-01	6.24E-09	6.24E-09	1.12E-11	1.12E-11
44	$CO(aq) + 1/2O_2(aq) + H_2O \rightarrow HCO_3^- + H^+$	2	4.52E-11	5.27E-11	1.22E-08	1.34E-01	6.24E-09	6.24E-01	1.13E-11	1.13E-11
Nitrate as an electron acceptor										

45	$H_2(aq) + NO_3^- \rightarrow NO_2^- + H_2O$	2	4.00E-07		2.82E-09		1.45E-09		1.43E-11	
46	$2H_2S(aq) + NO_3^- + Fe^{+2} \rightarrow$ pyrite $+ NO_2^- + 2H^+ + H_2O$	2	1.16E-08	1.91E-01	3.52E-08	4.32E-01	5.20E-09		3.67E-11	
47	$H_2S(aq) + NO_3^- \rightarrow$ sulfur $+ NO_2^- + H_2O$	2	1.84E-08	2.59E-01	1.83E-07	2.17E-01	6.53E-09		1.66E-09	
48	$2H_2S(aq) + 4NO_3^- \rightarrow S_2O_3^{-2} + 4NO_2^- + 2H^+ + H_2O$	8	4.74E-08	5.86E-01	2.09E-07	2.40E-01	1.48E-08	1.58E-01	3.73E-09	3.95E-09
49	$H_2S(aq) + 4NO_3^- \rightarrow SO_4^{-2} + 4NO_2^- + 2H^+$	8	1.08E-07	1.16E-01	2.26E-07	2.35E-01	3.17E-08		7.90E-09	
50	pyrite $+ NO_3^- + 2H^+ \rightarrow$ 2sulfur $+ Fe^{+2} + NO_2^- + H_2O$	2	1.23E-05		6.98E-08		6.26E-07		5.65E-07	
51	pyrite $+ 3NO_3^- \rightarrow S_2O_3^{-2} + 3NO_2^- + Fe^{+2}$	6	2.16E-05	2.38E-01	1.79E-07	1.98E-01	1.50E-06	1.65E-01	8.80E-07	9.55E-01
52	pyrite $+ 7NO_3^- + H_2O \rightarrow Fe^{+2} + 2SO_4^{-2} + 7NO_2^- + 2H^+$	14	2.49E-05		2.15E-07		1.78E-06		9.75E-07	
53	2sulfur $+ 2NO_3^- + H_2O \rightarrow S_2O_3^{-2} + 2NO_2^- + 2H^+$	4	2.62E-05	2.96E-01	2.34E-07	2.62E-01	1.94E-06	2.16E-01	1.04E-06	1.15E-01
54	sulfur $+ 3NO_3^- + H_2O \rightarrow SO_4^{-2} + 3NO_2^- + 2H^+$	6	2.70E-05		2.40E-07		1.97E-06		1.04E-06	
55	$S_2O_3^{-2} + 4NO_3^- + H_2O \rightarrow 2SO_4^{-2} + 4NO_2^- + 2H^+$	8	1.14E-07	1.22E-01	1.20E-07	1.28E-01	1.23E-07	1.37E-01	1.32E-07	1.40E-01
56	$3Fe^{+2} + NO_3^- + 3H_2O \rightarrow$ magnetite $+ NO_2^- + 6H^+$	2	1.93E-06		8.38E-09		8.72E-09		5.72E-12	
57	$2Fe^{+2} + NO_3^- + 2H_2O \rightarrow$ hematite $+ NO_2^- + 4H^+$	2	3.61E-06		1.31E-08		1.36E-08		1.18E-11	
58	$2Fe^{+2} + NO_3^- + 2H_2O \rightarrow$ maghemite $+ NO_2^- + 4H^+$	2	3.13E-06		1.17E-08		1.23E-08		1.02E-11	
59	$2Fe^{+2} + NO_3^- + 3H_2O \rightarrow$ 2goethite $+ NO_2^- + 4H^+$	2	3.62E-06		1.32E-08		1.37E-08		1.18E-11	
60	$2Fe^{+2} + NO_3^- + 3H_2O \rightarrow$ 2lepidocrocite $+ NO_2^- + 4H^+$	2	3.03E-06		1.15E-08		1.20E-08		9.88E-12	

61	$2Fe^{+2} + NO_3^- + 5H_2O \rightarrow$ 2ferrihydrite + $NO_2^- + 4H^+$	2	2.67E-06		1.04E-08		1.10E-08		8.74E-12	
62	3fayalite + $2NO_3^- \rightarrow$ 2magnetite + $2NO_2^-$ + $3SiO_2$(aq)	4	3.12E-05	3.62E-01	2.54E-07	2.70E-01	2.23E-06		1.20E-06	
63	3ferrosilite + $NO_3^- \rightarrow$ magnetite + NO_2^- + $3SiO_2$(aq)	2	2.79E-05	3.89E-01	2.27E-07	2.59E-01	2.14E-06		1.15E-06	
64	2magnetite + $NO_3^- \rightarrow$ 3hematite + NO_2^-	2	2.96E-05		2.41E-07		1.99E-06		1.09E-06	
65	2magnetite + $NO_3^- \rightarrow$ 3maghemite + NO_2^-	2	2.12E-05		1.70E-07		1.43E-06		8.08E-07	
66	2magnetite + NO_3^- + $3H_2O \rightarrow$ 6goethite + NO_2^-	2	2.97E-05		2.43E-07		2.01E-06		1.09E-06	
67	2magnetite + NO_3^- + $3H_2O \rightarrow$ 6lepidocrocite + NO_2^-	2	1.93E-05		1.56E-07		1.31E-06		7.49E-07	
68	2magnetite + NO_3^- + $9H_2O \rightarrow$ 6ferrihydrite + NO_2^-	2	1.30E-05		1.05E-07		9.04E-07		5.44E-07	
69	CH_4(aq) + $3NO_3^- \rightarrow$ CO(aq) + $3NO_2^-$ + $2H_2O$	6	8.65E-08	9.27E-01	5.96E-08	5.97E-01	8.84E-10	8.84E-01	2.81E-11	2.86E-11
70	CH_4(aq) + $4NO_3^- \rightarrow$ CO_2(aq) + $4NO_2^-$ + $2H_2O$	8	1.24E-07		9.20E-08		1.36E-09		4.10E-11	
71	CH_4(aq) + $4NO_3^- \rightarrow$ HCO_3^- + $4NO_2^-$ + H^+ + H_2O	8	1.24E-07		9.20E-08		1.36E-09		4.10E-11	
72	CO(aq) + $NO_3^- \rightarrow$ CO_2(aq) + NO_2^-	2	3.37E-11	3.75E-11	9.47E-09	9.47E-09	4.52E-09	4.52E-09	8.64E-12	8.64E-12
73	CO(aq) + NO_3^- + $H_2O \rightarrow$ HCO_3^- + NO_2^- + H^+	2	3.37E-11	3.75E-11	9.47E-09	9.47E-01	4.52E-09	4.52E-09	8.64E-12	8.64E-12
74	NH_4^+ + $3NO_3^- \rightarrow$ $2H^+$ + $4NO_2^-$ + H_2O	6	3.89E-06		3.49E-08		2.94E-07		5.00E-09	
75	N_2(aq) + $3NO_3^-$ + $H_2O \rightarrow$ $5NO_2^-$ + $2H^+$	6	-8.35E-07		-1.53E-07		-1.13E-06		-3.91E-07	
76	N_2O(aq) + $2NO_3^-$ + $H_2O \rightarrow 4NO_2^-$ + $2H^+$	4	-1.52E-06	-1.52E-01	-2.95E-08	-2.22E-01	-2.72E-08	-1.97E-01	-1.39E-08	-6.38E-09
77	2NO(aq) + NO_3^- + $H_2O \rightarrow 3NO_2^-$ + $2H^+$	2	-5.72E-09	1.78E-09	-2.22E-09	5.28E-09	-1.65E-09	5.86E-09	3.23E-09	1.79E-01
78	$NO_3^- \rightarrow$ NO_2^- +	2	-1.38E-05	-1.43E-01	-1.36E-07	-9.55E-01	-1.02E-06		-3.92E-07	

	$1/2O_2(aq)$										
79	$3H_2(aq) + 2H^+ + 2NO_3^- \rightarrow 2NO(aq) + 4H_2O$	6	3.87E-07	4.40E-01	2.53E-09	2.94E-09	1.29E-09	1.50E-09	1.15E-11	1.35E-11
80	$6H_2S(aq) + 3Fe^{+2} + 2NO_3^- \rightarrow$ 3pyrite + $2NO(aq) + 4H_2O + 4 H^+$	6	1.10E-08	2.13E-01	3.20E-08	4.45E-01	4.69E-09	5.34E-09	2.95E-11	3.46E-11
81	$3H_2S(aq) + 2NO_3^- + 2H^+ \rightarrow$ 3sulfur + $2NO(aq) + 4H_2O$	6	1.72E-08	2.97E-01	2.35E-07	3.43E-01	5.52E-09	6.82E-09	1.23E-09	1.53E-09
82	$6H_2S(aq) + 8NO_3^- + 2H^+ \rightarrow 3S_2O_3^{-2} + 8NO(aq) + 7H_2O$	24	4.50E-08	6.63E-01	2.73E-07	3.77E-01	1.28E-08	1.63E-01	2.87E-09	3.70E-09
83	$3H_2S(aq) + 8NO_3^- + 2H^+ \rightarrow 8NO(aq) + 3SO_4^{-2} + 4H_2O$	24	1.03E-07	1.39E-01	2.98E-07	3.68E-01	2.77E-08	3.29E-01	6.18E-09	7.38E-09
84	$3pyrite + 2NO_3^- + 8H^+ \rightarrow$ 6sulfur + $3Fe^{+2} + 4H_2O + 2NO(aq)$	6	1.68E-05	2.36E-01	6.46E-08	1.22E-01	5.84E-07	1.40E-01	5.24E-07	7.55E-01
85	$pyrite + 2H^+ + 2NO_3^- \rightarrow S_2O_3^{-2} + Fe^{+2} + 2NO(aq) + H_2O$	6	3.07E-05	4.95E-01	2.29E-07	3.15E-01	1.89E-06	2.58E-01	9.96E-07	1.34E-01
86	$3pyrite + 14NO_3^- + 8H^+ \rightarrow 6SO_4^{-2} + 14NO(aq) + 4H_2O + 3Fe^{+2}$	42	3.58E-05	4.26E-01	2.83E-07	3.40E-01	2.31E-06	2.76E-01	1.14E-06	1.37E-01
87	$6sulfur + 4NO_3^- + H_2O \rightarrow 3S_2O_3^{-2} + 4NO(aq) + 2H^+$	12	3.77E-05	4.95E-01	3.11E-07	4.13E-01	2.55E-06	3.35E-01	1.23E-06	1.63E-01
88	$sulfur + 2NO_3^- \rightarrow SO_4^{-2} + 2NO(aq)$	6	3.90E-05	4.57E-01	3.19E-07	3.76E-01	2.60E-06	3.52E-01	1.24E-06	1.47E-01
89	$3S_2O_3^{-2} + 8NO_3^- + 2H^+ \rightarrow 6SO_4^{-2} + 8NO(aq) + H_2O$	24	1.09E-07	1.37E-01	1.06E-07	1.34E-01	1.08E-07	1.35E-01	1.03E-07	1.39E-01
90	$9Fe^{+2} + 2NO_3^- + 8H_2O \rightarrow$ 3magnetite + $2NO(aq) + 16H^+$	6	1.81E-06	2.32E-01	7.33E-09	8.83E-09	7.55E-09	9.48E-09	3.32E-12	5.76E-12
91	$6Fe^{+2} + 2NO_3^- + 5H_2O \rightarrow$ 3hematite + $2NO(aq) + 10H^+$	6	3.43E-06	4.20E-01	1.16E-08	1.38E-01	1.19E-08	1.41E-01	8.16E-12	1.68E-11
92	$6Fe^{+2} + 2NO_3^- + 5H_2O \rightarrow$ 3maghemite + $2NO(aq) + 10H^+$	6	2.95E-06	3.72E-01	1.02E-08	1.24E-01	1.05E-08	1.27E-01	6.61E-12	9.13E-12

93	$3Fe^{+2} + NO_3^- + 4H_2O \rightarrow$ 3goethite + NO(aq) + $5H^+$	3	3.44E-06	4.26E-01	1.16E-08	1.39E-01	1.19E-08	1.42E-01	8.20E-12	1.71E-11
94	$3Fe^{+2} + NO_3^- + 4H_2O \rightarrow$ 3lepidocrocite + NO(aq) + $5H^+$	6	2.85E-06	3.62E-01	9.88E-09	1.21E-01	1.02E-08	1.25E-01	6.28E-12	8.87E-12
95	$3Fe^{+2} + NO_3^- + 7H_2O \rightarrow$ 3ferrihydrite + NO(aq) + $5H^+$	3	2.49E-06	3.26E-01	8.87E-09	1.11E-01	9.19E-09	1.14E-01	5.14E-12	7.66E-12
96	9/2fayalite + $2NO_3^-$ + $2H^+ \rightarrow$ 3magnetite + 2NO(aq) + $9/2SiO_2$(aq) + H_2O	6	4.51E-05	5.95E-01	3.41E-07	4.22E-01	2.98E-06	3.44E-01	1.47E-06	1.70E-01
97	9ferrosilite + $2NO_3^-$ + $2H^+ \rightarrow$ 3magnetite + 2NO(aq) + $9SiO_2$(aq) + H_2O	6	4.03E-05	6.23E-01	3.00E-07	4.47E-01	2.85E-06	3.34E-01	1.40E-06	1.62E-01
98	6magnetite + $2NO_3^-$ + $2H^+ \rightarrow$ 9hematite + 2NO(aq) + H_2O	6	4.28E-05	4.96E-01	3.21E-07	3.78E-01	2.63E-06	3.89E-01	1.31E-06	1.53E-01
99	6magnetite + $2NO_3^-$ + $2H^+ \rightarrow$ 9maghemite + 2NO(aq) + H_2O	6	3.02E-05	3.70E-01	2.16E-07	2.73E-01	1.79E-06	2.24E-01	8.89E-07	1.12E-01
100	3magnetite + NO_3^- + H^+ + $4H_2O \rightarrow$ 9goethite + NO(aq)	3	4.30E-05	4.98E-01	3.25E-07	3.82E-01	2.66E-06	3.12E-01	1.32E-06	1.54E-01
101	3magnetite + NO_3^- + H^+ + $4H_2O \rightarrow$ 9lepidocrocite + NO(aq)	3	2.74E-05	3.42E-01	1.94E-07	2.57E-01	1.61E-06	2.70E-01	7.99E-07	1.26E-01
102	3magnetite + NO_3^- + H^+ + $13H_2O \rightarrow$ 9ferrihydrite + NO(aq)	3	1.79E-05	2.47E-01	1.17E-07	1.74E-01	1.00E-06	1.46E-01	4.92E-07	7.19E-01
103	CH_4(aq) + $2NO_3^-$ + $2H^+ \rightarrow$ CO(aq) + 2NO(aq) + $3H_2O$	6	8.30E-08	1.17E-01	5.18E-08	6.30E-01	7.57E-10	9.20E-01	2.16E-11	2.61E-11
104	$3CH_4$(aq) + $8NO_3^-$ + $8H^+ \rightarrow$ $3CO_2$(aq) + 8NO(aq) + $10H_2O$	24	1.19E-07	1.39E-01	8.15E-08	9.64E-01	1.19E-09	1.42E-09	3.24E-11	3.84E-11
105	$3CH_4$(aq) + $8NO_3^-$ + $5H^+ \rightarrow$ $3HCO_3^-$ + 8NO(aq) + $7H_2O$	24	1.19E-07	1.39E-01	8.15E-08	9.64E-01	1.19E-09	1.42E-09	3.24E-11	3.84E-11

106	$3CO(aq) + 2NO_3^- + 2H^+ \rightarrow 3CO_2(aq) + 2NO(aq) + H_2O$	6	3.25E-11	4.12E-11	8.71E-09	9.80E-09	4.13E-09	4.64E-09	7.20E-12	8.28E-12
107	$3CO(aq) + 2NO_3^- + 2H^+ + 2H_2O \rightarrow 3HCO_3^- + 2NO(aq) + 3H^+$	6	3.25E-11	4.12E-11	8.71E-09	9.80E-01	4.13E-09	4.64E-09	7.20E-12	8.29E-12
108	$3NH_4^+ + 5NO_3^- + 2H^+ \rightarrow 8NO(aq) + 7H_2O$	15	4.43E-06	1.53E-01	-1.31E-09	8.99E-01	2.92E-08	3.69E-01	-2.11E-10	3.44E-09
109	$3N_2(aq) + 4NO_3^- + 4H^+ \rightarrow 10NO(aq) + 2H_2O$	12	-9.10E-07	-5.95E-01	-4.45E-07	-3.28E-01	-3.43E-06	-2.29E-01	-1.69E-06	-1.12E-01
110	$3N_2O(aq) + 2NO_3^- + 2H^+ \rightarrow 8NO(aq) + H_2O$	6	-1.79E-06	-6.18E-01	-4.36E-08	-1.69E-01	-4.28E-08	-1.53E-01	-4.27E-08	-1.55E-01
111	$2NO_3^- + 2H^+ \rightarrow 2NO(aq) + 3/2O_2(aq) + H_2O$	6	-2.23E-05	-1.47E-01	-2.44E-07	-1.26E-01	-1.88E-06	-1.43E-01	-9.11E-07	-6.84E-01
112	$4H_2(aq) + 2NO_3^- + 2H^+ \rightarrow N_2O(aq) + 5H_2O$	8	4.67E-07	4.67E-01	3.27E-09	3.43E-09	1.66E-09	1.74E-09	1.50E-11	1.57E-11
113	$8H_2S(aq) + 4Fe^{+2} + 2NO_3^- \rightarrow 6H^+ + N_2O(aq) + 4pyrite + 5H_2O$	8	1.48E-08	2.23E-01	4.01E-08	4.98E-01	5.84E-09	6.80E-09	3.83E-11	4.20E-11
114	$4H_2S(aq) + 2NO_3^- + 2H^+ \rightarrow N_2O(aq) + 4sulfur + 5H_2O$	8	2.49E-08	3.24E-01	4.50E-07	5.47E-01	7.81E-09	8.30E-09	1.76E-09	1.87E-09
115	$2H_2S(aq) + 2NO_3^- \rightarrow N_2O(aq) + S_2O_3^{-2} + 2H_2O$	8	6.03E-08	7.15E-01	5.01E-07	5.92E-01	1.74E-08	1.93E-01	3.92E-09	4.38E-09
116	$H_2S(aq) + 2NO_3^- \rightarrow SO_4^{-2} + N_2O(aq) + H_2O$	8	1.34E-07	1.41E-01	5.35E-07	5.82E-01	3.68E-08	3.88E-01	8.28E-09	8.73E-09
117	$4pyrite + 2NO_3^- + 10H^+ \rightarrow 8sulfur + 4Fe^{+2} + N_2O(aq) + 5H_2O$	8	3.63E-05	3.63E-01	2.23E-07	2.52E-01	1.85E-06	2.79E-01	1.23E-06	1.34E-01
118	$4pyrite + 6NO_3^- + 6H^+ \rightarrow 4S_2O_3^{-2} + 3N_2O(aq) + 4Fe^{+2} + 3H_2O$	24	5.48E-05	5.93E-01	4.42E-07	5.84E-01	3.60E-06	4.13E-01	1.86E-06	2.12E-01
119	$4pyrite + 14NO_3^- + 6H^+ \rightarrow 8SO_4^{-2} + 4Fe^{+2} + 7N_2O(aq) + 3H_2O$	56	6.15E-05	6.15E-01	5.14E-07	5.43E-01	4.15E-06	4.38E-01	2.05E-06	2.16E-01
120	$4sulfur + H_2O + 2NO_3^- \rightarrow N_2O(aq) + 2S_2O_3^{-2} + 2H^+$	8	6.40E-05	7.81E-01	5.51E-07	6.37E-01	4.47E-06	5.16E-01	2.17E-06	2.52E-01
121	$4sulfur + 6NO_3^- + H_2O \rightarrow 4SO_4^{-2} + 3N_2O(aq)$	24	6.57E-05	6.57E-01	5.63E-07	5.91E-01	4.53E-06	4.76E-01	2.18E-06	2.30E-01

	+ $2H^+$										
122	$S_2O_3^{-2}$ + $2NO_3^-$ → $2SO_4^{-2}$ + N_2O(aq)	8	1.40E-07	1.47E-01	1.42E-07	1.57E-01	1.43E-07	1.58E-01	1.38E-07	1.53E-01
123	$12Fe^{+2}$ + $2NO_3^-$ + 11H-$_2O$ → 4magnetite + N_2O(aq) + $22H^+$	8	2.59E-06	2.59E-01	1.00E-08	1.60E-01	1.02E-08	1.76E-01	6.25E-12	6.89E-12
124	$8Fe^{+2}$ + $2NO_3^-$ + $7H_2O$ → 4hematite + N_2O(aq) + $14H^+$	8	4.60E-06	4.63E-01	1.56E-08	1.65E-01	1.59E-08	1.67E-01	1.26E-11	1.35E-11
125	$8Fe^{+2}$ + $2NO_3^-$ + $7H_2O$ → 4maghemite + N_2O(aq) + $14H^+$	8	4.13E-06	4.13E-01	1.42E-08	1.57E-01	1.45E-08	1.53E-01	1.10E-11	1.20E-11
126	$8Fe^{+2}$ + $2NO_3^-$ + 11H-$_2O$ → 8goethite + N_2O(aq) + $14H^+$	8	4.61E-06	4.61E-01	1.57E-08	1.65E-01	1.59E-08	1.67E-01	1.26E-11	1.35E-11
127	$8Fe^{+2}$ + $2NO_3^-$ + 11H-$_2O$ → 8lepidocrocite + N_2O(aq) + $14H^+$	8	4.02E-06	4.21E-01	1.39E-08	1.48E-01	1.42E-08	1.53E-01	1.07E-11	1.16E-11
128	$8Fe^{+2}$ + $2NO_3^-$ + 19H-$_2O$ → 8ferrihydrite + N_2O(aq) + $14H^+$	8	3.66E-06	3.67E-01	1.29E-08	1.38E-01	1.32E-08	1.41E-01	9.54E-12	1.48E-11
129	6fayalite + $2NO_3^-$ + $2H^+$ → 4magnetite + N_2O(aq) + $6SiO_2$(aq) + H_2O	8	7.40E-05	8.41E-01	5.92E-07	6.52E-01	5.05E-06	5.28E-01	2.49E-06	2.61E-01
130	12ferrosilite + $2NO_3^-$ + $2H^+$ → 4magnetite + N_2O(aq) + $12SiO_2$(aq) + H_2O	8	6.75E-05	8.78E-01	5.37E-07	6.29E-01	4.87E-06	5.98E-01	2.39E-06	2.52E-01
131	8magnetite + $2NO_3^-$ + $2H^+$ → 12hematite + N_2O(aq) + H_2O	8	7.08E-05	7.83E-01	5.66E-07	5.94E-01	4.58E-06	4.81E-01	2.27E-06	2.38E-01
132	8magnetite + $2NO_3^-$ + $2H^+$ → 12maghemite + N_2O(aq) + H_2O	8	5.41E-05	5.47E-01	4.25E-07	4.54E-01	3.46E-06	3.69E-01	1.71E-06	1.83E-01
133	8magnetite + $2NO_3^-$ + $2H^+$ + $11H_2O$ → 24goethite + N_2O(aq)	8	7.11E-05	7.11E-01	5.70E-07	5.99E-01	4.62E-06	4.85E-01	2.28E-06	2.40E-01
134	8magnetite + $2NO_3^-$ + $2H^+$ + $11H_2O$ → 24lepidocrocite + N_2O(aq)	8	5.03E-05	5.35E-01	3.95E-07	4.24E-01	3.22E-06	3.45E-01	1.59E-06	1.76E-01
135	8magnetite + $2NO_3^-$ + $2H^+$ + $35H_2O$ →	8	3.77E-05	3.77E-01	2.93E-07	3.22E-01	2.41E-06	2.63E-01	1.18E-06	1.30E-01

	24ferrihydrite + N_2O(aq)										
136	$4CH_4$(aq) + $6NO_3^-$ + $6H^+$ → $4CO$(aq) + $3N_2O$(aq) + $11H_2O$	24	1.06E-07	1.96E-01	7.19E-08	7.64E-01	1.04E-09	1.14E-01	2.95E-11	3.12E-11
137	CH_4(aq) + $2NO_3^-$ + $2H^+$ →CO_2(aq) + N_2O(aq) + $3H_2O$	8	1.50E-07	1.50E-01	1.08E-07	1.14E-01	1.58E-09	1.66E-09	4.29E-11	4.52E-11
138	CH_4(aq) + $2NO_3^-$ + H^+ → HCO_3^- + N_2O(aq) + $2H_2O$	8	1.50E-07	1.50E-01	1.08E-07	1.14E-01	1.58E-09	1.66E-09	4.29E-11	4.53E-11
139	$4CO$(aq) + $2NO_3^-$ + $2H^+$ → $4CO_2$(aq) + N_2O(aq) + H_2O	8	4.01E-11	4.39E-11	1.07E-08	1.18E-01	5.03E-09	5.22E-09	8.96E-12	9.34E-12
140	$4CO$(aq) + $2NO_3^-$ + $3H_2O$ → $4HCO_3^-$ + N_2O(aq) + $2H^+$	8	4.01E-11	4.39E-11	1.07E-08	1.18E-01	5.03E-09	5.22E-09	8.96E-12	9.34E-12
141	NH_4^+ + NO_3^- → N_2O(aq) + $2H_2O$	4	3.50E-05	3.50E-01	2.72E-07	3.29E-01	6.28E-07	7.56E-01	6.15E-09	7.52E-09
142	$4N_2$(aq) + $2NO_3^-$ + $2H^+$ → $5N_2O$(aq) + H_2O	8	-4.29E-07	-4.29E-01	-5.02E-07	-3.59E-01	-3.79E-06	-2.65E-01	-1.87E-06	-1.39E-01
143	$2NO_3^-$ + $2H^+$→ N_2O(aq) + $2O_2$(aq) + H_2O	8	-1.60E-05	-9.23E-01	-1.89E-07	-7.89E-01	-1.44E-06	-1.21E-01	-6.87E-07	-5.74E-01
144	$5H_2$(aq) + $2NO_3^-$ + $2H^+$ → N_2(aq) + $6H_2O$	10	5.39E-07		3.82E-09		1.92E-09		1.75E-11	
145	$10H_2S$(aq) + $2NO_3^-$ + $5Fe^{+2}$ → 5pyrite + N_2(aq) + $8H^+$ + $6H_2O$	10	1.83E-08	2.58E-01	4.60E-08	5.50E-01	6.64E-09		4.45E-11	
146	$5H_2S$(aq) + $2NO_3^-$ + $2H^+$ → 5sulfur + N_2(aq) + $6H_2O$	10	3.17E-08	3.92E-01	6.88E-07	7.73E-01	9.43E-09		2.13E-09	
147	$10H_2S$(aq) + $8NO_3^-$ → $5S_2O_3^{-2}$ + $4N_2$(aq) + $2H^+$ + $9H_2O$	40	7.39E-08	8.52E-01	7.51E-07	8.29E-01	2.06E-08	2.16E-01	4.66E-09	4.89E-09
148	$5H_2S$(aq) + $8NO_3^-$ → $5SO_4^{-2}$ + $4N_2$(aq) + $2H^+$ + $4H_2O$	40	1.61E-07	1.69E-01	7.94E-07	8.15E-01	4.33E-08		9.77E-09	
149	5pyrite + $2NO_3^-$ + $12H^+$ → 10sulfur + $5Fe^{+2}$ + N_2(aq) + $6H_2O$	10	6.07E-05		4.04E-07		3.26E-06		2.00E-06	
150	5pyrite + $6NO_3^-$ + $6H^+$ → $5S_2O_3^{-2}$ + $3N_2$(aq) + $5Fe^{+2}$ + $3H_2O$	30	8.39E-05	8.95E-01	6.78E-07	7.25E-01	5.44E-06	5.82E-01	2.79E-06	2.97E-01

151	5pyrite + $14NO_3^-$ + $4H^+$ → $10SO_4^{-2}$ + $5Fe^{+2}$ + $7N_2(aq)$ + $2H_2O$	70	9.23E-05		7.68E-07		6.14E-06		3.02E-06	
152	10sulfur + $4NO_3^-$ + $3H_2O$ → $5S_2O_3^{-2}$ + $2N_2(aq)$ + $6H^+$	20	9.55E-05	1.39E-01	8.14E-07	8.86E-01	6.54E-06	7.16E-01	3.18E-06	3.46E-01
153	5sulfur + $6NO_3^-$ + $2H_2O$ → $5SO_4^{-2}$ + $3N_2(aq)$ + $4H^+$	30	9.76E-05		8.29E-07		6.61E-06		3.19E-06	
154	$5S_2O_3^{-2}$ + $8NO_3^-$ + H_2O → $10SO_4^{-2}$ + $4N_2(aq)$ + $2H^+$	40	1.67E-07	1.75E-01	1.69E-07	1.76E-01	1.68E-07	1.75E-01	1.63E-07	1.78E-01
155	$15Fe^{+2}$ + $2NO_3^-$ + $14H_2O$ → 5magnetite + $N_2(aq)$ + $28H^+$	10	3.29E-06		1.20E-08		1.21E-08		8.33E-12	
156	$10Fe^{+2}$ + $2NO_3^-$ + $9H_2O$ → 5hematite + $N_2(aq)$ + $18H^+$	10	5.65E-06		1.86E-08		1.87E-08		1.57E-11	
157	$10Fe^{+2}$ + $2NO_3^-$ + $9H_2O$ → 5maghemite + $N_2(aq)$ + $18H^+$	10	5.18E-06		1.72E-08		1.73E-08		1.41E-11	
158	$10Fe^{+2}$ + $2NO_3^-$ + $14H_2O$ → 10goethite + $N_2(aq)$ + $18H^+$	10	5.66E-06		1.86E-08		1.87E-08		1.57E-11	
159	$10Fe^{+2}$ + $2NO_3^-$ + $14H_2O$ → 10lepidocrocite + $N_2(aq)$ + $18H^+$	10	5.07E-06		1.69E-08		1.70E-08		1.38E-11	
160	$10Fe^{+2}$ + $2NO_3^-$ + $24H_2O$ → 10ferrihydrite + $N_2(aq)$ + $18H^+$	10	4.71E-06		1.59E-08		1.60E-08		1.27E-11	
161	15fayalite + $4NO_3^-$ + $4H^+$ → 10magnetite + $2N_2(aq)$ + $15SiO_2(aq)$ + $2H_2O$	20	1.08E-04	1.26E-01	8.65E-07	9.49E-01	7.26E-06		3.58E-06	
162	15ferrosilite + $2NO_3^-$ + $2H^+$ → 5magnetite + $N_2(aq)$ + $15SiO_2(aq)$ + H_2O	10	9.98E-05	1.25E-01	7.97E-07	8.76E-01	7.03E-06		3.45E-06	
163	10magnetite + $2NO_3^-$ + $2H^+$ → 15hematite + $N_2(aq)$ + H_2O	10	1.04E-04		8.32E-07		6.68E-06		3.30E-06	
164	10magnetite + $2NO_3^-$ + $2H^+$ → 15maghemite + $N_2(aq)$ + H_2O	10	8.30E-05		6.56E-07		5.27E-06		2.61E-06	

165	10magnetite + $2NO_3^-$ + $2H^+$ + $14H_2O$ → 30goethite + N_2(aq)	10	1.04E-04		8.38E-07		6.72E-06		3.32E-06	
166	10magnetite + $2NO_3^-$ + $2H^+$ + $14H_2O$ → 30lepidocrocite + N_2(aq)	10	7.84E-05		6.20E-07		4.98E-06		2.46E-06	
167	10magnetite + $2NO_3^-$ + $2H^+$ + $44H_2O$ → 30ferrihydrite + N_2(aq)	10	6.25E-05		4.92E-07		3.95E-06		1.95E-06	
168	$5CH_4$(aq) + $6NO_3^-$ + $6H^+$ → 5CO(aq) + $3N_2$(aq) + $13H_2O$	30	1.26E-07	1.37E-01	8.66E-08	8.66E-01	1.25E-09	1.25E-09	3.51E-11	3.51E-11
169	$5CH_4$(aq) + $8NO_3^-$ + $8H^+$ →$5CO_2$(aq) + $4N_2$(aq) + $14H_2O$	40	1.77E-07		1.28E-07		1.85E-09		5.04E-11	
170	$5CH_4$(aq) + $8NO_3^-$ + $3H^+$ → $5HCO_3^-$ + $4N_2$(aq) + $9H_2O$	40	1.77E-07		1.28E-07		1.85E-09		5.04E-11	
171	5CO(aq) + $2NO_3^-$ + $2H^+$ → $5CO_2$(aq) + N_2(aq) + H_2O	10	4.69E-11	5.67E-11	1.21E-08	1.30E-01	5.66E-09	5.66E-09	1.02E-11	1.24E-11
172	5CO(aq) + $2NO_3^-$ + $4H_2O$ → $5HCO_3^-$ + N_2(aq) + $3H^+$	10	4.69E-11	5.67E-11	1.21E-08	1.30E-01	5.66E-09	5.66E-09	1.02E-11	1.25E-11
173	$5NH_4^+$ + $3NO_3^-$ → $4N_2$(aq) + $2H^+$ + $9H_2O$	15	9.94E-05		7.88E-07		1.05E-06		1.07E-08	
174	$2NO_3^-$ + $2H^+$→ N_2(aq) + $5/2O_2$(aq) + H_2O	10	-4.56E-06	3.91E-01	-1.10E-07	-8.79E-09	-8.51E-07		-3.92E-07	
175	$4H_2$(aq) + NO_3^- + $2H^+$ → NH_4^+ + $3H_2O$	8	3.66E-07		2.54E-09		1.27E-09		1.16E-11	
176	$8H_2S$(aq) + NO_3^- + $4Fe^{+2}$ → 4pyrite + NH_4^+ + $6H^+$ + $3H_2O$	8	1.00E-08	1.75E-01	3.21E-08	4.20E-01	4.64E-09		2.98E-11	
177	$4H_2S$(aq) + NO_3^- + $2H^+$ → 4sulfur + NH_4^+ + $3H_2O$	8	1.52E-08	2.27E-01	6.28E-07	7.64E-01	5.41E-09		1.25E-09	
178	$2H_2S$(aq) + NO_3^- → $S_2O_3^{-2}$ + NH_4^+	8	4.09E-08	5.22E-01	7.29E-07	8.54E-01	1.26E-08	1.35E-01	2.90E-09	3.13E-09
179	H_2S(aq) + NO_3^- + H_2O → SO_4^{-2} + NH_4^+	8	9.53E-08	1.28E-01	7.97E-07	8.31E-01	2.72E-08		6.25E-09	
180	4pyrite + NO_3^- + $10H^+$ → 8sulfur + $4Fe^{+2}$ + NH_4^+ + $3H_2O$	8	3.75E-05		1.74E-07		1.45E-06		1.43E-06	

181	4pyrite + $3NO_3^-$ + $6H^+$ + $3H_2O$ → $4S_2O_3^{-2}$ + $3NH_4^+$ + $4Fe^{+2}$	24	7.46E-05	8.36E-01	6.12E-07	6.88E-01	4.95E-06	5.55E-01	2.69E-06	2.99E-01
182	4pyrite + $7NO_3^-$ + $6H^+$ + $11H_2O$ → $4Fe^{+2}$ + $8SO_4^{-2}$ + $7NH_4^+$	56	8.81E-05		7.57E-07		6.05E-06		3.07E-06	
183	4sulfur + NO_3^- + $3H_2O$ → NH_4^+ + $2S_2O_3^{-2}$ + $2H^+$	8	9.31E-05	1.67E-01	8.30E-07	9.44E-01	6.69E-06	7.65E-01	3.32E-06	3.77E-01
184	4sulfur + $3NO_3^-$ + $7H_2O$ → $4SO_4^{-2}$ + $3NH_4^+$ + $2H^+$	24	9.65E-05		8.54E-07		6.82E-06		3.35E-06	
185	$S_2O_3^{-2}$ + NO_3^- + $2H_2O$ → $2SO_4^{-2}$ + NH_4^+	8	1.01E-07	1.86E-01	1.06E-07	1.14E-01	1.06E-07	1.13E-01	1.04E-07	1.12E-01
186	$12Fe^{+2}$ + NO_3^- + $13H_2O$ → 4magnetite + NH_4^+ + $22H^+$	8	1.60E-06		7.35E-09		7.42E-09		3.42E-12	
187	$8Fe^{+2}$ + NO_3^- + $9H_2O$ → 4hematite + NH_4^+ + $14H^+$	8	3.11E-06		1.16E-08		1.17E-08		8.30E-12	
188	$8Fe^{+2}$ + NO_3^- + $9H_2O$ → 4maghemite + NH_4^+ + $14H^+$	8	2.64E-06		1.02E-08		1.03E-08		6.76E-12	
189	$8Fe^{+2}$ + NO_3^- + $13H_2O$ → 8goethite + NH_4^+ + $14H^+$	8	3.12E-06		1.16E-08		1.17E-08		8.34E-12	
190	$8Fe^{+2}$ + NO_3^- + $13H_2O$ → 8lepidocrocite + NH_4^+ + $14H^+$	8	2.53E-06		9.91E-09		1.00E-08		6.43E-12	
191	$8Fe^{+2}$ + NO_3^- + $21H_2O$ → 8ferrihydrite + NH_4^+ + $14H^+$	8	2.17E-06		8.90E-09		9.00E-09		5.29E-12	
192	6fayalite + NO_3^- + $2H^+$ + H_2O → 4magnetite + NH_4^+ + $6SiO_2(aq)$	8	1.13E-04	1.33E-01	9.12E-07	9.76E-01	7.85E-06		3.96E-06	
193	12ferrosilite + NO_3^- + $2H^+$ + H_2O → 4magnetite + NH_4^+ + $12SiO_2(aq)$	8	1.00E-04	1.47E-01	8.03E-07	9.29E-01	7.49E-06		3.76E-06	
194	8magnetite + NO_3^- + $2H^+$ + H_2O → 12hematite + NH_4^+	8	1.07E-04		8.59E-07		6.92E-06		3.52E-06	
195	8magnetite + NO_3^- + $2H^+$ + H_2O → 12maghemite + NH_4^+	8	7.32E-05		5.77E-07		4.67E-06		2.41E-06	

196	8magnetite + NO_3^- + $2H^+$ + $13H_2O$ → 24goethite + NH_4^+	8	1.07E-04		8.68E-07		6.99E-06		3.54E-06	
197	8magnetite + NO_3^- + $2H^+$ + $13H_2O$ → 24lepidocrocite + NH_4^+	8	6.57E-05		5.19E-07		4.20E-06		2.17E-06	
198	8magnetite + NO_3^- + $2H^+$ + $37H_2O$ → 24ferrihydrite + NH_4^+	8	4.04E-05		3.14E-07		2.56E-06		1.35E-06	
199	$4CH_4(aq)$ + $3NO_3^-$ + $6H^+$ → $4CO(aq)$ + $3NH_4^+$ + $5H_2O$	24	7.68E-08	8.59E-01	5.19E-08	5.19E-01	7.43E-10	7.43E-01	2.19E-11	2.19E-11
200	$CH_4(aq)$ + NO_3^- + $2H^+$ → $CO_2(aq)$ + NH_4^+ + H_2O	8	1.11E-07		8.18E-08		1.18E-09		3.27E-11	
201	$CH_4(aq)$ + NO_3^- + H^+ → HCO_3^- + NH_4^+	8	1.11E-07		8.18E-08		1.18E-09		3.27E-11	
202	$4CO(aq)$ + NO_3^- + $2H^+$ + H_2O → $4CO_2(aq)$ + NH_4^+	8	3.04E-11	3.42E-11	8.72E-09	8.72E-01	4.08E-09	4.82E-09	7.26E-12	7.26E-12
203	$4CO(aq)$ + NO_3^- + $5H_2O$ → $4HCO_3^-$ + NH_4^+ + $2H^+$	8	3.04E-11	3.42E-11	8.72E-09	8.72E-09	4.08E-09	4.82E-09	7.26E-12	7.26E-12
204	H_2O + NO_3^- + $2H^+$ → NH_4^+ + $2O_2(aq)$	8	-6.69E-05	-5.34E-01	-6.49E-07	-4.87E-01	-5.13E-06		-2.39E-06	
Nitrite as an electron acceptor										
205	$H_2(aq)$ + $2NO_2^-$ + $2H^+$ → $2NO(aq)$ + $2H_2O$	2	3.63E-07	5.20E-01	1.95E-09	3.19E-09	9.66E-10	1.59E-09	5.70E-12	1.17E-11
206	$2H_2S(aq)$ + $2NO_2^-$ + Fe^{+2} → pyrite + $2NO(aq)$ + $2H_2O$	2	9.84E-09	2.48E-01	2.07E-08	3.82E-01	3.68E-09	5.62E-09	7.57E-12	1.51E-11
207	$H_2S(aq)$ + $2NO_2^-$ + $2H^+$ → sulfur + $2NO(aq)$ + $2H_2O$	2	1.49E-08	3.74E-01	9.83E-09	2.40E-01	3.50E-09	7.39E-09	3.10E-12	1.65E-11
208	$2H_2S(aq)$ + $8NO_2^-$ + $6H^+$ → $S_2O_3^{-2}$ + $8NO(aq)$ + $5H_2O$	8	4.03E-08	8.15E-01	1.22E-08	2.70E-01	8.73E-09	1.75E-01	4.80E-12	1.33E-11
209	$H_2S(aq)$ + $8NO_2^-$ + $6H^+$ → SO_4^{-2} + $8NO(aq)$ + $4H_2O$	8	9.39E-08	1.61E-01	1.39E-08	2.55E-01	1.43E-08	2.56E-01	5.72E-12	1.33E-11
210	pyrite + $2NO_2^-$ + $4H^+$ → 2sulfur + Fe^{+2} + $2NO(aq)$ + $2H_2O$	2	1.19E-07	2.97E-01	-9.96E-10	9.88E-09	-1.06E-09	1.28E-01	-1.37E-12	6.18E-12

211	pyrite + $6NO_2^-$ + $6H^+$ → $S_2O_3^{-2}$ + 6NO(aq) + Fe^{+2} + $3H_2O$	6	2.41E-07	4.48E-01	9.43E-09	2.21E-01	9.81E-09	2.34E-01	3.87E-12	1.27E-11
212	pyrite + $14NO_2^-$ + $12H^+$ → $2SO_4^{-2}$ + Fe^{+2} + 14NO(aq) + $6H_2O$	14	2.85E-07	4.63E-01	1.29E-08	2.38E-01	1.32E-08	2.46E-01	5.46E-12	1.32E-11
213	2sulfur + $4NO_2^-$ + $2H^+$ → $S_2O_3^{-2}$ + 4NO(aq) + H_2O	4	3.01E-07	5.23E-01	1.46E-08	2.82E-01	1.52E-08	2.94E-01	6.50E-12	1.59E-11
214	sulfur + $6NO_2^-$ + $4H^+$ → $2H_2O$ + SO_4^{-2} + 6NO(aq)	6	3.12E-07	4.91E-01	1.52E-08	2.68E-01	1.56E-08	2.70E-01	6.60E-12	1.42E-11
215	$S_2O_3^{-2}$ + $8NO_2^-$ + $6H^+$ → $2SO_4^{-2}$ + 8NO(aq) + $3H_2O$	8	9.98E-08	1.67E-01	1.41E-08	2.64E-01	1.44E-08	2.72E-01	5.71E-12	1.43E-11
216	$3Fe^{+2}$ + $2NO_2^-$ + $2H_2O$ → magnetite + 2NO(aq) + $4H^+$	2	1.81E-07	3.58E-01	5.22E-09	9.72E-01	5.20E-09	9.77E-09	-1.47E-12	3.56E-12
217	$2Fe^{+2}$ + $2NO_2^-$ + H_2O → hematite + 2NO(aq) + $2H^+$	2	2.36E-07	4.13E-01	8.39E-09	1.51E-01	8.37E-09	1.51E-01	9.65E-13	8.53E-12
218	$2Fe^{+2}$ + $2NO_2^-$ + H_2O → maghemite + 2NO(aq) + $2H^+$	2	1.99E-07	3.77E-01	7.00E-09	1.37E-01	6.98E-09	1.37E-01	-5.79E-13	6.98E-12
219	Fe^{+2} + NO_2^- + H_2O → goethite + NO(aq) + H^+	1	2.36E-07	4.14E-01	8.43E-09	1.52E-01	8.41E-09	1.52E-01	1.00E-12	8.56E-12
220	Fe^{+2} + NO_2^- + H_2O → lepidocrocite + NO(aq) + H^+	1	1.91E-07	3.69E-01	6.71E-09	1.35E-01	6.69E-09	1.34E-01	-9.11E-13	6.64E-12
221	Fe^{+2} + NO_2^- + $2H_2O$ → ferrihydrite + NO(aq) + H^+	1	1.63E-07	3.50E-01	5.70E-09	1.24E-01	5.68E-09	1.24E-01	-2.05E-12	5.56E-12
222	3fayalite + $4NO_2^-$ + $4H^+$ → 2magnetite + 4NO(aq) + $3SiO_2$(aq) + $2H_2O$	4	3.66E-07	6.18E-01	1.66E-08	2.90E-01	1.88E-08	3.17E-01	9.15E-12	1.67E-11
223	3ferrosilite + $2NO_2^-$ + $2H^+$ → magnetite + 2NO(aq) + $3SiO_2$(aq) + H_2O	2	3.24E-07	6.35E-01	1.40E-08	2.79E-01	1.77E-08	2.96E-01	8.32E-12	1.59E-11
224	2magnetite + $2NO_2^-$ + $2H^+$ → 3hematite + 2NO(aq) + H_2O	2	3.46E-07	5.24E-01	1.53E-08	2.63E-01	1.59E-08	2.73E-01	7.32E-12	1.49E-11

225	2magnetite + $2NO_2^-$ + $2H^+$ → 3maghemite + 2NO(aq) + H_2O	2	2.36E-07	4.14E-01	8.61E-09	1.95E-01	8.94E-09	2.27E-01	2.68E-12	1.24E-11
226	magnetite + NO_2^- + H^+ + H_2O → 3goethite + NO(aq)	1	3.48E-07	5.26E-01	1.56E-08	2.64E-01	1.62E-08	2.75E-01	7.43E-12	1.50E-11
227	magnetite + NO_2^- + H^+ + H_2O → 3lepidocrocite + NO(aq)	1	2.11E-07	3.89E-01	7.22E-09	1.89E-01	7.48E-09	1.88E-01	1.69E-12	9.24E-12
228	magnetite + NO_2^- + H^+ + $4H_2O$ → 3ferrihydrite + NO(aq)	1	1.28E-07	3.61E-01	2.33E-09	1.33E-01	2.39E-09	1.37E-01	-1.73E-12	5.83E-12
229	CH_4(aq) + $6NO_2^-$ + $6H^+$ → CO(aq) +6NO(aq) + $5H_2O$	6	7.59E-08	1.25E-01	1.18E-08	2.26E-01	5.04E-10	9.98E-01	4.80E-12	1.24E-11
230	CH_4(aq) + $8NO_2^-$ + $8H^+$ → CO_2(aq) +8NO(aq) + $6H_2O$	8	1.10E-07	1.70E-01	1.48E-08	2.57E-01	8.57E-10	1.56E-01	6.30E-12	1.39E-11
231	CH_4(aq) + $8NO_2^-$ + $7H^+$ → HCO_3^- + 8NO + $5H_2O$	8	1.10E-07	1.70E-01	1.48E-08	2.57E-01	8.57E-10	1.56E-09	6.30E-12	1.39E-11
232	CO(aq) + $2NO_2^-$ + $2H^+$ → CO_2(aq) + 2NO(aq) + H_2O	2	3.01E-11	4.89E-11	7.18E-09	1.43E-01	3.33E-09	4.86E-09	4.32E-12	7.35E-12
233	CO(aq) + $2NO_2^-$ + H^+ → HCO_3^- + 2NO(aq)	2	3.01E-11	4.89E-11	7.18E-09	1.43E-01	3.33E-09	4.86E-09	4.32E-12	7.35E-12
234	NH_4^+ + $5NO_2^-$ + $4H^+$ → 6NO(aq) + $4H_2O$	5	1.07E-08	2.24E-01	-5.19E-09	7.87E-09	-5.38E-09	8.23E-09	-7.43E-12	1.65E-12
235	N_2(aq) + $4NO_2^-$ + $4H^+$ → 6NO(aq) + $2H_2O$	4	-4.56E-07	-1.90E-01	-3.34E-08	-1.72E-01	-3.43E-08	-1.73E-01	-2.60E-11	-1.46E-11
236	N_2O(aq) + $2NO_2^-$ + $2H^+$ → 4NO(aq) + H_2O	2	-3.90E-07	-3.42E-01	-3.67E-08	-9.52E-09	-3.82E-08	-9.94E-09	-2.85E-11	-9.66E-12
237	$3NO_2^-$ + $2H^+$ → 2NO(aq) + NO_3^- + H_2O	2	-2.81E-08	9.43E-01	-5.10E-09	2.15E-09	-5.90E-09	1.66E-09	-7.19E-12	-2.16E-12
238	$2NO_2^-$ + $2H^+$→ 2NO(aq) + $1/2O_2$(aq) + H_2O	2	-2.23E-07	-1.38E-01	-2.06E-08	-5.89E-09	-2.15E-08	-1.17E-01	-1.73E-11	-9.77E-12
239	$2H_2$(aq) + $2NO_2^-$ + $2H^+$ → N_2O(aq) + $3H_2O$	4	5.35E-07	5.35E-01	3.73E-09	4.38E-01	1.86E-09	2.19E-09	1.56E-11	1.71E-11
240	$4H_2S$(aq) + $2NO_2^-$ + $2Fe^{+2}$ → 2pyrite + N_2O(aq) + $2H^+$ + $3H_2O$	4	1.81E-08	2.56E-01	4.51E-08	5.65E-01	6.47E-09	6.96E-09	3.99E-11	4.37E-11
241	$2H_2S$(aq) + $2NO_2^-$ + $2H^+$ → 2sulfur +	4	3.13E-08	3.88E-01	5.09E-08	6.29E-01	9.09E-09	1.59E-01	3.10E-11	3.47E-11

	$N_2O(aq) + 3H_2O$										
242	$2H_2S(aq) + 4NO_2^- + 2H^+ \rightarrow S_2O_3^{-2} + 2N_2O(aq) + 3H_2O$	8	7.32E-08	8.44E-01	5.58E-08	6.72E-01	1.99E-08	2.28E-01	3.44E-11	4.30E-11
243	$H_2S(aq) + 4NO_2^- + 2H^+ \rightarrow SO_4^{-2} + 2N_2O(aq) + 2H_2O$	8	1.60E-07	1.67E-01	5.90E-08	6.65E-01	4.19E-08	4.58E-01	3.62E-11	4.00E-11
244	$2pyrite + 2NO_2^- + 6H^+ \rightarrow 4sulfur + 2Fe^{+2} + N_2O(aq) + 3H_2O$	4	6.28E-07	6.28E-01	2.93E-08	3.47E-01	3.05E-08	3.61E-01	2.20E-11	2.58E-11
245	$2pyrite + 6NO_2^- + 6H^+ \rightarrow 2S_2O_3^{-2} + 3N_2O(aq) + 2Fe^{+2} + 3H_2O$	12	8.71E-07	9.30E-01	5.01E-08	5.92E-01	5.22E-08	6.16E-01	3.25E-11	3.88E-11
246	$2pyrite + 14NO_2^- + 10H^+ \rightarrow 4SO_4^{-2} + 2Fe^{+2} + 7N_2O(aq) + 5H_2O$	28	9.59E-07	9.59E-01	5.70E-08	6.25E-01	5.91E-08	6.47E-01	3.57E-11	3.95E-11
247	$2sulfur + 2NO_2^- \rightarrow S_2O_3^{-2} + N_2O(aq)$	4	9.92E-07	1.90E-01	6.06E-08	7.14E-01	6.31E-08	7.44E-01	3.78E-11	4.53E-11
248	$2sulfur + 6NO_2^- + 2H^+ \rightarrow H_2O + 2SO_4^{-2} + 3N_2O(aq)$	12	1.01E-06	1.14E-01	6.17E-08	6.71E-01	6.38E-08	6.95E-01	3.80E-11	4.17E-11
249	$S_2O_3^{-2} + 4NO_2^- + 2H^+ \rightarrow 2SO_4^{-2} + 2N_2O(aq) + H_2O$	8	1.66E-07	1.74E-01	5.95E-08	6.77E-01	6.14E-08	7.00E-01	3.62E-11	4.18E-11
250	$6Fe^{+2} + 2NO_2^- + 5H_2O \rightarrow 2magnetite + N_2O(aq) + 10H^+$	4	7.51E-07	7.60E-01	1.17E-08	1.28E-01	1.17E-08	1.28E-01	6.78E-12	8.42E-12
251	$4Fe^{+2} + 2NO_2^- + 3H_2O \rightarrow 2hematite + N_2O(aq) + 6H^+$	4	8.61E-07	8.62E-01	1.81E-08	1.98E-01	1.81E-08	1.98E-01	1.33E-11	1.52E-11
252	$4Fe^{+2} + 2NO_2^- + 3H_2O \rightarrow 2maghemite + N_2O(aq) + 6H^+$	4	7.88E-07	7.88E-01	1.67E-08	1.84E-01	1.67E-08	1.84E-01	1.18E-11	1.37E-11
253	$4Fe^{+2} + 2NO_2^- + 5H_2O \rightarrow 4goethite + N_2O(aq) + 6H^+$	4	8.62E-07	8.62E-01	1.81E-08	1.98E-01	1.81E-08	1.98E-01	1.34E-11	1.53E-11
254	$4Fe^{+2} + 2NO_2^- + 5H_2O \rightarrow 4lepidocrocite + N_2O(aq) + 6H^+$	4	7.72E-07	7.72E-01	1.64E-08	1.81E-01	1.64E-08	1.89E-01	1.15E-11	1.34E-11
255	$4Fe^{+2} + 2NO_2^- + 9H_2O \rightarrow 4ferrihydrite + N_2O(aq) + 6H^+$	4	7.16E-07	7.16E-01	1.54E-08	1.80E-01	1.54E-08	1.78E-01	1.03E-11	1.22E-11
256	$3fayalite + 2NO_2^- + 2H^+ \rightarrow 2magnetite +$	4	1.12E-06	1.26E-01	6.44E-08	7.30E-01	7.03E-08	7.59E-01	4.31E-11	4.68E-11

	$N_2O(aq) + 3SiO_2(aq) + H_2O$									
257	6ferrosilite + $2NO_2^-$ + $2H^+$ → 2magnetite + $N_2O(aq)$ + $6SiO_2(aq)$ + H_2O	4	1.04E-06	1.35E-01	5.92E-08	7.73E-01	6.80E-08	7.37E-01	4.14E-11	4.52E-11
258	4magnetite + $2NO_2^-$ + $2H^+$ → 6hematite + $N_2O(aq)$ + H_2O	4	1.08E-06	1.81E-01	6.19E-08	6.74E-01	6.45E-08	7.12E-01	3.94E-11	4.32E-11
259	4magnetite + $2NO_2^-$ + $2H^+$ → 6maghemite + $N_2O(aq)$ + H_2O	4	8.61E-07	8.61E-01	4.85E-08	5.39E-01	5.05E-08	5.61E-01	3.01E-11	3.39E-11
260	4magnetite + $2NO_2^-$ + $2H^+$ + $5H_2O$ → 12goethite + $N_2O(aq)$	4	1.09E-06	1.85E-01	6.24E-08	6.78E-01	6.49E-08	7.57E-01	3.96E-11	4.35E-11
261	4magnetite + $2NO_2^-$ + $2H^+$ + $5H_2O$ → 12lepidocrocite + $N_2O(aq)$	4	8.13E-07	8.13E-01	4.57E-08	5.11E-01	4.75E-08	5.32E-01	2.81E-11	3.19E-11
262	4magnetite + $2NO_2^-$ + $2H^+$ + $17H_2O$ → 12ferrihydrite + $N_2O(aq)$	4	6.46E-07	6.46E-01	3.59E-08	4.14E-01	3.74E-08	4.34E-01	2.13E-11	2.59E-11
263	$2CH_4(aq) + 6NO_2^- + 6H^+$ → $2CO(aq) + 3N_2O(aq) + 7H_2O$	12	1.25E-07	1.29E-01	5.48E-08	6.23E-01	1.20E-09	1.32E-01	3.09E-11	3.43E-11
264	$CH_4(aq) + 4NO_2^- + 4H^+$ → $CO_2(aq) + 2N_2O(aq) + 4H_2O$	8	1.75E-07	1.75E-01	6.09E-08	6.63E-01	1.79E-09	1.95E-09	3.74E-11	4.12E-11
265	$CH_4(aq) + 4NO_2^- + 3H^+$ → $HCO_3^- + 2N_2O(aq) + 3H_2O$	8	1.75E-07	1.75E-01	6.09E-08	6.63E-01	1.79E-09	1.95E-09	3.74E-11	4.12E-11
266	$2CO(aq) + 2NO_2^- + 2H^+$ → $2CO_2(aq) + N_2O(aq) + H_2O$	4	4.65E-11	5.30E-11	1.19E-08	1.27E-01	5.53E-09	5.91E-09	9.28E-12	1.33E-11
267	$2CO(aq) + 2NO_2^- + H_2O$ → $2HCO_3^- + N_2O(aq)$	4	4.65E-11	5.30E-11	1.19E-08	1.27E-01	5.53E-09	5.91E-09	9.28E-12	1.34E-11
268	$2NH_4^+ + 4NO_2^- + 2H^+$ → $3N_2O(aq) + 5H_2O$	8	6.11E-07	6.11E-01	3.39E-08	4.30E-01	3.54E-08	4.39E-01	1.86E-11	2.43E-11
269	$2N_2(aq) + 2NO_2^- + 2H^+$ → $3N_2O(aq) + H_2O$	4	-3.48E-07	-3.48E-01	-3.99E-08	-2.36E-01	-3.97E-08	-2.27E-01	-2.95E-11	-1.82E-11
270	$4NO_2^- + 2H^+$ → $N_2O(aq) + 2NO_3^- + H_2O$	4	1.53E-07	1.53E-01	7.98E-09	1.72E-01	7.44E-09	1.28E-01	1.60E-12	3.48E-12

271	$2NO_2^- + 2H^+ \rightarrow N_2O(aq) + O_2(aq) + H_2O$	4	-5.68E-08	3.28E-01	-1.00E-08	3.18E-09	-1.04E-08	-4.78E-09	-9.86E-12	-6.84E-12
272	$3H_2(aq) + 2NO_2^- + 2H^+ \rightarrow N_2(aq) + 4H_2O$	6	6.31E-07		4.48E-09		2.23E-09		1.95E-11	
273	$6H_2S(aq) + 2NO_2^- + 3Fe^{+2} \rightarrow$ 3pyrite + $N_2(aq) + 4H^+ + 4H_2O$	6	2.27E-08	3.17E-01	5.33E-08	6.14E-01	7.61E-09		4.97E-11	
274	$3H_2S(aq) + 2NO_2^- + 2H^+ \rightarrow$ 3sulfur + $N_2(aq) + 4H_2O$	6	4.05E-08	4.83E-01	9.63E-08	1.67E-01	1.14E-08		6.12E-11	
275	$6H_2S(aq) + 8NO_2^- + 2H^+ \rightarrow 3S_2O_3^{-2} + 4N_2(aq) + 7H_2O$	24	9.16E-08	1.29E-01	1.04E-07	1.13E-01	2.44E-08	2.54E-01	6.63E-11	6.91E-11
276	$3H_2S(aq) + 8NO_2^- + 2H^+ \rightarrow 3SO_4^{-2} + 4N_2(aq) + 4H_2O$	24	1.97E-07	2.41E-01	1.08E-07	1.19E-01	5.10E-08		6.91E-11	
277	3pyrite + $2NO_2^- + 8H^+ \rightarrow$ 6sulfur + $3Fe^{+2} + N_2(aq) + 4H_2O$	6	1.27E-06		6.38E-08		6.55E-08		4.78E-11	
278	pyrite + $2NO_2^- + 2H^+ \rightarrow S_2O_3^{-2} + N_2(aq) + Fe^{+2} + H_2O$	6	1.63E-06	1.72E-01	9.51E-08	1.58E-01	9.81E-08	1.38E-01	6.35E-11	6.73E-11
279	3pyrite + $14NO_2^- + 8H^+ \rightarrow 6SO_4^{-2} + 3Fe^{+2} + 7N_2(aq) + 4H_2O$	42	1.77E-06		1.06E-07		1.08E-07		6.83E-11	
280	6sulfur + $4NO_2^- + H_2O \rightarrow 3S_2O_3^{-2} + 2N_2(aq) + 2H^+$	12	1.82E-06	1.95E-01	1.11E-07	1.19E-01	1.14E-07	1.23E-01	7.14E-11	7.78E-11
281	sulfur + $2NO_2^- \rightarrow SO_4^{-2} + N_2(aq)$	6	1.85E-06		1.12E-07		1.16E-07		7.17E-11	
282	$3S_2O_3^{-2} + 8NO_2^- + 2H^+ \rightarrow 6SO_4^{-2} + 4N_2(aq) + H_2O$	24	2.02E-07	3.00E-01	1.09E-07	1.13E-01	1.12E-07	1.16E-01	6.90E-11	7.19E-11
283	$9Fe^{+2} + 2NO_2^- + 8H_2O \rightarrow$ 3magnetite + $N_2(aq) + 16H^+$	6	1.45E-06		1.44E-08		1.43E-08		1.01E-11	
284	$6Fe^{+2} + 2NO_2^- + 5H_2O \rightarrow$ 3hematite + $N_2(aq) + 10H^+$	6	1.62E-06		2.22E-08		2.20E-08		1.83E-11	
285	$6Fe^{+2} + 2NO_2^- + 5H_2O \rightarrow$ 3maghemite + $N_2(aq) + 10H^+$	6	1.51E-06		2.08E-08		2.06E-08		1.67E-11	
286	$6Fe^{+2} + 2NO_2^- + 8H_2O \rightarrow$ 6goethite + $N_2(aq)$	6	1.62E-06		2.23E-08		2.21E-08		1.83E-11	

	+ $10H^+$									
287	$6Fe^{+2} + 2NO_2^- + 8H_2O$ → 6lepidocrocite + $N_2(aq) + 10H^+$	6	1.49E-06		2.05E-08		2.03E-08		1.64E-11	
288	$6Fe^{+2} + 2NO_2^- + 14H_2O$ → 6ferrihydrite + $N_2(aq) + 10H^+$	6	1.40E-06		1.95E-08		1.93E-08		1.53E-11	
289	9fayalite + $4NO_2^-$ + $4H^+$ → 6magnetite + $2N_2(aq)$ + $9SiO_2(aq)$ + $2H_2O$	12	2.01E-06	2.21E-01	1.17E-07	1.21E-01	1.25E-07		7.94E-11	
290	9ferrosilite + $2NO_2^-$ + $2H^+$ → 3magnetite + $N_2(aq)$ + $9SiO_2(aq)$ + H_2O	6	1.88E-06	2.28E-01	1.09E-07	1.18E-01	1.22E-07		7.69E-11	
291	6magnetite + $2NO_2^-$ + $2H^+$ → 9hematite + $N_2(aq) + H_2O$	6	1.95E-06		1.13E-07		1.17E-07		7.39E-11	
292	6magnetite + $2NO_2^-$ + $2H^+$ → 9maghemite + $N_2(aq) + H_2O$	6	1.62E-06		9.27E-08		9.55E-08		6.00E-11	
293	6magnetite + $2NO_2^-$ + $2H^+$ + $8H_2O$ → 18goethite + $N_2(aq)$	6	1.96E-06		1.13E-07		1.17E-07		7.42E-11	
294	6magnetite + $2NO_2^-$ + $2H^+$ + $8H_2O$ → 18lepidocrocite + $N_2(aq)$	6	1.55E-06		8.85E-08		9.11E-08		5.70E-11	
295	6magnetite + $2NO_2^-$ + $2H^+$ + $26H_2O$ → 18ferrihydrite + $N_2(aq)$	6	1.30E-06		7.38E-08		7.59E-08		4.67E-11	
296	$CH_4(aq)$ + $2NO_2^-$ + $2H^+$ → $CO(aq)$ + $N_2(aq) + 3H_2O$	6	1.53E-07	1.57E-01	1.02E-07	1.21E-01	1.49E-09	1.49E-09	3.98E-11	3.98E-11
297	$3CH_4(aq)$ + $8NO_2^-$ + $8H^+$ → $3CO_2(aq)$ + $4N_2(aq)$ + $10H_2O$	24	2.12E-07		1.11E-07		2.17E-09		5.67E-11	
298	$3CH_4(aq)$ + $8NO_2^-$ + $5H^+$ → $3HCO_3^-$ + $4N_2(aq) + 7H_2O$	24	2.12E-07		1.11E-07		2.17E-09		5.67E-11	
299	$3CO(aq)$ + $2NO_2^-$ + $2H^+$ → $3CO_2(aq)$ + $N_2(aq) + H_2O$	6	5.58E-11	5.95E-11	1.38E-08	1.38E-01	6.42E-09	6.42E-09	1.12E-11	1.12E-11

300	$3CO(aq) + 2NO_2^- + 2H_2O \rightarrow 3HCO_3^- + N_2(aq) + H^+$	6	5.58E-11	5.95E-11	1.38E-08	1.38E-01	6.42E-09	6.42E-09	1.12E-11	1.12E-11
301	$NH_4^+ + NO_2^- \rightarrow N_2(aq) + 2H_2O$	3	1.88E-06		1.08E-07		1.11E-07		6.67E-11	
302	$5NO_2^- + 2H^+ \rightarrow N_2(aq) + 3NO_3^- + H_2O$	6	3.14E-07		1.76E-08		1.69E-08		7.82E-12	
303	$2NO_2^- + 2H^+ \rightarrow N_2(aq) + 3/2O_2(aq) + H_2O$	6	2.43E-07	3.76E-01	4.93E-09	1.65E-01	4.16E-09		-2.82E-14	
304	$3H_2(aq) + NO_2^- + 2H^+ \rightarrow NH_4^+ + 2H_2O$	6	3.55E-07		2.44E-09		1.21E-09		1.07E-11	
305	$6H_2S(aq) + NO_2^- + 3Fe^{+2} \rightarrow 3pyrite + NH_4^+ + 4H^+ + 2H_2O$	6	9.47E-09	1.70E-01	3.10E-08	3.97E-01	4.45E-09		2.75E-11	
306	$3H_2S(aq) + NO_2^- + 2H^+ \rightarrow 3sulfur + NH_4^+ + 2H_2O$	6	1.41E-08	2.16E-01	8.49E-08	1.44E-01	5.04E-09		5.57E-11	
307	$6H_2S(aq) + 4NO_2^- + 2H^+ + H_2O \rightarrow 3S_2O_3^{-2} + 4NH_4^+$	24	3.88E-08	5.37E-01	9.94E-08	1.17E-01	1.18E-08	1.28E-01	6.59E-11	7.16E-11
308	$3H_2S(aq) + 4NO_2^- + 2H^+ + 4H_2O \rightarrow 3SO_4^{-2} + 4NH_4^+$	24	9.09E-08	9.84E-01	1.09E-07	1.14E-01	2.57E-08		7.15E-11	
309	$3pyrite + NO_2^- + 8H^+ \rightarrow 6sulfur + 3Fe^{+2} + NH_4^+ + 2H_2O$	6	6.61E-07		1.99E-08		2.05E-08		2.89E-11	
310	$pyrite + NO_2^- + 2H^+ + H_2O \rightarrow S_2O_3^{-2} + Fe^{+2} + NH_4^+$	6	1.39E-06	1.57E-01	8.25E-08	9.35E-01	8.57E-08	9.77E-01	6.04E-11	6.79E-11
311	$3pyrite + 7NO_2^- + 8H^+ + 10H_2O \rightarrow 6SO_4^{-2} + 3Fe^{+2} + 7NH_4^+$	42	1.66E-06		1.03E-07		1.06E-07		6.99E-11	
312	$6sulfur + 2NO_2^- + 5H_2O \rightarrow 3S_2O_3^{-2} + 2NH_4^+ + 2H^+$	12	1.75E-06	2.26E-01	1.14E-07	1.31E-01	1.18E-07	1.35E-01	7.61E-11	8.74E-11
313	$sulfur + NO_2^- + 2H_2O \rightarrow SO_4^{-2} + NH_4^+$	6	1.82E-06		1.17E-07		1.21E-07		7.67E-11	
314	$3S_2O_3^{-2} + 4NO_2^- + 2H^+ + 7H_2O \rightarrow 6SO_4^{-2} + 4NH_4^+$	24	9.68E-08	1.43E-01	1.02E-07	1.92E-01	1.00E-07	1.76E-01	7.14E-11	7.74E-11
315	$9Fe^{+2} + NO_2^- + 10H_2O \rightarrow 3magnetite + NH_4^+ + 16H^+$	6	1.03E-06		7.00E-09		6.98E-09		2.65E-12	
316	$6Fe^{+2} + NO_2^- + 7H_2O \rightarrow 3hematite + NH_4^+ +$	6	1.36E-06		1.11E-08		1.10E-08		7.15E-12	

	$10H^+$									
317	$6Fe^{+2} + NO_2^- + 7H_2O \rightarrow$ 3maghemite + $NH_4^+ + 10H^+$	6	1.14E-06		9.68E-09		9.65E-09		5.61E-12	
318	$6Fe^{+2} + NO_2^- + 10H_2O \rightarrow$ 6goethite + $NH_4^+ + 10H^+$	6	1.36E-06		1.11E-08		1.11E-08		7.19E-12	
319	$6Fe^{+2} + NO_2^- + 10H_2O \rightarrow$ 6lepidocrocite + $NH_4^+ + 10H^+$	6	1.09E-06		9.39E-09		9.36E-09		5.28E-12	
320	$6Fe^{+2} + NO_2^- + 16H_2O \rightarrow$ 6ferrihydrite + $NH_4^+ + 10H^+$	6	9.26E-07		8.38E-09		8.35E-09		4.14E-12	
321	9fayalite + $2NO_2^- + 4H^+ + 2H_2O \rightarrow$ 6magnetite + $2NH_4^+ + 9SiO_2(aq)$	12	2.14E-06	2.54E-01	1.25E-07	1.35E-01	1.40E-07		9.20E-11	
322	9ferrosilite + $NO_2^- + 2H^+ + H_2O \rightarrow$ 3magnetite + $NH_4^+ + 9SiO_2(aq)$	6	1.89E-06	2.69E-01	1.10E-07	1.29E-01	1.33E-07		8.70E-11	
323	6magnetite + $NO_2^- + 2H^+ + H_2O \rightarrow$ 9hematite + NH_4^+	6	2.02E-06		1.18E-07		1.23E-07		8.10E-11	
324	6magnetite + $NO_2^- + 2H^+ + H_2O \rightarrow$ 9maghemite + NH_4^+	6	1.36E-06		7.76E-08		8.05E-08		5.32E-11	
325	6magnetite + $NO_2^- + 2H^+ + 10H_2O \rightarrow$ 18goethite + NH_4^+	6	2.03E-06		1.19E-07		1.24E-07		8.17E-11	
326	6magnetite + $NO_2^- + 2H^+ + 10H_2O \rightarrow$ 18lepidocrocite + NH_4^+	6	1.22E-06		6.92E-08		7.18E-08		4.73E-11	
327	6magnetite + $NO_2^- + 2H^+ + 28H_2O \rightarrow$ 18ferrihydrite + NH_4^+	6	7.17E-07		3.99E-08		4.12E-08		2.68E-11	
328	$CH_4(aq) + NO_2^- + 2H^+ \rightarrow CO(aq) + NH_4^+ + H_2O$	6	7.36E-08	7.74E-01	4.94E-08	4.94E-01	6.97E-10	6.97E-01	1.98E-11	1.98E-11
329	$3CH_4(aq) + 4NO_2^- + 8H^+ \rightarrow 3CO_2(aq) + 4NH_4^+ + 2H_2O$	24	1.07E-07		7.83E-08		1.11E-09		3.00E-11	
330	$3CH_4(aq) + 4NO_2^- + 5H^+ + H_2O \rightarrow 3HCO_3^-$	24	1.07E-07		7.83E-08		1.11E-09		3.00E-11	

	+ $4NH_4^+$										
331	$3CO(aq) + NO_2^- + 2H^+ + H_2O \rightarrow 3CO_2(aq) + NH_4^+$	6	2.94E-11	3.32E-11	8.47E-09	8.47E-09	3.93E-09	3.93E-09	6.80E-12	6.80E-12
332	$3CO(aq) + NO_2^- + 4H_2O \rightarrow 3HCO_3^- + NH_4^+ + H^+$	6	2.94E-11	3.32E-11	8.47E-09	8.47E-09	3.93E-09	3.93E-09	6.80E-12	6.83E-12
333	$H_2O + 4NO_2^- + 2H^+ \rightarrow NH_4^+ + 3NO_3^-$	6	-7.65E-08		-5.00E-09		-6.55E-09		-6.90E-12	
334	$H_2O + NO_2^- + 2H^+ \rightarrow NH_4^+ + 3/2O_2(aq)$	6	-1.39E-06	-1.13E-01	-9.79E-08	-7.47E-01	-1.02E-07		-6.68E-11	
Nitric oxide as an electron acceptor										
335	$H_2(aq) + 2NO(aq) \rightarrow N_2O(aq) + H_2O$	2	2.63E-08	3.38E-01	4.27E-09	6.13E-09	2.14E-09	3.73E-09	1.95E-11	2.85E-11
336	$2H_2S(aq) + 2NO(aq) + Fe^{+2} \rightarrow$ pyrite $+ N_2O(aq) + 2H^+ + H_2O$	2	1.88E-08	3.38E-01	2.83E-08	4.44E-01	7.32E-09	1.25E-01	4.96E-11	7.22E-11
337	$H_2S(aq) + 2NO(aq) \rightarrow$ sulfur $+ N_2O(aq) + H_2O$	2	1.64E-08	2.76E-01	2.08E-08	3.43E-01	1.08E-08	1.66E-01	2.43E-09	3.78E-01
338	$2H_2S(aq) + 8NO(aq) \rightarrow S_2O_3^{-2} + 4N_2O(aq) + 2H^+ + H_2O$	8	1.90E-08	2.93E-01	2.25E-08	3.58E-01	2.25E-08	3.47E-01	5.26E-09	8.22E-09
339	$H_2S(aq) + 8NO(aq) \rightarrow SO_4^{-2} + 4N_2O(aq) + 2H^+$	8	2.07E-08	2.91E-01	2.36E-08	3.54E-01	2.35E-08	3.48E-01	1.10E-08	1.64E-01
340	pyrite $+ 2NO(aq) + 2H^+ \rightarrow$ 2sulfur $+ Fe^{+2} + N_2O(aq) + H_2O$	2	1.40E-08	2.15E-01	1.34E-08	2.46E-01	1.34E-08	2.46E-01	1.58E-08	2.72E-01
341	pyrite $+ 6NO(aq) \rightarrow S_2O_3^{-2} + Fe^{+2} + 3N_2O(aq)$	6	1.91E-08	2.78E-01	2.06E-08	3.37E-01	2.06E-08	3.38E-01	2.11E-08	3.37E-01
342	pyrite $+ 14NO(aq) + H_2O \rightarrow 2SO_4^{-2} + 2H^+ + Fe^{+2} + 7N_2O(aq)$	14	2.10E-08	2.85E-01	2.30E-08	3.42E-01	2.28E-08	3.41E-01	2.27E-08	3.48E-01
343	2sulfur $+ 4NO(aq) + H_2O \rightarrow S_2O_3^{-2} + 2N_2O(aq) + 2H^+$	4	2.17E-08	3.13E-01	2.42E-08	3.73E-01	2.42E-08	3.74E-01	2.37E-08	3.69E-01
344	sulfur $+ 6NO(aq) + H_2O \rightarrow SO_4^{-2} + 3N_2O(aq) + 2H^+$	6	2.21E-08	2.96E-01	2.45E-08	3.58E-01	2.44E-08	3.57E-01	2.38E-08	3.51E-01
345	$S_2O_3^{-2} + 8NO(aq) + H_2O \rightarrow 2SO_4^{-2} +$	8	2.14E-08	2.99E-01	2.38E-08	3.60E-01	2.36E-08	3.58E-01	2.29E-08	3.52E-01

	$4N_2O(aq) + 2H^+$									
346	$3Fe^{+2} + 2NO(aq) + 3H_2O \rightarrow$ magnetite $+ N_2O(aq) + 6H^+$	2	1.66E-08	2.46E-01	1.37E-08	2.46E-01	1.36E-08	2.47E-01	1.00E-11	1.76E-11
347	$2Fe^{+2} + 2NO(aq) + 2H_2O \rightarrow$ hematite $+ N_2O(aq) + 4H^+$	2	1.89E-08	2.64E-01	2.10E-08	3.12E-01	2.10E-08	3.12E-01	1.82E-11	2.95E-11
348	$2Fe^{+2} + 2NO(aq) + 2H_2O \rightarrow$ maghemite $+ N_2O(aq) + 4H^+$	2	1.73E-08	2.48E-01	1.97E-08	2.98E-01	1.96E-08	2.98E-01	1.66E-11	2.80E-11
349	$2Fe^{+2} + 2NO(aq) + 3H_2O \rightarrow$ 2goethite $+ N_2O(aq) + 4H^+$	2	1.89E-08	2.64E-01	2.11E-08	3.12E-01	2.11E-08	3.12E-01	1.82E-11	2.95E-11
350	$2Fe^{+2} + 2NO(aq) + 3H_2O \rightarrow$ 2lepidocrocite $+ N_2O(aq) + 4H^+$	2	1.70E-08	2.45E-01	1.94E-08	2.95E-01	1.93E-08	2.95E-01	1.63E-11	2.76E-11
351	$2Fe^{+2} + 2NO(aq) + 5H_2O \rightarrow$ 2ferrihydrite $+ N_2O(aq) + 4H^+$	2	1.58E-08	2.33E-01	1.84E-08	2.85E-01	1.83E-08	2.85E-01	1.52E-11	2.65E-11
352	3fayalite $+ 4NO(aq) \rightarrow$ 2magnetite $+ 2 N_2O(aq) + 3SiO_2(aq)$	4	2.44E-08	3.47E-01	2.55E-08	3.78E-01	2.65E-08	3.78E-01	2.64E-08	3.77E-01
353	3ferrosilite $+ 2NO(aq) \rightarrow$ magnetite $+ N_2O(aq) + 3SiO_2(aq)$	2	2.26E-08	3.57E-01	2.37E-08	3.75E-01	2.58E-08	3.76E-01	2.55E-08	3.69E-01
354	2magnetite $+ 2NO(aq) \rightarrow$ 3hematite $+ N_2O(aq)$	2	2.35E-08	3.13E-01	2.46E-08	3.59E-01	2.46E-08	3.59E-01	2.45E-08	3.59E-01
355	2magnetite $+ 2NO(aq) \rightarrow$ 3maghemite $+ N_2O(aq)$	2	1.89E-08	2.64E-01	2.00E-08	3.13E-01	2.00E-08	3.12E-01	1.99E-08	3.12E-01
356	2magnetite $+ 2NO(aq) + 3H_2O \rightarrow$ 6goethtite $+ N_2O(aq)$	2	2.36E-08	3.11E-01	2.48E-08	3.64E-01	2.48E-08	3.63E-01	2.46E-08	3.60E-01
357	2magnetite $+ 2NO(aq) + 3H_2O \rightarrow$ 6lepidocrocite $+ N_2O(aq)$	2	1.79E-08	2.54E-01	1.90E-08	3.29E-01	1.90E-08	3.29E-01	1.89E-08	3.23E-01
358	2magnetite $+ 2NO(aq) + 9H_2O \rightarrow$ 6ferrihydrite $+ N_2O(aq)$	2	1.44E-08	2.19E-01	1.57E-08	2.69E-01	1.57E-08	2.69E-01	1.55E-08	2.68E-01
359	$CH_4(aq) + 6NO(aq) \rightarrow CO(aq) + 3N_2O(aq) +$	6	2.16E-08	2.97E-01	2.22E-08	3.34E-01	1.42E-09	2.15E-09	3.96E-11	6.28E-11

	$2H_2O$									
360	$CH_4(aq) + 8NO(aq) \rightarrow CO_2(aq) + 4N_2O(aq) + 2H_2O$	8	2.27E-08	3.16E-01	2.43E-08	3.55E-01	2.07E-09	3.45E-09	5.64E-11	8.36E-11
361	$CH_4(aq) + 8NO(aq) \rightarrow HCO_3^- + 4N_2O(aq) + H^+ + H_2O$	8	2.27E-08	3.16E-01	2.43E-08	3.55E-01	2.07E-09	3.45E-09	5.64E-11	8.36E-11
362	$CO(aq) + 2NO(aq) \rightarrow CO_2(aq) + N_2O(aq)$	2	4.80E-11	6.67E-11	1.33E-08	1.82E-01	6.20E-09	8.50E-09	1.12E-11	1.57E-11
363	$CO(aq) + 2NO(aq) + H_2O \rightarrow HCO_3^- + N_2O(aq) + H^+$	2	4.80E-11	6.67E-11	1.33E-08	1.82E-01	6.20E-09	8.50E-09	1.12E-11	1.57E-11
364	$2NO(aq) \rightarrow N_2O(aq) + 1/2O_2(aq)$	4	-4.78E-10	8.90E-09	-1.67E-10	1.38E-01	-1.79E-10	1.18E-01	-1.02E-10	1.12E-01
365	$2NH_4^+ + 8NO(aq) \rightarrow 5N_2O(aq) + 2H^+ + 3H_2O$	8	1.36E-08	2.11E-01	1.50E-08	2.72E-01	1.50E-08	2.72E-01	1.02E-08	1.91E-01
366	$N_2(aq) + 2NO(aq) \rightarrow 2N_2O(aq)$	2	-1.31E-08	-5.61E-09	-1.05E-08	4.54E-09	-9.85E-09	5.16E-09	-9.94E-09	5.17E-09
367	$4NO(aq) + H_2O \rightarrow N_2O(aq) + 2NO_2^- + 2H^+$	2	7.21E-10	8.22E-09	3.28E-09	1.27E-01	3.28E-09	1.27E-01	4.83E-09	1.43E-01
368	$H_2O + 8NO(aq) \rightarrow 3N_2O(aq) + 2NO_3^- + 2H^+$	6	3.94E-09	1.14E-01	6.03E-09	1.63E-01	5.74E-09	1.67E-01	5.63E-09	1.62E-01
369	$2H_2(aq) + 2NO(aq) \rightarrow N_2(aq) + 2H_2O$	4	6.56E-08	7.31E-01	5.13E-09	5.75E-09	2.55E-09	2.86E-09	2.34E-11	2.65E-11
370	$4H_2S(aq) + 2NO(aq) + 2Fe^{+2} \rightarrow 2pyrite + N_2(aq) + 4H^+ + 2H_2O$	4	2.53E-08	3.66E-01	6.04E-08	7.52E-01	8.60E-09	9.57E-09	5.95E-11	6.75E-11
371	$2H_2S(aq) + 2NO(aq) \rightarrow 2sulfur + N_2(aq) + 2H_2O$	4	4.59E-08	6.86E-01	5.22E-08	6.41E-01	1.33E-08	1.53E-01	3.02E-09	3.48E-09
372	$2H_2S(aq) + 4NO(aq) \rightarrow S_2O_3^{-2} + 2N_2(aq) + 2H^+ + H_2O$	8	5.11E-08	6.43E-01	5.55E-08	6.79E-01	2.84E-08	3.33E-01	6.45E-09	7.58E-09
373	$H_2S(aq) + 4NO(aq) \rightarrow SO_4^{-2} + 2N_2(aq) + 2H^+$	8	5.45E-08	6.39E-01	5.77E-08	6.63E-01	5.69E-08	6.44E-01	1.34E-08	1.52E-01
374	$2pyrite + 2NO(aq) + 4H^+ \rightarrow 4sulfur + 2Fe^{+2} + N_2(aq) + 2H_2O$	4	4.10E-08	4.86E-01	3.72E-08	4.47E-01	3.66E-08	4.49E-01	4.16E-08	4.92E-01
375	$2pyrite + 6NO(aq) \rightarrow 2S_2O_3^{-2} + 2Fe^{+2} + 3N_2(aq)$	12	5.13E-08	6.13E-01	5.16E-08	6.17E-01	5.10E-08	6.99E-01	5.21E-08	6.22E-01

376	2pyrite + 14NO(aq) + $2H_2O \rightarrow 4SO_4^{-2} + 4H^+ + 2Fe^{+2} + 7N_2(aq)$	28	5.50E-08	6.25E-01	5.64E-08	6.39E-01	5.55E-08	6.34E-01	5.53E-08	6.28E-01
377	2sulfur + 2NO(aq) + $H_2O \rightarrow S_2O_3^{-2} + N_2(aq) + 2H^+$	4	5.64E-08	6.77E-01	5.88E-08	7.53E-01	5.82E-08	6.94E-01	5.74E-08	6.87E-01
378	2sulfur + 6NO(aq) + $2H_2O \rightarrow 2SO_4^{-2} + 3N_2(aq) + 4H^+$	12	5.74E-08	6.49E-01	5.96E-08	6.76E-01	5.87E-08	6.62E-01	5.76E-08	6.51E-01
379	$S_2O_3^{-2}$ +4NO(aq) + $H_2O \rightarrow 2SO_4^{-2} + 2N_2(aq) + 2H^+$	8	5.60E-08	6.53E-01	5.81E-08	6.74E-01	5.71E-08	6.65E-01	5.58E-08	6.52E-01
380	$6Fe^{+2}$ + 2NO(aq) + $6H_2O \rightarrow$ 2magnetite + $N_2(aq) + 12H^+$	4	4.62E-08	5.37E-01	1.68E-08	1.95E-01	1.66E-08	1.89E-01	1.33E-11	1.58E-11
381	$4Fe^{+2}$ + 2NO(aq) + $4H_2O \rightarrow$ 2hematite + $N_2(aq) + 8H^+$	4	5.09E-08	5.84E-01	2.58E-08	2.91E-01	2.55E-08	2.88E-01	2.31E-11	2.69E-11
382	$4Fe^{+2}$ + 2NO(aq) + $4H_2O \rightarrow$ 2maghemite + $N_2(aq) + 8H^+$	4	4.78E-08	5.53E-01	2.44E-08	2.77E-01	2.41E-08	2.75E-01	2.16E-11	2.54E-11
383	$4Fe^{+2}$ + 2NO(aq) + $6H_2O \rightarrow$ 4goethite + $N_2(aq) + 8H^+$	4	5.09E-08	5.84E-01	2.58E-08	2.92E-01	2.55E-08	2.89E-01	2.32E-11	2.70E-11
384	$4Fe^{+2}$ + 2NO(aq) + $6H_2O \rightarrow$ 4lepidocrocite + $N_2(aq) + 8H^+$	4	4.71E-08	5.47E-01	2.41E-08	2.75E-01	2.38E-08	2.72E-01	2.13E-11	2.55E-11
385	$4Fe^{+2}$ + 2NO(aq) + $10H_2O \rightarrow$ 4ferrihydrite + $N_2(aq) + 8H^+$	4	4.48E-08	5.23E-01	2.31E-08	2.64E-01	2.28E-08	2.62E-01	2.01E-11	2.39E-11
386	3fayalite + 2NO(aq) $\rightarrow$ 2magnetite + $N_2(aq)$ + $3SiO_2(aq)$	4	6.19E-08	7.54E-01	6.15E-08	7.16E-01	6.29E-08	7.44E-01	6.27E-08	7.21E-01
387	6ferrosilite + 2NO(aq) $\rightarrow$ 2magnetite + $N_2(aq)$ + $6SiO_2(aq)$	4	5.83E-08	7.78E-01	5.79E-08	6.96E-01	6.15E-08	6.90E-01	6.10E-08	6.86E-01
388	4magnetite + 2NO(aq) $\rightarrow$ 6hematite + $N_2(aq)$	4	6.02E-08	6.77E-01	5.97E-08	6.72E-01	5.91E-08	6.66E-01	5.90E-08	6.65E-01
389	4magnetite + 2NO(aq) $\rightarrow$ 6maghemite + $N_2(aq)$	4	5.09E-08	5.84E-01	5.05E-08	5.80E-01	4.98E-08	5.73E-01	4.97E-08	5.73E-01
390	4magnetite + 2NO(aq) + $6H_2O \rightarrow$ 12goethtite + $N_2(aq)$	4	6.03E-08	6.78E-01	6.00E-08	6.75E-01	5.94E-08	6.69E-01	5.92E-08	6.68E-01

391	4magnetite + 2NO(aq) + $6H_2O$ → 12lepidocrocite + N_2(aq)	4	4.88E-08	5.63E-01	4.85E-08	5.65E-01	4.79E-08	5.55E-01	4.77E-08	5.53E-01
392	4magnetite + 2NO(aq) + $18H_2O$ → 12ferrihydrite + N_2(aq)	4	4.18E-08	4.93E-01	4.18E-08	4.93E-01	4.12E-08	4.87E-01	4.09E-08	4.85E-01
393	$2CH_4$(aq) + 6NO(aq) → 2CO(aq) + $3N_2$(aq) + $4H_2O$	12	5.63E-08	6.53E-01	5.48E-08	6.23E-01	1.74E-09	1.98E-09	4.86E-11	5.54E-11
394	CH_4(aq) + 4NO(aq) → CO_2(aq) + $2N_2$(aq) + $2H_2O$	8	5.84E-08	6.59E-01	5.90E-08	6.65E-01	2.50E-09	2.82E-09	6.84E-11	7.74E-11
395	CH_4(aq) + 4NO(aq) → HCO_3^- + $2N_2$(aq) + H^+ + H_2O	8	5.84E-08	6.59E-01	5.90E-08	6.65E-01	2.50E-09	2.82E-01	6.84E-11	7.74E-11
396	2CO(aq) + 2NO(aq) → $2CO_2$(aq) + N_2(aq)	4	6.11E-11	7.24E-11	1.56E-08	1.72E-01	7.20E-09	7.97E-01	1.32E-11	1.48E-11
397	2CO(aq) + 2NO(aq) + $2H_2O$ → $2HCO_3^-$ + N_2(aq) + $2H^+$	4	6.11E-11	7.24E-11	1.56E-08	1.72E-01	7.20E-09	7.97E-09	1.32E-11	1.48E-11
398	$4NH_4^+$ + 6NO(aq) → $5N_2$(aq) + $4H^+$ + $6H_2O$	12	5.82E-08	6.57E-01	5.74E-08	6.50E-01	5.64E-08	6.40E-01	1.47E-08	1.68E-01
399	6NO(aq) + $2H_2O$ → N_2(aq) + $4NO_2^-$ + $4H^+$	4	5.33E-09	1.28E-01	7.86E-09	1.54E-01	7.66E-09	1.52E-01	9.75E-09	1.74E-01
400	$2H_2O$ + 10NO(aq) → $3N_2$(aq) + $4NO_3^-$ + $4H^+$	12	1.42E-08	2.17E-01	1.59E-08	2.34E-01	1.51E-08	2.27E-01	1.50E-08	2.25E-01
401	2NO(aq) → N_2(aq) + O_2(aq)	4	1.22E-08	2.35E-01	1.01E-08	2.30E-01	9.49E-09	1.72E-01	9.73E-09	1.73E-01
402	$5H_2$(aq) + 2NO(aq) + $2H^+$ → $2NH_4^+$ + $2H_2O$	10	7.68E-08	8.43E-01	2.29E-09	2.54E-09	1.14E-09	1.26E-09	1.04E-11	1.16E-11
403	$10H_2S$(aq) + 2NO(aq) + $5Fe^{+2}$ → 5pyrite + $2NH_4^+$ + $8H^+$ + $2H_2O$	10	7.89E-09	1.69E-01	2.94E-08	4.14E-01	4.21E-09	4.62E-09	2.70E-11	3.00E-11
404	$5H_2S$(aq) + 2NO(aq) + $2H^+$ → 5sulfur + $2NH_4^+$ + $2H_2O$	10	1.10E-08	2.15E-01	4.43E-08	6.30E-01	4.57E-09	5.34E-09	1.08E-09	1.26E-09
405	$10H_2S$(aq) + 8NO(aq) + $7H_2O$ → $5S_2O_3^{-2}$ + $8NH_4^+$ + $2H^+$	40	3.25E-08	4.97E-01	5.26E-08	7.37E-01	1.09E-08	1.34E-01	2.56E-09	3.15E-09
406	$5H_2S$(aq) + 8NO(aq) + $12H_2O$ → $5SO_4^{-2}$ + $8NH_4^+$+ $2H^+$	40	4.90E-08	6.12E-01	5.82E-08	6.85E-01	2.39E-08	2.70E-01	5.57E-09	6.29E-09
407	5pyrite + 2NO(aq) + $12H^+$ → 10sulfur +	10	1.54E-08	2.29E-01	6.94E-09	1.44E-01	6.79E-09	1.43E-01	2.27E-08	3.27E-01

	$5Fe^{+2} + 2NH_4^+ + 2H_2O$									
408	5pyrite + 6NO(aq) + $6H^+ + 9H_2O \rightarrow 5S_2O_3^{-2} + 5Fe^{+2} + 6NH_4^+$	30	4.10E-08	5.47E-01	4.29E-08	5.67E-01	4.28E-08	5.65E-01	4.89E-08	6.28E-01
409	5pyrite + 14NO(aq) + $4H^+ + 26H_2O \rightarrow 10SO_4^{-2} + 5Fe^{+2} + 14NH_4^+$	70	5.03E-08	5.78E-01	5.48E-08	6.23E-01	5.42E-08	6.17E-01	5.69E-08	6.44E-01
410	10sulfur + 4NO(aq) + $11H_2O \rightarrow 5S_2O_3^{-2} + 4NH_4^+ + 6H^+$	20	5.38E-08	7.67E-01	6.09E-08	7.78E-01	6.08E-08	7.77E-01	6.21E-08	7.96E-01
411	5sulfur + 6NO(aq) + $14H_2O \rightarrow 5SO_4^{-2} + 6NH_4^+ + 4H^+$	30	5.61E-08	6.36E-01	6.28E-08	7.31E-01	6.21E-08	6.96E-01	6.26E-08	7.13E-01
412	$5S_2O_3^{-2}$ +8NO(aq) + $17H_2O \rightarrow 10SO_4^{-2} + 8NH_4^+ + 2H^+$	40	5.26E-08	6.48E-01	5.91E-08	7.13E-01	5.80E-08	7.22E-01	5.81E-08	7.39E-01
413	$15Fe^{+2}$ +2NO(aq) + $18H_2O \rightarrow$ 5magnetite + $2NH_4^+ + 28H^+$	10	2.84E-08	3.59E-01	6.46E-09	7.36E-01	6.44E-09	7.34E-09	2.47E-12	3.48E-12
414	$10Fe^{+2}$ + 2NO(aq) + $13H_2O \rightarrow$ 5hematite + $2NH_4^+ + 18H^+$	10	4.00E-08	4.75E-01	1.03E-08	1.17E-01	1.02E-08	1.16E-01	6.88E-12	8.39E-12
415	$10Fe^{+2}$ + 2NO(aq) + $13H_2O \rightarrow$ 5maghemite + $2NH_4^+ + 18H^+$	10	3.22E-08	3.97E-01	8.87E-09	1.22E-01	8.83E-09	1.18E-01	5.34E-12	6.85E-12
416	$5Fe^{+2}$ + NO(aq) + $9H_2O \rightarrow$ 5goethite + $NH_4^+ + 9H^+$	5	4.01E-08	4.76E-01	1.03E-08	1.17E-01	1.03E-08	1.16E-01	6.92E-12	8.43E-12
417	$5Fe^{+2}$ + NO(aq) + $9H_2O \rightarrow$ 5lepidocrocite + $NH_4^+ + 9H^+$	5	3.05E-08	3.83E-01	8.58E-09	9.93E-09	8.54E-09	9.89E-09	5.00E-12	6.52E-12
418	$5Fe^{+2}$ + NO(aq) + $14H_2O \rightarrow$ 5ferrihydrite + $NH_4^+ + 9H^+$	5	2.47E-08	3.22E-01	7.57E-09	8.92E-09	7.53E-09	8.88E-09	3.87E-12	5.38E-12
419	15fayalite + 4NO(aq) + $4H^+ + 6H_2O \rightarrow$ 10magnetite + $4NH_4^+ + 15SiO_2$(aq)	20	6.75E-08	8.92E-01	6.76E-08	8.30E-01	7.27E-08	8.18E-01	7.53E-08	8.29E-01
420	15ferrosilite + 2NO(aq) + $2H^+ + 3H_2O \rightarrow$ 5magnetite + $2NH_4^+ + 15SiO_2$(aq)	10	5.86E-08	9.43E-01	5.86E-08	7.65E-01	6.90E-08	7.65E-01	7.12E-08	7.87E-01

421	10magnetite + 2NO(aq) + $2H^+$ + $3H_2O$ → 15hematite + $2NH_4^+$	10	6.32E-08	7.71E-01	6.32E-08	7.74E-01	6.31E-08	7.58E-01	6.62E-08	7.38E-01
422	10magnetite + 2NO(aq) + $2H^+$ + $3H_2O$ → 15maghemite + $2NH_4^+$	10	4.00E-08	4.75E-01	4.01E-08	4.76E-01	3.99E-08	4.74E-01	4.30E-08	5.54E-01
423	5magnetite + NO(aq) + H^+ + $9H_2O$ → 15goethtite + NH_4^+	5	6.36E-08	7.11E-01	6.40E-08	7.16E-01	6.38E-08	7.13E-01	6.67E-08	7.43E-01
424	5magnetite + NO(aq) + H^+ + $9H_2O$ → 15lepidocrocite + NH_4^+	5	3.49E-08	4.24E-01	3.53E-08	4.28E-01	3.51E-08	4.26E-01	3.80E-08	4.56E-01
425	5magnetite + NO(aq) + H^+ + $24H_2O$ → 15ferrihydrite + NH_4^+	5	1.73E-08	2.48E-01	1.84E-08	2.59E-01	1.82E-08	2.57E-01	2.09E-08	2.85E-01
426	$5CH_4$(aq) + 6NO(aq) + $6H^+$ → 5CO(aq) + $6NH_4^+$ + H_2O	30	5.35E-08	6.50E-01	4.54E-08	5.23E-01	6.38E-10	7.35E-01	1.93E-11	2.22E-11
427	$5CH_4$(aq) + $8NO$(aq) + $8H^+$ + $2H_2O$ → $5CO_2$(aq) + $8NH_4^+$	40	5.88E-08	6.63E-01	6.15E-08	6.90E-01	1.03E-09	1.16E-09	2.93E-11	3.30E-11
428	$5CH_4$(aq) + $8NO$(aq) + $3H^+$ + $7H_2O$ → $5HCO_3^-$ + $8NH_4^+$	40	5.88E-08	6.63E-01	6.15E-08	6.90E-01	1.03E-09	1.16E-09	2.93E-11	3.30E-11
429	5CO(aq) + 2NO(aq) + $2H^+$ + $3H_2O$ → $5CO_2$(aq) + $2NH_4^+$	10	2.62E-11	3.30E-11	8.08E-09	8.74E-09	3.75E-09	4.56E-09	6.69E-12	7.29E-12
430	5CO(aq) + 2NO(aq) + $8H_2O$ → $5HCO_3^-$ + $2NH_4^+$ + $3H^+$	10	2.62E-11	3.30E-11	8.08E-09	8.74E-09	3.75E-09	4.56E-09	6.69E-12	7.30E-12
431	6NO(aq) + $4H_2O$ → NH_4^+ + $5NO_2^-$ + $4H^+$	5	-7.88E-09	-3.75E-01	-4.52E-09	2.98E-09	-4.54E-09	2.97E-09	-1.37E-09	6.19E-09
432	$7H_2O$ + 8NO(aq) → $3NH_4^+$ + $5NO_3^-$ + $2H^+$	15	-1.06E-08	-3.64E-09	-7.39E-09	1.88E-01	-8.16E-09	-6.48E-01	-7.12E-09	4.37E-01
433	$3H_2O$ + 2NO(aq) + $2H^+$ → $2NH_4^+$ + $5/2O_2$(aq)	10	-5.68E-08	-4.00E-01	-6.08E-08	-3.99E-01	-6.09E-08	-5.34E-01	-5.70E-08	-4.94E-01
Nitrous Oxide as an electron acceptor										
434	H_2(aq) + N_2O(aq) → N_2(aq) + H_2O	2	8.24E-07	8.24E-01	5.38E-09	6.00E-09	2.64E-09	2.96E-01	2.44E-11	2.74E-11
435	$2H_2S$(aq) + N_2O(aq) + Fe^{+2} → pyrite + N_2(aq)	2	3.19E-08	3.94E-01	6.31E-08	7.79E-01	8.90E-09	9.88E-09	6.19E-11	6.94E-11

	$+ 2H^+ + H_2O$									
436	$H_2S(aq) + N_2O(aq) \rightarrow$ sulfur $+ N_2(aq) + H_2O$	2	5.90E-08	6.65E-01	5.51E-08	6.80E-01	1.39E-08	1.59E-01	3.17E-09	3.62E-09
437	$2H_2S(aq) + 4N_2O(aq) \rightarrow S_2O_3^{-2} + 4N_2(aq) + 2H^+ + H_2O$	8	1.29E-07	1.40E-01	5.84E-08	7.58E-01	2.96E-08	3.45E-01	6.74E-09	7.87E-09
438	$H_2S(aq) + 4N_2O(aq) \rightarrow SO4^{-2} + 4N_2(aq) + 2H^+$	8	2.70E-07	2.78E-01	6.07E-08	6.93E-01	5.92E-08	6.67E-01	1.39E-08	1.57E-01
439	pyrite $+ N_2O(aq) + 2H^+ \rightarrow$ 2sulfur $+ Fe^{+2} + N_2(aq) + H_2O$	2	3.18E-06	3.18E-01	4.02E-08	4.77E-01	3.89E-08	4.64E-01	4.40E-08	5.16E-01
440	pyrite $+ 3N_2O(aq) \rightarrow S_2O_3^{-2} + Fe^{+2} + 3N_2(aq)$	6	3.79E-06	3.93E-01	5.46E-08	6.46E-01	5.33E-08	6.33E-01	5.45E-08	6.46E-01
441	pyrite $+ 7N_2O(aq) + H_2O \rightarrow 2SO_4^{-2} + Fe^{+2} + 7N_2(aq) + 2H^+$	14	4.01E-06	4.66E-01	5.93E-08	6.68E-01	5.79E-08	6.54E-01	5.77E-08	6.52E-01
442	2sulfur $+ 2N_2O(aq) + H_2O \rightarrow S_2O_3^{-2} + 2N_2(aq) + 2H^+$	4	4.09E-06	4.39E-01	6.18E-08	7.32E-01	6.05E-08	7.18E-01	5.97E-08	7.17E-01
443	sulfur $+ 3N_2O(aq) + H_2O \rightarrow SO_4^{-2} + 3N_2(aq) + 2H^+$	6	4.14E-06	4.14E-01	6.25E-08	7.30E-01	6.10E-08	6.85E-01	5.99E-08	6.75E-01
444	$S_2O_3^{-2} + 4N_2O(aq) + H_2O \rightarrow 2SO_4^{-2} + 4N_2(aq) + 2H^+$	8	2.76E-07	2.84E-01	6.10E-08	7.42E-01	5.94E-08	6.88E-01	5.82E-08	6.76E-01
445	$3Fe^{+2} + N_2O(aq) + 3H_2O \rightarrow$ magnetite $+ N_2(aq) + 6H^+$	2	3.49E-06	3.49E-01	1.77E-08	1.99E-01	1.73E-08	1.96E-01	1.41E-11	1.66E-11
446	$2Fe^{+2} + N_2O(aq) + 2H_2O \rightarrow$ hematite $+ N_2(aq) + 4H^+$	2	3.76E-06	3.76E-01	2.71E-08	3.47E-01	2.65E-08	2.99E-01	2.43E-11	2.81E-11
447	$2Fe^{+2} + N_2O(aq) + 2H_2O \rightarrow$ maghemite $+ N_2(aq) + 4H^+$	2	3.58E-06	3.58E-01	2.57E-08	2.97E-01	2.51E-08	2.86E-01	2.28E-11	2.66E-11
448	$2Fe^{+2} + N_2O(aq) + 3H_2O \rightarrow$ 2goethite $+ N_2(aq) + 4H^+$	2	3.77E-06	3.77E-01	2.71E-08	3.51E-01	2.66E-08	2.99E-01	2.44E-11	2.82E-11
449	$2Fe^{+2} + N_2O(aq) + 3H_2O \rightarrow$ 2lepidocrocite $+ N_2(aq) + 4H^+$	2	3.54E-06	3.54E-01	2.54E-08	2.88E-01	2.48E-08	2.82E-01	2.25E-11	2.62E-11
450	$2Fe^{+2} + N_2O(aq) + 5H_2O \rightarrow$ 2ferrihydrite $+ N_2(aq) + 4H^+$	2	3.40E-06	3.44E-01	2.44E-08	2.78E-01	2.38E-08	2.73E-01	2.13E-11	2.52E-11

451	3fayalite + $2N_2O(aq)$ → 2magnetite + $2N_2(aq) + 3SiO_2(aq)$	4	4.41E-06	4.74E-01	6.44E-08	7.43E-01	6.53E-08	7.28E-01	6.50E-08	7.26E-01
452	3ferrosilite + $N_2O(aq)$ → magnetite + $N_2(aq)$ + $3SiO_2(aq)$	2	4.20E-06	4.86E-01	6.09E-08	7.25E-01	6.38E-08	7.14E-01	6.34E-08	7.93E-01
453	2magnetite + $N_2O(aq)$ → 3hematite + $N_2(aq)$	2	4.31E-06	4.39E-01	6.27E-08	7.27E-01	6.14E-08	6.89E-01	6.14E-08	6.89E-01
454	2magnetite + $N_2O(aq)$ → 3maghemite + $N_2(aq)$	2	3.76E-06	3.76E-01	5.34E-08	6.93E-01	5.22E-08	5.97E-01	5.21E-08	5.97E-01
455	2magnetite + $N_2O(aq)$ + $3H_2O$ → 6goethtite + $N_2(aq)$	2	4.32E-06	4.32E-01	6.30E-08	7.51E-01	6.17E-08	6.92E-01	6.16E-08	6.92E-01
456	2magnetite + $N_2O(aq)$ + $3H_2O$ → 6lepidocrocite + $N_2(aq)$	2	3.64E-06	3.64E-01	5.15E-08	5.91E-01	5.02E-08	5.78E-01	5.01E-08	5.77E-01
457	2magnetite + $N_2O(aq)$ + $9H_2O$ → 6ferrihydrite + $N_2(aq)$	2	3.23E-06	3.24E-01	4.48E-08	5.23E-01	4.35E-08	5.20E-01	4.33E-08	5.85E-01
458	$CH_4(aq)$ + $3N_2O(aq)$ → $CO(aq) + 3N_2(aq) + 2H_2O$	6	2.08E-07	2.12E-01	5.78E-08	6.53E-01	1.81E-09	2.54E-09	5.07E-11	5.75E-11
459	$CH_4(aq)$ + $4N_2O(aq)$ → $CO_2(aq) + 4N_2(aq) + 2H_2O$	8	2.86E-07	2.86E-01	6.20E-08	6.95E-01	2.60E-09	2.92E-09	7.12E-11	8.29E-11
460	$CH_4(aq)$ + $4N_2O(aq)$ → HCO_3^- + $4N_2(aq)$ + $H^+ + H_2O$	8	2.86E-07	2.86E-01	6.20E-08	6.95E-01	2.60E-09	2.92E-09	7.12E-11	8.29E-11
461	$CO(aq) + N_2O(aq)$ → $CO_2(aq) + N_2(aq)$	2	7.42E-11	7.80E-11	1.62E-08	1.78E-01	7.44E-09	8.29E-09	1.37E-11	1.52E-11
462	$CO(aq) + N_2O(aq) + H_2O$ → HCO_3^- + $N_2(aq) + H^+$	2	7.42E-11	7.80E-11	1.62E-08	1.78E-01	7.44E-09	8.29E-09	1.37E-11	1.52E-11
463	$2NH_4^+ + 3N_2O(aq)$ → $4N_2(aq) + 2H^+ + 3H_2O$	6	4.19E-06	4.20E-01	6.04E-08	6.79E-01	5.88E-08	6.63E-01	1.54E-08	1.74E-01
464	$N_2O(aq)$ → $N_2(aq)$ + $1/2O_2(aq)$	2	1.49E-06	1.76E-01	1.31E-08	2.59E-01	1.18E-08	1.93E-01	1.21E-08	1.97E-01
465	$2N_2O(aq)$ → $N_2(aq)$ + $2NO(aq)$	2	3.30E-07	7.71E-01	-4.54E-09	1.47E-01	-5.16E-09	9.85E-09	-5.17E-09	9.94E-09
466	$3N_2O(aq) + H_2O$ → $2N_2(aq) + 2NO_2^- + 2H^+$	4	1.08E-06	1.85E-01	1.08E-08	1.83E-01	1.00E-08	1.76E-01	1.21E-08	1.97E-01
467	H_2O + $5N_2O(aq)$ → $4N_2(aq) + 2NO_3^- + 2H^+$	8	1.60E-06	1.65E-01	1.89E-08	2.65E-01	1.74E-08	2.50E-01	1.73E-08	2.49E-01

468	$4H_2(aq) + N_2O(aq) + 2H^+ \rightarrow 2NH_4^+ + H_2O$	8	2.65E-07	2.65E-01	1.64E-09	1.80E-09	8.09E-10	8.87E-01	7.42E-12	8.17E-12
469	$8H_2S(aq) + N_2O(aq) + 4Fe^{+2} \rightarrow$ 4pyrite $+ 2NH_4^+ + 6H^+ + H_2O$	8	5.17E-09	1.27E-01	2.23E-08	3.24E-01	3.19E-09	3.44E-09	1.94E-11	2.13E-11
470	$4H_2S(aq) + N_2O(aq) + 2H^+ \rightarrow$ 4sulfur $+ 2NH_4^+ + H_2O$	8	5.52E-09	1.32E-01	3.94E-08	6.48E-01	2.52E-09	3.14E-09	6.27E-10	7.43E-01
471	$2H_2S(aq) + N_2O(aq) + 2H_2O \rightarrow S_2O_3^{-2} + 2NH_4^+$	8	2.16E-08	3.28E-01	5.27E-08	7.66E-01	6.78E-09	8.72E-09	1.66E-09	2.11E-09
472	$H_2S(aq) + N_2O(aq) + 3H_2O \rightarrow SO_4^{-2} + 2NH_4^+$	8	5.66E-08	6.46E-01	6.16E-08	7.36E-01	1.57E-08	1.76E-01	3.77E-09	4.22E-09
473	4pyrite $+ N_2O(aq) + 10H^+ \rightarrow$ 8sulfur $+ 4Fe^{+2} + 2NH_4^+ + H_2O$	8	1.67E-07	1.67E-01	-2.04E-08	-1.29E-01	-2.07E-08	-1.31E-01	6.19E-09	1.37E-01
474	4pyrite $+ 3N_2O(aq) + 6H^+ + 9H_2O \rightarrow 4S_2O_3^{-2} + 4Fe^{+2} + 6NH_4^+$	24	2.58E-06	3.16E-01	3.72E-08	5.47E-01	3.69E-08	5.44E-01	4.82E-08	6.58E-01
475	4pyrite $+ 7N_2O(aq) + 6H^+ + 25H_2O \rightarrow 8SO_4^{-2} + 4Fe^{+2} + 14NH_4^+$	56	3.45E-06	3.45E-01	5.62E-08	6.37E-01	5.51E-08	6.26E-01	6.09E-08	6.85E-01
476	4sulfur $+ N_2O(aq) + 5H_2O \rightarrow 2S_2O_3^{-2} + 2NH_4^+ + 2H^+$	8	3.78E-06	4.66E-01	6.60E-08	8.85E-01	6.57E-08	8.82E-01	6.91E-08	9.18E-01
477	4sulfur $+ 3N_2O(aq) + 13H_2O \rightarrow 4SO_4^{-2} + 6NH_4^+ + 2H^+$	24	4.00E-06	4.17E-01	6.90E-08	7.65E-01	6.78E-08	7.53E-01	7.00E-08	7.75E-01
478	$S_2O_3^{-2} + N_2O(aq) + 4H_2O \rightarrow 2SO_4^{-2} + 2NH_4^+$	8	6.24E-08	6.99E-01	6.30E-08	7.83E-01	6.13E-08	7.64E-01	6.28E-08	7.79E-01
479	$12Fe^{+2} + N_2O(aq) + 15H_2O \rightarrow$ 4magnetite $+ 2NH_4^+ + 22H^+$	8	6.06E-07	6.57E-01	4.10E-09	4.66E-09	4.07E-09	4.64E-09	-4.28E-14	5.87E-13
480	$8Fe^{+2} + N_2O(aq) + 11H_2O \rightarrow$ 4hematite $+ 2NH_4^+ + 14H^+$	8	1.62E-06	1.62E-01	6.72E-09	7.56E-09	6.68E-09	7.52E-09	3.11E-12	4.55E-12
481	$8Fe^{+2} + N_2O(aq) + 11H_2O \rightarrow$ 4maghemite $+ 2NH_4^+ + 14H^+$	8	1.15E-06	1.15E-01	5.32E-09	6.17E-09	5.28E-09	6.13E-09	1.57E-12	2.51E-12
482	$8Fe^{+2} + N_2O(aq) + 15H_2O \rightarrow$ 8goethite $+ 2NH_4^+ + 14H^+$	8	1.63E-06	1.63E-01	6.76E-09	7.65E-09	6.72E-09	7.57E-09	3.15E-12	4.93E-12

483	$8Fe^{+2} + N_2O(aq) + 15H_2O \rightarrow 8lepidocrocite + 2NH_4^+ + 14H^+$	8	1.04E-06	1.42E-01	5.04E-09	5.88E-09	5.00E-09	5.85E-09	1.24E-12	2.18E-12
484	$8Fe^{+2} + N_2O(aq) + 23H_2O \rightarrow 8ferrihydrite + 2NH_4^+ + 14H^+$	8	6.82E-07	6.82E-01	4.03E-09	4.87E-09	3.98E-09	4.83E-09	9.73E-14	1.42E-12
485	$6fayalite + N_2O(aq) + 2H^+ + 3H_2O \rightarrow 4magnetite + 2NH_4^+ + 6SiO_2(aq)$	8	5.07E-06	6.40E-01	7.67E-08	9.25E-01	8.47E-08	9.23E-01	9.03E-08	9.79E-01
486	$12ferrosilite + N_2O(aq) + 2H^+ + 3H_2O \rightarrow 4magnetite + 2NH_4^+ + 12SiO_2(aq)$	8	4.23E-06	6.88E-01	6.23E-08	8.65E-01	7.88E-08	8.63E-01	8.37E-08	9.13E-01
487	$8magnetite + N_2O(aq) + 2H^+ + 3H_2O \rightarrow 12hematite + 2NH_4^+$	8	4.67E-06	4.67E-01	6.97E-08	7.73E-01	6.94E-08	7.69E-01	7.57E-08	8.32E-01
488	$8magnetite + N_2O(aq) + 2H^+ + 3H_2O \rightarrow 12maghemite + 2NH_4^+$	8	2.48E-06	2.48E-01	3.26E-08	4.12E-01	3.23E-08	3.98E-01	3.86E-08	4.62E-01
489	$8magnetite + N_2O(aq) + 2H^+ + 15H_2O \rightarrow 24goethtite + 2NH_4^+$	8	4.70E-06	4.74E-01	7.09E-08	7.84E-01	7.06E-08	7.89E-01	7.66E-08	8.42E-01
490	$8magnetite + N_2O(aq) + 2H^+ + 15H_2O \rightarrow 24lepidocrocite + 2NH_4^+$	8	2.00E-06	2.00E-01	2.49E-08	3.24E-01	2.46E-08	3.22E-01	3.07E-08	3.82E-01
491	$8magnetite + N_2O(aq) + 2H^+ + 39H_2O \rightarrow 24ferrihydrite + 2NH_4^+$	8	3.50E-07	3.50E-01	-2.00E-09	5.50E-09	-2.37E-09	5.15E-09	3.36E-09	1.92E-01
492	$4CH_4(aq) + 3N_2O(aq) + 6H^+ + H_2O \rightarrow 4CO(aq) + 6NH_4^+$	24	4.78E-08	5.16E-01	2.78E-08	3.21E-01	3.82E-10	4.43E-01	1.25E-11	1.43E-11
493	$CH_4(aq) + N_2O(aq) + 2H^+ + H_2O \rightarrow CO_2(aq) + 2NH_4^+$	8	7.23E-08	7.23E-01	4.96E-08	5.52E-01	6.94E-10	7.75E-01	2.03E-11	2.25E-11
494	$CH_4(aq) + N_2O(aq) + H^+ + 2H_2O \rightarrow HCO_3^- + 2NH_4^+$	8	7.23E-08	7.23E-01	4.96E-08	5.52E-01	6.94E-10	7.75E-01	2.03E-11	2.25E-11
495	$4CO(aq) + N_2O(aq) + 2H^+ + 3H_2O \rightarrow 4CO_2(aq) + 2NH_4^+$	8	2.08E-11	2.46E-11	6.37E-09	6.78E-09	2.95E-09	3.14E-01	5.18E-12	5.56E-12
496	$4CO(aq) + N_2O(aq) + 7H_2O \rightarrow 4HCO_3^- +$	8	2.08E-11	2.46E-11	6.37E-09	6.78E-09	2.95E-09	3.14E-09	5.18E-12	5.56E-12

	$2NH_4^+ + 2H^+$									
497	$3H_2O + N_2O(aq) + 2H^+ \rightarrow 2NH_4^+ + 2O_2(aq)$	8	-6.63E-06	-5.75E-01	-1.29E-07	-9.99E-01	-1.29E-07	-1.22E-01	-1.21E-07	-1.14E-01
498	$5N_2O(aq) + 2H^+ + 3H_2O \rightarrow 2NH_4^+ + 8NO(aq)$	8	-1.99E-06	-1.29E-01	-4.35E-08	-2.40E-01	-4.35E-08	-2.42E-01	-4.22E-08	-2.26E-01
499	$3N_2O(aq) + 5H_2O \rightarrow 2NH_4^+ + 4NO_2^- + 2H^+$	8	-2.02E-06	-2.22E-01	-3.87E-08	-3.12E-01	-3.88E-08	-3.13E-01	-3.23E-08	-2.48E-01
500	$2H_2O + N_2O(aq) \rightarrow NH_4^+ + NO_3^-$	4	-2.27E-06	-2.27E-01	-4.33E-08	-3.59E-01	-4.46E-08	-3.77E-01	-4.15E-08	-3.40E-01
Nitrogen as an electron acceptor										
501	$3H_2(aq) + N_2(aq) + 2H^+ \rightarrow 2NH_4^+$	6	7.82E-08		3.97E-10		1.98E-10		1.76E-12	
502	$6H_2S(aq) + N_2(aq) + 3Fe^{+2} \rightarrow$ 3pyrite $+ 2NH_4^+ + 4H^+$	6	-3.74E-09	3.76E-09	8.72E-09	1.68E-01	1.29E-09		5.27E-12	
503	$3H_2S + N_2(aq) + 2H^+ \rightarrow$ 3sulfur $+ 2NH_4^+$	6	-1.23E-08	-4.80E-09	-9.87E-07	-1.46E-01	-1.28E-09		-2.19E-10	
504	$6H_2S + 4N_2(aq) + 2H^+ + 9H_2O \rightarrow 3S_2O_3^{-2} + 8NH_4^+$	24	-1.40E-08	-2.80E-01	-3.62E-07	4.11E-01	-8.35E-10	1.37E-01	-3.17E-11	1.94E-01
505	$3H_2S + 4N_2(aq) + 2H^+ + 12H_2O \rightarrow 3SO_4^{-2} + 8NH_4^+$	24	-1.47E-08	-7.28E-09	5.78E-08	2.68E-01	4.61E-10		3.80E-10	
506	3pyrite $+ N_2(aq) + 8H^+ \rightarrow$ 6sulfur $+ 3Fe^{+2} + 2NH_4^+$	6	-6.46E-07		-3.80E-06		-3.74E-05		-2.23E-05	
507	pyrite $+ N_2(aq) + 2H^+ + 3H_2O \rightarrow S_2O_3^{-2} + Fe^{+2} + 2NH_4^+$	6	-2.59E-07	-1.65E-01	-1.09E-06	-6.22E-01	-1.03E-05	-5.58E-01	-3.74E-06	7.22E-01
508	3pyrite $+ 7N_2(aq) + 8H^+ + 24H_2O \rightarrow 6SO_4^{-2} + 3Fe^{+2} + 14NH_4^+$	42	-1.18E-07		-1.94E-07		-1.72E-06		1.88E-06	
509	6sulfur $+ 2N_2(aq) + 9H_2O \rightarrow 3S_2O_3^{-2} + 4NH_4^+ + 2H^+$	12	-6.59E-08	7.57E-01	2.63E-07	9.68E-01	3.25E-06	1.38E-01	5.55E-06	1.22E-01
510	sulfur $+ N_2(aq) + 4H_2O \rightarrow SO_4^{-2} + 2NH_4^+$	6	-3.04E-08		4.06E-07		4.22E-06		5.91E-06	
511	$3S_2O_3^{-2} + 4N_2(aq) + 2H^+ + 15H_2O \rightarrow 6SO_4^{-2} + 8NH_4^+$	24	-8.83E-09	-1.33E-09	2.65E-09	1.16E-01	2.50E-09	1.78E-01	6.22E-09	1.38E-01
512	$9Fe^{+2} + N_2(aq) + 12H_2O \rightarrow$ 3magnetite	6	-4.50E-07		-4.27E-10		-3.36E-10		-4.76E-12	

	+ $2NH_4^+$ +$16H^+$								
513	$6Fe^{+2}$ + N_2(aq) + $9H_2O$ → 3hematite + $2NH_4^+$ + $10H^+$	6	-2.75E-07		-7.67E-11		6.16E-11		-3.96E-12	
514	$6Fe^{+2}$ + N_2(aq) + $9H_2O$ → 3maghemite + $2NH_4^+$ + $10H^+$	6	-3.91E-07		-1.47E-09		-1.33E-09		-5.51E-12	
515	$6Fe^{+2}$ + N_2(aq) + $12H_2O$ → 6goethite + $2NH_4^+$ + $10H^+$	6	-2.73E-07		-3.08E-11		1.07E-10		-3.93E-12	
516	$6Fe^{+2}$ + N_2(aq) + $12H_2O$ → 6lepidocrocite + $2NH_4^+$ + $10H^+$	6	-4.17E-07		-1.76E-09		-1.62E-09		-5.84E-12	
517	$6Fe^{+2}$ + N_2(aq) + $18H_2O$ → 6ferrihydrite + $2NH_4^+$ + $10H^+$	6	-5.06E-07		-2.77E-09		-2.63E-09		-6.98E-12	
518	9fayalite + $2N_2$(aq) + $4H^+$ + $6H_2O$ → 6magnetite + $4NH_4^+$ + $9SiO_2$(aq)	12	1.42E-07	3.54E-01	7.66E-07	1.16E-01	1.22E-05		1.49E-05	
519	9ferrosilite + N_2(aq) + $2H^+$ + $3H_2O$ → 3magnetite + $2NH_4^+$ + $9SiO_2$(aq)	6	6.36E-09	4.31E-01	9.14E-08	8.76E-01	9.42E-06		1.20E-05	
520	6magnetite + N_2(aq) + $2H^+$ + $3H_2O$ → 9hematite + $2NH_4^+$	6	7.62E-08		4.39E-07		4.98E-06		8.45E-06	
521	6magnetite + N_2(aq) + $2H^+$ + $3H_2O$ → 9maghemite + $2NH_4^+$	6	-2.74E-07		-1.31E-06		-1.25E-05		-7.95E-06	
522	6magnetite + N_2(aq) + $2H^+$ + $12H_2O$ → 18goethtite + $2NH_4^+$	6	8.25E-08		4.97E-07		5.54E-06		8.85E-06	
523	6magnetite + N_2(aq) + $2H^+$ + $12H_2O$ → 18lepidocrocite + $2NH_4^+$	6	-3.52E-07		-1.67E-06		-1.61E-05		-1.15E-05	
524	6magnetite + N_2(aq) + $2H^+$ + $30H_2O$ → 18ferrihydrite + $2NH_4^+$	6	-6.17E-07		-2.93E-06		-2.88E-05		-2.36E-05	
525	CH_4(aq) + N_2(aq) + $2H^+$ + H_2O → $2NH_4^+$ + CO(aq)	6	-5.63E-09	-1.88E-09	-5.76E-09	-5.76E-01	-9.38E-11	-9.38E-11	-2.30E-13	-2.35E-13

526	$3CH_4(aq) + 4N_2(aq) + 8H^+ + 6H_2O \rightarrow 8NH_4^+ + 3CO_2(aq)$	24	1.06E-09		4.83E-09		5.93E-11		3.30E-12	
527	$3CH_4(aq) + 4N_2(aq) + 5H^+ + 9H_2O \rightarrow 8NH_4^+ + 3HCO_3^-$	24	1.06E-09		4.83E-09		5.93E-11		3.30E-12	
528	$3CO(aq) + N_2(aq) + 2H^+ + 3H_2O \rightarrow 3CO_2(aq) + 2NH_4^+$	6	2.94E-12	6.69E-12	3.10E-09	3.97E-09	1.45E-09	1.45E-01	2.35E-12	2.35E-12
529	$3CO(aq) + N_2(aq) + 2H^+ + 6H_2O \rightarrow 3HCO_3^- + 2NH_4^+ + 3H^+$	6	2.94E-12	6.69E-12	3.10E-09	3.97E-09	1.45E-09	1.45E-09	2.35E-12	2.35E-12
530	$3H_2O + N_2(aq) + 2H^+ \rightarrow 2NH_4^+ + 3/2O_2(aq)$	6	-1.74E-06	-1.60E-01	-8.89E-06	-7.89E-01	-8.83E-05		-7.87E-05	
531	$4N_2(aq) + 2H^+ + 3H_2O \rightarrow 2NH_4^+ + 3N_2O(aq)$	6	-6.73E-07	-6.73E-01	-3.19E-06	-2.84E-01	-3.12E-05	-2.76E-01	-2.84E-05	-2.55E-01
532	$5N_2(aq) + 4H^+ + 6H_2O \rightarrow 4NH_4^+ + 6NO(aq)$	12	-9.92E-07	-8.79E-01	-4.88E-06	-4.32E-01	-4.81E-05	-4.25E-01	-4.37E-05	-3.84E-01
533	$N_2(aq) + 2H_2O \rightarrow NH_4^+ + NO_2^-$	3	-9.98E-07		-4.66E-06		-4.59E-05		-3.94E-05	
534	$9H_2O + 4N_2(aq) + 2H^+ \rightarrow 5NH_4^+ + 3NO_3^-$	15	-1.04E-06		-4.88E-06		-4.86E-05		-4.34E-05	
Sulfate as an electron acceptor										
535	$4H_2(aq) + 2SO_4^{-2} + 2H^+ \rightarrow S_2O_3^{-2} + 5H_2O$	8	8.17E-08	1.14E-01	1.88E-10	3.43E-01	9.35E-11	1.72E-01	3.82E-13	1.14E-12
536	$8NH_4^+ + 6SO_4^{-2} \rightarrow 3S_2O_3^{-2} + 4N_2(aq) + 2H^+ + 15H_2O$	24	1.07E-06	7.12E-01	-4.96E-08	-1.30E-01	-6.36E-08	-1.59E-01	-9.35E-10	-4.22E-01
537	$2NH_4^+ + 2SO_4^{-2} \rightarrow S_2O_3^{-2} + N_2O(aq) + 4H_2O$	8	-7.51E-05	-6.76E-01	-5.08E-07	-4.16E-01	-6.47E-07	-5.19E-01	-7.05E-09	-5.69E-09
538	$8NH_4^+ + 10SO_4^{-2} + 2H^+ \rightarrow 5S_2O_3^{-2} + 8NO(aq) + 17H_2O$	40	-1.39E-04	-1.14E-01	-9.28E-07	-7.70E-01	-1.19E-06	-9.83E-01	-1.27E-08	-1.52E-01
539	$4NH_4^+ + 6SO_4^{-2} \rightarrow 3S_2O_3^{-2} + 4NO_2^- + 2H^+ + 7H_2O$	24	-1.68E-04	-1.56E-01	-1.07E-06	-9.94E-01	-1.37E-06	-1.27E-01	-1.39E-08	-1.29E-01
540	$NH_4^+ + 2SO_4^{-2} \rightarrow S_2O_3^{-2} + NO_3^- + 2H_2O$	8	-2.33E-04	-2.17E-01	-1.48E-06	-1.39E-01	-1.92E-06	-1.79E-01	-2.03E-08	-1.89E-01
541	$4N_2(aq) + 2SO_4^{-2} + 2H^+ \rightarrow S_2O_3^{-2} + 4N_2O(aq) + H_2O$	8	-8.93E-07	-8.70E-01	-4.41E-06	-3.83E-01	-4.31E-05	-3.73E-01	-3.99E-05	-3.43E-01
542	$2N_2(aq) + 2SO_4^{-2} + 2H^+ \rightarrow S_2O_3^{-2} +$	8	-1.64E-06	-1.49E-01	-8.46E-06	-7.28E-01	-4.29E-05	-3.69E-01	-7.70E-05	-6.58E-01

	$4NO(aq) + H_2O$									
543	$4N_2(aq) + 6SO_4^{-2} + H_2O \rightarrow 3S_2O_3^{-2} + 8NO_2^- + 2H^+$	24	-1.98E-06	-1.91E-01	-8.55E-06	-8.24E-01	-3.31E-05	-3.19E-01	-8.48E-05	-8.15E-01
544	$4N_2(aq) + 10SO_4^{-2} + 2H^+ \rightarrow 5S_2O_3^{-2} + 8NO_3^- + H_2O$	40	-2.75E-06	-2.63E-01	-7.23E-06	-6.92E-01	-2.83E-05	-2.71E-01	-1.26E-04	-1.24E-01
545	$4N_2O(aq) + 2SO_4^{-2} + 2H^+ \rightarrow S_2O_3^{-2} + 8NO(aq) + H_2O$	8	-3.51E-06	-2.52E-01	-7.20E-08	-4.76E-01	-7.16E-08	-4.72E-01	-7.04E-08	-4.58E-01
546	$2N_2O(aq) + 2SO_4^{-2} + H_2O \rightarrow S_2O_3^{-2} + 4NO_2^- + 2H^+$	8	-5.09E-06	-4.87E-01	-9.33E-08	-8.28E-01	-9.26E-08	-8.13E-01	-8.37E-08	-7.24E-01
547	$N_2O(aq) + 2SO_4^{-2} \rightarrow S_2O_3^{-2} + 2NO_3^-$	8	-8.66E-06	-8.23E-01	-1.57E-07	-1.42E-01	-1.58E-07	-1.43E-01	-1.53E-07	-1.38E-01
548	$8NO + 2SO_4^{-2} + 3H_2O \rightarrow S_2O_3^{-2} + 8NO_2^- + 6H^+$	8	-2.09E-08	-1.25E-01	-1.82E-08	-9.74E-09	-1.80E-08	-9.54E-09	-1.42E-08	-5.77E-09
549	$8NO + 6SO_4^{-2} + H_2O \rightarrow 3S_2O_3^{-2} + 8NO_3^- + 2H^+$	24	-5.13E-08	-4.99E-01	-5.01E-08	-3.98E-01	-5.07E-08	-4.35E-01	-4.91E-08	-3.87E-01
550	$4NO_2^- + 2SO_4^{-2} + 2H^+ \rightarrow S_2O_3^{-2} + 4NO_3^- + H_2O$	8	-7.20E-07	-6.76E-01	-4.63E-08	-4.35E-01	-4.93E-08	-4.65E-01	-3.49E-11	-3.30E-11
551	$12Fe^{+2} + 2SO_4^{-2} + 11H_2O \rightarrow S_2O_3^{-2} + 4magnetite + 22H^+$	8	-1.19E-06	-9.97E-01	-1.19E-09	-6.26E-01	-1.09E-09	-5.23E-01	-5.91E-12	-5.28E-12
552	$8Fe^{+2} + 2SO_4^{-2} + 7H_2O \rightarrow S_2O_3^{-2} + 4hematite + 14H^+$	8	-1.07E-06	-7.83E-01	-1.22E-09	-3.75E-01	-1.06E-09	-2.19E-01	-5.69E-12	-4.74E-12
553	$8Fe^{+2} + 2SO_4^{-2} + 7H_2O \rightarrow S_2O_3^{-2} + 4maghemite + 14H^+$	8	-1.54E-06	-1.26E-01	-2.61E-09	-1.77E-09	-2.46E-09	-1.61E-09	-7.23E-12	-6.29E-12
554	$8Fe^{+2} + 2SO_4^{-2} + 11H_2O \rightarrow S_2O_3^{-2} + 8goethite + 14H^+$	8	-1.06E-06	-7.71E-01	-1.17E-09	-3.29E-01	-1.02E-09	-1.75E-01	-5.65E-12	-4.74E-12
555	$8Fe^{+2} + 2SO_4^{-2} + 11H_2O \rightarrow S_2O_3^{-2} + 8lepidocrocite + 14H^+$	8	-1.65E-06	-1.36E-01	-2.90E-09	-2.55E-09	-2.74E-09	-1.90E-09	-7.56E-12	-6.62E-12
556	$8Fe^{+2} + 2SO_4^{-2} + 19H_2O \rightarrow S_2O_3^{-2} + 8ferrihydrite + 14H^+$	8	-2.01E-06	-1.72E-01	-3.91E-09	-3.65E-09	-3.75E-09	-2.91E-09	-8.70E-12	-7.76E-12
557	$6fayalite + 2SO_4^{-2} + 2H^+ \rightarrow S_2O_3^{-2} +$	8	4.77E-04	1.35E-01	2.52E-07	9.19E-01	2.58E-06	3.79E-01	2.78E-04	3.84E-01

	4magnetite + $6SiO_2(aq) + H_2O$									
558	12ferrosilite + $2SO_4^{-2}$ + $2H^+ \rightarrow S_2O_3^{-2}$ + 4magnetite + $12SiO_2(aq) + H_2O$	8	5.86E-05	1.59E-01	-3.37E-07	6.56E-01	1.62E-06	2.83E-01	1.86E-04	2.91E-01
559	8magnetite + $2SO_4^{-2}$ + $2H^+ \rightarrow S_2O_3^{-2}$ + 12hematite + H_2O	8	2.74E-04	4.93E-01	-3.36E-08	2.74E-01	9.44E-08	1.37E-01	7.41E-05	1.80E-01
560	8magnetite + $2SO_4^{-2}$ + $2H^+ \rightarrow S_2O_3^{-2}$ + 12maghemite + H_2O	8	-8.09E-04	-5.90E-01	-1.56E-06	-1.25E-01	-5.90E-06	-4.68E-01	-4.43E-04	-3.37E-01
561	8mganetite + $2SO_4^{-2}$ + $2H^+ + 11H_2O \rightarrow S_2O_3^{-2}$ + 24goethtite	8	2.94E-04	5.13E-01	1.68E-08	3.25E-01	2.88E-07	1.57E-01	8.68E-05	1.92E-01
562	8mganetite + $2SO_4^{-2}$ + $2H^+ + 11H_2O \rightarrow S_2O_3^{-2}$ + 24lepidocrocite	8	-1.05E-03	-8.32E-01	-1.87E-06	-1.56E-01	-7.14E-06	-5.93E-01	-5.54E-04	-4.48E-01
563	8mganetite + $2SO_4^{-2}$ + $2H^+ + 35H_2O \rightarrow S_2O_3^{-2}$ + 24ferrihydrite	8	-1.87E-03	-1.65E-01	-2.98E-06	-2.67E-01	-1.15E-05	-1.29E-01	-9.35E-04	-8.29E-01
564	$4CH_4(aq) + 6SO_4^{-2}$ + $6H^+ \rightarrow 3S_2O_3^{-2}$ + $4CO(aq) + 11H_2O$	24	-4.63E-09	4.74E-09	-1.14E-08	-7.24E-09	-1.75E-10	-1.15E-01	-3.33E-12	-1.63E-12
565	$CH_4(aq) + 2SO_4^{-2}$ + $2H^+ \rightarrow S_2O_3^{-2}$ + $CO_2(aq) + 3H_2O$	8	2.39E-09	9.89E-01	-2.70E-09	2.87E-09	-4.88E-11	3.24E-11	-8.34E-13	1.43E-12
566	$CH_4(aq) + 2SO_4^{-2} + H^+ \rightarrow S_2O_3^{-2} + HCO_3^- + 2H_2O$	8	2.39E-09	9.89E-09	-2.70E-09	2.87E-09	-4.88E-11	3.23E-11	-8.32E-13	1.43E-12
567	$4CO(aq) + 2SO_4^{-2}$ + $2H^+ \rightarrow S_2O_3^{-2}$ + $4CO_2(aq) + H_2O$	8	3.27E-12	8.90E-12	2.55E-09	2.95E-09	1.19E-09	1.38E-09	1.66E-12	2.41E-12
568	$4CO(aq) + 2SO_4^{-2}$ + $3H_2O \rightarrow S_2O_3^{-2}$ + $4HCO_3^- + 2H^+$	8	3.27E-12	8.90E-12	2.55E-09	2.95E-09	1.19E-09	1.38E-09	1.66E-12	2.42E-12
569	$2SO_4^{-2} + 2H^+ \rightarrow S_2O_3^{-2}$ + $2O_2(aq) + H_2O$	6	-5.33E-03	-4.68E-01	-8.18E-06	-6.99E-01	-3.19E-05	-3.74E-01	-2.67E-03	-2.57E-01
570	$H_2S(aq) + SO_4^{-2} \rightarrow S_2O_3^{-2} + H_2O$	4	-1.34E-08	1.63E-09	-7.33E-07	2.54E-01	-2.13E-09	-1.87E-01	-4.43E-10	8.34E-12
571	4pyrite + $6SO_4^{-2}$ + $6H^+ \rightarrow 7S_2O_3^{-2} + 4Fe^{+2}$ + $3H_2O$	24	-7.63E-04	-2.53E-01	-1.37E-06	-6.54E-01	-5.15E-06	-2.32E-01	-3.10E-04	-6.40E-01
572	4sulfur + $2SO_4^{-2} + H_2O \rightarrow 3S_2O_3^{-2} + 2H^+$	8	-1.65E-04	4.92E-01	-1.88E-07	7.37E-01	-5.01E-07	3.14E-01	-1.72E-05	2.99E-01

573	$3H_2(aq) + SO_4^{-2} + 2H^+ \rightarrow sulfur + 4H_2O$	6	8.67E-08		2.19E-10		1.04E-10		4.23E-13	
574	$2NH_4^+ + SO_4^{-2} \rightarrow sulfur + N_2(aq) + 4H_2O$	6	2.59E-06		-4.22E-08		-5.70E-08		-9.07E-10	
575	$6NH_4^+ + 4SO_4^{2-} + 2H^+ \rightarrow 4sulfur + 3N_2O(aq) + 13H_2O$	24	-7.31E-05	-7.39E-01	-4.98E-07	-4.50E-01	-6.38E-07	-5.74E-01	-7.02E-09	-6.33E-09
576	$6NH_4^+ + 5SO_4^{2-} + 4H^+ \rightarrow 6NO(aq) + 14H_2O + 5sulfur$	30	-1.37E-04	-1.27E-01	-9.16E-07	-8.18E-01	-1.18E-06	-1.52E-01	-1.27E-08	-1.13E-01
577	$NH_4^+ + SO_4^{-2} \rightarrow sulfur + NO_2^- + 2H_2O$	6	-1.65E-04		-1.05E-06		-1.35E-06		-1.39E-08	
578	$3NH_4^+ + 4SO_4^{-2} + 2H^+ \rightarrow 4sulfur + 3NO_3^- + 7H_2O$	24	-2.29E-04		-1.46E-06		-1.90E-06		-2.02E-08	
579	$3N_2(aq) + SO_4^{-2} + 2H^+ \rightarrow sulfur + 3N_2O(aq) + H_2O$	6	-8.87E-07	-8.87E-01	-4.39E-06	-3.93E-01	-4.30E-05	-3.83E-01	-3.98E-05	-3.54E-01
580	$3N_2(aq) + 2SO_4^{-2} + 4H^+ \rightarrow 2sulfur + 6NO(aq) + 2H_2O$	12	-1.63E-06	-1.44E-01	-8.41E-06	-7.47E-01	-6.41E-05	-5.69E-01	-7.68E-05	-6.79E-01
581	$N_2(aq) + SO_4^{-2} \rightarrow sulfur + 2NO_2^-$	6	-1.96E-06		-9.72E-06		-4.95E-05		-8.46E-05	
582	$3N_2(aq) + 5SO_4^{-2} + 4H^+ \rightarrow 5sulfur + 6NO_3^- + 2H_2O$	30	-2.72E-06		-1.07E-05		-4.22E-05		-1.26E-04	
583	$3N_2O(aq) + SO_4^{-2} + 2H^+ \rightarrow sulfur + 6NO(aq) + H_2O$	6	-3.48E-06	-2.61E-01	-7.16E-08	-5.00E-01	-7.14E-08	-4.88E-01	-7.03E-08	-4.76E-01
584	$3N_2O(aq) + 2SO_4^{-2} + H_2O \rightarrow 2sulfur + 6NO_2^- + 2H^+$	12	-5.03E-06	-5.33E-01	-9.26E-08	-8.57E-01	-9.21E-08	-8.46E-01	-8.35E-08	-7.59E-01
585	$3N_2O(aq) + 4SO_4^{-2} + 2H^+ \rightarrow 4sufur + 6NO_3^- + H_2O$	24	-8.54E-06	-8.54E-01	-1.55E-07	-1.48E-01	-1.57E-07	-1.49E-01	-1.53E-07	-1.45E-01
586	$6NO(aq) + SO_4^{-2} + 2H_2O \rightarrow sulfur + 6NO_2^- + 4H^+$	6	-2.07E-08	-1.32E-01	-1.80E-08	-1.48E-01	-1.79E-08	-1.35E-01	-1.42E-08	-6.60E-09
587	$2NO(aq) + SO_4^{-2} \rightarrow sulfur + 2NO_3^-$	6	-5.06E-08	-4.39E-01	-4.95E-08	-4.27E-01	-5.03E-08	-4.28E-01	-4.89E-08	-4.14E-01
588	$3NO_2^- + SO_4^{-2} + 2H^+ \rightarrow sulfur + 3NO_3^- + H_2O$	6	-7.09E-07		-4.57E-08		-4.90E-08		-3.48E-11	
589	$9Fe^{+2} + SO_4^{-2} + 8H_2O \rightarrow sulfur + 3magnetite$	6	-1.14E-06		-1.07E-09		-1.01E-09		-5.87E-12	

	+ $16H^+$									
590	$6Fe^{+2} + SO_4^{-2} + 5H_2O$ → sulfur + 3hematite + $10H^+$	6	-9.96E-07		-1.05E-09		-9.48E-10		-5.63E-12	
591	$6Fe^{+2} + SO_4^{-2} + 5H_2O$ → sulfur + 3maghemite + $10H^+$	6	-1.47E-06		-2.44E-09		-2.34E-09		-7.18E-12	
592	$6Fe^{+2} + SO_4^{-2} + 8H_2O$ → sulfur + 6goethite + $10H^+$	6	-9.88E-07		-1.00E-09		-9.03E-10		-5.60E-12	
593	$6Fe^{+2} + SO_4^{-2} + 8H_2O$ → sulfur + 6lepidocrocite + $10H^+$	6	-1.58E-06		-2.73E-09		-2.63E-09		-7.51E-12	
594	$6Fe^{+2} + SO_4^{-2} + 14H_2O$ → sulfur + 6ferrihydrite + $10H^+$	6	-1.94E-06		-3.74E-09		-3.64E-09		-8.65E-12	
595	9fayalite + $2SO_4^{-2}$ + $4H^+$ → 2sulfur + 6magnetite + $9SiO_2(aq) + 2H_2O$	12	7.98E-04	1.78E-01	4.71E-07	9.85E-01	4.11E-06		4.26E-04	
596	9ferrosilite + SO_4^{-2} + $2H^+$ → sulfur + 3magnetite + $9SiO_2(aq) + H_2O$	6	1.70E-04	2.14E-01	-4.12E-07	6.15E-01	2.68E-06		2.87E-04	
597	6magnetite + SO_4^{-2} + $2H^+$→ sulfur + 9hematite + H_2O	6	4.94E-04		4.34E-08		3.92E-07		1.20E-04	
598	6magnetite + SO_4^{-2} + $2H^+$→ sulfur + 9maghemite + H_2O	6	-1.13E-03		-2.24E-06		-8.59E-06		-6.56E-04	
599	6mganetite + SO_4^{-2} + $2H^+$ + $8H_2O$ → sulfur + 18goethtite	6	5.23E-04		1.19E-07		6.83E-07		1.39E-04	
600	6mganetite + SO_4^{-2} + $2H^+$ + $8H_2O$ → sulfur + 18lepidocrocite	6	-1.49E-03		-2.71E-06		-1.05E-05		-8.22E-04	
601	6mganetite + SO_4^{-2} + $2H^+$ + $26H_2O$ → sulfur + 18ferrihydrite	6	-2.72E-03		-4.37E-06		-1.70E-05		-1.39E-03	
602	$CH_4(aq) + SO_4^{-2} + 2H^+$ → sulfur + CO(aq) + $3H_2O$	6	-3.22E-09	5.29E-01	-1.06E-08	-1.56E-01	-1.67E-10	-1.67E-01	-3.24E-12	-3.24E-12
603	$3CH_4(aq) + 4SO_4^{-2}$ + $8H^+$ → 4sulfur +	24	4.27E-09		-1.57E-09		-3.76E-11		-7.11E-13	

	$3CO_2(aq) + 10H_2O$									
604	$3CH_4(aq) + 4SO_4^{-2} + 5H^+ \rightarrow 4sulfur + 3HCO_3^- + 7H_2O$	24	4.27E-09		-1.57E-09		-3.76E-11		-7.09E-13	
605	$3CO(aq) + SO_4^{-2} + 2H^+ \rightarrow sulfur + 3CO_2(aq) + H_2O$	6	3.74E-12	7.50E-12	2.63E-09	2.63E-09	1.22E-09	1.22E-09	1.68E-12	1.68E-12
606	$3CO(aq) + SO_4^{-2} + 2H_2O \rightarrow sulfur + 3HCO_3^- + H^+$	6	3.75E-12	7.50E-12	2.63E-09	2.63E-09	1.22E-09	1.22E-09	1.68E-12	1.68E-12
607	$SO_4^{-2} + 2H^+ \rightarrow sulfur + 3/2O_2(aq) + H_2O$	6	-7.92E-03	-7.26E-01	-1.22E-05	-1.86E-01	-4.77E-05		-4.00E-03	
608	$3H_2S(aq) + SO_4^{-2} + 2H^+ \rightarrow 4sulfur + 4H_2O$	6	-1.15E-08	-3.99E-09	-1.82E-06	-7.22E-01	-1.86E-09		-4.19E-10	
609	$3pyrite + SO_4^{-2} + 8H^+ \rightarrow 3Fe^{+2} + 7sulfur + 4H_2O$	6	-2.86E-03		-5.50E-06		-2.14E-05		-1.33E-03	
610	$7H_2(aq) + 2SO_4^{-2} + Fe^{+2} + 2H^+ \rightarrow pyrite + 8H_2O$	14	1.11E-07		4.83E-10		2.36E-10		1.33E-12	
611	$3Fe^{+2} + 6SO_4^{-2} + 14NH_4^+ \rightarrow 3pyrite + 7N_2(aq) + 8H^+ + 24H_2O$	42	6.76E-06		6.51E-09		5.76E-09		-7.44E-12	
612	$4Fe^{2+} + 8SO_4^{-2} + 14NH_4^+ \rightarrow 4pyrite + 7N_2O(aq) + 6H^+ + 25H_2O$	56	-3.17E-05	-3.17E-01	-1.00E-07	-8.86E-01	-9.87E-08	-8.68E-01	-1.20E-10	-1.65E-01
613	$5Fe^{2+} + 10SO_4^{-2} + 14NH_4^+ \rightarrow 5pyrite + 14NO(aq) + 4H^+ + 26H_2O$	70	-4.99E-05	-4.35E-01	-1.57E-07	-1.38E-01	-1.55E-07	-1.36E-01	-1.80E-10	-1.59E-01
614	$3Fe^{+2} + 6SO_4^{-2} + 7NH_4^+ \rightarrow 3pyrite + 7NO_2^- + 8H^+ + 10H_2O$	42	-5.02E-05		-1.50E-07		-1.48E-07		-1.63E-10	
615	$4Fe^{+2} + 8SO_4^{-2} + 7NH_4^+ \rightarrow 4pyrite + 7NO_3^- + 6H^+ + 11\ H_2O$	56	-5.25E-05		-1.57E-07		-1.57E-07		-1.79E-10	
616	$Fe^{+2} + 2SO_4^{-2} + 7N_2(aq) + 2H^+ \rightarrow pyrite + 7N_2O(aq) + H_2O$	14	-8.58E-07	-8.58E-01	-4.21E-07	-3.74E-01	-4.12E-07	-3.65E-01	-4.57E-10	-4.37E-01
617	$2Fe^{+2} + 4SO_4^{-2} + 7N_2(aq) + 4H^+ \rightarrow$	28	-1.57E-06	-1.39E-01	-4.02E-07	-3.55E-01	-3.97E-07	-3.50E-01	-4.40E-10	-3.87E-01

	2pyrite + 14NO(aq) + $2H_2O$									
618	$3Fe^{+2}$ + $6SO_4^{-2}$ + $7N_2$(aq) + $4H_2O$ → 3pyrite + $14NO_2^-$ + $8H^+$	42	-1.88E-06		-3.06E-07		-3.02E-07		-3.19E-10	
619	$5Fe^{+2}$ + $10SO_4^{-2}$ + $7N_2$(aq) + $2H_2O$ → 5pyrite + $14NO_3^-$ + $4H^+$	70	-2.57E-06		-2.55E-07		-2.55E-07		-2.82E-10	
620	Fe^{+2} + $2SO_4^{-2}$ + $7N_2O$(aq) + $2H^+$ → pyrite + 14NO + H_2O	14	-3.35E-06	-2.46E-01	-6.84E-08	-4.60E-01	-6.82E-08	-4.57E-01	-4.76E-10	-3.17E-01
621	$2Fe^{+2}$ + $4SO_4^{-2}$ + $7N_2O$(aq) + $5H_2O$ → 2pyrite + $14NO_2^-$ + $10H^+$	28	-4.76E-06	-4.76E-01	-8.62E-08	-7.87E-01	-8.58E-08	-7.82E-01	-2.76E-10	-2.50E-01
622	$4Fe^{+2}$ + $8SO_4^{-2}$ + $7N_2O$(aq) + $3H_2O$ → 4pyrite + $14NO_3^-$ + $6H^+$	56	-8.00E-06	-8.33E-01	-1.43E-07	-1.35E-01	-1.44E-07	-1.37E-01	-2.52E-10	-2.39E-01
623	Fe^{+2} + $2SO_4^{-2}$ + 14NO(aq) + $6H_2O$ → pyrite + $14NO_2^-$ + $12H^+$	14	-1.95E-08	-1.21E-01	-1.64E-08	-8.89E-09	-1.63E-08	-8.77E-01	-1.82E-10	-7.65E-11
624	$3Fe^{+2}$ + $6SO_4^{-2}$ + 14NO(aq) + $4H_2O$ → 3pyrite + $14NO_3^-$ + $8H^+$	42	-4.71E-08	-3.96E-01	-4.47E-08	-3.72E-01	-4.55E-08	-3.84E-01	-2.12E-10	-1.77E-01
625	Fe^{+2} + $2SO_4^{-2}$ + $7NO_2^-$ + $2H^+$ → pyrite + $7NO_3^-$ + H_2O	14	-6.54E-07		-4.11E-08		-4.42E-08		-3.25E-11	
626	$22Fe^{+2}$ + $2SO_4^{-2}$ + $20H_2O$ → pyrite + 7magnetite + $40H^+$	14	-8.61E-07		-1.11E-10		-5.84E-11		-4.88E-12	
627	$15Fe^{+2}$ + $2SO_4^{-2}$ + $13H_2O$ → pyrite + 7hematite + $26H^+$	14	-5.95E-07		3.63E-10		4.42E-10		-4.20E-12	
628	$15Fe^{+2}$ + $2SO_4^{-2}$ + $13H_2O$ → pyrite + 7maghemite + $26H^+$	14	-1.04E-06		-9.36E-10		-8.56E-10		-5.64E-12	
629	$15Fe^{+2}$ + $2SO_4^{-2}$ + $20H_2O$ → pyrite + 14goethite + $26H^+$	14	-5.87E-07		4.06E-10		4.84E-10		-4.16E-12	

630	$15Fe^{+2} + 2SO_4^{-2} + 20H_2O \rightarrow$ pyrite + 14lepidocrocite + $26H^+$	14	-1.14E-06		-1.20E-09		-1.13E-09		-5.95E-12	
631	$15Fe^{+2} + 2SO_4^{-2} + 34H_2O \rightarrow$ pyrite + 14ferrihydrite + $26H^+$	14	-1.47E-06		-2.15E-09		-2.07E-09		-7.01E-12	
632	21fayalite + $4SO_4^{-2} + 2Fe^{+2} + 4H^+ \rightarrow$ 14magnetite + 2pyrite + $21SiO_2(aq) + 2H_2O$	28	1.48E-05	2.70E-01	3.22E-08	4.53E-01	4.66E-08		5.16E-11	
633	21ferrosilite + $2SO_4^{-2} + Fe^{+2} + 2H^+ \rightarrow$ 7magnetite + pyrite + $21SiO_2(aq) + H_2O$	14	7.12E-06	3.14E-01	9.58E-09	3.58E-01	3.73E-08		4.00E-11	
634	14magnetite + $Fe^{+2} + 2SO_4^{-2} + 2H^+ \rightarrow$ pyrite + 21hematite + H_2O	14	1.11E-05		2.12E-08		2.24E-08		2.60E-11	
635	14magnetite + $Fe^{+2} + 2SO_4^{-2} + 2H^+ \rightarrow$ pyrite + 21maghemite + H_2O	14	-8.89E-06		-3.72E-08		-3.60E-08		-3.89E-11	
636	14magnetite + $Fe^{+2} + 2SO_4^{-2} + 2H^+ + 20H_2O \rightarrow$ pyrite + 42goethite	14	1.15E-05		2.32E-08		2.43E-08		2.76E-11	
637	14magnetite + $Fe^{+2} + 2SO_4^{-2} + 2H^+ + 20H_2O \rightarrow$ pyrite + 42lepidocrocite	14	-1.33E-05		-4.93E-08		-4.81E-08		-5.28E-11	
638	14magnetite + $Fe^{+2} + 2SO_4^{-2} + 2H^+ + 62H_2O \rightarrow$ pyrite + 42ferrihydrite	14	-2.85E-05		-9.17E-08		-9.06E-08		-1.01E-10	
639	$7CH_4(aq) + 6SO_4^{-2} + 6H^+ + 3Fe^{+2} \rightarrow$ 3pyrite + $7CO(aq) + 17H_2O$	42	3.77E-09	7.52E-09	-3.46E-09	-3.46E-01	-6.42E-11	-6.42E-11	-1.19E-12	-1.19E-12
640	$7CH_4(aq) + 8SO_4^{-2} + 8H^+ + 4Fe^{+2} \rightarrow$ 4pyrite + $7CO_2(aq) + 18H_2O$	56	1.36E-08		7.90E-09		9.88E-11		2.02E-12	
641	$7CH_4(aq) + 8SO_4^{-2} + H^+ + 4Fe^{+2} \rightarrow$ 4pyrite + $7HCO_3^- + 11H_2O$	56	1.36E-08		7.90E-09		9.88E-11		2.02E-12	
642	$7CO(aq) + 2SO_4^{-2} + 2H^+ + Fe^{+2} \rightarrow$ pyrite + $7CO_2(aq) + H_2O$	14	6.07E-12	9.82E-12	3.32E-09	3.32E-09	1.54E-09	1.54E-09	2.14E-12	2.14E-12
643	$7CO(aq) + 2SO_4^{-2} + Fe^{+2} + 6H_2O \rightarrow$ pyrite	14	6.07E-12	9.83E-12	3.32E-09	3.32E-09	1.54E-09	1.54E-09	2.14E-12	2.15E-12

	+ $7HCO_3^-$ + $5H^+$									
644	Fe^{+2} + $2SO_4^{-2}$ + $2H^+$ → pyrite + $7/2O_2$(aq) + H_2O	14	-9.24E-05	-8.43E-01	-2.91E-07	-2.58E-01	-2.90E-07		-3.19E-10	
645	$7H_2S$(aq) + SO_4^{-2} + $4Fe^{+2}$ → 4pyrite + $6H^+$ + $4H_2O$	7	-2.17E-09	5.33E-09	8.45E-09	1.55E-01	1.41E-09		3.68E-12	
646	$4H_2$(aq) + SO_4^{-2} + $2H^+$ → H_2S(aq) + $4H_2O$	8	9.71E-08	1.17E-01	2.80E-10	3.72E-01	1.79E-10		1.12E-12	
647	$8NH_4^+$ + $3SO_4^{-2}$ → $3H_2S$ + $4N_2$(aq) + $2H^+$ + $12H_2O$	24	5.81E-06	1.18E-01	-2.79E-08	-6.33E-09	-1.13E-08		-4.31E-10	
648	$2NH_4^+$ + SO_4^{-2} → H_2S + N_2O(aq) + $3H_2O$	8	-6.88E-05	-6.75E-01	-4.79E-07	-4.13E-01	-5.77E-07	-5.13E-01	-6.38E-09	-5.70E-09
649	$8NH_4^+$ + $5SO_4^{-2}$ + $2H^+$ → $5H_2S$ + 8NO(aq) + $12H_2O$	40	-1.31E-04	-1.52E-01	-8.92E-07	-7.58E-01	-1.10E-06	-9.76E-01	-1.19E-08	-1.53E-01
650	$4NH_4^+$ + $3SO_4^{-2}$ → $3H_2S$(aq) + $4NO_2^-$ + $2H^+$ + $4H_2O$	24	-1.59E-04	-1.47E-01	-1.02E-06	-9.83E-01	-1.26E-06		-1.29E-08	
651	NH_4^+ + SO_4^{-2} → H_2S(aq) + NO_3^- + H_2O	8	-2.21E-04	-2.46E-01	-1.43E-06	-1.37E-01	-1.78E-06		-1.89E-08	
652	$4N_2$(aq) + SO_4^{-2} + $2H^+$ → H_2S(aq) + $4N_2O$(aq)	8	-8.75E-07	-8.51E-01	-4.34E-06	-3.85E-01	-4.18E-05	-3.71E-01	-3.88E-05	-3.43E-01
653	$2N_2$(aq) + SO_4^{-2} + $2H^+$ → H_2S(aq) + 4NO(aq)	8	-1.61E-06	-1.37E-01	-8.32E-06	-7.24E-01	-8.08E-05	-7.13E-01	-7.48E-05	-6.59E-01
654	$4N_2$(aq) + $3SO_4^{-2}$ + $4H_2O$ → $3H_2S$(aq) + $8NO_2^-$ + $2H^+$	24	-1.93E-06	-1.86E-01	-9.59E-06	-9.38E-01	-6.36E-05		-8.15E-05	
655	$4N_2$(aq) + $5SO_4^{-2}$ + $2H^+$ + $4H_2O$ → $5H_2S$(aq) + $8NO_3^-$	40	-2.66E-06	-2.54E-01	-1.34E-05	-1.40E-01	-5.40E-05		-1.20E-04	
656	$4N_2O$(aq) + SO_4^{-2} + $2H^+$ → H_2S(aq) + 8NO(aq)	8	-3.42E-06	-2.43E-01	-7.09E-08	-4.72E-01	-6.96E-08	-4.74E-01	-6.85E-08	-4.59E-01
657	$2N_2O$(aq) + SO_4^{-2} + $2H_2O$ → H_2S(aq) + $4NO_2^-$ + $2H^+$	8	-4.92E-06	-4.70E-01	-9.11E-08	-8.14E-01	-8.85E-08	-8.96E-01	-8.00E-08	-7.24E-01
658	N_2O(aq) + SO_4^{-2} + H_2O → H_2S(aq) + $2NO_3^-$	8	-8.32E-06	-7.88E-01	-1.53E-07	-1.47E-01	-1.50E-07	-1.42E-01	-1.46E-07	-1.38E-01
659	8NO(aq) + SO_4^{-2} + $4H_2O$ → H_2S(aq) + $8NO_2^-$ + $6H^+$	8	-2.02E-08	-1.17E-01	-1.76E-08	-9.56E-09	-1.70E-08	-9.45E-09	-1.33E-08	-5.72E-09

660	$8NO(aq) + 3SO_4^{-2} + 4H_2O \rightarrow 3H_2S(aq) + 8NO_3^- + 2H^+$	24	-4.91E-08	-3.88E-01	-4.84E-08	-3.92E-01	-4.76E-08	-4.75E-01	-4.63E-08	-3.88E-01
661	$4NO_2^- + SO_4^{-2} + 2H^+ \rightarrow H_2S(aq) + 4NO_3^-$	8	-6.85E-07	-6.48E-01	-4.46E-08	-4.33E-01	-4.62E-08		-3.30E-11	
662	$12Fe^{+2} + SO_4^{-2} + 12H_2O \rightarrow$ 4magnetite $+ H_2S(aq) + 22H^+$	8	-1.04E-06	-8.46E-01	-8.54E-10	-5.19E-01	-4.69E-10		-5.29E-12	
663	$8Fe^{+2} + SO_4^{-2} + 8H_2O \rightarrow$ 4hematite $+ H_2S(aq) + 14H^+$	8	-8.43E-07	-5.54E-01	-7.18E-10	-2.15E-01	-1.38E-10		-4.76E-12	
664	$8Fe^{+2} + SO_4^{-2} + 8H_2O \rightarrow$ 4maghemite $+ H_2S(aq) + 14H^+$	8	-1.32E-06	-1.30E-01	-2.11E-09	-1.66E-09	-1.53E-09		-6.30E-12	
665	$8Fe^{+2} + SO_4^{-2} + 12H_2O \rightarrow$ 8goethite $+ H_2S(aq) + 14H^+$	8	-8.34E-07	-5.45E-01	-6.72E-10	-1.69E-01	-9.34E-11		-4.72E-12	
666	$8Fe^{+2} + SO_4^{-2} + 12H_2O \rightarrow$ 8lepidocrocite $+ H_2S(aq) + 14H^+$	8	-1.42E-06	-1.14E-01	-2.40E-09	-1.89E-01	-1.82E-09		-6.63E-12	
667	$8Fe^{+2} + SO_4^{-2} + 20H_2O \rightarrow$ 8ferrihydrite $+ H_2S(aq) + 14H^+$	8	-1.78E-06	-1.50E-01	-3.41E-09	-2.94E-09	-2.83E-09		-7.77E-12	
668	6fayalite $+ SO_4^{-2} + 2H^+ \rightarrow$ 4magnetite $+ H_2S(aq) + 6SiO_2(aq)$	8	1.30E-03	3.50E-01	8.69E-07	1.93E-01	7.81E-06		7.64E-04	
669	12ferrosilite $+ SO_4^{-2} + 2H^+ \rightarrow$ 4magnetite $+ H_2S(aq) + 12SiO_2(aq)$	8	4.60E-04	3.53E-01	-3.08E-07	1.43E-01	5.90E-06		5.79E-04	
670	8magnetite $+ SO_4^{-2} + 2H^+ \rightarrow$ 12hematite $+ H_2S(aq)$	8	8.92E-04	1.34E-01	2.99E-07	6.66E-01	2.85E-06		3.55E-04	
671	8magnetite $+ SO_4^{-2} + 2H^+ \rightarrow$ 12maghemite $+ H_2S(aq)$	8	-1.27E-03	-8.36E-01	-2.75E-06	-2.38E-01	-9.13E-06		-6.79E-04	
672	8magnetite $+ SO_4^{-2} + 2H^+ + 12H_2O \rightarrow$ 24goethite $+ H_2S(aq)$	8	9.31E-04	1.37E-01	3.99E-07	7.67E-01	3.23E-06		3.81E-04	
673	8magnetite $+ SO_4^{-2} + 2H^+ + 12H_2O \rightarrow$ 24lepidocrocite $+ H_2S(aq)$	8	-1.76E-03	-1.32E-01	-3.38E-06	-3.96E-01	-1.16E-05		-9.01E-04	
674	8magnetite $+ SO_4^{-2} + 2H^+ + 36H_2O \rightarrow$ 24ferrihydrite $+$	8	-3.39E-03	-2.96E-01	-5.59E-06	-5.22E-01	-2.03E-05		-1.66E-03	

	$H_2S(aq)$									
675	$4CH_4(aq) + 3SO_4^{-2} + 6H^+ \rightarrow 4CO(aq) + 3H_2S(aq) + 8H_2O$	24	-2.28E-10	9.15E-09	-8.93E-09	-6.44E-09	-1.08E-10	-1.82E-01	-1.66E-12	-1.66E-12
676	$CH_4(aq) + SO_4^{-2} + 2H^+ \rightarrow CO_2(aq) + H_2S(aq) + 2H_2O$	8	8.27E-09	1.58E-01	6.01E-10	3.92E-09	4.01E-11		1.39E-12	
677	$CH_4(aq) + SO_4^{-2} + H^+ \rightarrow HCO_3^- + H_2S(aq) + H_2O$	8	8.27E-09	1.58E-01	6.01E-10	3.92E-09	4.01E-11		1.39E-12	
678	$4CO(aq) + SO_4^{-2} + 2H^+ \rightarrow 4CO_2(aq) + H_2S(aq)$	8	4.74E-12	1.37E-11	2.79E-09	3.33E-09	1.40E-09	1.42E-09	2.03E-12	2.34E-12
679	$4CO(aq) + SO_4^{-2} + 4H_2O \rightarrow 4HCO_3^- + H_2S(aq) + 2H^+$	8	4.74E-12	1.37E-11	2.79E-09	3.33E-09	1.40E-09	1.41E-09	2.04E-12	2.35E-12
680	$2H^+ + SO_4^{-2} \rightarrow H_2S(aq) + 2O_2(aq)$	8	-1.03E-02	-9.20E-01	-1.60E-05	-1.39E-01	-6.12E-05		-5.14E-03	
Thiosulfate as an electron acceptor										
681	$2H_2(aq) + S_2O_3^{-2} + 2H^+ \rightarrow 2sulfur + 3H_2O$	4	1.09E-08	1.84E-01	-2.71E-11	2.82E-01	-3.04E-11	1.26E-01	-1.01E-12	5.57E-13
682	$4NH_4^+ + 3S_2O_3^{-2} + 2H^+ \rightarrow 6sulfur + 2N_2(aq) + 9H_2O$	12	-4.01E-09	3.49E-09	-1.03E-08	-2.79E-09	-1.10E-08	-3.45E-09	-1.88E-09	-8.51E-01
683	$2NH_4^+ + 2S_2O_3^{-2} + 2H^+ \rightarrow 4sulfur + N_2O(aq) + 5H_2O$	8	-3.96E-08	-3.21E-01	-4.42E-08	-3.30E-01	-4.41E-08	-3.28E-01	-8.31E-09	-6.26E-09
684	$4NH_4^+ + 5S_2O_3^{-2} + 6H^+ \rightarrow 10sulfur + 4NO(aq) + 11H_2O$	20	-5.65E-08	-4.34E-01	-6.22E-08	-4.87E-01	-6.21E-08	-4.87E-01	-1.43E-08	-1.12E-01
685	$2NH_4^+ + 3S_2O_3^{-2} + 2H^+ \rightarrow 6sulfur + 2NO_2^- + 5H_2O$	12	-5.68E-08	-4.93E-01	-5.98E-08	-5.23E-01	-5.98E-08	-5.22E-01	-1.58E-08	-1.38E-01
686	$NH_4^+ + 2S_2O_3^{-2} + 2H^+ \rightarrow 4sulfur + NO_3^- + 3H_2O$	8	-5.90E-08	-5.15E-01	-6.21E-08	-5.46E-01	-6.26E-08	-5.51E-01	-2.28E-08	-2.34E-01
687	$2N_2(aq) + S_2O_3^{-2} + 2H^+ \rightarrow 2sulfur + 2N_2O(aq) + H_2O$	4	-1.47E-07	-1.40E-01	-1.46E-07	-1.24E-01	-1.44E-07	-1.21E-01	-1.42E-07	-1.19E-01
688	$N_2(aq) + S_2O_3^{-2} + 2H^+ \rightarrow 2sulfur + 2NO(aq) + H_2O$	4	-1.35E-07	-1.13E-01	-1.40E-07	-1.18E-01	-1.39E-07	-1.16E-01	-1.37E-07	-1.15E-01
689	$2N_2(aq) + 3S_2O_3^{-2} + 2H^+ \rightarrow 6sulfur + 4NO_2^-$	12	-1.10E-07	-1.22E-01	-1.09E-07	-1.19E-01	-1.09E-07	-1.13E-01	-1.03E-07	-9.52E-01

	+ H_2O									
690	$2N_2(aq) + 5S_2O_3^{-2} + 6H^+ \rightarrow 10sulfur + 4NO_3^- + 3H_2O$	20	-9.20E-08	-8.45E-01	-9.32E-08	-8.57E-01	-9.37E-08	-8.61E-01	-9.23E-08	-8.48E-01
691	$2N_2O(aq) + S_2O_3^{-2} + 2H^+ \rightarrow 2sulfur + 4NO(aq) + H_2O$	4	-1.24E-07	-8.66E-01	-7.46E-08	-4.83E-01	-7.46E-08	-4.83E-01	-7.39E-08	-4.74E-01
692	$N_2O(aq) + S_2O_3^{-2} \rightarrow 2sulfur + 2NO_2^-$	4	-9.12E-08	-8.37E-01	-9.85E-08	-8.35E-01	-9.85E-08	-8.35E-01	-9.06E-08	-7.55E-01
693	$N_2O(aq) + 2S_2O_3^{-2} + 2H^+ \rightarrow 4sulfur + H_2O + 2NO_3^-$	8	-7.83E-08	-7.83E-01	-8.38E-08	-7.25E-01	-8.49E-08	-7.37E-01	-8.37E-08	-7.23E-01
694	$4NO(aq) + S_2O_3^{-2} + H_2O \rightarrow 2sulfur + 4NO_2^- + 2H^+$	4	-2.21E-08	-1.28E-01	-1.95E-08	-1.13E-01	-1.95E-08	-1.93E-01	-1.59E-08	-6.50E-01
695	$4NO(aq) + 3S_2O_3^{-2} + 2H^+ \rightarrow 6sulfur + 4NO_3^- + H_2O$	12	-5.48E-08	-4.17E-01	-5.40E-08	-4.86E-01	-5.51E-08	-4.20E-01	-5.43E-08	-4.17E-01
696	$2NO_2^- + S_2O_3^{-2} + 2H^+ \rightarrow 2sulfur + 2NO_3^- + H_2O$	4	-6.54E-08	-5.79E-01	-5.00E-08	-4.46E-01	-5.38E-08	-4.82E-01	-3.83E-11	-3.46E-11
697	$6Fe^{+2} + S_2O_3^{-2} + 5H_2O \rightarrow 2sulfur + 2magnetite + 10H^+$	4	-2.78E-08	-2.35E-01	-1.97E-09	-8.46E-01	-1.98E-09	-8.53E-01	-7.06E-12	-5.85E-12
698	$4Fe^{+2} + S_2O_3^{-2} + 3H_2O \rightarrow 2sulfur + 2hematite + 6H^+$	4	-1.86E-08	-1.16E-01	-2.39E-09	-7.49E-01	-2.40E-09	-7.15E-01	-7.42E-12	-5.53E-12
699	$4Fe^{+2} + S_2O_3^{-2} + 3H_2O \rightarrow 2sulfur + 2maghemite + 6H^+$	4	-2.47E-08	-1.72E-01	-3.78E-09	-2.96E-09	-3.80E-09	-2.16E-09	-8.97E-12	-7.76E-12
700	$4Fe^{+2} + S_2O_3^{-2} + 5H_2O \rightarrow 2sulfur + 4goethite + 6H^+$	4	-1.84E-08	-1.94E-01	-2.35E-09	-6.59E-01	-2.36E-09	-6.74E-01	-7.38E-12	-5.49E-12
701	$4Fe^{+2} + S_2O_3^{-2} + 5H_2O \rightarrow 2sulfur + 4lepidocrocite + 6H^+$	4	-2.61E-08	-1.86E-01	-4.07E-09	-2.38E-09	-4.08E-09	-2.39E-01	-9.30E-12	-7.48E-12
702	$4Fe^{+2} + S_2O_3^{-2} + 9H_2O \rightarrow 2sulfur + 4ferrihydrite + 6H^+$	4	-3.08E-08	-2.33E-01	-5.08E-09	-3.39E-09	-5.10E-09	-3.46E-09	-1.04E-11	-8.55E-12
703	$3fayalite + S_2O_3^{-2} + 2H^+ \rightarrow 2sulfur + 2magnetite + 3SiO_2(aq) + H_2O$	4	3.50E-09	2.22E-01	-2.15E-09	9.53E-09	2.02E-09	9.53E-09	3.04E-09	1.60E-01

704	6ferrosilite + $S_2O_3^{-2}$ + $2H^+$ → 2sulfur + 2magnetite + $6SiO_2(aq)$ + H_2O	4	-3.67E-09	2.63E-01	-9.32E-09	6.52E-09	-9.45E-10	6.56E-09	-2.78E-10	7.28E-09
705	4magnetite + $S_2O_3^{-2}$ + $2H^+$ → 2sulfur + 6hematite + H_2O	4	2.29E-11	7.52E-09	-5.62E-09	1.88E-09	-5.66E-09	1.84E-09	-4.28E-09	3.27E-09
706	4magnetite + $S_2O_3^{-2}$ + $2H^+$ → 2sulfur + 6maghemite + H_2O	4	-1.85E-08	-1.12E-01	-2.42E-08	-1.67E-01	-2.42E-08	-1.67E-01	-2.28E-08	-1.53E-01
707	4mganetite + $S_2O_3^{-2}$ + $2H^+$ + $5H_2O$ → 2sulfur + 12goethtite	4	3.58E-10	7.86E-09	-5.01E-09	2.49E-09	-5.06E-09	2.44E-09	-3.83E-09	3.73E-09
708	4mganetite + $S_2O_3^{-2}$ + $2H^+$ + $5H_2O$ → 2sulfur + 12lepidocrocite	4	-2.26E-08	-1.51E-01	-2.80E-08	-2.56E-01	-2.81E-08	-2.55E-01	-2.68E-08	-1.92E-01
709	4mganetite + $S_2O_3^{-2}$ + $2H^+$ + $17H_2O$ → 2sulfur + 12ferrihydrite	4	-3.67E-08	-2.92E-01	-4.15E-08	-3.40E-01	-4.15E-08	-3.43E-01	-4.04E-08	-3.29E-01
710	$2CH_4(aq)$ + $3S_2O_3^{-2}$ + $6H^+$ → 6sulfur + $2CO(aq)$ + $7H_2O$	12	-7.77E-09	2.24E-09	-1.55E-08	-7.97E-09	-2.71E-10	-1.50E-01	-6.45E-12	-3.52E-12
711	$CH_4(aq)$ + $2S_2O_3^{-2}$ + $4H^+$ → 4sulfur + $CO_2(aq)$ + $4H_2O$	8	-3.48E-09	4.20E-09	-7.04E-09	4.63E-01	-1.77E-10	-1.52E-11	-5.00E-12	-4.64E-13
712	$CH_4(aq)$ + $2S_2O_3^{-2}$ + $3H^+$ → 4sulfur + HCO_3^- + $3H_2O$	8	-3.48E-09	4.20E-09	-7.04E-09	4.63E-01	-1.77E-10	-1.52E-11	-5.00E-12	-4.63E-13
713	$2CO(aq)$ + $S_2O_3^{-2}$ + $2H^+$ → 2sulfur + $2CO_2(aq)$ + H_2O	4	9.36E-13	8.44E-12	1.98E-09	2.79E-09	8.87E-10	1.27E-09	9.69E-13	1.72E-12
714	$2CO(aq)$ + $S_2O_3^{-2}$ + H_2O → 2sulfur + $2HCO_3^-$	4	9.36E-13	8.44E-12	1.98E-09	2.79E-09	8.88E-10	1.27E-09	9.70E-13	1.73E-12
715	$S_2O_3^{-2}$ + $2H^+$ → 2sulfur + $O_2(aq)$ + H_2O	4	-9.60E-08	-8.11E-01	-1.05E-07	-8.67E-01	-1.05E-07	-9.74E-01	-1.03E-07	-9.53E-01
716	$2H_2S(aq)$ + $S_2O_3^{-2}$ + $2H^+$ → 4sulfur + $3H_2O$	4	-1.43E-08	-3.50E-09	-2.08E-08	-4.34E-09	-2.70E-09	-1.73E-09	-6.33E-10	-4.67E-01
717	2pyrite + $S_2O_3^{-2}$ + $6H^+$ → $2Fe^{+2}$ + 6sulfur + $3H_2O$	4	-3.82E-08	-3.73E-01	-5.07E-08	-4.32E-01	-5.07E-08	-4.32E-01	-3.90E-08	-3.15E-01
718	$3S_2O_3^{-2}$ + $2H^+$ → 4sulfur + $2SO_4^{-2}$ + H_2O	8	-5.62E-09	1.88E-09	-5.98E-09	1.52E-09	-6.47E-09	1.35E-09	-7.15E-09	4.13E-01
719	$3H_2(aq)$ + $S_2O_3^{-2}$ + Fe^{+2} → pyrite + $3H_2O$	6	3.55E-08	4.32E-01	6.69E-10	8.76E-01	3.21E-10	4.25E-01	1.60E-12	2.64E-12

720	$Fe^{+2} + S_2O_3^{-2} + 2NH_4^+ \rightarrow$ pyrite + N_2(aq) + $2H^+ + 3H_2O$	6	1.31E-08	2.61E-01	8.90E-09	1.57E-01	8.01E-09	1.48E-01	-1.22E-12	6.33E-12
721	$4Fe^{+2} + 4S_2O_3^{-2} + 6NH_4^+ \rightarrow$ 4pyrite + $3N_2O$(aq) + $6H^+ + 9H_2O$	24	-4.04E-08	-3.29E-01	-3.69E-08	-2.60E-01	-3.67E-08	-2.49E-01	-4.93E-11	-3.61E-11
722	$5Fe^{+2} + 5S_2O_3^{-2} + 6NH_4^+ \rightarrow$ 5pyrite + 6NO(aq) + $6H^+ + 9H_2O$	30	-6.57E-08	-4.92E-01	-6.12E-08	-4.63E-01	-6.11E-08	-4.62E-01	-7.54E-11	-5.87E-11
723	$Fe^{+2} + S_2O_3^{-2} + NH_4^+ \rightarrow$ pyrite + $NO_2^- + 2H^+ + H_2O$	6	-6.61E-08	-5.86E-01	-5.80E-08	-5.12E-01	-5.79E-08	-5.20E-01	-6.79E-11	-6.37E-11
724	$4Fe^{+2} + 4S_2O_3^{-2} + 3NH_4^+ \rightarrow$ 4pyrite + $3NO_3^- + 6H^+ + 3H_2O$	24	-6.94E-08	-6.19E-01	-6.11E-08	-5.43E-01	-6.18E-08	-5.52E-01	-7.48E-11	-6.73E-11
725	$Fe^{+2} + S_2O_3^{-2} + 3N_2$(aq) $\rightarrow$ pyrite + $3N_2O$(aq)	6	-2.01E-07	-1.93E-01	-1.74E-07	-1.47E-01	-1.71E-07	-1.44E-01	-1.94E-10	-1.63E-01
726	$2Fe^{+2} + 2S_2O_3^{-2} + 3N_2$(aq) $\rightarrow$ 2pyrite + 6NO(aq)	12	-1.84E-07	-1.54E-01	-1.66E-07	-1.39E-01	-1.65E-07	-1.38E-01	-1.87E-10	-1.56E-01
727	$Fe^{+2} + S_2O_3^{-2} + N_2$(aq) + $H_2O \rightarrow$ pyrite + $2NO_2^- + 2H^+$	6	-1.45E-07	-1.38E-01	-1.25E-07	-1.18E-01	-1.24E-07	-1.17E-01	-1.35E-10	-1.28E-01
728	$5Fe^{+2} + 5S_2O_3^{-2} + 3N_2$(aq) + $3H_2O \rightarrow$ 5pyrite + $6NO_3^- + 6H^+$	30	-1.19E-07	-1.11E-01	-1.03E-07	-9.63E-01	-1.04E-07	-9.69E-01	-1.19E-10	-1.11E-01
729	$Fe^{+2} + S_2O_3^{-2} + 3N_2O$(aq) $\rightarrow$ pyrite + 6NO(aq)	6	-1.67E-07	-1.15E-01	-6.61E-08	-4.11E-01	-6.62E-08	-4.11E-01	-2.02E-10	-1.27E-01
730	$2Fe^{+2} + 2S_2O_3^{-2} + 3N_2O$(aq) + $3H_2O \rightarrow$ 2pyrite + $6NO_2^- + 6H^+$	12	-1.18E-07	-1.12E-01	-8.17E-08	-6.92E-01	-8.16E-08	-6.91E-01	-1.16E-10	-9.76E-11
731	$4Fe^{+2} + 4S_2O_3^{-2} + 3N_2O$(aq) + $3H_2O \rightarrow$ 4pyrite + $6NO_3^- + 6H^+$	24	-9.84E-08	-9.88E-01	-9.03E-08	-7.85E-01	-9.18E-08	-8.21E-01	-1.06E-10	-9.28E-11
732	$Fe^{+2} + S_2O_3^{-2} + 6NO$(aq) + $3H_2O \rightarrow$ pyrite + $6NO_2^- + 6H^+$	6	-1.89E-08	-1.15E-01	-1.53E-08	-6.56E-09	-1.53E-08	-6.49E-09	-7.61E-11	-2.32E-11
733	$Fe^{+2} + S_2O_3^{-2} + 2NO$(aq) + $H_2O \rightarrow$ pyrite + $2NO_3^- + 2H^+$	6	-4.52E-08	-3.40E-01	-4.13E-08	-3.75E-01	-4.25E-08	-3.12E-01	-8.91E-11	-6.65E-11

734	$Fe^{+2} + S_2O_3^{-2} + 3NO_2^- \rightarrow$ pyrite + $3NO_3^-$	6	-7.91E-08	-7.16E-01	-3.78E-08	-3.42E-01	-4.11E-08	-3.73E-01	-3.18E-11	-2.93E-11
735	$10Fe^{+2} + S_2O_3^{-2} + 9H_2O \rightarrow$ pyrite + 3magnetite + $18H^+$	6	-2.27E-08	-1.52E-01	5.06E-10	1.18E-09	4.99E-10	1.17E-09	-4.41E-12	-3.65E-12
736	$7Fe^{+2} + S_2O_3^{-2} + 6H_2O \rightarrow$ pyrite + 3hematite + $12H^+$	6	-8.72E-09	-1.22E-09	1.21E-09	2.17E-01	1.20E-09	2.16E-09	-3.57E-12	-2.49E-12
737	$7Fe^{+2} + S_2O_3^{-2} + 6H_2O \rightarrow$ pyrite + 3maghemite + $12H^+$	6	-1.80E-08	-1.49E-01	1.37E-11	9.78E-01	5.17E-12	9.76E-01	-4.90E-12	-3.82E-12
738	$7Fe^{+2} + S_2O_3^{-2} + 9H_2O \rightarrow$ pyrite + 6goethite + $12H^+$	6	-8.55E-09	-1.53E-09	1.25E-09	2.30E-09	1.24E-09	2.21E-09	-3.54E-12	-2.47E-12
739	$7Fe^{+2} + S_2O_3^{-2} + 9H_2O \rightarrow$ pyrite + 6lepidoocrocite + $12H^+$	6	-2.01E-08	-1.26E-01	-2.33E-10	7.32E-01	-2.42E-10	7.24E-01	-5.18E-12	-4.12E-12
740	$7Fe^{+2} + S_2O_3^{-2} + 15H_2O \rightarrow$ pyrite + 6ferrihydrite + $12H^+$	6	-2.71E-08	-1.96E-01	-1.10E-09	-1.35E-01	-1.11E-09	-1.44E-01	-6.16E-12	-5.77E-12
741	$9fayalite + 2S_2O_3^{-2} + 2Fe^{+2} \rightarrow$ 6magnetite + 2pyrite + $9SiO_2(aq)$	12	2.44E-08	4.87E-01	1.99E-08	3.23E-01	2.55E-08	3.23E-01	2.41E-11	3.16E-11
742	$9ferrosilite + S_2O_3^{-2} + Fe^{+2} \rightarrow$ 3magnetite + pyrite + $9SiO_2(aq)$	6	1.36E-08	5.49E-01	1.02E-08	2.82E-01	2.15E-08	2.83E-01	1.91E-11	2.67E-11
743	$6magnetite + Fe^{+2} + S_2O_3^{-2} \rightarrow$ pyrite + 9hematite	6	1.91E-08	2.67E-01	1.52E-08	2.20E-01	1.52E-08	2.19E-01	1.31E-11	2.65E-11
744	$6magnetite + Fe^{+2} + S_2O_3^{-2} \rightarrow$ pyrite + 9maghemite	6	-8.67E-09	-1.17E-01	-9.83E-09	-3.90E-09	-9.87E-09	-3.12E-09	-1.47E-11	-7.15E-12
745	$6magnetite + Fe^{+2} + S_2O_3^{-2} + 9H_2O \rightarrow$ pyrite + 18goethite	6	1.97E-08	2.72E-01	1.60E-08	2.28E-01	1.60E-08	2.27E-01	1.38E-11	2.13E-11
746	$6magnetite + Fe^{+2} + S_2O_3^{-2} + 9H_2O \rightarrow$ pyrite + 18lepidocrocite	6	-1.48E-08	-7.34E-09	-1.50E-08	-8.26E-09	-1.51E-08	-8.31E-09	-2.07E-11	-1.31E-11
747	$6magnetite + Fe^{+2} + S_2O_3^{-2} + 27H_2O \rightarrow$ pyrite + 18ferrihydrite	6	-3.59E-08	-2.84E-01	-3.32E-08	-2.64E-01	-3.33E-08	-2.65E-01	-4.12E-11	-3.36E-11
748	$CH_4(aq) + S_2O_3^{-2} + Fe^{+2} \rightarrow$ pyrite + $CO(aq) + 2H_2O$	6	7.47E-09	1.87E-01	1.58E-09	7.15E-09	2.28E-12	8.34E-11	-5.97E-13	1.67E-12

749	$3CH_4(aq) + 4S_2O_3^{-2} + 4Fe^{+2} \rightarrow 4pyrite + 3CO_2(aq) + 6H_2O$	24	1.39E-08	2.14E-01	1.33E-08	2.48E-01	1.87E-10	2.96E-01	2.81E-12	5.83E-12
750	$3CH_4(aq) + 4S_2O_3^{-2} + 4Fe^{+2} \rightarrow 4pyrite + 3HCO_3^- + 3H^+ + 3H_2O$	24	1.39E-08	2.14E-01	1.33E-08	2.48E-01	1.87E-10	2.96E-01	2.81E-12	5.83E-12
751	$3CO(aq) + S_2O_3^{-2} + Fe^{+2} \rightarrow pyrite + 3CO_2(aq)$	6	7.31E-12	1.36E-11	3.81E-09	4.36E-09	1.75E-09	2.43E-09	2.27E-12	2.77E-12
752	$3CO(aq) + S_2O_3^{-2} + Fe^{+2} + 3H_2O \rightarrow pyrite + 3HCO_3^- + 3H^+$	6	7.31E-12	1.36E-11	3.81E-09	4.36E-09	1.75E-09	2.44E-09	2.27E-12	2.78E-12
753	$Fe^{+2} + S_2O_3^{-2} \rightarrow pyrite + 3/2O_2(aq)$	6	-1.25E-07	-1.62E-01	-1.19E-07	-9.76E-01	-1.19E-07	-1.12E-01	-1.35E-10	-1.27E-01
754	$6H_2S(aq) + S_2O_3^{-2} + 4Fe^{+2} \rightarrow 4pyrite + 6H^+ + 3H_2O$	6	-1.56E-09	7.19E-09	8.77E-09	1.65E-01	1.67E-09	2.00E-09	3.65E-12	5.54E-12
755	$7S_2O_3^{-2} + 4Fe^{+2} + 3H_2O \rightarrow 4pyrite + 6SO_4^{-2} + 6H^+$	24	3.70E-09	1.13E-01	6.79E-09	1.43E-01	6.16E-09	1.37E-01	3.44E-12	1.67E-11
756	$4H_2(aq) + S_2O_3^{-2} + 2H^+ \rightarrow 2H_2S(aq) + 3H_2O$	8	3.55E-08	5.80E-01	2.17E-10	5.56E-01	1.87E-10	2.65E-01	1.11E-12	1.87E-12
757	$8NH_4^+ + 3S_2O_3^{-2} \rightarrow 6H_2S(aq) + 4N_2(aq) + 2H^+ + 9H_2O$	24	5.58E-09	2.88E-01	-8.75E-09	7.70E-09	-1.06E-09	6.45E-09	-4.41E-10	7.19E-11
758	$2NH_4^+ + S_2O_3^{-2} \rightarrow 2H_2S(aq) + N_2O(aq) + 2H_2O$	8	-6.57E-08	-4.32E-01	-7.66E-08	-5.27E-01	-6.74E-08	-5.23E-01	-6.39E-09	-5.27E-09
759	$8NH_4^+ + 5S_2O_3^{-2} + 2H^+ \rightarrow 10H_2S(aq) + 8NO(aq) + 7H_2O$	40	-9.95E-08	-6.50E-01	-1.13E-07	-8.42E-01	-1.03E-07	-8.39E-01	-1.19E-08	-9.69E-09
760	$4NH_4^+ + 3S_2O_3^{-2} \rightarrow 6H_2S(aq) + 4NO_2^- + 2H^+ + H_2O$	24	-1.00E-07	-7.76E-01	-1.08E-07	-9.14E-01	-9.86E-08	-9.11E-01	-1.30E-08	-1.19E-01
761	$NH_4^+ + S_2O_3^{-2} \rightarrow 2H_2S(aq) + NO_3^-$	8	-1.04E-07	-8.19E-01	-1.12E-07	-9.60E-01	-1.04E-07	-9.69E-01	-1.89E-08	-1.76E-01
762	$4N_2(aq) + S_2O_3^{-2} + H_2O + 2H^+ \rightarrow 2H_2S(aq) + 4N_2O(aq)$	8	-2.80E-07	-2.58E-01	-2.80E-07	-2.34E-01	-2.66E-07	-2.29E-01	-2.63E-07	-2.25E-01
763	$2N_2(aq) + S_2O_3^{-2} + H_2O + 2H^+ \rightarrow 2H_2S(aq) + 4NO(aq)$	8	-2.57E-07	-2.46E-01	-2.68E-07	-2.22E-01	-2.57E-07	-2.19E-01	-2.54E-07	-2.16E-01
764	$4N_2(aq) + 3S_2O_3^{-2} + 7H_2O \rightarrow 6H_2S(aq) + 8NO_2^- + 2H^+$	24	-2.06E-07	-1.83E-01	-2.07E-07	-1.95E-01	-1.96E-07	-1.89E-01	-1.84E-07	-1.77E-01

765	$4N_2(aq) + 5S_2O_3^{-2} + 2H^+ + 9H_2O \rightarrow 10H_2S(aq) + 8NO_3^-$	40	-1.70E-07	-1.48E-01	-1.75E-07	-1.58E-01	-1.66E-07	-1.59E-01	-1.64E-07	-1.56E-01
766	$4N_2O(aq) + S_2O_3^{-2} + 2H^+ + H_2O \rightarrow 2H_2S(aq) + 8NO(aq)$	8	-2.35E-07	-1.52E-01	-7.16E-08	-4.52E-01	-6.94E-08	-4.50E-01	-6.86E-08	-4.42E-01
767	$2N_2O(aq) + S_2O_3^{-2} + 3H_2O \rightarrow 2H_2S(aq) + 4NO_2^- + 2H^+$	8	-1.69E-07	-1.46E-01	-9.26E-08	-7.69E-01	-8.81E-08	-7.68E-01	-8.01E-08	-6.87E-01
768	$N_2O(aq) + S_2O_3^{-2} + 2H_2O \rightarrow 2H_2S(aq) + 2NO_3^-$	8	-1.43E-07	-1.26E-01	-1.56E-07	-1.32E-01	-1.49E-07	-1.34E-01	-1.46E-07	-1.32E-01
769	$8NO(aq) + S_2O_3^{-2} + 5H_2O \rightarrow 2H_2S(aq) + 8NO_2^- + 6H^+$	8	-2.04E-08	-1.80E-01	-1.80E-08	-8.44E-09	-1.69E-08	-8.42E-09	-1.33E-08	-4.80E-09
770	$8NO(aq) + 3S_2O_3^{-2} + 7H_2O \rightarrow 6H_2S(aq) + 8NO_3^- + 2H^+$	24	-4.97E-08	-3.38E-01	-4.96E-08	-3.59E-01	-4.73E-08	-3.70E-01	-4.64E-08	-3.60E-01
771	$4NO_2^- + S_2O_3^{-2} + 2H^+ + H_2O \rightarrow 2H_2S(aq) + 4NO_3^-$	8	-1.17E-07	-9.48E-01	-4.58E-08	-3.98E-01	-4.60E-08	-4.31E-01	-3.31E-11	-3.12E-11
772	$12Fe^{+2} + S_2O_3^{-2} + 13H_2O \rightarrow$ 4magnetite $+ 2H_2S(aq) + 22H^+$	8	-4.21E-08	-1.96E-01	-1.08E-09	1.55E-01	-4.15E-10	1.48E-01	-5.30E-12	-4.67E-12
773	$8Fe^{+2} + S_2O_3^{-2} + 9H_2O \rightarrow$ 4hematite $+ 2H_2S(aq) + 14H^+$	8	-2.35E-08	-1.20E-09	-1.06E-09	7.89E-01	-5.72E-11	7.87E-01	-4.78E-12	-3.83E-12
774	$8Fe^{+2} + S_2O_3^{-2} + 9H_2O \rightarrow$ 4maghemite $+ 2H_2S(aq) + 14H^+$	8	-3.59E-08	-1.34E-01	-2.45E-09	-6.17E-01	-1.45E-09	-6.34E-01	-6.32E-12	-5.38E-12
775	$8Fe^{+2} + S_2O_3^{-2} + 13H_2O \rightarrow$ 8goethite $+ 2H_2S(aq) + 14H^+$	8	-2.33E-08	-7.89E-01	-1.01E-09	8.35E-01	-1.23E-11	8.32E-01	-4.74E-12	-3.79E-12
776	$8Fe^{+2} + S_2O_3^{-2} + 13H_2O \rightarrow$ 8lepidocrocite $+ 2H_2S(aq) + 14H^+$	8	-3.86E-08	-1.61E-01	-2.74E-09	-8.89E-01	-1.74E-09	-8.92E-01	-6.65E-12	-5.78E-12
777	$8Fe^{+2} + S_2O_3^{-2} + 21H_2O \rightarrow$ 8ferrihydrite $+ 2H_2S(aq) + 14H^+$	8	-4.80E-08	-2.55E-01	-3.75E-09	-1.90E-09	-2.75E-09	-1.93E-09	-7.79E-12	-6.85E-12
778	6fayalite $+ S_2O_3^{-2} + 2H^+ + H_2O \rightarrow$ 4magnetite $+ 2H_2S(aq) + 6SiO_2(aq)$	8	2.06E-08	6.56E-01	7.54E-09	3.23E-01	2.49E-08	3.25E-01	2.72E-08	3.48E-01

779	12ferrosilite + $S_2O_3^{-2}$ + $2H^+$ + H_2O → 4magnetite + $2H_2S$(aq) + 12SiO_2(aq)	8	6.25E-09	7.38E-01	-6.80E-09	2.63E-01	1.90E-08	2.65E-01	2.06E-08	2.82E-01
780	8magnetite + $S_2O_3^{-2}$ + $2H^+$ + H_2O → 12hematite + $2H_2S$(aq)	8	1.36E-08	3.61E-01	5.92E-10	1.74E-01	9.54E-09	1.74E-01	1.26E-08	2.15E-01
781	8magnetite + $S_2O_3^{-2}$ + $2H^+$ + H_2O → 12maghemite + $2H_2S$(aq)	8	-2.34E-08	-9.43E-01	-3.65E-08	-2.57E-01	-2.76E-08	-2.44E-01	-2.45E-08	-1.69E-01
782	8magnetite + $S_2O_3^{-2}$ + $2H^+$ + 13H_2O → 24goethite + $2H_2S$(aq)	8	1.43E-08	3.68E-01	1.82E-09	1.83E-01	1.07E-08	1.82E-01	1.35E-08	2.16E-01
783	8magnetite + $S_2O_3^{-2}$ + $2H^+$ + 13H_2O → 24lepidocrocite + $2H_2S$(aq)	8	-3.17E-08	-9.18E-09	-4.42E-08	-2.77E-01	-3.53E-08	-2.77E-01	-3.24E-08	-2.49E-01
784	8magnetite + $S_2O_3^{-2}$ + $2H^+$ + 37H_2O → 24ferrihydrite + $2H_2S$(aq)	8	-5.97E-08	-3.72E-01	-7.11E-08	-5.47E-01	-6.22E-08	-5.48E-01	-5.97E-08	-5.22E-01
785	4CH_4(aq) + 3$S_2O_3^{-2}$ + $6H^+$ → 6H_2S(aq) + 4CO(aq) + 5H_2O	24	-1.45E-09	1.92E-01	-1.06E-08	-1.48E-09	-1.02E-10	-4.16E-11	-1.69E-12	8.39E-15
786	CH_4(aq) + $S_2O_3^{-2}$ + $2H^+$ → $2H_2S$(aq) + CO_2(aq) + H_2O	8	6.64E-09	2.91E-01	-1.66E-09	1.54E-01	4.79E-11	1.29E-01	1.35E-12	3.62E-12
787	CH_4(aq) + $S_2O_3^{-2}$ + H^+ → $2H_2S$(aq) + HCO_3^-	8	6.64E-09	2.91E-01	-1.66E-09	1.54E-01	4.79E-11	1.29E-01	1.35E-12	3.62E-12
788	4CO(aq) + $S_2O_3^{-2}$ + $2H^+$ + H_2O → 4CO_2(aq) + $2H_2S$(aq)	8	4.34E-12	1.37E-11	2.62E-09	3.51E-09	1.42E-09	1.62E-09	2.03E-12	2.45E-12
789	4CO(aq) + $S_2O_3^{-2}$ + 5H_2O → 4HCO_3^- + $2H_2S$(aq) + $2H^+$	8	4.34E-12	1.37E-11	2.62E-09	3.51E-09	1.42E-09	1.61E-09	2.03E-12	2.47E-12
790	$2H^+$ + H_2O + $S_2O_3^{-2}$ → $2H_2S$(aq) + $2O_2$(aq)	8	-1.78E-07	-1.49E-01	-1.98E-07	-1.64E-01	-1.89E-07	-1.81E-01	-1.84E-07	-1.77E-01
791	$S_2O_3^{-2}$ + H_2O → H_2S(aq) + SO_4^{-2}	4	-1.63E-09	1.34E-01	-3.05E-09	8.93E-09	7.21E-10	8.23E-09	-1.39E-10	7.42E-09
Sulfur as an electron acceptor										
792	H_2(aq) + 2sulfur + Fe^{+2} → pyrite + $2H^+$	2	2.57E-07		2.06E-09		1.02E-09		6.80E-12	

793	$2NH_4^+ + 6sulfur + 3Fe^{+2} \rightarrow 3pyrite + N_2(aq) + 8H^+$	6	5.27E-06		1.82E-08		1.79E-08		1.26E-11	
794	$2NH_4^+ + 8sulfur + 4Fe^{+2} + H_2O \rightarrow 4pyrite + N_2O(aq) + 10H^+$	8	-2.18E-07	-2.19E-01	2.90E-09	4.58E-09	2.96E-09	4.65E-09	-3.44E-12	-1.55E-12
795	$2NH_4^+ + 10sulfur + 5Fe^{+2} + 2H_2O \rightarrow 5pyrite + 2NO(aq) + 12H^+$	10	-2.82E-06	-1.90E-01	-5.20E-09	-2.50E-09	-5.15E-09	-2.45E-01	-1.21E-11	-9.85E-12
796	$NH_4^+ + 6sulfur + 3Fe^{+2} + 2H_2O \rightarrow 3pyrite + NO_2^- + 8H^+$	6	-2.87E-06		-4.13E-09		-4.08E-09		-9.63E-12	
797	$NH_4^+ + 8sulfur + 4Fe^{+2} + 3H_2O \rightarrow 4pyrite + NO_3^- + 10H^+$	8	-3.20E-06		-5.16E-09		-5.38E-09		-1.19E-11	
798	$N_2(aq) + 2sulfur + Fe^{+2} + H_2O \rightarrow pyrite + N_2O(aq) + 2H^+$	2	-6.82E-07	-6.82E-01	-4.29E-08	-3.62E-01	-4.18E-08	-3.54E-01	-5.16E-11	-4.40E-11
799	$N_2(aq) + 4sulfur + 2Fe^{+2} + 2H_2O \rightarrow 2pyrite + 2NO(aq) + 4H^+$	4	-1.22E-06	-1.34E-01	-4.02E-08	-3.35E-01	-3.97E-08	-3.29E-01	-4.92E-11	-4.16E-11
800	$N_2(aq) + 6sulfur + 3Fe^{+2} + 4H_2O \rightarrow 3pyrite + 2NO_2^- + 8H^+$	6	-1.35E-06		-2.64E-08		-2.60E-08		-3.19E-11	
801	$N_2(aq) + 10sulfur + 5Fe^{+2} + 6H_2O \rightarrow 5pyrite + 2NO_3^- + 12H^+$	10	-1.69E-06		-1.92E-08		-1.93E-08		-2.67E-11	
802	$N_2O(aq) + 2sulfur + Fe^{+2} + H_2O \rightarrow pyrite + 2NO(aq) + 2H^+$	2	-2.52E-06	-1.64E-01	-4.43E-08	-2.48E-01	-4.43E-08	-2.46E-01	-5.43E-11	-3.17E-11
803	$N_2O(aq) + 4sulfur + 2Fe^{+2} + 3H_2O \rightarrow 2pyrite + 2NO_2^- + 6H^+$	4	-3.12E-06	-3.12E-01	-2.15E-08	-1.82E-01	-2.15E-08	-1.82E-01	-2.58E-11	-2.22E-11
804	$N_2O(aq) + 8sulfur + 4Fe^{+2} + 5H_2O \rightarrow 4pyrite + 2NO_3^- + 10H^+$	8	-4.72E-06	-4.72E-01	-1.49E-08	-1.32E-01	-1.54E-08	-1.37E-01	-2.23E-11	-2.43E-11
805	$2NO(aq) + 2sulfur + Fe^{+2} + 2H_2O \rightarrow pyrite + 2NO_2^- + 4H^+$	2	-1.25E-08	-5.27E-09	-6.81E-09	6.87E-01	-6.81E-09	7.79E-01	-1.24E-11	2.74E-12
806	$2NO(aq) + 6sulfur + 3Fe^{+2} + 4H_2O \rightarrow$	6	-2.61E-08	-1.86E-01	-9.60E-09	-5.96E-09	-1.03E-08	-5.78E-01	-1.67E-11	-1.16E-11

	3pyrite + $2NO_3^-$ + $8H^+$							
807	NO_2^- + 2sulfur + Fe^{+2} + H_2O → pyrite + NO_3^- + $2H^+$	2	-3.23E-07		-8.26E-09		-9.29E-09	-1.88E-11
808	$4Fe^{+2}$ + 2sulfur + $4H_2O$ → pyrite + magnetite + $8H^+$	2	4.00E-07		4.22E-09		4.22E-09	-4.19E-13
809	$3Fe^{+2}$ + 2sulfur + $3H_2O$ → pyrite + hematite + $6H^+$	2	1.01E-06		6.00E-09		6.00E-09	1.56E-12
810	$3Fe^{+2}$ + 2sulfur + $3H_2O$ → pyrite + maghemite + $6H^+$	2	6.93E-07		5.08E-09		5.07E-09	5.29E-13
811	$3Fe^{+2}$ + 2sulfur + $4H_2O$ → pyrite + 2goethite + $6H^+$	2	1.02E-06		6.03E-09		6.03E-09	1.58E-12
812	$3Fe^{+2}$ + 2sulfur + $4H_2O$ → pyrite + 2lepidocrocite + $6H^+$	2	6.22E-07		4.89E-09		4.88E-09	3.08E-13
813	$3Fe^{+2}$ + 2sulfur + $6H_2O$ → pyrite + 2ferrihydrite + $6H^+$	2	3.82E-07		4.21E-09		4.21E-09	-4.51E-13
814	3fayalite + 4sulfur + $2Fe^{+2}$ + $2H_2O$ → 2pyrite + 2magnetite + $3SiO_2(aq)$ + $4H^+$	4	6.43E-06	8.16E-01	2.18E-08	2.38E-01	2.37E-08	2.10E-11
815	3ferrosilite + 2sulfur + Fe^{+2} + H_2O → pyrite + magnetite + $3SiO_2(aq)$ + $2H^+$	2	5.32E-06	8.79E-01	1.86E-08	2.24E-01	2.24E-08	1.94E-11
816	2magnetite + 2sulfur + Fe^{+2} + H_2O → pyrite + 3hematite + $2H^+$	2	5.89E-06		2.03E-08		2.03E-08	1.74E-11
817	2magnetite + 2sulfur + Fe^{+2} + H_2O → pyrite + 3maghemite + $2H^+$	2	3.03E-06		1.19E-08		1.19E-08	8.11E-12
818	2magnetite + 2sulfur + Fe^{+2} + $4H_2O$ → pyrite + 6goethite + $2H^+$	2	5.94E-06		2.05E-08		2.05E-08	1.76E-11
819	2magnetite + 2sulfur + Fe^{+2} + $4H_2O$ → pyrite + 6lepidocrocite + $2H^+$	2	2.40E-06		1.02E-08		1.02E-08	6.12E-12
820	2magnetite + 2sulfur + Fe^{+2} + $10H_2O$ → pyrite	2	2.40E-07		4.13E-09		4.11E-09	-7.06E-13

	+ 6ferrihydrite + $2H^+$									
821	CH_4(aq) + 6sulfur + $3Fe^{+2}$ + H_2O → 3pyrite + CO(aq) + $6H^+$	6	4.57E-08	4.94E-01	1.58E-08	1.58E-01	5.50E-10	5.50E-01	1.11E-11	1.11E-11
822	CH_4(aq) + 8sulfur + $4Fe^{+2}$ + $2H_2O$ → 4pyrite + CO_2(aq) + $8H^+$	8	6.95E-08		1.96E-08		9.17E-10		1.54E-11	
823	CH_4(aq) + 8sulfur + $4Fe^{+2}$ + $3H_2O$ → 4pyrite + HCO_3^- + $9H^+$	8	6.95E-08		1.96E-08		9.17E-10		1.54E-11	
824	CO(aq) + 2sulfur + Fe^{+2} + H_2O → pyrite + CO_2(aq) + $2H^+$	2	2.01E-11	2.38E-11	7.48E-09	7.48E-09	3.47E-09	3.47E-09	4.87E-12	4.87E-12
825	CO(aq) + 2sulfur + Fe^{+2} + $2H_2O$ → pyrite + HCO_3^- + $3H^+$	2	2.01E-11	2.38E-11	7.48E-09	7.48E-09	3.47E-09	3.47E-09	4.87E-12	4.87E-12
826	Fe^{+2} + 2sulfur + H_2O → pyrite + $2H^+$ +1/2O-$_2$(aq)	2	-8.90E-06	-7.74E-01	-2.44E-08	-1.96E-01	-2.44E-08		-3.19E-11	
827	$2Fe^{+2}$ + 6sulfur + $3H_2O$ → 2pyrite + $S_2O_3^{-2}$ + $6H^+$	4	4.73E-06	5.89E-01	1.94E-08	2.28E-01	1.94E-08	2.29E-01	1.57E-11	1.95E-11
828	$3Fe^{+2}$ + 7sulfur + $4H_2O$ → 3pyrite + SO_4^{-2} + $8H^+$	6	5.02E-06		2.01E-08		1.99E-08		1.59E-11	
829	H_2S(aq) + Fe^{+2} + sulfur → pyrite + $2H^+$	1	4.81E-09	1.23E-01	1.34E-08	1.75E-01	3.86E-09		8.94E-12	
830	H_2(aq) + sulfur → H_2S(aq)	2	1.28E-07	2.70E-01	4.61E-10	8.32E-01	4.04E-10		3.23E-12	
831	$2NH_4^+$ + 3sulfur → $3H_2S$(aq) + N_2(aq) + $2H^+$	6	1.55E-05	3.96E-01	1.51E-08	1.25E-01	1.26E-07		9.95E-10	
832	$2NH_4^+$ + 4sulfur + H_2O → $4H_2S$(aq) + N_2O(aq) + $2H^+$	8	-5.59E-05	-2.37E-01	-4.22E-07	-2.57E-01	-3.94E-07	-3.34E-01	-4.48E-09	-3.80E-09
833	$2NH_4^+$ + 5sulfur + $2H_2O$ → $5H_2S$(aq) + 2NO(aq) + $2H^+$	10	-1.15E-04	-5.89E-01	-8.21E-07	-5.77E-01	-8.74E-07	-7.47E-01	-9.52E-09	-8.16E-09
834	NH_4^+ + 3sulfur + $2H_2O$ → $3H_2S$(aq) + NO_2^- + $2H^+$	6	-1.39E-04	-9.97E-01	-9.38E-07	-7.63E-01	-9.89E-07		-1.01E-08	
835	NH_4^+ + 4sulfur + $3H_2O$ → $4H_2S$(aq) + NO_3^- +	8	-1.95E-04	-1.35E-01	-1.31E-06	-1.78E-01	-1.42E-06		-1.51E-08	

	$2H^+$									
836	$N_2(aq)$ + sulfur + H_2O → $H_2S(aq)$ + $N_2O(aq)$	2	-8.37E-07	-7.43E-01	-4.21E-06	-3.46E-01	-3.85E-05	-3.38E-01	-3.57E-05	-3.12E-01
837	$N_2(aq)$ + 2sulfur + $2H_2O$ → $2H_2S(aq)$ + 2NO(aq)	4	-1.53E-06	-1.15E-01	-8.04E-06	-6.55E-01	-7.40E-05	-6.46E-01	-6.86E-05	-5.97E-01
838	$N_2(aq)$ + 3sulfur + $4H_2O$ → $3H_2S(aq)$ + $2NO_2^-$ + $2H^+$	6	-1.81E-06	-1.54E-01	-9.17E-06	-8.33E-01	-8.25E-05		-7.22E-05	
839	$N_2(aq)$ + 5sulfur + $6H_2O$ → $5H_2S(aq)$ + $2NO_3^-$ + $2H^+$	10	-2.47E-06	-1.99E-01	-1.28E-05	-1.14E-01	-1.14E-04		-1.05E-04	
840	$N_2O(aq)$ + sulfur + H_2O → $H_2S(aq)$ + 2NO(aq)	2	-3.25E-06	-1.93E-01	-6.87E-08	-4.17E-01	-6.42E-08	-4.16E-01	-6.33E-08	-4.63E-01
841	$N_2O(aq)$ + 2sulfur + $3H_2O$ → $2H_2S(aq)$ + $2NO_2^-$ + $2H^+$	4	-4.56E-06	-3.68E-01	-8.67E-08	-7.27E-01	-7.77E-08	-7.17E-01	-6.95E-08	-6.19E-01
842	$N_2O(aq)$ + 4sulfur + $5H_2O$ → $4H_2S(aq)$ + $2NO_3^-$ + $2H^+$	8	-7.61E-06	-5.85E-01	-1.44E-07	-1.19E-01	-1.28E-07	-1.26E-01	-1.25E-07	-1.17E-01
843	2NO(aq) + sulfur + $2H_2O$ → $H_2S(aq)$ + $2NO_2^-$ + $2H^+$	2	-1.87E-08	-7.43E-09	-1.65E-08	-6.78E-09	-1.43E-08	-6.75E-01	-1.07E-08	-3.97E-09
844	2NO(aq) + 3sulfur + $4H_2O$ → $3H_2S(aq)$ + $2NO_3^-$ + $2H^+$	6	-4.46E-08	-2.59E-01	-4.51E-08	-3.93E-01	-3.95E-08	-3.20E-01	-3.84E-08	-3.87E-01
845	NO_2^- + sulfur + H_2O → $H_2S(aq)$ + NO_3^-	2	-6.14E-07	-4.37E-01	-4.15E-08	-3.50E-01	-3.81E-08		-2.78E-11	
846	$3Fe^{+2}$ + sulfur + $4H_2O$ → magnetite + $H_2S(aq)$ + $6H^+$	2	-7.31E-07	3.87E-01	-1.95E-10	1.15E-09	1.15E-09		-3.54E-12	
847	$2Fe^{+2}$ + sulfur + $3H_2O$ → hematite + $H_2S(aq)$ + $4H^+$	2	-3.82E-07	7.74E-01	2.71E-10	2.28E-01	2.29E-09		-2.13E-12	
848	$2Fe^{+2}$ + sulfur + $3H_2O$ → maghemite + $H_2S(aq)$ + $4H^+$	2	-8.58E-07	2.97E-01	-1.12E-09	8.92E-01	8.99E-10		-3.68E-12	
849	$2Fe^{+2}$ + sulfur + $4H_2O$ → 2goethite + $H_2S(aq)$ + $4H^+$	2	-3.73E-07	7.82E-01	3.18E-10	2.33E-09	2.34E-09		-2.09E-12	
850	$2Fe^{+2}$ + sulfur + $4H_2O$ → 2lepidocrocite + $H_2S(aq)$ + $4H^+$	2	-9.63E-07	1.92E-01	-1.41E-09	6.49E-01	6.11E-10		-4.01E-12	

851	$2Fe^{+2}$ + sulfur + $6H_2O$ → 2ferrihydrite + $H_2S(aq)$ + $4H^+$	2	-1.32E-06	-1.68E-01	-2.42E-09	-4.54E-01	-4.01E-10		-5.15E-12	
852	3fayalite + 2sulfur + $2H_2O$ → 2magnetite + $2H_2S(aq)$ + $3SiO_2(aq)$	4	0.00E+00		0.00E+00		0.00E+00		0.00E+00	
853	3ferrosilite + sulfur + H_2O → magnetite + $H_2S(aq)$ + $3SiO_2(aq)$	2	0.00E+00		0.00E+00		0.00E+00		0.00E+00	
854	2magnetite + sulfur + H_2O → 3hematite + $H_2S(aq)$	2	0.00E+00		0.00E+00		0.00E+00		0.00E+00	
855	2magnetite + sulfur + H_2O → 3maghemite + $H_2S(aq)$	2	0.00E+00		0.00E+00		0.00E+00		0.00E+00	
856	2magnetite + sulfur + $4H_2O$ → 6goethite + $H_2S(aq)$	2	0.00E+00		0.00E+00		0.00E+00		0.00E+00	
857	2magnetite + sulfur + $4H_2O$ → 6lepidocrocite + $H_2S(aq)$	2	0.00E+00		0.00E+00		0.00E+00		0.00E+00	
858	2magnetite + sulfur + $10H_2O$ → 6ferrihydrite + $H_2S(aq)$	2	0.00E+00		0.00E+00		0.00E+00		0.00E+00	
859	$CH_4(aq)$ + 3sulfur + H_2O → $CO(aq)$ + $3H_2S(aq)$	6	8.75E-09	3.55E-01	-4.04E-09	5.92E-09	6.66E-11	6.66E-11	3.07E-12	3.69E-12
860	$CH_4(aq)$ + 4sulfur + $2H_2O$ → $CO_2(aq)$ + $4H_2S(aq)$	8	2.02E-08	5.24E-01	7.13E-09	2.40E-01	2.73E-10		7.70E-12	
861	$CH_4(aq)$ + 4sulfur + $3H_2O$ → HCO_3^- + $4H_2S(aq)$ + H^+	8	2.02E-08	5.24E-01	7.13E-09	2.40E-01	2.73E-10		7.70E-12	
862	$CO(aq)$ + sulfur + H_2O → $CO_2(aq)$ + $H_2S(aq)$	2	7.74E-12	1.90E-11	3.26E-09	4.24E-01	1.95E-09	1.95E-09	3.09E-12	3.85E-12
863	$CO(aq)$ + sulfur + $2H_2O$ → HCO_3^- + $H_2S(aq)$ + H^+	2	7.74E-12	1.90E-11	3.27E-09	4.24E-09	1.95E-09	1.95E-09	3.09E-12	3.86E-12
864	sulfur + H_2O → $H_2S(aq)$ + $1/2O_2(aq)$	2	0.00E+00		0.00E+00		0.00E+00		0.00E+00	
865	$3H_2O$ + 4sulfur → $S_2O_3^{-2}$ + $2H_2S(aq)$ + $2H^+$	4	0.00E+00		0.00E+00		0.00E+00		0.00E+00	
866	$4H_2O$ + 4sulfur → SO_4^{-2} + $3H_2S(aq)$ + $2H^+$	6	0.00E+00		0.00E+00		0.00E+00		0.00E+00	

Pyrite as an electron acceptor										
867	$H_2(aq) + pyrite + 2H^+ \rightarrow Fe^{+2} + 2H_2S(aq)$	2	-4.82E-10	1.57E-01	-1.14E-09	-4.24E-01	-2.17E-10		-3.50E-13	
868	$2NH_4^+ + 3pyrite + 4H^+ \rightarrow 6H_2S(aq) + N_2(aq) + 3Fe^{+2}$	6	-2.42E-05	2.42E-01	-3.64E-07	-1.89E-01	-2.53E-07		-1.43E-09	
869	$2NH_4^+ + 4pyrite + 6H^+ + H_2O \rightarrow 8H_2S(aq) + N_2O(aq) + 4Fe^{+2}$	8	-1.09E-04	-4.44E-01	-9.28E-07	-6.46E-01	-8.99E-07	-8.36E-01	-7.72E-09	-7.32E-09
870	$2NH_4^+ + 5pyrite + 8H^+ + 2H_2O \rightarrow 10H_2S(aq) + 2NO(aq) + 5Fe^{+2}$	10	-1.81E-04	-8.47E-01	-1.45E-06	-1.64E-01	-1.51E-06	-1.38E-01	-1.36E-08	-1.23E-01
871	$NH_4^+ + 3pyrite + 4H^+ + 2H_2O \rightarrow 6H_2S(aq) + NO_2^- + 3Fe^{+2}$	6	-2.19E-04	-1.22E-01	-1.70E-06	-1.35E-01	-1.75E-06		-1.49E-08	
872	$NH_4^+ + 4pyrite + 6H^+ + 3H_2O \rightarrow 8H_2S(aq) + NO_3^- + 4Fe^{+2}$	8	-3.01E-04	-1.72E-01	-2.32E-06	-1.86E-01	-2.43E-06		-2.16E-08	
873	$N_2(aq) + pyrite + 2H^+ + H_2O \rightarrow 2H_2S(aq) + N_2O(aq) + Fe^{+2}$	2	-9.92E-07	-8.31E-01	-5.42E-06	-4.39E-01	-4.78E-05	-4.32E-01	-4.10E-05	-3.66E-01
874	$N_2(aq) + 2pyrite + 4H^+ + 2H_2O \rightarrow 4H_2S(aq) + 2NO(aq) + 2Fe^{+2}$	4	-1.84E-06	-1.28E-01	-1.05E-05	-8.41E-01	-9.27E-05	-8.33E-01	-7.91E-05	-7.25E-01
875	$N_2(aq) + 3pyrite + 4H^+ + 4H_2O \rightarrow 6H_2S(aq) + 2NO_2^- + 3Fe^{+2}$	6	-2.28E-06	-1.71E-01	-1.28E-05	-1.11E-01	-1.11E-04		-8.80E-05	
876	$N_2(aq) + 5pyrite + 8H^+ + 6H_2O \rightarrow 10H_2S(aq) + 2NO_3^- + 5Fe^{+2}$	10	-3.24E-06	-2.30E-01	-1.88E-05	-1.64E-01	-1.61E-04		-1.31E-04	
877	$N_2O(aq) + pyrite + 2H^+ + H_2O \rightarrow 2H_2S(aq) + 2NO(aq) + Fe^{+2}$	2	-3.97E-06	-2.29E-01	-8.81E-08	-5.66E-01	-7.91E-08	-5.66E-01	-7.22E-08	-4.96E-01
878	$N_2O(aq) + 2pyrite + 2H^+ + 3H_2O \rightarrow 4H_2S(aq) + 2NO_2^- + 2Fe^{+2}$	4	-6.01E-06	-4.25E-01	-1.26E-07	-1.14E-01	-1.07E-07	-1.00E+00	-8.74E-08	-7.98E-01
879	$N_2O(aq) + 4pyrite + 6H^+ + 5H_2O \rightarrow 8H_2S(aq) + 2NO_3^- + 4Fe^{+2}$	8	-1.05E-05	-6.98E-01	-2.22E-07	-1.78E-01	-1.88E-07	-1.83E-01	-1.61E-07	-1.53E-01
880	$2NO(aq) + pyrite + 2H_2O \rightarrow 2H_2S(aq) + Fe^{+2} + 2NO_2^-$	2	-2.48E-08	-9.85E-09	-2.62E-08	-1.43E-01	-2.17E-08	-1.43E-01	-1.51E-08	-7.57E-09

881	$2NO(aq) + 3pyrite + 4H^+ + 4H_2O \rightarrow 6H_2S(aq) + 3Fe^{+2} + 2NO_3^-$	6	-6.31E-08	-3.38E-01	-7.42E-08	-5.33E-01	-6.19E-08	-5.43E-01	-5.18E-08	-4.43E-01
882	$NO_2^- + pyrite + 2H^+ + H_2O \rightarrow 2H_2S(aq) + Fe^{+2} + NO_3^-$	2	-9.06E-07	-5.57E-01	-6.96E-08	-5.66E-01	-6.06E-08		-3.67E-11	
883	$2Fe^{+2} + pyrite + 4H_2O \rightarrow magnetite + 2H_2S(aq) + 4H^+$	2	-2.99E-06	-6.83E-01	-9.03E-09	-5.28E-09	-4.98E-09		-9.78E-12	
884	$Fe^{+2} + pyrite + 3H_2O \rightarrow hematite + 2H_2S(aq) + 2H^+$	2	-4.56E-06	6.50E-01	-1.69E-08	-8.88E-09	-8.84E-09		-1.32E-11	
885	$Fe^{+2} + pyrite + 3H_2O \rightarrow maghemite + 2H_2S(aq) + 2H^+$	2	-5.51E-06	-8.88E-01	-1.97E-08	-1.17E-01	-1.16E-08		-1.63E-11	
886	$Fe^{+2} + pyrite + 4H_2O \rightarrow 2goethite + 2H_2S(aq) + 2H^+$	2	-4.54E-06	8.14E-01	-1.68E-08	-8.79E-09	-8.75E-09		-1.31E-11	
887	$Fe^{+2} + pyrite + 4H_2O \rightarrow 2lepidocrocite + 2H_2S(aq) + 2H^+$	2	-5.72E-06	-1.99E-01	-2.03E-08	-1.22E-01	-1.22E-08		-1.70E-11	
888	$Fe^{+2} + pyrite + 6H_2O \rightarrow 2ferrihydrite + 2H_2S(aq) + 2H^+$	2	-6.44E-06	-1.82E-01	-2.23E-08	-1.43E-01	-1.42E-08		-1.92E-11	
889	$fayalite + pyrite + 2H_2O \rightarrow magnetite + 2H_2S(aq) + SiO_2(aq)$	2	0.00E+00		0.00E+00		0.00E+00		0.00E+00	
890	$2ferrosilite + pyrite + 2H_2O \rightarrow magnetite + 2H_2S(aq) + 2SiO_2(aq)$	2	0.00E+00		0.00E+00		0.00E+00		0.00E+00	
891	$magnetite + pyrite + 2H_2O \rightarrow 2hematite + 2H_2S(aq)$	2	-1.01E-08	4.85E-09	-1.76E-08	-8.61E-09	-8.57E-09		0.00E+00	
892	$magnetite + pyrite + 2H_2O \rightarrow 2maghemite + 2H_2S(aq)$	2	-1.63E-08	-1.33E-09	-2.37E-08	-1.48E-01	-1.47E-08		0.00E+00	
893	$magnetite + pyrite + 4H_2O \rightarrow 4goethtite + 2H_2S(aq)$	2	-1.00E-08	4.97E-09	-1.74E-08	-8.48E-01	-8.37E-09		0.00E+00	
894	$magnetite + pyrite + 4H_2O \rightarrow 4lepidocrocite + 2H_2S(aq)$	2	-1.77E-08	-2.75E-09	-2.50E-08	-1.67E-01	-1.60E-08		0.00E+00	
895	$magnetite + pyrite + 8H_2O \rightarrow 4ferrihydrite$	2	-2.24E-08	-7.38E-09	-2.95E-08	-2.56E-01	-2.05E-08		0.00E+00	

	+ $2H_2S(aq)$									
896	$CH_4(aq)$ + 3pyrite + $6H^+ + H_2O \rightarrow CO(aq) + 3Fe^{+2} + 6H_2S(aq)$	6	-2.82E-08	2.56E-01	-4.72E-08	-2.73E-01	-4.16E-10	-4.16E-01	-4.98E-12	-4.98E-12
897	$CH_4(aq)$ + 4pyrite + $8H^+ + 2H_2O \rightarrow CO_2(aq) + 4Fe^{+2} + 8H_2S(aq)$	8	-2.90E-08	3.99E-01	-5.05E-08	-2.39E-01	-3.71E-10		-3.03E-12	
898	$CH_4(aq)$ + 4pyrite + $7H^+ + 3H_2O \rightarrow HCO_3^- + 4Fe^{+2} + 8H_2S(aq)$	8	-2.90E-08	3.99E-01	-5.05E-08	-2.39E-01	-3.71E-10		-3.03E-12	
899	$CO(aq)$ + pyrite + $2H^+ + H_2O \rightarrow Fe^{+2} + CO_2(aq) + 2H_2S(aq)$	2	-4.58E-12	1.42E-11	-9.47E-10	9.93E-01	4.31E-10	4.38E-01	1.30E-12	1.30E-12
900	$CO(aq)$ + pyrite + $H^+ + 2H_2O \rightarrow Fe^{+2} + HCO_3^- + 2H_2S(aq)$	2	-4.58E-12	1.42E-11	-9.47E-10	9.93E-01	4.31E-10	4.37E-01	1.30E-12	1.30E-12
901	H_2O + pyrite + $2H^+ \rightarrow Fe^{+2} + 2H_2S(aq) + 1/2O_2(aq)$	2	-5.35E-08	-3.48E-01	-6.59E-08	-5.16E-01	-5.69E-08		0.00E+00	
902	pyrite + $2H^+ \rightarrow$ sulfur + $H_2S(aq) + Fe^{+2}$	1	-1.23E-08	-4.81E-09	-1.94E-08	-1.49E-01	-1.49E-08		0.00E+00	
903	$3H_2O$ + 4pyrite + $6H^+ \rightarrow S_2O_3^{-2} + 6H_2S(aq) + 4Fe^{+2}$	6	-1.08E-08	2.34E-09	-1.83E-08	-9.74E-09	-1.16E-08	-9.69E-09	0.00E+00	
904	$4H_2O$ + 4pyrite + $6H^+ \rightarrow SO_4^{-2} + 7H_2S(aq) + 4Fe^{+2}$	7	-9.32E-09	3.85E-01	-1.72E-08	-9.39E-09	-9.51E-09		0.00E+00	
Magnetite as an electron acceptor										
905	$H_2(aq)$ + magnetite + $6H^+ \rightarrow 3Fe^{+2} + 4H_2O$	2	2.03E-07		5.15E-10		2.44E-10		7.47E-12	
906	$2NH_4^+$ + 3magnetite + $16H^+ \rightarrow 9Fe^{+2} + N_2(aq) + 12H_2O$	6	3.84E-05		2.78E-08		2.84E-08		3.88E-09	
907	$2NH_4^+$ + 4magnetite + $22H^+ \rightarrow 12Fe^{+2} + N_2O(aq) + 15H_2O$	8	-2.53E-05	-2.53E-01	-4.05E-07	-3.56E-01	-5.24E-07	-4.63E-01	-6.37E-10	4.66E-11
908	$2NH_4^+$ + 5magnetite + $28H^+ \rightarrow 15Fe^{+2} + 2NO(aq) + 18H_2O$	10	-7.70E-05	-6.92E-01	-7.99E-07	-7.16E-01	-1.04E-06	-9.94E-01	-4.72E-09	-3.35E-09
909	NH_4^+ + 3magnetite + $16H^+ \rightarrow 9Fe^{+2} + NO_2^- + 10H_2O$	6	-9.34E-05		-9.13E-07		-1.18E-06		-4.32E-09	

910	NH_4^+ + 4magnetite + $22H^+ \rightarrow 12Fe^{+2} + NO_3^- + 13H_2O$	8	-1.34E-04		-1.28E-06		-1.68E-06		-7.43E-09	
911	N_2(aq) + magnetite + $6H^+ \rightarrow 3Fe^{+2} + N_2O$(aq) + $3H_2O$	2	-7.47E-07	-7.47E-01	-4.17E-06	-3.70E-01	-4.09E-05	-3.62E-01	-2.94E-05	-2.50E-01
912	N_2(aq) + 2magnetite + $12H^+ \rightarrow 6Fe^{+2} + 2NO$(aq) + $6H_2O$	4	-1.35E-06	-1.16E-01	-7.96E-06	-7.22E-01	-7.88E-05	-6.94E-01	-5.60E-05	-4.71E-01
913	N_2(aq) + 3magnetite + $16H^+ \rightarrow 9Fe^{+2} + 2NO_2^- + 8H_2O$	6	-1.55E-06		-9.05E-06		-8.97E-05		-5.34E-05	
914	N_2(aq) + 5magnetite + $28H^+ \rightarrow 15Fe^{+2} + 2NO_3^- + 14H_2O$	10	-2.02E-06		-1.26E-05		-1.26E-04		-7.37E-05	
915	N_2O(aq) + magnetite + $6H^+ \rightarrow 3Fe^{+2} + 2NO$(aq) + $3H_2O$	2	-2.83E-06	-1.95E-01	-6.80E-08	-4.55E-01	-6.80E-08	-4.55E-01	-5.27E-08	-3.73E-01
916	N_2O(aq) + 2magnetite + $10H^+ \rightarrow 6Fe^{+2} + 2NO_2^- + 5H_2O$	4	-3.73E-06	-3.73E-01	-8.54E-08	-7.80E-01	-8.53E-08	-7.78E-01	-4.83E-08	-4.70E-01
917	N_2O(aq) + 4magnetite + $22H^+ \rightarrow 12Fe^{+2} + 2NO_3^- + 11H_2O$	8	-5.94E-06	-5.94E-01	-1.41E-07	-1.34E-01	-1.43E-07	-1.36E-01	-8.26E-08	-7.51E-01
918	2NO(aq) + magnetite + $4H^+ \rightarrow 3Fe^{+2} + 2NO_2^- + 2H_2O$	2	-1.51E-08	-7.62E-09	-1.62E-08	-8.69E-09	-1.62E-08	-8.67E-09	-5.35E-09	2.21E-09
919	2NO(aq) + 3magnetite + $16H^+ \rightarrow 9Fe^{+2} + 2NO_3^- + 8H_2O$	6	-3.39E-08	-2.64E-01	-4.41E-08	-3.66E-01	-4.52E-08	-3.77E-01	-2.25E-08	-1.49E-01
920	NO_2^- + magnetite + $6H^+ \rightarrow 3Fe^{+2} + NO_3^- + 3H_2O$	2	-4.46E-07		-4.05E-08		-4.39E-08		-1.72E-11	
921	$2H_2S$(aq) + magnetite + $4H^+ \rightarrow$ pyrite + $2Fe^{+2} + 4H_2O$	2	2.22E-09	9.72E-09	5.56E-06	1.32E-01	1.43E-09		5.85E-10	
922	H_2S(aq) + magnetite + $6H^+ \rightarrow 3Fe^{+2}$ + sulfur + $4H_2O$	2	-3.77E-10	7.12E-09	-3.82E-06	6.50E-01	-9.93E-10		6.35E-10	
923	$2H_2S$(aq) + 4magnetite + $22H^+ \rightarrow 12Fe^{+2} + S_2O_3^{-2} + 13H_2O$	8	9.80E-09	2.15E-01	-1.00E-06	7.22E-01	-2.56E-10	7.16E-01	1.68E-09	1.92E-09
924	H_2S(aq) + 4magnetite + $22H^+ \rightarrow SO_4^{-2} + 12Fe^{+2} + 12H_2O$	8	3.30E-08	4.47E-01	6.92E-06	1.14E-01	1.62E-09		3.80E-09	

925	pyrite + magnetite + $8H^+ \rightarrow 4Fe^{+2} + 2sulfur + 4H_2O$	2	-5.19E-09		-1.88E-08		-1.87E-08		0.00E+00	
926	pyrite + 3magnetite + $18H^+ \rightarrow 10Fe^{+2} + S_2O_3^{-2} + 9H_2O$	6	1.52E-08	2.27E-01	-1.31E-08	-5.62E-09	-1.31E-08	-5.55E-01	0.00E+00	
927	pyrite + 7magnetite + $40H^+ \rightarrow 2SO_4^{-2} + 22Fe^{+2} + 20H_2O$	14	6.15E-08		2.72E-09		1.43E-09		0.00E+00	
928	2sulfur + 2magnetite + $10H^+ \rightarrow 6Fe^{+2} + S_2O_3^{-2} + 5H_2O$	4	0.00E+00		0.00E+00		0.00E+00		0.00E+00	
929	sulfur + 3magnetite + $16H^+ \rightarrow SO_4^{-2} + 9Fe^{+2} + 8H_2O$	6	0.00E+00		0.00E+00		0.00E+00		0.00E+00	
930	$S_2O_3^{-2}$ + 4magnetite + $22H^+ \rightarrow 12Fe^{+2} + 2SO_4^{-2} + 11H_2O$	8	3.88E-08	4.63E-01	8.35E-09	1.58E-01	6.97E-09	1.45E-01	6.33E-08	7.89E-01
931	CH_4(aq) + 3magnetite + $18H^+ \rightarrow$ CO(aq) + $9Fe^{+2} + 11H_2O$	6	3.01E-08	3.39E-01	-2.59E-09	-2.59E-01	-5.76E-11	-5.77E-11	1.26E-11	1.26E-11
932	CH_4(aq) + 4magnetite + $24H^+ \rightarrow CO_2$(aq) + $12Fe^{+2} + 14H_2O$	8	4.87E-08		9.05E-09		1.08E-10		2.04E-11	
933	CH_4(aq) + 4magnetite + $23H^+ \rightarrow HCO_3^- + 12Fe^{+2} + 13H_2O$	8	4.87E-08		9.05E-09		1.08E-10		2.04E-11	
934	CO(aq) + magnetite + $6H^+ \rightarrow CO_2$(aq) + $3Fe^{+2} + 3H_2O$	2	1.49E-11	1.87E-11	3.41E-09	3.46E-09	1.56E-09	1.57E-09	5.21E-12	5.28E-12
935	CO(aq) + magnetite + $5H^+ \rightarrow HCO_3^- + 3Fe^{+2} + 2H_2O$	2	1.49E-11	1.86E-11	3.41E-09	3.46E-09	1.56E-09	1.57E-09	5.21E-12	5.29E-12
936	$6H^+$ + magnetite $\rightarrow 3Fe^{+2} + 1/2O_2$(aq) + $3H_2O$	2	-1.10E-05	-9.77E-01	-1.48E-05	-1.34E-01	-1.48E-05		-1.21E-11	
Hematite as an electron acceptor										
937	H_2(aq) + hematite + $4H^+ \rightarrow 2Fe^{+2} + 3H_2O$	2	1.54E-07		4.12E-10		1.92E-10		4.93E-12	
938	$2NH_4^+$ + 3hematite + $10H^+ \rightarrow 6Fe^{+2} + N_2$(aq) + $9H_2O$	6	2.34E-05		3.33E-09		-3.48E-09		2.15E-09	
939	$2NH_4^+$ + 4hematite + $14H^+ \rightarrow 8Fe^{+2}$ +	8	-4.53E-05	-4.53E-01	-4.38E-07	-3.89E-01	-5.67E-07	-5.29E-01	-2.94E-09	-2.25E-09

	$N_2O(aq) + 11H_2O$									
940	$2NH_4^+ + 5hematite + 18H^+ \rightarrow 10Fe^{+2} + 2NO(aq) + 13H_2O$	10	-1.02E-04	-8.59E-01	-8.40E-07	-7.42E-01	-1.09E-06	-9.63E-01	-7.59E-09	-6.23E-09
941	$NH_4^+ + 3hematite + 10H^+ \rightarrow 6Fe^{+2} + NO_2^- + 7H_2O$	6	-1.23E-04		-9.62E-07		-1.25E-06		-7.77E-09	
942	$NH_4^+ + 4hematite + 14H^+ \rightarrow 8Fe^{+2} + NO_3^- + 9H_2O$	8	-1.74E-04		-1.34E-06		-1.76E-06		-1.20E-08	
943	$N_2(aq) + hematite + 4H^+ \rightarrow 2Fe^{+2} + N_2O(aq) + 2H_2O$	2	-8.06E-07	-8.57E-01	-4.24E-06	-3.77E-01	-4.17E-05	-3.69E-01	-3.32E-05	-2.87E-01
944	$N_2(aq) + 2hematite + 8H^+ \rightarrow 4Fe^{+2} + 2NO(aq) + 4H_2O$	4	-1.47E-06	-1.28E-01	-8.12E-06	-7.18E-01	-8.04E-05	-7.96E-01	-6.35E-05	-5.46E-01
945	$N_2(aq) + 3hematite + 10H^+ \rightarrow 6Fe^{+2} + 2NO_2^- + 5H_2O$	6	-1.72E-06		-9.29E-06		-9.20E-05		-6.47E-05	
946	$N_2(aq) + 5hematite + 18H^+ \rightarrow 10Fe^{+2} + 2NO_3^- + 9H_2O$	10	-2.31E-06		-1.29E-05		-1.30E-04		-9.24E-05	
947	$N_2O(aq) + hematite + 4H^+ \rightarrow 2Fe^{+2} + 2NO(aq) + 2H_2O$	2	-3.10E-06	-2.22E-01	-6.93E-08	-4.68E-01	-6.93E-08	-4.67E-01	-5.90E-08	-3.64E-01
948	$N_2O(aq) + 2hematite + 6H^+ \rightarrow 4Fe^{+2} + 2NO_2^- + 3H_2O$	4	-4.27E-06	-4.27E-01	-8.79E-08	-8.41E-01	-8.79E-08	-8.35E-01	-6.10E-08	-5.34E-01
949	$N_2O(aq) + 4hematite + 14H^+ \rightarrow 8Fe^{+2} + 2NO_3^- + 7H_2O$	8	-7.03E-06	-7.30E-01	-1.46E-07	-1.39E-01	-1.48E-07	-1.50E-01	-1.08E-07	-1.42E-01
950	$2NO(aq) + hematite + 2H^+ \rightarrow 2Fe^{+2} + 2NO_2^- + H_2O$	2	-1.74E-08	-9.94E-09	-1.68E-08	-9.32E-09	-1.68E-08	-9.30E-09	-8.52E-09	-9.65E-01
951	$2NO(aq) + 3hematite + 10H^+ \rightarrow 6Fe^{+2} + 2NO_3^- + 5H_2O$	6	-4.09E-08	-3.34E-01	-4.60E-08	-3.85E-01	-4.71E-08	-3.96E-01	-3.20E-08	-2.45E-01
952	$NO_2^- + hematite + 4H^+ \rightarrow 2Fe^{+2} + NO_3^- + 2H_2O$	2	-5.56E-07		-4.23E-08		-4.58E-08		-2.35E-11	
953	$2H_2S(aq) + hematite + 2H^+ \rightarrow pyrite + Fe^{+2} + 3H_2O$	2	-1.04E-10	7.40E-09	4.93E-06	9.44E-01	1.27E-09		3.95E-10	

954	$H_2S(aq) + hematite + 4H^+ \rightarrow 2Fe^{+2} + sulfur + 3H_2O$	2	-5.02E-09	2.48E-09	-5.07E-06	-6.33E-01	-1.32E-09		2.55E-10	
955	$2H_2S(aq) + 4hematite + 14H^+ \rightarrow 8Fe^{+2} + S_2O_3^{-2} + 9H_2O$	8	5.05E-10	1.18E-01	-3.51E-06	4.71E-01	-9.06E-10	6.59E-11	9.17E-10	1.14E-09
956	$H_2S(aq) + 4hematite + 14H^+ \rightarrow 8Fe^{+2} + SO_4^{-2} + 8H_2O$	8	1.44E-08	2.19E-01	1.91E-06	6.38E-01	3.19E-10		2.28E-09	
957	$pyrite + hematite + 6H^+ \rightarrow 3Fe^{+2} + 2sulfur + 3H_2O$	2	-9.84E-09		-2.00E-08		-2.00E-08		0.00E+00	
958	$pyrite + 3hematite + 12H^+ \rightarrow 7Fe^{+2} + S_2O_3^{-2} + 6H_2O$	6	1.22E-09	8.72E-01	-1.69E-08	-9.38E-09	-1.68E-08	-9.31E-09	0.00E+00	
959	$pyrite + 7hematite + 26H^+ \rightarrow 15Fe^{+2} + 2SO_4^{-2} + 13H_2O$	14	2.90E-08		-6.04E-09		-7.36E-09		0.00E+00	
960	$2sulfur + 2hematite + 6H^+ \rightarrow 4Fe^{+2} + S_2O_3^{-2} + 3H_2O$	4	0.00E+00		0.00E+00		0.00E+00		0.00E+00	
961	$sulfur + 3hematite + 10H^+ \rightarrow 6Fe^{+2} + SO_4^{-2} + 5H_2O$	6	0.00E+00		0.00E+00		0.00E+00		0.00E+00	
962	$S_2O_3^{-2} + 4hematite + 14H^+ \rightarrow 8Fe^{+2} + 2SO_4^{-2} + 7H_2O$	8	2.03E-08	2.78E-01	3.34E-09	1.84E-01	1.95E-09	9.46E-09	3.79E-08	4.55E-01
963	$CH_4(aq) + 3hematite + 12H^+ \rightarrow CO(aq) + 6Fe^{+2} + 8H_2O$	6	1.62E-08	1.99E-01	-5.38E-09	-5.38E-01	-9.83E-11	-9.83E-11	6.91E-12	6.96E-12
964	$CH_4(aq) + 4hematite + 16H^+ \rightarrow CO_2(aq) + 8Fe^{+2} + 10H_2O$	8	3.02E-08		5.34E-09		5.34E-11		1.28E-11	
965	$CH_4(aq) + 4hematite + 15H^+ \rightarrow HCO_3^- + 8Fe^{+2} + 9H_2O$	8	3.02E-08		5.34E-09		5.34E-11		1.28E-11	
966	$CO(aq) + hematite + 4H^+ \rightarrow CO_2(aq) + 2Fe^{+2} + 2H_2O$	2	1.02E-11	1.40E-11	3.13E-09	3.13E-09	1.43E-09	1.43E-09	3.94E-12	3.94E-12
967	$CO(aq) + hematite + 3H^+ \rightarrow HCO_3^- + 2Fe^{+2} + H_2O$	2	1.02E-11	1.40E-11	3.13E-09	3.13E-09	1.43E-09	1.43E-09	3.94E-12	3.94E-12
968	$4H^+ + hematite \rightarrow 2Fe^{+2} + 1/2O_2(aq) + 2H_2O$	2	-1.25E-05	-1.13E-01	-1.52E-05	-1.34E-01	-1.52E-05		-1.46E-11	

969	$H_2(aq) + 3hematite \rightarrow 2magnetite + H_2O$	2	5.71E-08		2.05E-10		8.75E-11		-1.50E-13	
970	$2NH_4^+ + 9hematite \rightarrow 6magnetite + N_2(aq) + 2H^+ + 3H_2O$	6	-6.50E-06		-4.56E-08		-6.73E-08		-1.30E-09	
971	$2NH_4^+ + 12hematite \rightarrow 8magnetite + N_2O(aq) + 2H^+ + 3H_2O$	8	-8.52E-05	-8.53E-01	-5.03E-07	-4.54E-01	-6.52E-07	-5.88E-01	-7.53E-09	-6.85E-09
972	$2NH_4^+ + 15hematite \rightarrow 10magnetite + 2NO(aq) + 2H^+ + 3H_2O$	10	-1.52E-04	-1.36E-01	-9.22E-07	-8.24E-01	-1.20E-06	-1.69E-01	-1.33E-08	-1.20E-01
973	$NH_4^+ + 9hematite \rightarrow 6magnetite + NO_2^- + 2H^+ + H_2O$	6	-1.83E-04		-1.06E-06		-1.38E-06		-1.47E-08	
974	$NH_4^+ + 12hematite \rightarrow 8magnetite + NO_3^- + 2H^+ + H_2O$	8	-2.54E-04		-1.47E-06		-1.93E-06		-2.12E-08	
975	$N_2(aq) + 3hematite \rightarrow 2magnetite + N_2O(aq)$	2	-9.23E-07	-9.23E-01	-4.40E-06	-3.93E-01	-4.32E-05	-3.85E-01	-4.07E-05	-3.62E-01
976	$N_2(aq) + 6hematite \rightarrow 4magnetite + 2NO(aq)$	4	-1.70E-06	-1.52E-01	-8.43E-06	-7.49E-01	-8.35E-05	-7.41E-01	-7.85E-05	-6.96E-01
977	$N_2(aq) + 9hematite + H_2O \rightarrow 6magnetite + 2NO_2^- + 2H^+$	6	-2.07E-06		-9.76E-06		-9.68E-05		-8.72E-05	
978	$N_2(aq) + 15hematite + H_2O \rightarrow 10magnetite + 2NO_3^- + 2H^+$	10	-2.90E-06		-1.37E-05		-1.38E-04		-1.30E-04	
979	$N_2O(aq) + 3hematite \rightarrow 2magnetite + 2NO(aq)$	2	-3.65E-06	-2.77E-01	-7.18E-08	-4.93E-01	-7.18E-08	-4.92E-01	-7.17E-08	-4.96E-01
980	$N_2O(aq) + 6hematite + H_2O \rightarrow 4magnetite + 2NO_2^- + 2H^+$	4	-5.37E-06	-5.37E-01	-9.29E-08	-8.54E-01	-9.29E-08	-8.54E-01	-8.64E-08	-7.88E-01
981	$N_2O(aq) + 12hematite + H_2O \rightarrow 8magnetite + 2NO_3^- + 2H^+$	8	-9.21E-06	-9.21E-01	-1.56E-07	-1.49E-01	-1.59E-07	-1.51E-01	-1.59E-07	-1.51E-01
982	$2NO(aq) + 3hematite + H_2O \rightarrow 2magnetite + 2NO_2^- + 2H^+$	2	-2.21E-08	-1.46E-01	-1.81E-08	-1.57E-01	-1.81E-08	-1.55E-01	-1.49E-08	-7.32E-09
983	$2NO(aq) + 9hematite + H_2O \rightarrow 6magnetite + 2NO_3^- + 2H^+$	6	-5.48E-08	-4.73E-01	-4.98E-08	-4.23E-01	-5.09E-08	-4.34E-01	-5.11E-08	-4.35E-01
984	$NO_2^- + 3hematite \rightarrow 2magnetite + NO_3^-$	2	-7.76E-07		-4.60E-08		-4.96E-08		-3.62E-11	

985	$2H_2S(aq) + 2hematite \rightarrow pyrite + magnetite + 2H_2O$	2	-2.43E-09	5.75E-09	4.31E-06	8.78E-01	1.11E-09		2.05E-10	
986	$H_2S(aq) + 3hematite \rightarrow 2magnetite + sulfur + H_2O$	2	-1.43E-08	-6.81E-09	-7.58E-06	-3.18E-01	-1.97E-09		-5.05E-10	
987	$2H_2S(aq) + 12hematite \rightarrow 8magnetite + S_2O_3^{-2} + 2H^+ + H_2O$	8	-1.81E-08	-6.82E-09	-8.52E-06	-2.96E-01	-2.21E-09	-1.23E-09	-6.02E-10	-3.77E-01
988	$H_2S(aq) + 12hematite \rightarrow 8magnetite + SO_4^{-2} + 2H^+$	8	-2.28E-08	-1.53E-01	-8.11E-06	-3.64E-01	-2.28E-09		-7.61E-10	
989	$pyrite + 3hematite + 2H^+ \rightarrow 2magnetite + 2sulfur + Fe^{+2} + H_2O$	2	-1.91E-08		-2.25E-08		-2.25E-08		0.00E+00	
990	$pyrite + 9hematite \rightarrow 6magnetite + Fe^{+2} + S_2O_3^{-2}$	6	-2.67E-08	-1.91E-01	-2.44E-08	-1.69E-01	-2.44E-08	-1.68E-01	0.00E+00	
991	$pyrite + 21hematite + H_2O \rightarrow 14magnetite + Fe^{+2} + 2SO_4^{-2} + 2H^+$	14	-3.60E-08		-2.36E-08		-2.49E-08		0.00E+00	
992	$2sulfur + 6hematite + H_2O \rightarrow 4magnetite + S_2O_3^{-2} + 2H^+$	4	0.00E+00		0.00E+00		0.00E+00		0.00E+00	
993	$sulfur + 9hematite + H_2O \rightarrow 6magnetite + SO_4^{-2} + 2H^+$	6	0.00E+00		0.00E+00		0.00E+00		0.00E+00	
994	$S_2O_3^{-2} + 12hematite + H_2O \rightarrow 8magnetite + 2SO_4^{-2} + 2H^+$	8	-1.69E-08	-9.40E-09	-6.68E-09	8.17E-01	-8.09E-09	-5.85E-01	-1.29E-08	-5.31E-09
995	$CH_4(aq) + 9hematite \rightarrow 6magnetite + CO(aq) + 2H_2O$	6	-1.17E-08	-7.93E-09	-1.10E-08	-1.96E-01	-1.80E-10	-1.80E-01	-4.52E-12	-4.52E-12
996	$CH_4(aq) + 12hematite \rightarrow 8magnetite + CO_2(aq) + 2H_2O$	8	-7.01E-09		-2.10E-09		-5.51E-11		-2.43E-12	
997	$CH_4(aq) + 12hematite \rightarrow 8magnetite + HCO_3^- + H^+ + H_2O$	8	-7.01E-09		-2.10E-09		-5.51E-11		-2.43E-12	
998	$CO(aq) + 3hematite \rightarrow 2magnetite + CO_2(aq)$	2	9.24E-13	4.67E-12	2.59E-09	2.59E-09	1.18E-09	1.18E-01	1.40E-12	1.40E-12
999	$CO(aq) + 3hematite + H_2O \rightarrow 2magnetite + HCO_3^- + H^+$	2	9.24E-13	4.67E-12	2.59E-09	2.59E-09	1.18E-09	1.18E-09	1.40E-12	1.40E-12

1000	3hematite → 2magnetite + $1/2O_2$(aq)	2	-5.15E-06	-4.75E-01	-5.32E-06	-4.75E-01	-5.32E-06		-6.57E-12	
Maghemite as an electron acceptor										
1001	H_2(aq) + maghemite + $4H^+$ → $2Fe^{+2}$ + $3H_2O$	2	1.87E-07		6.67E-10		3.20E-10		6.17E-12	
1002	$2NH_4^+$ + 3maghemite + $10H^+$ → $6Fe^{+2}$ + N_2(aq) + $9H_2O$	6	3.34E-05		6.37E-08		7.51E-08		2.99E-09	
1003	$2NH_4^+$ + 4maghemite + $14H^+$ → $8Fe^{+2}$ + N_2O(aq) + $11H_2O$	8	-3.20E-05	-3.22E-01	-3.57E-07	-3.83E-01	-4.62E-07	-3.98E-01	-1.82E-09	-1.13E-09
1004	$2NH_4^+$ + 5maghemite + $18H^+$ → $10Fe^{+2}$ + 2NO(aq) + $13H_2O$	10	-8.54E-05	-6.93E-01	-7.39E-07	-6.42E-01	-9.59E-07	-8.32E-01	-6.20E-09	-4.83E-09
1005	NH_4^+ + 3maghemite + $10H^+$ → $6Fe^{+2}$ + NO_2^- + $7H_2O$	6	-1.03E-04		-8.41E-07		-1.09E-06		-6.09E-09	
1006	NH_4^+ + 4maghemite + $14H^+$ → $8Fe^{+2}$ + NO_3^- + $9H_2O$	8	-1.47E-04		-1.18E-06		-1.55E-06		-9.79E-09	
1007	N_2(aq) + maghemite + $4H^+$ → $2Fe^{+2}$ + N_2O(aq) + $2H_2O$	2	-7.67E-07	-7.67E-01	-4.05E-06	-3.59E-01	-3.97E-05	-3.60E-01	-3.14E-05	-2.69E-01
1008	N_2(aq) + 2maghemite + $8H^+$ → $4Fe^{+2}$ + 2NO(aq) + $4H_2O$	4	-1.39E-06	-1.23E-01	-7.73E-06	-6.79E-01	-7.65E-05	-6.79E-01	-5.99E-05	-5.98E-01
1009	N_2(aq) + 3maghemite + $10H^+$ → $6Fe^{+2}$ + $2NO_2^-$ + $5H_2O$	6	-1.60E-06		-8.71E-06		-8.62E-05		-5.92E-05	
1010	N_2(aq) + 5maghemite + $18H^+$ → $10Fe^{+2}$ + $2NO_3^-$ + $9H_2O$	10	-2.12E-06		-1.20E-05		-1.20E-04		-8.33E-05	
1011	N_2O(aq) + maghemite + $4H^+$ → $2Fe^{+2}$ + 2NO(aq) + $2H_2O$	2	-2.92E-06	-2.39E-01	-6.62E-08	-4.37E-01	-6.62E-08	-4.36E-01	-5.59E-08	-3.33E-01
1012	N_2O(aq) + 2maghemite + $6H^+$ → $4Fe^{+2}$ + $2NO_2^-$ + $3H_2O$	4	-3.91E-06	-4.00E-01	-8.17E-08	-7.42E-01	-8.17E-08	-7.42E-01	-5.48E-08	-4.72E-01
1013	N_2O(aq) + 4maghemite + $14H^+$ → $8Fe^{+2}$ + $2NO_3^-$ + $7H_2O$	8	-6.30E-06	-6.33E-01	-1.34E-07	-1.26E-01	-1.36E-07	-1.29E-01	-9.56E-08	-8.86E-01
1014	2NO(aq) + maghemite + $2H^+$ → $2Fe^{+2}$ + $2NO_2^-$ + H_2O	2	-1.59E-08	-8.40E-09	-1.53E-08	-7.77E-09	-1.53E-08	-7.75E-09	-6.98E-09	5.79E-01

1015	$2NO(aq) + 3maghemite + 10H^+ \rightarrow 6Fe^{+2} + 2NO_3^- + 5H_2O$	6	-3.63E-08	-2.88E-01	-4.14E-08	-3.39E-01	-4.25E-08	-3.50E-01	-2.74E-08	-1.98E-01
1016	$NO_2^- + maghemite + 4H^+ \rightarrow 2Fe^{+2} + NO_3^- + 2H_2O$	2	-4.82E-07		-3.79E-08		-4.11E-08		-2.04E-11	
1017	$2H_2S(aq) + maghemite + 2H^+ \rightarrow pyrite + Fe^{+2} + 3H_2O$	2	1.44E-09	8.94E-09	6.48E-06	1.95E-01	1.67E-09		4.87E-10	
1018	$H_2S(aq) + maghemite + 4H^+ \rightarrow 2Fe^{+2} + sulfur + 3H_2O$	2	-1.93E-09	5.57E-09	-1.98E-06	2.49E-01	-5.17E-10		4.40E-10	
1019	$2H_2S(aq) + 4maghemite + 14H^+ \rightarrow 8Fe^{+2} + S_2O_3^{-2} + 9H_2O$	8	6.69E-09	1.79E-01	2.67E-06	1.90E-01	6.95E-10	1.67E-09	1.29E-09	1.51E-09
1020	$H_2S(aq) + 4maghemite + 14H^+ \rightarrow 8Fe^{+2} + SO_4^{-2} + 8H_2O$	8	2.68E-08	3.43E-01	1.43E-05	1.87E-01	3.52E-09		3.02E-09	
1021	$pyrite + maghemite + 6H^+ \rightarrow 3Fe^{+2} + 2sulfur + 3H_2O$	2	-6.75E-09		-1.69E-08		-1.69E-08		0.00E+00	
1022	$pyrite + 3maghemite + 12H^+ \rightarrow 7Fe^{+2} + S_2O_3^{-2} + 6H_2O$	6	1.05E-08	1.80E-01	-7.61E-09	-1.69E-01	-7.55E-09	-4.19E-11	0.00E+00	
1023	$pyrite + 7maghemite + 26H^+ \rightarrow 15Fe^{+2} + 2SO_4^{-2} + 13H_2O$	14	5.06E-08		1.56E-08		1.43E-08		0.00E+00	
1024	$2sulfur + 2maghemite + 6H^+ \rightarrow 4Fe^{+2} + S_2O_3^{-2} + 3H_2O$	4	0.00E+00		0.00E+00		0.00E+00		0.00E+00	
1025	$sulfur + 3maghemite + 10H^+ \rightarrow 6Fe^{+2} + SO_4^{-2} + 5H_2O$	6	0.00E+00		0.00E+00		0.00E+00		0.00E+00	
1026	$S_2O_3^{-2} + 4maghemite + 14H^+ \rightarrow 8Fe^{+2} + 2SO_4^{-2} + 7H_2O$	8	3.26E-08	4.12E-01	1.57E-08	2.32E-01	1.43E-08	2.18E-01	5.03E-08	5.78E-01
1027	$CH_4(aq) + 3maghemite + 12H^+ \rightarrow CO(aq) + 6Fe^{+2} + 8H_2O$	6	2.55E-08	2.92E-01	1.50E-09	1.51E-09	1.85E-12	1.85E-12	9.69E-12	9.69E-12
1028	$CH_4(aq) + 4maghemite + 16H^+ \rightarrow CO_2(aq) + 8Fe^{+2} + 10H_2O$	8	4.25E-08		1.45E-08		1.87E-10		1.65E-11	
1029	$CH_4(aq) + 4maghemite + 15H^+ \rightarrow HCO_3^- +$	8	4.25E-08		1.45E-08		1.87E-10		1.65E-11	

	$8Fe^{+2} + 9H_2O$									
1030	$CO(aq) + maghemite + 4H^+ \rightarrow CO_2(aq) + 2Fe^{+2} + 2H_2O$	2	1.33E-11	1.76E-11	3.80E-09	3.85E-09	1.75E-09	1.75E-09	4.56E-12	4.56E-12
1031	$CO(aq) + maghemite + 3H^+ \rightarrow HCO_3^- + 2Fe^{+2} + H_2O$	2	1.33E-11	1.76E-11	3.80E-09	3.85E-09	1.75E-09	1.75E-09	4.56E-12	4.56E-12
1032	$4H^+ + maghemite \rightarrow 2Fe^{+2} + 1/2O_2(aq) + 2H_2O$	2	-1.15E-05	-1.27E-01	-1.42E-05	-1.25E-01	-1.42E-05		-1.34E-11	
1033	$H_2(aq) + 3maghemite \rightarrow 2magnetite + H_2O$	2	1.54E-07		9.70E-10		4.73E-10		3.56E-12	
1034	$2NH_4^+ + 9maghemite \rightarrow 6magnetite + N_2(aq) + 2H^+ + 3H_2O$	6	2.34E-05		1.36E-07		1.68E-07		1.22E-09	
1035	$2NH_4^+ + 12maghemite \rightarrow 8magnetite + N_2O(aq) + 2H^+ + 3H_2O$	8	-4.54E-05	-4.54E-01	-2.61E-07	-2.12E-01	-3.37E-07	-2.74E-01	-4.18E-09	-3.50E-09
1036	$2NH_4^+ + 15maghemite \rightarrow 10magnetite + 2NO(aq) + 2H^+ + 3H_2O$	10	-1.02E-04	-8.60E-01	-6.20E-07	-5.22E-01	-8.03E-07	-6.77E-01	-9.15E-09	-7.79E-09
1037	$NH_4^+ + 9maghemite \rightarrow 6magnetite + NO_2^- + 2H^+ + H_2O$	6	-1.23E-04		-6.97E-07		-9.04E-07		-9.63E-09	
1038	$NH_4^+ + 12maghemite \rightarrow 8magnetite + NO_3^- + 2H^+ + H_2O$	8	-1.74E-04		-9.89E-07		-1.30E-06		-1.45E-08	
1039	$N_2(aq) + 3maghemite \rightarrow 2magnetite + N_2O(aq)$	2	-8.06E-07	-8.60E-01	-3.82E-06	-3.35E-01	-3.74E-05	-3.28E-01	-3.52E-05	-3.74E-01
1040	$N_2(aq) + 6maghemite \rightarrow 4magnetite + 2NO(aq)$	4	-1.47E-06	-1.28E-01	-7.27E-06	-6.33E-01	-7.19E-05	-6.25E-01	-6.76E-05	-5.87E-01
1041	$N_2(aq) + 9maghemite + H_2O \rightarrow 6magnetite + 2NO_2^- + 2H^+$	6	-1.72E-06		-8.01E-06		-7.93E-05		-7.08E-05	
1042	$N_2(aq) + 15maghemite + H_2O \rightarrow 10magnetite + 2NO_3^- + 2H^+$	10	-2.31E-06		-1.08E-05		-1.09E-04		-1.03E-04	
1043	$N_2O(aq) + 3maghemite \rightarrow 2magnetite + 2NO(aq)$	2	-3.10E-06	-2.22E-01	-6.25E-08	-4.25E-01	-6.25E-08	-4.00E-01	-6.25E-08	-3.98E-01

1044	$N_2O(aq) + 6maghemite + H_2O \rightarrow 4magnetite + 2NO_2^- + 2H^+$	4	-4.27E-06	-4.27E-01	-7.44E-08	-6.69E-01	-7.43E-08	-6.68E-01	-6.78E-08	-6.27E-01
1045	$N_2O(aq) + 12maghemite + H_2O \rightarrow 8magnetite + 2NO_3^- + 2H^+$	8	-7.03E-06	-7.34E-01	-1.19E-07	-1.12E-01	-1.21E-07	-1.14E-01	-1.22E-07	-1.14E-01
1046	$2NO(aq) + 3maghemite + H_2O \rightarrow 2magnetite + 2NO_2^- + 2H^+$	2	-1.75E-08	-9.95E-09	-1.34E-08	-5.94E-09	-1.34E-08	-5.92E-09	-1.02E-08	-2.68E-09
1047	$2NO(aq) + 9maghemite + H_2O \rightarrow 6magnetite + 2NO_3^- + 2H^+$	6	-4.09E-08	-3.34E-01	-3.59E-08	-2.84E-01	-3.70E-08	-2.95E-01	-3.72E-08	-2.96E-01
1048	$NO_2^- + 3maghemite + \rightarrow 2magnetite + NO_3^-$	2	-5.56E-07		-3.25E-08		-3.56E-08		-2.69E-11	
1049	$2H_2S(aq) + 2maghemite \rightarrow pyrite + magnetite + 2H_2O$	2	6.64E-10	8.16E-09	7.40E-06	1.19E-01	1.91E-09		3.90E-10	
1050	$H_2S(aq) + 3maghemite \rightarrow 2magnetite + sulfur + H_2O$	2	-5.04E-09	2.46E-09	1.69E-06	6.17E-01	4.33E-10		4.95E-11	
1051	$2H_2S(aq) + 12maghemite \rightarrow 8magnetite + S_2O_3^{-2} + 2H^+ + H_2O$	8	4.71E-10	1.17E-01	1.00E-05	1.83E-01	2.60E-09	3.57E-09	5.06E-10	7.32E-01
1052	$H_2S(aq) + 12maghemite \rightarrow 8magnetite + SO_4^{-2} + 2H^+$	8	1.43E-08	2.18E-01	2.90E-05	3.35E-01	7.32E-09		1.45E-09	
1053	$pyrite + 3maghemite + 2H^+ \rightarrow 2magnetite + 2sulfur + Fe^{+2} + H_2O$	2	-9.85E-09		-1.32E-08		-1.32E-08		0.00E+00	
1054	$pyrite + 9maghemite \rightarrow 6magnetite + Fe^{+2} + S_2O_3^{-2}$	6	1.17E-09	8.67E-09	3.42E-09	1.92E-01	3.46E-09	1.98E-01	0.00E+00	
1055	$pyrite + 21maghemite + H_2O \rightarrow 14magnetite + Fe^{+2} + 2SO_4^{-2} + 2H^+$	14	2.89E-08		4.13E-08		4.00E-08		0.00E+00	
1056	$2sulfur + 6maghemite + H_2O \rightarrow 4magnetite + S_2O_3^{-2} + 2H^+$	4	0.00E+00		0.00E+00		0.00E+00		0.00E+00	
1057	$sulfur + 9maghemite + H_2O \rightarrow 6magnetite +$	6	0.00E+00		0.00E+00		0.00E+00		0.00E+00	

	$SO_4^{-2} + 2H^+$									
1058	$S_2O_3^{-2}$ + 12maghemite + H_2O → 8magnetite + $2SO_4^{-2} + 2H^+$	8	2.02E-08	2.77E-01	3.04E-08	3.79E-01	2.90E-08	3.65E-01	2.42E-08	3.17E-01
1059	CH_4(aq) + 9maghemite → 6magnetite + CO(aq) + $2H_2O$	6	1.61E-08	1.99E-01	9.69E-09	9.69E-09	1.21E-10	1.28E-01	3.81E-12	3.81E-12
1060	CH_4(aq) + 12maghemite → 8magnetite + CO_2(aq) + $2H_2O$	8	3.01E-08		2.54E-08		3.45E-10		8.69E-12	
1061	CH_4(aq) + 12maghemite → 8magnetite + HCO_3^- + H^+ + H_2O	8	3.01E-08		2.54E-08		3.45E-10		8.69E-12	
1062	CO(aq) + 3maghemite → 2magnetite + CO_2(aq)	2	1.02E-11	1.39E-11	4.60E-09	4.63E-09	2.12E-09	2.12E-09	3.25E-12	3.26E-12
1063	CO(aq) + 3maghemite + H_2O → 2magnetite + HCO_3^- + H^+	2	1.02E-11	1.39E-11	4.60E-09	4.63E-09	2.12E-09	2.12E-09	3.25E-12	3.25E-12
1064	3maghemite → 2magnetite + $1/2O_2$(aq)	2	-4.16E-06	-3.76E-01	-4.33E-06	-3.76E-01	-4.33E-06		-5.33E-12	
Goethite as an electron acceptor										
1065	$1/2H_2$(aq) + goethite + $2H^+$ → Fe^{+2} + $2H_2O$	1	1.54E-07		4.03E-10		1.88E-10		4.90E-12	
1066	$2NH_4^+$ + 6goethite + $10H^+$ → $6Fe^{+2}$ + N_2(aq) + $12H_2O$	6	2.33E-05		1.34E-09		-6.02E-09		2.13E-09	
1067	$2NH_4^+$ + 8goethite + $14H^+$ → $8Fe^{+2}$ + N_2O(aq) + $15H_2O$	8	-4.55E-05	-4.55E-01	-4.40E-07	-3.92E-01	-5.70E-07	-5.63E-01	-2.96E-09	-2.28E-01
1068	NH_4^+ + 5goethite + $9H^+$ → $5Fe^{+2}$ + NO(aq) + $9H_2O$	5	-1.02E-04	-8.62E-01	-8.44E-07	-7.46E-01	-1.09E-06	-9.67E-01	-7.63E-09	-6.27E-09
1069	NH_4^+ + 6goethite + $10H^+$ → $6Fe^{+2}$ + NO_2^- + $10H_2O$	6	-1.24E-04		-9.66E-07		-1.25E-06		-7.81E-09	
1070	NH_4^+ + 8goethite + $14H^+$ → $8Fe^{+2}$ + NO_3^- + $13H_2O$	8	-1.74E-04		-1.35E-06		-1.77E-06		-1.21E-08	
1071	N_2(aq) + 2goethite + $4H^+$ → $2Fe^{+2}$ +	2	-8.06E-07	-8.64E-01	-4.25E-06	-3.79E-01	-4.17E-05	-3.71E-01	-3.32E-05	-2.88E-01

	$N_2O(aq) + 3H_2O$									
1072	$N_2(aq) + 4goethite + 8H^+ \rightarrow 4Fe^{+2} + 2NO(aq) + 6H_2O$	4	-1.47E-06	-1.28E-01	-8.13E-06	-7.19E-01	-8.05E-05	-7.18E-01	-6.36E-05	-5.47E-01
1073	$N_2(aq) + 6goethite + 10H^+ \rightarrow 6Fe^{+2} + 2NO_2^- + 8H_2O$	6	-1.72E-06		-9.31E-06		-9.22E-05		-6.48E-05	
1074	$N_2(aq) + 10goethite + 18H^+ \rightarrow 10Fe^{+2} + 2NO_3^- + 14H_2O$	10	-2.31E-06		-1.30E-05		-1.30E-04		-9.26E-05	
1075	$N_2O(aq) + 2goethite + 4H^+ \rightarrow 2Fe^{+2} + 2NO(aq) + 3H_2O$	2	-3.11E-06	-2.22E-01	-6.94E-08	-4.69E-01	-6.94E-08	-4.68E-01	-5.91E-08	-3.64E-01
1076	$N_2O(aq) + 4goethite + 6H^+ \rightarrow 4Fe^{+2} + 2NO_2^- + 5H_2O$	4	-4.28E-06	-4.28E-01	-8.81E-08	-8.62E-01	-8.81E-08	-8.55E-01	-6.11E-08	-5.36E-01
1077	$N_2O(aq) + 8goethite + 14H^+ \rightarrow 8Fe^{+2} + 2NO_3^- + 11H_2O$	8	-7.04E-06	-7.43E-01	-1.47E-07	-1.39E-01	-1.49E-07	-1.41E-01	-1.08E-07	-1.72E-01
1078	$NO(aq) + goethite + H^+ \rightarrow Fe^{+2} + NO_2^- + H_2O$	1	-1.75E-08	-9.97E-09	-1.69E-08	-9.37E-09	-1.69E-08	-9.35E-09	-8.56E-09	-1.39E-09
1079	$NO(aq) + 3goethite + 5H^+ \rightarrow 3Fe^{+2} + NO_3^- + 4H_2O$	3	-4.10E-08	-3.35E-01	-4.62E-08	-3.87E-01	-4.73E-08	-3.98E-01	-3.21E-08	-2.46E-01
1080	$NO_2^- + 2goethite + 4H^+ \rightarrow 2Fe^{+2} + NO_3^- + 3H_2O$	2	-5.57E-07		-4.25E-08		-4.59E-08		-2.36E-11	
1081	$2H_2S(aq) + 2goethite + 2H^+ \rightarrow Fe^{+2} + pyrite + 4H_2O$	2	-1.32E-10	7.37E-09	4.88E-06	9.35E-01	1.26E-09		3.93E-10	
1082	$H_2S(aq) + 2goethite + 4H^+ \rightarrow 2Fe^{+2} + sulfur + 4H_2O$	2	-5.08E-09	2.42E-09	-5.18E-06	-7.58E-01	-1.34E-09		2.50E-10	
1083	$2H_2S(aq) + 8goethite + 14H^+ \rightarrow 8Fe^{+2} + S_2O_3^{-2} + 13H_2O$	8	3.94E-10	1.16E-01	-3.71E-06	4.59E-01	-9.58E-10	1.42E-11	9.08E-10	1.13E-01
1084	$H_2S(aq) + 8goethite + 14H^+ \rightarrow 8Fe^{+2} + SO_4^{-2} + 12H_2O$	8	1.42E-08	2.17E-01	1.50E-06	5.97E-01	2.15E-10		2.26E-09	
1085	$pyrite + 2goethite + 6H^+ \rightarrow 3Fe^{+2} + 2sulfur + 4H_2O$	2	-9.89E-09		-2.01E-08		-2.01E-08		0.00E+00	

1086	pyrite + 6goethite + $12H^+ \rightarrow 7Fe^{+2} + S_2O_3^{-2} + 9H_2O$	6	1.05E-09	8.55E-01	-1.72E-08	-9.69E-09	-1.71E-08	-9.61E-09	0.00E+00	
1087	pyrite + 14goethite + $26H^+ \rightarrow 2SO_4^{-2} + 15Fe^{+2} + 20H_2O$	14	2.86E-08		-6.76E-09		-8.06E-09		0.00E+00	
1088	2sulfur + 4goethite + $6H^+ \rightarrow 4Fe^{+2} + S_2O_3^{-2} + 5H_2O$	4	0.00E+00		0.00E+00		0.00E+00		0.00E+00	
1089	sulfur + 6goethite + $10H^+ \rightarrow 6Fe^{+2} + SO_4^{-2} + 8H_2O$	6	0.00E+00		0.00E+00		0.00E+00		0.00E+00	
1090	$S_2O_3^{-2}$ + 8goethite + $14H^+ \rightarrow 8Fe^{+2} + 2SO_4^{-2} + 11H_2O$	8	2.00E-08	2.75E-01	2.93E-09	1.43E-01	1.55E-09	9.68E-01	3.76E-08	4.52E-01
1091	CH_4(aq) + 6goethite + $12H^+ \rightarrow$ CO(aq) + $6Fe^{+2} + 11H_2O$	6	1.60E-08	1.98E-01	-5.61E-09	-5.68E-09	-1.02E-10	-1.15E-01	6.84E-12	6.84E-12
1092	CH_4(aq) + 8goethite + $16H^+ \rightarrow CO_2$(aq) + $8Fe^{+2} + 14H_2O$	8	2.99E-08		5.03E-09		4.91E-11		1.27E-11	
1093	CH_4(aq) + 8goethite + $15H^+ \rightarrow HCO_3^- + 8Fe^{+2} + 13H_2O$	8	2.99E-08		5.03E-09		4.91E-11		1.27E-11	
1094	CO(aq) + 2goethite + $4H^+ \rightarrow CO_2$(aq) + $2Fe^{+2} + 3H_2O$	2	1.02E-11	1.40E-11	3.11E-09	3.11E-01	1.42E-09	1.42E-09	3.92E-12	3.92E-12
1095	CO(aq) + 2goethite + $3H^+ \rightarrow HCO_3^- + 2Fe^{+2} + 2H_2O$	2	1.02E-11	1.40E-11	3.11E-09	3.11E-09	1.42E-09	1.42E-09	3.92E-12	3.92E-12
1096	$2H^+$ + goethite $\rightarrow Fe^{+2} + 1/4O_2$(aq)+ $3/2H_2O$	1	-6.24E-06	-5.65E-01	-7.60E-06	-6.74E-01	-7.60E-06		-7.33E-12	
1097	H_2(aq) + 6goethite $\rightarrow$ 2magnetite + $4H_2O$	2	5.54E-08		1.80E-10		7.50E-11		-2.41E-13	
1098	$2NH_4^+$ + 18goethtite $\rightarrow$ 6magnetite + N_2(aq) + $2H^+ + 12H_2O$	6	-7.04E-06		-5.16E-08		-7.49E-08		-1.36E-09	
1099	$2NH_4^+$ + 24goethtite $\rightarrow$ 8magnetite + N_2O(aq) + $2H^+ + 15H_2O$	8	-8.59E-05	-8.59E-01	-5.11E-07	-4.62E-01	-6.62E-07	-5.98E-01	-7.62E-09	-6.93E-09
1100	NH_4^+ + 15goethtite $\rightarrow$ 5magnetite + NO(aq) + $H^+ + 9H_2O$	5	-1.53E-04	-1.37E-01	-9.32E-07	-8.34E-01	-1.21E-06	-1.82E-01	-1.34E-08	-1.28E-01
1101	NH_4^+ + 18goethite $\rightarrow$ 6magnetite + NO_2^- +	6	-1.84E-04		-1.07E-06		-1.39E-06		-1.48E-08	

	$2H^+ + 10H_2O$									
1102	NH_4^+ + 24goethite → 8magnetite + NO_3^- + $2H^+ + 13H_2O$	8	-2.55E-04		-1.49E-06		-1.95E-06		-2.14E-08	
1103	N_2(aq) + 6goethite → 2magnetite + N_2O(aq) + $3H_2O$	2	-9.25E-07	-9.25E-01	-4.42E-06	-3.96E-01	-4.34E-05	-3.87E-01	-4.08E-05	-3.63E-01
1104	N_2(aq) + 12goethite → 4magnetite + 2NO(aq) + $6H_2O$	4	-1.71E-06	-1.52E-01	-8.47E-06	-7.53E-01	-8.39E-05	-7.45E-01	-7.88E-05	-6.99E-01
1105	N_2(aq) + 18goethite → 6magnetite + $2NO_2^-$ + $2H^+ + 8H_2O$	6	-2.08E-06		-9.82E-06		-9.73E-05		-8.76E-05	
1106	N_2(aq) + 30goethite → 10magnetite + $2NO_3^-$ + $2H^+ + 14H_2O$	10	-2.91E-06		-1.38E-05		-1.39E-04		-1.31E-04	
1107	N_2O(aq) + 6goethite → 2magnetite + 2NO(aq) + $3H_2O$	2	-3.66E-06	-2.78E-01	-7.21E-08	-4.96E-01	-7.21E-08	-4.95E-01	-7.20E-08	-4.93E-01
1108	N_2O(aq) + 12goethite → 4magnetite + $2NO_2^-$ + $2H^+ + 5H_2O$	4	-5.38E-06	-5.38E-01	-9.35E-08	-8.63E-01	-9.35E-08	-8.60E-01	-8.68E-08	-7.93E-01
1109	N_2O(aq) + 24goethite → 8magnetite + $2NO_3^-$ + $2H^+ + 11H_2O$	8	-9.25E-06	-9.25E-01	-1.58E-07	-1.55E-01	-1.60E-07	-1.52E-01	-1.60E-07	-1.52E-01
1110	NO(aq) + 3goethite → magnetite + NO_2^- + $H_2O + H^+$	1	-2.22E-08	-1.47E-01	-1.82E-08	-1.73E-01	-1.82E-08	-1.73E-01	-1.50E-08	-7.43E-09
1111	NO(aq) + 9goethite → 3magnetite + NO_3^- + $4H_2O + H^+$	3	-5.51E-08	-4.76E-01	-5.02E-08	-4.27E-01	-5.13E-08	-4.38E-01	-5.14E-08	-4.39E-01
1112	NO_2^- + 6goethite → 2magnetite + NO_3^- + $3H_2O$	2	-7.80E-07		-4.64E-08		-5.00E-08		-3.64E-11	
1113	$2H_2S$(aq) + 4goethite → pyrite + magnetite + $4H_2O$	2	-2.48E-09	5.18E-09	4.20E-06	8.68E-01	1.08E-09		2.00E-10	
1114	H_2S(aq) + 6goethite → 2magnetite + sulfur + $4H_2O$	2	-1.45E-08	-6.98E-09	-7.89E-06	-3.42E-01	-2.05E-09		-5.18E-10	
1115	$2H_2S$(aq) + 24goethite → 8magnetite + $S_2O_3^{-2}$ + $2H^+ + 13H_2O$	8	-1.84E-08	-7.16E-09	-9.13E-06	-9.99E-01	-2.36E-09	-1.39E-09	-6.30E-10	-4.37E-01

1116	$H_2S(aq) + 24goethite \rightarrow 8magnetite + SO_4^{-2} + 2H^+ + 12H_2O$	8	-2.34E-08	-1.59E-01	-9.34E-06	-4.87E-01	-2.59E-09		-8.16E-10	
1117	$pyrite + 6goethite + 2H^+ \rightarrow 2magnetite + 2sulfur + Fe^{+2} + 4H_2O$	2	-1.93E-08		-2.28E-08		-2.28E-08		0.00E+00	
1118	$pyrite + 18goethite \rightarrow 6magnetite + Fe^{+2} + S_2O_3^{-2} + 9H_2O$	6	-2.72E-08	-1.97E-01	-2.53E-08	-1.78E-01	-2.53E-08	-1.77E-01	0.00E+00	
1119	$pyrite + 42goethite \rightarrow 14magnetite + Fe^{+2} + 2SO_4^{-2} + 2H^+ + 20H_2O$	14	-3.72E-08		-2.57E-08		-2.70E-08		0.00E+00	
1120	$2sulfur + 12goethite \rightarrow 4mganetite + S_2O_3^{-2} + 2H^+ + 5H_2O$	4	0.00E+00		0.00E+00		0.00E+00		0.00E+00	
1121	$sulfur + 18goethite \rightarrow 6magnetite + SO_4^{-2} + 2H^+ + 8H_2O$	6	0.00E+00		0.00E+00		0.00E+00		0.00E+00	
1122	$S_2O_3^{-2} + 24goethite \rightarrow 8mganetite + 2SO_4^{-2} + 2H^+ + 11H_2O$	8	-1.76E-08	-1.69E-01	-7.91E-09	-4.17E-01	-9.29E-09	-1.78E-09	-1.38E-08	-6.23E-09
1123	$CH_4(aq) + 18goethite \rightarrow 6magnetite + CO(aq) + 11H_2O$	6	-1.22E-08	-8.43E-09	-1.16E-08	-1.16E-01	-1.89E-10	-1.89E-01	-4.73E-12	-4.73E-12
1124	$CH_4(aq) + 24goethite \rightarrow 8magnetite + CO_2(aq) + 14H_2O$	8	-7.68E-09		-3.01E-09		-6.80E-11		-2.70E-12	
1125	$CH_4(aq) + 24goethite \rightarrow 8magnetite + H^+ + HCO_3^- + 13H_2O$	8	-7.68E-09		-3.01E-09		-6.80E-11		-2.70E-12	
1126	$CO(aq) + 6goethite \rightarrow 2magnetite + CO_2(aq) + 3H_2O$	2	7.58E-13	4.58E-12	2.52E-09	2.52E-09	1.15E-09	1.15E-09	1.35E-12	1.35E-12
1127	$CO(aq) + 6goethite \rightarrow 2magnetite + HCO_3^- + H^+ + 2H_2O$	2	7.58E-13	4.58E-12	2.52E-09	2.52E-09	1.15E-09	1.15E-09	1.35E-12	1.35E-12
1128	$6goethite \rightarrow 2magnetite + 1/2O_2(aq) + 3H_2O$	2	-2.59E-06	-2.38E-01	-2.68E-06	-2.39E-01	-2.68E-06		-3.30E-12	
Lepidocrocite as an electron acceptor										
1129	$1/2H_2(aq) + lepidocrocite + 2H^+ \rightarrow Fe^{+2} + 2H_2O$	1	1.94E-07		7.19E-10		3.47E-10		6.43E-12	

1130	$2NH_4^+ + 6lepidocrocite + 10H^+ \rightarrow 6Fe^{+2} + N_2(aq) + 12H_2O$	6	3.56E-05		7.62E-08		9.14E-08		3.17E-09	
1131	$2NH_4^+ + 8lepidocrocite + 14H^+ \rightarrow 8Fe^{+2} + N_2O(aq) + 15H_2O$	8	-2.91E-05	-2.97E-01	-3.41E-07	-2.92E-01	-4.40E-07	-3.76E-01	-1.58E-09	-8.94E-01
1132	$NH_4^+ + 5lepidocrocite + 9H^+ \rightarrow 5Fe^{+2} + NO(aq) + 9H_2O$	5	-8.17E-05	-6.56E-01	-7.19E-07	-6.29E-01	-9.32E-07	-8.44E-01	-5.90E-09	-4.53E-09
1133	$NH_4^+ + 6lepidocrocite + 10H^+ \rightarrow 6Fe^{+2} + NO_2^- + 10H_2O$	6	-9.90E-05		-8.16E-07		-1.06E-06		-5.73E-09	
1134	$NH_4^+ + 8lepidocrocite + 14H^+ \rightarrow 8Fe^{+2} + NO_3^- + 13H_2O$	8	-1.41E-04		-1.15E-06		-1.51E-06		-9.31E-09	
1135	$N_2(aq) + 2lepidocrocite + 4H^+ \rightarrow 2Fe^{+2} + N_2O(aq) + 3H_2O$	2	-7.58E-07	-7.58E-01	-4.01E-06	-3.55E-01	-3.93E-05	-3.47E-01	-3.10E-05	-2.65E-01
1136	$N_2(aq) + 4lepidocrocite + 8H^+ \rightarrow 4Fe^{+2} + 2NO(aq) + 6H_2O$	4	-1.38E-06	-1.19E-01	-7.65E-06	-6.79E-01	-7.57E-05	-6.63E-01	-5.91E-05	-5.20E-01
1137	$N_2(aq) + 6lepidocrocite + 10H^+ \rightarrow 6Fe^{+2} + 2NO_2^- + 8H_2O$	6	-1.58E-06		-8.58E-06		-8.50E-05		-5.80E-05	
1138	$N_2(aq) + 10lepidocrocite + 18H^+ \rightarrow 10Fe^{+2} + 2NO_3^- + 14H_2O$	10	-2.07E-06		-1.18E-05		-1.18E-04		-8.14E-05	
1139	$N_2O(aq) + 2lepidocrocite + 4H^+ \rightarrow 2Fe^{+2} + 2NO(aq) + 3H_2O$	2	-2.88E-06	-2.00E-01	-6.55E-08	-4.34E-01	-6.55E-08	-4.30E-01	-5.53E-08	-3.27E-01
1140	$N_2O(aq) + 4lepidocrocite + 6H^+ \rightarrow 4Fe^{+2} + 2NO_2^- + 5H_2O$	4	-3.83E-06	-3.83E-01	-8.05E-08	-7.29E-01	-8.04E-08	-7.29E-01	-5.35E-08	-4.59E-01
1141	$N_2O(aq) + 8lepidocrocite + 14H^+ \rightarrow 8Fe^{+2} + 2NO_3^- + 11H_2O$	8	-6.14E-06	-6.14E-01	-1.31E-07	-1.24E-01	-1.34E-07	-1.26E-01	-9.30E-08	-8.55E-01
1142	$NO(aq) + lepidocrocite + H^+ \rightarrow Fe^{+2} + NO_2^- + H_2O$	1	-1.56E-08	-8.56E-01	-1.50E-08	-7.45E-09	-1.49E-08	-7.43E-09	-6.64E-09	9.19E-01
1143	$NO(aq) + 3lepidocrocite + 5H^+$	3	-3.52E-08	-2.77E-01	-4.04E-08	-3.29E-01	-4.15E-08	-3.42E-01	-2.64E-08	-1.88E-01

	→ $3Fe^{+2}$ + NO_3^- + $4H_2O$									
1144	NO_2^- + 2lepidocrocite + $4H^+$ → $2Fe^{+2}$ + NO_3^- + $3H_2O$	2	-4.66E-07		-3.69E-08		-4.01E-08		-1.98E-11	
1145	$2H_2S$(aq) + 2lepidocrocite + $2H^+$ → Fe^{+2} + pyrite + $4H_2O$	2	1.78E-09	9.29E-01	6.80E-06	1.13E-01	1.76E-09		5.07E-10	
1146	H_2S(aq) + 2lepidocrocite + $4H^+$ → $2Fe^{+2}$ + sulfur + $4H_2O$	2	-1.25E-09	6.25E-09	-1.34E-06	3.13E-01	-3.52E-10		4.79E-10	
1147	$2H_2S$(aq) + 8lepidocrocite + $14H^+$ → $8Fe^{+2}$ + $S_2O_3^{-2}$ + $13H_2O$	8	8.06E-09	1.93E-01	3.95E-06	1.22E-01	1.03E-09	2.00E-09	1.37E-09	1.59E-09
1148	H_2S(aq) + 8lepidocrocite + $14H^+$ → $8Fe^{+2}$ + SO_4^{-2} + $12H_2O$	8	2.95E-08	3.70E-01	1.68E-05	2.13E-01	4.19E-09		3.17E-09	
1149	pyrite + 2lepidocrocite + $6H^+$ → $3Fe^{+2}$ + 2sulfur + $4H_2O$	2	-6.06E-09		-1.63E-08		-1.63E-08		0.00E+00	
1150	pyrite + 6lepidocrocite + $12H^+$ → $7Fe^{+2}$ + $S_2O_3^{-2}$ + $9H_2O$	6	1.26E-08	2.53E-01	-5.69E-09	1.82E-09	-5.62E-09	1.88E-09	0.00E+00	
1151	pyrite + 14lepidocrocite + $26H^+$ → $2SO_4^{-2}$ + $15Fe^{+2}$ + $20H_2O$	14	5.54E-08		2.01E-08		1.88E-08		0.00E+00	
1152	2sulfur + 4lepidocrocite + $6H^+$ → $4Fe^{+2}$ + $S_2O_3^{-2}$ + $5H_2O$	4	0.00E+00		0.00E+00		0.00E+00		0.00E+00	
1153	sulfur + 6lepidocrocite + $10H^+$ → $6Fe^{+2}$ + SO_4^{-2} + $8H_2O$	6	0.00E+00		0.00E+00		0.00E+00		0.00E+00	
1154	$S_2O_3^{-2}$ + 8lepidocrocite + $14H^+$ → $8Fe^{+2}$ + $2SO_4^{-2}$ + $11H_2O$	8	3.54E-08	4.29E-01	1.83E-08	2.58E-01	1.69E-08	2.44E-01	5.29E-08	6.49E-01
1155	CH_4(aq) + 6lepidocrocite + $12H^+$ → CO(aq) + $6Fe^{+2}$ + $11H_2O$	6	2.75E-08	3.13E-01	2.92E-09	2.92E-01	2.26E-11	2.26E-11	1.03E-11	1.28E-11

1156	$CH_4(aq) + 8lepidocrocite + 16H^+ \rightarrow CO_2(aq) + 8Fe^{+2} + 14H_2O$	8	4.53E-08		1.64E-08		2.15E-10		1.73E-11	
1157	$CH_4(aq) + 8lepidocrocite + 15H^+ \rightarrow HCO_3^- + 8Fe^{+2} + 13H_2O$	8	4.53E-08		1.64E-08		2.15E-10		1.73E-11	
1158	$CO(aq) + 2lepidocrocite + 4H^+ \rightarrow CO_2(aq) + 2Fe^{+2} + 3H_2O$	2	1.40E-11	1.77E-11	3.94E-09	3.94E-09	1.81E-09	1.81E-09	4.69E-12	4.69E-12
1159	$CO(aq) + 2lepidocrocite + 3H^+ \rightarrow HCO_3^- + 2Fe^{+2} + 2H_2O$	2	1.40E-11	1.77E-11	3.94E-09	3.94E-09	1.81E-09	1.81E-01	4.69E-12	4.69E-12
1160	$2H^+ + lepidocrocite \rightarrow Fe^{+2} + 1/4O_2(aq) + 3/2 H_2O$	1	-5.63E-06	-5.23E-01	-6.98E-06	-6.12E-01	-6.98E-06		-6.56E-12	
1161	$H_2(aq) + 6lepidocrocite \rightarrow 2magnetite + 4H_2O$	2	1.76E-07		1.13E-09		5.53E-10		4.35E-12	
1162	$2NH_4^+ + 18lepidocrocite \rightarrow 6magnetite + N_2(aq) + 2H^+ + 12H_2O$	6	3.00E-05		1.73E-07		2.17E-07		1.76E-09	
1163	$2NH_4^+ + 24lepidocrocite \rightarrow 8magnetite + N_2O(aq) + 2H^+ + 15H_2O$	8	-3.65E-05	-3.65E-01	-2.11E-07	-1.62E-01	-2.72E-07	-2.85E-01	-3.46E-09	-2.78E-09
1164	$NH_4^+ + 15lepidocrocite \rightarrow 5magnetite + NO(aq) + H^+ + 9H_2O$	5	-9.10E-05	-7.50E-01	-5.57E-07	-4.59E-01	-7.22E-07	-5.95E-01	-8.25E-09	-6.89E-09
1165	$NH_4^+ + 18lepidocrocite \rightarrow 6magnetite + NO_2^- + 2H^+ + 10H_2O$	6	-1.10E-04		-6.22E-07		-8.06E-07		-8.55E-09	
1166	$NH_4^+ + 24lepidocrocite \rightarrow 8magnetite + NO_3^- + 2H^+ + 13H_2O$	8	-1.56E-04		-8.89E-07		-1.17E-06		-1.31E-08	
1167	$N_2(aq) + 6lepidocrocite \rightarrow 2magnetite + N_2O(aq) + 3H_2O$	2	-7.80E-07	-7.84E-01	-3.70E-06	-3.23E-01	-3.62E-05	-3.15E-01	-3.40E-05	-2.96E-01
1168	$N_2(aq) + 12lepidocrocite \rightarrow 4magnetite + 2NO(aq) + 6H_2O$	4	-1.42E-06	-1.23E-01	-7.03E-06	-6.88E-01	-6.95E-05	-6.65E-01	-6.52E-05	-5.63E-01

1169	N_2(aq) + 18lepidocrocite → 6magnetite + $2NO_2^-$ + $2H^+$ + $8H_2O$	6	-1.64E-06		-7.65E-06		-7.57E-05		-6.72E-05	
1170	N_2(aq) + 30lepidocrocite → 10magnetite + $2NO_3^-$ + $2H^+$ + $14H_2O$	10	-2.18E-06		-1.02E-05		-1.03E-04		-9.67E-05	
1171	N_2O(aq) + 6lepidocrocite → 2magnetite + 2NO(aq) + $3H_2O$	2	-2.98E-06	-2.11E-01	-6.06E-08	-3.88E-01	-6.06E-08	-3.85E-01	-6.05E-08	-3.78E-01
1172	N_2O(aq) + 12lepidocrocite → 4magnetite + $2NO_2^-$ + $2H^+$ + $5H_2O$	4	-4.03E-06	-4.33E-01	-7.05E-08	-6.34E-01	-7.05E-08	-6.30E-01	-6.38E-08	-5.63E-01
1173	N_2O(aq) + 24lepidocrocite → 8magnetite + $2NO_3^-$ + $2H^+$ + $11H_2O$	8	-6.55E-06	-6.55E-01	-1.12E-07	-1.45E-01	-1.14E-07	-1.62E-01	-1.14E-07	-1.62E-01
1174	NO(aq) + 3lepidocrocite → magnetite + NO_2^- + H_2O + H^+	1	-1.64E-08	-8.92E-09	-1.25E-08	-4.98E-09	-1.25E-08	-4.96E-09	-9.24E-09	-1.69E-01
1175	NO(aq) + 9lepidocrocite → 3magnetite + NO_3^- + $4H_2O$ + H^+	3	-3.78E-08	-3.33E-01	-3.30E-08	-2.55E-01	-3.41E-08	-2.66E-01	-3.42E-08	-2.66E-01
1176	NO_2^- + 6lepidocrocite → 2magnetite + NO_3^- + $3H_2O$	2	-5.07E-07		-2.97E-08		-3.27E-08		-2.50E-11	
1177	$2H_2S$(aq) + 4lepidocrocite → pyrite + magnetite + $4H_2O$	2	1.35E-09	8.85E-09	8.04E-06	1.26E-01	2.08E-09		4.29E-10	
1178	H_2S(aq) + 6lepidocrocite → 2magnetite + sulfur + $4H_2O$	2	-2.98E-09	4.52E-09	3.61E-06	8.83E-01	9.32E-10		1.69E-10	
1179	$2H_2S$(aq) + 24lepidocrocite → 8magnetite + $S_2O_3^{-2}$ + $2H^+$ + $13H_2O$	8	4.59E-09	1.58E-01	1.39E-05	2.29E-01	3.59E-09	4.56E-09	7.44E-10	9.70E-01
1180	H_2S(aq) + 24lepidocrocite →	8	2.26E-08	3.52E-01	3.67E-05	4.11E-01	9.32E-09		1.93E-09	

	8magnetite + SO_4^{-2} + $2H^+ + 12H_2O$									
1181	pyrite + 6lepidocrocite + $2H^+ \rightarrow$ 2magnetite + 2sulfur + $Fe^{+2} + 4H_2O$	2	-7.79E-09		-1.13E-08		-1.13E-08		0.00E+00	
1182	pyrite + 18lepidocrocite $\rightarrow$ 6magnetite + Fe^{+2} + $S_2O_3^{-2} + 9H_2O$	6	7.34E-09	1.48E-01	9.18E-09	1.67E-01	9.24E-09	1.67E-01	0.00E+00	
1183	pyrite + 42lepidocrocite $\rightarrow$ 14magnetite + Fe^{+2} + $2SO_4^{-2} + 2H^+ + 20H_2O$	14	4.33E-08		5.48E-08		5.34E-08		0.00E+00	
1184	2sulfur + 12lepidocrocite $\rightarrow$ 4mganetite + $S_2O_3^{-2}$ + $2H^+ + 5H_2O$	4	0.00E+00		0.00E+00		0.00E+00		0.00E+00	
1185	sulfur + 18lepidocrocite $\rightarrow$ 6magnetite + SO_4^{-2} + $2H^+ + 8H_2O$	6	0.00E+00		0.00E+00		0.00E+00		0.00E+00	
1186	$S_2O_3^{-2}$ + 24lepidocrocite $\rightarrow$ 8mganetite + $2SO_4^{-2}$ + $2H^+ + 11H_2O$	8	2.84E-08	3.59E-01	3.81E-08	4.56E-01	3.67E-08	4.42E-01	3.21E-08	3.97E-01
1187	CH_4(aq) + 18lepidocrocite $\rightarrow$ 6magnetite + CO(aq) + $11H_2O$	6	2.23E-08	2.66E-01	1.40E-08	1.40E-01	1.83E-10	1.83E-01	5.60E-12	5.65E-12
1188	CH_4(aq) + 24lepidocrocite $\rightarrow$ 8magnetite + CO_2(aq) + $14H_2O$	8	3.83E-08		3.11E-08		4.29E-10		1.11E-11	
1189	CH_4(aq) + 24lepidocrocite $\rightarrow$ 8magnetite + H^+ + $HCO_3^- + 13H_2O$	8	3.83E-08		3.11E-08		4.29E-10		1.11E-11	
1190	CO(aq) + 6lepidocrocite $\rightarrow$ 2magnetite + CO_2(aq) + $3H_2O$	2	1.23E-11	1.67E-11	5.02E-09	5.20E-09	2.32E-09	2.32E-09	3.65E-12	3.65E-12
1191	CO(aq) + 6lepidocrocite $\rightarrow$ 2magnetite + HCO_3^- + $H^+ + 2H_2O$	2	1.23E-11	1.67E-11	5.02E-09	5.19E-09	2.32E-09	2.32E-01	3.65E-12	3.65E-12

1192	6lepidocrocite → 2magnetite + $1/2O_2$(aq) + $3H_2O$	2	-1.97E-06	-1.77E-01	-2.06E-06	-1.78E-01	-2.06E-06		-2.53E-12	
Ferrihydrite as an electron acceptor										
1193	H_2(aq) + 2ferrihydrite + $4H^+$ → $2Fe^{+2}$ + $6H_2O$	2	2.18E-07		9.05E-10		4.41E-10		7.34E-12	
1194	$2NH_4^+$ + 6ferrihydrite + $10H^+$ → $6Fe^{+2}$ + N_2(aq) + $18H_2O$	6	4.31E-05		1.20E-07		1.49E-07		3.79E-09	
1195	$2NH_4^+$ + 8ferrihydrite + $14H^+$ → $8Fe^{+2}$ + N_2O(aq) + $23H_2O$	8	-1.90E-05	-1.93E-01	-2.82E-07	-2.33E-01	-3.64E-07	-3.20E-01	-7.54E-10	-7.45E-11
1196	NH_4^+ + 5ferrihydrite + $9H^+$ → $5Fe^{+2}$ + NO(aq) + $14H_2O$	5	-6.91E-05	-5.33E-01	-6.46E-07	-5.48E-01	-8.36E-07	-7.93E-01	-4.87E-09	-3.50E-09
1197	NH_4^+ + 6ferrihydrite + $10H^+$ → $6Fe^{+2}$ + NO_2^- + $16H_2O$	6	-8.39E-05		-7.28E-07		-9.43E-07		-4.50E-09	
1198	NH_4^+ + 8ferrihydrite + $14H^+$ → $8Fe^{+2}$ + NO_3^- + $21H_2O$	8	-1.21E-04		-1.03E-06		-1.36E-06		-7.66E-09	
1199	N_2(aq) + 2ferrihydrite + $4H^+$ → $2Fe^{+2}$ + N_2O(aq) + $5H_2O$	2	-7.29E-07	-7.29E-01	-3.87E-06	-3.40E-01	-3.79E-05	-3.32E-01	-2.96E-05	-2.52E-01
1200	N_2(aq) + 4ferrihydrite + $8H^+$ → $4Fe^{+2}$ + 2NO(aq) + $10H_2O$	4	-1.32E-06	-1.13E-01	-7.37E-06	-6.43E-01	-7.29E-05	-6.35E-01	-5.64E-05	-4.75E-01
1201	N_2(aq) + 6ferrihydrite + $10H^+$ → $6Fe^{+2}$ + $2NO_2^-$ + $14H_2O$	6	-1.49E-06		-8.16E-06		-8.08E-05		-5.40E-05	
1202	N_2(aq) + 10ferrihydrite + $18H^+$ → $10Fe^{+2}$ + $2NO_3^-$ + $24H_2O$	10	-1.93E-06		-1.11E-05		-1.11E-04		-7.46E-05	
1203	N_2O(aq) + 2ferrihydrite + $4H^+$ → $2Fe^{+2}$ + 2NO(aq) + $5H_2O$	2	-2.74E-06	-1.86E-01	-6.33E-08	-4.79E-01	-6.33E-08	-4.75E-01	-5.30E-08	-3.34E-01
1204	N_2O(aq) + 4ferrihydrite + $6H^+$ → $4Fe^{+2}$ + $2NO_2^-$ + $9H_2O$	4	-3.55E-06	-3.55E-01	-7.60E-08	-6.85E-01	-7.59E-08	-6.84E-01	-4.89E-08	-4.13E-01
1205	N_2O(aq) + 8ferrihydrite + $14H^+$ → $8Fe^{+2}$ + $2NO_3^-$ + $19H_2O$	8	-5.59E-06	-5.59E-01	-1.22E-07	-1.15E-01	-1.25E-07	-1.18E-01	-8.39E-08	-7.64E-01

1206	NO(aq) + ferrihydrite + $H^+ \rightarrow Fe^{+2} + NO_2^- + 2H_2O$	1	-1.44E-08	-6.89E-09	-1.38E-08	-6.33E-09	-1.38E-08	-6.39E-09	-5.51E-09	2.49E-01
1207	NO(aq) + 3ferrihydrite + $5H^+ \rightarrow 3Fe^{+2} + NO_3^- + 7H_2O$	3	-3.17E-08	-2.42E-01	-3.71E-08	-2.96E-01	-3.82E-08	-3.65E-01	-2.30E-08	-1.54E-01
1208	NO_2^- + 2ferrihydrite + $4H^+ \rightarrow 2Fe^{+2} + NO_3^- + 5H_2O$	2	-4.11E-07		-3.37E-08		-3.67E-08		-1.75E-11	
1209	$2H_2S$(aq) + 2ferrihydrite + $2H^+ \rightarrow Fe^{+2}$ + pyrite + $6H_2O$	2	2.95E-09	1.45E-01	7.92E-06	1.24E-01	2.05E-09		5.75E-10	
1210	H_2S(aq) + 2ferrihydrite + $4H^+ \rightarrow 2Fe^{+2}$ + sulfur + $6H_2O$	2	1.09E-09	8.59E-09	9.01E-07	5.37E-01	2.31E-10		6.15E-10	
1211	$2H_2S$(aq) + 8ferrihydrite + $14H^+ \rightarrow 8Fe^{+2} + S_2O_3^{-2} + 21H_2O$	8	1.27E-08	2.40E-01	8.44E-06	1.67E-01	2.19E-09	3.16E-09	1.64E-09	1.86E-09
1212	H_2S(aq) + 8ferrihydrite + $14H^+ \rightarrow 8Fe^{+2} + SO_4^{-2} + 20H_2O$	8	3.88E-08	4.63E-01	2.58E-05	3.29E-01	6.51E-09		3.72E-09	
1213	pyrite + 2ferrihydrite + $6H^+ \rightarrow 3Fe^{+2}$ + 2sulfur + $6H_2O$	2	-3.72E-09		-1.40E-08		-1.40E-08		0.00E+00	
1214	pyrite + 6ferrihydrite + $12H^+ \rightarrow 7Fe^{+2} + S_2O_3^{-2} + 15H_2O$	6	1.96E-08	2.77E-01	1.05E-09	8.55E-09	1.12E-09	8.63E-09	0.00E+00	
1215	pyrite + 14ferrihydrite + $26H^+ \rightarrow 15Fe^{+2} + 2SO_4^{-2} + 34H_2O$	14	7.18E-08		3.58E-08		3.45E-08		0.00E+00	
1216	2sulfur + 4ferrihydrite + $6H^+ \rightarrow 4Fe^{+2} + S_2O_3^{-2} + 9H_2O$	4	0.00E+00		0.00E+00		0.00E+00		0.00E+00	
1217	sulfur + 6ferrihydrite + $10H^+ \rightarrow 6Fe^{+2} + SO_4^{-2} + 14H_2O$	6	0.00E+00		0.00E+00		0.00E+00		0.00E+00	
1218	$S_2O_3^{-2}$ + 8ferrihydrite + $14H^+ \rightarrow 8Fe^{+2} + 2SO_4^{-2} + 19H_2O$	8	4.47E-08	5.22E-01	2.72E-08	3.47E-01	2.59E-08	3.34E-01	6.20E-08	6.96E-01
1219	CH_4(aq) + 6ferrihydrite + $12H^+ \rightarrow 6Fe^{+2}$ + CO(aq) + $17H_2O$	6	3.45E-08	3.83E-01	7.92E-09	7.92E-09	9.54E-11	9.54E-11	1.23E-11	1.23E-11
1220	CH_4(aq) + 8ferrihydrite + $16H^+ \rightarrow 8Fe^{+2}$ +	8	5.46E-08		2.31E-08		3.12E-10		2.00E-11	

	$CO_2(aq) + 22H_2O$									
1221	$CH_4(aq) + 8ferrihydrite + 15H^+ \rightarrow 8Fe^{+2} + HCO_3^- + 21H_2O$	8	5.46E-08		2.31E-08		3.12E-10		2.00E-11	
1222	$CO(aq) + 2ferrihydrite + 4H^+ \rightarrow 2Fe^{+2} + CO_2(aq) + 5H_2O$	2	1.63E-11	2.85E-11	4.43E-09	4.44E-09	2.04E-09	2.42E-09	5.14E-12	5.14E-12
1223	$CO(aq) + 2ferrihydrite + 3H^+ \rightarrow 2Fe^{+2} + HCO_3^- + 4H_2O$	2	1.63E-11	2.86E-11	4.43E-09	4.44E-09	2.04E-09	2.42E-09	5.14E-12	5.14E-12
1224	$ferrihydrite + 2H^+ \rightarrow Fe^{+2} + 1/4O_2(aq) + 5/2H_2O$	1	-5.25E-06	-4.65E-01	-6.62E-06	-5.76E-01	-6.62E-06		-6.11E-12	
1225	$H_2(aq) + 6ferrihydrite \rightarrow 2magnetite + 10H_2O$	2	2.49E-07		1.68E-09		8.34E-10		7.08E-12	
1226	$2NH_4^+ + 18ferrihydrite \rightarrow 6magnetite + N_2(aq) + 2H^+ + 30H_2O$	6	5.26E-05		3.05E-07		3.89E-07		3.61E-09	
1227	$2NH_4^+ + 24ferrihydrite \rightarrow 8magnetite + N_2O(aq) + 2H^+ + 39H_2O$	8	-6.39E-06	-6.39E-01	-3.58E-08	1.35E-01	-4.36E-08	2.69E-01	-9.88E-10	-3.41E-01
1228	$NH_4^+ + 15ferrihydrite \rightarrow 5magnetite + NO(aq) + H^+ + 24H_2O$	5	-5.33E-05	-3.72E-01	-3.38E-07	-2.44E-01	-4.36E-07	-3.89E-01	-5.16E-09	-3.79E-09
1229	$NH_4^+ + 18ferrihydrite \rightarrow 6magnetite + NO_2^- + 2H^+ + 28H_2O$	6	-6.50E-05		-3.59E-07		-4.63E-07		-4.85E-09	
1230	$NH_4^+ + 24ferrihydrite \rightarrow 8magnetite + NO_3^- + 2H^+ + 37H_2O$	8	-9.59E-05		-5.38E-07		-7.15E-07		-8.13E-09	
1231	$N_2(aq) + 6ferrihydrite \rightarrow 2magnetite + N_2O(aq) + 9H_2O$	2	-6.92E-07	-6.92E-01	-3.28E-06	-2.88E-01	-3.20E-05	-2.73E-01	-3.00E-05	-2.55E-01
1232	$N_2(aq) + 12ferrihydrite \rightarrow 4magnetite + 2NO(aq) + 18H_2O$	4	-1.24E-06	-1.53E-01	-6.18E-06	-5.24E-01	-6.10E-05	-5.16E-01	-5.72E-05	-4.83E-01
1233	$N_2(aq) + 18ferrihydrite \rightarrow 6magnetite + 2NO_2^- + 2H^+ + 26H_2O$	6	-1.38E-06		-6.39E-06		-6.30E-05		-5.52E-05	
1234	$N_2(aq) + 30ferrihydrite \rightarrow 10magnetite + 2NO_3^- + 2H^+ + 44H_2O$	10	-1.74E-06		-8.11E-06		-8.17E-05		-7.65E-05	

1235	N_2O(aq) + 6ferrihydrite → 2magnetite + 2NO(aq) + $9H_2O$	2	-2.57E-06	-1.69E-01	-5.38E-08	-3.13E-01	-5.38E-08	-3.13E-01	-5.36E-08	-3.98E-01
1236	N_2O(aq) + 12ferrihydrite → 4magnetite + $2NO_2^-$ + $2H^+$ + $17H_2O$	4	-3.21E-06	-3.27E-01	-5.71E-08	-4.96E-01	-5.70E-08	-4.95E-01	-5.02E-08	-4.26E-01
1237	N_2O(aq) + 24ferrihydrite → 8magnetite + $2NO_3^-$ + $2H^+$ + $35H_2O$	8	-4.90E-06	-4.90E-01	-8.46E-08	-7.72E-01	-8.68E-08	-7.93E-01	-8.64E-08	-7.89E-01
1238	NO(aq) + 3ferrihydrite → magnetite + NO_2^- + $4H_2O$ + H^+	1	-1.29E-08	-5.42E-09	-9.11E-09	-1.68E-09	-9.09E-09	-1.58E-09	-5.83E-09	1.73E-09
1239	NO(aq) + 9ferrihydrite → 3magnetite + NO_3^- + $13H_2O$ + H^+	3	-2.73E-08	-1.98E-01	-2.29E-08	-1.54E-01	-2.40E-08	-1.65E-01	-2.40E-08	-1.64E-01
1240	NO_2^- + 6ferrihydrite → 2magnetite + NO_3^- + $9H_2O$	2	-3.41E-07		-2.00E-08		-2.25E-08		-1.81E-11	
1241	$2H_2S$(aq) + 4ferrihydrite → magnetite + pyrite + $8H_2O$	2	3.69E-09	1.12E-01	1.03E-05	1.48E-01	2.66E-09		5.65E-10	
1242	H_2S(aq) + 6ferrihydrite → 2magnetite + sulfur + $10H_2O$	2	4.03E-09	1.15E-01	1.03E-05	1.48E-01	2.68E-09		5.77E-10	
1243	$2H_2S$(aq) + 24ferrihydrite → 8magnetite + $S_2O_3^{-2}$ + $2H^+$ + $37H_2O$	8	1.86E-08	2.99E-01	2.73E-05	3.56E-01	7.08E-09	8.57E-09	1.56E-09	1.79E-09
1244	H_2S(aq) + 24ferrihydrite → 8magnetite + SO_4^{-2} + $2H^+$ + $36H_2O$	8	5.06E-08	5.81E-01	6.36E-05	6.87E-01	1.63E-08		3.56E-09	
1245	pyrite + 6ferrihydrite + $2H^+$ → 2magnetite + 2sulfur + Fe^{+2} + $10H_2O$	2	-7.79E-10		-4.59E-09		-4.57E-09		0.00E+00	
1246	pyrite + 18ferrihydrite → 6magnetite + Fe^{+2} + $S_2O_3^{-2}$ + $27H_2O$	6	2.84E-08	3.59E-01	2.94E-08	3.69E-01	2.95E-08	3.70E-01	0.00E+00	
1247	pyrite + 42ferrihydrite → 14magnetite + Fe^{+2} + $2SO_4^{-2}$ + $2H^+$ +	14	9.24E-08		1.02E-07		1.01E-07		0.00E+00	

	$62H_2O$									
1248	2sulfur + 12ferrihydrite → 4mganetite + $S_2O_3^{-2}$ + $2H^+$ + $17H_2O$	4	0.00E+00		0.00E+00		0.00E+00		0.00E+00	
1249	sulfur + 18ferrihydrite → 6mganetite + SO_4^{-2} + $2H^+$ + $26H_2O$	6	0.00E+00		0.00E+00		0.00E+00		0.00E+00	
1250	$S_2O_3^{-2}$ + 24ferrihydrite → 8mganetite + $2SO_4^{-2}$ + $2H^+$ + $35H_2O$	8	5.65E-08	6.40E-01	6.50E-08	7.25E-01	6.37E-08	7.12E-01	5.95E-08	6.71E-01
1251	CH_4(aq) + 18ferrihydrite → 6magnetite + CO(aq) + $29H_2O$	6	4.34E-08	4.72E-01	2.90E-08	2.90E-01	4.02E-10	4.15E-01	1.17E-11	1.17E-11
1252	CH_4(aq) + 24ferrihydrite → 8magnetite + CO_2(aq) + $38H_2O$	8	6.64E-08		5.11E-08		7.20E-10		1.93E-11	
1253	CH_4(aq) + 24ferrihydrite → 8magnetite + HCO_3^- + H^+ + $37H_2O$	8	6.64E-08		5.11E-08		7.20E-10		1.93E-11	
1254	CO(aq) + 6ferrihydrite → 2magnetite + CO_2(aq) + $9H_2O$	2	1.93E-11	2.32E-11	6.48E-09	6.49E-09	3.01E-09	3.61E-09	5.01E-12	5.14E-12
1255	CO(aq) + 6ferrihydrite → 2magnetite + HCO_3^- + H^+ + $8H_2O$	2	1.93E-11	2.32E-11	6.48E-09	6.49E-01	3.01E-09	3.61E-09	5.02E-12	5.15E-12
1256	6ferrihydrite → 2magnetite + $1/2O_2$(aq) + $9H_2O$	2	-1.59E-06	-1.39E-01	-1.70E-06	-1.41E-01	-1.70E-06		-2.08E-12	
Carbon monoxide as an electron acceptor										
1257	$3H_2$(aq) + CO(aq) → CH_4(aq) + H_2O	6	2.43E-11	2.85E-11	6.11E-10	6.19E-01	3.18E-10	3.19E-01	1.86E-12	1.86E-12
1258	$2NH_4^+$ + CO(aq) → N_2(aq) + CH_4(aq) + H_2O + $2H^+$	6	1.88E-12	5.63E-12	1.68E-09	1.68E-09	8.86E-10	8.86E-01	1.53E-13	1.53E-13
1259	$6NH_4^+$ + 4CO(aq) → $3N_2O$(aq) + $4CH_4$(aq) + H_2O + $6H^+$	24	-5.16E-11	-4.78E-11	-9.36E-09	-8.14E-09	-4.19E-09	-3.61E-09	-9.47E-12	-8.34E-12
1260	$6NH_4^+$ + 5CO(aq) + H_2O → 6NO(aq) + $5CH_4$(aq) + $6H^+$	30	-7.69E-11	-6.42E-11	-1.52E-08	-1.33E-01	-6.94E-09	-6.23E-09	-1.47E-11	-1.29E-11

1261	$NH_4^+ + CO(aq) + H_2O \rightarrow NO_2^- + CH_4(aq) + 2H^+$	6	-7.74E-11	-7.37E-11	-1.44E-08	-1.44E-01	-6.58E-09	-6.58E-09	-1.32E-11	-1.32E-11
1262	$3NH_4^+ + 4CO(aq) + 5H_2O \rightarrow 3NO_3^- + 4CH_4(aq) + 6H^+$	24	-8.06E-11	-7.68E-11	-1.52E-08	-1.52E-01	-7.02E-09	-7.22E-09	-1.46E-11	-1.46E-11
1263	$3N_2(aq) + CO(aq) + 2H_2O \rightarrow 3N_2O(aq) + CH_4(aq)$	6	-2.12E-10	-2.82E-01	-4.25E-08	-3.76E-01	-1.94E-08	-1.71E-01	-3.83E-11	-3.39E-11
1264	$3N_2(aq) + 2CO(aq) + 4H_2O \rightarrow 6NO(aq) + 2CH_4(aq)$	12	-1.95E-10	-1.69E-01	-4.06E-08	-3.57E-01	-1.87E-08	-1.64E-01	-3.69E-11	-3.24E-11
1265	$N_2(aq) + CO(aq) + 3H_2O \rightarrow 2NO_2^- + CH_4(aq) + 2H^+$	6	-1.57E-10	-1.53E-01	-3.06E-08	-3.57E-01	-1.40E-08	-1.44E-01	-2.65E-11	-2.65E-11
1266	$3N_2(aq) + 5CO(aq) + 13H_2O \rightarrow 6NO_3^- + 5CH_4(aq) + 6H^+$	30	-1.30E-10	-1.26E-01	-2.53E-08	-2.53E-01	-1.18E-08	-1.18E-01	-2.34E-11	-2.34E-11
1267	$3N_2O(aq) + CO(aq) + 2H_2O \rightarrow 6NO + CH_4(aq)$	6	-1.78E-10	-1.30E-01	-4.35E-08	-2.89E-01	-2.03E-08	-1.34E-01	-4.00E-11	-2.64E-11
1268	$3N_2O(aq) + 2CO(aq) + 7H_2O \rightarrow 6NO_2^- + 2CH_4(aq) + 6H^+$	12	-1.29E-10	-1.25E-01	-2.70E-08	-2.46E-01	-1.25E-08	-1.14E-01	-2.29E-11	-2.62E-11
1269	$3N_2O(aq) + 4CO(aq) + 11H_2O \rightarrow 6NO_3^- + 4CH_4(aq) + 6H^+$	24	-1.10E-10	-1.58E-01	-2.22E-08	-2.12E-01	-1.04E-08	-9.86E-09	-2.08E-11	-1.97E-11
1270	$6NO(aq) + CO(aq) + 5H_2O \rightarrow CH_4(aq) + 6NO_2^- + 6H^+$	6	-1.25E-10	-7.59E-11	-1.56E-08	-8.11E-09	-9.36E-09	-4.76E-01	-1.48E-11	-5.76E-12
1271	$2NO(aq) + CO(aq) + 3H_2O \rightarrow 2NO_3^- + CH_4(aq) + 2H^+$	6	-1.02E-10	-8.30E-11	-1.84E-08	-1.51E-01	-8.68E-09	-7.15E-09	-1.74E-11	-1.44E-11
1272	$3NO_2^- + CO(aq) + 2H_2O \rightarrow 3NO_3^- + CH_4(aq)$	6	-9.03E-11	-8.65E-11	-1.74E-08	-1.74E-01	-8.35E-09	-8.35E-09	-1.87E-11	-1.88E-11
1273	$6H_2S(aq) + 3Fe^{+2} + CO(aq) \rightarrow 3pyrite + CH_4(aq) + 6H^+ + H_2O$	6	-2.06E-11	2.82E-11	8.00E-09	1.38E-01	1.66E-09	1.66E-09	3.32E-12	3.32E-12
1274	$3H_2S(aq)\ CO(aq) \rightarrow 3sulfur + CH_4(aq) + H_2O$	6	-3.50E-11	-8.75E-12	-1.73E-09	1.19E-01	-5.32E-10	-5.32E-01	-2.05E-12	-2.46E-12
1275	$6H_2S(aq) + 4CO(aq) + 5H_2O \rightarrow 3S_2O_3^{-2} + 4CH_4(aq) + 6H^+$	24	-1.92E-11	1.45E-12	4.31E-10	3.18E-09	3.93E-10	9.67E-01	-5.59E-15	1.13E-12

1276	$3H_2S(aq) + 4CO(aq) + 8H_2O \rightarrow 3SO_4^{-2} + 4CH_4(aq) + 6H^+$	24	-9.15E-12	2.28E-13	1.88E-09	2.61E-09	1.02E-09	1.22E-09	1.11E-12	1.17E-12
1277	$3pyrite + CO(aq) + 6H^+ \rightarrow 6sulfur + CH_4(aq) + 3Fe^{+2} + H_2O$	6	-4.94E-11	-4.57E-11	-1.15E-08	-1.15E-01	-5.19E-09	-5.19E-09	-7.41E-12	-7.49E-12
1278	$pyrite + CO(aq) + 2H_2O \rightarrow S_2O_3^{-2} + CH_4(aq) + Fe^{+2}$	6	-1.87E-11	-7.47E-12	-2.09E-09	-4.62E-01	-7.87E-10	-2.15E-11	-1.11E-12	3.98E-13
1279	$3pyrite + 7CO(aq) + 17H_2O \rightarrow 6SO_4^{-2} + 7CH_4(aq) + 6H^+ + 3Fe^{+2}$	42	-7.52E-12	-3.77E-12	1.01E-09	1.11E-09	6.06E-10	6.65E-01	7.91E-13	7.91E-13
1280	$6sulfur + 2CO(aq) + 7H_2O \rightarrow 3S_2O_3^{-2} + 2CH_4(aq) + 6H^+$	12	-3.35E-12	1.16E-11	2.59E-09	5.35E-09	1.41E-09	2.56E-09	2.03E-12	4.31E-12
1281	$sulfur + CO(aq) + 3H_2O \rightarrow SO_4^{-2} + CH_4(aq) + 2H^+$	6	-5.29E-13	3.22E-12	3.09E-09	3.89E-09	1.57E-09	1.57E-09	2.16E-12	2.16E-12
1282	$3S_2O_3^{-2} + 4CO(aq) + 11H_2O \rightarrow 6SO_4^{-2} + 4CH_4(aq) + 6H^+$	24	-4.74E-12	4.63E-12	2.12E-09	3.34E-09	1.08E-09	1.65E-09	1.09E-12	2.22E-12
1283	$9Fe^{+2} + CO(aq) + 11H_2O \rightarrow 3magnetite + CH_4(aq) + 18H^+$	6	-3.39E-11	-3.12E-11	3.49E-10	3.49E-01	5.33E-10	5.33E-01	-4.67E-12	-4.67E-12
1284	$6Fe^{+2} + CO(aq) + 8H_2O \rightarrow 3hematite + CH_4(aq) + 12H^+$	6	-1.99E-11	-1.62E-11	1.09E-09	1.88E-09	9.28E-10	9.28E-01	-3.84E-12	-3.84E-12
1285	$6Fe^{+2} + CO(aq) + 8H_2O \rightarrow 3maghemite + CH_4(aq) + 12H^+$	6	-2.92E-11	-2.55E-11	-3.03E-10	-3.35E-01	-1.74E-11	-1.74E-11	-5.38E-12	-5.39E-12
1286	$6Fe^{+2} + CO(aq) + 11H_2O \rightarrow 6goethite + CH_4(aq) + 12H^+$	6	-1.98E-11	-1.62E-11	1.13E-09	1.13E-09	9.59E-10	9.59E-01	-3.80E-12	-3.80E-12
1287	$6Fe^{+2} + CO(aq) + 11H_2O \rightarrow 6lepidocrocite + CH_4(aq) + 12H^+$	6	-3.13E-11	-2.75E-11	-5.91E-10	-5.91E-01	-2.14E-10	-2.14E-01	-5.71E-12	-5.71E-12
1288	$6Fe^{+2} + CO(aq) + 17H_2O \rightarrow 6ferrihydrite + CH_4(aq) + 12H^+$	6	-3.83E-11	-3.45E-11	-1.60E-09	-1.62E-09	-9.01E-10	-9.14E-01	-6.85E-12	-6.85E-12
1289	$9fayalite + 2CO + 4H_2O \rightarrow 6magnetite + 2CH_4(aq) + 9SiO_2(aq)$	12	1.31E-11	3.38E-11	4.33E-09	5.69E-09	2.87E-09	2.87E-09	5.21E-12	5.21E-12

1290	9ferrosilite + CO + $2H_2O$ → 3magnetite + $CH_4(aq)$ + $9SiO_2(aq)$	6	2.39E-12	3.99E-11	2.00E-09	4.72E-09	2.42E-09	2.42E-09	4.22E-12	4.22E-12
1291	6magnetite + $CO(aq)$ + $2H_2O$ → 9hematite + $CH_4(aq)$	6	7.93E-12	1.17E-11	3.20E-09	3.24E-09	1.70E-09	1.70E-09	3.02E-12	3.16E-12
1292	6magnetite + $CO(aq)$ + $2H_2O$ → 9maghemite + $CH_4(aq)$	6	-1.99E-11	-1.61E-11	-2.83E-09	-2.83E-09	-1.14E-09	-1.15E-09	-2.54E-12	-2.54E-12
1293	6magnetite + $CO(aq)$ + $11H_2O$ → 18goethite + $CH_4(aq)$	6	8.43E-12	1.22E-11	3.40E-09	3.44E-09	1.79E-09	1.79E-09	3.15E-12	3.15E-12
1294	6magnetite + $CO(aq)$ + $11H_2O$ → 18lepidocrocite + $CH_4(aq)$	6	-2.61E-11	-2.23E-11	-4.08E-09	-4.82E-09	-1.73E-09	-1.73E-09	-3.74E-12	-3.74E-12
1295	6magnetite + $CO(aq)$ + $29H_2O$ → 18ferrihydrite + $CH_4(aq)$	6	-4.71E-11	-4.34E-11	-8.47E-09	-8.47E-09	-3.79E-09	-3.79E-09	-7.83E-12	-7.83E-12
1296	$2H_2O$ + $CO(aq)$ → $CH_4(aq)$ + $3/2O_2(aq)$	6	-1.36E-10	-1.21E-01	-2.91E-08	-2.56E-01	-1.35E-08	-1.35E-01	-2.65E-11	-2.65E-11
1297	$2H_2O$ + $4CO(aq)$ → $CH_4(aq)$ + $3CO_2(aq)$	6	2.68E-12	6.43E-12	2.74E-09	2.74E-09	1.31E-09	1.36E-09	1.80E-12	1.82E-12
1298	$5H_2O$ + $4CO(aq)$ → $CH_4(aq)$ + $3HCO_3^-$ + $3H^+$	6	2.68E-12	6.43E-12	2.74E-09	2.74E-09	1.31E-09	1.36E-09	1.80E-12	1.83E-12
Carbon dioxide as an electron acceptor										
1299	$H_2(aq)$ + $CO_2(aq)$ → $CO(aq)$ + H_2O	2	8.19E-09	4.75E-01	-7.80E-10	-7.80E-01	-3.92E-10	-3.92E-01	-2.94E-12	-2.94E-12
1300	$2NH_4^+$ + $3CO_2(aq)$ → $3CO(aq)$ + $N_2(aq)$ + $2H^+$ + $3H_2O$	6	-2.16E-05	-9.48E-01	-1.31E-07	-1.36E-01	-1.28E-07	-1.28E-01	-3.19E-09	-3.19E-09
1301	$2NH_4^+$ + $4CO_2(aq)$ → $4CO(aq)$ + $N_2O(aq)$ + $2H^+$ + $3H_2O$	8	-1.05E-04	-8.92E-01	-2.86E-07	-2.69E-01	-2.78E-07	-2.66E-01	-1.01E-08	-9.38E-09
1302	$2NH_4^+$ + $5CO_2(aq)$ → $5CO(aq)$ + $2NO(aq)$ + $2H^+$ + $3H_2O$	10	-1.77E-04	-1.47E-01	-3.68E-07	-3.47E-01	-3.59E-07	-3.32E-01	-1.65E-08	-1.51E-01
1303	NH_4^+ + $3CO_2(aq)$ → $3CO(aq)$ + NO_2^- + $2H^+$ + H_2O	6	-2.13E-04	-1.89E-01	-3.57E-07	-3.57E-01	-3.48E-07	-3.48E-01	-1.85E-08	-1.85E-01
1304	NH_4^+ + $4CO_2(aq)$ → $4CO(aq)$ + NO_3^- + $2H^+$	8	-2.94E-04	-2.61E-01	-3.68E-07	-3.68E-01	-3.61E-07	-3.61E-01	-2.63E-08	-2.63E-01

	+ H_2O									
1305	$N_2(aq) + CO_2(aq) \rightarrow CO(aq) + N_2O(aq)$	2	-9.82E-07	-9.34E-01	-7.52E-07	-6.83E-01	-7.26E-07	-6.58E-01	-4.48E-05	-4.33E-01
1306	$N_2(aq) + 2CO_2(aq) \rightarrow 2CO(aq) + 2NO(aq)$	4	-1.82E-06	-1.54E-01	-7.24E-07	-6.56E-01	-7.05E-07	-6.37E-01	-8.68E-05	-7.79E-01
1307	$N_2(aq) + 3CO_2(aq) + H_2O \rightarrow 3CO(aq) + 2NO_2^- + 2H^+$	6	-2.25E-06	-2.16E-01	-5.84E-07	-5.84E-01	-5.68E-07	-5.68E-01	-9.95E-05	-9.95E-01
1308	$N_2(aq) + 5CO_2(aq) + H_2O \rightarrow 5CO(aq) + 2NO_3^- + 2H^+$	10	-3.19E-06	-2.95E-01	-5.10E-07	-5.14E-01	-5.01E-07	-5.17E-01	-1.17E-04	-1.17E-01
1309	$N_2O(aq) + CO_2(aq) \rightarrow CO(aq) + 2NO(aq)$	2	-3.92E-06	-2.82E-01	-8.37E-08	-6.12E-01	-8.33E-08	-6.78E-01	-7.87E-08	-5.65E-01
1310	$N_2O(aq) + 2CO_2(aq) + H_2O \rightarrow 2CO(aq) + 2NO_2^- + 2H^+$	4	-5.91E-06	-5.47E-01	-1.17E-07	-1.93E-01	-1.16E-07	-1.84E-01	-1.00E-07	-9.28E-01
1311	$N_2O(aq) + 4CO_2(aq) + H_2O \rightarrow 4CO(aq) + 2NO_3^- + 2H^+$	8	-1.03E-05	-9.43E-01	-2.04E-07	-1.97E-01	-2.05E-07	-1.97E-01	-1.87E-07	-1.79E-01
1312	$2NO(aq) + CO_2(aq) + H_2O \rightarrow CO(aq) + 2NO_2^- + 2H^+$	2	-2.44E-08	-1.55E-01	-2.40E-08	-1.65E-01	-2.38E-08	-1.63E-01	-1.84E-08	-1.89E-01
1313	$2NO(aq) + 3CO_2(aq) + H_2O \rightarrow 3CO(aq) + 2NO_3^- + 2H^+$	6	-6.18E-08	-4.88E-01	-6.77E-08	-6.18E-01	-6.82E-08	-6.68E-01	-6.16E-08	-5.47E-01
1314	$NO_2^- + CO_2(aq) \rightarrow CO(aq) + NO_3^-$	2	-8.87E-07	-7.98E-01	-6.33E-08	-6.33E-01	-6.70E-08	-6.70E-01	-4.32E-11	-4.32E-11
1315	$2H_2S(aq) + Fe^{+2} + CO_2(aq) \rightarrow CO(aq) + pyrite + 2H^+ + H_2O$	2	-7.09E-09	2.29E-09	-4.12E-09	3.93E-09	-5.47E-10	-5.47E-01	-6.49E-12	-6.49E-12
1316	$H_2S(aq) + CO_2(aq) \rightarrow CO(aq) + sulfur + H_2O$	2	-1.90E-08	-7.74E-09	-1.79E-07	-1.38E-01	-4.96E-09	-4.96E-01	-9.22E-10	-9.22E-01
1317	$2H_2S(aq) + 4CO_2(aq) \rightarrow 4CO(aq) + S_2O_3^{-2} + 2H^+ + H_2O$	8	-2.74E-08	-8.67E-09	-1.48E-07	-1.16E-01	-8.18E-09	-7.29E-09	-1.44E-09	-1.21E-09
1318	$H_2S(aq) + 4CO_2(aq) \rightarrow 4CO(aq) + SO_4^{-2} + 2H^+$	8	-4.15E-08	-1.90E-01	-1.28E-07	-1.18E-01	-1.42E-08	-1.42E-01	-2.43E-09	-2.43E-09
1319	$pyrite + CO_2(aq) + 2H^+ \rightarrow CO(aq) + 2sulfur + Fe^{+2} + H_2O$	2	-2.11E-04	-1.78E-01	-3.15E-07	-3.15E-01	-3.07E-07	-3.72E-01	-5.60E-05	-5.64E-01
1320	$pyrite + 3CO_2(aq) \rightarrow 3CO(aq) + S_2O_3^{-2} + Fe^{+2}$	6	-1.20E-04	-6.47E-01	-1.84E-07	-1.68E-01	-1.77E-07	-1.55E-01	-3.19E-05	-2.61E-01

1321	pyrite + $7CO_2(aq)$ + H_2O → $7CO(aq)$ + $2SO_4^{-2}$ + $2H^+$ + Fe^{+2}	14	-8.70E-05	-5.38E-01	-1.40E-07	-1.45E-01	-1.36E-07	-1.36E-01	-2.46E-05	-2.46E-01
1322	2sulfur + $2CO_2(aq)$ + H_2O → $2CO(aq)$ + $S_2O_3^{-2}$ + $2H^+$	4	-7.47E-05	-8.29E-01	-1.18E-07	-8.35E-01	-1.12E-07	-7.86E-01	-1.98E-05	-1.11E-01
1323	sulfur + $3CO_2(aq)$ + H_2O → $3CO(aq)$ + SO_4^{-2} + $2H^+$	6	-6.64E-05	-3.32E-01	-1.11E-07	-1.18E-01	-1.08E-07	-1.77E-01	-1.94E-05	-1.94E-01
1324	$S_2O_3^{-2}$ + $4CO_2(aq)$ + H_2O → $4CO(aq)$ + $2SO_4^{-2}$ + $2H^+$	8	-3.56E-08	-1.40E-01	-5.44E-08	-4.69E-01	-5.42E-08	-4.67E-01	-4.08E-08	-3.33E-01
1325	$3Fe^{+2}$ + $CO_2(aq)$ + $3H_2O$ → magnetite + $CO(aq)$ + $6H^+$	2	-1.91E-06	-1.53E-01	-4.71E-09	-4.78E-09	-4.59E-09	-4.59E-09	-8.68E-12	-8.68E-12
1326	$2Fe^{+2}$ + $CO_2(aq)$ + $2H_2O$ → hematite + $CO(aq)$ + $4H^+$	2	-2.15E-06	-1.57E-01	-6.50E-09	-6.50E-09	-6.32E-09	-6.32E-09	-9.84E-12	-9.84E-12
1327	$2Fe^{+2}$ + $CO_2(aq)$ + $2H_2O$ → maghemite + $CO(aq)$ + $4H^+$	2	-2.63E-06	-2.49E-01	-7.89E-09	-7.89E-09	-7.71E-09	-7.71E-09	-1.14E-11	-1.14E-11
1328	$2Fe^{+2}$ + $CO_2(aq)$ + $3H_2O$ → 2goethite + $CO(aq)$ + $4H^+$	2	-2.14E-06	-1.56E-01	-6.45E-09	-6.45E-09	-6.27E-09	-6.27E-09	-9.81E-12	-9.86E-12
1329	$2Fe^{+2}$ + $CO_2(aq)$ + $3H_2O$ → 2lepidocrocite + $CO(aq)$ + $4H^+$	2	-2.73E-06	-2.15E-01	-8.18E-09	-8.18E-09	-8.00E-09	-8.00E-09	-1.17E-11	-1.17E-11
1330	$2Fe^{+2}$ + $CO_2(aq)$ + $5H_2O$ → 2ferrihydrite + $CO(aq)$ + $4H^+$	2	-3.09E-06	-2.51E-01	-9.19E-09	-9.19E-09	-9.01E-09	-9.17E-09	-1.29E-11	-1.29E-11
1331	3fayalite + $2CO_2(aq)$ → 2magnetite + $2CO(aq)$ + $3SiO_2(aq)$	4	-2.60E-05	5.74E-01	-9.33E-08	-7.43E-01	-6.94E-08	-6.95E-01	-7.65E-06	-7.65E-01
1332	3ferrosilite + $CO_2(aq)$ → magnetite + $CO(aq)$ + $3SiO_2(aq)$	2	-5.78E-05	7.51E-01	-1.26E-07	-8.80E-01	-8.28E-08	-8.28E-01	-1.15E-05	-1.15E-01
1333	2magnetite + $CO_2(aq)$ → 3hematite + $CO(aq)$	2	-4.14E-05	-8.19E-01	-1.09E-07	-1.92E-01	-1.04E-07	-1.47E-01	-1.61E-05	-1.67E-01
1334	2magnetite + $CO_2(aq)$ → 3maghemite + $CO(aq)$	2	-1.24E-04	-9.35E-01	-1.94E-07	-1.95E-01	-1.88E-07	-1.88E-01	-3.74E-05	-3.74E-01
1335	2magnetite + $CO_2(aq)$ + $3H_2O$ → 6goethite + $CO(aq)$	2	-3.99E-05	-6.71E-01	-1.06E-07	-1.64E-01	-1.01E-07	-1.14E-01	-1.55E-05	-1.55E-01

1336	2magnetite + CO_2(aq) + $3H_2O$ → 6lepidoocrocite + CO(aq)	2	-1.42E-04	-1.86E-01	-2.12E-07	-2.12E-01	-2.05E-07	-2.52E-01	-4.20E-05	-4.20E-01
1337	2magnetite + CO_2(aq) + $9H_2O$ → 6ferrihydrite + CO(aq)	2	-2.04E-04	-1.77E-01	-2.73E-07	-2.73E-01	-2.66E-07	-2.66E-01	-5.77E-05	-5.77E-01
1338	CH_4(aq) + $3CO_2$(aq) → $4CO$(aq) + $2H_2O$	6	-2.57E-08	-1.76E-01	-3.75E-08	-3.75E-01	-5.53E-10	-5.53E-01	-1.08E-11	-1.81E-11
1339	CO_2(aq) → CO(aq) + $1/2O_2$(aq)	2	-4.67E-04	-4.42E-01	-5.63E-07	-5.14E-01	-5.52E-07	-5.52E-01	-1.29E-04	-1.29E-01
1340	$4H_2$(aq) + CO_2(aq) → CH_4(aq) + $2H_2O$	8	7.55E-08		2.63E-10		1.40E-10		6.60E-13	
1341	$8NH_4^+$ + $3CO_2$(aq) → $4N_2$(aq) + $3CH_4$(aq) + $8H^+$ + $6H_2O$	24	-8.51E-07		-3.18E-08		-3.49E-08		-7.46E-10	
1342	$2NH_4^+$ + CO_2(aq) → N_2O(aq) + CH_4(aq) + $2H^+$ + H_2O	8	-7.77E-05	-7.77E-01	-4.85E-07	-4.36E-01	-6.08E-07	-5.45E-01	-6.80E-09	-6.12E-09
1343	$8NH_4^+$ + $5CO_2$(aq) → 8NO(aq) + $5CH_4$(aq) + $8H^+$ + $2H_2O$	40	-1.42E-04	-1.26E-01	-8.99E-07	-8.12E-01	-9.73E-07	-8.65E-01	-1.24E-08	-1.16E-01
1344	$4NH_4^+$ + $3CO_2$(aq) + $2H_2O$ → $4NO_2^-$ + $3CH_4$(aq) + $8H^+$	24	-1.72E-04		-9.66E-07		-9.30E-07		-1.36E-08	
1345	NH_4^+ + CO_2(aq) + H_2O → NO_3^- + CH_4(aq) + $2H^+$	8	-2.38E-04		-1.01E-06		-9.82E-07		-1.98E-08	
1346	$4N_2$(aq) + CO_2(aq) + $2H_2O$ → $4N_2O$(aq) + CH_4(aq)	8	-9.01E-07	-9.65E-01	-2.54E-06	-2.27E-01	-2.44E-06	-2.17E-01	-3.95E-05	-3.52E-01
1347	$2N_2$(aq) + CO_2(aq) + $2H_2O$ → 4NO(aq) + CH_4(aq)	8	-1.66E-06	-1.47E-01	-2.44E-06	-2.17E-01	-2.36E-06	-2.88E-01	-7.61E-05	-6.72E-01
1348	$4N_2$(aq) + $3CO_2$(aq) + $10H_2O$ → $8NO_2^-$ + $3CH_4$(aq) + $8H^+$	24	-2.01E-06		-1.87E-06		-1.81E-06		-8.36E-05	
1349	$4N_2$ + $5CO_2$(aq) + $14H_2O$ → $8NO_3^-$ + $5CH_4$(aq) + $8H^+$	40	-2.79E-06		-1.58E-06		-1.54E-06		-1.24E-04	
1350	$4N_2O$(aq) + CO_2(aq) + $2H_2O$ → 8NO(aq) + CH_4(aq)	8	-3.55E-06	-2.66E-01	-7.11E-08	-4.86E-01	-7.05E-08	-4.80E-01	-6.97E-08	-4.73E-01
1351	$2N_2O$(aq) + CO_2(aq) + $4H_2O$ → $4NO_2^-$ +	8	-5.16E-06	-5.16E-01	-9.15E-08	-8.46E-01	-9.03E-08	-8.28E-01	-8.23E-08	-7.48E-01

	$CH_4(aq) + 4H^+$									
1352	$N_2O(aq) + CO_2(aq) + 3H_2O \rightarrow 2NO_3^- + CH_4(aq) + 2H^+$	8	-8.80E-06	-8.82E-01	-1.53E-07	-1.46E-01	-1.53E-07	-1.46E-01	-1.51E-07	-1.43E-01
1353	$8NO(aq) + CO_2(aq) + 6H_2O \rightarrow 8NO_2^- + CH_4(aq) + 8H^+$	8	-2.12E-08	-1.37E-01	-1.77E-08	-1.22E-01	-1.74E-08	-9.92E-09	-1.39E-08	-6.34E-09
1354	$8NO(aq) + 3CO_2(aq) + 10H_2O \rightarrow 8NO_3^- + 3CH_4(aq) + 8H^+$	24	-5.22E-08	-4.47E-01	-4.87E-08	-4.12E-01	-4.90E-08	-4.15E-01	-4.80E-08	-4.49E-01
1355	$4NO_2^- + CO_2(aq) + 2H_2O \rightarrow 4NO_3^- + CH_4(aq)$	8	-7.34E-07		-4.49E-08		-4.76E-08		-3.42E-11	
1356	$8H_2S(aq) + 4Fe^{+2} + CO_2(aq) \rightarrow 4pyrite + CH_4(aq) + 8H^+ + 2H_2O$	8	-3.87E-09	3.63E-09	7.26E-09	1.54E-01	1.11E-09		2.53E-12	
1357	$4H_2S(aq) + CO_2(aq) \rightarrow 4sulfur + CH_4(aq) + 2H_2O$	8	-1.26E-08	-5.60E-01	-2.52E-07	-8.79E-01	-1.64E-09		-3.84E-10	
1358	$2H_2S(aq) + CO_2(aq) + H_2O \rightarrow S_2O_3^{-2} + CH_4(aq) + 2H^+$	8	-1.46E-08	-3.32E-09	-1.30E-07	2.45E-01	-1.55E-09	-5.74E-01	-3.60E-10	-1.34E-01
1359	$H_2S(aq) + CO_2(aq) + 2H_2O \rightarrow SO_4^{-2} + CH_4(aq) + 2H^+$	8	-1.58E-08	-8.27E-09	-4.83E-08	-7.41E-09	-9.62E-10		-2.77E-10	
1360	$4pyrite + CO_2(aq) + 8H^+ \rightarrow 8sulfur + CH_4(aq) + 4Fe^{+2} + 2H_2O$	8	-6.16E-04		-7.98E-07		-7.66E-07		-1.41E-04	
1361	$4pyrite + 3CO_2(aq) + 6H_2O \rightarrow 4S_2O_3^{-2} + 3CH_4(aq) + 4Fe^{+2}$	24	-2.53E-04	-1.64E-01	-2.72E-07	-1.82E-01	-2.47E-07	-1.57E-01	-4.47E-05	-2.15E-01
1362	$4pyrite + 7CO_2(aq) + 18H_2O \rightarrow 8SO_4^{-2} + 7CH_4(aq) + 8H^+ + 4Fe^{+2}$	56	-1.20E-04		-9.74E-08		-8.26E-08		-1.55E-05	
1363	$4sulfur + CO_2(aq) + 4H_2O \rightarrow 2S_2O_3^{-2} + CH_4(aq) + 4H^+$	8	-7.12E-05	6.17E-01	-8.47E-09	1.29E-01	1.27E-08	1.48E-01	3.56E-06	3.83E-01
1364	$4sulfur + 3CO_2(aq) + 10H_2O \rightarrow 4SO_4^{-2} + 3CH_4(aq) + 8H^+$	24	-3.79E-05		1.94E-08		3.14E-08		5.45E-06	
1365	$S_2O_3^{-2} + CO_2(aq) + 3H_2O \rightarrow 2SO_4^{-2} +$	8	-9.89E-09	-2.39E-09	-3.86E-09	3.65E-09	-2.99E-09	4.52E-09	-4.78E-09	2.79E-09

	$CH_4(aq) + 2H^+$							
1366	$12Fe^{+2} + CO_2(aq) + 14H_2O \rightarrow$ 4magnetite $+ CH_4(aq) + 24H^+$	8	-1.25E-06		-9.15E-10		-7.47E-10	-5.68E-12
1367	$8Fe^{+2} + CO_2(aq) + 10H_2O \rightarrow$ 4hematite $+ CH_4(aq) + 16H^+$	8	-1.16E-06		-8.09E-10		-5.56E-10	-5.34E-12
1368	$8Fe^{+2} + CO_2(aq) + 10H_2O \rightarrow$ 4maghemite $+ CH_4(aq) + 16H^+$	8	-1.64E-06		-2.20E-09		-1.95E-09	-6.88E-12
1369	$8Fe^{+2} + CO_2(aq) + 14H_2O \rightarrow$ 8goethite $+ CH_4(aq) + 16H^+$	8	-1.15E-06		-7.63E-10		-5.11E-10	-5.30E-12
1370	$8Fe^{+2} + CO_2(aq) + 14H_2O \rightarrow$ 8lepidocrocite $+ CH_4(aq) + 16H^+$	8	-1.74E-06		-2.49E-09		-2.24E-09	-7.21E-12
1371	$8Fe^{+2} + CO_2(aq) + 22H_2O \rightarrow$ 8ferrihydrite $+ CH_4(aq) + 16H^+$	8	-2.10E-06		-3.50E-09		-3.25E-09	-8.35E-12
1372	6fayalite $+ CO_2(aq) + 2H_2O \rightarrow$ 4magnetite $+ 6SiO_2(aq) + CH_4(aq)$	8	1.24E-04	3.23E-01	8.94E-08	1.66E-01	1.85E-07	5.23E-05
1373	12ferrosilite $+ CO_2(aq) + 2H_2O \rightarrow$ 4magnetite $+ 12SiO_2(aq) + CH_4(aq)$	8	-3.41E-06	3.95E-01	-4.18E-08	1.18E-01	1.31E-07	3.70E-05
1374	8magnetite $+ CO_2(aq) + 2H_2O \rightarrow$ 12hematite $+ CH_4(aq)$	8	6.21E-05		2.59E-08		4.60E-08	1.86E-05
1375	8magnetite $+ CO_2(aq) + 2H_2O \rightarrow$ 12maghemite $+ CH_4(aq)$	8	-2.67E-04		-3.14E-07		-2.89E-07	-6.66E-05
1376	8magnetite $+ CO_2(aq) + 14H_2O \rightarrow$ 24goethite $+ CH_4(aq)$	8	6.80E-05		3.71E-08		5.68E-08	2.07E-05
1377	8magnetite $+ CO_2(aq) + 14H_2O \rightarrow$ 24lepidocrocite $+ CH_4(aq)$	8	-3.39E-04		-3.84E-07		-3.58E-07	-8.49E-05
1378	8magnetite $+ CO_2(aq) + 38H_2O \rightarrow$ 24ferrihydrite +	8	-5.88E-04		-6.30E-07		-6.01E-07	-1.48E-04

	$CH_4(aq)$										
1379	$2H_2O + CO_2(aq) \rightarrow CH_4(aq) + 2O_2(aq)$	8	-1.64E-03	-1.57E-01	-1.79E-06	-1.59E-01	-1.74E-06		-4.35E-04	
Bicarbonate as an electron acceptor										
1380	$H_2(aq) + HCO_3^- + H^+ \rightarrow CO(aq) + 2H_2O$	2	8.19E-09	4.75E-01	-7.80E-10	-7.80E-01	-3.92E-10	-3.92E-01	-2.95E-12	-2.95E-12
1381	$2NH_4^+ + 3HCO_3^- + H^+ \rightarrow 3CO(aq) + N_2(aq) + 6H_2O$	6	-2.16E-05	-9.48E-01	-2.79E-07	-2.79E-01	-3.61E-07	-3.66E-01	-3.19E-09	-3.19E-09
1382	$2NH_4^+ + 4HCO_3^- + 2H^+ \rightarrow 4CO(aq) + N_2O(aq) + 7H_2O$	8	-1.05E-04	-8.92E-01	-8.14E-07	-7.65E-01	-1.04E-06	-9.79E-01	-1.01E-08	-9.38E-09
1383	$2NH_4^+ + 5HCO_3^- + 3H^+ \rightarrow 5CO(aq) + 2NO(aq) + 8H_2O$	10	-1.77E-04	-1.47E-01	-1.31E-06	-1.21E-01	-1.68E-06	-1.56E-01	-1.65E-08	-1.51E-01
1384	$NH_4^+ + 3HCO_3^- + H^+ \rightarrow 3CO(aq) + NO_2^- + 4H_2O$	6	-2.13E-04	-1.89E-01	-1.53E-06	-1.53E-01	-1.96E-06	-1.96E-01	-1.85E-08	-1.85E-01
1385	$NH_4^+ + 4HCO_3^- + 2H^+ \rightarrow 4CO(aq) + NO_3^- + 5H_2O$	8	-2.94E-04	-2.61E-01	-2.09E-06	-2.95E-01	-2.71E-06	-2.71E-01	-2.63E-08	-2.63E-01
1386	$N_2(aq) + HCO_3^- + H^+ \rightarrow CO(aq) + N_2O(aq) + H_2O$	2	-9.82E-07	-9.34E-01	-5.15E-06	-4.68E-01	-5.05E-05	-4.58E-01	-4.48E-05	-4.34E-01
1387	$N_2(aq) + 2HCO_3^- + 2H^+ \rightarrow 2CO(aq) + 2NO(aq) + 2H_2O$	4	-1.82E-06	-1.54E-01	-9.93E-06	-8.99E-01	-5.29E-05	-4.78E-01	-8.68E-05	-7.79E-01
1388	$N_2(aq) + 3HCO_3^- + H^+ \rightarrow 3CO(aq) + 2NO_2^- + 2H_2O$	6	-2.25E-06	-2.16E-01	-1.20E-05	-1.23E-01	-4.26E-05	-4.26E-01	-7.25E-05	-7.25E-01
1389	$N_2(aq) + 5HCO_3^- + 3H^+ \rightarrow 5CO(aq) + 2NO_3^- + 4H_2O$	10	-3.19E-06	-2.95E-01	-1.75E-05	-1.75E-01	-3.76E-05	-3.76E-01	-6.58E-05	-6.58E-01
1390	$N_2O(aq) + HCO_3^- + H^+ \rightarrow CO(aq) + 2NO(aq) + H_2O$	2	-3.92E-06	-2.82E-01	-8.37E-08	-6.12E-01	-8.33E-08	-6.78E-01	-7.87E-08	-5.65E-01
1391	$N_2O(aq) + 2HCO_3^- \rightarrow 2CO(aq) + 2NO_2^- + H_2O$	4	-5.91E-06	-5.47E-01	-1.17E-07	-1.93E-01	-1.16E-07	-1.84E-01	-1.00E-07	-9.28E-01
1392	$N_2O(aq) + 4HCO_3^- + 2H^+ \rightarrow 4CO(aq) + 2NO_3^- + 3H_2O$	8	-1.03E-05	-9.43E-01	-2.04E-07	-1.97E-01	-2.05E-07	-1.97E-01	-1.87E-07	-1.79E-01

1393	$2NO(aq) + HCO_3^- \rightarrow CO(aq) + 2NO_2^- + H^+$	2	-2.44E-08	-1.55E-01	-2.40E-08	-1.65E-01	-2.38E-08	-1.63E-01	-1.84E-08	-1.81E-01
1394	$2NO(aq) + 3HCO_3^- + 3H^+ \rightarrow 3CO(aq) + 2NO_3^- + 2H_2O + 2H^+$	6	-6.18E-08	-4.87E-01	-6.77E-08	-6.18E-01	-6.82E-08	-6.68E-01	-6.16E-08	-5.41E-01
1395	$NO_2^- + HCO_3^- + H^+ \rightarrow CO(aq) + NO_3^- + H_2O$	2	-8.87E-07	-7.98E-01	-6.33E-08	-6.33E-01	-6.70E-08	-6.70E-01	-4.32E-11	-4.32E-11
1396	$2H_2S(aq) + Fe^{+2} + HCO_3^- \rightarrow CO(aq) +$ pyrite $+ H^+ + 2H_2O$	2	-7.09E-09	2.29E-09	-4.12E-09	3.93E-09	-5.47E-10	-5.47E-01	-6.49E-12	-6.49E-12
1397	$H_2S(aq) + HCO_3^-(aq) + H^+ \rightarrow CO(aq) +$ sulfur $+ 2H_2O$	2	1.02E-07	1.30E-01	1.10E-04	1.19E-01	2.86E-08	2.86E-01	6.75E-09	6.75E-09
1398	$2H_2S(aq) + 4HCO_3^- + 2H^+ \rightarrow 4CO(aq) + S_2O_3^{-2} + 5H_2O$	8	-2.74E-08	-8.67E-09	-1.10E-05	-8.24E-01	-8.18E-09	-7.29E-09	-1.44E-09	-1.21E-09
1399	$H_2S(aq) + 4HCO_3^- + 2H^+ \rightarrow 4CO(aq) + SO_4^{-2} + 4H_2O$	8	-4.15E-08	-1.90E-01	-9.52E-06	-8.75E-01	-1.42E-08	-1.42E-01	-2.43E-09	-2.43E-09
1400	pyrite $+ HCO_3^- + 3H^+ \rightarrow CO(aq) +$ 2sulfur $+ Fe^{+2} + 2H_2O$	2	-2.54E-04	-2.14E-01	-2.35E-05	-2.35E-01	-2.31E-05	-2.36E-01	-3.14E-05	-3.14E-01
1401	pyrite $+ 3HCO_3^- + 3H^+ \rightarrow 3CO(aq) + S_2O_3^{-2} + Fe^{+2} + 3H_2O$	6	-1.45E-04	-7.85E-01	-1.37E-05	-1.20E-01	-1.33E-05	-1.16E-01	-1.79E-05	-1.46E-01
1402	pyrite $+ 7HCO_3^- + 5H^+ \rightarrow 7CO(aq) + 2SO_4^{-2} + Fe^{+2} + 6H_2O$	14	-1.05E-04	-6.49E-01	-1.04E-05	-1.43E-01	-1.02E-05	-1.22E-01	-1.38E-05	-1.38E-01
1403	$2sulfur + 2HCO_3^- \rightarrow 2CO(aq) + S_2O_3^{-2} + H_2O$	4	-9.01E-05	-1.00E+00	-8.77E-06	-6.22E-01	-8.43E-06	-5.89E-01	-1.11E-05	-6.25E-01
1404	sulfur $+ 3HCO_3^- + H^+ \rightarrow 3CO(aq) + SO_4^{-2} + 2H_2O$	6	-8.01E-05	-4.00E-01	-8.25E-06	-8.25E-01	-8.08E-06	-8.83E-01	-1.09E-05	-1.86E-01
1405	$S_2O_3^{-2} + 4HCO_3^- + 2H^+ \rightarrow 4CO(aq) + 2SO_4^{-2} + 3H_2O$	8	-3.56E-08	-1.40E-01	-5.44E-08	-4.69E-01	-5.42E-08	-4.67E-01	-4.08E-08	-3.33E-01
1406	$3Fe^{+2} + HCO_3^- + 2H_2O \rightarrow CO(aq) +$ magnetite $+ 5H^+$	2	-1.91E-06	-1.53E-01	-4.71E-09	-4.78E-09	-4.59E-09	-4.59E-09	-8.68E-12	-8.68E-12
1407	$2Fe^{+2} + HCO_3^- + H_2O \rightarrow CO(aq) +$ hematite $+ 3H^+$	2	-2.15E-06	-1.57E-01	-6.50E-09	-6.50E-01	-6.32E-09	-6.32E-09	-9.85E-12	-9.85E-12
1408	$2Fe^{+2} + HCO_3^- + H_2O \rightarrow CO(aq) +$	2	-2.63E-06	-2.49E-01	-7.89E-09	-7.89E-01	-7.71E-09	-7.72E-09	-1.14E-11	-1.14E-11

	maghemite + $3H^+$									
1409	$2Fe^{+2} + HCO_3^- + 2H_2O$ → CO(aq) + 2goethite + $3H^+$	2	-2.14E-06	-1.56E-01	-6.45E-09	-6.45E-01	-6.28E-09	-6.28E-01	-9.81E-12	-9.89E-12
1410	$2Fe^{+2} + HCO_3^- + 2H_2O$ → CO(aq) + 2lepidocrocite + $3H^+$	2	-2.73E-06	-2.15E-01	-8.18E-09	-8.18E-09	-8.00E-09	-8.00E-09	-1.17E-11	-1.17E-11
1411	$2Fe^{+2} + HCO_3^- + 4H_2O$ → CO(aq) + 2ferrihydrite + $3H^+$	2	-3.09E-06	-2.51E-01	-9.19E-09	-9.19E-09	-9.01E-09	-9.15E-09	-1.29E-11	-1.29E-11
1412	3fayalite + $2HCO_3^-$ + $2H^+$ → 2CO(aq) + 2magnetite + $3SiO_2(aq) + 2H_2O$	4	-3.14E-05	6.88E-01	-6.95E-06	-5.53E-01	-5.21E-06	-5.29E-01	-4.29E-06	-4.29E-01
1413	3ferrosilite + HCO_3^- + H^+ → CO(aq) + magnetite + $3SiO_2(aq)$ + H_2O	2	-6.97E-05	9.55E-01	-9.39E-06	-6.55E-01	-6.21E-06	-6.21E-01	-6.43E-06	-6.43E-01
1414	2magnetite + HCO_3^- + H^+ → CO(aq) + 3hematite + H_2O	2	-4.99E-05	-9.87E-01	-8.13E-06	-8.13E-01	-7.81E-06	-7.89E-01	-9.01E-06	-9.14E-01
1415	2magnetite + HCO_3^- + H^+ → CO(aq) + 3maghemite + H_2O	2	-1.49E-04	-1.90E-01	-1.45E-05	-1.45E-01	-1.41E-05	-1.49E-01	-2.10E-05	-2.96E-01
1416	2magnetite + HCO_3^- + H^+ + $2H_2O$ → CO(aq) + 6goethite	2	-4.81E-05	-8.99E-01	-7.93E-06	-7.93E-01	-7.61E-06	-7.67E-01	-8.72E-06	-8.73E-01
1417	2magnetite + HCO_3^- + H^+ + $2H_2O$ → CO(aq) + 6lepidocrocite	2	-1.71E-04	-1.39E-01	-1.58E-05	-1.58E-01	-1.54E-05	-1.54E-01	-2.35E-05	-2.35E-01
1418	2magnetite + HCO_3^- + H^+ + $8H_2O$ → CO(aq) + 6ferrihydrite	2	-2.46E-04	-2.58E-01	-2.04E-05	-2.35E-01	-2.00E-05	-2.00E-01	-3.23E-05	-3.23E-01
1419	HCO_3^- + H^+ → CO(aq) + $1/2O_2(aq)$ + H_2O	2	-5.63E-04	-4.83E-01	-4.19E-05	-3.83E-01	-4.14E-05	-4.14E-01	-7.25E-05	-7.25E-01
1420	$CH_4(aq)$ + $3HCO_3^-$ + $3H^+$ → 4CO(aq) + $5H_2O$	6	-2.57E-08	-1.77E-01	-3.75E-08	-3.75E-01	-5.53E-10	-5.53E-01	-1.08E-11	-1.82E-11
1421	$4H_2(aq)$ + HCO_3^- + H^+ → $CH_4(aq)$ + $3H_2O$	8	7.55E-08		2.63E-10		1.40E-10		6.59E-13	
1422	$8NH_4^+$ + $3HCO_3^-$ → $4N_2(aq)$ + $3CH_4(aq)$ + $5H^+$ + $9H_2O$	24	-8.52E-07		-3.18E-08		-3.49E-08		-7.47E-10	

1423	$2NH_4^+ + HCO_3^- \rightarrow N_2O(aq) + CH_4(aq) + H^+ + 2H_2O$	8	-7.77E-05	-7.77E-01	-4.85E-07	-4.36E-01	-6.08E-07	-5.45E-01	-6.80E-09	-6.12E-09
1424	$8NH_4^+ + 5HCO_3^- \rightarrow 8NO(aq) + 5CH_4(aq) + 3H^+ + 7H_2O$	40	-1.42E-04	-1.26E-01	-8.99E-07	-8.11E-01	-1.14E-06	-1.15E-01	-1.24E-08	-1.16E-01
1425	$4NH_4^+ + 3HCO_3^- \rightarrow 4NO_2^- + 3CH_4(aq) + 5H^+ + H_2O$	24	-1.72E-04		-1.03E-06		-1.31E-06		-1.36E-08	
1426	$NH_4^+ + HCO_3^- \rightarrow NO_3^- + CH_4(aq) + H^+$	8	-2.38E-04		-1.44E-06		-1.85E-06		-1.98E-08	
1427	$4N_2(aq) + HCO_3^- + H^+ + H_2O \rightarrow 4N_2O + CH_4(aq)$	8	-9.01E-07	-9.65E-01	-4.36E-06	-3.89E-01	-4.24E-05	-3.77E-01	-3.95E-05	-3.52E-01
1428	$2N_2(aq) + HCO_3^- + H^+ + H_2O \rightarrow 4NO + CH_4(aq)$	8	-1.66E-06	-1.47E-01	-8.34E-06	-7.43E-01	-8.19E-05	-7.26E-01	-7.61E-05	-6.72E-01
1429	$4N_2(aq) + 3HCO_3^- + 7H_2O \rightarrow 8NO_2^- + 3CH_4(aq) + 5H^+$	24	-2.01E-06		-9.62E-06		-9.44E-05		-8.36E-05	
1430	$4N_2(aq) + 5HCO_3^- + 9H_2O \rightarrow 8NO_3^- + 5CH_4(aq) + 3H^+$	40	-2.79E-06		-1.35E-05		-1.16E-04		-1.24E-04	
1431	$4N_2O(aq) + HCO_3^- + H_2O + H^+ \rightarrow 8NO + CH_4(aq)$	8	-3.55E-06	-2.66E-01	-7.11E-08	-4.86E-01	-7.05E-08	-4.80E-01	-6.97E-08	-4.74E-01
1432	$2N_2O(aq) + HCO_3^- + 3H_2O \rightarrow 4NO_2^- + CH_4(aq) + 3H^+$	8	-5.16E-06	-5.16E-01	-9.15E-08	-8.46E-01	-9.03E-08	-8.28E-01	-8.23E-08	-7.48E-01
1433	$N_2O(aq) + HCO_3^- + 2H_2O \rightarrow 2NO_3^- + CH_4(aq) + H^+$	8	-8.80E-06	-8.82E-01	-1.53E-07	-1.46E-01	-1.53E-07	-1.46E-01	-1.51E-07	-1.43E-01
1434	$8NO(aq) + HCO_3^- + 5H_2O \rightarrow 8NO_2^- + CH_4(aq) + 7H^+$	8	-2.12E-08	-1.37E-01	-1.77E-08	-1.22E-01	-1.74E-08	-9.92E-09	-1.39E-08	-6.34E-09
1435	$8NO(aq) + 3HCO_3^- + 7H_2O \rightarrow 3CH_4(aq) + 8NO_3^- + 5H^+$	24	-5.22E-08	-4.47E-01	-4.87E-08	-4.12E-01	-4.90E-08	-4.15E-01	-4.80E-08	-4.49E-01
1436	$4NO_2^- + HCO_3^- + H^+ + H_2O \rightarrow 4NO_3^- + CH_4(aq)$	8	-7.34E-07		-4.49E-08		-4.76E-08		-3.42E-11	
1437	$8H_2S(aq) + 4Fe^{+2} + HCO_3^- \rightarrow 4pyrite + CH_4(aq) + 7H^+ + 3H_2O$	8	-3.87E-09	3.63E-09	7.26E-09	1.54E-01	1.11E-09		2.52E-12	

1438	$4H_2S(aq) + HCO_3^- + H^+ \rightarrow 4sulfur + CH_4(aq) + 3H_2O$	8	-1.26E-08	-5.60E-09	-6.87E-06	-2.41E-01	-1.64E-09		-3.84E-10	
1439	$2H_2S(aq) + HCO_3^- \rightarrow S_2O_3^{-2} + CH_4(aq) + H^+$	8	-1.46E-08	-3.32E-09	-7.10E-06	1.12E-01	-1.55E-09	-5.74E-01	-3.61E-10	-1.35E-01
1440	$H_2S(aq) + HCO_3^- + H_2O \rightarrow SO_4^{-2} + CH_4(aq) + H^+$	8	-1.58E-08	-8.27E-09	-3.60E-06	-5.53E-01	-9.62E-10		-2.78E-10	
1441	$4pyrite + HCO_3^- + 9H^+ \rightarrow 8sulfur + CH_4(aq) + 4Fe^{+2} + 3H_2O$	8	-7.42E-04		-5.95E-05		-5.75E-05		-7.92E-05	
1442	$4pyrite + 3HCO_3^- + 3H^+ + 3H_2O \rightarrow 4S_2O_3^{-2} + 3CH_4(aq) + 4Fe^{+2}$	24	-3.05E-04	-1.98E-01	-2.02E-05	-1.34E-01	-1.85E-05	-1.18E-01	-2.51E-05	-1.28E-01
1443	$4pyrite + 7HCO_3^- + 11H_2O \rightarrow 8SO_4^{-2} + 7CH_4(aq) + H^+ + 4Fe^{+2}$	56	-1.45E-04		-7.25E-06		-6.20E-06		-8.70E-06	
1444	$4sulfur + HCO_3^- + 3H_2O \rightarrow CH_4(aq) + 2S_2O_3^{-2} + 3H^+$	8	-8.59E-05	7.44E-01	-6.31E-07	9.59E-01	9.55E-07	1.11E-01	1.99E-06	2.15E-01
1445	$4sulfur + 3HCO_3^- + 7H_2O \rightarrow 4SO_4^{-2} + 3CH_4(aq) + 5H^+$	24	-4.57E-05		1.45E-06		2.36E-06		3.05E-06	
1446	$S_2O_3^{-2} + HCO_3^- + 2H_2O \rightarrow 2SO_4^{-2} + CH_4(aq) + H^+$	8	-9.89E-09	-2.39E-01	-3.86E-09	3.65E-09	-2.99E-09	4.52E-09	-4.78E-09	2.77E-09
1447	$12Fe^{+2} + HCO_3^- + 13H_2O \rightarrow 4magnetite + CH_4(aq) + 23H^+$	8	-1.25E-06		-9.15E-10		-7.47E-10		-5.68E-12	
1448	$8Fe^{+2} + HCO_3^- + 9H_2O \rightarrow 4hematite + CH_4(aq) + 15H^+$	8	-1.16E-06		-8.09E-10		-5.56E-10		-5.34E-12	
1449	$8Fe^{+2} + HCO_3^- + 9H_2O \rightarrow 4maghemite + CH_4(aq) + 15H^+$	8	-1.64E-06		-2.20E-09		-1.95E-09		-6.88E-12	
1450	$8Fe^{+2} + HCO_3^- + 13H_2O \rightarrow 8goethite + CH_4(aq) + 15H^+$	8	-1.15E-06		-7.63E-10		-5.11E-10		-5.30E-12	
1451	$8Fe^{+2} + HCO_3^- + 13H_2O \rightarrow 8lepidocrocite + CH_4(aq) + 15H^+$	8	-1.74E-06		-2.49E-09		-2.24E-09		-7.22E-12	
1452	$8Fe^{+2} + HCO_3^- + 21H_2O \rightarrow 8ferrihydrite + CH_4(aq) + 15H^+$	8	-2.10E-06		-3.50E-09		-3.25E-09		-8.35E-12	

1453	6fayalite + HCO_3^- + H^+ + H_2O → 4magnetite + 6SiO_2(aq) + CH_4(aq)	8	1.49E-04	3.89E-01	6.66E-06	1.23E-01	1.39E-05	2.93E-05
1454	12ferrosilite + HCO_3^- + H^+ + H_2O → 4magnetite + 12SiO_2(aq) + CH_4(aq)	8	-4.11E-06	4.77E-01	-3.11E-06	8.25E-01	9.84E-06	2.07E-05
1455	8magnetite + HCO_3^- + H^+ + H_2O → 12hematite + CH_4(aq)	8	7.49E-05		1.93E-06		3.45E-06	1.04E-05
1456	8magnetite + HCO_3^- + H^+ + H_2O → 12maghemite + CH_4(aq)	8	-3.21E-04		-2.33E-05		-2.17E-05	-3.73E-05
1457	8magnetite + HCO_3^- + H^+ + 13H_2O → 24goethite + CH_4(aq)	8	8.20E-05		2.76E-06		4.26E-06	1.16E-05
1458	8magnetite + HCO_3^- + H^+ + 13H_2O → 24lepidocrocite + CH_4(aq)	8	-4.09E-04		-2.86E-05		-2.69E-05	-4.76E-05
1459	8magnetite + HCO_3^- + H^+ + 37H_2O → 24ferrihydrite + CH_4(aq)	8	-7.09E-04		-4.69E-05		-4.51E-05	-8.28E-05
1460	H_2O + HCO_3^- + H^+ → CH_4(aq) + 2O_2(aq)	8	-1.98E-03	-1.82E-01	-1.33E-04	-1.19E-01	-1.31E-04	-2.44E-04

APPENDIX F

RETRIVAL OF THE REVISED HELGESON-KIRKHAM-FLOWERS EQUATION OF STATE MODEL PARAMETERS FOR AQUEOUS NITRIC AND NITROUS OXIDE

F1. Introduction

As important intermediaries in the nitrogen cycle during nitrification and denitrification, nitrous oxide (N_2O) and nitric oxide (NO) have been measured at many different field locations across the world. Their thermodynamic properties have also been examined in the lab under a wide variety of conditions. This has led to a firm understanding of the thermodynamic properties of the gaseous forms of nitrous oxide and nitric oxide and how they interact with other species; however, thermodynamic data for characterizing their behavior in the most biorelevent state, the aqueous state, have yet to be determined. In order to remedy this, a literature search for applicable experimental values and theoretical correlation strategies were employed to derive a set of thermodynamic properties that will be consistent with the SUPCRT92 Slop07/10 database. This will allow researchers to calculate affinities for metabolic reaction pathways employed by microorganisms associated with the nitrogen cycle across the broad range of P-T conditions at which these organisms have been found to exist.

F2. Background

Using correlation strategies from Plyasunov and Shock (2001) parameters for the revised Helgeson-Kirkham-Flowers (HKF) equations of state (EoS) can be determined. Many of these correlation strategies rely on accurately knowing the Gibbs energy of hydration ($\Delta_h G^o$), defined as:

$$\Delta_h^v G^o = RTln\left(\Phi_2^\rho \frac{PV_1^o}{RT}\right) \quad \text{(F1)}$$

$\Delta_h^v G^o$ is the energy of transfer of a solute from the gas phase to an equal volume of solution (see Lin and Wood (1996) for more information on this representation); Φ_2^o and V_1^o stand for a fugacity coefficient of the infinitely dilute solute (subscript 2) and the molar volume of water (subscript 1), respectively. The power behind this approach lies in the relation between the Born charging energy (G_{Born}) and the $\Delta_h G^o$. The Born energy is the difference between the energy of charging a sphere of radius r (the approximation for an ion) from zero charge to Z_e in an incompressible continuum of dielectric constant ε and in a vacuum; and it is integral to continuum models and to the HKF EoS. G_{Born} is defined as follows (Born, 1920):

$$G_{Born} = -\left(\frac{(Z_e)N_A}{2r}\right)\left(\frac{1-\varepsilon}{\varepsilon}\right) \tag{F2}$$

Where Z designates the ionic charge of a species, $_e$ stands for the charge of an electron, and N_A is Avogadro's number. The Born charging energy process corresponds to the isochoric transfer process (Friedman and Krishnan, 1973; Ben-Naim, 1987). The Gibbs energy of hydration and the Born charging process are related to each other via the following relation:

$$\Delta_h G^o = G_{Born} + RTln\left(\frac{RT}{V_1^0 P^{\otimes}}\right) - RTln\left(\frac{1000}{M_w}\right) \tag{F3}$$

where V_1^0 represents the molar volume of water at the temperature and pressure of interest, $P^{\otimes}$ = 0.1 MPa or 1 bar and designates the standard pressure of the ideal gas state, where M_w = 18.015268 g mol^{-1} (Wagner and Pruß, 2002), the molar mass of water.

The following expression:

$$\Delta_h G^o(T) = RTln\ k_h - RTln\left(\frac{1000}{M_w}\right) \approx\ RTln\ k_h - RTln(55.51)$$

(F4)

relates the $\Delta_h G^o$ data of Willhelm et al. (1977) and others to that employed here for the correlation strategies that are to be imployed. It is the second term in the expression that is needed for conversion between the molality concentration scale employed for the Gibbs energy of hydration and the mole fraction concentration scale, that is used for Henry's constant. Note that the value of k_h has to be converted into the bar pressure units, because the standard pressure for the ideal gas is 0.1 MPa = 1 bar. Through this process, literature values from various sources can be used to drive the correlations and determine the HKF parameters necessary for performing thermodynamic calculations at temperatures and pressures other than 25 ^oC and 1 bar (standard temperature and pressure, STP).

The following is a summary of the correlations used in in Plyasunov and Shock (2001) that are employed here for N species. The values are in joules and the Gibbs energy of hydration is in kJ mol^{-1} (For the purposes of this work, final values for use in SupCrt92 have been converted to calories using the thermochemical calorie(4.184 J/cal) conversion factor.).

$$\omega \cdot 10^{-5} = 2.61 + \frac{324.1}{\Delta_h G^o - 90.6}$$

(F5)

$$\sigma = 1.069 V_2^o$$

(F6)

$$\frac{10 \cdot a_1}{V_2^o} = 0.820 - 1.85 \cdot 10^{-3} \cdot \Delta_h G^o$$

(F7)

$$\frac{10^{-2} \cdot a_2}{V_2^o} = 0.648 - 4.81 \cdot 10^{-3} \cdot \Delta_h G^o$$

(F8)

$$10^{-4} \cdot a_4 = 8.10 - 0.746 \cdot 10^{-2} a_2 + 0.219 \cdot \Delta_h G^o$$

(F9)

$$a_3 = -11.9 - 3.09 \cdot 10^{-4} \cdot a_4$$

(F10)

$$10^{-4} \cdot c_2 = 2.14 + 0.849\, \Delta_h G^o$$

(F11)

The last parameter in the HKF EoS (not introduced yet in this section), c_1, can then be solved using experimental values of the standard partial molal heat capacity, $\bar{C}_p^o$, and the following relation from the HKF EoS (Helgeson and Kirkham (1976), Helgeson et al. (1981), Shock and Helgeson (1988), Tanger and Helgeson (1988), Shock et al. (1989), etc.) :

$$\bar{C}_p^o = \Delta\bar{C}_{p,n}^o + \Delta\bar{C}_{p,s}^o$$

$$= c_1 + \frac{c_2}{(T-\Theta)^2} - \left(\frac{2T}{(T-\Theta)^3}\right)\left(a_3(P - P_r) + a_4 ln\left(\frac{\Psi + P}{\Psi + P_r}\right)\right)$$

$$+ \omega TX + 2TY\left(\frac{\partial \omega}{\partial T}\right)_P - T\left(\frac{1}{\varepsilon} - 1\right)\left(\frac{\partial^2 \omega}{\partial T^2}\right)_P$$

(F12)

In this formulation $\Delta\bar{C}^{o}_{p,n}$ and $\Delta\bar{C}^{o}_{p,s}$ are the nonsolvation and solvation contributions to the heat capacity; c_1, c_2, and a_1 through a_4 are the species-dependent nonsolvation parameters; T_r, P_r, P, and T are the reference temperature of 298.15 K, the reference pressure of 1 bar, and the temperature and pressure of interest, respectively; ε stands for the dielctric constant of water. Ψ and Θ refer to solvent parameters equal to 2600 bars and 228 K respectively. The terms X and Y denote Born functions given by:

$$X \equiv \frac{1}{\varepsilon}\left(\left(\frac{\partial^2 ln\varepsilon}{\partial T^2}\right)_P - \left(\frac{\partial ln\varepsilon}{\partial T}\right)_P^2\right) \tag{F13}$$

and

$$Y \equiv \frac{1}{\varepsilon}\left(\frac{\partial ln\varepsilon}{\partial T}\right)_P \tag{F14}$$

ω is the conventional Born coefficient defined for the *j*th aqueous species by:

$$\omega_j \equiv \omega_j^{abs} - Z_j\omega_{H^+}^{abs} \tag{F15}$$

where Z_j stands for the formal charge on the *j*th aqueous species, $\omega_{H^+}^{abs}$ refers to the absolute Born coefficient of the hydrogen ion, which is taken to be 0.5387×10^5 cal mol^{-1} at 25 ^{o}C and 1 bar (Helgeson and Kirkham, 1976) and ω_j^{abs} is the absolute Born coefficient of the *j*th species. ω_j^{abs} is given by:

$$\omega_j^{abs} \equiv \frac{N_A\, e^2 Z_j^2}{2r_{e,j}} = \frac{\eta\, Z_j^2}{r_{e,j}} \tag{F16}$$

where N_A is Avogardro's number, e stands for the absolute electronic charge (4.80298 × 10^{-10} esu), η = 1.66027 × 10^5 Å cal mol^{-1} , and $r_{e,j}$ denotes the effective electrostatic radius of the *j*th species. $r_{e,j}$ is given by:

$$r_{e,j} = r_{x,j} + |Z_j|\Gamma_{\pm}$$

(F17)

where $r_{x,j}$ is the crystallographic radius of the *j*th species and $\Gamma_{\pm}$ is given by:

$$\Gamma_{\pm} \equiv k_z + g$$

(F18)

k_z represents a charge-dependent constant equivalent to 0.0 for anions and 0.94 for cations and g designates a solvent function of temperature and density. Finally, the g function has been experimentally determined and treated in several other publications (Tanger and Helgeson, 1988; Shock et al. 1989, etc.) and the reader is encouraged to explore these resources for further information since this is beyond the scope for the material being treated here. It should be noted that at lower temperatures and pressures, the g function and its partial derivatives approach zero. Moreover, below 175 ^oC and 2450 bars Eqn F12 simplifies to the isobaric form of the heat capacity equation; for aqueous nonelectrolytes the isobaric form is given by Shock et al. (1989):

$$\bar{C}_p^o = c_1 + \frac{c_2}{(T-\Theta)^2} + \omega_e TX$$

(F19)

where ω_e is the effective Born coefficient determined either by the previously mentioned correlations from Plyasunov and Shock (2001) or by alternate methodsthat may include,

but are not limited, to other correlation strategies, group contribution algorithms, etc. From Eqn. (F19) c_1 is readily solvable using the previously determined values for ω and c_2 from the correlation strategies and $\bar{C}_p^o$ from experimental data sources.

Tables F1 through F3 display the standard partial molal thermodynamic properties of aqueous nitric and nitrous oxide as well as the gaseous properties. Figure F1 displays the Gibbs energy of formation and heat capacity of nitric and nitrous oxides with respect to dissolved nitrogen and carbon dioxide across the liquid vapor saturation curve.

Table F1. Standard state thermodynamic properties of aqueous nitric oxide and nitrous oxide.

Specie name	Formula	$\Delta\bar{G}_f^o$ [a,d]	$\Delta\bar{H}_f^o$ [a,e]	$\bar{S}^o$ [b,f]	$\bar{C}_p^o$ [b,g]	V^o [c,h]
Nitric oxide	NO(aq)	24390.	18750.	28.5	54.4	27.
Nitrous oxide	N_2O(aq)	27100.	14660.	28.6	6.8	36.

[a] cal mol^{-1}, [b] cal mol^{-1} K^{-1}, [c] cm^3 mol^{-1}, [d] calculated from $\Delta\bar{G}_h^o$ (g ←→ aq) given by Wilhelm et al. (1977) and Cabani and Gianni (1986), and $\Delta\bar{G}_f^o$ (g) from Wagman et al. (1982). [e] calculated from $\Delta\bar{H}_h^o$ (g ←→ aq) given by Wilhelm et al. (1977) and Cabani and Gianni (1986), and $\Delta\bar{H}_f^o$ (g) from Wagman et al. (1982), [f] calculated from values of $\Delta\bar{G}_f^o$ and $\Delta\bar{H}_f^o$ in the table, together with the values of $\bar{S}^o$ of the elements from Cox et al. (1989), [g] Values of $\bar{C}_p^o$ for the aqueous species are calculated from $\Delta\bar{C}_p^o$ (g ←→ aq) given by Wilhelm et al. (1977) and Cabani and Gianni (1986), and $\bar{C}_p^o$ (g) from Wagman et al. (1982), [h] estimated by Plyasunov et al. (2000a)

Table F2. Fitting parameters for the Helgeson-Kirkham-Flowers equations of state for aqueous nitric oxide and nitrous oxide.

Specie name	Formula	$a_1 * 10$ [a]	$a_2 * 10^{-2}$ [b]	a_3 [c]	$a_4 * 10^{-4}$ [d]	c_1 [e]	$c_2 * 10^{-4}$ [d]	$\omega * 10^{-5}$ [b]
Nitric oxide	NO(aq)	5.107	4.662	1.670	-1.461	33.91	8.258	-0.4075
Nitrous oxide	N_2O(aq)	6.909	5.957	4.757	-2.460	-10.38	6.983	-0.3279

HKF parameters determined using the correlation strategies described in Plyasunov and Shock (2001), [a] cal mol^{-1} bar^{-1}, [b] cal mol^{-1}, [c] cal K mol^{-1} bar^{-1}, [d] cal mol^{-1} K, [e] cal mol^{-1} K^{-1},

Table F3. Standard molar thermodynamic properties of gaseous nitric oxide and nitrous oxide.

Specie Name	Specie Formula	ΔG_f^o [a]	ΔH_f^o [a]	S_f^o [b]	V^o [c]	C_p^o [b]	a [b]	b * 10^3 [d]	c * 10^{-5} [e]	T_{MAX} [f]
Nitric Oxide,g	NO(g)	20690.[g]	21570.[g]	50.373[g]	-	7.1[h]	6.295[i]	1.836[i]	0.249[i]	1000.[j]
Nitrous Oxide,g	N_2O(g)	24900.[g]	19610.[g]	52.545[g]	-	9.2[h]	9.833[i]	3.512[i]	-1.492[i]	1000.[j]

[a] cal mol^{-1}, [b] cal mol^{-1} K^{-1}, [c] cm^3 mol^{-1}, [d] cal mol^{-1} K^{-2}, [e] cal mol^{-1} K, [f] maximum temperature of validity for Maier-Kelley coefficients in degrees Kelvin, [g] Wagman et al. (1982), [h] calculated from the Maier-Kelley equation at 298.15 K, [i] Maier-Kelley Coefficients calculated from fitting a curve of the Maier-Kelley equation to the C_p^o data from Stull et al. (1969) as found in Amend and Shock (1995), [j] Stull et al. (1969).

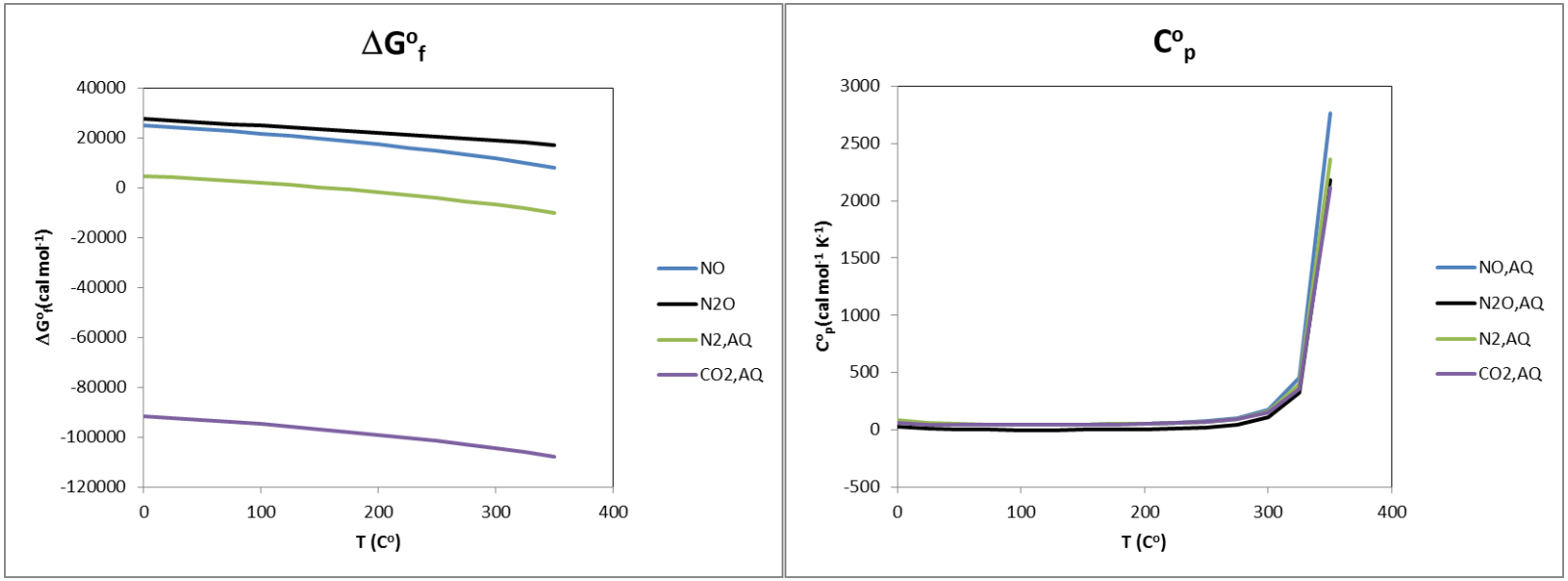

Figure F1. Gibbs energy of formation and heat capacity of nitric oxide and nitrous oxide with respect to dissolved nitrogen and carbon dioxide across the liquid vapor saturation curve.

APPENDIX G

CRITICAL ASSESMENT OF THE STANDARD PARTIAL MOLAR THERMODYNAMIC PROPERTIES OF GOETHITE (α-FeOOH), LEPIDOCROCITE (γ-FeOOH), MAGHEMITE (γ-Fe_2O_3), AND FERRIHYDRITE (FeOOH•XH_2O)

G1. Introduction

Iron oxides and (oxy)hydroxides are ubiquitous across all known biologically relevant environments as well as many geological settings where life may or may not be present. The role of iron oxides in biogeochemical processes is directly linked to microbial metabolisms, weathering, alteration, element, and nutrient cycling. With this in mind, understanding their thermodynamic properties allows investigations that elucidate how geochemical and biological processes interact to shape the physical, chemical, and energetic landscape of the natural environment.

Often times, iron oxides in the natural environment occur as hydrated, poorly crystalline nanoparticles with high surface energies. This makes it difficult to characterize their composition, their extent of hydration, and their thermodynamic properties. Many studies have shown that there is correlations between iron oxide surface area and excess water, as well as enthalpy making characterization and determination of the thermodynamic properties even more difficult to determine (Mazeina and Navrotsky, 2005; Bomatí-Miguel et al., 2008; Laberty and Navrotsky, 1998; Majzlan et al., 2007; Majzlan et al., 2003a,b; Schwertmann, 1988; etc.). In 2003 an extensive review of iron oxide crystallography, chemistry, mineralogy, and technological applications was performed by Cornell and Schwertmann and may be of use to readers seeking further information.

Here we analyze the best data sets available for these minerals and normalize them to the thermodynamic data from Helgeson et al. (1978), Shock et al. (1989, 1992, 1997a,b), Shock and McKinnon (1993), and Sverjensky et al. (1997), which are all part

of an internally consistent database of thermodynamic properties for use with the SUPCRT92 computer code (Johnson et al., 1992). We use the revised Helgeson-Kirkham-Flowers equation of state (Shock et al., 1992, 1997a) and are consistent with standard Gibbs energies for metabolic reactions summarized by Amend and Shock (2001) so thermodynamic calculations across a range of temperatures and pressures can be performed to assess the feasibility of reactions involving these species as constituents. Table G1 summarizes the thermodynamic properties of these minerals used with other internally consistent data.

G2. Goethite (α-FeOOH), Lepidocrocite (γ-FeOOH), and Maghemite (γ-Fe_2O_3)

G2.1. Entropy, Heat Capacity, and Volume

The entropy, heat capacity, and volume (Table G1) for goethite, lepidocrocite, and maghemite, are taken from Majzlan et al. (2003a). The authors use heat capacity data that were corrected for excess water using a Debye-Einstein representation of the C_p of hexagonal ice. Heat capacity was expressed as a function of temperature and inserted into equation 1 to calculate the entropy at standard temperature and pressure (STP, 1 bar and 25 ^{o}C):

$$S_m = \int_0^T \frac{C_{p,m}}{T}\, dT \qquad \text{(G1)}$$

where S_m is the standard molar entropy, T is the temperature in Kelvin, and $C_{p,m}$ is the molar isobaric heat capacity. While the measured data for entropy, heat capacity and volume were taken in this work, the Maier-Kelley coefficients were retrieved by

regressing the heat capacity data via non-linear least squares fit method from Kemmer and Keller (2010). Coefficients were regressed for the following functional form:

$$C^o_{P_r,i} = a_i + b_i T + c_i T^{-2} \quad \text{(G2)}$$

where $C^o_{P_r,i}$ is the molar isobaric heat capacity, T is the temperature in Kelvin and a_i, b_i, and c_i are fitting parameters reported in the format consistent with entry into the SupCrt92 software package (Johnson et al. 1992).

G2.2. Enthalpy of Formation and Gibbs Free Energy of Formation

To derive the enthalpy of formation (ΔH^o_f) of the iron (oxy)hydroxides of interest with zero surface area and nominal composition it is necessary to regress the enthalpy data of several samples with different surface areas and hydration states. Data from Mazeina and Navrotsky (2005), Majzlan et al. (2003b, 2007), Bomatí-Miguel et al. (2008) were regressed after being normalized to the previously mentioned data sources by using values of water, steam, hematite, the elements, etc., from Helgeson et al. (1978) and Wagman et al. (1982). Therefore, values calculated in this work for the enthalpy of formation and the Gibbs free energy of formation (ΔG^o_f) differ slightly from the values previsously obtained due to our use of thermodynamic data values (Table G2) to provide consistency as opposed to using data from Robie and Hemingway (1995). An example of this difference can be found in Figure G1. We note that the slope of the regression (i.e., the surface enthalpy) does not change because the corrections are universal across each sample, resulting in only a difference in the y-intercept (i.e., the standard molar enthalpy of formation). The differences between this work and that of previous authors for the standard enthalpy of formation of goethite, lepidocrocite, and maghemite are

approximately -125, -144, and -280 cal mol^{-1}, respectively. The standard Gibbs energy of formation (ΔG_f^o) can be calculated as follows:

$$\Delta G_f^o = \Delta H_f^o - T\Delta S_f^o \quad \text{(G3)}$$

$$\Delta S_f^o = S^o{}_{(\mathrm{Fe(III)-min,cr})} - aS_{Fe,cr}^o - bS_{O_2,g}^o - cS_{H_2,g}^o \quad \text{(G4)}$$

Where T = 298.15 K, and $S_{Fe,cr}^o$, $S_{O_2,g}^o$, and $S_{H_2,g}^o$ are the entropies of the subscripted elements; a, b, and c are the appropriate coefficients for the formation of the iron (oxy)hydroxide of interest, and $S^o{}_{(\mathrm{Fe(III)-min,cr})}$ is the entropy of the iron (oxy)hydroxide of interest. Equations 3 & 4 provide the ΔG_f^o presented in Table G1.

G3. Ferrihydrite ($FeOOH \bullet XH_2O$)

G3.1. Entropy and Heat Capacity

Entropy and heat capacity data for two line ferrihydrite ($FeOOH \bullet 0.027H_2O$) is taken from Snow et al. (2013) and used to estimate the properties for various states of hydration. The entropy of completely hydrated two line ferrihydrite ($Fe(OH)_3$) was estimated using isostructural pairs of Fe(III) and Al(III) phases: corundum-hematite, γ-alumina-maghemite, diaspore-goethite, boehmite-lepidocrocite, and gibbsite-ferrihydrite ($Fe(OH)_3$). These were plotted against each other (Fig. G2) in an approach similar to that of Majzlan et al. (2004). This entropy estimation for fully hydrated ferrihydrite was then combined with ferrihydrite ($FeOOH \bullet 0.027H_2O$) to estimate the fully anhydrous form (FeOOH) as depicted in Fig. G3. With this estimation, one could derive values of entropy for any ferrihydrite hydration state. An analogous approach was taken for the

heat capacities, whereby the isostructural pairs of Fe(III) and Al(III) phases were used to derive the heat capacity for the fully hydrated for of ferrihydrite (Fig. G4) and then used with the heat capacities for two line ferrihydrite ($FeOOH \bullet 0.027H_2O$) to estimate the anhydrous form (Fig. G5). Data used for these estimations can be found in Table G3.

The Maier-Kelley coefficients for two line ferrihydrite ($FeOOH \bullet 0.027H_2O$) were retrieved by regressing the heat capacity data from Snow et al. (2013) in the same manner as for goethite, lepidocrocite, and maghemite. In order to estimate the Maier-Kelley coefficients for the fully hydrated and anhydrous forms of ferrihydritewe followed the assumption from Helgeson et al. (1978): that the contribution of structural and zeolitic water to the standard molal heat capacities of minerals can be estimated by assuming it to be zero. Specifically,

$$\psi + \ n_{H_2O_{(z)}} H_2O_{(z)} \rightleftharpoons \ \psi \bullet n_{H_2O_{(z)}} H_2O_{(z)} \tag{G5}$$

and $\Delta S^o_{r.P_r,T_r} = \Delta C^o_{p,r.P_r,T_r} = 0$; where ψ is a dehydrated mineral, $n_{H_2O_{(z)}}$ is the reaction coefficient for water, and $\psi \bullet n_{H_2O_{(z)}} H_2O_{(z)}$ is the hydrated equivalent of ψ in which the water molecules are bound. If the $\Delta C^o_{p,r.P_r,T_r}$ of (G5) is taken to be zero, then the Maier-Kelley coefficients can be estimated for other forms of ferrihydrite by solving for the a_i term in equation G2 using the $C^o_{p,r.P_r,T_r}$ and the same b_i and c_i terms from ferrihydrite ($FeOOH \bullet 0.027H_2O$) in equation 2.

G3.2. Molar Volume

The molar volume for ferrihydrite was estimated using data and correlation strategies from Hiemstra and Riemsdijk (2009). Reconstructing their figure six (also Fig.

G6 in this work) allows the density of ferrihydrite to be determined and put in the context of only ferrihydrite (Fig. G7). Using data from Hiemstra and Riemsdijk (2009) the relationship between density and the molar mass (expressed per mole oxygen) can be expressed between density and the extent of hydration for both 2 and 6 line ferrihydrite (Fig. G8) and subsequently, just 2-line ferrihydrite (Fig. G9). Given that the density (in g cm^{-3}) is known, as well as the gram formula molar mass, the molar volume can be calculated.

G3.3. Enthalpy of Formation and Gibbs Free Energy of Formation

The enthalpy of formation for ferrihydrite ($FeOOH \bullet 0.027H_2O$) from Snow et al. (2013) was recalculated and normalized analogous to goethite, lepidocrocite, and maghemite. The enthalpy of formation for anhydrous and fully hydrated ferrihydrite was estimated using the values derived in this work from Snow et al. (2013), as well as recalculated and normalized using the data from Majzlan et al. (2004) for 2-line ferrihydrite (Fig.G10). Using the values estimated from the correlation in Fig. G10 and the previous entropies; Gibbs energies of formation were calculated for ferrihydrite ($FeOOH \bullet 0.027H_2O$), ferrihydrite ($FeOOH \bullet 1.0H_2O$), and ferrihydrite ($FeOOH \bullet 0.0H_2O$) using equations G3 and G4.

Table G1. Thermodynamic data for iron (oxy)hydroxides consistent with data for aqueous iron ions and other iron minerals in the SUPCRT92 database (Johnson et al. 1992); Coefficients a, b, and c are from the Maier-Kelley equation for the temperature dependence of the heat capacity (Helgeson et al 1978).

Mineral Name	Mineral Formula	ΔG_f^o [a]	ΔH_f^o [a]	S_f^o [b]	V^o [c]	C_p^o [b]	a [b]	b(10^3) [d]	c(10^{-5}) [e]	T_{MAX} [f]
Goethtite	α-FeOOH	-117363[k]	-134327[m]	14.27[h]	20.88[h]	17.77[h]	-4.016[t]	64.72[t]	2.17041[t]	375[h]
Lepidocrocite	γ-FeOOH	-115480[k]	-132062[n]	15.55[h]	22.40[h]	16.52[h]	12.92[t]	17.22[t]	-1.35237[t]	390[h]
Maghemite	γ-Fe_2O_3	-175097[k]	-194233[o]	22.24[h]	32.80[h]	25.02[h]	25.78[t]	15.23[t]	-4.66232[t]	760[h]
Ferrihydrite, 2l	FeOOH ·0.027 H_2O [g]	-115184[k]	-129797[i]	17.14[i]	21.66[j]	18.99[i]	11.03[u]	32.51[u]	-1.54166[u]	300[i]
	FeOOH	-111474[k]	-127680[p]	16.81[l]	21.45[j]	18.66[r]	10.70[v]	32.51[v]	-1.54166[v]	300[i]
	$Fe(OH)_3$	-170972[k]	-200115[p]	29.17[q]	33.70[j]	30.96[s]	23.00[v]	32.51[v]	-1.54166[v]	300[i]

[a] cal mol^{-1}, [b] cal mol^{-1} K^{-1}, [c] cm^3 mol^{-1}, [d] cal mol^{-1} K^{-2}, [e] cal mol^{-1} K, [f] maximum temperature of validity for Maier-Kelley coefficients in degrees Kelvin, [g] composition of synthetic 2-line Ferrihydrite from Snow et al. (2013), [h] Majzlan et al. (2003a), [i] Snow et al. (2013), [j] estimated using correlation strategies modified from Heimstra and Riemdijk (2009) as described in the text and Figs. G 6-G10, [k] calculated from the enthalpy and entropy data from the table along with the entropy of the elements from Wagman et al. 1982, [l] estimated using correlation in Figure G3 for the estimated entropy of formation of $Fe(OH)_3$ and FeOOH ·0.027 H_2O in the above table, [m] data from Mazeina and Navrotsky (2005) recalculated and normalized to be consistent with other data sources described in the text, [n] data from Majzlan et al. (2003b, 2007) recalculated and normalized to be consistent with other data sources described in the text, [o] data from Bomatí-Miguel et al. (2008) recalculated and normalized to be consistent with other data sources described in the text, [p] estimated via the correlation in Figure G10 using data for 2-line ferrihydrite from Snow et al. (2013) and Majzlan et al. (2004) that was recalculated and normalized to be consistent with other data sources described in the text, [q] estimated using the correlation in Figure G2 using entropy of formation data for iron and alumina analogs, [r] estimated using correlation in Figure G5 for the estimated heat capacity of $Fe(OH)_3$ and FeOOH ·0.027 H_2O in the above table, [s] estimated using the correlation in Figure G4 using heat capacity data for iron and alumina analogs, [t] regressed using data from Majzlan et al. (2003a), [u] regressed using data from Snow et al. 2013, [v] calculated by holding the b_i and c_i parameters of the Maier-Kelly power function constant and solving for the a_i parameter from the estimated heat capacity.

Table G2. Thermodynamic data used in this study to normalize thermodynamic values to those of other studies and provide internal consistency for thermodynamic calculations. All data in the table are from Helgeson et al. 1978, Wagman et al. 1982, or calculated using SUPCRT92 (Johnson et al. 1992) and a database utilizing the previous reference values.

Specie Name	Specie Formula	$\Delta\overline{G_f^o}$ [a]	$\Delta\overline{H_f^o}$ [a]	$\overline{S_f^o}$ [b]
Hydrogen gas	H_2 , g			31.234
Oxygen gas	O_2 , g			49.029
Oxygen gas (700°C)	O_2 , g (700 °C)	-36626	5169	58
Carbon	C_{xl}			1.4
Carbon dioxide gas	CO_2, g			51.1
Carbon dioxide gas (700 °C)	CO_2, g , (700 °C)	-133706	-86494	64
Water	H_2O,l	-56688	-68317	16.712
Steam	H_2O,g	-54524.8	-57935.1	44.763
Steam, (700/701°C)	H_2O,g (700/701°C)	-89104 / -89160	-51851 / -51842	55.4 / 55.4
Iron metal	Fe_{xl}			6.52
Hematite	α-Fe_2O_3	-178155	-197720	20.94

[a] cal mol^{-1}, [b] cal mol^{-1} K^{-1},

Table G3. Summary of the standard partial molar thermodynamic properties of iron and aluminum (oxy)hydroxides and oxides.

Mineral Name	Mineral Formula	$\Delta\overline{G_f^o}$ [a]	$\Delta\overline{H_f^o}$ [a]	$\overline{S_f^o}$ [b]	$\overline{C_p^o}$ [b]
Hematite	α–Fe_2O_3	-178155[c]	-197720[c]	20.94[c]	25.04[c]
Maghemite	γ–Fe_2O_3	-175097[d]	-194233[e]	22.40[f]	25.02[f]
Goethite	α–FeOOH	-117363[d]	-134327[g]	14.27[f]	17.77[f]
Lepidocrocite	γ–FeOOH	-115480[d]	-132062[h]	15.55[f]	16.52[f]
Ferrihydrite, 2l	FeOOH ·0.027 H_2O [i]	-115184[d]	-129797[j]	17.14[k]	18.99[k]
	FeOOH	-111474[d]	-127680[l]	16.81[m]	18.66[n]
	$Fe(OH)_3$	-170972[d]	-200115[l]	29.17[o]	30.96[p]
Corundum	α–Al_2O_3	-374824[c]	-397145[c]	12.17[q]	18.9[c]
Gamma-alumina	γ–Al_2O_3	-373769[r]	-396000[r]	12.5[r]	19.77[r]
Diaspore	α–AlOOH	-218402[c]	-237170[c]	8.44[q]	15.7[c]
Boehmite	γ–AlOOH	-217250[c]	-235078[c]	8.89[q]	15.7[c]
Gibbsite	$Al(OH)_3$	-276168[c]	-309065[c]	16.35[q]	22.2[c]

[a] cal mol^{-1}, [b] cal mol^{-1} K^{-1}, [c] data from Helgeson et al. (1978), [d] calculated from the enthalpy and entropy data in the table along with the entropy of the elements from Wagman et al. 1982, [e] data from Bomatí-Miguel et al. (2008) recalculated and normalized to be consistent with other data sources described in the text, [f] Majzlan et al. (2003a), [g] data from Mazeina and Navrotsky (2005) recalculated and normalized to be consistent with other data sources described in the text, [h] data from Majzlan et al. (2003b, 2007) recalculated and normalized to be consistent with other data sources described in the text, [i] composition of synthetic 2-line ferrihydrite from Snow et al. (2013), [j] data from Snow et al. (2013) recalculated and normalized to be consistent with other data sources described in the text, [k] data from Snow et al. (2013), [l] estimated via the correlation in Figure 10 using data for 2-line ferrihydrite from Snow et al. (2013) and Majzlan et al. (2004) that was recalculated and normalized to be consistent with other data sources described in the text e, [m] estimated using correlation in Figure 3 for the estimated entropy of formation of $Fe(OH)_3$ and FeOOH ·0.027 H_2O in the above table, [n] estimated using correlation in Figure 5 for the estimated heat capacity of $Fe(OH)_3$ and FeOOH ·0.027 H_2O in the above table, [o] estimated using the correlation in Figure 2 using entropy of formation data for iron and alumina analogs from the above table, [p] estimated using the correlation in Figure 4 using heat capacity data for iron and alumina analogs from the above table, [q] data from Robie and Hemingway (1995), [r] data from Chase (1998).

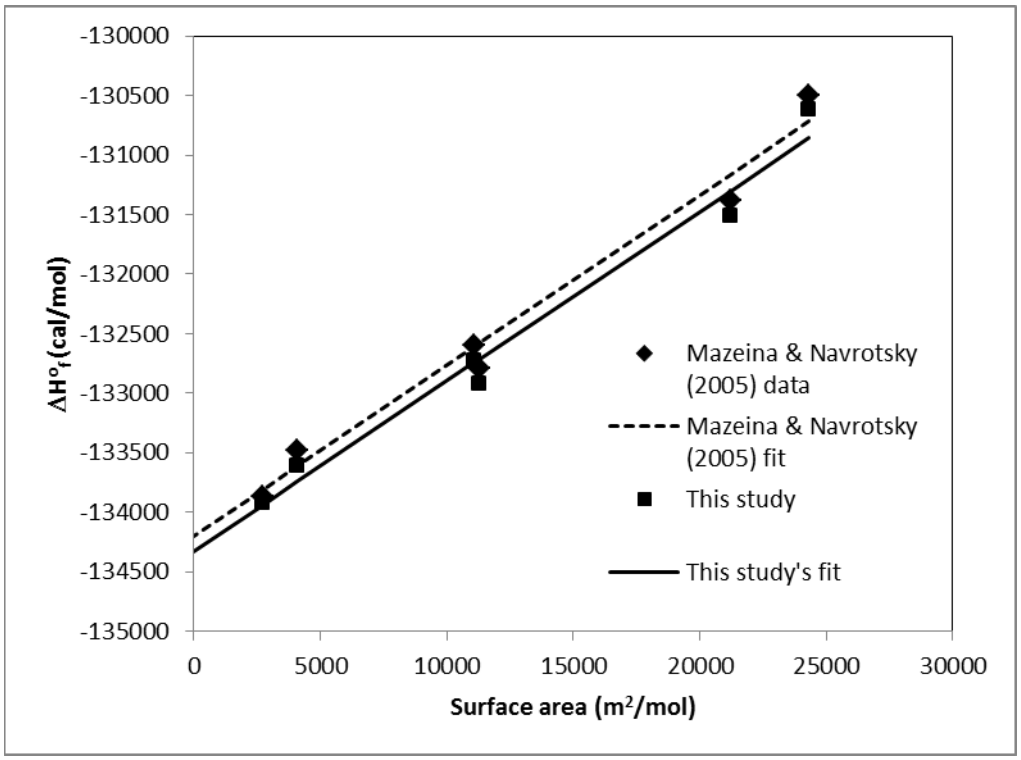

Figure G1. Enthalpy of formation (ΔH_f^o) of goethite recalculated using high-temperature calorimetry data as a function of surface area from Mazeina and Navrotsky (2005). The data points that are diamonds and the dashed regression line are from the original work, while the data points that are squares and the solid regression line were re-calculated here to be consistent with other data sources described in the text of Appendix G above. The offset is approximately 125 cal mol^{-1} due to the difference in values used for hematite, steam, and water.

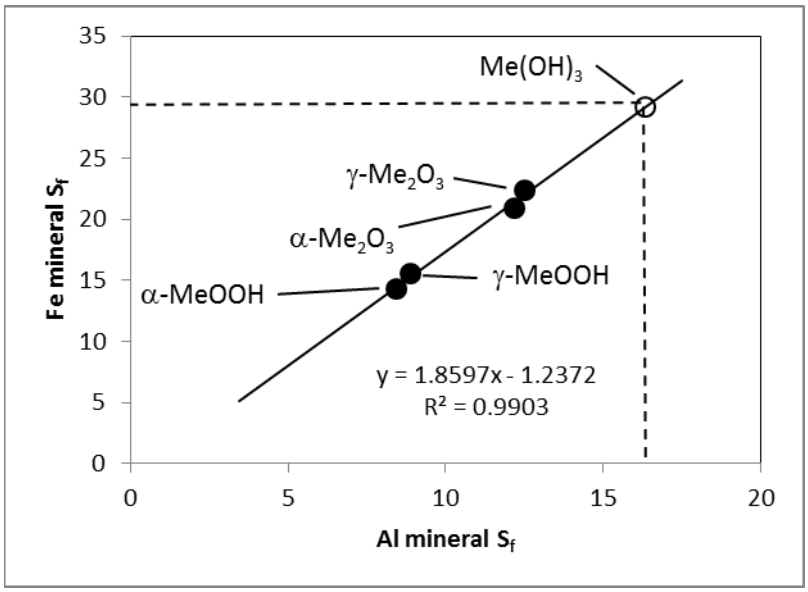

Figure G2. Entropy of formation for isostructural pairs of Fe(III) and Al(III) phases: corundum-hematite, gamma alumina – maghemite, diaspore-goethtite, boehmite-lepidocrocite, and gibbsite-ferrihydrite as $Fe(OH)_3$, data located in Table G3 (After Majzlan et al., 2004). Closed symbols are isostructural pairs with known thermodynamic data, open symbols are estimated from correlations based on the known value for gibbsite.

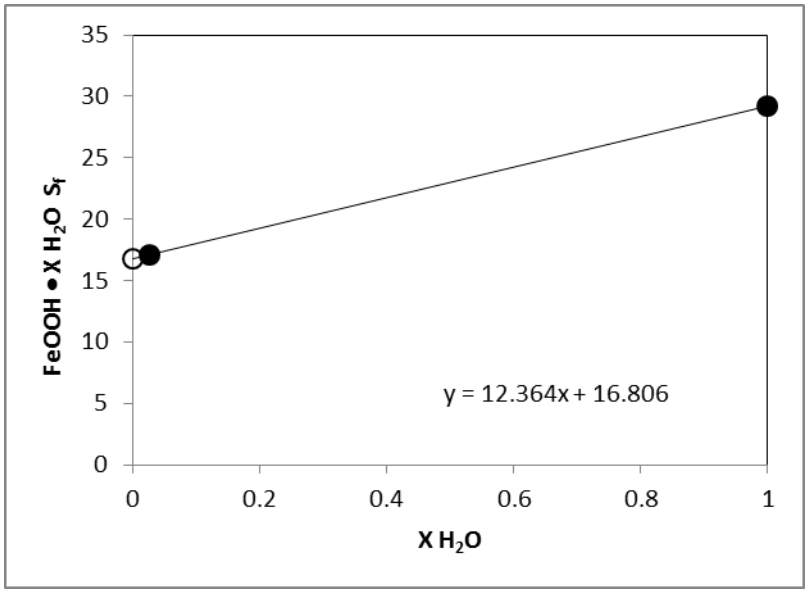

Figure G3. Entropy of formation for ferrihydrite as a function of water content using the 2-line ferrihydrite value from Snow et al. (2013) and the value estimated from the correlation depicted in Figure G2. The solid circles represent values that have known values from measurements, open circles represent the values estimated from the correlation in the figure and used in subsequent calculations.

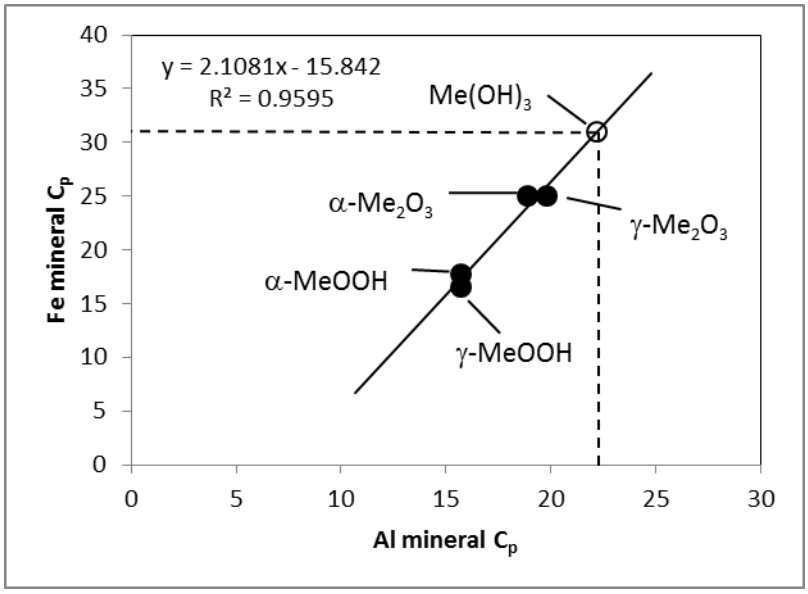

Figure G4. Heat capacities for isostructural pairs of Fe(III) and Al(III) phases: corundum-hematite, gamma alumina – maghemite, diaspore-goethtite, boehmite-lepidocrocite, and gibbsite-ferrihydrite as $Fe(OH)_3$; data located in Table G3. Closed symbols are isostructural pairs with known thermodynamic data; the open symbol is estimated from the correlation based on the known value for gibbsite.

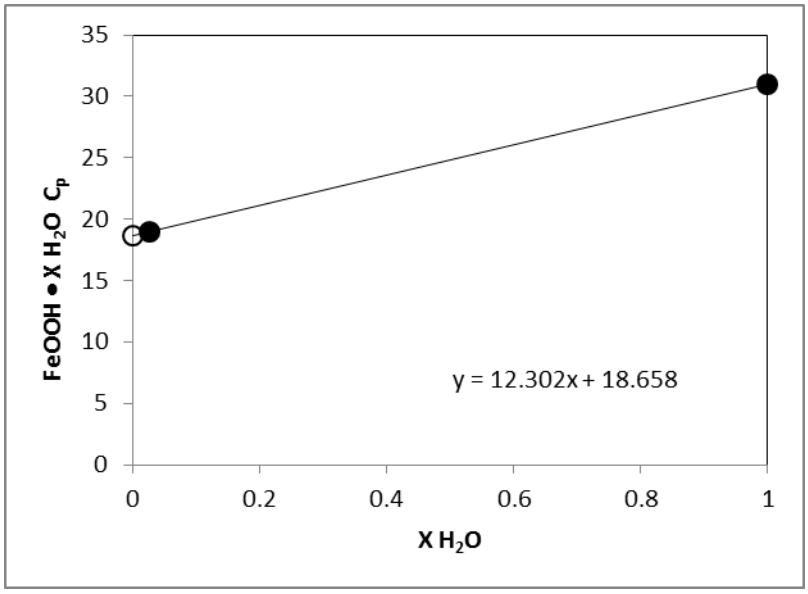

Figure G5. Heat capacity of ferrihydrite as a function of water content using the 2-line ferrihydrite value from Snow et al. (2013) and the value estimated from the correlation depicted in Figure G4. The closed circles have data associated with them or have been estimated previously; open circle represents the value estimated from the correlation on the figure and is used in subsequent calculations.

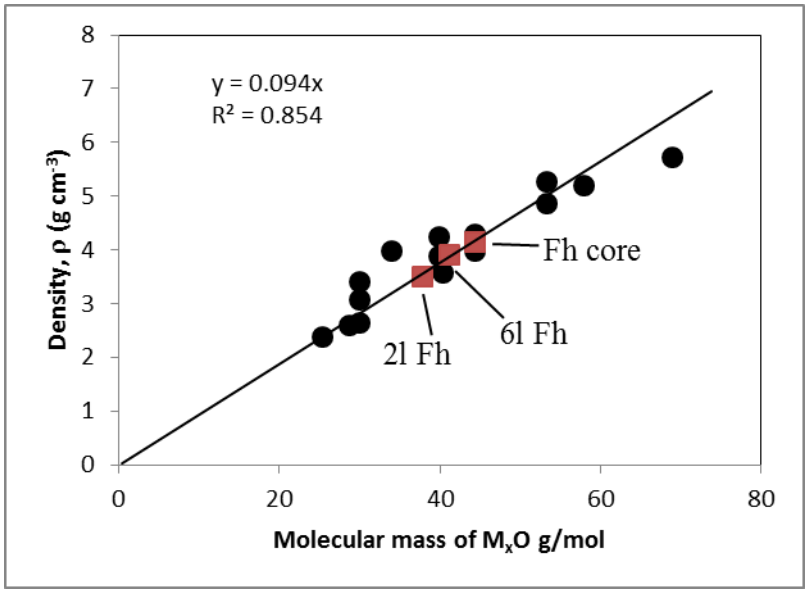

Figure G6. Correlation of density with molecular mass for oxides and (oxy)hydroxides normalized to one oxygen after Hiemstra and Riemsdijk (2009). Minerals included in the figure are: hematite, corundum, diaspora, boehmite, gibbsite, goethite, lepidocrocite, maghemite, kaolinite, quartz, periclase, anatase, rutile, feroxyte, wustite, magnetite, 2-line ferrihydrite (with nominal composition of $FeOOH \bullet 0.67H_2O$ denoted as 2l Fh), 6-line ferrihydrite(with nominal composition of $FeOOH \bullet 0.28H_2O$ denoted as 6l Fh), and the ferrihydrite core (with nominal composition of $FeOOH \bullet 0.0H_2O$ denoted as Fh core). Data for anatase and wustite are from Robie and Hemingway (1995); data for feroxyte is from Hiemstra and Riemsdijk (2009); all other data are from Wagman et al. (1982) and/or Helgeson et al. (1978). The three ferrihydrites are displayed as red squares while all other minerals are black dots. There is a direct correlation between the number of oxygens and mineral density. This trend is also apparent for the different states of hydration for ferrihydrite, as well as the slight differences in ordering between 2 and 6-line ferrihydrite. Various ice phases have been left out of the figure for simplicity.

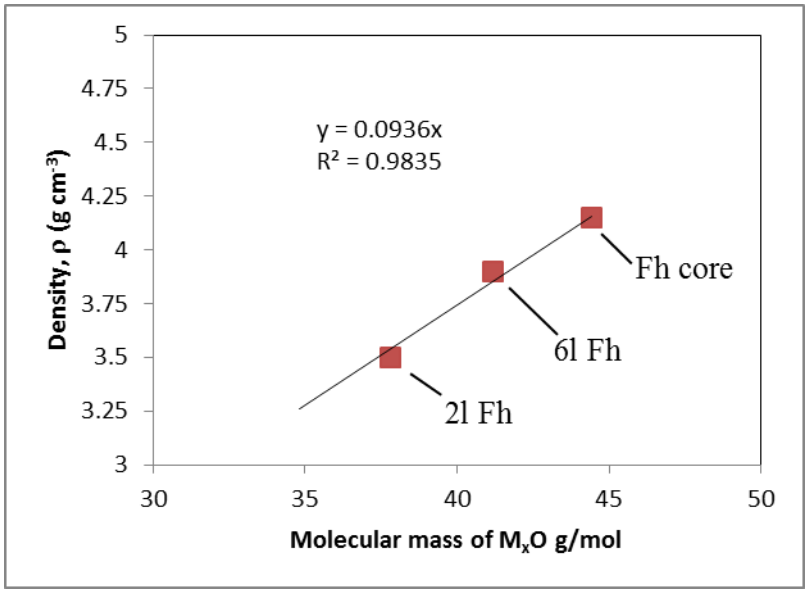

Figure G7. Density of ferrihydrite as a function of molecular mass normalized to one oxygen. The line is a linear fit to the correlation. The correlation allows one to predict the density, and therefore the volume minerals like ferrihydrite that do not have a static M_xO ratio.

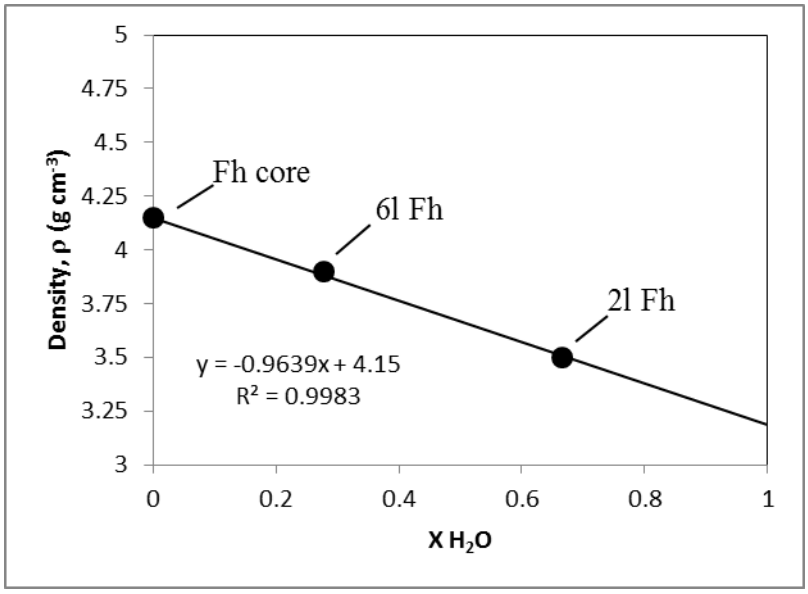

Figure G8. Relationship between density and the extent of hydration (XH_2O) for ferrihydrite. The extent of hydration can be used as a proxy for M_xO within the same mineral system because the fundamental formula for the mineral is the same and therefore the excess oxygen among minerals in different hydration states is directly dependent on the extent of hydration.

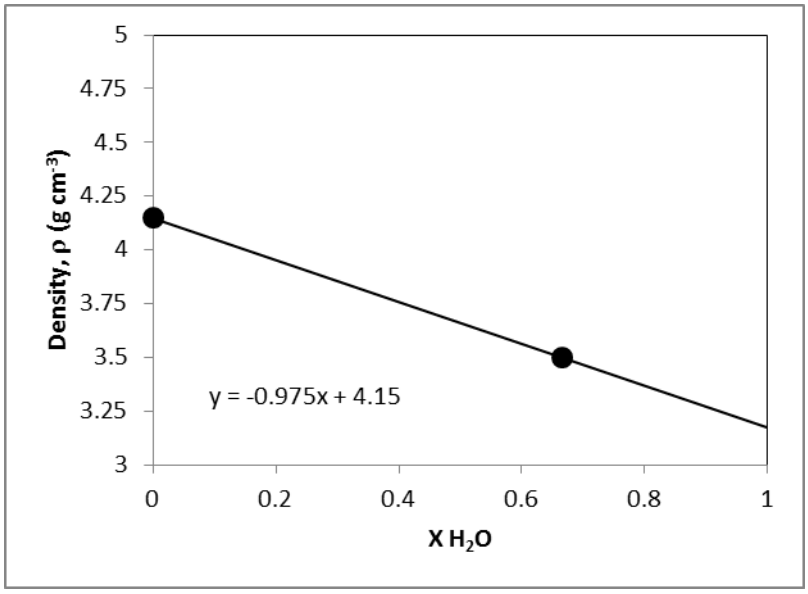

Figure G9. Relationship between density and the extent of hydration for 2-line ferrihydrite.

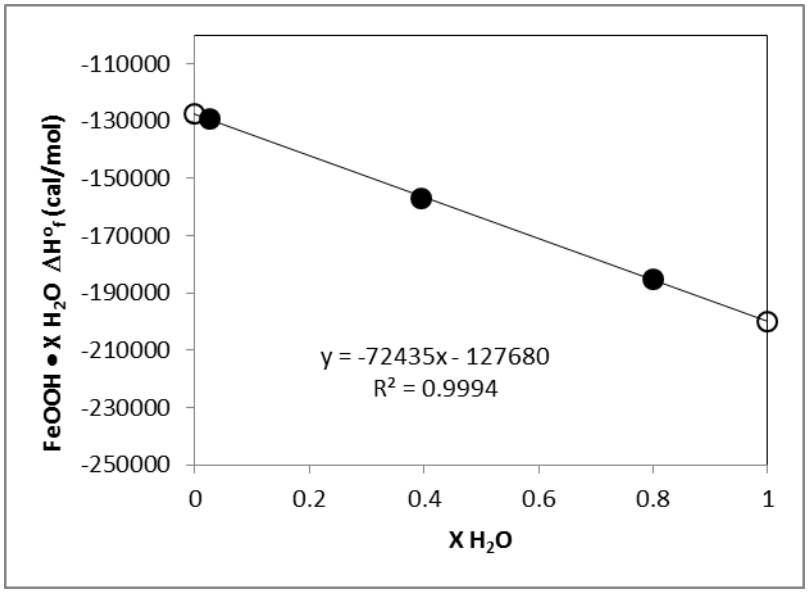

Figure G10. Enthalpy of formation of ferrihydrite (after Majzlan et al., 2004) as a function of water content using only 2-line ferrihydrite values from Majzlan et al. (2004) and Snow et al. (2013) that have been recalculated and normalized to be consistent with data from Wagman et al. (1982) and Helgeson et al. (1978). Open circles represent the values estimated from the correlation on the figure.

APPENDIX H

SET OF FIGURES FOR RANKED AFFINITIES IN CAL PER MILLILITER FOR ELECTRON ACCEPTORS FROM APPENDIX E

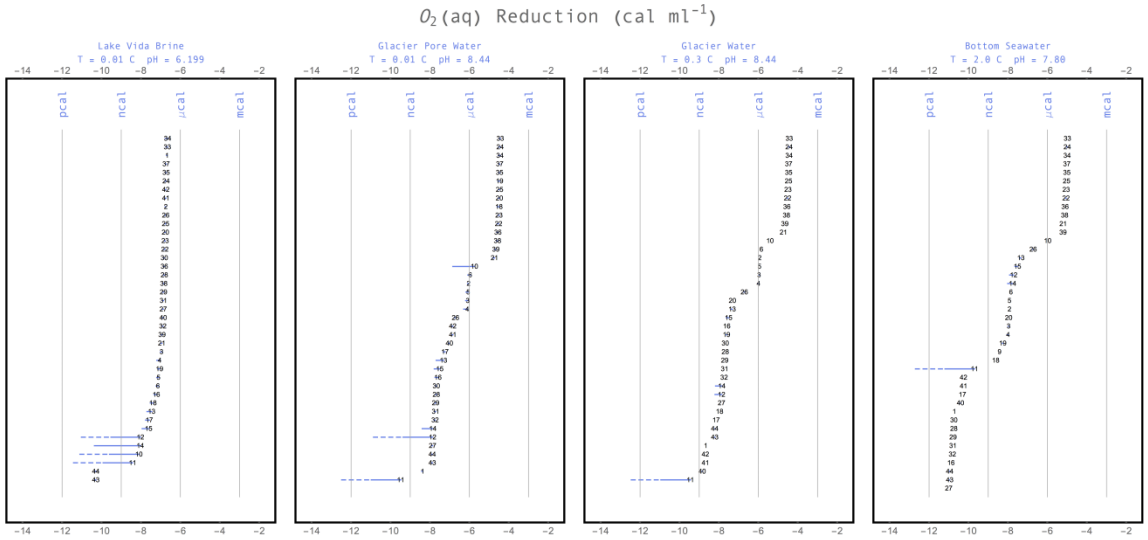
O_2(aq) Reduction (cal ml^{-1})
Lake Vida Brine
T = 0.01 C pH = 6.199
Glacier Pore Water
T = 0.01 C pH = 8.44
Glacier Water
T = 0.3 C pH = 8.44
Bottom Seawater
T = 2.0 C pH = 7.80
pcal
ncal
µcal
mcal
−14 −12 −10 −8 −6 −4 −2

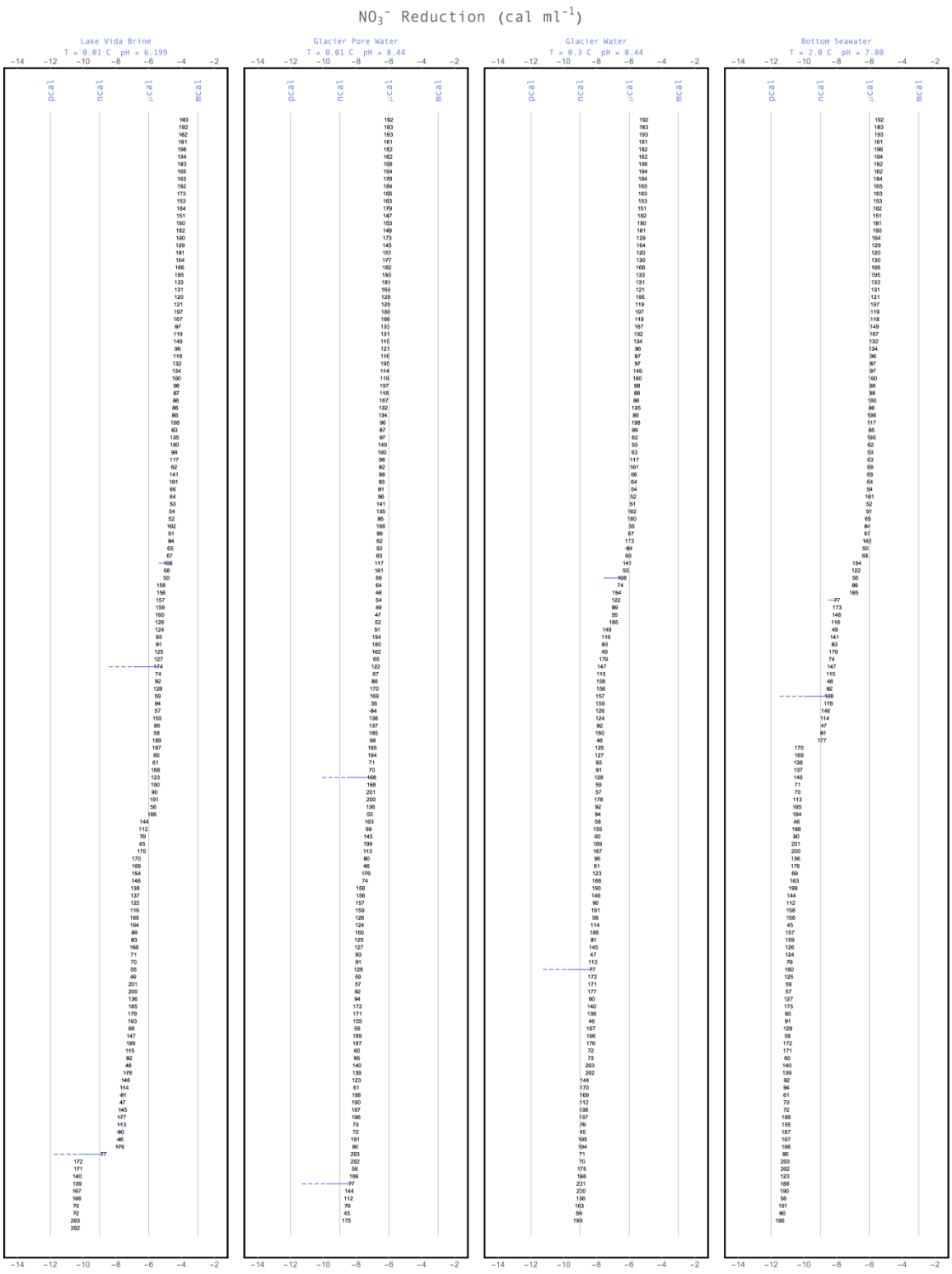
NO_3^- Reduction (cal ml^{-1})
Lake Vida Brine
T = 0.01 C pH = 6.199
Glacier Pore Water
T = 0.01 C pH = 8.44
Glacier Water
T = 0.3 C pH = 8.44
Bottom Seawater
T = 2.0 C pH = 7.80
pcal
ncal
µcal
mcal
−14
−12
−10
−8
−6
−4
−2

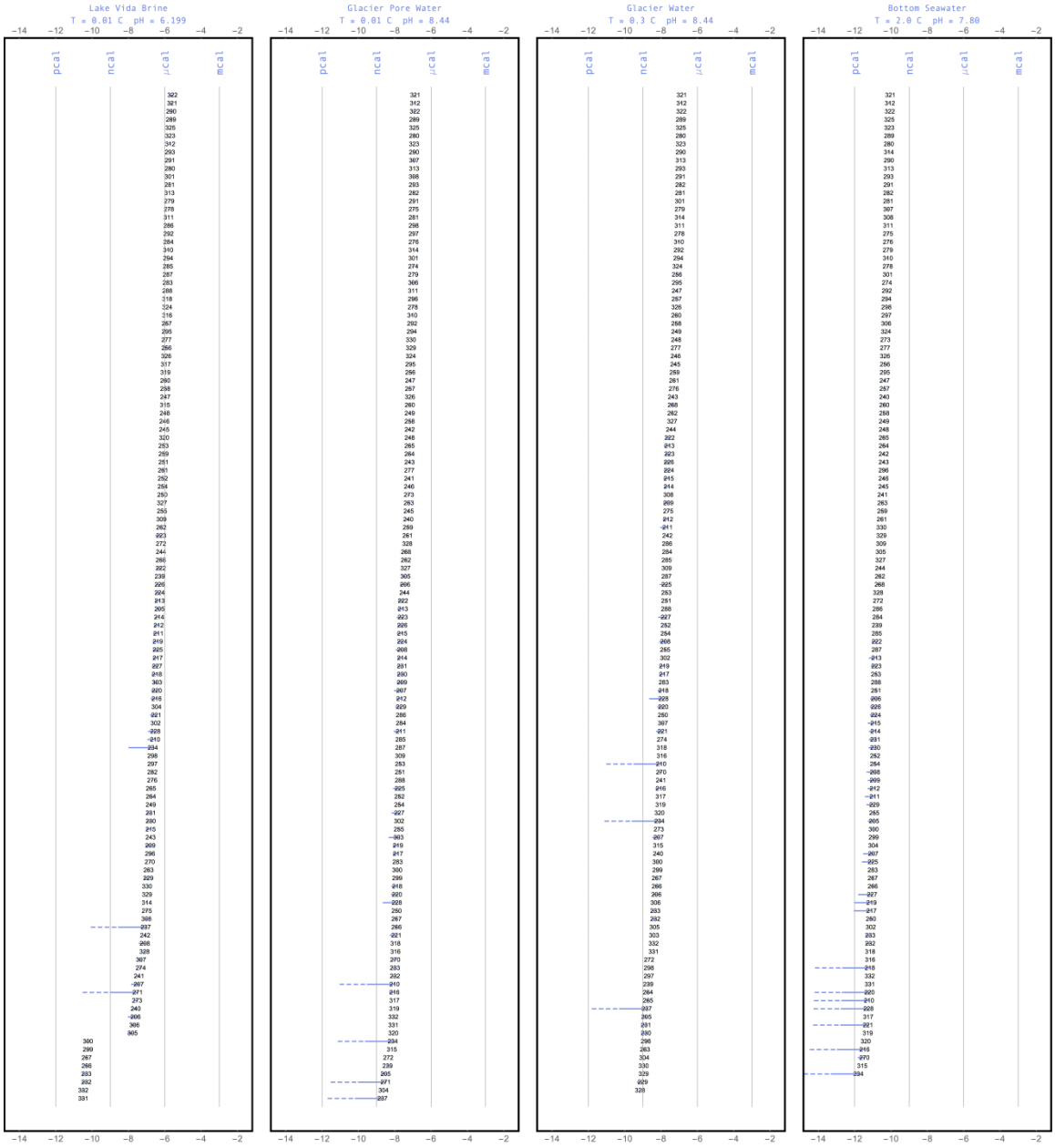
NO_2^- Reduction (cal ml^{-1})
Lake Vida Brine
T = 0.01 C pH = 6.199
Glacier Pore Water
T = 0.01 C pH = 8.44
Glacier Water
T = 0.3 C pH = 8.44
Bottom Seawater
T = 2.0 C pH = 7.80
pCal
nCal
µCal
mCal
−14 −12 −10 −8 −6 −4 −2

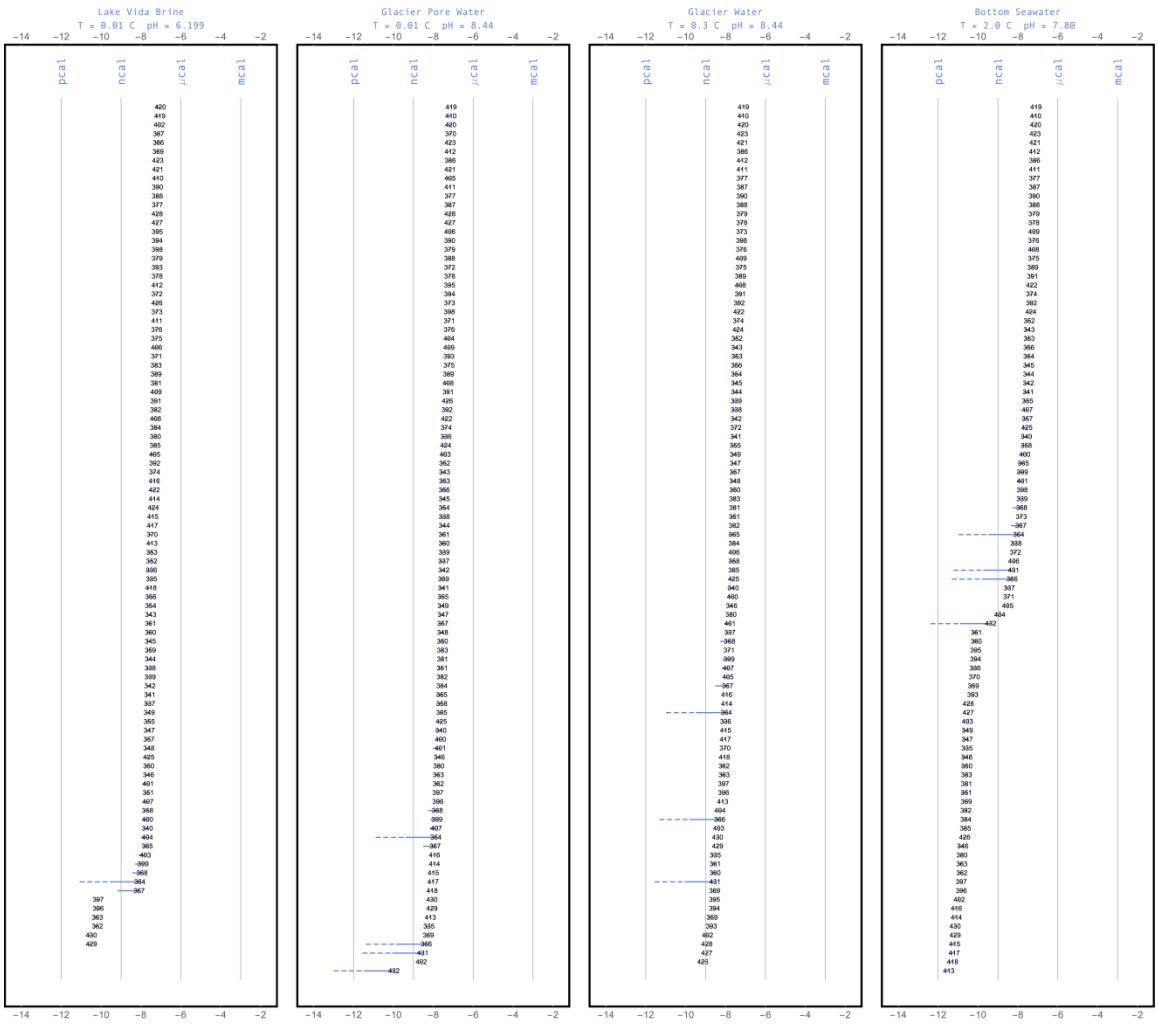
NO(aq) Reduction (cal ml^{-1})
Lake Vida Brine
T = 0.01 C pH = 6.199
Glacier Pore Water
T = 0.01 C pH = 8.44
Glacier Water
T = 0.3 C pH = 8.44
Bottom Seawater
T = 2.0 C pH = 7.80
pcal
ncal
μcal
mcal
−14 −12 −10 −8 −6 −4 −2

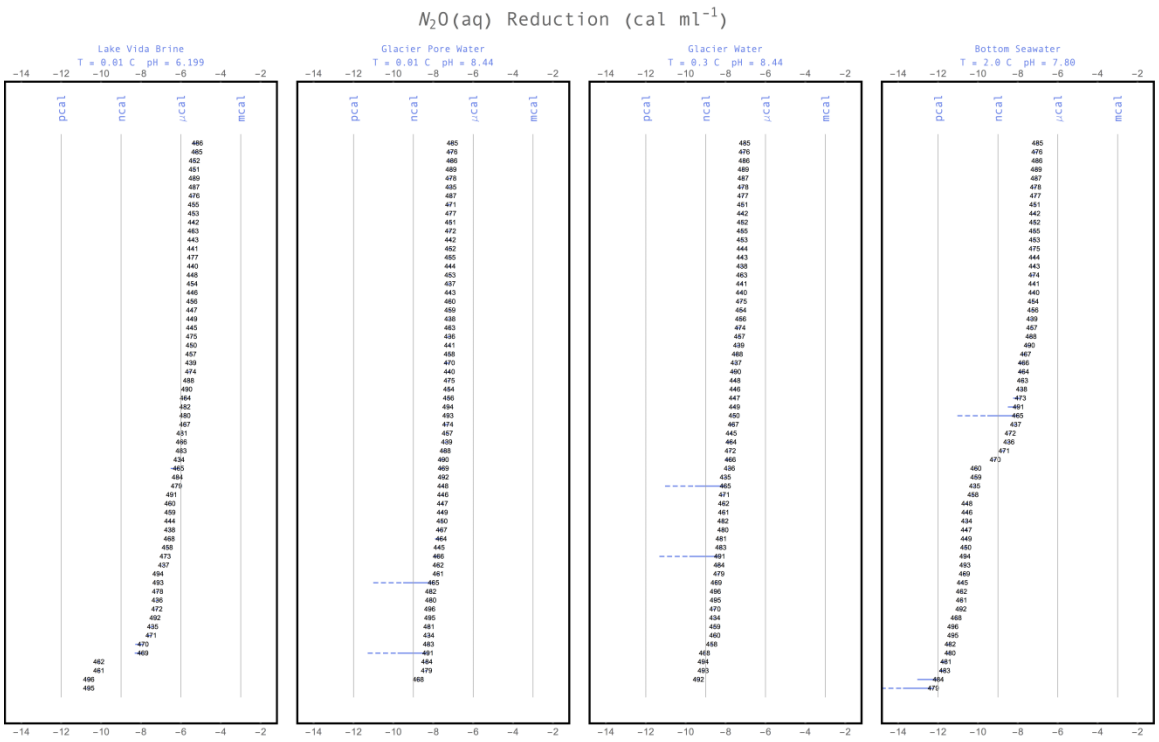
N_2O(aq) Reduction (cal ml^{-1})
Lake Vida Brine
T = 0.01 C pH = 6.199
Glacier Pore Water
T = 0.01 C pH = 8.44
Glacier Water
T = 0.3 C pH = 8.44
Bottom Seawater
T = 2.0 C pH = 7.80
pcal
ncal
µcal
mcal
−14
−12
−10
−8
−6
−4
−2

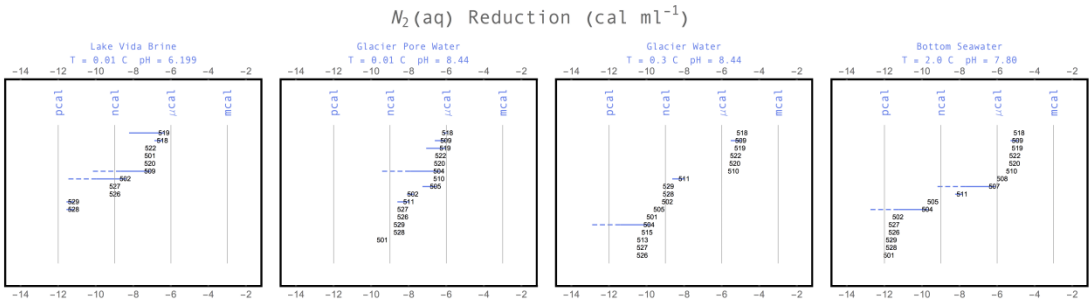
N_2(aq) Reduction (cal ml^{-1})
Lake Vida Brine
T = 0.01 C pH = 6.199
Glacier Pore Water
T = 0.01 C pH = 8.44
Glacier Water
T = 0.3 C pH = 8.44
Bottom Seawater
T = 2.0 C pH = 7.80
pcal
ncal
µcal
mcal
−14 −12 −10 −8 −6 −4 −2

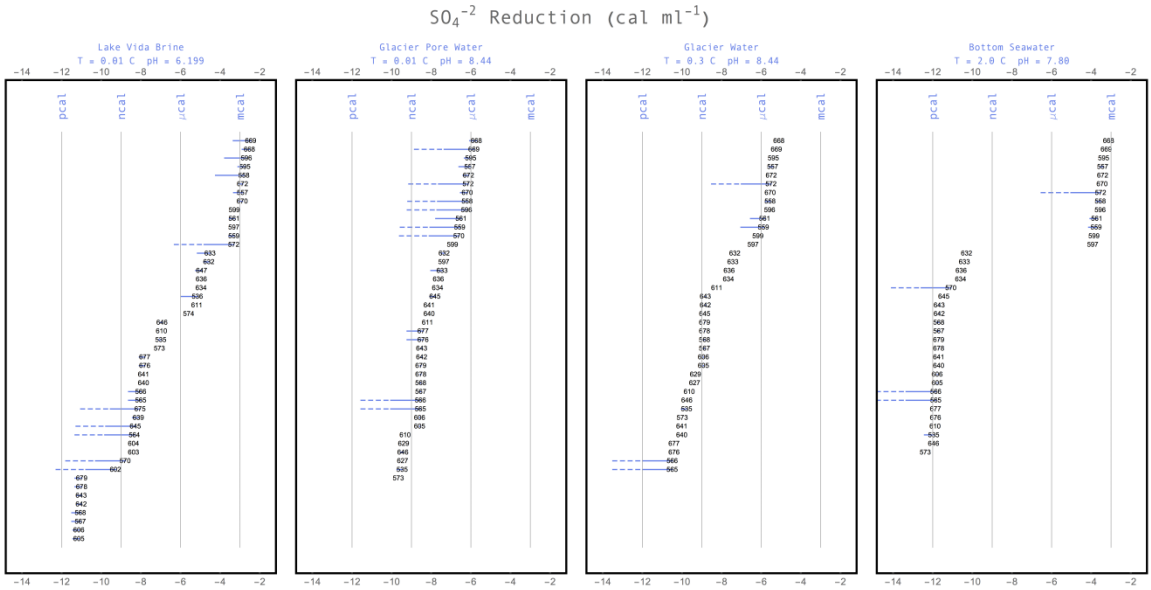
SO4-2 Reduction (cal ml-1)
Lake Vida Brine
T = 0.01 C pH = 6.199
Glacier Pore Water
T = 0.01 C pH = 8.44
Glacier Water
T = 0.3 C pH = 8.44
Bottom Seawater
T = 2.0 C pH = 7.80
pcal
ncal
µCal
mcal
−14
−12
−10
−8
−6
−4
−2

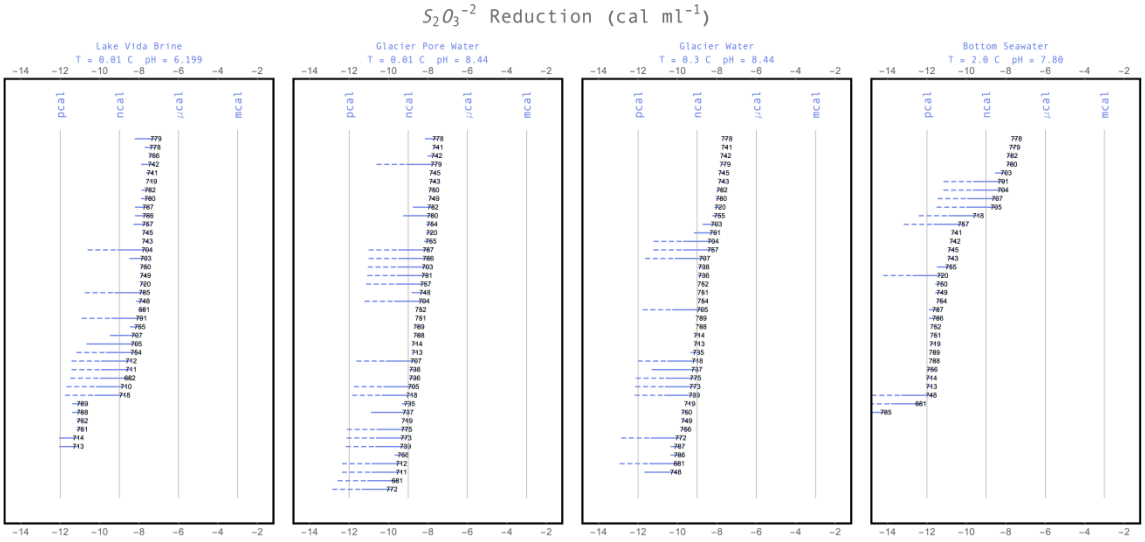
$S_2O_3^{-2}$ Reduction (cal ml^{-1})
Lake Vida Brine
T = 0.01 C pH = 6.199
Glacier Pore Water
T = 0.01 C pH = 8.44
Glacier Water
T = 0.3 C pH = 8.44
Bottom Seawater
T = 2.0 C pH = 7.80
pcal
ncal
µcal
mcal
−14 −12 −10 −8 −6 −4 −2

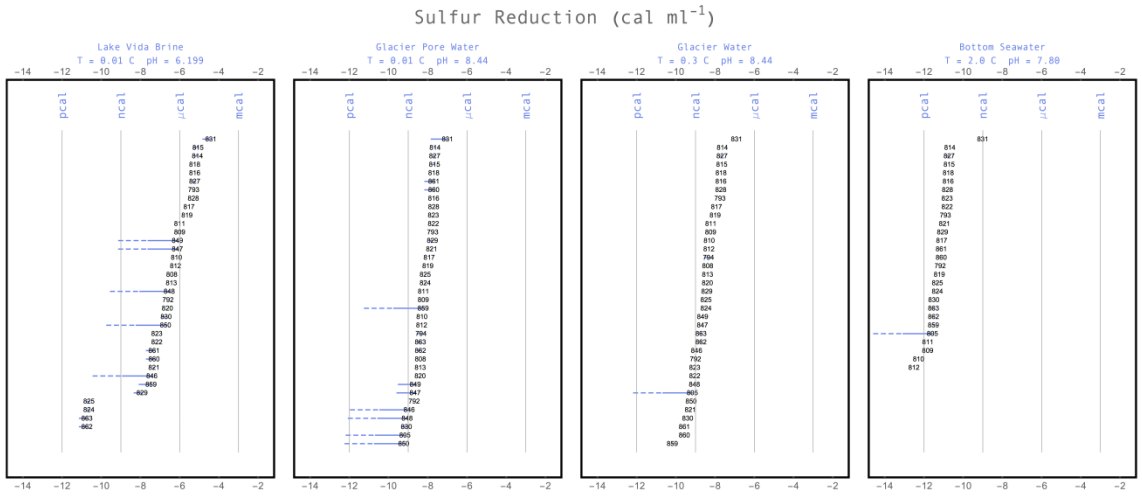
Sulfur Reduction (cal ml^{-1})
Lake Vida Brine
T = 0.01 C pH = 6.199
Glacier Pore Water
T = 0.01 C pH = 8.44
Glacier Water
T = 0.3 C pH = 8.44
Bottom Seawater
T = 2.0 C pH = 7.80
pcal
ncal
µcal
mcal
−14
−12
−10
−8
−6
−4
−2

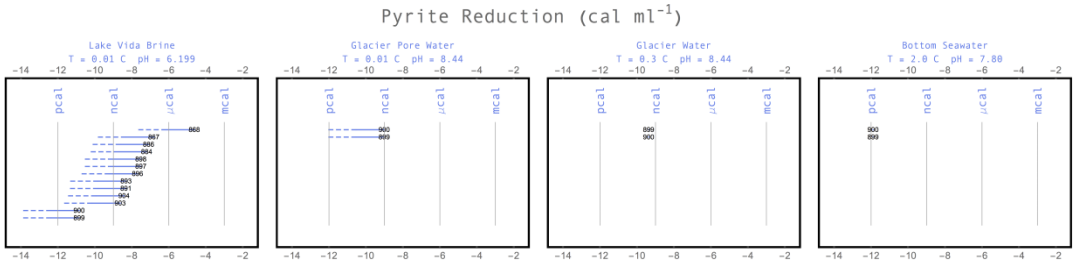
Pyrite Reduction (cal ml^{-1})
Lake Vida Brine
T = 0.01 C pH = 6.199
Glacier Pore Water
T = 0.01 C pH = 8.44
Glacier Water
T = 0.3 C pH = 8.44
Bottom Seawater
T = 2.0 C pH = 7.80
pcal
ncal
µcal
mcal
−14 −12 −10 −8 −6 −4 −2
868
867
886
884
895
897
896
893
891
904
903
900
899

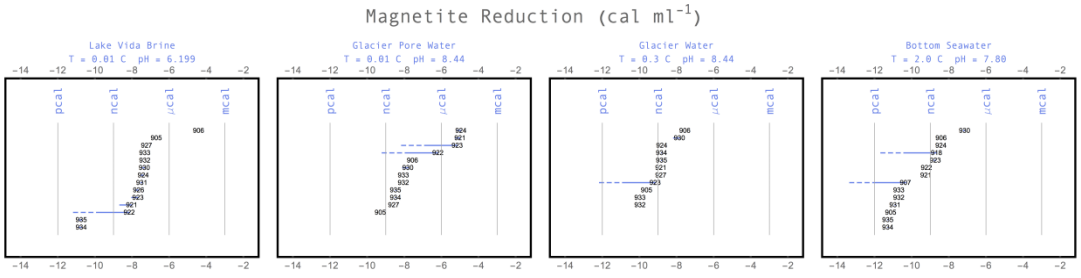
Magnetite Reduction (cal ml^{-1})
Lake Vida Brine
T = 0.01 C pH = 6.199
Glacier Pore Water
T = 0.01 C pH = 8.44
Glacier Water
T = 0.3 C pH = 8.44
Bottom Seawater
T = 2.0 C pH = 7.80
pcal
ncal
µcal
mcal
−14 −12 −10 −8 −6 −4 −2

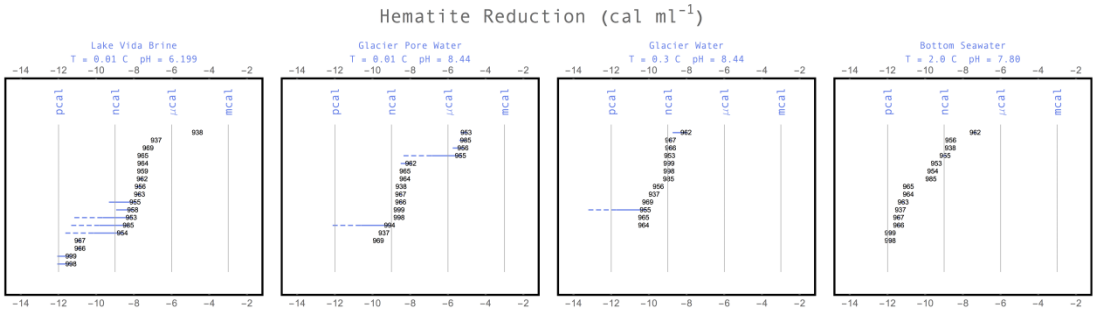
Hematite Reduction (cal ml^{-1})
Lake Vida Brine
T = 0.01 C pH = 6.199
Glacier Pore Water
T = 0.01 C pH = 8.44
Glacier Water
T = 0.3 C pH = 8.44
Bottom Seawater
T = 2.0 C pH = 7.80
pcal
ncal
µcal
mcal
−14 −12 −10 −8 −6 −4 −2

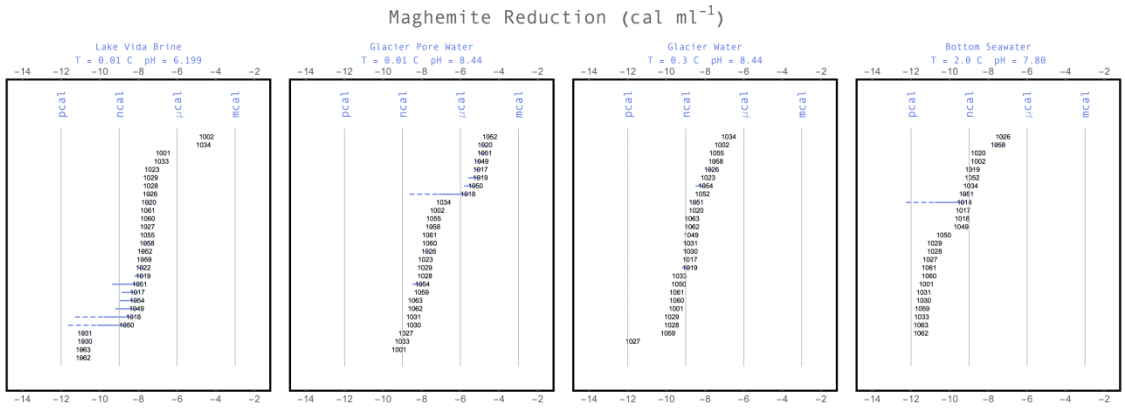
Maghemite Reduction (cal ml^{-1})
Lake Vida Brine
T = 0.01 C pH = 6.199
Glacier Pore Water
T = 0.01 C pH = 8.44
Glacier Water
T = 0.3 C pH = 8.44
Bottom Seawater
T = 2.0 C pH = 7.80
pcal
ncal
µcal
mcal
−14 −12 −10 −8 −6 −4 −2

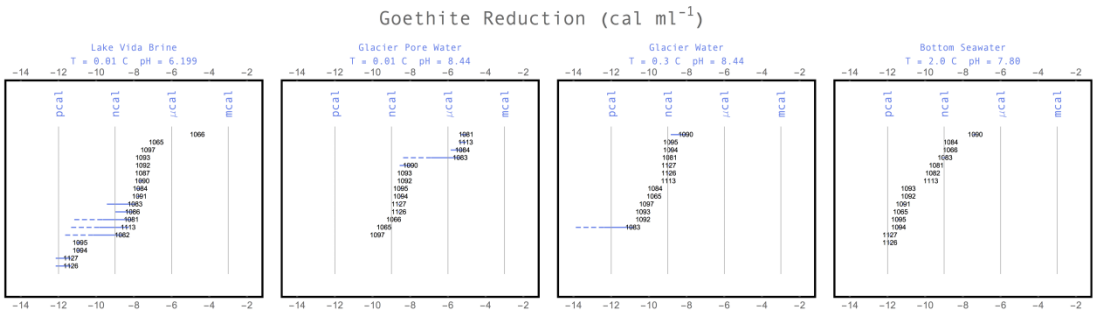
Goethite Reduction (cal ml^{-1})
Lake Vida Brine
T = 0.01 C pH = 6.199
Glacier Pore Water
T = 0.01 C pH = 8.44
Glacier Water
T = 0.3 C pH = 8.44
Bottom Seawater
T = 2.0 C pH = 7.80
pcal
ncal
µcal
mcal
−14 −12 −10 −8 −6 −4 −2

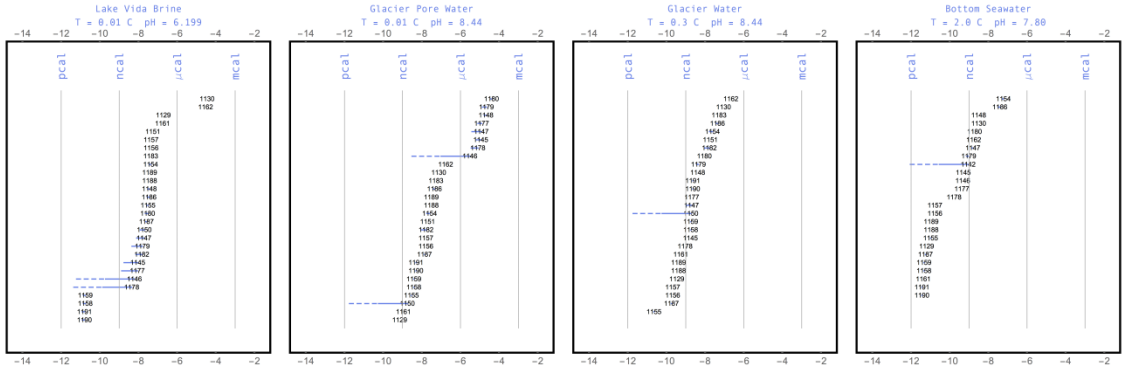
Lepidocrocite Reduction (cal ml^{-1})
Lake Vida Brine
T = 0.01 C pH = 6.199
Glacier Pore Water
T = 0.01 C pH = 8.44
Glacier Water
T = 0.3 C pH = 8.44
Bottom Seawater
T = 2.0 C pH = 7.80
pcal
ncal
µcal
mcal
−14 −12 −10 −8 −6 −4 −2

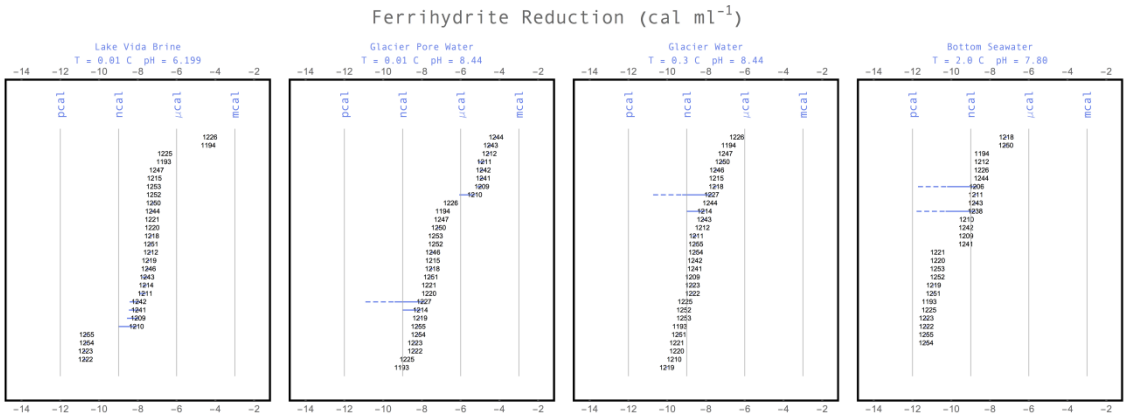
Ferrihydrite Reduction (cal ml^{-1})
Lake Vida Brine
T = 0.01 C pH = 6.199
Glacier Pore Water
T = 0.01 C pH = 8.44
Glacier Water
T = 0.3 C pH = 8.44
Bottom Seawater
T = 2.0 C pH = 7.80
pcal
ncal
µcal
mcal
−14 −12 −10 −8 −6 −4 −2

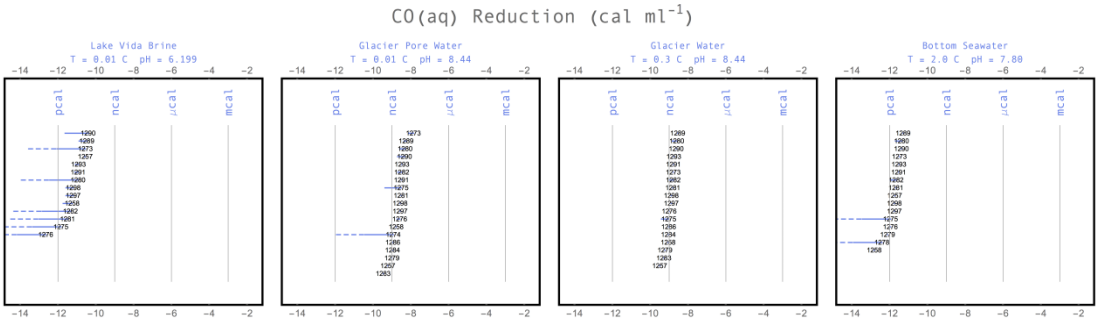
CO(aq) Reduction (cal ml^{-1})
Lake Vida Brine
T = 0.01 C pH = 6.199
Glacier Pore Water
T = 0.01 C pH = 8.44
Glacier Water
T = 0.3 C pH = 8.44
Bottom Seawater
T = 2.0 C pH = 7.80
pcal
ncal
µcal
mcal
−14 −12 −10 −8 −6 −4 −2

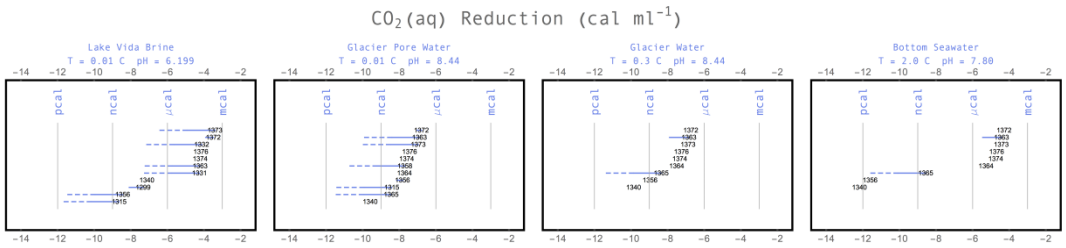
CO_2(aq) Reduction (cal ml^{-1})
Lake Vida Brine
T = 0.01 C pH = 6.199
Glacier Pore Water
T = 0.01 C pH = 8.44
Glacier Water
T = 0.3 C pH = 8.44
Bottom Seawater
T = 2.0 C pH = 7.80
pcal
ncal
µcal
mcal
−14 −12 −10 −8 −6 −4 −2

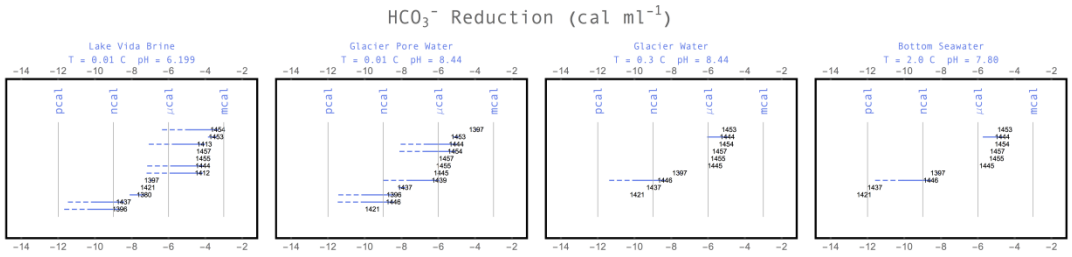
HCO3- Reduction (cal ml-1)
Lake Vida Brine
T = 0.01 C pH = 6.199
Glacier Pore Water
T = 0.01 C pH = 8.44
Glacier Water
T = 0.3 C pH = 8.44
Bottom Seawater
T = 2.0 C pH = 7.80
pcal
ncal
µcal
mcal
−14 −12 −10 −8 −6 −4 −2

APPENDIX I

CONSTRUCTION OF P-T-D FIGURES FOR THE SUBSURFACE BIOSPHERE

Pressure estimates were made in cases where enough data existed for the system that a reliable calculation could be made. Marine samples often included a seawater depth, which was converted to pressure assuming that a column of seawater of 10.3 m would exert 1 atm or 1.013 bar of pressure. For continental samples, pressure was calculated as overburden using either lithostatic or hydrostatic pressure, whichever was appropriate for the system. Overburden was calculated as follows:

$$P_{ob} = \rho * g * d$$

where P_{ob} is overburden pressure in Pa, ρ is density in kg m^{-3}, g is the gravitational constant, (9.806 m s^{-2}) and d is the depth in meters. This provides a fair estimation of the pressure beyond that which the atmosphere exerts on a sample at depth. If the density of a particular rock type was unavailable for a sampling site from literature sources, an average density was used, i.e., 2.65 g/cc for granite, 2.55 g/cc for sandstone, and 0.92 g/cc for ice. Some ground water pressures required an extra step to estimate the *in situ* down-borehole pressures because the only available information was the depth and the artesian head. For example, one sampling site came from a depth of 1270 m from an artesian well with a head pressure of 466 ft or ~142 m. This indicates the ability of the well pressure to sustain a column of water 142 m above the surface, making the total pressure at the sampling locale that of a column of water under hydrostatic pressure with a depth of 1412m plus the one bar of pressure for the atmosphere at that spot or a total of ~140 bars.

References for data and pressure estimates:

Amend and Shock (2001), Apps (2010), Arcuri and Ehrlich (1977), Ask et al. (2001), Bakermans et al. (2006), Bale et al. (1997), Bartlett (2002), Bernhardt et al. (1988), Bonch-Osmolovskaya et al. (2003), Böning et al. (2004), Brazelton and Baross (2009), Breezee et al. (2004), Byers et al. (1998), Canganella et al. (1997), Carvalho (2013), Chivian et al (2008), Collins et al. (2010), D'Elia et al. (2008), Daumas et al. (1986), Daumas et al. (1988), DeLong et al. (1997), Delwiche et al. (1996), Deming and Baross (1986), Deming et al. (1988), Ehrlich et al. (1972), Ekendahl and Pedersen (1994), Ellis and Ege (1975), Erauso et al. (1993), Fardeau et al. (2000), Fell (1967), Grabowski et al. (2005), Greene et al. (1997), Grossman and Shulman (1995), Haldeman et al. (1993), Havig et al. (2011), Inagaki et al. (2003), Johnson et al. (1992), Kaksonen et al. (2006a), Kaksonen et al. (2006b), Kato et al (1995), Kato et al (1996), Kato et al (1997), Kato et al (1998), Kieft et al. (1999), Kieft et al. (2005), Kimura et al. (2005), Klouche et al. (2007), Kotelnikova and Pedersen (1998), Kotelnikova et al. (1998), Kotlar et al. (2011), L'Haridon et al. (1995), Li et al. (2006), Li et al. (2007), Li et al. (2010), Liesack et al. (1991), Lui et al. (1997), Loiacono et al. (2012), Love et al. (1993), Marteinsson et al. (1999), Marteinsson et al. (2012), Meersman et al. (2013), Myer-Dombard et al. (2011), Milller et al. (1998), Miyoshi et al. (2005), Mochimaru et al. (2007), Mori et al. (2002), Morita and ZoBell (1955), Motamedi and Pedersen (1998), Nakai et al. (2011), Nazina et al. (2007), Nilsen and Torsvik (1996), Nilsen et al. (1996a), Nilsen et al. (1996b), Nogi et al. (1998), Nunoura et al. (2005), Olson et al. (1981), Onstott et al. (1997), Onstott et al. (1998), Panikov and Sizova (2007), Parkes et al. (1994), Pedersen (1997), Pedersen and Ekendahl (1990), Pope et al. (1975), Price and Sowers (2004), Rivkina et al. (2000),

Rosnes et al. (1991), Russell et al. (1994), Sahl et al. (2008), Salamatin et al. (1998), Salisbury et al. (2002), Schippers and Neretin (2006), Scholander et al. (1965), Schwarz and Colwell (1975), Schwarz and Colwell (1975), Schwarz et al. (1975), Sharma et al. (2002), Shi et al. (1997), Shock (2009), Stetter et al. (1993), Steurer and Underwood (2003), Stevens et al. (1993), Stevens and McKinley (1995), Szewzyk et al. (1994), Szewzyk et al. (1997), Takai et al. (2001a), Takai et al. (2001b), Takai et al. (2002), Takai et al. (2005), Takai et al. (2008), Tanaka et al. (2001), Tardy-Jacquenod et al. (1998), Tobal (1993), Trimarco et al. (2006), Turley (2000), Vanlint et al. (2011), Wanger et al. (2012), Winnock and Pontalier (1970), Wouters et al. (2013), Wynter et al. (1996), Ynagibayashi et al. (1999), Yayanos et al. (1981), Yayanos and Dietz (1982), Yayanos et al. (1982), Yayanos (1986), Yoshioka et al (2009), Zhan et al. (2005), Zhan et al. (2006), Zimov et al. (2006), Zink et al. (2003), ZoBell (1952), ZoBell and Morita (1957), ZoBell (1958).